50 Copies

NATIONAL AERONAUTICS AND SPACE ADMINISTRATION

Technical Report 32-1249

Mariner Venus 67 Spacecraft Environmental Test Results

George C. Ragsdale
Donald C. Mesnard

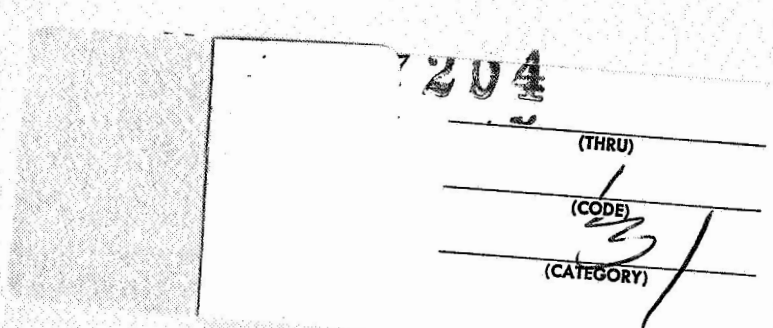

JET PROPULSION LABORATORY
CALIFORNIA INSTITUTE OF TECHNOLOGY
PASADENA, CALIFORNIA

June 15, 1968

NATIONAL AERONAUTICS AND SPACE ADMINISTRATION

Technical Report 32-1249

Mariner Venus 67 Spacecraft Environmental Test Results

George C. Ragsdale
Donald C. Mesnard

Approved by:

W. S. Shipley, *Manager*
Environmental Requirements Section

D. Schneiderman, *Project Manager*
Mariner Venus 67

JET PROPULSION LABORATORY
CALIFORNIA INSTITUTE OF TECHNOLOGY
PASADENA, CALIFORNIA

June 15, 1968

TECHNICAL REPORT 32-1249

Prepared Under Contract No. NAS 7-100
National Aeronautics & Space Administration

Foreword

The authors – George C. Ragsdale, Spacecraft Environmental Requirements Engineer during the post-launch phase of the *Mariner* Venus 67 Project, and Donald C. Mesnard – prepared this report because of the clear value in having a single reference volume documenting the various types of information pertaining to the spacecraft environmental test program for the *Mariner* Venus 67 Project.

The success of the overall environmental program is evidenced by the *Mariner V* flight record. However, to provide a report of greatest worth, the program has been critically reviewed in this document. Contained is information relating to type-approval and flight-acceptance tests at the subsystem and system levels, and to special developmental tests – which are generally performed at the subsystem level, as well as data from magnetic control.

It is anticipated that the readers' deductions, together with the conclusions and recommendations contained in this report, will serve advantageously in the development of future projects.

Acknowledgment

Valuable contributions were made to this report and to the environmental test program by James E. Maclay, who was the Spacecraft Environmental Requirements Engineer during the prelaunch phase of the *Mariner* Venus 67 Project, and by Jay D. Schmuecker, who was the Engineering and Mechanics Division Representative during the *Mariner* Venus 67 Project. Appreciation is expressed to these individuals and to John Schlue and George L. Parker, who performed the final check of this documentation.

Also acknowledged are the contributions from the following listed group supervisors, cognizant engineers, and other supporting personnel who made the environmental test program so successful:

B. Anspaugh	A. Delgadillo	G. Kunkel
P. Barnett	T. De Vries	D. Miller
J. Bastow	L. Dumas	M. O'Neill
R. Becker	E. Floyd	J. Randolph
A. Campbell	D. Frankos	W. Read
W. Carroll	R. Freeland	D. Swenson
J. Chisholm	T. Gindorf	M. Trummel
G. Coyle	J. Goldsmith	H. Von Delden
R. Dawe	L. Keeler	D. Wiksten

Contents

Contents (contd)

Contents (contd)

Contents (contd)

Tables

Contents (contd)

Tables (contd)

Contents (contd)

Tables (contd)

Figures

Contents (contd)

Figures (contd)

Contents (contd)

Figures (contd)

Contents (contd)

Figures (contd)

Contents (contd)

Figures (contd)

Contents (contd)

Figures (contd)

Contents (contd)

Figures (contd)

Contents (contd)

Figures (contd)

Abstract

This report details the *Mariner* Venus 67 environmental program, which included type-approval (TA) testing, developmental and special investigative testing, and flight-acceptance (FA) testing at both the subsystem and system levels. First, the overall test program is described and summarized; then the development and qualification of the spacecraft are discussed; and finally, the FA testing of each spacecraft and its subsystem is described. Within each section, the tests are described in detail and results are given. Problems encountered during testing and anomalies resulting from the tests are discussed, and summaries of all waivers and test deviations are included. A section is included that discusses the magnetic control test program, and the appendixes contain information on special tests and subjects related to the spacecraft environmental test program. The depth of coverage of the report allows an evaluation of the philosophy forming a basis for the test program. Recommendations for future programs result from these evaluations and are included in the final section of the report.

Mariner Venus 67 Spacecraft Environmental Test Results

I. Description of Environmental Test Program

The objective of the *Mariner* Venus 67 environmental test program was to provide high assurance of achieving a successful flight mission. Since there was no flight-test program, the ground tests had to provide adequate evaluation of all achievable variables of spacecraft functions and environments that were expected to occur in flight.

To accomplish this objective, the convention evolved at JPL has been to demonstrate design adequacy by requiring successful type approval (TA) tests of flight quality subsystems and of a flight quality system. The TA test levels are intended to be in excess of environmental conditions predicted for the mission. Subsystem TA tests qualify the units for all mission environments of significance, including those experienced prior to, and following, their assembly into the system configuration. System TA tests are generally accomplished using a proof test model (PTM) spacecraft, and are limited to those mission environments which may result in significant intra-system interactions with those environments. Flight acceptance (FA) tests of flight and spare subsystems and systems are accomplished to identify workmanship and manufacturing flaws and to assure that the flight equipment is representative of the qualified design. FA test levels are intended to equal the extremes of the predicted mission environments.

In establishing the test program for *Mariner* Venus 67, several modifications to JPL Flight Project convention were made because of the Project's concept of using the basic *Mariner* Mars 1964 spacecraft design and hardware to the greatest extent possible. The modified program included the FA testing of a flight spacecraft and a flight support spacecraft at both the subsystem and system levels. Type approval testing was generally conducted at the subsystem level, only, since no proof test model (PTM) was provided for system level TA testing. Both a structural test model (STM) and a temperature control model (TCM) were provided, and these were used for their usual purposes. Additionally, the STM was used for the TA vibration testing of some subsystems whose vibration environment was greatly affected by spacecraft system interaction. The deletion of system-level TA testing and the corresponding lack of a PTM were based on the consideration of the *Mariner* Mars 1964 spacecraft as an environmentally qualified design. This same judgement resulted in the requiring of subsystem TA testing of only those items whose changes in design or predicted environment dictated new TA tests. In certain instances, the changes in mission parameters—resulting in either modifications to the environmental test requirements or hardware design changes—dictated a requirement for special tests for the requalification of portions of the spacecraft system whose qualification was rendered invalid by the changes. Also, hardware that was FA tested for the *Mariner* Mars 1964 project and used on the *Mariner* Venus 67 without change was generally not retested. Type-approval and flight-acceptance testing usually consisted of vibration tests and thermal vacuum tests.

In this report, an attempt is made to show the relationship between the testing philosophy and the results. Variations in the behavior of subsystems and/or systems in the same environment are pointed out when possible.

A. Objectives of *Mariner* Venus 67 Environmental Test Program

At the start of the *Mariner* Venus 67 Project, goals for the test program were established. In general, the philosophy of the Project was to provide a Venus fly-by mission capability in 1967, using the basic *Mariner* Mars 1964 spacecraft design[1] and hardware to the greatest practical extent. The basic plan was to have a flight[2] spacecraft (M67-2) and a flight-support[3] spacecraft (M67-1) completely FA tested, both at the subsystem and system levels. The design was to be adequately TA tested at the assembly level. However, no PTM was provided for system-level TA testing.

The goal of the environmental test program, then, was to ensure that the policies were realized – obtaining maximum results without a PTM. The general approach of the environmental testing program was to consider the *Mariner* Venus 67 design (Fig. 1) a derivation of the adequately qualified *Mariner* Mars 1964 design, making optimum use of the earlier *Mariner* test experience. After a reexamination of the general TA and FA test levels, it was felt that they were still appropriate for the Venus mission; however, certain procedural changes, which had negligible effects on the test level, were made to facilitate testing. The *Mariner IV*[4] testing program was critically reviewed to determine what parts of the spacecraft were invalidated by design and mission changes.

Following the evaluation, requalification testing was performed at the subsystem level. As a result of the subsystem assessments, of the 38 assemblies that were environmentally tested during the *Mariner* Mars 1964 test program, it was decided that 25 of these assemblies should be subjected again to some degree of TA testing – 10 because they were new designs, 12 because of design change between the *Mariner* Mars 1964 and *Mariner* Venus 67 (including 2 that would have required retesting for new environments, independent of the design change), and 3 because their new environment would exceed *Mariner* Mars 1964 test levels. Because there was no PTM, several items, whose environments were strongly influenced by the spacecraft system, were either partially, or wholly, qualified for vibration aboard the STM; these were: solar panels, solar-panel-tip dampers, dual-frequency receiver (DFR) antennas, temperature-control references, high-gain antenna deployment assembly, and numerous thermal-control shields and blankets.

Of the 38 assemblies for each of the spacecraft, all but 3 (on each spacecraft) were FA tested at the subsystem level prior to delivery to the spacecraft assembly facility (SAF); the *Mariner* Mars 1964 testing on those 3 was still valid. In the event of subsequent rework because of Engineering Change Requests (ECRs) or Problem/Failure Reports (PFRs), each assembly was carefully reviewed to determine the degree of FA retesting required.

After assembly, both spacecraft were FA tested to conservative levels for vibration, thermal–vacuum and electromagnetic interference (EMI), and all the important pyrotechnic devices were fired.

B. Realization of Test Program Objectives

All of the goals regarding the *Mariner* Venus 67 test program were realized – in fact, in many cases, more satisfactorily so than those for the *Mariner II* and the *Mariner IV* test programs. A greater depth of penetration was possible – and necessary – on the *Mariner* Venus 67 program, because of the fact that the spacecraft hardware and gross design had been previously qualified, permitting emphasis to be placed on specific hardware items for which either the hardware or the environment had changed.

The current success of *Mariner V* could not have been achieved without a highly successful environmental test

[1]The *Mariner* Mars 1964 spacecraft were the *Mariners III* and *IV*, from the *Mariner C* block. The various spacecraft were: the MC-1, proof test model; MC-2, which became *Mariner III;* MC-3, which became *Mariner IV;* MC-4, the flight spare; and MC-5, which comprised a partial set of critical spare units.

[2]The flight spacecraft (M67-2) was made up of the MC-4 frame with new subsystem hardware, if available; the remainder of the subsystem comprised hardware, first, from MC-5, which was a partial spacecraft made up of selected spares, and then, from the MC-4, the spare spacecraft for the *Mariner* Mars 1964.

[3]The flight spare spacecraft (M67-1) was made up of the MC-1 frame with the best remaining subsystems from MC-4, as well as subsystems from MC-1 (the PTM for the *Mariner* Mars 1964), and some TA subsystems. (MC-3 spacecraft became the *Mariner IV.*)

[4]The *Mariner* Mars 1964 spacecraft was referred to as *Mariner IV* after launch; the *Mariner* Venus 67 spacecraft was designated *Mariner V* following launch.

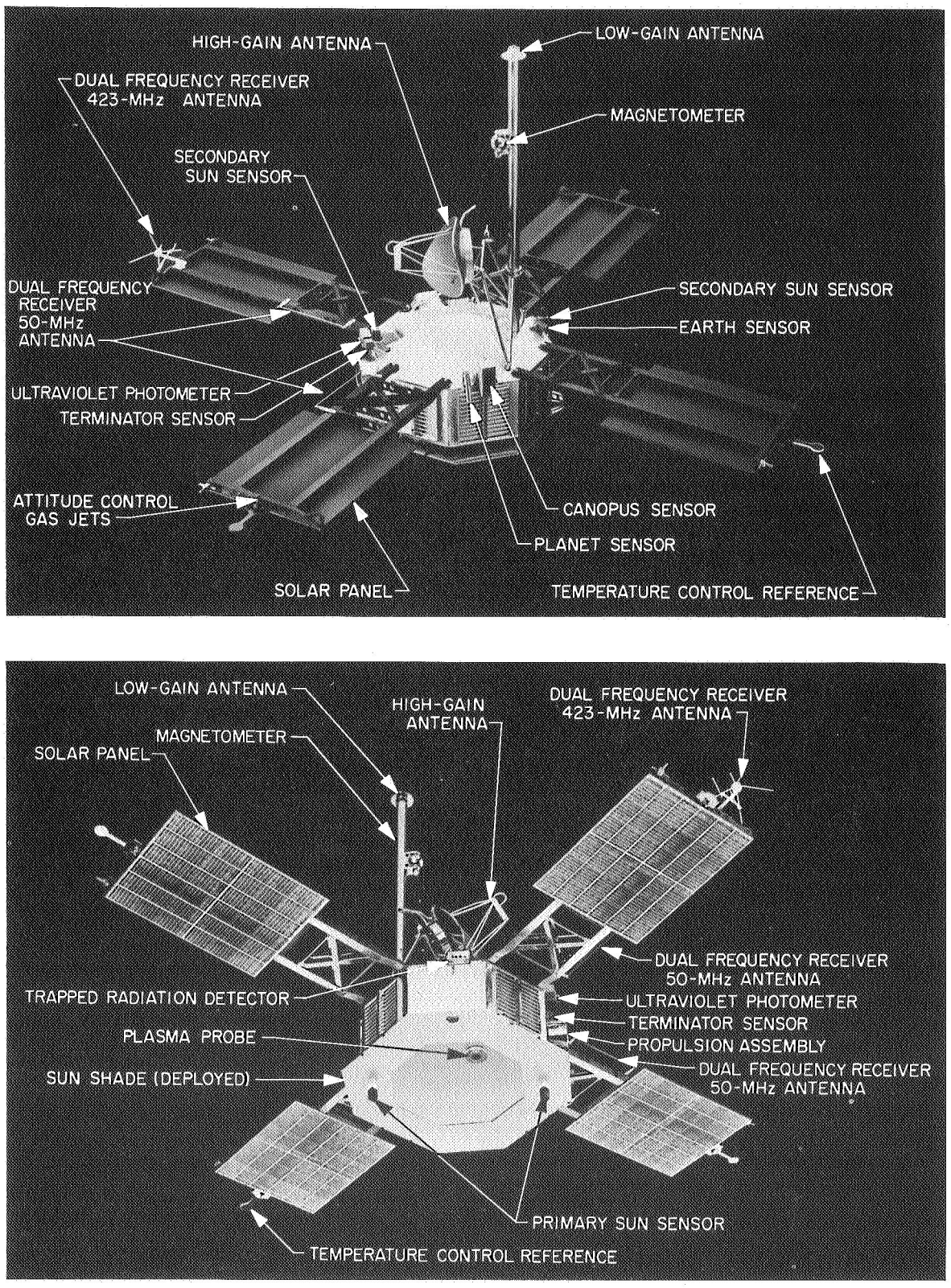

Fig. 1. *Mariner* Venus 67 spacecraft

program designed with the capability to identify potentially dangerous problems. However, this report is necessarily critical of the complete environmental testing program. The inclusion of failure information – as well as data on successes – and the discussion of major problems permits this assessment.

During the system-level FA environmental tests of the two *Mariner* Venus 67 spacecraft, seven significant anomalies and/or failures were noted; they are summarized below:

(1) During the M67-1 system vibration test and, again, during the thermal–vacuum systems test, the data automation system (DAS) was intermittent. It was concluded that the most likely reason for the anomalous operation was the noise at the status bit OR gate (RSL98). This expander gate input was not filtered; and since it was only used for status information and was not part of the science data, it was not considered worthwhile to filter it.

(2) During the M67-1 thermal–vacuum system test, the spacecraft temperatures were lower than expected. Changes in the thermal shield eliminated most of the discrepancy. Even though M67-2 had the new shield design, its temperatures also ran somewhat low during the system test, but not low enough to warrant further changes. The PFR that was written has been closed.

(3) During the M67-1 thermal–vacuum test, the plasma probe sensor and the sun sensors dropped slightly below their predicted lower FA temperature during the simulated midcourse maneuver. A similar drop occurred during the M67-2 thermal–vacuum system test. From past developmental testing, it was known that neither item was sensitive to even considerably lower temperatures; hence, the PFRs that were written were satisfactorily closed.

(4) During the M67-1 thermal–vacuum systems test, the plasma probe experiment data appeared noisy. The M67-2 plasma probe also experienced noisy data but to a lesser extent. The problem, which was established as being fairly common to this unit (i.e., it was seen on the *Mariner* Mars 1964 Project, as well as on another project where the unit was flown), was definitely not related to the *Mariner IV* plasma probe failure. Historically, the problem is a short-lived condition, and both of the PFRs that were written have been closed.

The numerical results of the *Mariner* Venus 67 subsystem level testing for vibration and thermal–vacuum are presented in Table 1, where they are compared with *Mariner* Mars 1964 results. It should be noted that the failure-rate percentages for FA tests were fairly close on the two projects. The FA vibration failure rate was slightly higher on the *Mariner* Venus 67 program, whereas the FA thermal–vacuum rate of failure was slightly lower. Also of interest, however, is the fact that the TA failure rate was higher for both vibration and thermal–vacuum on the *Mariner* Venus 67 Project. This fact most likely reflects the use of old hardware on the *Mariner* Venus 67 Project, which was left from the *Mariner* Mars 1964 Project, since the test levels were essentially the same for both projects. Another reason for the higher TA failure rate may be the lack of developmental testing.

Table 1. Comparison of *Mariner* Mars 1964 and *Mariner* Venus 67 assembly-level environmental test failures

Type	Vibration			Thermal–vacuum			Overall failure rate, %
	Number of tests	Failures	Failure rate, %	Number of tests	Failures	Failure rate, %	
Mariner Venus 67							
TA	21	5	23.8	22	7	31.8	27.9
FA	117	7	6.0	81	7	8.6	7.1
Mariner Mars 1964							
TA	244	30	12.3	95	19	20.0	14.5
FA	538	26	4.8	310	28	9.0	6.4

In Table 2, each of the 26 assembly-level environmental test failures that occurred during the *Mariner* Venus 67 test program is briefly described with a subjective assessment of the degree of concern for each. In this table, a failure is considered to be one unique problem; for instance, if several units failed due to the same problem, it was considered to be one failure. As an example, the FA vibration failures on the radio (Table 2)

Table 2. *Mariner* Venus 67 major environmentally induced test failure summary, assembly level

Subsystem	Test type	Test	Failure		Problem evaluation
			Cause	Description	
Plasma probe	TA	Thermal–vacuum	Design deficiency	At low temperatures, the unit did not sequence properly. This problem, which had also been noted on a flight unit prior to delivery from the vendor, was corrected by a design change in the circuitry.	The design change was verified as curing the problem and all flight units were modified accordingly.
Pyro control assembly	TA	Thermal–vacuum	Age	The assembly passed TA testing on *Mariner* Mars 1964, but for *Mariner* Venus 67 was modified by the addition of a terminator-sensor amplifier. In TA thermal–vacuum testing, a partial failure of an energy storage capacitor was noted. The *Mariner* Venus 67 TA unit is *not* the *Mariner* C TA unit, but is one of the *leftover* flight units. Even though this problem has not been noted in any flight units, this TA unit was dissected to analyze the failed capacitor, since all flight units are the same age. Analysis showed that capacitors were not secured properly in can and that continued vibration could cause lead line to break.	Because this portion of the pyro control passed TA testing on *Mariner* C, there was no real concern over the adequacy of the design. There was concern, however, over the possibility that the energy storage capacitors were affected by age, hence flight units were frequently examined. Further, multiple redundancy existed in this function.
Radio Serial No. 2	TA	Vibration	Design deficiency and age	The *Mariner* Venus 67 TA unit is the old *Mariner* C PTM unit. It was not rebuilt to eliminate a design problem with Johansen capacitors. Its TA testing is incomplete at this time and has been plagued by capacitor problems and by problems localized to the receiver, only, which are attributable to the unit's age and excessive test history. The RF amplifiers have experienced no problems during *Mariner* Venus 67 testing. A PFR was written because an RF cable was loose, and the connector was retorqued.	There was no concern over this problem as to mission success because RF amplifier portions of the radio experienced no difficulty during *Mariner* Venus 67 testing, and the receiver passed TA testing on *Mariner* C. The problem with Johansen capacitors was one that was expected, and the other problems in the receiver were not surprising for a unit with as excessive a history of qualification-level testing as this one had.
Low-gain antenna	TA	Thermal–vacuum	Design deficiency	On the *Mariner* Venus 67 mission, it was determined that this item would experience much lower temperatures than it was designed for. During testing to these low temperatures, cable clamp bonding failed. Development work was conducted to find a different bond material that would be better at low temperatures, and one was found. The bonding on flight antennas could not be changed because, at room temperatures, the bonds had full strength and could not be removed.	This failure was not a risk to the mission; no bonding problems were observed on the flight antennas during testing, and if these bonds had failed during flight, it would have been past the launch phase, at which time the support of the cable clamps would no longer be needed.

show that there were two distinct problems, but three units were affected by the failure; PFRs were actually written against each unit. None of the assembly-level environmental test failures recurred during system-level environmental testing, and all subsystem FA failures were followed by a successful rerun of the FA test.

It should be pointed out that Table 2 is all inclusive, covering TA and FA testing, as well as any test failures that occurred on spare units. Therefore, a direct correspondence does not exist between Table 2 and subsequent tables appearing later in the text that cover only the TA testing or the FA testing.

Table 2 (contd)

Subsystem	Test type	Test	Failure		Problem evaluation
			Cause	Description	
Battery Serial Nos. 27, 28, and 29	TA	Vibration	Design deficiency	At very low frequencies (approximately 2 Hz), the battery plates go through a slosh mode which broke some header wires inside the battery. The same condition was known to exist on the *Mariner* C batteries. This problem occurred on all three units.	This was not a serious problem because failures occurred under unique vibration conditions (slowly swept low-frequency sine) that do not exist in flight. The test requirements were attempting to simulate transient conditions, but they were known to be overly severe. Even though a similar failure were to occur in flight, the battery had sufficient capability (based on a design qualified by multiple past use) to still function.
Tape recorder	TA	Thermal–vacuum	Design deficiency	Following test, failure of a discrete component was noted. This component is one that the Component Parts people recommended be changed for a more reliable type. The problem is felt to be from wrong choice of pieceparts, rather than a deficiency in circuit design.	After review, the Project Office decision was that part type replacement was not warranted, since the TA unit was built with unscreened parts, and the screening process for flight parts was very effective at detecting this particular flaw. The unit has since been successfully tested to TA levels because of potting problems discovered on the flight unit.
Dual-frequency receiver	TA	Vibration	Design deficiency and faulty workmanship	During vibration, a spot bond on a lead broke loose and allowed motion of the wire to break the solder terminal. The unit was satisfactorily repaired, and more attention given to the spot bonding on flight units.	No concern over this failure because, since the TA unit was satisfactorily reshaken, no flight unit exhibited this problem, and the flight units were verified as being better quality bonding.
Dual-frequency receiver	TA	Thermal–vacuum	Faulty workmanship	At high temperature, the unit exhibited improper data readout. This was traced to two discrete components that were not within tolerance.	Following replacement of components, the unit was satisfactorily retested.
Solar panels	TA	Thermal–vacuum	Faulty procedures	During TA testing in the space simulator at Venus intensities, the lamps went off because of a Laboratory-wide power failure. The resulting thermal transient damaged the solar panel beyond repair.	Prior to the accident, it had been established that the panel was not affected by thermal transients that would be experienced during midcourse maneuvers when solar intensity is nearer that of earth. Immediately following the accident, extensive work was done on samples of panels, and it was reconfirmed that thermal transients appropriate for midcourse maneuver conditions would not affect the panel. It was also verified that thermal transients occurring at Venus intensity conditions would cause the observed panel degradation. This test is considered to have been passed, in spite of the accident.

Table 2 (contd)

Subsystem	Test type	Test	Failure		Problem evaluation
			Cause	Description	
Radio Serial Nos. 2, 7, 8 Serial No. 7	FA	Vibration	Design deficiency	An L-shaped tuning cavity was not supported at its ends. The overhanging end contacted the chassis under vibration and caused an adjacent crystal to fluctuate in frequency. This design condition existed on all radios but was not as noticeable on others as on the SN 2, 7, and 8 radios. A fillet of bonding was put around the perimeter of the cavity and verified that it cured the problem. Crystal and capacitor failed on SN 7 and were replaced.	There was no concern over the tuning cavity PFR; in fact, at one time, a decision had been reached to launch without correcting the problem, which was known to occur only under certain levels of vibration and always return to its original condition at the end of vibration. Since the design remedy was simple, however, it was instituted on all units. A piecepart failure was responsible for crystal and capacitor failure.
Dual-frequency receiver VHF antennas Serial No. 3 Serial No. 4	FA	Vibration	Design deficiency	Following vibration, a crack between a phenolic fitting and the aluminum mast was noted. It was determined that differences in expansion coefficients between the fittings and the mast caused separation during curing, and a fiberglass dowel pin was added to the design to retain the fitting on the mast. Failure occurred on SN 3 and 4; however, units SN 3 through 6 were reworked.	Since TA tests had occurred prior to FA, this failure should have been noted at that time. It was not; but after the FA failures, when the TA was reexamined, a crack was found that had not previously been noted. An antenna test model that had experienced no environmental testing was examined, and it also exhibited the same crack. The addition of the dowel pin was felt to be an adequate correction, and no concern remained over this failure.
Thrust-vector-control assembly	FA	Vibration	Faulty workmanship	The potentiometer brush block came loose on the shaft during vibration.	Although the unit successfully passed the test following retightening of the locking screw, enough concern remained to institute null position checks during Pasadena and AFETR operations.
Thrust-vector-control assembly	FA	Thermal–vacuum	Design deficiency	At low temperature, the shaft motion was erratic. The cause of the problem was traced to the original lubricant, which was replaced with one with better low-temperature properties.	Following this design change, it was learned that the flight environment of the TVCAs was even lower than the test temperature at which problems occurred. Tests were run at 0°F with the new lubricant and no problem was experienced.
Thrust-vector-control assembly	FA	Thermal–vacuum	Faulty workmanship	This unit lost torque gain during T/V test. The problem was ultimately traced to a defective magnet in the unit.	The actuator was rejected.
Temperature-control reference	FA	Thermal–vacuum	Faulty workmanship	This unit, which had been reworked once before for the same problem, exhibited excessive thermal gradients across its sensor surface during test.	The particular unit was scrapped, and no other unit has exhibited this problem.
Tape recorder	FA	Thermal–vacuum	Faulty workmanship	Erratic performance during test was noted. This was traced to a potted module which was only partially filled with potting compound. On further checking, this same condition existed in several potted modules. This condition also existed in the TA unit but did not give any problems when the TA unit was satisfactorily tested.	All suspected modules were replaced with newly fabricated modules and FA retested. An abbreviated TA was also rerun to verify that the modules (3 in each tape recorder subsystem) were still qualified.

Table 2 (contd)

Subsystem	Test type	Test	Failure		Problem evaluation
			Cause	Description	
Separation-initiated timer	FA	Vibration	Faulty workmanship	A dimensional problem on a bracket allowed switch contacts to chatter in vibration. The bracket was replaced and the unit successfully retested.	No concern.
Separation-initiated timer	FA	Temperature	Design deficiency	The timing was not within specification due to viscosity of oil in the damper.	It was determined that the specification time limits were needlessly tight.
Thrust-vector-control assembly	FA	Vibration	Faulty procedures	Following vibration it was noted that all 4 actuators in the vane assembly had experienced a loss of torque. This problem was ultimately traced to a procedural error in magnetizing the torquer magnets in the actuators.	The new magnetizing procedure gave superior results to the procedure used on *Mariner* Mars 1964. This new procedure resulted in adequate gain under all conditions.
Magnetometer		Thermal–vacuum	Faulty procedures	Malfunction of unit at low temperature was traced to an improper tuning condition of an RF section. It was retuned correctly, then passed the test.	Correct tuning of this device was at variance with the instruction manual. The proper tuning method is now known.
Pyro-arming switch Serial No. C110 Serial No. C111		Vibration	Faulty workmanship	During vibration, contact chatter was observed. This was traced to improper adjustment of spring load on switch levels. Both units experienced the same problem.	Discrepancy was corrected and the unit satisfactorily retested.
Data automation system		Thermal–vacuum	Faulty workmanship	All magnetometer Z-axis works in the DAS 420-bit format indicated that the seventh most significant bit was always a one. This problem disappeared for approximately 16 h, then reappeared.	The failure was isolated to a single flatpack, which was replaced. The DAS was then subjected to TA level and duration high-temperature thermal–vacuum test. The failed flatpack was tested separately, but in the same chamber and at the same time as the DAS. The DAS operated normally throughout the test and failure was repeated in the flatpack. In view of the above, it was agreed that the DAS had met the Mariner Venus 67 TA test requirements.
Plasma probe		Vibration	Age	Following the special repeat of TA sine and random vibration of module 32A3 only, the plasma probe failed to sequence properly.	This module had previously passed TA vibration. The test was repeated to check the integrity of the diode board added as a result of PFR. The failure was in old circuitry which had been successfully TA tested twice before, so did not affect the validity of this test.
Dual-frequency receiver		Thermal–vacuum	Faulty procedures	A crystal had been replaced as a precaution for a manufacturing potential defect. A circuit trimming capacitor was not aligned properly.	Tuning was corrected and the unit successfully retested.

C. Detailed Review of Typical Subsystem Qualification

To illustrate the general process used on *Mariner* Venus 67 to go from *Mariner IV* qualification status to *Mariner V* flight status, the attitude-control (A/C) jet valve assemblies are chosen as being representative of the methodology followed for all subsystems.[5]

Preliminary estimates of maximum valve temperature for *Mariner* Venus 67 was 215°F. However, at this temperature, the valve opening time was not satisfactory; therefore, the valve's pintle assembly was modified slightly. Thus, a possible need for requalification testing arose from two causes: a change in design and a change in expected assembly environment.

Two of these valves were successfully TA tested to general test levels for humidity, shock, and vibration. These two valves were then tested to special thermal–vacuum test levels of 14 and 255°F. Also, twelve of the valves that were designated for use on the M67-1 spacecraft were FA tested to vibration and special thermal–vacuum test levels of 32 and 215°F.

Before the valve testing for the flight spacecraft (M67-2) and the spare valve began, it was learned (from solar-panel tests in the space simulator) that the operating temperature range would run low, not high. Test temperatures were then revised to accommodate the lower operating range. The TA valves were successfully retested to the new, revised, lower thermal–vacuum temperature of −65°F but were not subjected to further vibration testing. The eighteen valves for the M67-2 spacecraft and six spares were FA tested to normal vibration levels and to the new, revised, thermal–vacuum temperatures of −45 and 131°F.

The problem then arose that, strictly speaking, the valves should have been removed from the M67-1 spacecraft for new FA tests to the new low temperature. However, because there was never any problem during any temperature testing (two TA valves and twelve flight valves to extra-high temperature; the same two TA valves and eighteen flight valves to extra-low temperature), the retesting of the twelve valves for the M67-1 spacecraft to the new, lower FA temperature was waived.

[5]The solar panel qualification, which was one of the most important subsystem qualifications because of the lack of a PTM, is discussed in Section II.

Environmental testing of the attitude-control jet valve assemblies illustrates several characteristics of the *Mariner* Venus 67 environmental test program:

(1) The mission change necessitated a design change; this led to requalification requirements because *Mariner* Mars 1964 testing had been compromised.

(2) Independent of the design change, the mission change resulted in an expected environment sufficiently different from *Mariner* Mars 1964 to warrant augmenting these tests with tests to new levels.

(3) For lack of a PTM, this item went aboard the solar panel for a portion of its qualification testing. There it was tested for acoustics and thermal shock. Although it experienced a thermal–vacuum environment, the main output of this facet of test was a better estimate for assembly-level testing (i.e., its formal TA thermal–vacuum test was as an assembly).

(4) With many tests moving in parallel, rather than in series (e.g., assembly-level thermal–vacuum tests slightly preceded the above tests in the space simulator), late information had to be incorporated into the test levels in the midst of the environmental testing program. Hence, the question of whether to repeat previous tests was settled by careful consideration of the circumstances.

(5) Units passed tests of deliberately conservative levels with no difficulty.

Some subsystems were simpler, and testing of these was routine. Others were more complex; and for a few, it was necessary to accept test results that, in an exact sense, had failed the test but had satisfied the intent of the test – e.g., battery, data automation system (DAS), and plasma probe results as given in Table 2. These examples are good illustrations of the subjective judgments that are often required during the qualification of a flight spacecraft. However, the jet valves give a typical representation and illustrate the process of going from *Mariner* Mars 1964 qualification status to *Mariner* Venus 67 flight status.

II. Type-Approval Environmental Testing

The purpose of type-approval (TA) testing is to verify a design; the tests establish that the assembly can satisfactorily operate in an environment that is in excess of

that expected in use. The tests also validate the environmental test technique for use in flight-acceptance (FA) testing.

To provide assurance of locating design inadequacies, a margin is established such that the imposed tests are more severe than operational conditions, but it is not so severe that reasonable safety limits are exceeded or that unrealistic failure modes are excited. Type-approval tests are not intended to be destructive tests; to pass them successfully, the equipment shall suffer no performance degradation. A meaningful TA test is one that combines the environmental stimulus with the appropriate performance tests necessary to determine satisfactory operation.

Since the *Mariner* Venus 67 design was considered to be a derivative of the adequately qualified *Mariner* Mars 1964 design, the Project Management decided early in the program to eliminate the proof test model (PTM) in an effort to save both time and money. The philosophy of the test program then was to requalify items with design changes sufficiently significant to invalidate *Mariner* Mars 1964 testing. Because of the lack of a PTM, most of the requalification occurred at the subsystem level. In some cases, however, the structural test model was used as a substitute for the PTM to qualify assemblies whose vibration environment is strongly influenced by the spacecraft system. System level test objectives could not always be satisfied on the STM, and this sometimes led to an unusual system-level test, special testing on the spare spacecraft (M67-1), or in rare cases, an unavoidable deficiency in the testing program.

In addition to verifying the design of the structural subsystem, the dynamic testing of the STM qualified the following assemblies for vibration:

(1) Octagon structure, including miscellaneous mounting brackets

(2) Bay II shear web

(3) Temperature control louvers

(4) Upper thermal blanket

(5) Lower thermal blanket

(6) Deployable sunshade, including deployment hardware

(7) Fixed sunshades

(8) Side thermal shields

(9) Temperature-control references (TCR)

(10) Solar panel structures

(11) Separation-initiated timer (SIT)

(12) Pyrotechnics arming switch (PAS)

(13) Upper-ring harnesses (9W1 and 9W2) and cable trough structure

(14) Lower-ring harness (9W19)

(15) Squib-firing harnesses (9W8, 9W28, 9W38)

(16) Post-injection propulsion system (PIPS) wiring harnesses (9W10, 9W11)

(17) Superstructure

(18) High-gain antenna structure

(19) High-gain antenna deployment hardware, including deploy switch

(20) PIPS support structure and adjustment pads

(21) Sun-sensor pedestal (Bays II and VI)

(22) Umbilical connector bracket

(23) Plasma-probe support bracket

(24) Trapped radiation detector (TRD) support bracket

(25) Dual-frequency receiver (DFR) antennas

(26) Attitude-control-jet sunshade

(27) Low-gain antenna structure

(28) Low-gain antenna dampers

(29) Solar-panel boost dampers

(30) Solar-panel deploy springs and switches

(31) Solar-panel cruise damper and latch assemblies

(32) Science signal harnesses (9W22, 9W24, 9W26)

(33) Magnetometer coaxial cables (9W29, 9W34)

The STM tests were repeated later, following changes to the solar-panel boost dampers, attitude control (A/C) jets, sunshades, and sunshade deployment hardware. The STM tests and thermal control model (TCM) tests yielded environmental data needed for confirming subsystem-level test requirements.

A special testing of the solar panel system was conducted because most of the qualification status from the

Mariner Mars 1964 testing was voided due to the fact that the change in mission affected many of the spacecraft appendages. (Solar panel system is defined as the solar panel with A/C jets, sunshades, pinpullers, dampers, cabling, temperature control references, and DFR antennas.) This testing program was partially conducted on the aforementioned STM test. There were also dynamic, acoustic, and thermal–vacuum tests in the space simulator of the solar panel system as an entity. Additional details on these tests appear later in this section.

Because of its dual role as PTM and spare flight spacecraft, the M67-1 spacecraft was subjected to limited qualification-type tests over and above M67-2 tests. In general, these test levels were some modest margin over the M67-2 test levels but were not equivalent to the *Mariner* Mars 1964 PTM test levels. These tests included additional margin in solar simulation, the firing of all spacecraft pyro devices, RF irradiation with live squibs installed, and approximately a 5-dB increase in random noise test levels below 800 Hz. These test levels do not invalidate the M67-1 spacecraft's flightworthiness.

Subsystems that had been TA tested were retested to varying degrees as a result of their design changes. The following subsystems either had major design changes or were completely new designs and, therefore, underwent complete TA testing. Items 3, 5, 6, and 7 were vibration tested on the STM in addition to subsystem level tests; the vibration environment of the other items is more independent of spacecraft system and, hence, needed no system-level testing.

(1) Data automation subsystem (DAS)

(2) Dual-frequency receiver (DFR)

(3) DFR UHF antenna

(4) DFR VHF antenna

(5) Planet sensor

(6) Solar panel

(7) High-gain antenna-deployment mechanism

(8) Thermal-control references (TCRs)

(9) UV photometer

(10) Solar-panel-tip dampers

The subsystems listed in Table 3 had less extensive design changes and underwent partial TA retesting. The degree of TA retesting was determined by the subsystem cognizant engineer and the spacecraft environmental requirements engineer at the time the subsystem environmental test specification was prepared.[6]

Table 3. Subsystems retested after design changes

Subsystem	Design change	Kind of test
Trapped radiation detector	New bracket	Vibration
Plasma probe	Product improvement	Vibration and thermal–vacuum
Tape recorder subsystem	Functional change	Vibration and thermal–vacuum
Canopus sensor	Mechanical change	Vibration, static acceleration
Power subsystem, bay I	Functional change	Vibration and thermal–vacuum
Power subsystem, bay II	Functional change	Vibration and thermal–vacuum
Radio subsystem	Functional change	Vibration and thermal–vacuum
Pyrotechnic control	Functional change	Vibration, thermal–vacuum, and EMI
Jet valve assemblies	Pintle modified	Vibration and thermal–vacuum
Structure	Structural change	Vibration
Battery	Product improvement	Vibration and thermal–vacuum
Thrust-vector-control assembly (TVCA)	Lubricant change	Temperature

The mission changes – flight direction change from Mars to Venus and a new science payload – resulted in environments for some assemblies that were significantly different from those considered in establishing *Mariner* Mars 1964 TA test requirements; for those assemblies, the past qualification testing was augmented by testing to new limits. The following items were tested to nonstandard tests or levels, accordingly:

(1) Plasma probe cup
(2) S-band antennas
(3) Attitude-control valves
(4) Attitude-control thrust-vector actuator

} Nonstandard temperature

(5) Squibs — Life tests and proton radiation

[6]A complete list of TA and FA Environmental Test Specifications is given in Appendix A.

(6) Dual-frequency receiver
(7) Data automation system
(8) Pyro control
(9) Power
(10) Radio

} Electromagnetic interference (EMI)

After careful analysis, some *Mariner* Mars 1964 PTM tests were felt to be still valid. The system level demagnetization, the system level acoustic test (as supplemented by special STM test), the system-level launch vehicle charging, and the umbilical-line transient tests were not repeated.

A deficiency in the test program was that the *Mariner* Venus 67 flight support spacecraft system (M67-1) was not tested to full PTM levels. To do so would have rendered the spare spacecraft unflightworthy.

A. System-Level Testing

1. Structural test model.

a. Objective. The STM vibration tests were intended to verify the spacecraft's capability to structurally withstand the boost environment. The STM was composed of flight structural items and structural simulations of all spacecraft components.

b. Initial vibration test. Low-frequency structural developmental and design ultimate-load tests (Appendix B) were run for torsional, lateral, and axial axes of excitation on the STM, starting in late July 1966. A typical test setup is illustrated in Fig. 2.

Low-frequency structural developmental and design ultimate-load tests were run for the following axes of excitation with a test structure containing four, uncelled solar panels:

Torsional	(1 setup, 10 runs)	July 25–29, 1966
Lateral	(3 setups, 17 runs)	August 2–4, 1966
Axial	(1 setup, 5 runs)	August 8, 1966

The following tests were performed to qualify one, celled solar panel at the system level for low frequency and complex wave excitation along one axial and two lateral axes:

Axial	(1 setup, 4 runs)	August 11, 1966
Lateral	(3 setups, 10 runs)	August 12–13, 1966

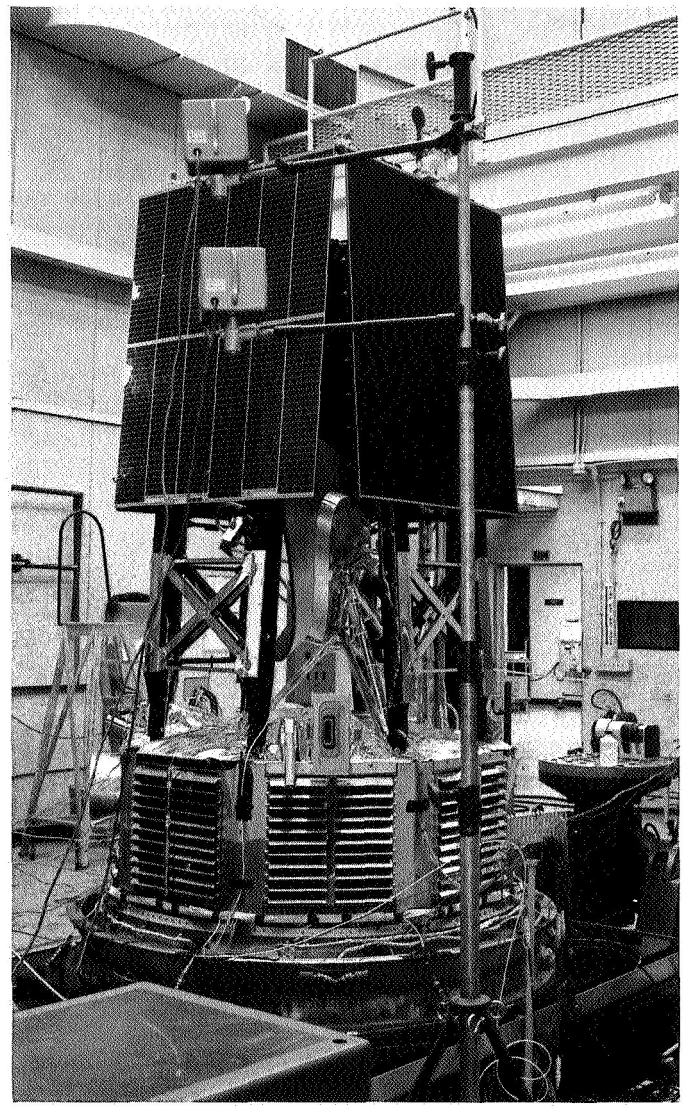

Fig. 2. Typical STM vibration test setup

Additional low-level runs were made to determine the dynamic response characteristics of the PIPS for fuel pressure configurations along its most critical axis of response. For this portion of the test, the STM contained four, uncelled solar panels:

Axial	(1 setup, 4 runs)	August 16, 1966

Two modifications were made on the solar-panel-tip dampers during the testing program. The initial damper test hardware was found to be unacceptable. Improved damping characteristics were brought about by changing the size of the sealing O-rings and changing the viscosity of the damping fluid. Qualification and design ultimate-load-level testing was performed, without failure, with

the modified hardware for torsional and x-axis excitation. During x-axis excitation at design ultimate-load level, large dynamic excursions of the dampers at 8 Hz resulted in boundary contact between the end of the damper piston and the damper housing. Even though the dynamic loads associated with this shock-type acceleration were not deleterious to the structure, the dampers were removed from the test structure and mechanically adjusted to provide for larger dynamic displacements. The boundary contact occurred only at STM design-ultimate-load level in the lateral axes of excitation and did not occur at FA or PTM test levels. Also, as a consequence of an action item that resulted from the second solar-panel design review, a flight-configuration tip damper was successfully subjected to a temperature and thermal shock test per JPL specification.

Two other pieces of hardware were repaired during the remainder of the testing program. The attitude-control jet sunshade was repaired in bays I and VII for spot-weld failures. One lexan tube fitting on the high-gain antenna feed support structure developed a crack during design ultimate-load-level testing in the z axis. After completion of the STM test and prior to use of the STM as a test fixture for the solar panel system-level qualification test, the fitting was preloaded in the hoop direction by using a wire wrapping potted with epoxy. A small hole was drilled at the apex of the crack to prevent a potential stress concentration. The crack appeared not to propagate during the remainder of the test program.

The STM successfully withstood design ultimate-load and structural-qualification dynamic-loads tests defined in JPL specifications (listed in Appendix A). The full 3 wk of allocated test time were required for completion of initial testing, and only minor delays resulted from hardware and test equipment problems. The actual total time for which the STM underwent the forced vibration excitation necessary to satisfy all the objectives of the test program was 208 min.

c. Final vibration test. A follow-up spacecraft composite vibration test (Ref. 1) of the modified *Mariner* Venus 67 STM was performed in early November 1966. The purpose of the follow-up STM test was to obtain supplemental dynamic response data required by late design changes in the basic spacecraft structure and to qualify structural hardware that either was not included on the previous STM or was modified since the previous tests. The solar-panel-tip damper is an example of hardware that was extensively redesigned between the tests. The follow-up STM test also provided an opportunity to verify the complex-wave vibration-control equipment operational procedure to be used on flight spacecraft testing. Verification of flight operational test procedures on the STM was mandatory because no PTM was available for the purposes of structural dynamic testing. The STM successfully withstood the qualification dynamic loads defined by JPL specification.

Low-frequency structural developmental and qualification dynamic load tests were run for the following axes of excitation.

Lateral X	(1 setup, 7 runs)	November 7, 1966
Lateral X-Y Bay II	(1 setup, 7 runs)	November 9, 1966
Axial	(1 setup, 11 runs)	November 11, 1966

One week of test time was required for completion of the testing. The actual total time for which the STM underwent forced vibration excitation necessary to satisfy the above objectives was 60 min.

Analysis of reduced test data indicated no major changes in the dynamic response characteristics of the modified test structure.

2. Temperature control model.

a. Objectives. There were four principal purposes of the TCM space simulator test[7]:

(1) To verify the adequacy of the basic thermal design. Basic design features include insulation blankets top and bottom, louvers, polished aluminum shields, and white paint around the periphery.

(2) To define empirically some features of the detailed temperature control design. Best estimates of electrical power dissipation and spacecraft configuration were tested to find an acceptable combination of louvers, side shields, surface preparations, thermal conductances, and heater sizes.

(3) To determine empirically the influence of various thermal parameters on spacecraft temperatures. This information is useful in estimating temperatures for conditions that cannot be tested (e.g.,

[7]Much of the material in this section has been derived from a JPL internal document by D. Miller, on the *Mariner* Venus temperature control model space simulator, April 1967.

some aspects of midcourse maneuver) and for changing the thermal design to accommodate changes in the spacecraft.

(4) To develop handling techniques for simulator operations with flight-type spacecraft.

b. Test configuration. The TCM test configuration (Fig. 3) was the thermal equivalent of the flight spacecraft (Fig. 1). The TCM included flight-like structure, exterior surfaces, louvers, shades, and thermal shields, and geometric mockups of all peripheral items except the solar panels, which were thermally mocked up. The chamber was not large enough to allow the solar panels to be used. The TCM contained no electronic equipment. The power dissipation of the electronics was simulated by electrical heaters. Because of the reversed flight solar attitude, a special inverting fixture was fabricated to rotate the spacecraft from the normal ground-handling attitude to the chamber-test attitude (the lights are in the top of the chamber).

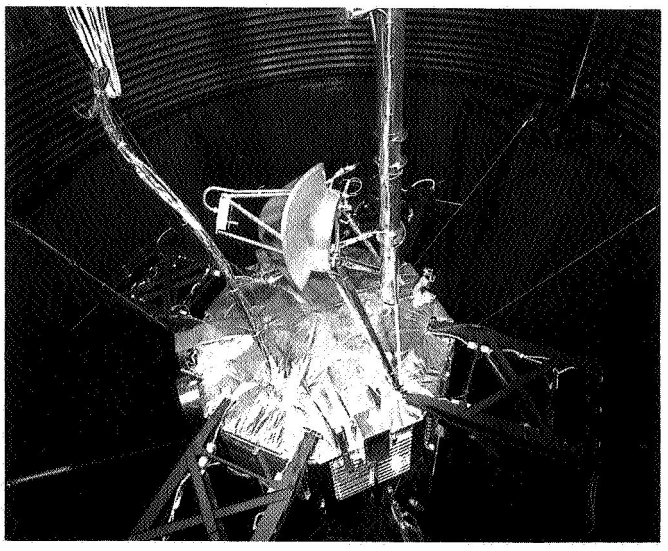

Fig. 3. Thermal control model test III

c. Test results. The TCM tests were conducted in the JPL 10-ft space simulator between June 24 and July 6, 1966 (Fig. 4). Table 4 presents a summary of the test results for the bus. *Mariner IV* flight temperatures and allowable temperature ranges are shown for comparison. The *Mariner* Venus 67 TCM and *Mariner IV* flight data are for different modes of internal power dissipation, but provide a *mean operating temperature* comparison.

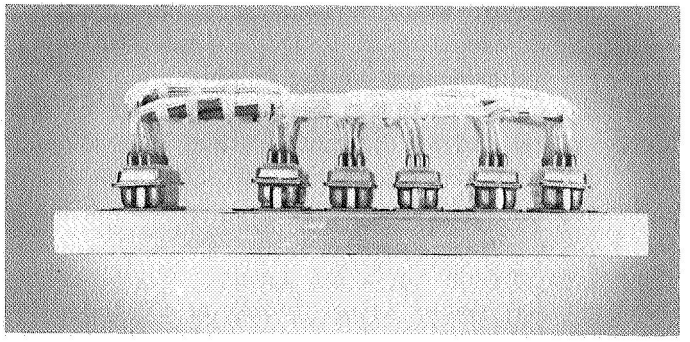

Fig. 4. *Mariner* Venus 67 TCM removal from 10-ft simulator

During the TCM testing, two modes were run in which the solar simulator lights were turned off and the TCM heater power was increased to reproduce the temperature profiles for the earth cruise mode and the gyros on encounter mode (TCM test II, modes 7 and 6). The difference in internal power with the lights off is equivalent to the solar heating input. Excluding the conductive input from the sun sensors and the radiative input from solar panels, the solar input at earth was found to be 18.5 W and at Venus 36 W. These inputs are small compared with the 150- to 250-W bus internal-power dissipation.

Without solar input and with the spacecraft on lowest cruise-mode power, the midcourse motor propellant tank had just dropped to freezing (TCM test II, mode 8). A solar intensity increase from 250 to 286 W/ft^2 caused only a 1.3°F average increase in bus temperature at Venus (TCM test I, modes 2 and 3). An extrapolation to perihelion showed that bus survival was not a problem.

The thermal effects of a catastrophic sunshade failure were investigated in TCM test III. The shade was completely stowed, and earth cruise and encounter modes were run. Analysis of the test data indicated that the bus would absorb an incremental 150 W at Venus with the sunshade stowed. This heat input raised the bus temperature 32.5°F at encounter and caused an undesirably high, but probably tolerable, temperature level.

Mariner Venus 67 is thermally a power-dependent spacecraft, so this parameter is of interest in design studies and in evaluating the effect of simulator error sources. For these reasons, tests were performed in which internal power was reduced 20% at earth and increased 20% at Venus (TCM test II, modes 9 and 4). The power variation produced a negligible effect for the Venus power-up case, but brought the midcourse motor

propellant near freezing for the earth power-down mode. Thus, the power margin at the cold end was about 30 W. The hot-end margin was deduced by a *louvers open* mode in which internal power was increased to force all louvers open and the drive temperatures near the upper limits (TCM test II, mode 5). The power increment above the gyros on encounter level was about 125 W.

d. Conclusions. The TCM tests showed that the basic thermal design could accommodate the hottest and coldest steady-state conditions for the spacecraft. A particular configuration of shields, louvers, and paint patterns was found that was satisfactory for flight.

Test III showed (Table 4) that if the sunshade failed to deploy, the mission would not be lost because of overheating. The thermal configuration purposely placed temperatures near the lower end of the allowable range to allow for maneuver heating, post-encounter operation as the spacecraft proceeds closer to the sun, margin for sunshade deployment failure, and favorable temperatures for long lifetime of electronics.

B. Subsystem-Level Testing

1. Type-approval testing. A type-approval subsystem test setup that is typical for this series of tests is that for the data automation system (DAS), shown in Fig. 5.

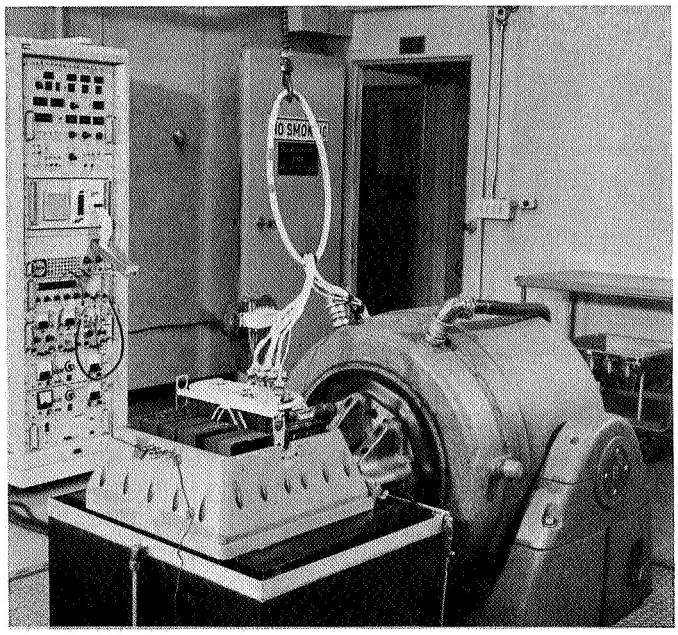

Fig. 5. Typical subsystem TA vibration test setup, DAS

A summary of the *Mariner* Venus 67 TA subsystem testing is presented in Table 5. The table shows each of the subsystems and notes significant past test history experienced by that unit during the *Mariner* Mars 1964 test program. A summary of *Mariner* Mars 1964 life tests appears in Appendix C.

a. Summary of TA waivers[8] *and test deviations.*

(1) *Data automation subsystem.* After the TA thermal–vacuum failure of a discrete component and the identification of the failed components in developmental tests at TA conditions, it was decided to repeat only the failed portion of the TA test and the retest was successful.

(2) *Trapped radiation detector.* The TA thermal–vacuum test was to be run to special temperature, but this was not possible, due to the lack of an electrically equivalent TA unit. Vibration test was run on a mechanically equivalent configuration only.

(3) *Plasma probe.* The thermal shock of sensor was waived because both the sensor and the electronics are tested in the same chamber. The 32A1 unit used a nonstandard operating temperature of 135°C in thermal–vacuum.

(4) *Magnetometer.* No TA tests were required of the unit because it was qualified on the *Mariner IV* program.

(5) *UV Photometer.* There were no waivers or deviations on this unit.

(6) *Dual-frequency receiver.* There were no waivers or deviations on this unit.

(7) *Transponder (radio), Cases V and VI.* The total retest of the radio after an RF connector became loose during Z-axis vibration was waived because of the test history of the receiver. It was required to repeat only the Z-axis portion of the test.

(8) *Tape recorder.* The test was repeated because of some redesign of the unit.

(9) *High-gain antenna.* A special low-temperature TA test at −283°F was performed to cover the change in the mission's environment.

(10) *Low-gain antenna.* A special low-temperature thermal-vacuum test (−200°F) qualified the antenna.

(11) *DFR antennas, UHF and VHF.* There were no waivers or deviations on these units.

[8]Appendix D lists *Mariner* Venus 67 test waivers, both TA and FA.

Table 4. *Mariner* Venus 67 TCM temperature test results summary; comparison with *Mariner IV* flight temperatures

Spacecraft bay	Test design temperature limits, °F	*Mariner IV* flight temperatures, °F			*Mariner* Venus 67 TCM temperatures, °F													
					Test I			Test II									Test III	
		Earth cruise, cavity battery charger *on*	Mars cruise, TWT, battery charger *off*	Playback, TWT, battery charger *off*	Mode 1, earth cruise, cavity, battery charger *off*	Mode 2, gyros *on* encounter	Mode 3, gyros *on* encounter at 286 W/ft²	Mode 1, cruise, TWT, battery charger *on*	Mode 2, cruise, no panel power	Mode 3, parametric	Mode 4, Venus cruise, 120% power	Mode 5, louvers open	Mode 6, encounter temperature match	Mode 7, earth cruise, temperature match	Mode 8, earth cruise, lights *off*	Mode 9, earth cruise, 80% power	Mode 1, earth cruise, shade stowed	Mode 2, gyros *on* encounter, shade stowed
I	14 to 167	76	60	54	64.4	80.4	81.8	77.4	75.2	77.8	80.8	104.0	80.4	63.6	53.2	47.4	75.0	111.8
II	35 to 125	72	41	33	48.0	64.5	67.5	62.5	61.0	63.5	65.5	89.5	63.5	46.0	32.0	30.5	74.0	119.0
III	14 to 122	70	51	34	63.8	74.8	75.6	74.8	73.0	75.2	75.4	97.2	75.8	63.0	45.4	41.2	75.2	103.8
IV	14 to 167	72	54	47	60.6	77.8	79.4	74.4	72.6	76.2	78.2	105.4	78.2	60.2	41.4	37.4	77.6	114.8
V	14 to 149	66	60	60	56.4	73.8	74.0	71.0	70.6	72.0	72.0	91.6	74.6	55.4	38.2	35.2	67.6	99.0
VI	14 to 167	71	70	69	64.4	86.0	86.8	83.0	82.2	84.0	88.8	110.4	86.0	63.4	47.8	41.8	72.4	110.0
VII	30 to 131	64	58	57	57.6	77.4	79.0	65.2	63.8	65.0	65.8	87.8	77.4	56.8	44.4	40.6	63.2	106.4
VIII	14 to 167	88[a]	81[a]	77[a]	67.5	85.3	86.5	73.8	72.3	72.5	76.3	99.5	84.8	66.5	63.0	57.5	72.0	115.8
Average		72.4	59.4	53.9	60.3	77.5	78.8	72.8	71.3	73.3	75.4	98.2	77.6	59.4	45.7	41.5	72.1	110.1

[a]Estimated by correlation with battery temperature.

Table 5. *Mariner* Venus 67 type-approval subsystem testing summary

Subsystem or assembly	Serial No.	Significant *Mariner* Mars 1964 TA test history	Design changes for *Mariner* Venus 67	*Mariner* Venus 67 TA testing summary				
				Vibration test		Thermal–vacuum test		Comments
				Date	Results	Date	Results	
Data automation subsystem	073	None.	New	1/30/67	Passed (1)	2/15/67 3/15/67	Failed Passed (2)	(1) IC lid fell off during vibration due to poor bonding operations, not to vibration test. (2) Flatpack failed; replaced flatpack and repeated test successfully. (3) Unit also passed shock and EMI TA tests.
Trapped radiation detector	*Mariner* Venus 67 TA	*Mariner* Mars 1964 TA unit passed all TA tests on *Mariner* Mars 1964 program.	Minor (1)	8/19/66	Passed	See Note (2)		(1) Change was mechanical in sensor bracketry, but temperature environment different too. (2) Thermal–vacuum to special temperature desirable; not possible because of lack of electrically equivalent TA unit.
Plasma probe	*Mariner* Venus 67 TA	Same unit that was TA tested on *Mariner* Mars 1964 and passed all TA tests on *Mariner* Mars 1964 program.	Significant	9/22/66 1/18/66	Passed Passed (2)	9/28/66 1/17/67	Failed (1,3) Passed (3)	(1) Failed to sequence at low temperature. (2) Unit 32A3 was vibrated to check integrity of diode board added as result of PFR. The failure was in old circuitry and did not affect validity of this test. (3) Assembly environmental test specification required nonstandard test temperature because of assembly flight environment for 32A1 unit.
Magnetometer	—	*Mariner* Mars 1964 TA unit passed all TA tests on *Mariner* Mars 1964 program.	None	*Mariner* Mars 1964 TA tests still valid on *Mariner* Venus 67				(1) The 33A3 SN 1 unit on the M67-1 spacecraft was a TA unit on *Mariner* Mars 1964 program.
UV photometer	3	*Mariner* Mars 1964 TA unit passed all TA tests on *Mariner* Mars 1964 program (1).	New	9/29/66	Passed	10/16/66	Passed	(1) Since photometer was dropped from *Mariner IV* because of a design problem, it was considered to be a new design for *Mariner* Venus 67. (2) The TA unit for *Mariner V* was an old MC-3 unit on *Mariner IV*. (3) Unit also passed static acceleration test.
Dual-frequency receiver	1	None.	New	1/25/67 1/28/67	Failed (1) Passed	2/6/67 3/6/67	Failed (2) Passed	(1) Transformer lead broke at solder joint—lead rebonded and resoldered to terminal. (2) A capacitor and transistor failed; both components were replaced and test repeated. (3) Unit also passed humidity and EMI tests.

Table 5 (contd)

Subsystem or assembly	Serial No.	Significant *Mariner* Mars 1964 TA test history	Design changes for *Mariner* Venus 67	*Mariner* Venus 67 TA testing summary				
				Vibration test		Thermal–vacuum test		Comments
				Date	Results	Date	Results	
DFR filters	1, 4	None.	New (1)	1/28/67	Passed	2/15/67	Passed	(1) These were added for an EMI problem and, although tested separately, are considered part of DFR. (2) Units also passed shock, EMI, and humidity tests.
Transponder (radio) cases V and VI	2	Same unit used as PTM on *Mariner* Mars 1964 program. This *Mariner* Mars 1964 TA unit passed all tests on *Mariner* Mars 1964 program.	Significant	2/24/67 3/1/67	Failed (1,2) Passed (3)	4/6/67	Passed	(1) PFR written for loose connector. (2) PFR written for gain loss associated with vibration failure; determined to be Johansen capacitors in frequency divider. (3) PFR written for leaking hermetic seal on tantalum capacitor.
Data encoder	—	*Mariner* Mars 1964 TA unit passed all TA tests on *Mariner* Mars 1964 program.	None	*Mariner* Mars 1964 TA tests still valid on *Mariner* Venus 67				
Command subsystem	—	*Mariner* Mars 1964 TA unit passed all TA tests on *Mariner* Mars 1964 program.	None	*Mariner* Mars 1964 TA tests still valid on *Mariner* Venus 67				
Tape recorder	2	Same unit that was TA tested on *Mariner* Mars 1964 passed all TA tests on *Mariner* Mars 1964 program.	Significant	11/21/66 4/20/67	Passed Passed (3)	12/6/66 4/24/67	Failed (1,2) Passed (1,3)	(1) Because of temperature limit on tape, used nonstandard test temperatures. (2) Following test, failure of discrete component noted. No retest for this reason, however, because unscreened parts were used and it was felt that flight screening process would eliminate this problem on flight units. (3) TA retesting due to workmanship probably associated with potting which was discovered on a flight unit. TA test repeated.

Table 5 (contd)

Subsystem or assembly	Serial No.	Significant *Mariner* Mars 1964 TA test history	Design changes for *Mariner* Venus 67	*Mariner* Venus 67 TA testing summary				
				Vibration test		Thermal–vacuum test		Comments
				Date	Results	Date	Results	
High-gain antenna	4	Same unit used as PTM on *Mariner* Mars 1964 program. This TA unit passed all TA tests.	None (1)	*Mariner* Mars 1964 vibration test still valid on *Mariner* Venus 67		10/25/66	Passed (2,3)	(1) *Mariner* Venus 67 temperature environment different from *Mariner IV*. (2) PFR written for nylon screw that became loose. ECR changed nylon screw to metal screw; performance test indicated problem solved. No additional test required. (3) Assembly environmental test specification required nonstandard test temperature because of assembly flight environment.
Low-gain antenna	C-106	None.	None (1)	*Mariner* Mars 1964 vibration test still valid on *Mariner* Venus 67		12/29/66	Passed (1,2)	(1) *Mariner* Venus 67 temperature environment different from *Mariner* Mars 1964. (2) Cable clamps became loose; internal communication 4/4/67 from E. Floyd stated that no clamp problem had occurred during FA tests and that antenna would be damaged in removing the clamps. He then recommended that TA retesting be abandoned. This was approved by spacecraft system manager and environmental requirements engineer.
DFR antenna, UHF	STM	None.	New	11/23/67	Passed	TA tests were accomplished during STM and solar panel TA testing		(1) Unit also passed shock and acoustic TA tests.
DFR antenna, VHF	—	None.	New	TA tests were accomplished during STM and solar panel TA testing				
A/C electronics 7A1	—	*Mariner* Mars 1964 TA unit passed all TA tests on *Mariner* Mars 1964 program.	None	*Mariner* Mars 1964 TA tests still valid on *Mariner* Venus 67				
A/C gyros 7A2	—	*Mariner* Mars 1964 TA unit passed all TA tests on *Mariner* Mars 1964 program.	None	*Mariner* Mars 1964 TA tests still valid on *Mariner* Venus 67				

Table 5 (contd)

Subsystem or assembly	Serial No.	Significant *Mariner* Mars 1964 TA test history	Design changes for *Mariner* Venus 67	*Mariner* Venus 67 TA testing summary				
				Vibration test		Thermal–vacuum test		Comments
				Date	Results	Date	Results	
A/C jet valve assembly	86, 88	These units used as TA units on *Mariner* Mars 1964 program and passed all TA tests.	Minor (1)	9/28/66	Passed	10/18/66	Passed (3)	(1) *Mariner* Venus 67 temperature environment different from *Mariner* Mars 1964. (2) These units also passed humidity and static acceleration tests. (3) Assembly environmental test specification required nonstandard test temperatures because of assembly flight environment.
A/C gas system	—	*Mariner* Mars 1964 TA unit passed all TA tests on *Mariner* Mars 1964 program.	None	*Mariner* Mars 1964 TA tests still valid on *Mariner* Venus 67				
Canopus sensor	103	Same unit used as TA unit on *Mariner* Mars 1964 program and passed all TA tests.	Minor	12/6/66	Passed	Not required on *Mariner* Venus 67		(1) Change was only mechanical; shutter was integrated into optics. (2) Unit also passed shock and static acceleration tests.
Sun sensors	—	*Mariner* Mars 1964 TA units passed all TA tests on *Mariner* Mars 1964 program.	None	*Mariner* Mars 1964 TA tests still valid on *Mariner* Venus 67				
Earth sensor	—	*Mariner* Mars 1964 TA unit passed all TA tests on *Mariner* Mars 1964 program.	None	*Mariner* Mars 1964 TA tests still valid on *Mariner* Venus 67				
Planet sensor	001	None.	New	8/30/66 9/2/66	Passed Passed (1)	9/21/66	Passed	(1) PFR written for excessive vibration levels from operator error; some sty-cast knocked off unit. Electrically and optically no damage. (2) Unit also passed shock and static-acceleration tests. (3) Same unit which was developmental tested under name of prototype. Disassembled and inspected before TA test.

Table 5 (contd)

Subsystem or assembly	Serial No.	Significant *Mariner* Mars 1964 TA test history	Design changes for *Mariner* Venus 67	*Mariner* Venus 67 TA testing summary				
				Vibration test		Thermal–vacuum test		Comments
				Date	Results	Date	Results	
Terminator sensor	—	*Mariner IV* TA unit passed all TA tests on *Mariner IV* program. Unit was *narrow-angle Mars* gate on *Mariner IV*.	None	*Mariner* Mars 1964 TA tests still valid on *Mariner* Venus 67				
Jet vane actuators	—	*Mariner IV* TA units passed all TA tests on *Mariner IV* program.	Minor (1)	*Mariner* Mars 1964 TA tests still valid on *Mariner* Venus 67				(1) *Mariner* Venus 67 temperature environment different from *Mariner IV*, so did special low temperature test (in air). This also covered change to lubricant with better low temperature properties.
Central computer & sequencer	—	*Mariner IV* TA units passed all TA tests on *Mariner IV* program.	None	*Mariner* Mars 1964 TA tests still valid on *Mariner* Venus 67				
Power, case I	02	Same unit used as TA unit on *Mariner IV* program and passed all TA tests.	Significant	1/24/66 4/4/67	Passed Passed (2)	1/27/66 4/7/67	Passed Passed (2)	(1) Unit also passed shock test. (2) TA unit was retested to FA levels per ECR.
Power regulator, case VIII	02	Same unit used as TA unit on *Mariner IV* program and passed all TA tests.	Significant	1/24/66	Passed	1/27/66	Passed	(1) Unit also passed shock test.
Battery	27, 28, 29	*Mariner IV* TA units passed all TA tests on *Mariner IV* program.	Minor (1)	11/4/66 11/4/66 11/4/66	Failed Failed Failed Waived (2)	12/12/66 12/12/66 12/12/66	Passed Passed Passed	(1) All new production runs of batteries have TA testing as a matter of policy. (2) Three PFRs written for failure that occurred during vibration but did not show up until thermal–vacuum test. Not felt to be serious problem in that failures occur under very unique vibration conditions (slowly swept low-frequency sine) which do not exist in flight. Further, battery has sufficient capability to still function given a similar failure would occur in flight. Same failures were noted on *Mariner IV* TA tests and no flight problems noted. Consistent with above, low-frequency portion of test verbally waived and battery tests considered complete.

Table 5 (contd)

Subsystem or assembly	Serial No.	Significant *Mariner* Mars 1964 TA test history	Design changes for *Mariner* Venus 67	*Mariner* Venus 67 TA testing summary				
				Vibration test		Thermal–vacuum test		Comments
				Date	Results	Date	Results	
Solar panel	002	None.	New	9/12/66	Passed	9/2/66	Passed (1)	(1) PFR written; during TA testing in space simulator, at Venus intensities, lamps went off because of Laboratory-wide power failure. Resulting thermal transient damaged the solar panel beyond repair. Prior to accident, sufficient test data were obtained to consider the test passed in spite of the accident. (2) Unit also passed acoustic test. (3) Assembly environmental test specification required nonstandard test temperature because of assembly flight environment.
Louver assembly	—	*Mariner IV* TA unit passed all TA tests on *Mariner IV* program.	None	*Mariner* Mars 1964 TA tests still valid on *Mariner* Venus 67				
Structure	—	*Mariner IV* STM unit passed all TA tests on *Mariner IV* program.	Significant	8/16/66	Passed (1)	Not required (2)		(1) Unit also passed acoustic tests. (2) No other environmental tests performed on STM. (3) Preliminary and follow-up reports written on STM vibration test.
Temperature control reference	11, 13	None.	New	Tested on STM		11/30/66 11/30/66	Passed Passed	(1) Units also passed acoustic and thermal shock tests.
Solar-panel-tip dampers	C-161	None.	New	8/16/66	Passed (1)	11/29/66	Passed (2)	(1) Preliminary and follow-up reports written on STM vibration test. (2) Thermal–vacuum and thermal shock tests added at time of design review.
Antenna-deployment mechanism	5	None.	New	8/16/66	Passed (1)	12/5/66 12/19/66	Failed (2) Passed	(1) Preliminary and follow-up reports written on STM vibration test. (2) Three PFRs for antenna failed to deploy due to cold-stiffened cables and latch bracket bearing shifting. Two ECRs written for design change.

Table 5 (contd)

Subsystem or assembly	Serial No.	Significant *Mariner* Mars 1964 TA test history	Design changes for *Mariner* Venus 67	*Mariner* Venus 67 TA testing summary				
				Vibration test		Thermal–vacuum test		Comments
				Date	Results	Date	Results	
Pyro control	1005, 1006	Same units used on *Mariner IV* PTM. The TA units passed all TA tests on *Mariner IV* program.	Significant	12/2/66	Passed (2)	3/14/67	Failed (1)	(1) PFR for storage capacitors voltage decay after third plane of vibration. Failure not reported until after thermal–vacuum test. Will not be able to rerun test. (2) Unit also passed humidity and EMI tests.
Post-injection propulsion system	—	*Mariner IV* TA units passed all TA tests on *Mariner IV* program.	None	*Mariner* Mars 1964 TA tests still valid on *Mariner* Venus 67				
Pin pullers	—	*Mariner IV* TA units passed all TA tests on *Mariner IV* program.	None	*Mariner* Mars 1964 TA tests still valid on *Mariner* Venus 67				
Squibs	—	*Mariner IV* TA units passed all TA tests on *Mariner IV* program.	None (1)	*Mariner* Mars 1964 TA tests still valid on *Mariner* Venus 67				(1) Tested for long vacuum life and proton radiation.

(12) *A/C jet valve assemblies.* An internal communication approved the testing of TA valves at nonstandard temperatures of −65 and +255°F.

(13) *Canopus sensor.* No TA thermal–vacuum test was required; there was no change in electrical design of unit from *Mariner* Mars 1964.

(14) *Planet sensor.* There were no waivers or deviations on this unit.

(15) *A/C thrust-vector actuator.* Minimum TA temperature was revised to 0°F.

(16) *Power, bay I.* A complete TA test sequence was performed on this bay because of the design change from *Mariner* Mars 1964 to *Mariner* Venus 67.

(17) *Power regulator, bay VIII.* A complete TA test sequence was performed on this bay because of the design change from *Mariner* Mars 1964 to *Mariner* Venus 67.

(18) *Battery.* Static acceleration test was waived February 3, 1967.

(19) *Solar panel.* An unscheduled thermal shock at high temperature made further TA tests impossible. Special tests were run, however, on representative panel specimens.

(20) *Structures.* There were no waivers or deviations on these units.

(21) *Temperature-control reference.* Utilization of TA unit SN 13 was made necessary by the poor quality of flight units.

(22) *Solar-panel-tip dampers.* There were no waivers or deviations on these units.

(23) *Antenna deployment.* There were no waivers or deviations on this unit.

(24) *Pyrotechnic control.* Thermal–vacuum could not be rerun because following a capacitor-bank voltage decay, the unit was cut up to remove capacitors for component evaluation.

(25) *Squibs.* There were no waivers or deviations on this unit.

b. Mariner Mars 1964 summary of TA test results.

(1) *Magnetometer.* The magnetometer passed all TA requirements on the *Mariner* Mars 1964 program without any failures or anomalies.

(2) *Data encoder.* The data encoder passed all TA requirements on the *Mariner* Mars 1964 program. All PFRs were satisfactorily closed.

(3) *Command subsystem.* The command unit passed all TA requirements on the *Mariner* Mars 1964 program. All PFRs were satisfactorily closed.

(4) *High-gain antenna.* The high-gain antenna passed all TA requirements on the *Mariner* Mars 1964 program. There were no PFRs or anomalies.

(5) *Low-gain antenna.* The low-gain antenna passed all TA requirements on the *Mariner* Mars 1964 program. There were no PFRs or anomalies.

(6) *Attitude-control thrust-vector control.* The thrust-vector control passed all TA requirements on the *Mariner* Mars 1964 program without any failures or anomalies.

(7) *Central computer and sequencer.* The central computer and sequencer (CC&S) passed all TA requirements on the *Mariner* Mars 1964 program. All PFRs were closed satisfactorily.

(8) *Attitude-control subsystem (7A1 and 7A2).* The A/C units passed all TA requirements on the *Mariner* Mars 1964 program. All PFRs were closed satisfactorily.

(9) *Canopus sensor.* The Canopus sensor passed the thermal–vacuum TA test on the *Mariner* Mars 1964 program without any failures or anomalies.

(10) *Sun, earth, and terminator sensors.* All three sensors passed TA requirements on *Mariner* Mars 1964 without any failures or anomalies.

(11) *Attitude-control equipment plate (7GA1 and 7GA2).* The A/C gas subsystem passed all TA requirements without any failures or anomalies.

(12) *Louver assemblies.* The louvers passed all TA requirements without any failures or anomalies.

(13) *Post-injection propulsion system.* The PIPS assembly passed all TA requirements on the *Mariner* Mars 1964 program. The one PFR was closed satisfactorily.

2. Special subsystem testing.

a. Electromagnetic interference tests.

Dual-frequency receiver (SN 01). The dual-frequency receiver (DFR) electromagnetic interference (EMI) testing was performed to verify that the DFR would function properly when subjected to an electromagnetic

environment similar to twice that expected to exist on the *Mariner* Venus 67 spacecraft. Figure 6 shows the test setup used for DFR EMI testing.

The *Mariner* Venus 67 DFR utilized a configuration which neither had flown on a spacecraft nor had been subjected to an electromagnetic environment similar to that expected to exist on the *Mariner* Venus 67 spacecraft. The electromagnetic interference testing levels that were used to verify that the DFR would function properly were derived from data acquired during the testing sequence of the *Mariner* Mars 1964 spacecraft and the expected electromagnetic environment for the *Mariner* Venus 67 spacecraft. The interference levels to which the DFR was subjected are detailed by environmental specification. In accordance with the above specification the DFR was tested per JPL test procedure. The radiated interference susceptibility testing as required by specification, and stipulated in the test procedure, was not performed from 0.15 through 25 MHz because of the inability to locate the required antenna. Table 6 lists the required tests and test limits as defined in the JPL test procedure.

The DFR (SN 01) was subjected to electromagnetic interference testing according to JPL TA procedure with the exception of radiated susceptibility testing from 0.15 through 25 MHz. The unit successfully passed the tests as specified and operated within its prescribed limits with no degradation to operation during the electromagnetic interference testing, with the exception of spurious response susceptibility. The required spurious response

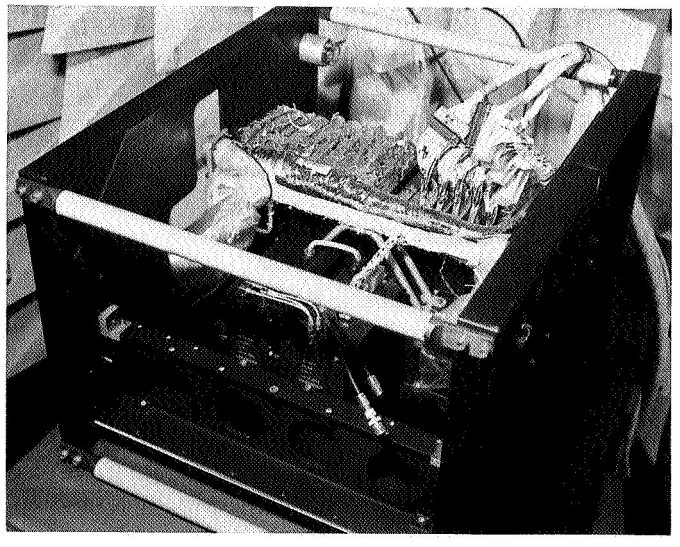

Fig. 6. Setup for dual-frequency receiver EMI testing

Table 6. EMI tests and limits for DFR

Electromagnetic interference	Interference limits	
	Environmental test specification	JPL test procedure
Generated interference		
Generated conducted transient	$<\pm 0.5$ V max	± 0.5 V max
Generated sinusoidal		
30 Hz to 15 kHz	<0.5 V peak to peak	<0.5 V peak to peak
15 to 150 kHz	<0.5 V peak to peak, decreasing at 20 dB/octave to 0.05 V peak to peak at 150 kHz	<0.5 V peak to peak
150 kHz to 25 MHz	<0.05 V peak to peak	<0.05 V peak to peak
Conducted interference susceptibility, power leads		
Transients	± 16 V amplitude ≤ 20 μs wide ≤ 7 μs rise time Repetition rate: 0.5 to 500 pulses/s	± 16 V amplitude
Sinusoidal		
30 Hz to 15 kHz	1.0 V peak to peak	1.0 V peak to peak
15 to 150 kHz	1.0 V peak to peak at 15 kHz, decreasing at 20 dB/decade to 0.1 V peak to peak at 150 kHz	1.0 V peak to peak
150 kHz to 25 MHz	0.1 V peak to peak	0.1 V peak to peak
Conducted interference susceptibility, signal lines		
Transients	± 400 mV amplitude ≤ 20 μs wide ≤ 7 μs rise time Repetition rate: 0.5 to 500 pulses/s	± 400 mV amplitude
Sinusoidal		
30 Hz to 15 kHz	0.1 V peak to peak	0.1 V peak to peak
15 to 150 kHz	0.1 V peak to peak at 15 kHz, decreasing at 20 dB/ decade to 0.01 V peak to peak at 150 kHz	0.1 V peak to peak
150 kHz to 25 MHz	0.01 V peak to peak	0.01 V peak to peak

Table 6 (contd)

Electromagnetic interference	Interference limits	
	Environmental test specification	JPL test procedure
Equipment enclosure radiated interference susceptibility test		
Frequency, MHz	Power density, $dBmW/m^2$	Power density, $dBmW/m^2$
0.15 to 100	2	
100 to 150	4	
225 to 260	36	
400 to 550	10	
1200 to 1400	30	
2200 to 2900	0	
5400 to 5900	28	
8500 to 10,000	30	
Spurious response susceptibility test		
Frequency, MHz 1.0 to 10,000	Signal level 0 dBmW	Signal level 0 dBmW
Oscillator radiation test		
Frequency, MHz 1.0 to 10,000	Signal level All energy detectable by sampling receiver	Signal level

susceptibility limits were exploratory limits representing expected prelaunch-to-separation electromagnetic environmental levels. Since the science equipment would not be turned on prior to separation and prelaunch checkout could be performed by careful planning (i.e., turnoff or scheduling), the susceptibility did not jeopardize the mission.

Data automation system. The data automation system (DAS) electromagnetic interference testing was performed to verify that the unit would function properly when subjected to an electromagnetic environment similar to twice that expected to exist on the *Mariner* Venus 67 spacecraft.

The *Mariner* Venus 67 DAS utilized a configuration which neither had flown on a spacecraft nor had been subjected to an electromagnetic environment similar to that expected to exist on the *Mariner* Venus 67 spacecraft. To verify that the DAS would function properly, electromagnetic interference testing levels were derived from data acquired during the testing sequence of the *Mariner C* spacecraft and from the expected electromagnetic environment for the *Mariner* Venus 67 spacecraft. The interference levels to which the DAS were subjected are listed in the environmental specification. In accordance with the specification, the DAS was tested per JPL test procedure. Table 7 lists the required test limits and the test limits as defined in the JPL test procedure.

The data automation system (SN 073) was subjected to electromagnetic interference testing per type-approval procedure as outlined in a JPL procedure. The unit successfully passed the tests as specified and operated within the prescribed limits with no degradation to operation during all electromagnetic interference testing.

Pyrotechnic control unit. The pyrotechnic control unit (PCU) electromagnetic interference testing (Fig. 6) was performed to verify that the unit would function properly when subjected to an electromagnetic environment similar to twice that expected to exist on the *Mariner* Venus 67 spacecraft.

The *Mariner* Venus 67 PCU utilized a configuration which neither had flown on a spacecraft nor had been subjected to an electromagnetic environment similar to that expected to exist on the *Mariner* Venus 67 spacecraft. To verify that the PCU would function properly, electromagnetic interference testing levels were derived from data acquired during the testing sequence of the *Mariner* Mars 1964 spacecraft and the expected electromagnetic environment for the *Mariner* Venus 67 spacecraft. The *Mariner* Project review specified that the PCU be subjected to the derived interference levels. The interference levels to which the PCU was subjected are specified in a JPL internal memorandum. In accordance with the above, the PCU was tested per JPL procedure. Table 8 lists the required test limits and the test limits as defined in the JPL test procedure.

Two PCUs (SN 1005 and 1006) were subjected to electromagnetic interference testing according to TA procedures. The units successfully passed the tests as specified and operated within the prescribed limits with no degradation to operation during all electromagnetic interference testing.

In summary, it should be pointed out that the subsystem electromagnetic interference tests did not adequately simulate the electromagnetic environment that

Table 7. EMI tests and limits for DAS

Electromagnetic interference	Interference limits	
	Environmental test specification	JPL test procedure
Generated interference		
Generated conducted transient	< ±0.5 V	±0.5 V max
Generated sinusoidal		
30 Hz to 15 kHz	<0.5 V peak to peak	0.5 V peak to peak
15 to 150 kHz	<0.5 V peak to peak, decreasing at 20 dB/octave to 0.05 V peak to peak at 150 kHz	0.5 V peak to peak
150 kHz to 25 MHz	<0.05 V peak to peak	0.5 V peak to peak
51.0 ±7 MHz, 423.3 ±3 MHz	<20,000 V across 50 Ω	Not tested[a]
Conducted interference susceptibility, power leads		
Transients	±16 V amplitude ≤20 μs wide ≤7 μs rise time Repetition rate: 0.5 to 500 pulses/s	±16 V amplitude
Sinusoidal		
30 Hz to 15 kHz	1 V peak to peak	1 V peak to peak
15 to 150 kHz	1 V peak to peak at 15 kHz, decreasing at 20 dB/ decade to 0.1 V peak to peak at 150 kHz	1 V peak to peak
150 kHz to 25 MHz	0.1 V peak to peak	0.1 V peak to peak
Conducted interference susceptibility, signal lines		
Transients	±400 mV amplitude ≤20 μs wide ≤7 μs rise time Repetition rate: 0.5 to 500 pulses/s	±400 mV amplitude
Sinusoidal		
30 Hz to 15 kHz	0.1 V peak to peak	0.1 V peak to peak
15 to 150 kHz	0.1 V peak to peak at 15 kHz, decreasing at 20 dB/decade to 0.01 V peak to peak at 150 kHz	0.1 V peak to peak
150 kHz to 25 MHz	0.01 V peak to peak	0.01 V peak to peak

[a]Due to the magnitude and harmonic content of the prime power source, it was not possible to instrument the pyrotechnic control unit for this measurement.

Table 8. EMI tests and limits for PCU

Electromagnetic interference	Interference limits	
	Environmental test specification	JPL test procedure
Generated interference		
Generated conducted transient	<±0.5 V max	±0.5 V max
30 Hz to 15 kHz	<0.5 V peak to peak	0.5 V peak to peak
15 to 150 kHz	<0.5 V peak to peak, decreasing at 20 dB/octave to 0.05 V peak to peak at 150 kHz	0.5 V peak to peak
150 kHz to 25 MHz	<0.05 V peak to peak	0.05 V peak to peak
51.0 ±7 MHz, 423.3 ±3 MHz	<20,000 V across 50 Ω	Not tested[a]
Conducted interference susceptibility, power leads		
Transients	±16 V amplitude ≤20 μs wide ≤7 μs rise time Repetition rate: 0.5 to 500 pulses/s	±16 V amplitude
Sinusoidal		
30 Hz to 15 kHz	1 V peak to peak	1 V peak to peak
15 to 150 kHz	1 V peak to peak at 15 kHz, decreasing at 20 dB/decade to 0.1 V peak to peak at 150 kHz	1 V peak to peak
150 kHz to 25 MHz	0.1 V peak to peak	0.1 V peak to peak
Conducted interference susceptibility, signal lines		
Transients	±400 mV amplitude ≤20 μs wide ≤7 μs rise time Repetition rate: 0.5 to 500 pulses/s	±400 mV amplitude
Sinusoidal		
30 Hz to 15 kHz	0.1 V peak to peak	0.1 V peak to peak
15 to 150 kHz	0.1 V peak to peak at 15 kHz, decreasing at 20 dB/decade to 0.01 V peak to peak at 150 kHz	0.1 V peak to peak
150 kHz to 25 MHz	0.01 V peak to peak	0.01 peak to peak

[a]Due to the magnitude and harmonic content of the prime power source, it was not possible to instrument the pyrotechnic control unit for this measurement.

the subsystem would experience during spacecraft system operation. Further study is necessary to develop tests that adequately simulate the *Mariner* spacecraft electrical environment.

b. Solar panel TA testing program.

Vibration testing. Prior to the start of testing, an overall test plan was formulated in consultation with cognizant structural and solar panel engineers. The planned sequence of tests and use of test results was to be the following:

First, qualify the TA panel under vibration by mounting the TA panel on the STM (using three STM panels) and conduct a PTM vibration test. Panel response data at selected locations was to be acquired.

Second, by use of the response data from the TA test (on the STM) and the results of modal testing of a structural model of the solar panel, a single panel test was to be developed. A representative response location on the solar panel was selected and by using the modal test data, a desired response in the single-panel test configuration in two corrugation modes was to be determined. The level of response for an equivalent single-panel TA test would be selected to produce stresses (panel curvature) in the two modes selected, which would equal the stress induced in the TA panel during its vibration test as part of the STM. An early estimate of the required input for this response in the single panel mode would be made using modal test data. The single-panel test configuration was to be with the panel supported at the damper attachment points by two struts rigidly attached to the floor at their other ends; vibration would be input at the input hinges from a rigid test fixture. The test would be mechanized by estimating an input level at the hinges required to give the desired response at the selected location. The actual response would be limited by stopping the test if the response exceeded the desired level by $>10\%$.

Third, when the TA panel (already qualified to vibration test levels on the STM spacecraft) had completed other required TA tests, a TA test of a single panel (Fig. 7) was to be conducted to provide confidence that the FA panels would pass the single-panel FA test. This test would also serve both to provide a better estimate of input required for desired response on FA test panels and to check out the single-panel test technique prior to the FA tests.

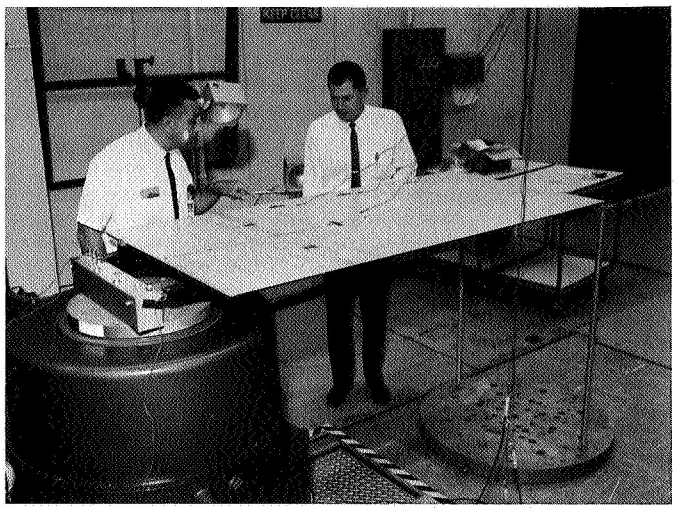

Fig. 7. Single solar panel for TA vibration test

The TA test on STM spacecraft was properly conducted to the levels required by the JPL specification. No physical damage to the panel was discovered; neither was electrical degradation found during or after the test. Based on response measurements during this test and single-panel modal tests, two corrugation modes at about 74 and 116 Hz were selected to be excited during single-panel testing. The required responses at the selected response control location (C4) were calculated to be 3.0 *g* peak at 74 Hz and 7.0 *g* peak at 111 Hz for the TA tests. Later, errors in the STM test data reduction were discovered, and the desired responses were increased by a factor of 1.4 to 4.2 *g* peak at 74 Hz and 9.9 *g* peak at 111 Hz. The accelerometer used to measure the desired response was located on the cell side of the panel.

Preliminary test plans called for the single-panel TA vibration test to be a part of the formal TA test program. Damage to the panel during thermal–vacuum testing (described later in this Section) precluded evaluation of the panel's electrical integrity, and therefore, the test was considered as developmental in purpose. With response data from this test, sweep ranges and input levels for the single-panel FA tests were selected as follows: (1) 67 to 83 Hz, input was 0.85 *g* rms; (2) 105 to 120 Hz, input was 1.4 *g* rms. The accelerometer used to develop the frequencies and amplitudes was located at the response control location, but on the cell side of the panel. In order to minimize damage to the flight panels, the response control accelerometer was to be located at the same point on the panel, but on the corrugation side. To discover any change in measured response due to this change in accelerometer location, data

were taken during this test at both locations and then compared. Unfortunately, upon reduction of the raw data, it was discovered that data from the corrugation side accelerometer was lost. At this point, it was assumed that, at these panel modes, the two locations should not differ greatly, although later testing (reported in Section IV) proved the assumption to be in error. A summary of solar-panel vibration qualification is presented in Table 9.

Acoustic testing. The original test plan was to expose the TA panel (SN 002) to the TA acoustic test level (JPL specification) and assess electrical and structural damage.

Test results showed that problems with the TA thermal–vacuum test affected the electrical integrity of the TA panel prior to the acoustic testing. Because of this, the acoustic test could not be considered a full TA test. The panel was actually tested two times – first, as a single panel, and second, mounted on the STM spacecraft (with three STM panels). The test had to be repeated because solar panel appendages were not included on the single panel test.

For the first solar panel acoustic test, the single panel was hung in its mounting frame by shock cord within the 930-ft^3 reverberant chamber and exposed to the FA acoustic test for 20 s, then inspected for damage. The TA acoustic test was then run for 60 s. Figure 8 shows the average sound-pressure-spectrum level (SPSL) of four microphones in the chamber during the TA test, compared with the specified spectrum. The test was

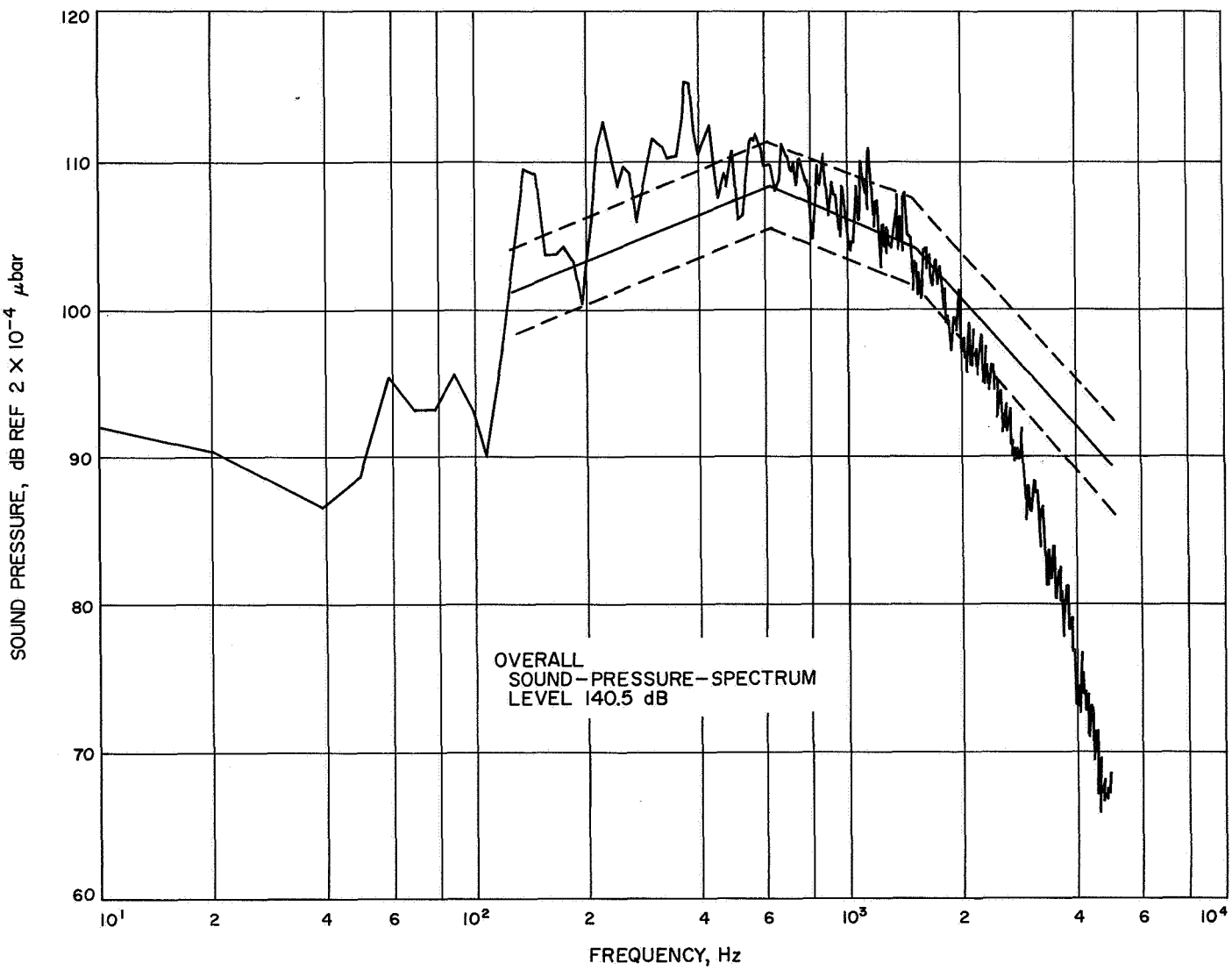

Fig. 8. Sound-pressure spectrum level for single-panel TA test

Table 9. Solar panel system qualification

Subsystem	Vibration	Acoustic	Thermal, steady-state	Thermal shock	Shock[a]	Remarks
Solar panel	Test extensive; see text for details.	Test extensive; see text for details.	Test extensive; see text for details.	Test extensive; see text for details.	None; not feasible on a test item this size.	
Tip dampers	Tested on STM to STM levels.	Tested to TA levels on STM acoustic test.	Tested as assemblies since they were not on during solar panel tests.	None	None	
A/C jets & plumbing	Tested on STM to STM levels. Jets TA tested only as assembly.	Tested to TA levels on STM acoustic test.	Jets tested on solar panel TA test in space simulator. Also TA tested as assembly.	Jets tested on solar panel TA test in space simulator.	Jets TA tested as assemblies.	
A/C jet sunshade	Tested on STM to STM levels. Many spot welds failed initially; satisfactorily retested following redesign on STM followup tests.	Tested to TA levels on STM acoustic test following redesign.	Tested on solar panel TA test in space simulator.	Tested on solar panel TA test in space simulator.	None	
Pinpuller, squibs & harnesses	Pinpullers and squibs TA tested as assemblies; harness was on STM.	Tested to TA levels on *Mariner* C PTM acoustic test.	Pinpullers (no squibs and harness) were on solar panel TA test in space simulator.	Pinpullers (no squibs and harness) were on solar panel TA test in space simulator.	Pinpullers and squibs TA tested as assemblies.	Pinpullers, squibs & harness EMI tested to ensure isolation from low-gain antenna.

DFR antenna, VHF	Tested on STM to STM levels.	Tested to TA levels on STM acoustic test.	Tested on solar panel TA test in space simulator.	Was on solar panel during TA steady-state thermal–vacuum test in space simulator when lights went off at Venus conditions. Since it was unaffected, it can be considered as being qualified to very conservative thermal-shock levels.	None	This item is not amenable to testing as an assembly.
DFR antenna, UHF	Developmental tested as assembly to levels determined from STM tests. TA assembly level also passed.	Tested to TA levels on STM acoustic test.	Tested on solar panel TA test in space simulator.	Same as VHF antenna.	Done during assembly-level TA.	
Temperature transducer	TA tested as assembly. Also tested on all solar panel TA tests.	Tested on solar panel TA test and on STM acoustic test.	Tested on solar panel TA test. Also TA tested as assembly.	Tested on solar panel TA test in space simulator.	TA tested as assembly.	
Temperature control reference	Tested on STM to STM levels.	Tested to TA levels on STM acoustic test.	Tested on solar panel TA test in space simulator.	Tested on solar panel TA test in space simulator. Had delamination failure; see PFR 011365. Failure attributed to poor bond repair.	None	

[a]These items experienced shock test during the pyro firing in the system-level testing. This system-level testing provides an excellent simulation of the boundary conditions and environment application but is deficient in that no TA to FA or FA to expected flight environment margins are provided.

specified in 1/3-octave bands and the analysis bandwidth used for the SPSLs with which it is compared was 20 Hz. The only damage to the panel during either test was that cell covers were broken. Most covers were broken during the FA test; only a small additional amount were broken during the TA test. Electrical performance could not be fairly evaluated.

For the second solar panel acoustic test, all solar panel appendages (omitted during the first test) were in place. To conduct this test, the panel was mounted in place on the STM spacecraft with three STM solar panels. Because of a test-facility error, the test was conducted in two sections. Following chamber equalization, in which a dummy of the spacecraft was used, some parts of the noise generators were cleaned or replaced. This modification greatly affected the noise spectrum and resulted in a test being conducted with the spectrum as shown on Fig. 9. It greatly exceeded the test specification in low frequencies but was an undertest at high frequencies. To complete the test, the chamber was equalized at a lower noise level to produce a spectrum up to that specified in the high frequencies but below test specification in low frequencies. The test was then repeated with the new spectra as shown in Fig. 10. This second test was considered to have filled in the high-frequency portion of the spectrum. Following the tests, no damage to the solar panel or its appendages was found. A summary of solar-panel acoustic qualification is presented in Table 9.

Thermal–vacuum. A detailed test plan was initiated prior to the start of the type-approval thermal–vacuum testing of the *Mariner* Venus 67 solar panel. The testing was accomplished in the JPL 10-ft space simulator with the panel (Fig. 11) completely assembled with all hardware that would be assembled to the panels during flight including the complete attitude control mechanisms and plumbing. Test requirements and specifications were defined in a JPL specification.

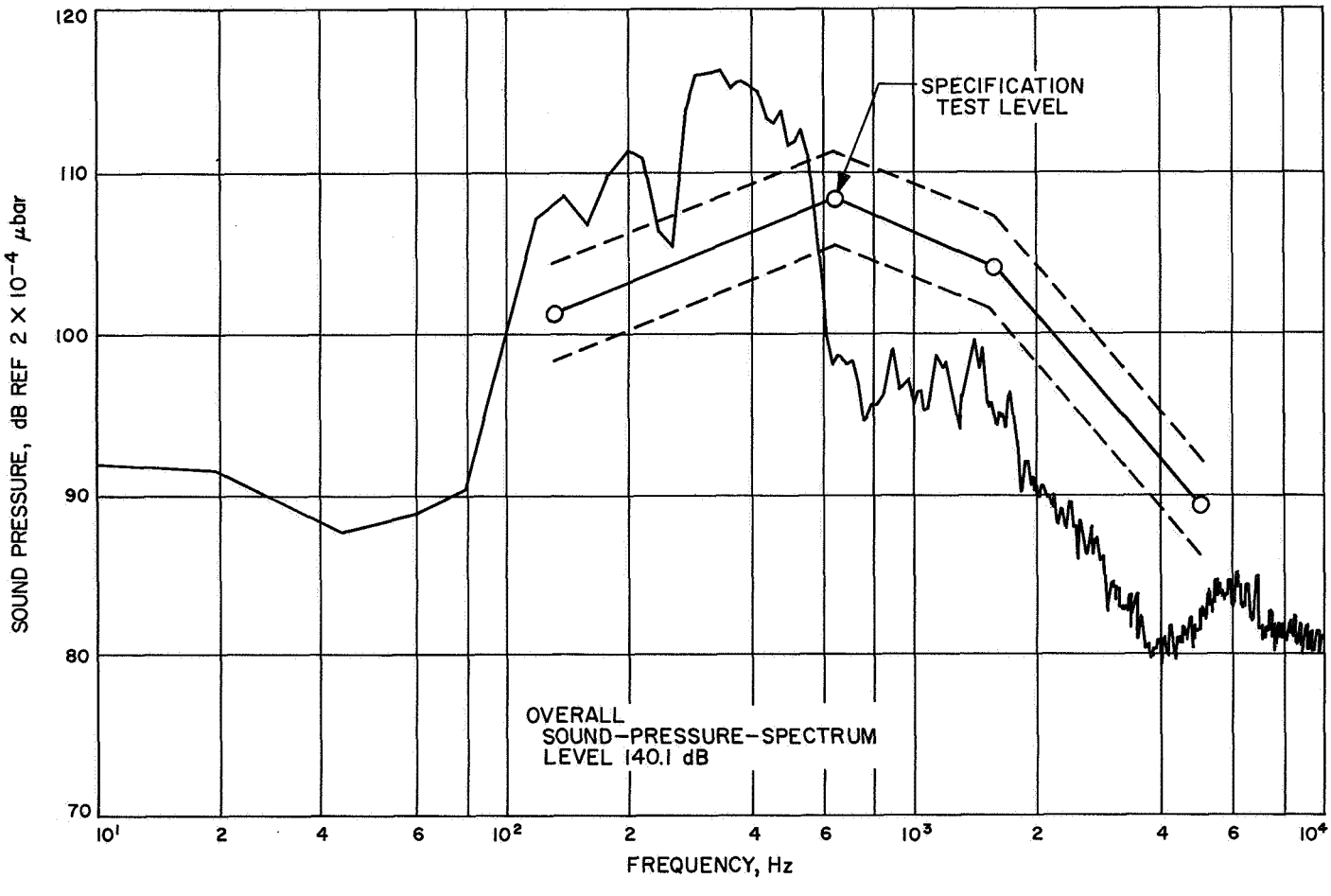

Fig. 9. Solar panel acoustic test following noise-generator cleanup or replacement

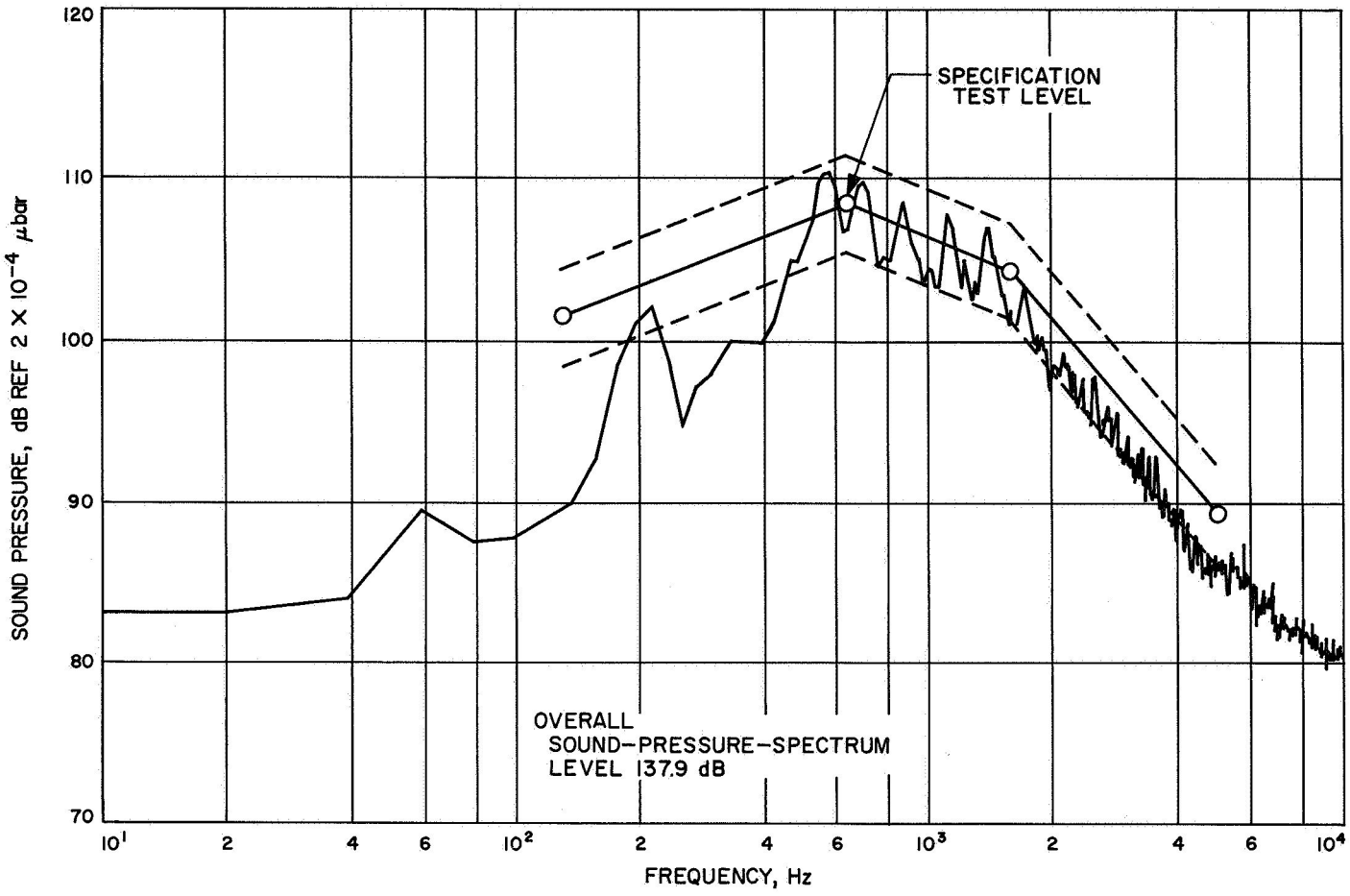

Fig. 10. Solar panel acoustic test after chamber equalization

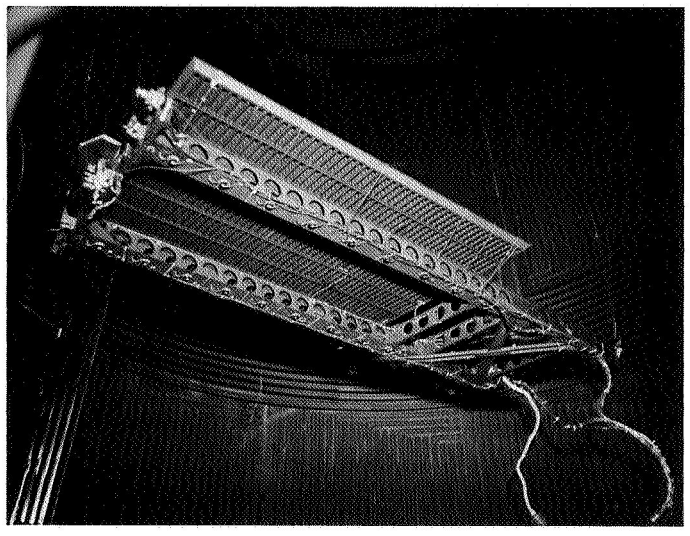

Fig. 11. Solar panel thermal shock test

It was the purpose of the TA thermal–vacuum test program to qualify the complete solar panel assembly by subjecting the unit to two thermal shocks, one from 135 to −180°F and the other from 160 to −180°F. The panel was then to experience a 100-h soak at 284°F. Before and after exposure to the thermal–vacuum environment the panel was to be visually inspected and electrically tested in sunlight at the JPL Table Mountain Test Facility near Wrightwood, California.

The solar panel configuration consisted of an attitude control jet and manifold assembly (exclusive of cabling and plumbing), an A/C sunshade, a pinpuller assembly (exclusive of cabling), and the temperature-control reference paddle. It is believed that the deletion of the cabling and plumbing associated with various items has a negligible effect on the results of the tests. It was initially intended to mount a damper assembly but, because of the possibility of oil leakage and subsequent contamination, this assembly was eliminated. It was also intended to mount the DFR antennas (50 and 425 MHz) but a delay in availability, due to a problem with paint curing, eliminated these items from the thermal shock test. However, the DFR antennas were on board, properly painted, for the high-temperature steady-state test.

The complete solar panel assembly was instrumented with chromel/constantan thermocouples coupled to a datex printout system. Table 10 and Figs. 12 and 13 illustrate the thermocouple locations. The panel was suspended by overhead cabling, at a height of approximately 5 ft from the lower shroud of the 10-ft solar simulation chamber, and positioned as advantageously as possible in the 6.5-ft beam pattern. Intensity mappings taken prior to the thermal-shock test are listed in Table 11, while those taken prior to the high-temperature steady-state test are given in Table 12. Mapping locations are shown in Fig. 14.

Table 10. Thermocouple and datex numbering system

Thermocouple No.	Position	Datex channel
2	Sunlit yaw valve	102
3	Roll valve	147
4	Shaped yaw valve	148
5	Spade lug, under screw of A/C jet manifold	149
6	TCR bracket	126
7	TCR channel	127
8	TCR sensor	128
9	A/C assembly mounting point (panel end)	150
—	Pinpuller	101
1	50 *Mariner IV* DFR antenna capacitor	222
10	425 *Mariner IV* DFR brace end point, sunward	223
11	425 *Mariner IV* DFR mast at brace attach	224

Table 11. Solar irradiance mapping values for thermal shock test

Location No.	Value, V
1	0.1727
2	0.1799
3	0.1789
4	0.1789
5	0.1800
6	0.1800
19	0.1834
20	0.1810
21	0.1839
22	0.1810
23	0.1810
24	0.1810
25	0.1810
26	0.1775
27	0.1802
28	0.1750
29	0.1722
32	0.1759
34	0.1789
35	0.1750
36	0.0028
37	0.1754
39	0.1830
40	0.1839
41	0.1820
42	0.1819
43	0.1798
44	0.1769
Eppley radiometer reading was 0.1793 V.	

FOLDOUT FRAME 1

FOLDOUT FRAME 2

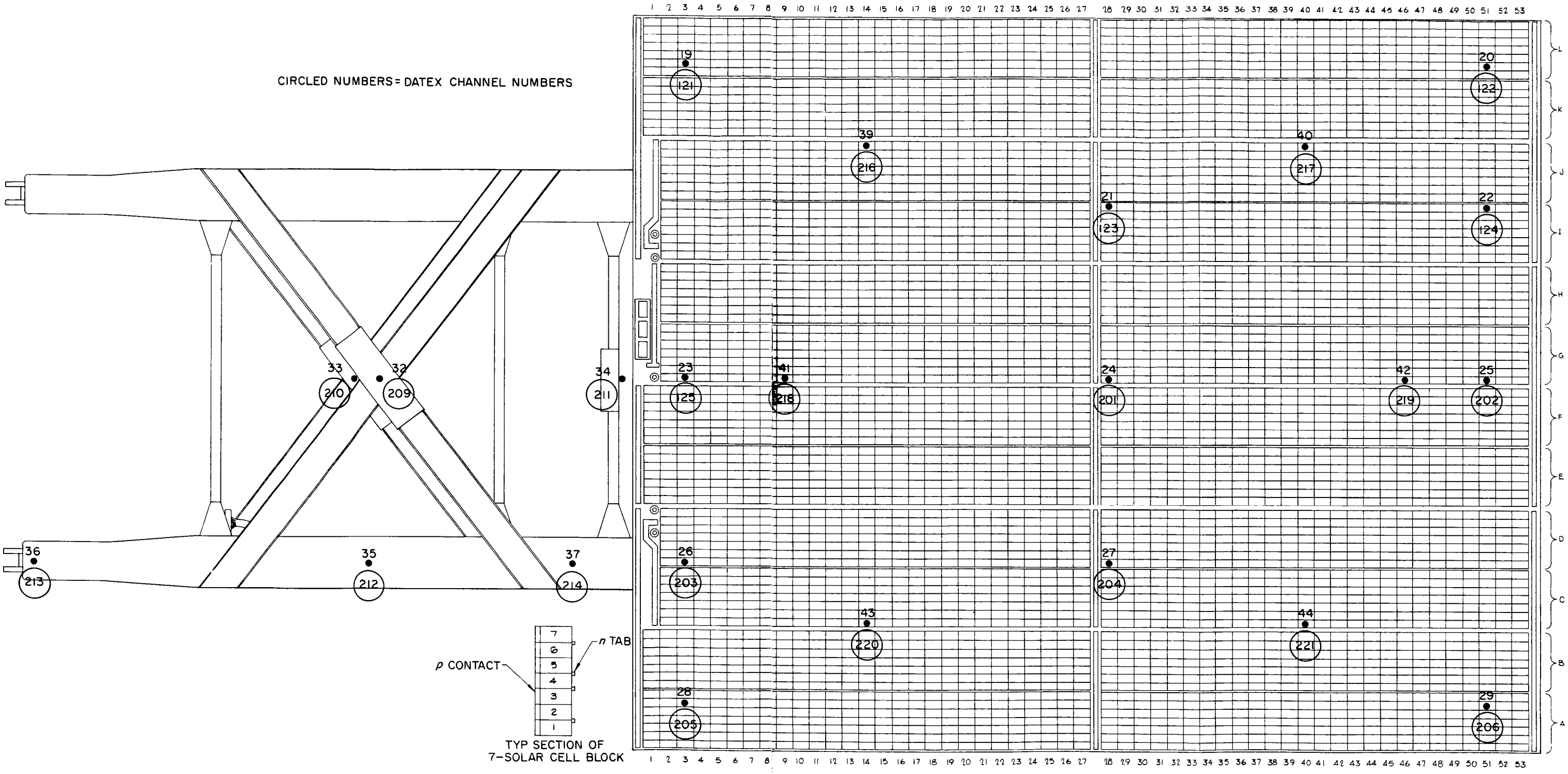

Fig. 12. Solar panel thermocouple locations, front side

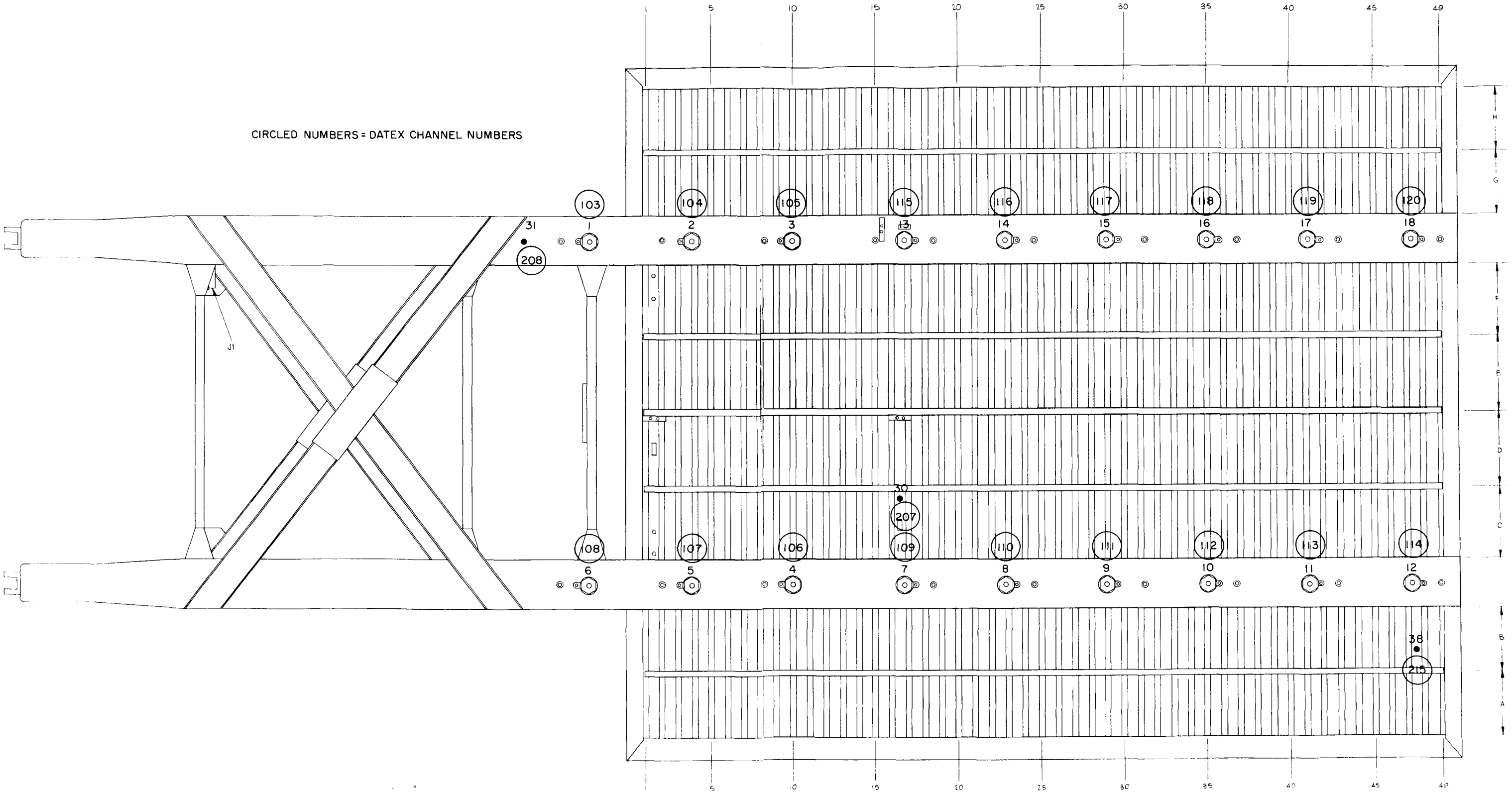

Fig. 13. Solar panel thermocouple locations, back side

FOLDOUT FRAME 1

FOLDOUT FRAME 2

FOLDOUT FRAME

FOLDOUT FRAME

MAP NOS. AT TC LOCATIONS

1	26
2	27
3	28
4	29
5	32
6	34
19	35
20	36
21	37
22	39
23	40
24	41
25	42
	43
	44

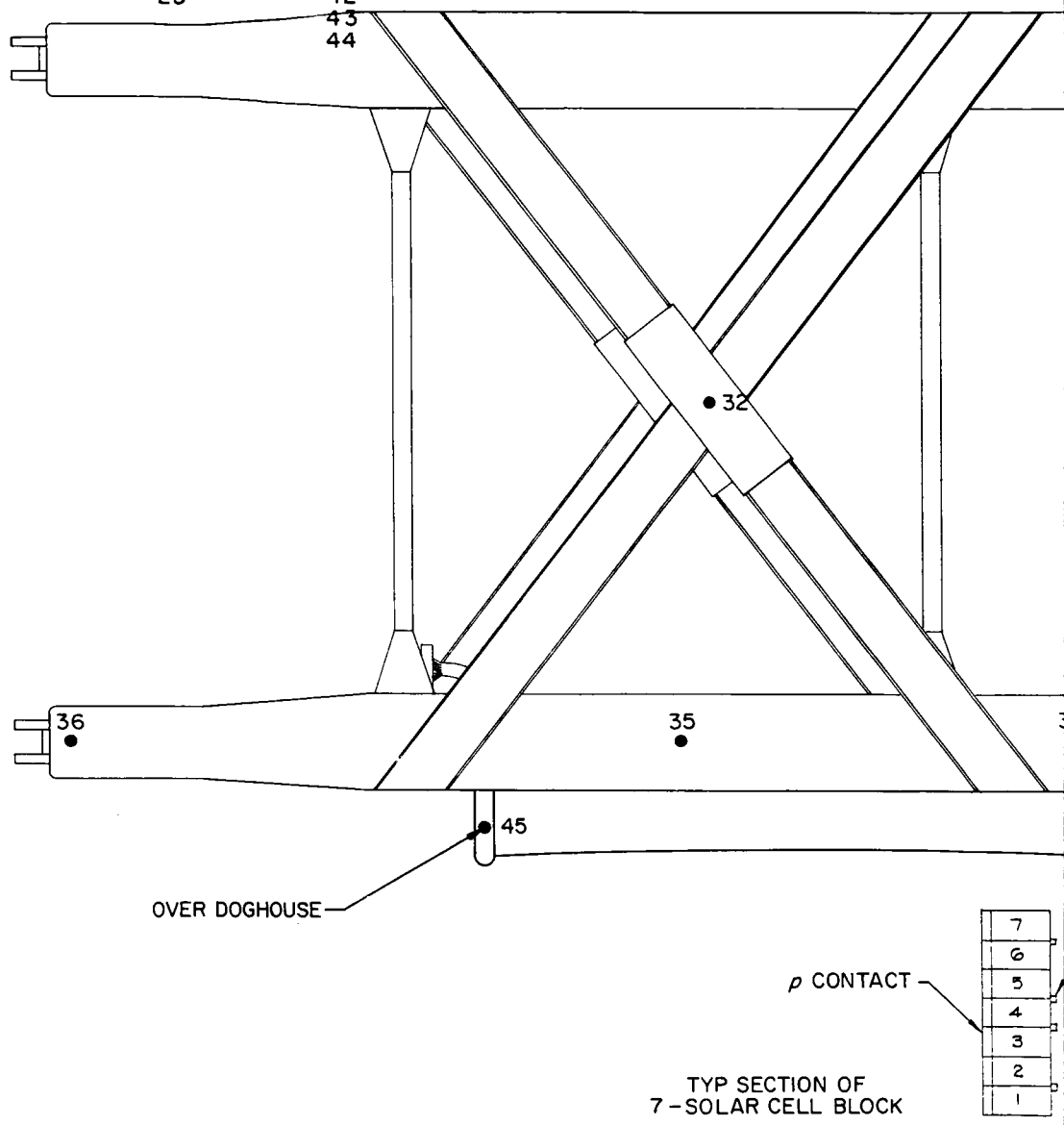

FOLDOUT FRAME 3

FOLDOUT FRAME 2

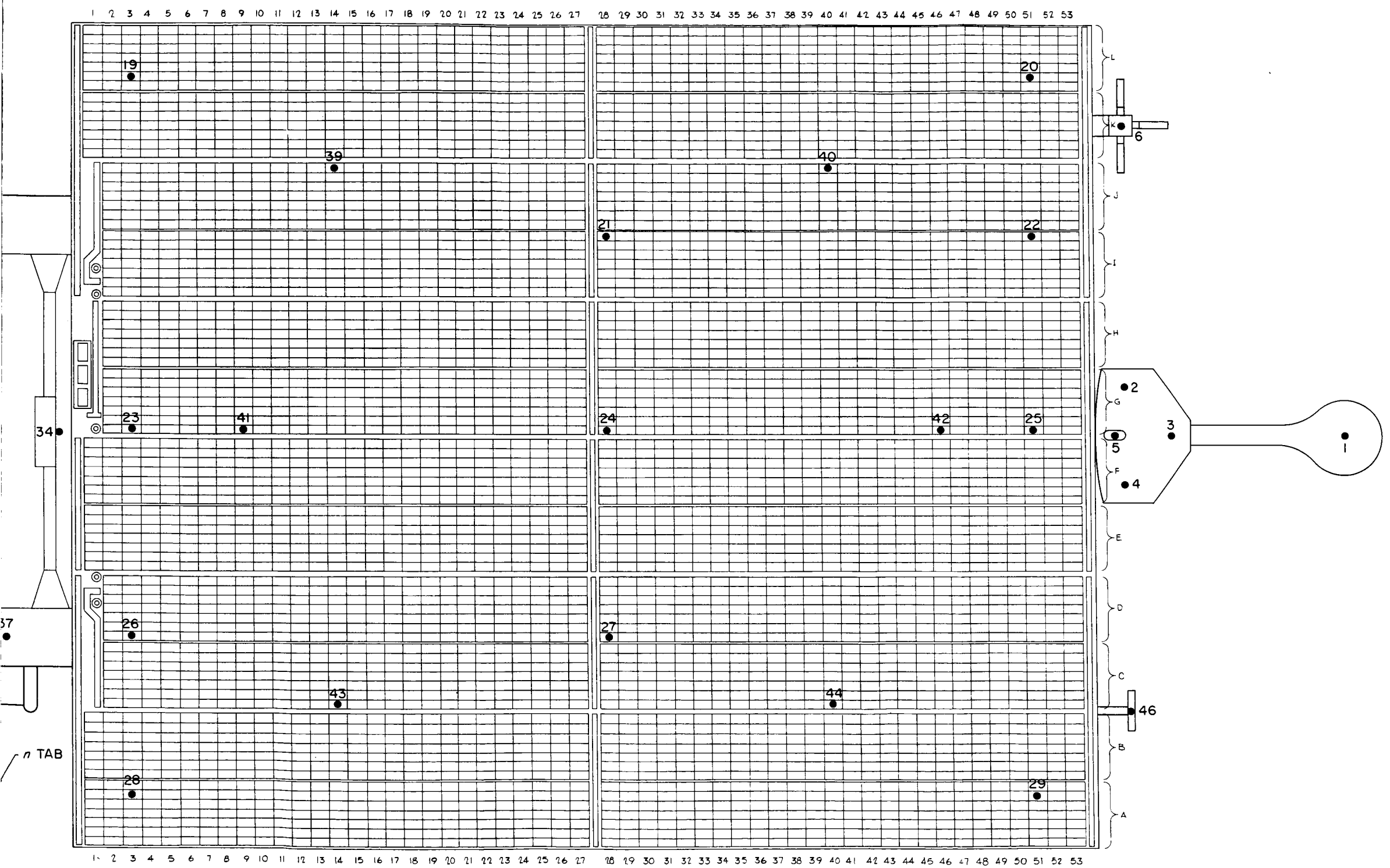

Fig. 14. Solar irradiance mapping locations

Table 12. Solar irradiance mapping values for high-temperature steady-state test

Location No.	Value, V
1	0.1699
2	0.1750
3	0.1746
4	0.1754
5	0.1769
6	0.1773
19	0.1789
20	0.1768
21	0.1789
22	0.1789
23	0.1790
24	0.1789
25	0.1796
26	0.1769
27	0.1799
28	0.1740
29	0.1499
32	0.1739
34	0.1762
35	0.1717
36	0.0040
37	0.1759
39	0.1779
40	0.1799
41	0.1797
42	0.1792
43	0.1779
44	0.1499
45	0.1607
46	0.1550
Eppley radiometer reading 0.1769.	

There were three *test levels* – (1) thermal shock, (2) high-temperature steady state, and (3) unscheduled thermal shock.

(1) Since thermal-shock-rate predictions for the panel are subject to many possible errors, it is more advantageous to simulate the conditions that determine the transient than duplicate a predicted transient rate. Based on this reasoning, it was originally planned to establish solar simulator intensities, corresponding to the sun's intensity at certain times during flight, then turn off the simulator and allow the panel to cool. However, because of the uncertainty of the spectral characteristics of the solar simulator and the spectral sensitivity of solar cells, it was decided to bring the panel, and the associated fittings, to a particular steady-state temperature corresponding to a predicted cruise temperature during flight. Once this steady-state temperature level was obtained, the lights would be turned off and the temperature allowed to decay to a predetermined level. At this low level the lights would be turned back on, at the settings obtained during the previous steady state, and the panel allowed to heat until it reached steady state again. Performing the thermal shock test in this manner provides a worst case simulation of midcourse maneuver – i.e., an instantaneous 90 deg turn of the spacecraft both out of and into the sun. The steady-state temperatures selected for the start of the transients were based upon predicted cruise temperatures for launch $L + 8$ days and $L + 50$ days. The rationale for choosing these particular days was that normally midcourse maneuver would occur at $\sim L + 8$ days, but the maneuver was unrestricted up to $L + 30$ days. Therefore, testing at $L + 8$ days was planned to provide a possibility of later correlation with flight data, while testing at $L + 50$ days to provide a TA level test more severe than the expected maximum of $L + 30$ days. A curve of the planned thermal-shock testing is shown in Fig. 15.

(2) The predicted solar-panel temperature for encounter $E + 10$ days is 260°F. An rms and worst-case error analysis was performed on this predicted number and resulted in establishing the solar panel steady-state TA test level at 300°F. However, subsequent discussion with the solar-panel cognizant engineer disclosed P-contact delamination problems at temperatures >284°F. Therefore, a decision was made to conduct the steady-state test at 284°F for a 60-h duration.

(3) Inherent in the planning of both the thermal shock and high-temperature steady-state tests was the intent to monitor the electrical performance of the solar panel at all times to ensure its proper qualification. It was learned, shortly before completion of the 60-h steady-state test, that this had not been done. It was, therefore, decided to extend the steady-state test an additional 24 h to provide adequate time to perform various electrical measurements. At 60 h and 28 min after the start of the steady-state test, an unexpected loss of electrical power

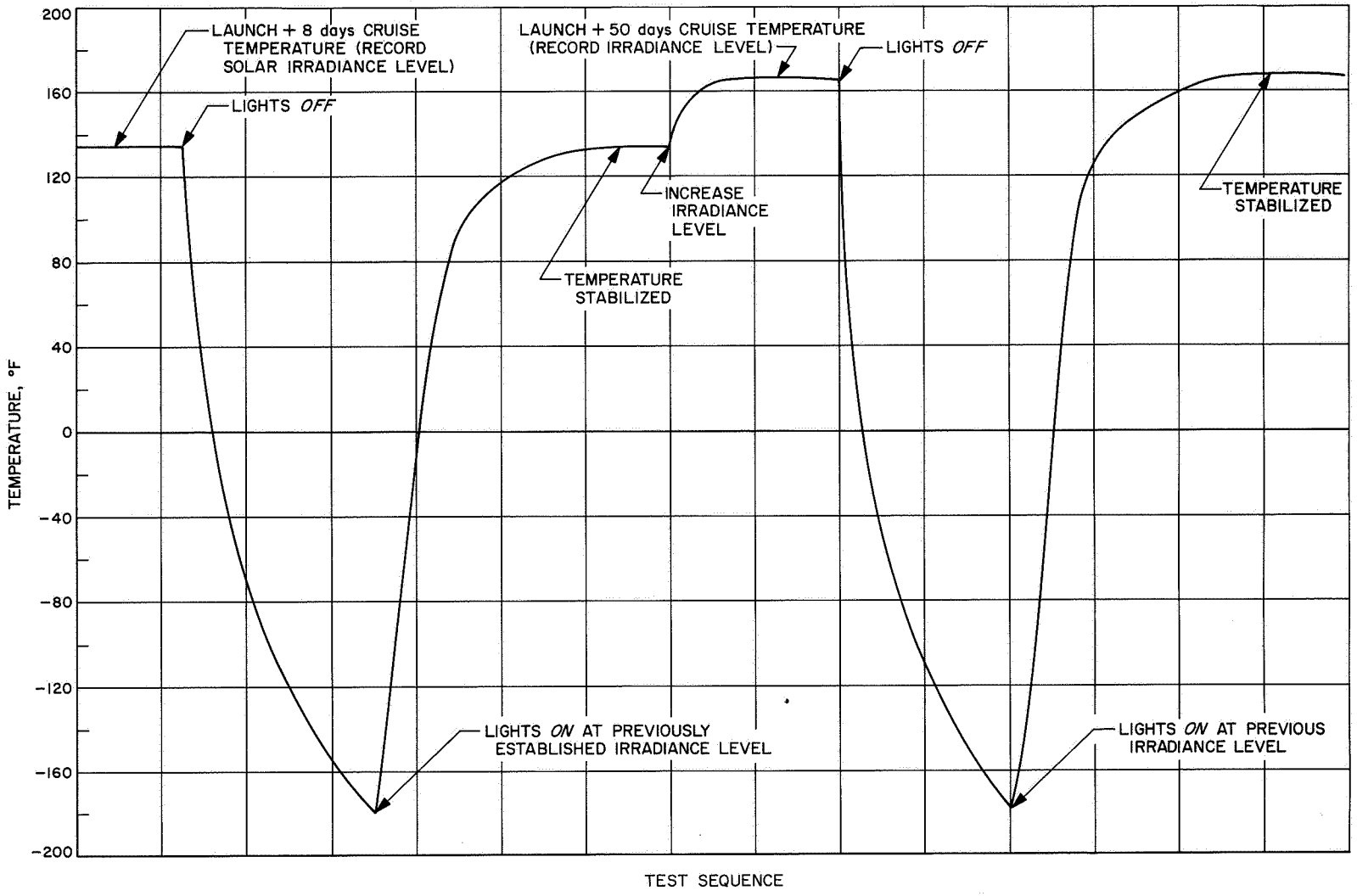

Fig. 15. Planned thermal shock routine

to the solar simulation lights occurred. Correspondingly, the solar panel experienced an unscheduled thermal shock from +284°F to −48°F before the lights were placed back in operation (see Fig. 16). The panel temperature was then raised to 284°F, and the balance of the steady-state testing was completed.

Test results for (1) the scheduled thermal shock, (2) the high-temperature steady state, and (3) the unscheduled thermal shock are given, respectively, in the following paragraphs.

(1) The scheduled thermal shock test was performed as planned with one exception. Because of an oversight, the items mounted on the solar panel did not always attain true steady-state temperature levels before or after the shock as had been planned. Therefore, maximum transient rates on these items were not obtained. However, the results still appear to be of definite value in determining the transient rates that would apply in any further testing of these items. The results of the scheduled thermal shock test are presented graphically for the solar panel, attitude-control assembly, and TCR in Figs. 17 through 19.

As shown in Fig. 17 the downward solar panel shock, from the L + 8 days level (133°F, 128 W/ft²), was 33°F/min for the first minute and 29°F/min over the first 3 min. The returning upward shock was 43°F/min

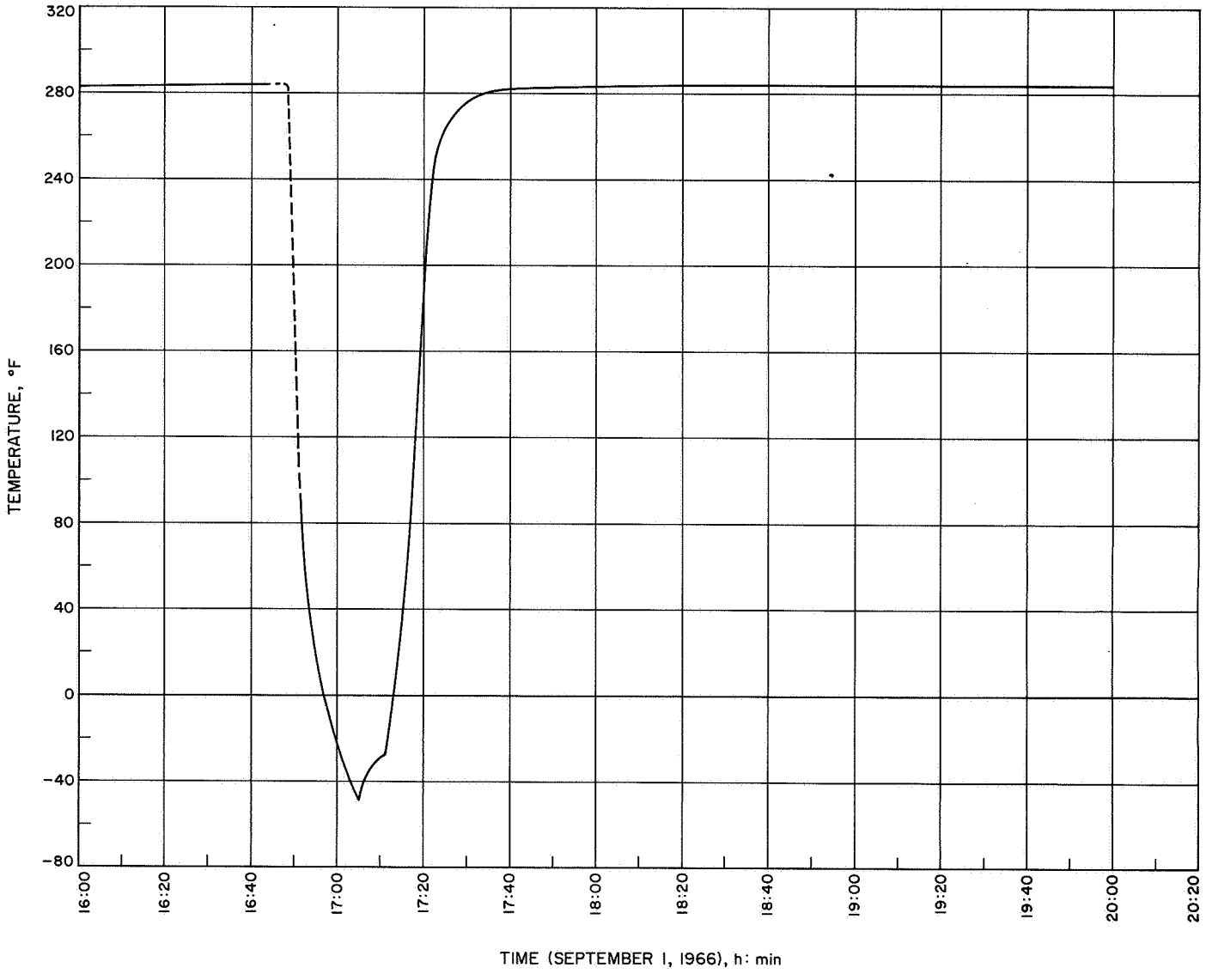

Fig. 16. Solar panel unscheduled thermal shock during steady state

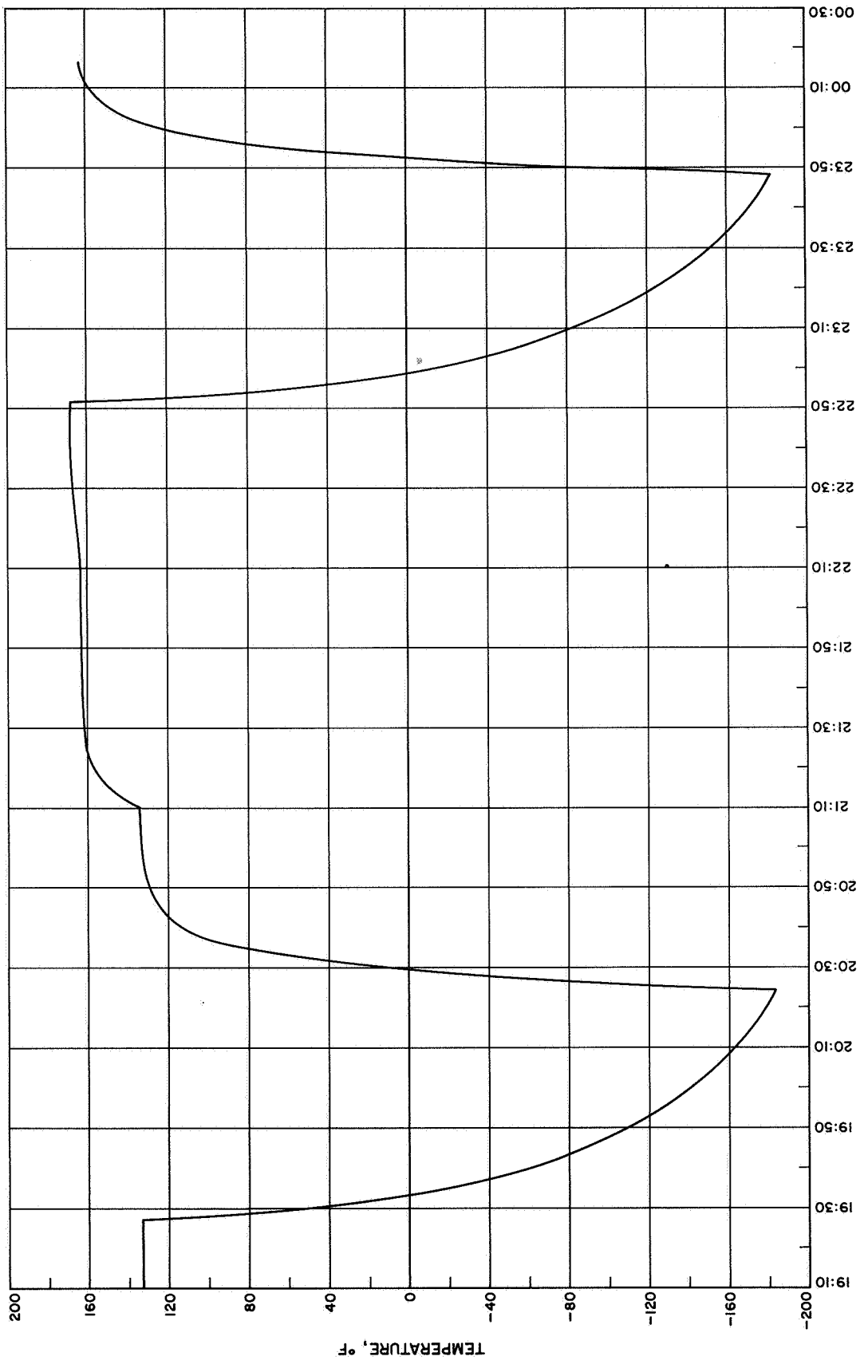

Fig. 17. Curve for solar panel during thermal shock

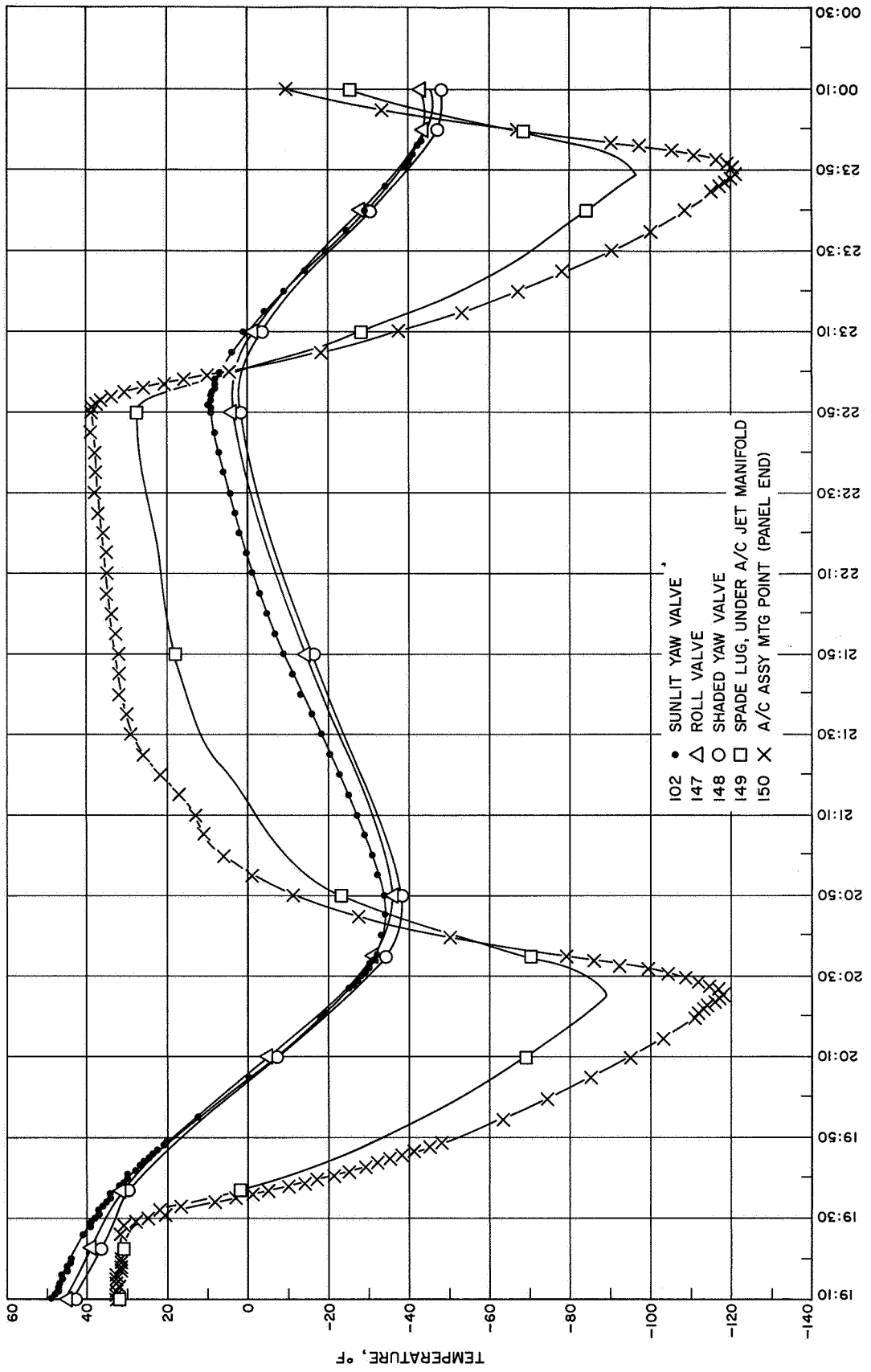

Fig. 18. Curve for attitude-control assembly during thermal shock

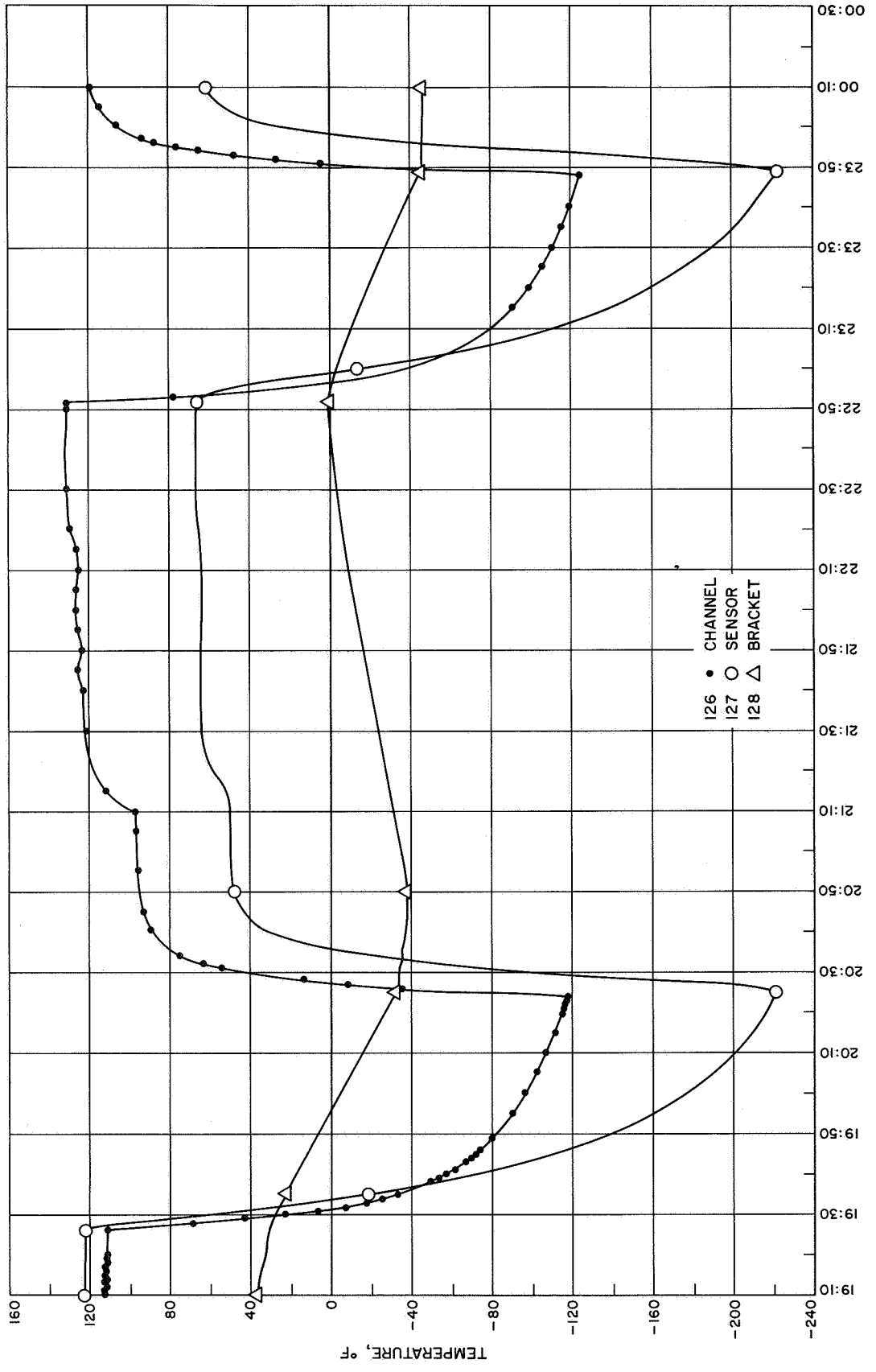

Fig. 19. Time–temperature curve for TCR during thermal shock

for the first minute and 41°F/min over the first 3 min. For the L + 50 days conditions (168°F, 159 W/ft²) the down shock was 46°F/min for the first minute and 32.6°F/min over the first 3 min, while the upward shock was 59°F/min for the first minute and 49°F/min over the first 3 min.

Figure 18 shows the results of the transient at various locations of the attitude-control assembly. The thermal shock for the attitude-control assembly is not as severe as that of the panel which is probably attributable to several reasons: The mass of the assembly is concentrated such that it has reasonably good heat capacity with a small radiating area; the upper portion of the assembly is shielded by a sunshade that reduces the effect of a sun-dependent transient; true steady-state conditions were not reached in the assembly prior to initiation of the transient. The two data curves of Fig. 18 that most nearly approach steady-state conditions are essentially solar-panel temperatures at the mounting area rather than attitude-control assembly temperatures. In reference to the curves presented, it should be noted that this data is for the non-operating mode, only, and no account was made for operation of the jets.

The data from the thermal control reference device is shown in Fig. 19. It should be noted that the thermal location designations and numbers appearing on Fig. 19 are different than those shown in Table 5. Discussion with the TCR cognizant engineer indicated that the leads had been hooked up in wrong order, and the designations on Fig. 19 have been corrected for this. This discussion also revealed that the failure of the sensor temperature to return to its original level after the first transient was due to delamination of the aluminum foil sensor that was discovered upon completion of transient testing. This delamination invalidates the temperature information obtained after the initial downward shock; however, the data for that initial down shock agrees well with the panel reference temperature rate: 34°F/min for the first minute vs 33°F/min for the panel, and 24.7°F/min over the first 3 min vs 29°F/min for the panel. The delamination was subsequently repaired, prior to steady-state testing.

(2) The steady-state tests were initially uneventful. A steady-state panel temperature of 284°F was reached with a solar simulator intensity of approximately 306 W/ft² (Eppley). An indication of the corresponding steady-state temperatures for the attached items can be seen in the steady-state portions of Figs. 16 and 20 through 22.

(3) As mentioned previously it was decided to extend the duration of the steady-state test to complete electrical measurements on the panel, and it was during this extension period that a complete electrical power failure occurred at JPL resulting in loss of power to the chamber's solar simulator. Without a heat source, the panel temperature fell rapidly, producing a severe thermal shock. When power was later restored, the panel was brought back gradually to 75°F, and the test was terminated until possible damage to the panel assembly could be assessed. Subsequent visual and electrical inspection revealed that 30% of the solar cells exhibited some damage, primarily in delamination of the electrical p-contact strip (the top contact) from the cell and that the panel power output capability had decreased approximately 25%.

The data for this shock are presented in Figs. 20 through 23. Since a steady-state run was in progress at the time, data for the initial portion of the shock had to be extrapolated because of the lower sampling rate used during steady state. A steady-state data sample was taken at 16:45 (9/1/66). According to the facility log book the power loss occurred at 16:48; data sampling on 1-min intervals was initiated at 16:51. Therefore, Figs. 17 through 20 show the portion from 16:45 to 16:51 in dashed lines. When power was restored, the lights were placed back in operation sequentially to regain the steady-state temperature.

Figure 16 indicates a transient rate of ~54°F/min for the first minute and ~63°F/min over the first 3 min for the solar panel. Figures 20 and 21 indicate the corresponding transients for the attitude control system and DFR antennas respectively. Figure 22 shows the transient data given by the TCR. This TCR data compares well with that of the solar panel reference thermocouple indicating ~52°F/min for the first minute and ~61°F/min over the first 3 min. As in the normal thermal shock tests, the TCR indicates a wider total span of temperatures than the solar panel reference thermocouple.

A detailed test and analysis program was conducted to investigate the solar panel failure. The cause of the problem was traced to mechanical stresses due to thermal shock induced into the panel during the chamber-light power failure. The solar-cell interconnecting wiring did not have the necessary compliance to protect the cells

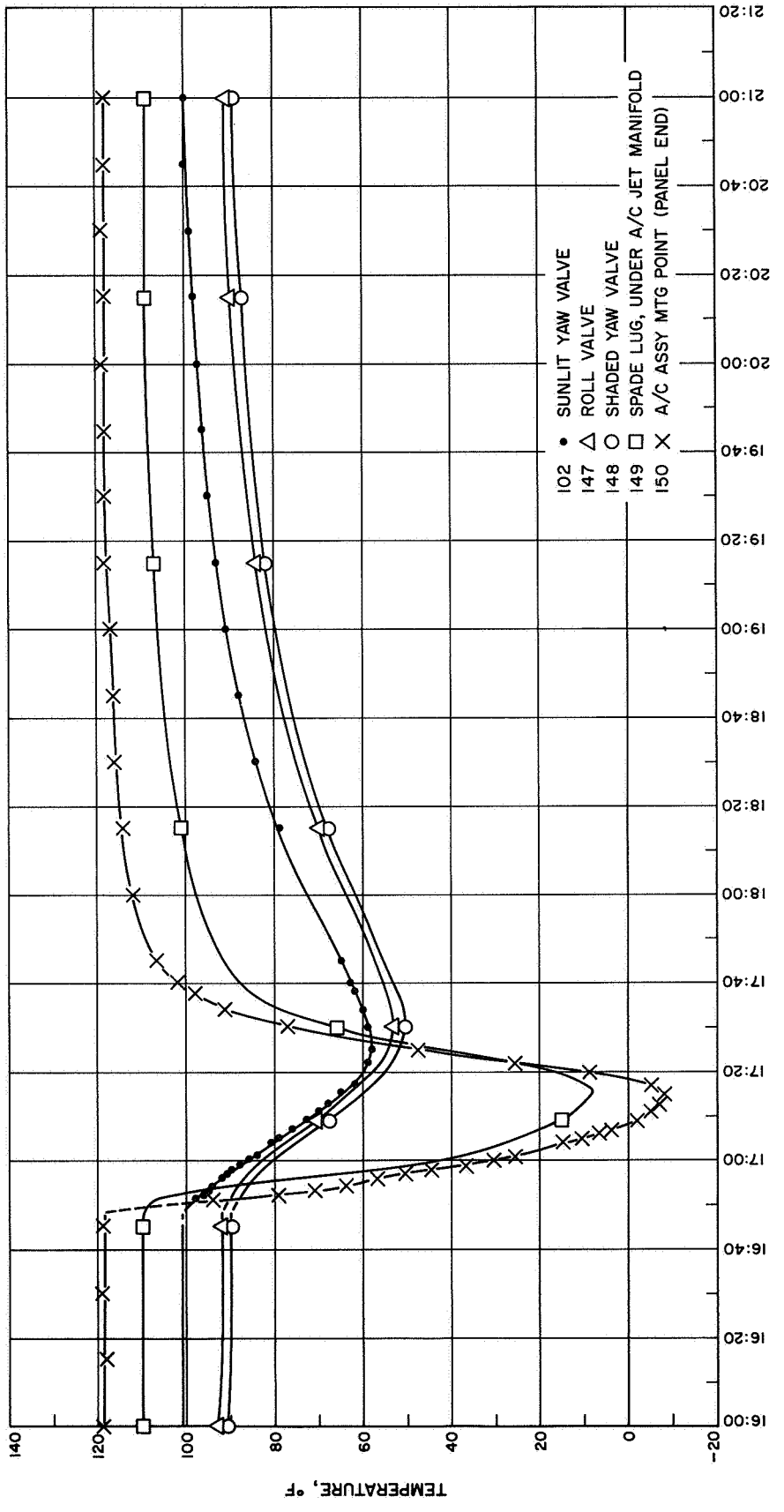

Fig. 20. Curves for attitude-control assembly undergoing unscheduled thermal shock during steady state

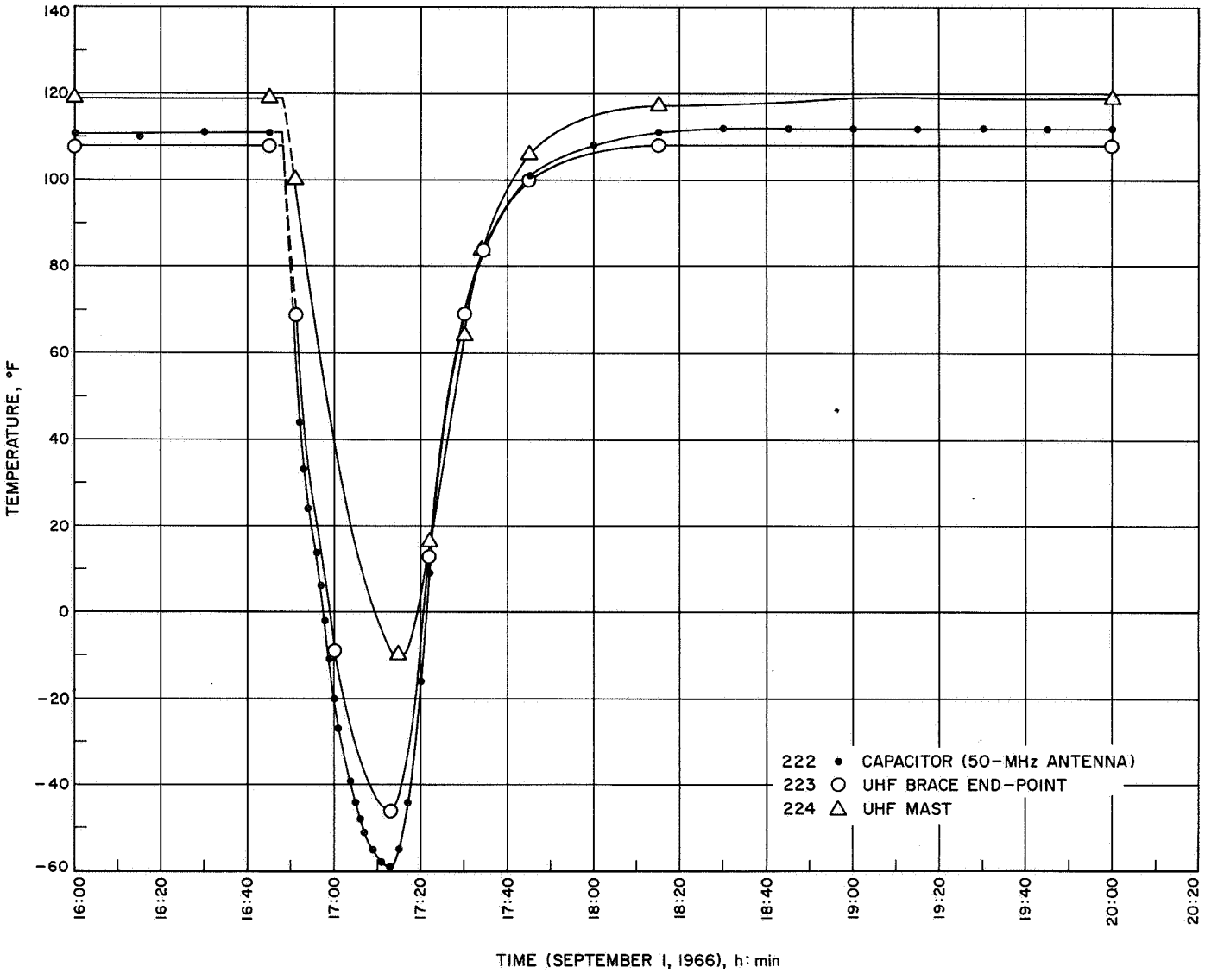

Fig. 21. Curves for DFR antennas undergoing unscheduled thermal shock during steady state

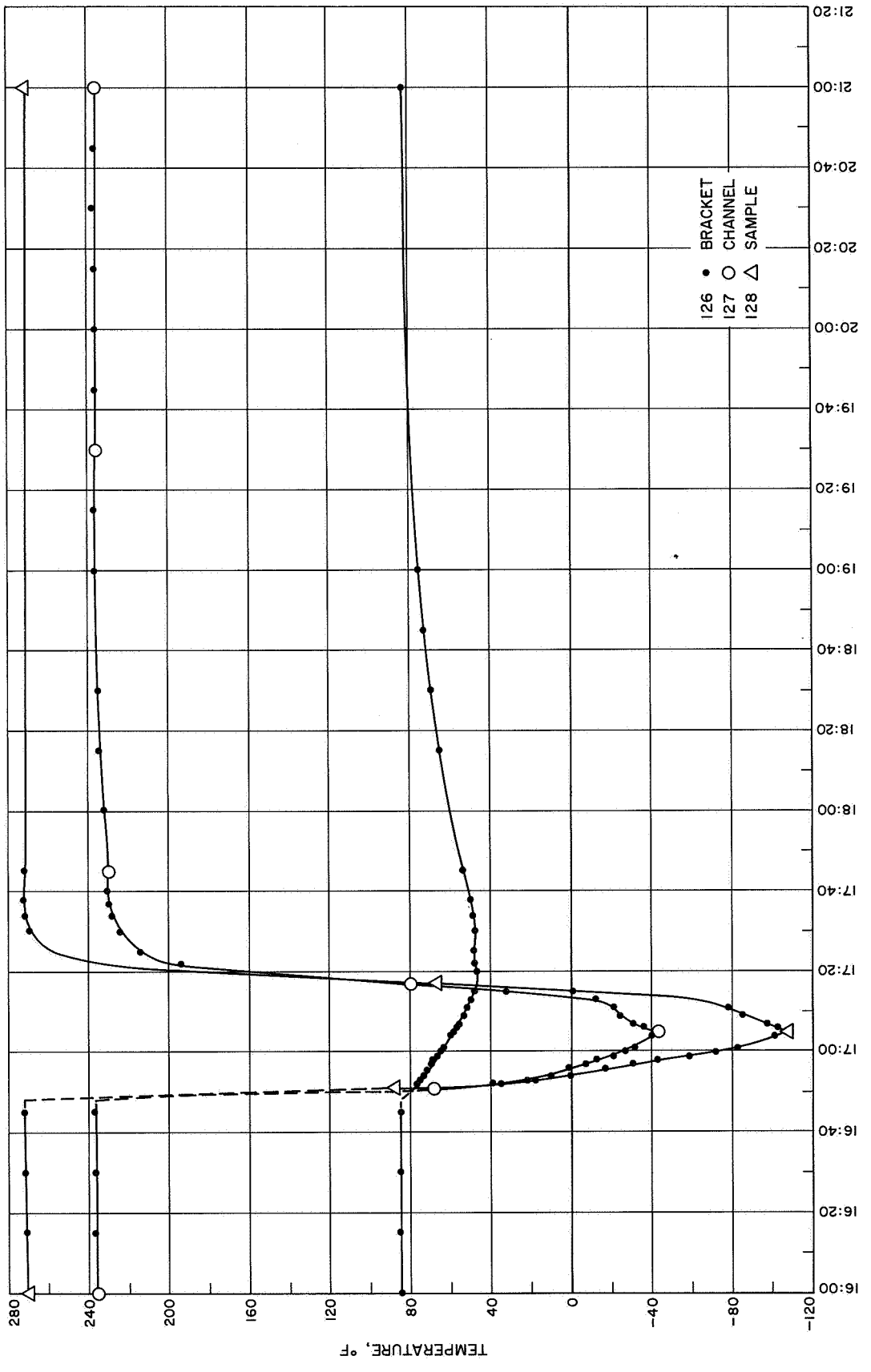

Fig. 22. Curves for TCR undergoing unscheduled thermal shock during steady state

during this period. An elaborate empirical testing program was conducted to test this analysis, the result of which indicated the analysis to be correct and that the panel probably would not have degraded significantly if light power failure had not occurred.

III. Developmental and Special Investigative Environmental Testing

For the *Mariner* Venus 67 program, many special developmental and investigative type tests were conducted to prove the feasibility and adequacy of the spacecraft hardware. A large majority of these tests were conducted at the subsystem level, using prototype or test hardware. Other tests were conducted on the structural test model (STM), the temperature control model (TCM), and in some cases, on the spare flight spacecraft (M67-1). The tests, which were not formal project requirements, were usually performed by cognizant organizations and/or systems personnel who felt that additional information was needed prior to formal testing. It is also pointed out that it would have been impossible to include all of the developmental and investigative type tests in this report. The tests that are described have been included in an effort to illustrate the scope of the environmental test program; generally, they fall into one of the following categories:

(1) Tests required to evaluate the expected environment

(2) Tests performed to evaluate anticipated problems

(3) Tests performed to determine compatibility between subsystems

(4) Tests resulting from other systems development problems

These tests were used to confirm analyses, verify problem solutions, and gather information essential to Project success.

A. System Level

1. Electromagnetic interference and electromagnetic compatibility tests.

a. Live squib/S-band transmitter safety. The objective of this test was to investigate the 2297-MHz power level to determine if the radiation from the omnidirectional antenna on *Mariner* Venus 67 would be hazardous to the pinpuller squibs. The solar panel pinpuller locations are closer to the low-gain antenna on *Mariner V* than they were on *Mariner IV*. This test was performed to determine the margin of safety for the new configuration without conducting a test on the M67-1 spacecraft that would require test time and test team manpower. It was important to obtain data early, in case a redesign was necessary.

Description. The test was conducted with the *Mariner* Mars 1964 STM spacecraft. Four (*Mariner IV* type) solar panels were installed in the *Mariner* Venus 67 configuration – facing away from the spacecraft. Pinpuller brackets were installed in each of the corners formed by the solar panels in their folded position. The cable harnesses used for the test were four 9W38 cables and one 9W8 cable. The shroud adapter and shroud were installed on the test spacecraft. The test was performed at JPL in the Spacecraft Assembly Facility.

Test instrumentation. For the EMI and electromagnetic capability (EMC) tests, a special RF power meter was built in the Laboratory. Previous measurements of the RF power that a squib would receive were subject to some uncertainty because of the measurement method used: An adapter from the squib harness connector to a type N coaxial fitting and a standard RF power meter thermistor mount was then temporarily fixed at the squib location, and power readings were made with the test RF power levels radiating the spacecraft. One uncertainty resulted because of the use of the standard 50 Ω thermistor mount replacing whatever impedance a squib would present to the wiring harness.

To eliminate the mismatch and reduce the uncertainty for these measurements, two thermistor mounts employing an actual squib and bridgewire were assembled. A bead thermistor with a low-temperature time constant (2 s) was selected and attached to the approximately 0.00175-in.-diam bridgewire with epoxy adhesive (no explosive was used). The thermistor was then incorporated as a leg of a resistance bridge. A calibration was performed by varying the current flow through the squib bridgewire, measuring the voltage drop across the bridgewire (in case the bridgewire resistance varied with temperature), and noting the corresponding reading on the resistance-bridge current meter. The first thermistor mount was made from a pinpuller assembly; the other was machined from a stock piece of aluminum. The unit made from the pinpuller preserved the dimensions of the anterior explosive cavity. A power dissipation of 1 mW on the bridgewire could easily be observed with either thermistor mount and with the resistance-bridge meter.

Since the maximum test power level was to be 31.6 W the maximum measurable power transfer ratio from the omnidirectional antenna to a squib bridgewire would be 31,600 to 1, or 45 dB. If no power could be noted as dissipated in the bridgewires, then the isolation would be assumed to be >45 dB. Approximately 387 mW is required to fire a squib.

Except for a high-power RF source, the equipment used in the test series was standard laboratory equipment.

Results. A preliminary measurement was made with the shroud removed before placing the spacecraft assembly in the test pit. The pit was to be used because live squibs would be installed for part of the testing. It was determined that the low-gain antenna should not radiate in excess of the 10-W level by more than 5 dB because of the possibility of damaging the unit. In the testing, a level of 31.6 W (5 dB above 10 W) was not exceeded.

The tests described below deviated from the test plan when it was determined that the cable harness attenuated the RF signal considerably.

Test I: Cable harness RF transmission-loss test. This portion was a preliminary test to determine the loss to an RF signal inserted into the bridgewire terminals at the 9W18J1 plug to verify that, in practice, an RF heating change could be detected with the power meter. Three tests were run. With one of the bridgewire leads grounded, two separate measurements were made. In the first, with 4.9 W of incident RF power (0.34 W reflected), an 0.8-mW reading was recorded at the bridgewire. This is a loss of 38 dB. In the second measurement, with 8.4-W incident power (0.56 W reflected) a 2.0-mW level was recorded. This is a loss of 36 dB. With one of the bridgewire leads not grounded, a loss of 39 dB was found.

If a 36-dB loss in the harness leads (the minimum measured loss) is assumed, it can be seen that even a 10-W input (approximately the maximum power from the transmitter) would supply only 2.38 mW to the bridgewire. Thus, it appears unlikely that any power picked up in the cabling could cause excessive heating in the bridgewire leads.

Test II: Low-power transfer ratio tests. This test was conducted with the two bridgewire thermistor mounts installed on the STM, attached directly on the pinpullers with C-clamps. With approximately 7.5 W radiated from the low-gain antenna, no power indication was measured in the bridgewire power meter. At the conclusion of this test the shroud was lifted, and a test was run to verify proper equipment operation. A level of 2 mW was recorded at the power meter with 8-W incident power. This results in a 36-dB loss, similar to the results of test I.

Since no power could be measured at all, the isolation from the omnidirectional antenna to the squib bridgewires was in excess of 38 dB.

Test III: High-power tests. This test was conducted with the maximum power, 31.6 W, radiated from the low-gain antenna with the shroud on. A pickup antenna was attached to pins f and r on plug 9W18J1, and a power reading was attempted again on the bridgewire power meter. No deflection could be observed.

Live squibs were then installed at each pinpuller location, and the cable harness was connected to each squib. At the 9W18J1 plug, an adapter was attached with an 18-in. lead on each pin that connected to a bridgewire terminal. The maximum level of 31.6 W was radiated for 16 min. At the end of that period, the squibs were removed and tested by cognizant personnel. No change to either the resistance or dielectric constant of each squib was noted; the squibs were subsequently test-fired and the results revealed no evidence of degradation.

Test IV: RF level measurements. In addition to the four pinpullers for the solar panels, one pinpuller was to be installed below the high-gain antenna. This location had not been determined at the time of the test, and a pinpuller or harness cable was not available.

Some measurements were made to obtain an idea of the field strength at different locations, including that below the high-gain antenna. These measurements were made by radiating a known RF level from the low-gain antenna and measuring the loss in that level at various locations with a test antenna and a field intensity meter. No exceptionally high levels were noted for the location under the high-gain antenna.

Conclusions. This series of tests indicated that there is no hazard to the pinpuller squibs in their new locations. The tests described under test I showed that, even in the improbable condition of 10 W at 2297 MHz being impressed across the bridgewire terminals at the harness main plug (JW18J1), no hazard would occur. The high-power tests then showed no other coupling paths for RF

into the squib. The coupling loss tests described under test IV show that no excessive power levels exist at a location under the high-gain antenna. There appears to be a safe condition for the squibs in all locations.

Cognizant pyrotechnics personnel formally investigated the squibs used in this test and determined that no evidence of degradation in their characteristics was apparent.

b. Antenna-coupling tests: DFR/S-band.

Description. As a result of preliminary bench compatibility tests of a *Pioneer* type dual-frequency receiver and an engineering model S-band transponder, it was desired to determine the RF coupling between the antennas of the two systems. No formal requirements were established. The coupling measurements were performed at the antenna range, using the *Mariner* Venus 67 antenna test model (ATM) spacecraft.

Results. The results obtained by the cognizant antenna personnel are shown in Table 13.

Recommendations. Based, in part, on the results of the RF coupling tests, RF filters were recommended for the DFR receiver to ensure a margin of confidence in the interference-free operation with other subsystems.

Follow-up activity. A bandpass filter for the VHF channel and a low-pass filter for the UHF channel of the DFR were procured and installed to ensure a sufficient noise-isolation margin.

c. Preliminary noise-level measurements on M67-1 spacecraft. The objective of these measurements was to attempt to identify RF noise sources that could degrade the performance of the DFR experiment at 49.8 MHz and at 423.3 MHz. Because this was a developmental type of test there were no formal requirements for permissible noise levels. The general requirement existed that the DFR should not be degraded by noise generated by spacecraft systems.

Description. These series of tests were performed prior to the formal delivery of the DFR to SAF. The measurement of RF noise levels were made with EMI equipment and with a DFR made available for a short period.

Results. It was determined that there were several subsystems generating noise that could degrade the sensitivity of the DFR VHF receiver. No noise was observed at the UHF frequency. Noise sources were determined to be the following:

(1) The power subsystem booster regulators

(2) The power subsystem battery charger

(3) The magnetometer during ignition

(4) The gas jets

(5) The DAS basic oscillator

(6) The transponder cavity power converter

(7) The transponder TWT power converter

Significant findings. It was observed in the course of testing that the DFR VHF antennas on the STM and flight spacecraft exhibited approximately 4-dB more gain to internally generated spacecraft signals. This effect was investigated independently by cognizant antenna personnel, and it was verified that this did, indeed, occur. The only apparent difference between the antennas is that the STM antenna is made with stainless steel conductor wires and the flight antenna has gold-plated wires.

Recommendations. In general, it was desired to suppress the noise from each of the above listed sources. Cognizant personnel recommended (1) that certain diodes within the power subsystem be changed to decrease the noise; (2) that the basic oscillator crystal frequency in the DAS could be shifted to move an interfering signal out of the DFR VHF passband; (3) that the noise generation of the transponder be investigated; and (4) that ferrite shielding beads be installed in the science case harness connections to the DAS and in the upper ring harness to suppress noise at the DFR VHF frequency. Wrapping of the DAS interconnect harness was also recommended as a noise reduction method.

Follow-up activity. The following changes were made to decrease the noise level at the VHF band:

(1) The 1N1583 diodes in the power regulator were removed and were replaced with 1N3892 diodes.

(2) Ferrite beads were installed in the ring harness close to the power regulators and in the science case harness connections to the DAS to suppress noise at the VHF band.

(3) The DAS master clock frequency was changed from 444.444 to 443.406 kHz.

Table 13. Antenna coupling test results

Frequency, MHz	Transmit antenna	Receive antenna	No mast Sept. 30, 1966		No mast Oct. 15, 1966		Metal mast (up) Oct. 19, 1966		Fiberglass mast (up) Nov. 30, 1966	
			Approx. power input, W	Isolation between transmit & receive antennas, dB	Approx. power input, W	Isolation between transmit & receive antennas, dB	Approx. power input, W	Isolation between transmit & receive antennas, dB	Approx. power input, W	Isolation between transmit & receive antennas, dB
2115.7	UHF	Low-gain antenna	3	72.0	2	76.0	—	—	3	69.2
	UHF	High-gain antenna 1	—	64.0	—	67.0	—	—	—	56.5
	UHF	High-gain antenna 2	—	—	—	61.5	—	—	—	54.5
	Low-gain antenna	UHF	—	—	—	—	—	—	—	68.5
	High-gain antenna 1	UHF	—	—	—	—	—	—	—	—
	High-gain antenna 2	UHF	—	—	—	—	—	—	—	54
2297.6	Low-gain antenna	VHF	4	70.0	2	—	2	57.0	3	68.0
	Low-gain antenna	UHF	—	74.0	—	76.0	—	—	—	68.0
	High-gain antenna 1	VHF	—	64.0	—	—	—	—	—	57.5
	High-gain antenna 1	UHF	—	65.0	—	68.0	—	—	—	62.5
	High-gain antenna 2	VHF	—	—	—	—	—	45.0	—	63.25
	High-gain antenna 2	UHF	—	—	—	70.0	—	—	—	63.5
423.3	Low-gain antenna	UHF	—	—	—	—	—	—	0.2	93.0
	High-gain antenna 1	UHF	—	—	—	—	—	—	—	79.0
	High-gain antenna 2	UHF	—	—	—	—	—	—	—	79.5
	UHF	Low-gain antenna	—	—	0.76	103.0	0.3	96.0	—	95.5
	UHF	High-gain antenna 1	—	—	—	84.0	—	80.0	—	79.0
	UHF	High-gain antenna 2	—	—	—	87.5	—	79.0	—	79.5
49.8	Low-gain antenna	VHF	0.1	105.0	—	—	—	—	0.2	78.0
	High-gain antenna 1	VHF	—	91.0	—	—	—	—	—	75.0
	High-gain antenna 2	VHF	—	—	—	—	—	—	—	73.0
	VHF	Low-gain antenna	—	—	—	—	0.2	114.0	—	77.5
	VHF	High-gain antenna 1	—	—	—	—	—	92.0	—	71.0
	VHF	High-gain antenna 2	—	—	—	—	—	93.0	—	70.0
2115.7	Low-gain antenna	VHF	3	67.0	—	—	—	—	—	—
	High-gain antenna 1	VHF	—	64.0	—	—	—	—	—	—

(4) The DAS interconnect harness (9W21) was wrapped with two-sided aluminum-coated mylar over a braided bleed wire to reduce RF noise emitted from the DAS.

In addition, special tests were performed in the laboratory on power subsystem items, the DAS, and the transponder. Some of these tests are described in other sections of this report.

d. Preliminary DFR/S-band EMC test on M67-1 spacecraft. The objective of this test was to determine (with the receiver installed on the spacecraft) the degree of degradation of the DFR experiment after several noise-suppression fixes had been installed. Because this was a developmental test, there were no formal test requirements; however, a letter from the DFR experiment scientist stated the maximum permissible degradation as 3 dB for the VHF channel and 1 dB for the UHF channel.

Description. This test was performed with the following modifications incorporated in the spacecraft: ferrite beads installed in cable 9W21, cable 9W20 wrapped, the DAS oscillators tuned to 443.900 MHz. The spacecraft was in a fully assembled condition and was raised by nylon cables to a height of approximately 15 ft during the test. The spacecraft was in a fully assembled configuration.

Results. It was determined that the degradation to the DFR VHF channel was approximately 3 to 4 dB, when the nonflight STM antennas were used, and 0.5 to 1.0 dB, when the flight antennas were used. This value is referenced to the expected cosmic noise of 8000°K.

Significant findings. An anomaly noted in this test was also observed during the preliminary noise investigations — i.e., the noise difference observed when using the two different antennas.

Recommendations. It was determined that all the fixes incorporated in the spacecraft should be added to the flight spacecraft and that a formal acceptance test should be performed on each spacecraft.

Follow-up activity. The effect of a difference in noise level observed with the STM steel conductor wire antenna and the flight gold-plated wires was investigated. The independent testing performed at the antenna range also showed this effect, and it was reported that the gold-plated feeds were measured to have a far-field gain that was 6 dB greater than the STM feeds. However, for a signal radiated within the *Mariner* Venus 67 mockup, the signal measured with the STM feeds was 4 dB higher than with the gold-plated feeds. This effect is attributed to differences in the near-field characteristics that occur when using the different feeds.

e. Umbilical line electromagnetic interference study. The objective of this study was to determine if conducted interference could couple to the umbilical lines and enter spacecraft circuitry to cause performance degradation of the spacecraft subsystems.

Description. A search of current literature, a review of launch complex cable drawings, and a study of spacecraft circuits associated with the umbilical wiring provided information on worst cases for transients, coupling between adjacent wiring in cables, and circuit sensitivity.

The worst-case power-line transient found on power lines in the launch complex exhibited the following characteristics: 1000-V amplitude, 100-μs duration, and rise and fall times of 1 μs. Coupling between wires (Figs. 23 and 24) was based on the results of a Boeing study

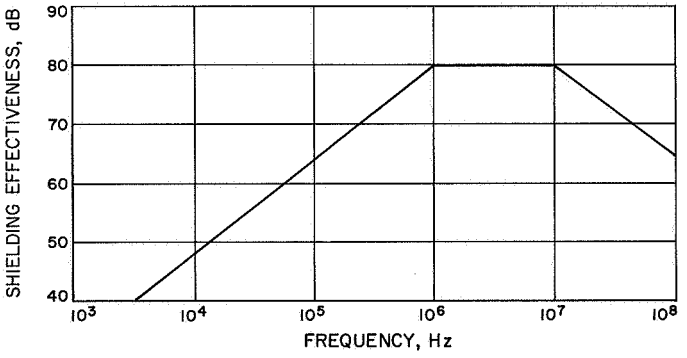

Fig. 23. Twisting and shielding effectiveness on magnetic-coupling attenuation spectrum

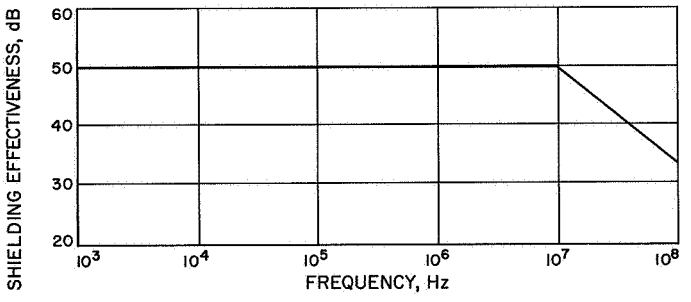

Fig. 24. Shielding effectiveness on capacitive-coupling attenuation spectrum

(Report D2-90642-1, Seattle, Washington, December 31, 1964). Typical circuits (Figs. 25 and 26) on the spacecraft side of the umbilical interface were classified and analyzed in terms of sensitivity characteristics (see Table 14).

The time domain transient waveform was converted to frequency domain representation, modified by appropriate coupling factors, reconstituted into the time domain and compared with the circuit threshold characteristics (Figs. 27–30).

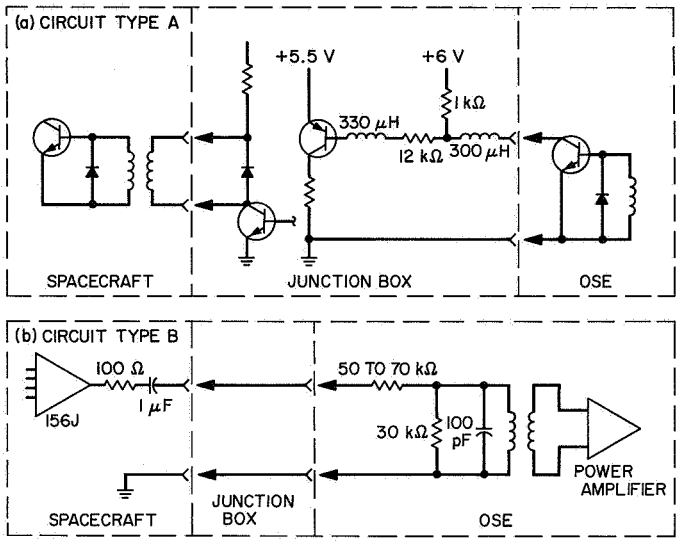

Fig. 25. Typical circuits A and B

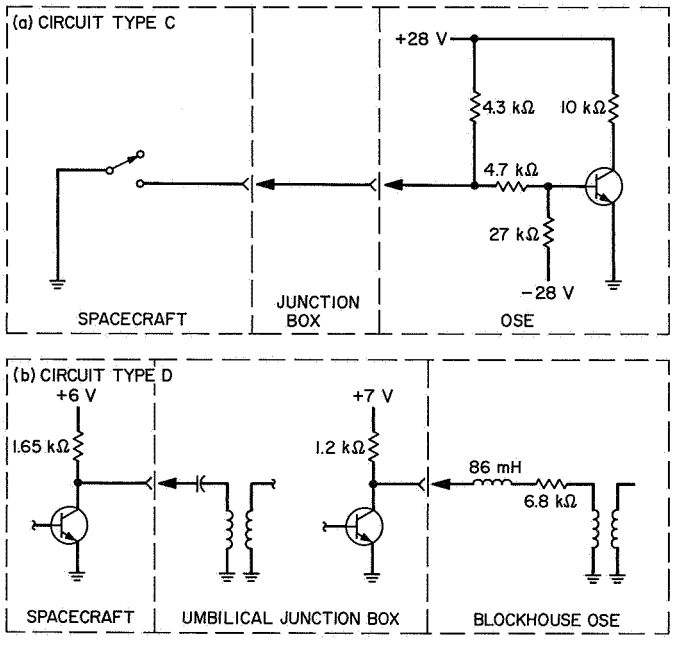

Fig. 26. Typical circuits C and D

Table 14. Sensitivity characteristics of typical circuits on spacecraft–umbilical interface

Fig. showing circuit diagram	Threshold sensitivity[a]					Fig. showing spectral plot
	Voltage, V	Current, mA	Power, mW peak	Time, μs	Energy, μJ	
25a	1.3	1.32	1.72	1	0.002	27
25b	2.1	≈0.035	≈0.07	2	0.0001	28
26a	5.6	4.15	23.2	0.2	0.005	29
26b	5	0.28	1.4	100	0.14	30

[a]Estimated values.

Results. This cursory worst-case analysis established the existence of a possible conducted interference problem on all but one of the four typical circuit types examined. It is worthy to note that this worst-case approach is *success* oriented; therefore, if the results indicated no interference problem, it would be a certainty. However, results indicating a marginal or definite interference problem require one or more iterations of a rigorous nature. Schedule and manpower limitations precluded a rigorous analysis and verification of the information used related to the interference transient level and coupling factors applied directly to the *Mariner* Venus 67 Program.

Significant findings. No problems were uncovered related to large transients appearing on the umbilical lines on *Mariner* Mars 1964, either at JPL or at the Cape. Furthermore, no problems of this nature occurred during *Mariner* Venus 67 spacecraft processing through most of the SAF testing. The transient utilized in this analysis was determined to be not typical for power lines adjacent to the umbilical cable runs. The coupling factors evolved by Boeing are only good as a first worst-case cull and can only verify a *no problem* certainty case.

Recommendations. It is recommended that future programs support effort to define typical interference levels that can appear on umbilical lines in the SAF Complex and the Launch Facility Complex. This will provide a realistic base for compatibility analysis of safety margin and/or establishing EMI environmental test requirements on umbilical lines.

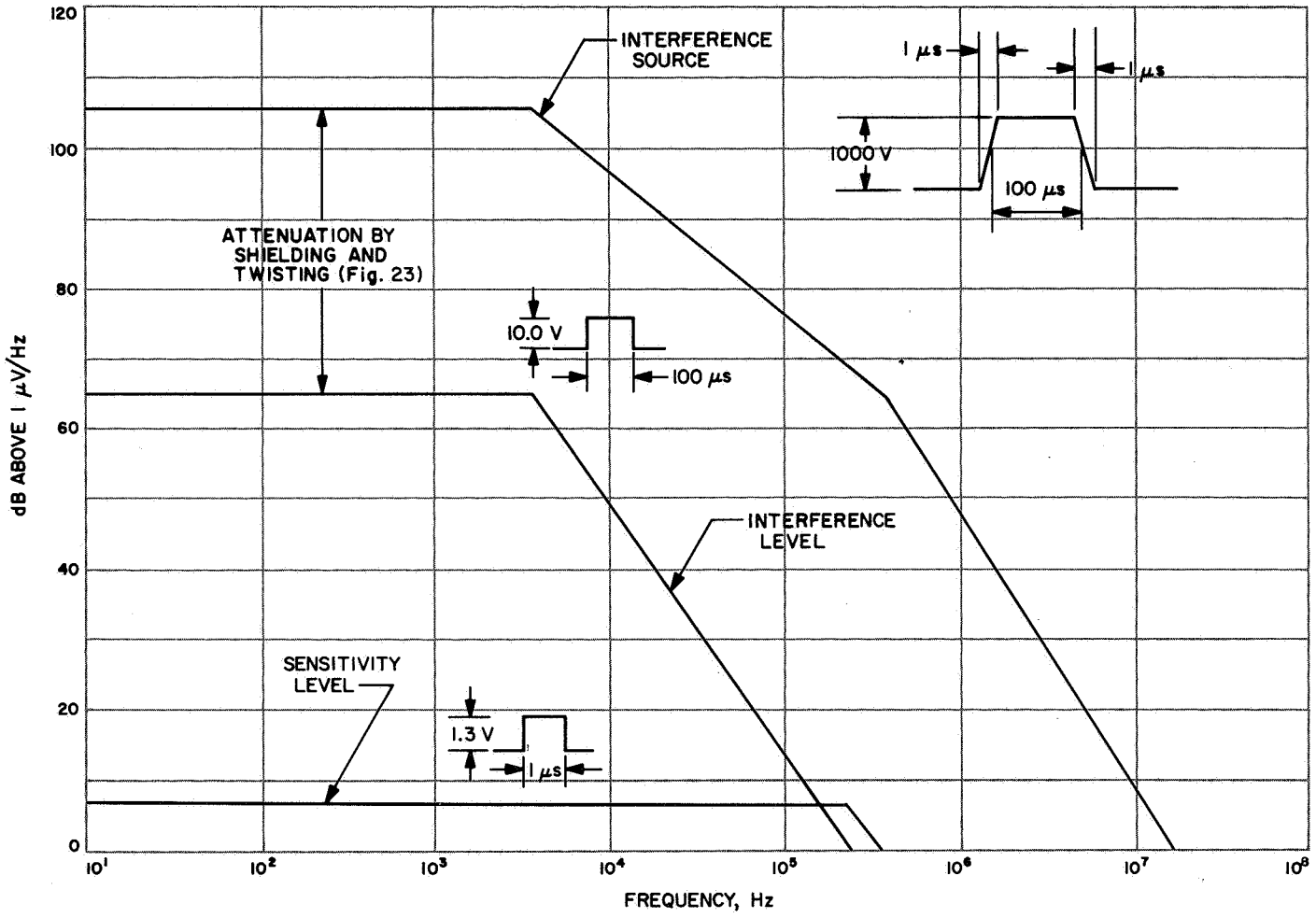

Fig. 27. Composite of interference and sensitivity of type A circuits

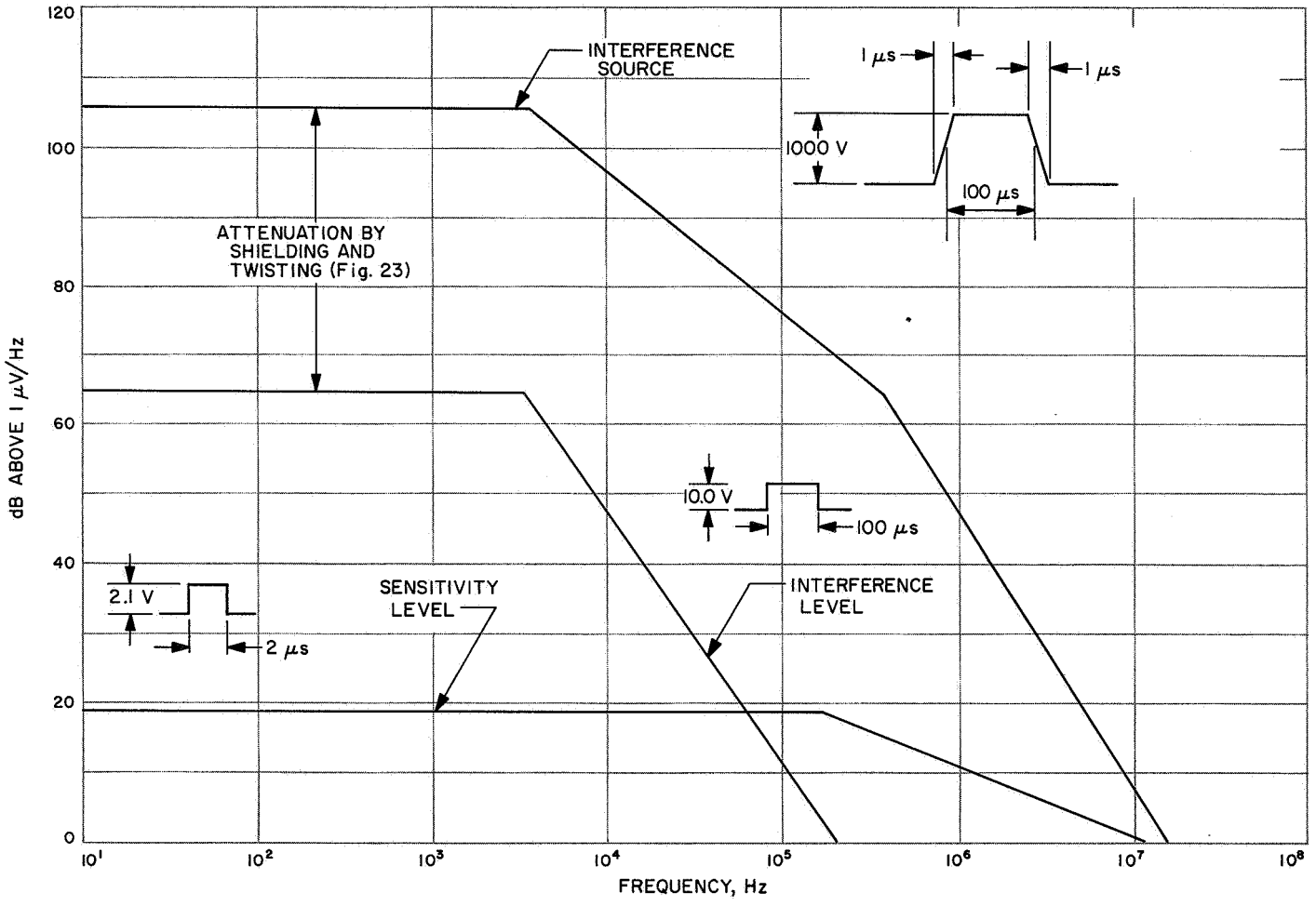

Fig. 28. Composite of interference and sensitivity of type B circuits

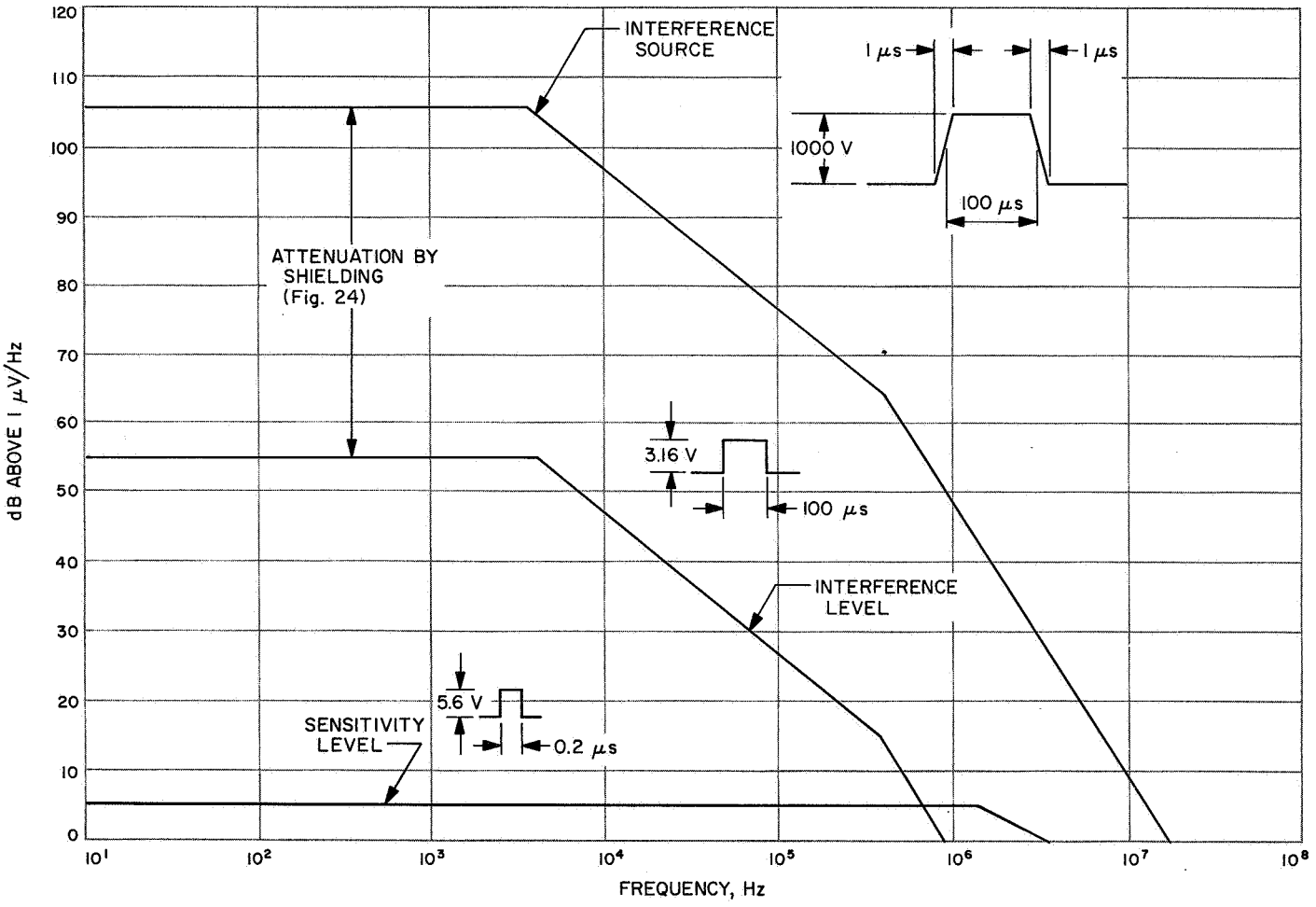

Fig. 29. Composite of interference and sensitivity of type C circuits

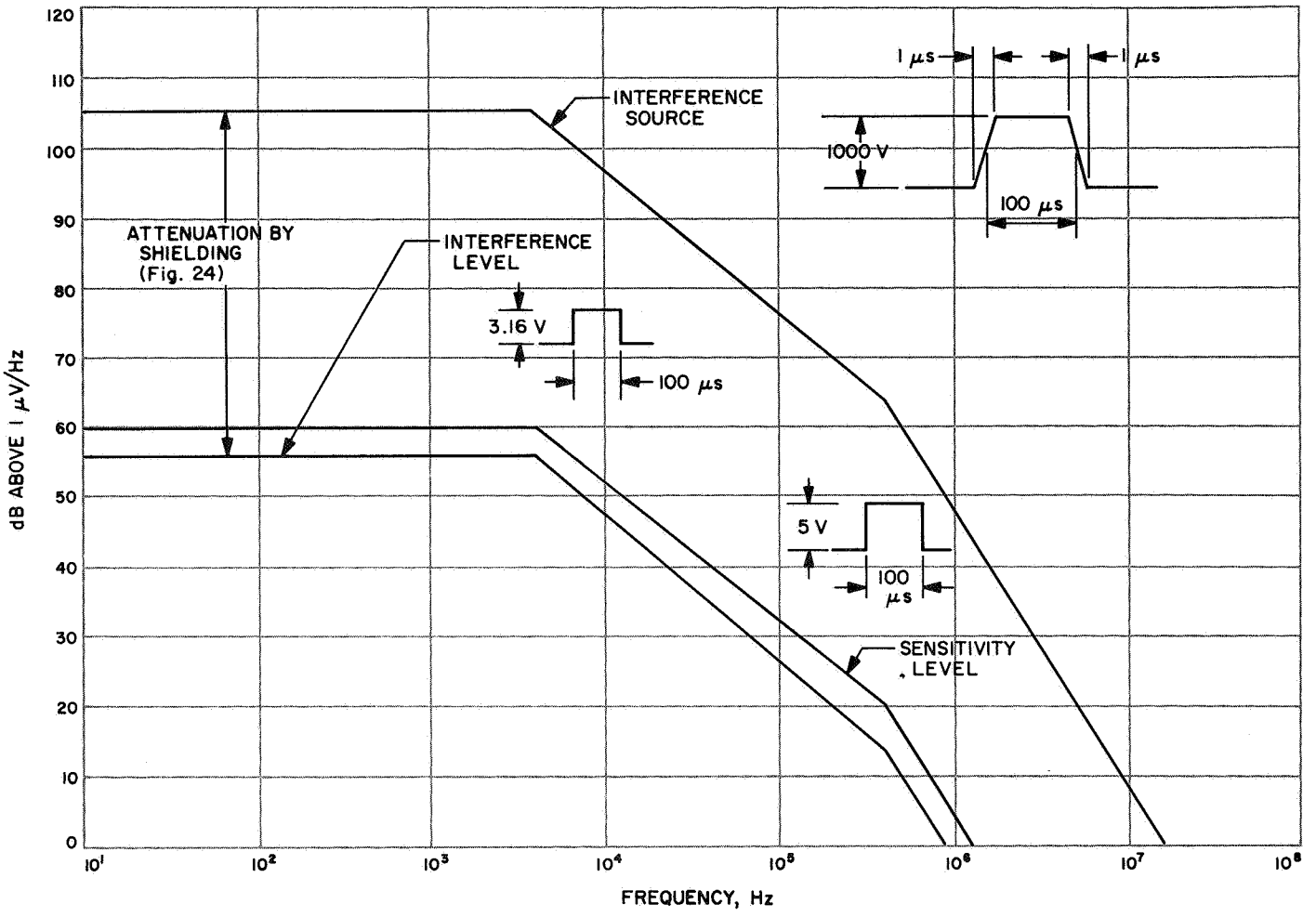

Fig. 30. Composite of interference and sensitivity of type D circuits

2. Solar-panel-deployment test.

a. Objective. The purpose of this test was to confirm the proper operation of the solar-panel-deployment mechanisms in light of the modifications to the system required to adapt to the *Mariner* Venus 67 configuration. In particular, it was necessary to verify (1) proper unlatching and separation of the solar panels from the revised boost damper attachment joints, (2) acceptable margin in available deployment spring torque to overcome the additional harnesses being routed across the hinge, (3) the dynamics of cruise damper latching resulting from revised panel system inertias, and (4) the proper operation, under simulated deployment conditions, of the sunshade-deployment lanyards.

b. Test configuration. The STM was mounted on a low-level positioner with the z axis of the spacecraft horizontal and bays I and V solar-panel-hinge axes vertical. The panels on bays III and VII were suspended by extension springs (1/3 lb/in.), adjusted to provide proper deployment simulation of these panels in the area of initial panel unlatching. The panels on bays I and V were fully ballasted and equipped with all harnesses and deployment hardware and a realistic simulation of the sunshade-deployment system. These two panels were allowed to fully deploy in this simulated zero-g position with the time to deploy recorded and proper separation and latching visually observed. The test setup in the deployed position is shown in Fig. 31.

Tests were run using pneumatic pinpullers and flight pyrotechnic pinpullers. Harnesses across the hinge were varied from the minimum case of no harnesses to the maximum case of the worst flight-panel-harness configuration with the harness temperature at a conservative −30°F. Deployment spring torques were varied over the complete tolerance range.

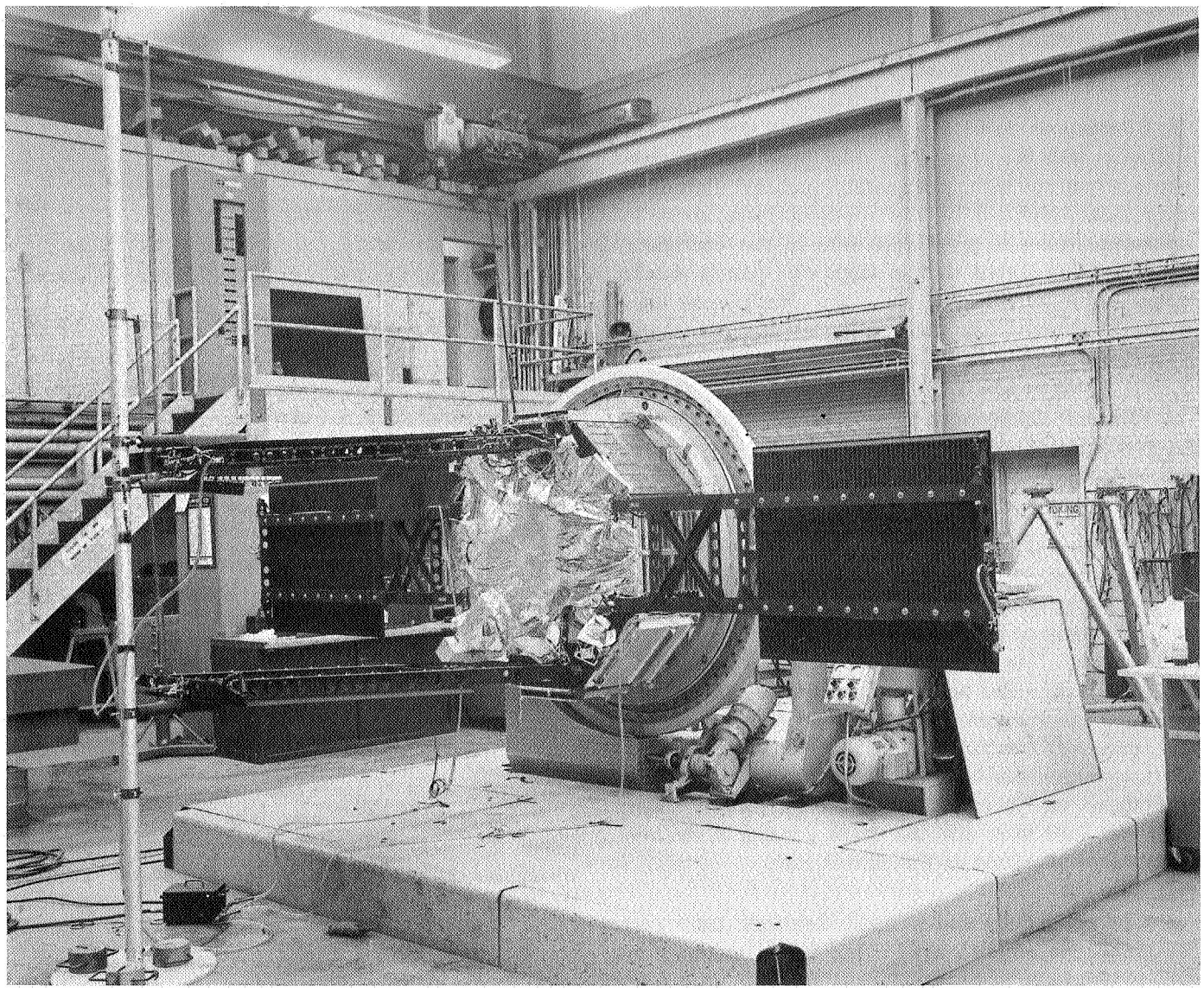

Fig. 31. STM solar-panel-deployment test

c. Test results. The visually observed boost latch separation and cruise damper latching at full deployment were satisfactory in all tests. The time to deploy a solar panel in the flight configuration was found to be an acceptable 6.0 s with a repeatability of ± 0.2 s. By varying panel-deployment spring torque over its full range in conjunction with varying the sunshade deployment torque from 0 to twice nominal, deploy times were affected by a maximum of 0.4 s. Varying harness configuration and temperature had negligible effect.

d. Conclusions. Satisfactory performance was observed in all tests with the changes in solar panel and deployment mechanisms being adequately qualified. Sufficient margin was exhibited by the apparent insensitivity in deployment times to gross variations in test configuration. It was predicted that in flight the panels should deploy smoothly and latch about 6 s after pyrotechnics are fixed. Actual flight data indicated that the panels deployed in slightly less than 6 s.

3. *Sunshade-deployment tests.* During the *Mariner* Venus 67 project, several series of sunshade-deployment tests were conducted.

a. Deployment tests on TCM. Sunshade-deployment tests were performed on the *Mariner* Venus 67 TCM using STM hardware. The purpose was to test a nominal deployment at TA level and investigate deployment failure modes. The spacecraft was mounted on a modified solar-panel stand and could rotate 360 deg about a horizontal axis supported by bays IV and VIII (Fig. 32). The spacecraft was rotated in 90-deg intervals to four positions during the test to study gravity effects on the deployment mechanics. A simulated solar-panel attach point was used to release the shade lanyard in the correct configuration and at the correct rate.

A total of 15 fully and partially deployed tests were performed. No anomalies were noted during the standard deployment modes.

Failure mode investigation. Additional tests were performed to investigate maximum shirttail ball retainer tension, lanyard out of top guide condition, and a deployment-spring-assembly failure.

A series of 7 tests determined that the maximum tension to release the Teflon ball from the retainer should not exceed 150 g.

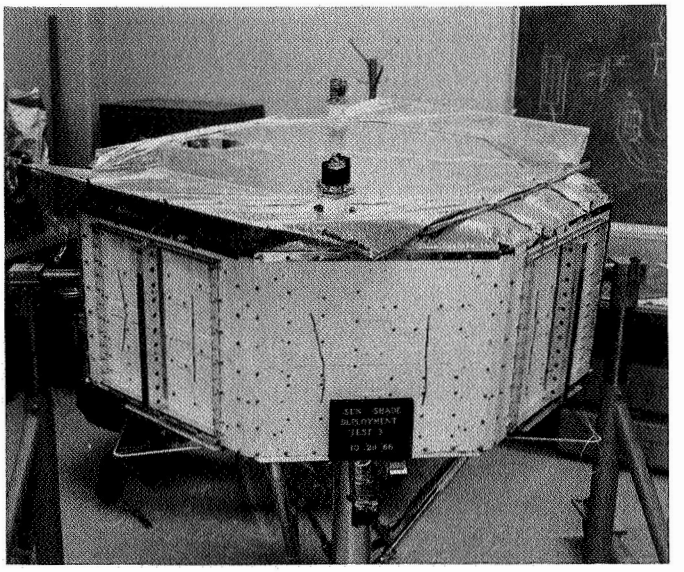

Fig. 32. TCM mounted for sunshade deployment tests

In subsequent failure mode tests, the shade in only one bay adjacent to the sun sensors was deployed. The usual result was that the shirttail retainer in bay VI released, while the one in bay II did not. This condition in bay VI resulted in a loose shirttail that could interfere with the primary sun sensor if this failure occurred. In subsequent testing, increasing the length of the tie from the shade to the ball prevented releasing in that failure mode. Full deployment tests were again run to verify release under normal conditions. As a result of these findings, the length between the teflon ball and the shade was adjusted and tied after the shade was installed on the spacecraft.

Another series of tests was performed to investigate a deployment-spring failure. The three failure modes tested were: (1) failure of the case bolt retaining the spring assembly, (2) failure of the screw attaching the shade to the spring, (3) one fractured spring. In this series of tests, the effect of gravity was very apparent, and the spacecraft was rolled about the $+X$, $-Y$ axis to determine the net effect.

Case 1 resulted in a partially deployed shade because the shirttail did not release. In cases 2 and 3 the shade deployed to its nominal position. Although it was difficult to ascertain the effect of gravity in this series of tests, it was concluded that the main body of the shade would still deploy if one spring broke, although the adjacent shirttail retainer would probably not release. The nondeployment of the shirttail would affect the bay

temperatures, but could not interfere with the TRD field of view in bay IV or the primary sun sensors in bays II and VI.

Conclusions. It was difficult, if not impossible, to produce a failure mode that would not allow the shade to assume a fully deployed position in bays I, III, V, and VII (discounting the failure of a solar panel to deploy). As a result of this series of tests and the MV-67 STM vibration tests 1 and 2, the shirttail-retainer release-force tolerance was established at a nominal 130 g. It was concluded that the shirttail in bays II, IV, VI, and VIII might not deploy in certain failure modes; however, test data indicated this was unlikely. Should the shirttail have failed to deploy in flight, it would not have affected the mission success.

Flight shade deployment tests. Midway through the M67-1 vibration test, it was necessary to remove the C-103 sunshade from the spacecraft for an inspection of the bus. During the process of removing the shade, the four bays were deploy-tested simultaneously by technicians releasing the individual lanyards. After the deployment, a fold was noted on the outer edge of the shade in bay VI, and the shade appeared loose in that bay, causing a PFR to be written. After reinstallation of the shade and completion of the vibration test, a similar deployment was performed in the SAF to verify the problem. Two deployments were performed in SAF without recurrence of the folded edge. It was noted, however, that the last 1/4 in. of travel in bays I and V was restricted by the lanyard tie configuration at the shade support tubes. The M67-1 flight sunshades SNs 103 and 104 were then removed from the SAF for further testing on the TCM bus in the shield shop.

Shade C-103.

(1) *Deployment tests.* The flight shade C-103, which had been through FA vibration and five installation-and-removal cycles to this point, was installed on the TCM and deployed two times in each of four positions. Each test was performed with a nominal deployment time of 6 s. The shade was deployed eight times without a fold being noted in bays II, IV, VI, or VIII. In each test, the lanyard tie to the shade support tube in bays I and V caused wrinkles in the shade.

(2) *Test summary.* The test failed to reproduce the folded-edge problem noted on the PFR, although it did uncover the cause of the excessive loose and wrinkled appearance of the shade in bay VI. Invesitgation of the failure to reproduce the folded edge revealed a similarity between this test and that of the STM shade C-102, which was used to perform TA deployment tests. Both shades had been subjected to several installation-and-removal cycles prior to the deployment tests, necessitating the shirttail being folded and unfolded; and this action could have affected the test results. To verify if any prior repeated folding of the shirttail were related to the problem, another deployment test was performed on the M67-1 spare shade, C-104.

Shade C-104.

(1) *Deployment test.* The installation of the C-104 shade on the TCM bus for this test represented the first time the shirttail was to be folded, except for the folding necessary to install it in the shipping container. The installation was identical to the previous test on C-103.

During testing there were four unreleased folds, two each in bays II and VIII. This configuration was not disturbed for 30 h to determine any movement caused by the deployment spring tension. After 30 h, the folds were still there, and no change was noticed. The test was repeated with the same results.

(2) *Test summary.* The initial deployment tests on the C-104 sunshade produced two edges with unreleased folds. Each of the four shirttails was folded slightly differently because of the spacecraft configuration (primary sun sensors, separation timer, and hole for the TRD). The shirttail fold and the extent of the crease in the aluminized tape-reinforced edge upon installation can affect the deployed condition. The loose and wrinkled appearance caused by the lanyard tie on the previous test was not noticed.

Conclusions. The following conclusions were drawn as a result of these tests:

(1) The 1-mil aluminum foil layer in the tape was weakened with repeated folding, which prevented the retention of the fold after deployment on the STM and the M67-1 C-103 sunshade tests.

(2) The lanyard tied over the teflon shade material at the support tubes could cause shade distortion and prevent the last 1/4 in. of travel in attaining the fully deployed position.

(3) The folds would not affect the mission success or the shade performance. The worst that could happen was the exposure of approximately 1 in. of the bay II shear-web can to solar radiation; and should the folds

be present, adequate margin existed not to expose any hardware in bays IV, VI, or VIII.

Corrective action.

(1) To ensure a more uniform installation of the sunshade and reduce the probability of the folds not releasing at deployment, the fold points were defined and a line scribed through the aluminum layer of the tape at that location to reduce the stiffness.

(2) The shade configuration at the lanyard attach point on the four support tubes was also modified, allowing a direct tie to the tube.

Sunshade C-103 was modified, and tests verified the fixes prior to modification of the flight shades C-104 and C-105.

b. Storage deployment test. This test was performed to evaluate a sunshade deployment after approximately 3 wk in the stowed position on a spacecraft. The time period approximates the period from installation of a shade on the spacecraft at the explosive-safe facility (ESF) to launch.

Configuration. The TCM bus and test hardware were identical to that used for the initial deployment test. The sunshade assembly tested was the M67-1 flight spare, and the deployment springs were a flight-spare set. The shade installation was performed according to assembly procedure.

Test summary. The configuration was stored for 20 days with the shade in the stowed prelaunch condition and the spacecraft in a vertical position. After this period of time, the shade lanyards were released, the shade was deployed in approximately 6 s, and the spacecraft was positioned with the Z axis horizontal. No anomalies were noted during, or after, deployment.

Conclusion. Thus, the 20-day storage time had no effect on the shade deployment and indications were that it could be stored for a much longer period with the same results.

4. Sunshade–adapter tests. Two series of tests were performed to determine the interactions between the *Agena* adapter and the spacecraft sunshade under various failure modes.

a. Preliminary sunshade hangup test. The preliminary hangup test was performed to investigate the failure modes of a premature sunshade deployment and its effect on the spacecraft separation from the *Agena* adapter.

Test configuration. The test configuration consisted of the STM less solar panels, antennas, upper thermal blanket, and *Agena* adapter EM 476 (with push-off springs).

The TCM lower thermal shield, 101, and a test sunshade with STM deployment springs were installed on the spacecraft (Fig. 33). In the absence of solar panels, the shade-release lanyards were taped to the louver housing in bays I, III, V, and VII to secure the shade in the stowed position.

The spacecraft was suspended from a hoist with short, attach cables. It was necessary that the spacecraft be level and balanced to depress adapter springs. This was done by placing lead-shot weights on the upper ring.

A 1000-lb-rated load cell was installed in the hoist cable to measure separation loads. A recorder was used to measure time vs load. Three cameras were equally spaced around the spacecraft to record its motion during separation.

Test sequence and results. A hoist pulled the spacecraft from the adapter with the sunshade in various conditions of deployment. Hoist loading was monitored with a load cell and recorded on an oscillograph. Photo coverage was obtained with three motion picture cameras, equally spaced around the STM. Camera speeds of 128 frames/s were used.

A total of seven separations were performed. The results are summarized in Table 15.

Conclusions. The test demonstrated that the addition of simple bumper brackets to the adapter PAS and in-flight disconnect bracketry would eliminate the possibility of spacecraft hangup if the sunshade were to be deployed early. Also, the adapter pressure transducer could be easily relocated to a position clear of the sunshade.

From the high-speed movies of the test, it was observed that the peak value of the drag force occurred right after the separation springs were fully extended.

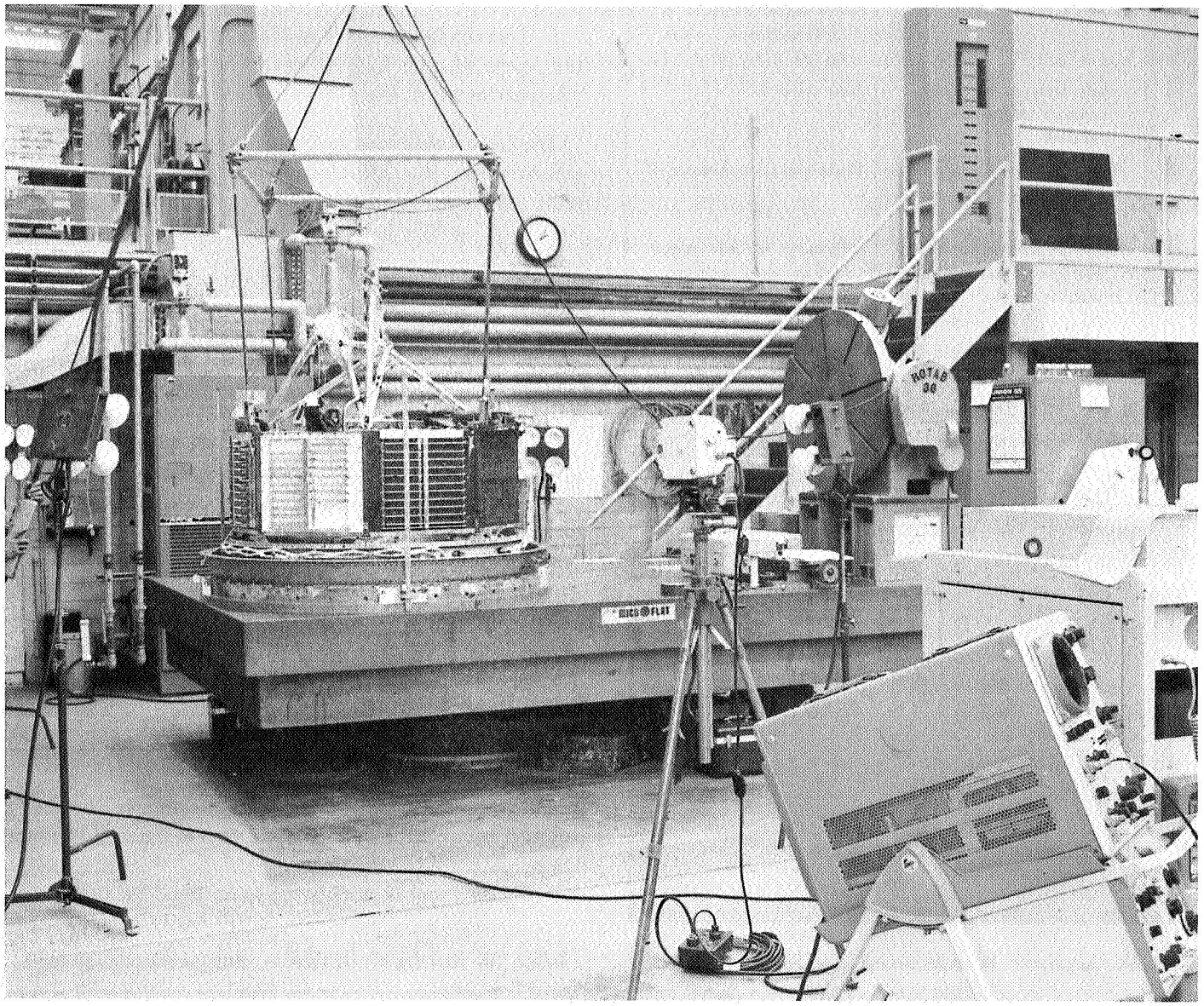

Fig. 33. Preliminary sunshade hangup test

Table 15. Preliminary sunshade-hangup-test results

Run	Test conditions	Results
1, 2	Shade stowed	Nominal separations used to obtain baseline load cell data
3	Shade deployed in adapter	Severe shade hangup on inflight disconnect bracket. Fig. 34
4	Shade deployed in adapter; rerun of run 3 with shade repaired	Same as run 3
5	Shade deployed in adapter; angled bumper fitted to in-flight bracket	Shade hangup on bumper
6	Shade deployed in adapter; near vertical skid rail fitted to in-flight bracket	No damage to shade; temporary snagging noted on PAS bracket and pushoff springs
7	Shade deployed on bay I (PAS bay) only; skid rail fitted to inflight bracket	Same as run 6, bay I only

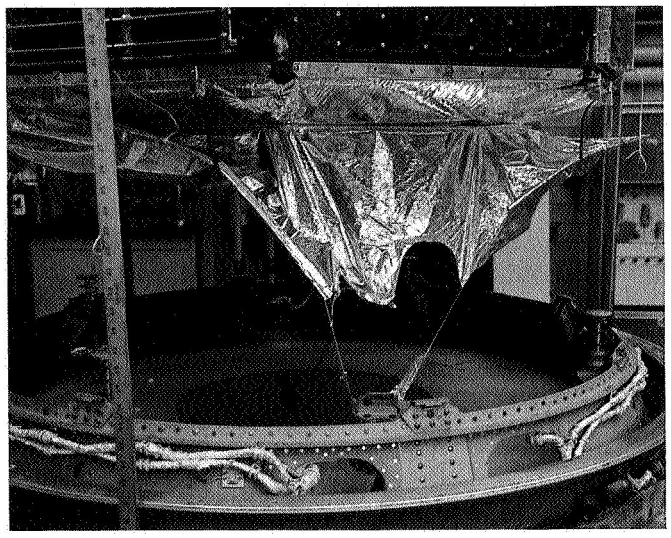

Fig. 34. Sunshade hangup on inflight disconnect bracket

From this information and the assumption that a real separation has the same drag force characteristics as that obtained from test, the result of the calculation showed that the maximum pitch rate would be 8.13 deg/s about the principal axis of the spacecraft. This worst case was very conservative, based on all the drag energy acting at one discrete point – the inflight disconnect bracket location.

b. Final sunshade hangup test. The final hangup tests were then performed (1) to verify Lockheed designed adapter sunshade guides on the inflight disconnect bracket and pyro arming switch bracket, and (2) to further investigate the failure modes of a premature sunshade deployment and its effect on the spacecraft separation dynamics.

c. Test configuration. The *Mariner* Venus 67 STM and the *Agena* adapter EM 476 were used for this test, which was conducted in the environmental test laboratory.

The hoist cable was instrumented with a 1000-lb-load cell to record the difference in loading when the spacecraft was lifted from the adapter with and without the sunshade deployed. The hoist's vertical lift speed was 2.35 in./s.

Two motion picture cameras were used – opposite bays V and I – to record the spacecraft motion. Five accelerometers[9] were located on the spacecraft's structure to record acceleration and dynamic-load data.

d. Test description. The spacecraft hoist cable was preloaded to 200 lb, and the four separation springs provided 280 lb preload, which provided a total of 480 lb, or a net difference of 60 lb additional force required to begin lifting the 540-lb spacecraft. The purpose of this preloading was to lift the spacecraft initially with minimum transient from the hoist mechanism. The output of the transducers was recorded on magnetic tape starting at the time that the hoist was switched on.

A total of five separation tests were performed. Table 16 gives a summary of the results.

As the spacecraft separated from the adapter, the shade support tubes in bays I, III, V, and VII came in contact

[9]Model 2213C manufactured by Endevco, Pasadena, Calif.

Table 16. Results of sunshade–adapter separation tests

Run	Test condition	Results
1 and 2	Shade stowed	Nominal separation to obtain baseline data
3 and 4	Shade deployed in adapter	Slight hangup on spring at corner F, resulting in bent rod on shade in bay V
5	Deployed bay V only	Same as runs 3 and 4

with the extended push-off springs at corners B, D, F, and H. The resulting effect, which is best described as similar to running a stick along a picket fence, occurred between the shade support tubes and the springs during separation. This condition resulted in bending the tube in bay V approximately 1 in. out of plane before the spacecraft was clear of the adapter. The bay V tube was the only one damaged in this manner, caused by its partially deployed position in the adapter. The peculiar position is caused by the other end of the tube bearing against the in-flight disconnect protective shield. The tube was straightened between runs and the same result was repeated in three runs. No other visible damage was apparent after each run.

During this test, acceleration and dynamic-load data relative to spacecraft separation dynamics was obtained.

e. Test results. The results of these tests were as follows:

(1) Separation of the spacecraft from the adapter with the sunshade deployed was completed without serious damage to the shade. The addition of the Lockheed hardware, as described, was successful in preventing the shade from snagging. The damage noted in bay V would have no effect on the mission success.

(2) It must be noted that the separation rate during these tests was limited to the hoist speed. The hoist constant velocity of approximately 3 in./s compares with the minimum differential velocity between the spacecraft and the *Agena* of 2 ft/s after separation. Although the time vs velocity profile was considerably different for the sunshade hangup test, it was believed to be conservative to shade damage.

(3) The maximum tip-off rate induced by the predeployed shade was 2.13 deg/s. Most of that rate was contributed by the shade support-tube's momentarily snagging in bay V.

(4) The combined tip-off rate caused by the shade prematurely deployed and the spacecraft *cg* offset would be 3.54 deg/s. This was in excess of the 3 deg/s limit given in an Engineering Document and did not account for any other effects on separation dynamics (e.g., push-off spring tolerance).

5. Full-scale antenna-pattern tests. Mechanical support was provided for obtaining preliminary and final *Mariner* Venus 67 spacecraft full-scale antenna patterns.

a. Hardware description.

Antenna test model. Early in the program an antenna test model (ATM), which was a crude flight-type mockup of a *Mariner V* spacecraft, was constructed and tested to determine as early as possible if any major antenna pattern problems existed. This mockup (Fig. 35) was built mostly of sheet metal and wire screen.

Second antenna model. The final full-scale antenna patterns for more precise records were measured with the developmental test model (DTM) spacecraft. The DTM was assembled as a flight-type spacecraft, except that the cases did not contain electronics, the solar cells were not included on the solar panels and most of the experiments were detailed mockups. The external configuration (Fig. 36) was well within 0.1 in. of flight-hardware dimensions.

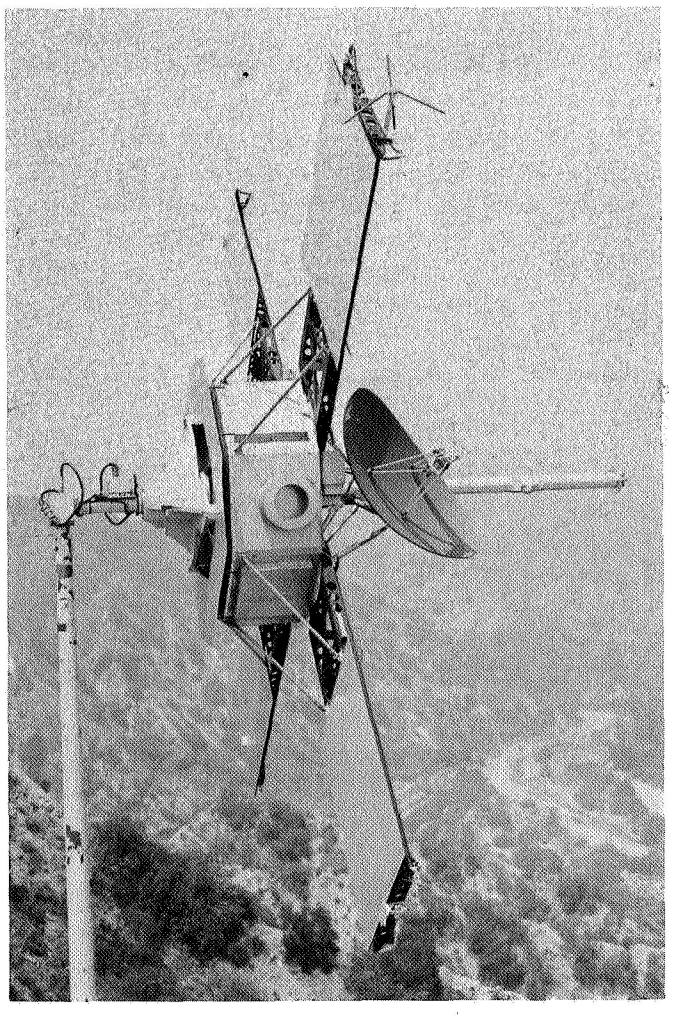

Fig. 35. Antenna test model

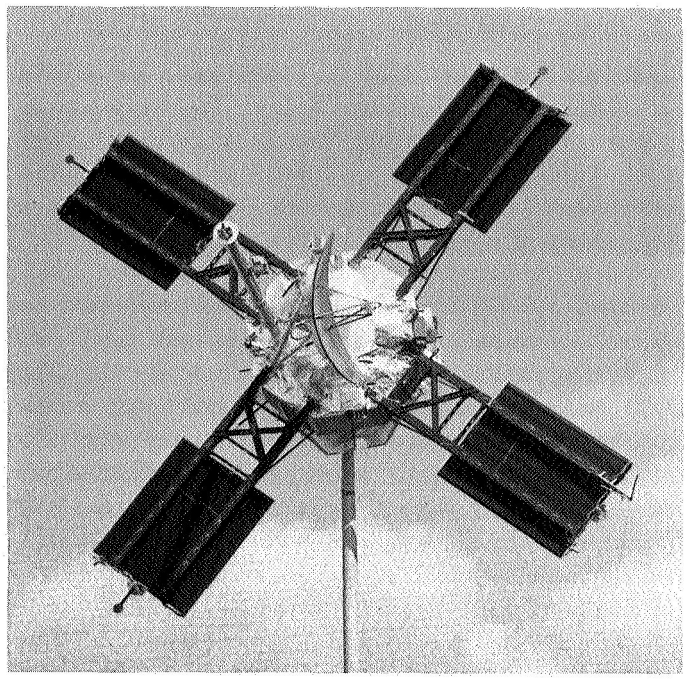

Fig. 36. Developmental test model

Agena adapter and forward equipment rack. A mockup of the *Agena* adapter and a portion of the forward equipment rack were constructed for S-band full-scale antenna patterns taken with the spacecraft in the launch configuration. The mockup was basically 1/2-in. aluminum tubular frames covered with wire structure cloth (Fig. 37). This mockup was secured to the steel mast. It was mounted stationary, but still allowed the spacecraft to rotate independently in the roll direction.

Spacecraft roll positions. The spacecraft roll positioner permitted remote control of spacecraft roll position while the DTM was mounted to either of the two existing support masts. (The steel mast was used in the S-band antenna measurements and the antenna laboratory fiberglass mast was used in the DFR antenna measurements.) The structure consisted of a steel spider weldment made up of eight square-tube legs welded radially to a center hub that mounted over the shaft of the mast. The ends of each of the legs were secured to the lower ring of the spacecraft. A drive mechanism mounted to the spider rotated it with the spacecraft.

Steel mast erection system. A mast erection system was designed and adapted to the spacecraft support steel mast to ensure a safer raising and lowering of the DTM spacecraft as well as to expedite the stowing of the spacecraft in case strong damaging wind or rain were encountered during antenna pattern measurement. The system, shown in Fig. 37, consists of a hydraulic pump and motor assembly, regulators, check valves, control valves, plumbing and a large hydraulic jack. The hydraulic jack raises and lowers the mast by acting on a steel arm welded to the mast.

Fig. 37. Mockup of *Agena* adapter and part of forward equipment rack

Spacecraft-support-mast proof tests.

(1) Antenna fiberglass mast. A static proof test of the Antlab positioner and fiberglass mast setup was successfully performed. The purpose of this test was to determine

that the positioner and mast could withstand wind loading. For a wind velocity of 67 mi/h with the solar panels deployed, the loading would be approximately 45,000 ft-lb.

(2) Roll positioner. A simulated dynamic test of the mast and spider mounting assembly was successfully conducted to ensure safety when raising or lowering the DTM. A dead-weight load factor of 3.5 × the actual weight (372 lb) of the spider assembly and DTM was established as the total load required for the simulated, dynamic proof test.

(3) Steel mast hydraulic erection system. This hydraulic erection system was proof tested to ensure a safe raising and lowering of the DTM and (looking into the future) the *Mariner* Mars 1969 antenna model spacecraft. The proof test was done in two phases: in the first phase, the erection system was subjected to a static load equivalent to 3½ × the sum of the estimated weight (350 lb) of the *Mariner* Mars 1969 antenna model, plus the weight (200 lb) of the roll-positioner assembly; in the second phase, the erection system was subjected to a static load (independently in two opposite directions) equivalent to 1¾ × the force created by a 65 mi/h wind velocity acting on the greatest wind-resistant surface area of *Mariner* Mars 1969. The mast was not mechanically locked during these tests, other than through its own hydraulic system.

Mechanical alignment. Measurements were made to establish the proper spacecraft and spacecraft positioner orientation and angular references for S-band and DFR antenna patterns. The alignments were made to establish a zero reference for spacecraft roll (clock angle), pitch, and azimuth relative to either of the transmitting antennas (the 9-ft dish illuminator antenna at the 730-ft DFR range and the 10-ft illuminator antenna for S-band at the 3600-ft East Mesa range).

The relationship of the high-gain antenna to the *X*, *Y*, and Z axes of the DTM bus was established, and coordinate lines were scribed on the upper and lower bus rings.

The zero-degree spacecraft cone angle (azimuth) was obtained with a K & E transit modified into a bore sight fixture. This fixture was mounted and aligned onto bay VI such that the plane cut by the transit's line of sight coincided with the plane established by the set of scribed coordinate lines of bays VI and II. After the spacecraft Z axis was set to the correct clock angle, the zero-degree spacecraft cone angle was established when the spacecraft was moved in azimuth until the vertical hairline of the transit fell in line with the centerline of the transmitting antenna.

b. Test description.

DFR full-scale antenna patterns. The 730-ft range on the Mesa was used for the DFR (49.8 and 423.3 MHz) full-scale antenna patterns. The ATM antenna model was used for the preliminary measurements, and the DTM was used for the final measurements. In general, the antenna model was mounted to the Antlab erected fiberglass mast and was in the cruise configuration. The solar panels were deployed and held in that position by fiberglass support rods. The sunshade on the DTM antenna model was alternately nested and deployed for these measurements.

S-band full-scale antenna patterns. The 3600-ft East Mesa range was used for the S-band full-scale antenna patterns. In general, the antenna model was mounted to the erected steel mast in the cruise configuration. The solar panels and sunshade were deployed. Data were also taken with the DTM in the launch configuration with solar panels and sunshade nested and with the *Agena* adapter and forward equipment rack in place.

6. Stray-light-reflection tests. Two series of spacecraft-reflection tests were performed in the celestarium to check the stray light interactions of the spacecraft, primarily the sunshade, with the optical sensors.

a. Preliminary sun sensor–thermal-shield compatibility test. The purpose of this test was to determine the sun-sensor null offset caused by sunlight reflecting into the detector cavities from the *Mariner* Venus 67 thermal shield.

Test description. The DTM bus containing a prototype lower thermal shield and sunshade was used. One primary sun sensor was mounted to its regular pedestal; the other one was moved to within 6 in. of the first one to allow both sensors to be illuminated by the heliostat, which provides a 24-in.-diam sun bundle (Fig. 38). The second sun sensor was also elevated 6 in. above its normal position to avoid reflections into its detector.

The DTM was tilted by means of screw jacks to achieve a sun sensor null condition while the sunlit portions of the thermal shield were covered with coffin cloth. After achieving a null output, the coffin cloth was removed and the null offset readings were taken. This

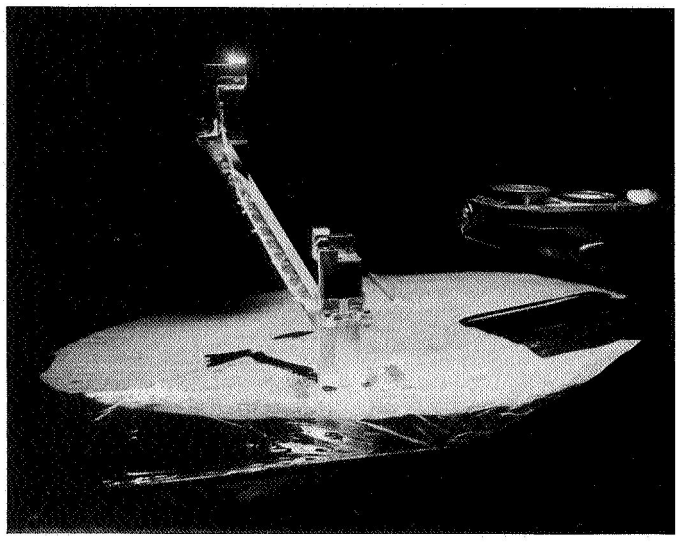

Fig. 38. DTM preliminary sun sensor test

technique was used to evaluate the following sunshade configurations:

(1) Loosely draped

(2) Taut

(3) Heavily sagged

(4) Folded into the retracted position

(5) Outer edges lowered approximately 1.5 in.

(6) Partially extended (failure mode)

(7) Thermal shield removed

Results. It was found that, by manually raising the outer edge of the sunshade, light could be reflected directly into the sensor detectors, causing large null offsets. This could not happen unless the shade broke loose from its supports.

This test, which approximated a worst-case condition, indicated that null offsets of <130 mV were caused by the sunshade. This offset represents 0.7 min of arc as compared with the 2-min tolerance allowed the primary sun sensor at room temperature. The addition of this effect to all other tolerances that could contribute to the sensor error results in a worst-case offset of approximately 3.8 mrad. The *Mariner* Venus 67 tolerance on the null offset is 5.5 mrad.

It was also found that raising the sunshade in an area immediately adjacent to the sensor pedestal caused the light to be reflected away from the detectors because of the angle induced in the shade.

Conclusion. The test indicated that the sunshade could be designed so that its effect on sun-sensor performance would be tolerable.

b. Final spacecraft reflectance test. The purpose of this reflectance test was to map the spacecraft with the existing light source to determine sources of stray light that might degrade the performance of the sun sensors, planet sensor, terminator sensor, and Canopus sensor.

Description. The TCM containing all exterior hardware except for antennas and upper thermal shield was installed on a portable stand; two solar panels were also provided (Fig. 39). The effects of the stowed and deployed flight sunshade on the primary sun sensors were evaluated under various failure modes. The same approach was used as during the preliminary test.

The effects of stray light through the sunshade and off spacecraft sunlit items were accurately measured at the other celestial sensor locations.

Results. The normal folded- and extended-sunshade configurations produced only slight null offsets on the sun sensors. Two failure modes, however, produced up to 5.0 V offset which is far above the established acceptable error of 1.2 V. The first failure mode was simulated by extending one thermal shade panel approximately half way, as might occur if an extension spring broke.

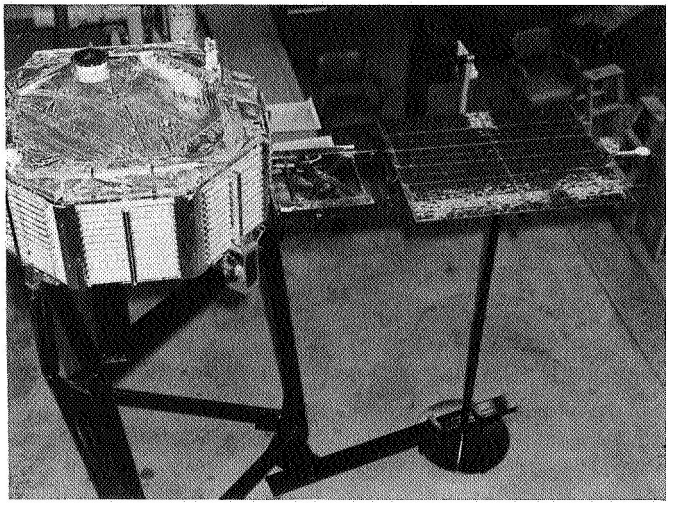

Fig. 39. TCM for final spacecraft reflectance test

This allowed the loose shade material to assume various positions, if a zero gravity field is assumed. Some of these positions intersected the sensor's field of view. Various positions and configurations were checked by supporting the shade material with tissue paper to overcome the 1-g field. The worst possible configuration produced approximately 5-V offset.

The second failure mode that caused a 5-V error was a so-called shirttail failure. This would occur if the two shade panels adjacent to a sun sensor remained in the folded position and the shade material between these panels was extended toward the sun sensor.

There was no significant stray light impingement on the other celestial sensor locations sufficient to affect their performance.

Conclusion. There was a possibility of serious degradation of sun-sensor performance resulting from a sunshade failure. The out-of-tolerance sun sensor null offset would affect the midcourse maneuver, accordingly. The performance of the other celestial sensors would not be impaired by stray light from the spacecraft in the nominal case. If the sunshade failed to deploy, the performance of the planet sensor could be impaired.

B. Subsystem Level

1. Electromagnetic interference–electromagnetic capability tests.

a. Bench compatibility test on Mariner Venus 67 S-band transponder and Pioneer DFR. The DFR and S-band transponder tests had the following objectives:

(1) To evaluate the performance of each subsystem while operating with a common power supply

(2) To evaluate the RF interactions between the two receivers for each channel

(3) To obtain RF spectrum signature data on the two subsystems to be utilized in evaluating compatibility with other spacecraft subsystems

The tests were desired because of the late delivery of a DFR. It was desired to obtain, at an early date, results that would show the possibility of interference between the two RF systems on the spacecraft.

Description. The two subsystems were operated with checkout equipment. The test was performed in a shielded enclosure with the subsystems placed in close proximity on a conducting surface. Each subsystem was calibrated, and its operation was determined to be nominal while the other test subsystem was turned off. After cognizant personnel were convinced that the operation of the equipment was nominal, the two subsystems were adjusted to operation close to threshold.

Various test configurations were used to determine the degree of interaction between the two subsystems. Figure 40 shows a typical test configuration used in this sequence of tests.

In particular, the sequence of tests was intended to determine the following characteristics:

(1) The interference coupling through a mutual power supply

(2) The interaction of local oscillator harmonics between the S-band receiver and the DFR-UHF receiver

(3) The interaction of local oscillator harmonics between the S-band receiver and the DFR-VHF receiver

(4) The interactions between the S-band transmitter power level at 2295 MHz and the DFR VHF channel

(5) The interactions between the S-band transmitter power level at 2295 MHz and the DFR VHF channel

(6) The interference effects to the DFR 423.3 MHz (UHF) channel from the following intermodulation products:

$$2115.699800 \text{ MHz} - 4 \times 423.300000 \text{ MHz} = 422.499800 \text{ MHz}$$

$$6 \times 423.300000 \text{ MHz} - 2115.699800 \text{ MHz} = 424.100200 \text{ MHz}$$

(7) A radiated spectrum measurement of the S-band transponder

(8) A radiated spectrum measurement of the DFR

Results. A summary of the results for each of the planned tests is given below:

(1) It was not possible to operate the two RF systems from a common power supply because the DFR was a

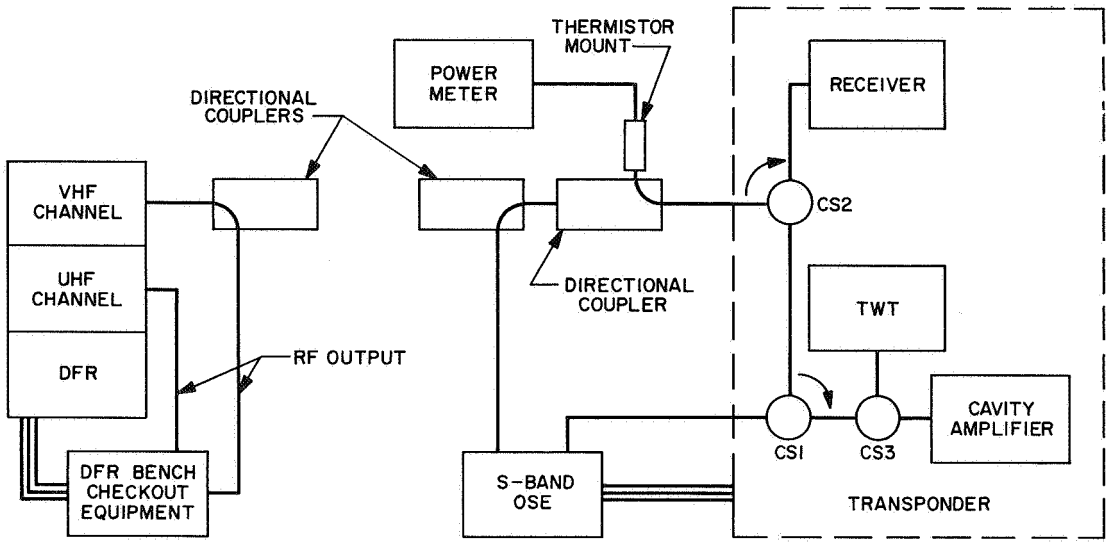

Fig. 40. Typical test configuration, DFR/S-band transponder

Pioneer configuration model. The two units were operated in close proximity on a common ground plane and no interference was observed.

(2), (3) No local oscillator interference was observed. However, it was determined that the 2295-MHz downlink signal should be isolated by at least 60 dB from the inputs to the DFR to avoid degradation.

(4) With the ranging loop *on* in the S-band transponder, there was interference with the DFR UHF channel. This interference apparently requires that an S-band RF level at downlink frequency enter the DFR and that RF levels generated within the DFR UHF receiver enter the transponder. This interference occurs as a self-lock problem within the S-band system. No interference occurs with the ranging loop *off* or with at least 13 dB of isolation between the two units.

(5) No interactions were observed between the DFR VHF receiver and the S-band transponder.

(6) No interference to the intermodulation products was noted.

(7) Noise at 49.8 MHz was observed to be generated by the transponder TWT. Lack of time precluded an extensive spectrum signature.

(8) A lack of time prevented a spectrum signature of the DFR at this time. (A signature was made of a *Mariner* Venus 67 DFR during the subsystem qualification tests.)

Significant findings. A significant finding in this test was that the S-band transponder could be jammed by noise or discrete components from the DFR when the ranging loop was operated.

Recommendations. The following recommendations were made based on the results of this test:

(1) A filter, preferably a bandpass, at the input to each DFR channel would prevent the 2297.5-MHz level from degrading the DFR. If such a filter were bidirectional in the 423.3-MHz channel, it would also isolate the spurious signals generated within the DFR at the S-band receiver frequency. Bandpass filters would also prevent noise from entering at the image frequencies.

(2) A filter at the output of the S-band transmitter to prevent radiation of noise at 49.8 MHz and 423.3 MHz would ensure that the DFR channels would not be degraded in sensitivity.

(3) The following antenna coupling measurements should be made to analyze the potential mutual interference between the two RF subsystems:

(a) The coupling of 2297.5 MHz from the S-band antennas to each DFR antenna should be determined.

(b) The coupling between the S-band antennas and the corresponding DFR antennas at 49.8 MHz and 423.3 MHz should be determined.

(c) The coupling between the DFR 423.3 MHz antenna and the S-band antennas at 2115.7 MHz should be determined.

It was also recommended that in a spacecraft compatibility test of the flight transponder and the DFR the following should be included in the test plan:

(1) Determine whether the new S-band filters installed in the transponder would alleviate the interference to the DFR.

(2) Determine degradation to the DFR with 2297.5 MHz and noise present.

(a) Determine the degradation of the DFR when a *clean* 2297.5-MHz signal (filtered to remove noise at the DFR frequencies) is coupled to the DFR.

(b) Determine the degradation of the DFR in the absence of the 2297.5-MHz signal. Allow only the noise from the transmitter to couple to the DFR.

(3) Determine the degradation of the S-band receiver when tightly coupled to DFR with ranging *off* and with ranging *on*.

(4) Determine in a bench test of the DFR alone the degradation with a power level at 2297.5 MHz inserted at the input to each channel.

Follow-up activity.

(1) Filters were procured by DFR cognizant personnel. A bandpass filter was selected for the VHF channel and a low-pass filter was selected for the UHF channel. These filters were installed external to the DFR.

(2) Antenna coupling tests were performed by cognizant personnel.

(3) A series of system compatibility tests was performed to verify compatible operation. These tests are reported elsewhere in this report.

b. Bench compatibility test of Mariner Venus 67 S-band transponder and flight-type DFR. This test was performed to verify that the VHF and UHF filters obtained for the DFR did, indeed, reduce the interference caused by the 2297-MHz S-band signal and that the interference to the ranging loop was eliminated.

Description. The first test with a Pioneer-type DFR and the prototype S-band transponder showed that, when the two units are tightly coupled with direct coaxial lines, the transponder is jammed when the ranging loop is *on*. This interference may be caused by discrete RF levels generated within the UHF channel when a strong-level S-band signal is present. The filter selected to eliminate this trouble associated with the UHF channel was a low-pass filter. A later test, using the *Mariner* Venus 67 S-band transponder and flight-type DFR was conducted by physically connecting the DFR and the engineering model transponder SN 3. Figure 41 shows the configuration used for the test. The S-band receiver was operated in the receive low, transmit high, RF power-up mode with a received signal level of −130 dBmW. The tuning stub shown in Fig. 41 is required for proper termination. The stub was adjusted to permit a 0-dBmW incident RF level to the DFR. The S-band system was monitored by the transponder OSE.

Results. When the S-band transponder is operated while connected in a tight configuration as shown in Fig. 41 there is an immediate jamming when connected to the UHF receiver without the low-pass filter. Insertion of the filter eliminates the interactions. The jamming is manifested by a large positive voltage occurring on the S-band receiver phase-detector and the AGC voltage decreases as it would for an increased signal strength. Without the filter, 55 dB isolation was required to eliminate the interference.

A 30-dB degradation was observed on both DFR channels with the filters inserted or removed. The degradation occurred with the TWT *on* and did not occur with the S-band cavity amplifier.

Significant findings. The degradation observed with the filters installed appeared to indicate that the TWT amplifier was emitting noise at the VHF and UHF frequency bands that would affect the DFR sensitivity.

Recommendations. No formal recommendations resulted, but an additional test to determine whether noise was generated by the TWT at the VHF band was considered necessary.

Follow-up activity. This test was performed at the VHF frequency only because at the time a sufficiently sensitive receiver for the UHF band was not available. A test on the engineering model (SN 3) transponder showed that the level of noise at 49.8 MHz emitted by the TWT was −100 dBm in a 45-kHz bandwidth. Since

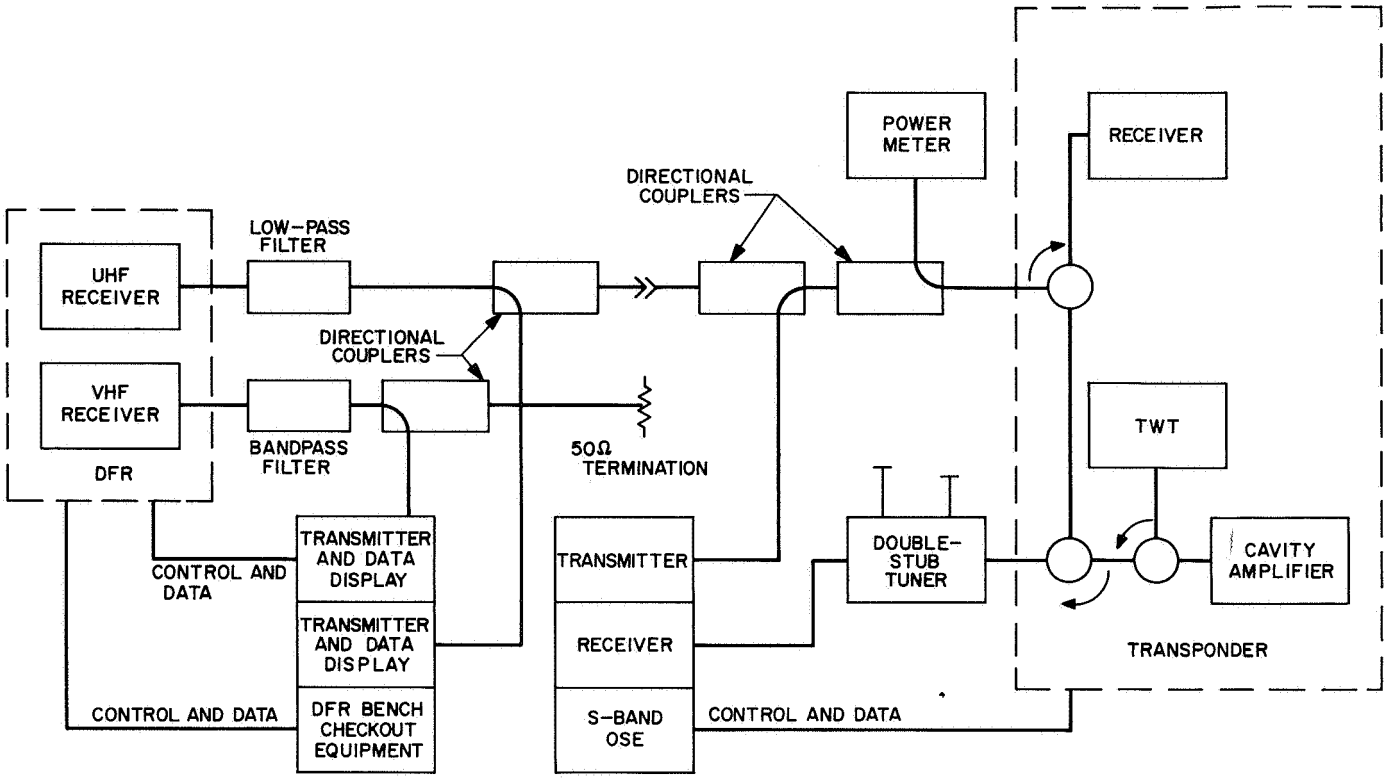

Fig. 41. Bench compatibility test of transponder and DFR

the antenna isolation was expected to be >73 dB, the degree of DFR VHF degradation contributed by the TWT would be negligible.

c. Power subsystem noise measurements.

Regulators. A series of measurements was made of a breadboard model power regulator to determine the reduction in noise at 49.8 MHz with a change of diodes. A reduction of noise at this frequency was desired to reduce the degradation of the DFR VHF receiver. Power cognizant personnel had suggested the replacement of the diodes as a means of reducing RF noise.

This test provided only qualitative information on the degree of noise reduction with a change in diode components. Measurements were made using a tuned probe, a current probe[10] and a portable receiver assembled by Stanford University personnel. The measurements were made in a test laboratory on a breadboard model power regulator (case 8). Measurements were first made with the original diodes (1N1583) and then again after replacement with faster diodes (1N3892). The readings were taken at various chassis points and each cable.

The readings showed that there was a significant reduction in the noise at 49.8 MHz. Because the tuned probe measurements were made in close proximity to the chassis, no attempt was made to convert the readings to field strength values. The current probe readings showed that previous high levels on the receiver were reduced to undetectable values. The noise figure of the receiver was estimated at 5 dB.

Although there were no significant test findings, it was recommended that the faster 1N3892 diodes replace the 1N1583 diodes. Tests subsequently performed on M67-1 and M67-2 demonstrated that the noise level had been reduced to an acceptable level.

Battery charger. Measurements were made of the noise level at 49.8 MHz generated by the 1N1583 diodes and the faster 1N3892 diodes when installed in the battery charger. This data was desired to determine the degree of noise reduction that would be possible at 49.8 MHz, the DFR VHF frequency.

[10]Model 91550-1, manufactured by Stoddart Electro Systems, Division of Tamar Electronics, Inc., Gardena, Calif.

This test provided qualitative data taken with both a tuned probe and a current probe and a portable hand assembled receiver. The battery charger tested was operated with 40 V impressed and 640-mA output and also in the boost mode with 30 V impressed and 330-mA output with each set of diodes.

The qualitative results showed that the 1N3892 faster diodes definitely reduced the noise level at 49.8 MHz. It was, therefore, recommended that these faster diodes replace the 1N1583s. However, the recommendation was not carried out; the fact that the operation of the battery charger is a controlled function was considered by the Project in not approving a change in the diodes.

d. DAS oscillator frequency incompatibility tests. It was discovered in compatibility tests (discussed elsewhere in this report) that the science data automation system (DAS) basic oscillator frequency interfered with the VHF receiver of the DFR. The basic frequency of the DAS was 444.444 kHz. The frequency multiplication scheme of the DAS caused the 112th harmonic to be of sufficient amplitude to degrade the DFR 49.8-MHz receiver. The nominal passband of the DFR VHF receiver is 45 kHz, and the 112th harmonic occurred at 49.777728 MHz. In addition, spaced at $\frac{1}{8} \times 444.444$ kHz there are discrete levels of a lower magnitude between the principal harmonics. There were two objectives of these tests – the first was to determine the amplitude of the 112th harmonic and the second was to verify that a temporary frequency change had removed the harmonic from the VHF passband sufficiently to permit compatibility tests of the DFR and spacecraft to proceed.

Description. The measurement of RF level at the 112th harmonic was performed on a partially assembled spacecraft (M67-1) that had the DFR VHF antenna installed. The measurement was made by substitution in the following manner. The harmonic was first found with the EMI test receiver equipment that included an R390A/URR military receiver, and a reference level was determined. The signal in question was connected directly from the spacecraft DFR antenna to the test receiver. The level was, therefore, that which would be coupled from the DAS system wiring to the RF antenna. The level obtained on the test receiver system was then duplicated with a test signal generator. Other tests performed with the DFR experiment had determined that the interfering signal entered through the RF input, not through the power or signal leads. The frequency verification test was conducted using the EMI test equipment.

Results. The power measurements showed a level of approximately −80 dBmW for the 112th harmonic and levels 30 dB lower for the harmonics spaced at $\frac{1}{8} \times 444.444$ kHz. The frequency verification measurements showed that the temporary oscillator change had pulled the frequency to 49.73 MHz, which was out of the 45-kHz bandpass.

Significant findings. Additional tests were also made to determine whether the harmonics extended to the UHF and S-band frequency ranges. The harmonics were not found in those ranges. (At S-band, a receiver with a noise figure of approximately 4 dB was used with a horn antenna at close proximity to the DAS breadboard model.)

Recommendations. Cognizant DAS personnel determined that the basic oscillator frequency could be changed to 443.406 kHz without degrading the operation of the unit. Their recommendation for the frequency change was carried out. In addition, recommendations for the placement of ferrite beads and for wrapping of the DAS interconnect harness (9W21) with two-sided aluminum-coated Mylar were approved. The beads and the wrapping were intended to reduce the level of all the harmonics that could leak into the DFR VHF antenna.

Follow-up activity. The selected frequency of 443.406 kHz placed the 112th harmonic at 49.66 MHz. This frequency is approximately 140 kHz removed from the center frequency. One of the harmonics spaced at $\frac{1}{8} \times 443.406$ kHz falls at the edge of the 45-kHz receiver bandpass but apparently is of insufficient magnitude to degrade the DFR.

e. Canopus sensor electromagnetic interference tests.

Description. The EMI tests were performed on the TA Canopus sensor 103 and the flight spare Canopus sensor 107 to determine the degradation in performance due to RF magnetic fields and conducted interference. These tests were performed as a result of an anomaly in the flight unit's operation on May 9, 1967 at Cape Kennedy. Essentially, the anomaly was that the intensity output of the Canopus sensor (106) on the flight spacecraft (M67-2) varied from dark input to roughly 1/14 of Canopus intensity with no light stimulus.

Test results. The subsystem EMI testing performed above showed that the units named did exhibit a susceptibility to RF magnetic fields and RF conducted interference within discrete frequency bands if the applied interference was modulated with the proper range

of frequencies. However, when a systems test was performed using the 107 unit, the anomaly was no longer present. Based on the testing results, the cause of the initial anomaly cannot be absolutely defined as an EMI problem; however, the tests did show that the units are susceptible to EMI. A detailed description of the tests which were performed can be found in Ref. 2.

Recommendations. To ensure that questions relating to EMI during future spacecraft development and testing are answered with a maximum confidence level, the below-listed recommendations are presented. Implementation of these recommendations would provide accurate information, specifically, on the electromagnetic environment generated by the spacecraft and the response of spacecraft components to this environment. Accurate knowledge of the magnitude of spacecraft electromagnetic environment and the response of equipment to this environment could result in elimination of possible problems with minimum effect on the spacecraft system processing and could save money and time.

(1) During the initial spacecraft design phase, work should be initiated to evaluate and analyze each spacecraft subsystem to determine the spectral distribution of critical, generated, and susceptible frequencies and/or waveforms and to cull for those combinations that could result in degradation to any portion of the spacecraft system.

(2) Based on (1), above, limited EMI tests should be performed on subsystems to obtain generated interference and interference-susceptibility levels. This would permit analyses to determine spacecraft compatibility. The tests should be accomplished before spacecraft assembly and made a part of the environmental requirements for subsystems.

(3) Specific compatibility tests should be performed at the intersubsystem level or at the spacecraft system level as warranted by compatibility analysis from (2) above.

f. Ferrite bead investigation. The objectives of this investigation were (1) to determine the utility of ferrite beads (similar to those[11] used on the *Mariner* Venus 67 spacecraft) as low-pass filters for the suppression of RF energy within a given system and (2) to determine the acceptance of a permanent residual magnetization by the ferrite beads.

[11]Ferroxcube 5659065/3B, manufactured by Ferroxcube Corporation of America, Saugerties, New York.

Description. The following investigations were performed to quantify the independent variables that determine the advantage of using ferrite beads for the two purposes noted above:

(1) A 2^n factorial experiment with center points, using $n = 2$ for the number of variables (the number of beads and frequency of interest), was performed to obtain an expected mean and variance of the resistance and reactance coefficients of the tested ferrite beads.

(2) A circuit analysis using transmission-line theory was performed on a typical simple circuit to quantify the independent variables associated with the use of ferrite beads as low-pass filters for maximum insertion loss between a source and load.

(3) A circuit analysis using transmission-line theory was performed on a typical simple circuit to quantify the independent variables associated with the use of ferrite beads as low-pass filters for reducing electromagnetic coupling between the source circuit and an adjacent secondary circuit. An experimental test was performed to verify the results.

(4) An experimental test was performed to determine the acceptance of a permanent residual magnetization by the ferrite beads. The experiment consisted of subjecting 32 ferrite beads (one bead on each of 32 separate lines that made up a 12-in. length of cable) to a 100-G field, then measuring the permanent residual magnetization.

Significant findings. From the 2^2 factorial experiment with center points, the *resistance coefficient* of the impedance of the sample of the ferrite beads was determined to be:

$$R = 54.1 + 6.3X_1 + 26.1X_2 - 1.9X_1^2 - 1.9X_2^2 + 3.5X_1X_2$$

for values of $X_1 = -1, 0, 1$, where

$-1 <=> 25$ MHz,

$0 <=> 50$ MHz,

$1 <=> 75$ MHz

for values of $X_2 = -1, 0, 1$, where

$-1 <=> 1$ bead,

$0 <=> 2$ beads,

$1 <=> 3$ beads

The variance of the resistance coefficient for the experiment was calculated to be 9.37 (i.e., $3\sigma = 9.18$). Figure 43 illustrates the variation of the mean reactance coefficient for the 1-, 2-, and 3-bead case as a function of frequency.

The *reactance coefficient* of the impedance of the sample of ferrite beads tested was:

$$X_L = 18.9 - 2.5X_1 + 4.8X_2 + 0.6X_1^2 + 0.6X_2^2 - 4.1X_1X_2$$

for values of $X_1 = -1, 0, 1$, where

$-1 <=> 25$ MHz,

$0 <=> 50$ MHz,

$1 <=> 75$ MHz

for values of $X_2 = -1, 0, 1$, where

$-1 <=> 1$ bead,

$0 <=> 2$ beads,

$1 <=> 3$ beads

The variance of the reactance coefficient for the experiment was calculated to be 3.16 (i.e., $3\sigma = 5.33$).

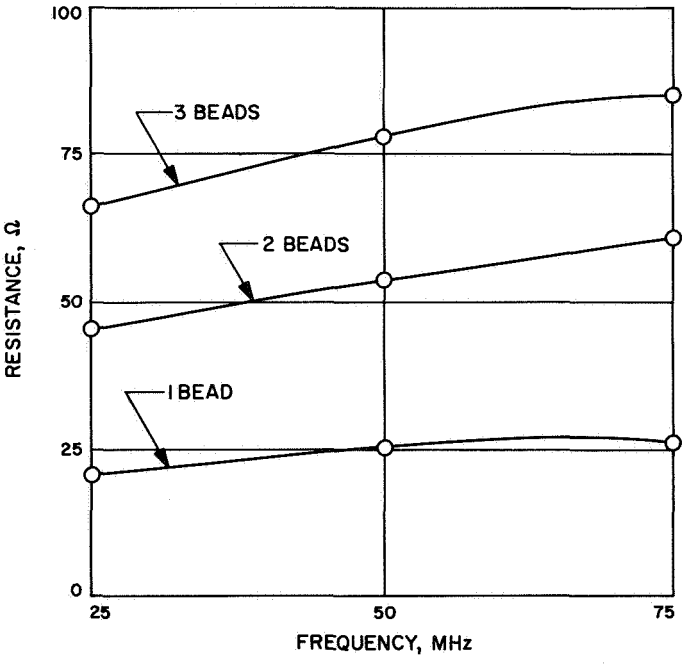

Fig. 42. Resistance of ferrite beads vs frequency

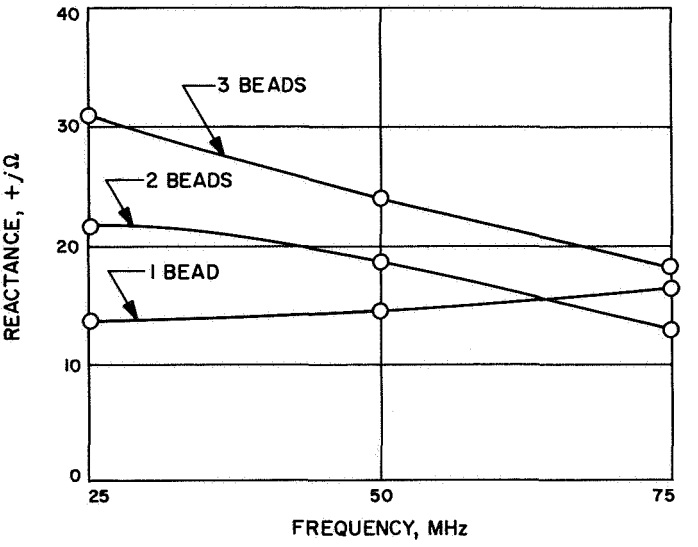

Fig. 43. Reactance of ferrite beads vs frequency

Figure 43 illustrates the variation of the mean reactance coefficient for the 1-, 2-, and 3-bead case as a function of frequency.

In general, the insertion loss of the ferrite beads in a circuit will be small (<10 dB) because of the relatively low impedance of the ferrite beads and is dependent on (1) the impedance of the ferrite beads used, (2) the source impedance, (3) the load impedance, (4) the frequency of interest, (5) the length of the wire, (6) the characteristic impedance of the wire, and (7) the location of the ferrite bead on the wire. The maximum insertion-loss results when the bead (or beads) is placed on the wire at the maximum-current point for the frequency of interest.

In general, the reduction of electromagnetic coupling obtained by using ferrite beads is small (<10 dB) and is dependent on (1) the impedance of the ferrite beads used, (2) the source impedance, (3) the load impedance, (4) the frequency of interest, (5) the length of the wire, (6) the characteristic impedance of the wire and, (7) the location of the ferrite beads on the wire. The maximum reduction of coupled electromagnetic energy from the use of ferrite beads will exist by placing the ferrite bead (or beads) on the lines such that

$$\int_0^L I(f)\,dl \cdot \int_0^L V(f)\,dl$$

is minimized where $I(f)$ and $V(f)$ are functions of l, and L is the length of the wire.

The permanent residual magnetization acquired by the 32 ferrite beads when subjected to an exposure of 100 G was $<1\gamma$ at 12 in.

Recommendations. Ferrite beads similar to those used on the *Mariner* Venus 67 spacecraft, are recommended for suppressing RF energy where weight, size, and magnetic contamination must be minimized and the desired suppression is relatively small (<10 dB).

It is recommended that other classes of ferrite beads be investigated for their interference suppression and magnetic contamination properties.

2. Solar-panel-deployment test.

a. Static test. A static test was conducted on a single solar panel to determine the panel's torsional stiffness, in-plane stiffness, and shear center.

Description. For these tests, the panel was pinned, supported at its two hinge points – one at the bottom of each spar. Torsional and in-plane loads were applied at the top of the spars, and the corresponding deflection was measured. The shear center was determined by applying loads in a plane parallel to the solar-panel corrugations and obtaining the distance between the two planes for a loading that produced *zero* torsional deflection of the panel.

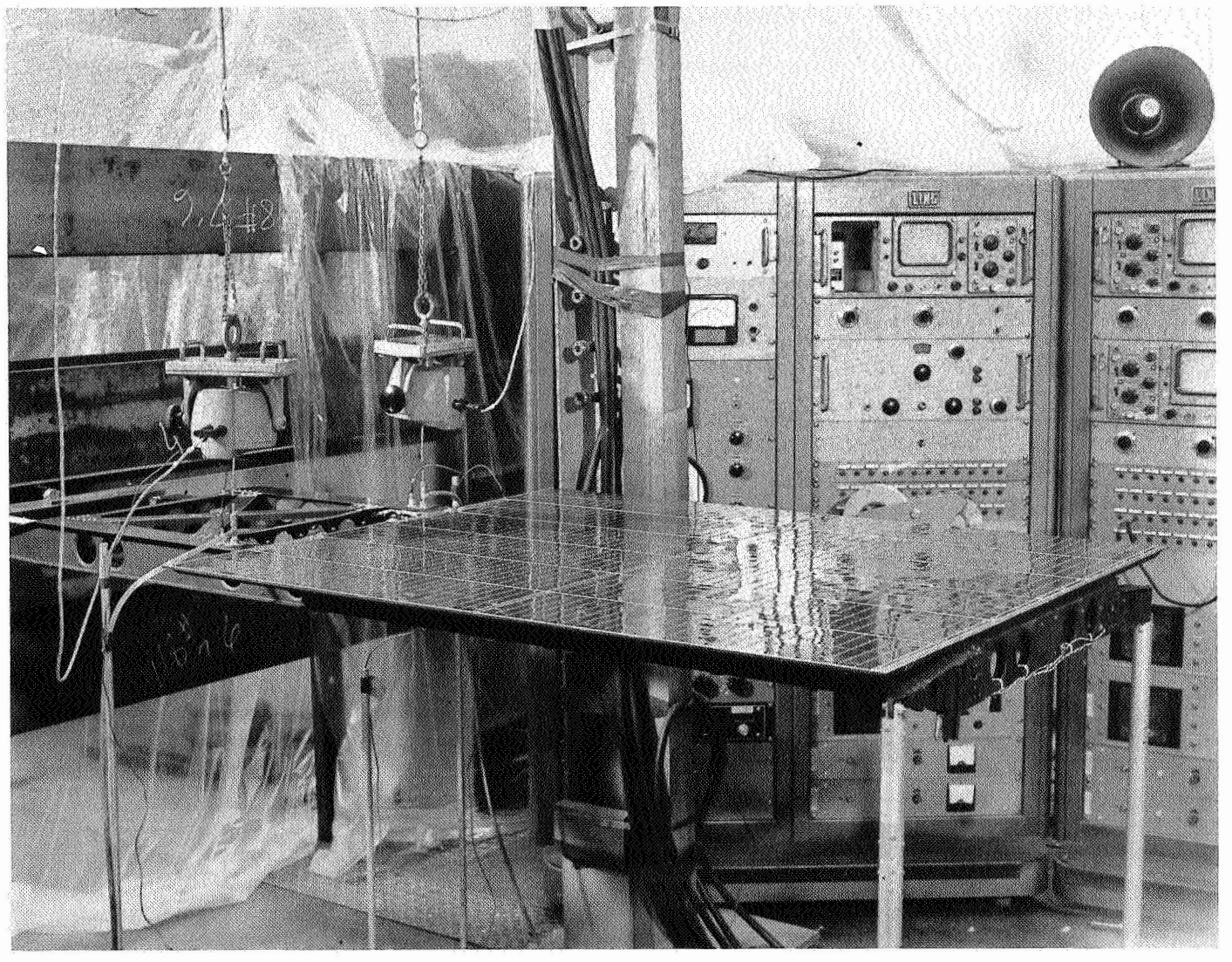

Fig. 44. Setup for modal vibration test

Test results. The in-plane test stiffness was high compared with analysis, as it should be, since both beams were prevented from in-plane sliding in the test setup. The measured value was 3.91×10^6 in.-lb/rad about the center of rotation, which is about 12 in. below the solar-panel hinge axis. The torsional stiffness was 1.33×10^4 in.-lb/rad, and the shear center was 0.60 in. from the face of the corrugations toward the spars. The latter two values verified analysis reasonably well.

Table 17. Summary of modal test data and comparison with analysis

Analysis frequency, Hz	Test frequency, Hz	Damping ratio[a] c/c_c from test	Comment
22.4	26.7	0.0048	In-plane mode; neither leg sliding in test
30.8	30.6	0.0045	Symmetric beam bending
39.1	40.6	0.0032	Antisymmetric beam bending
69.3	70 ± 2	>0.05	In-plane mode; impossible to excite due to high damping
87.0	80.9	0.008	Coupled beam and corrugation
94.8	73.9	0.0024	Symmetric corrugation mode analysis *EI*, 20% high

[a]In the ratio c/c_c, c = damping, and c_c = critical damping.

b. Modal vibration test.

Description. A modal test was conducted on one solar panel for a pinned-pinned support condition to verify dynamic analysis. Two small modal shakers were used to excite the normal modes for this support condition; Fig. 44 shows the test setup. Frequency and mode shapes were measured with extremely light accelerometers so that the mass of the response transducer would have minimal effect on the panel dynamics. Structural damping was obtained from acceleration logarithmic decrements and resonance curves of the normal modes. Minor difficulty was encountered during the test with backlash in the monoball bearings used to support the panel. Improved bearing tolerances reduced this problem to acceptable limits.

Test results. To a reasonable degree, the modal tests verified the panel properties predicted by analysis (Table 17). Existing discrepancies were at least partially explained by known differences between test parts and the analytic model. Also listed in Table 17 are the values, measured during test, of the damping ratios at small amplitudes used in later analysis. The quality of the test is indicated by the degree to which the test mass matrix is diagonal, as is shown in Table 18. The analytic mass matrix is also given, based on only those masses whose motions were measured in the test; and as can be seen, the discrepancy from a unit matrix is of the same order as the error of the test mass matrix.

Table 18. Mass matrix, solar panel structure

Data source	Test						Analysis					
Test	1.0	0.07	−0.08	[a]	0.07	0.01	0.96	0.11	0.07	−0.05	0.11	0.06
	0.07	1.0	0.04		0.08	0.08	−0.07	0.98	0.11	0.05	−0.04	−0.01
	−0.08	0.04	1.0		0.08	0.02	−0.03	0.14	−0.94	0.04	−0.01	−0.03
	0.07	0.08	0.08		1.0	0.18	0.03	−0.02	−0.14	−0.08	−0.71	0.16
	0.01	0.08	0.02		0.18	1.0	−0.03	0.08	0.03	0.01	−0.15	0.91
Analysis	0.96	−0.07	−0.03		0.03	−0.03	0.97	−0.01	0.01	0.02	0.10	0.05
	0.11	0.98	0.14		−0.02	0.08	−0.01	1.00	0.00	0.01	0.00	0.00
	0.07	0.11	−0.94		−0.14	0.03	0.01	0.00	1.00	0.02	−0.01	0.00
	−0.05	0.05	0.04		−0.08	0.01	0.02	0.01	0.02	0.80	−0.08	−0.04
	0.11	−0.04	−0.01		−0.71	−0.15	0.10	0.00	−0.01	−0.08	0.96	−0.02
	0.06	−0.01	−0.03		0.16	0.91	0.05	0.00	0.00	−0.04	−0.02	0.99

[a]Mode not verified by test.

Another measure of the comparison of the test results to analysis is the degree to which the test analytic coupling partition of the mass matrix approaches a unit matrix (Table 18); negative values on the diagonal imply only negative normalization. The decoupling exhibited by the analytic fourth mode and the test modes is an excellent indication of the existence of a highly damped mode that was impossible to excite with two shakers during the modal test.

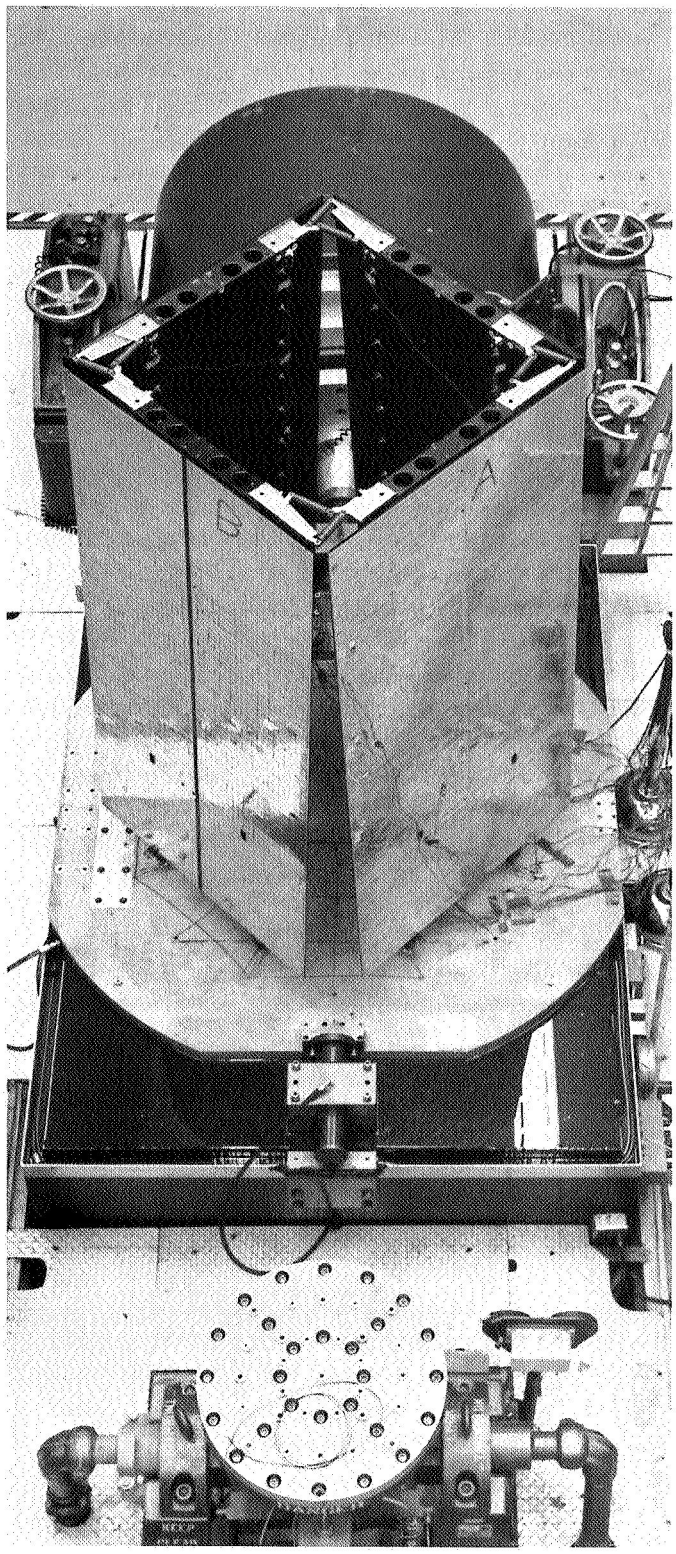

Fig. 45. Solar-panel latching feasibility test setup

c. Latching feasibility test.

Description. Early in the program, tests were conducted with four *Mariner* Mars 1964 panels that had dummy cells; these were modified to include tip latching to verify the suitability of such a latching scheme. The modifications were such that the line of action of the tip spring dampers was the same as that for the *Mariner* Venus 67 configuration. The four panels were mounted to a slider plate (Fig. 45) and excitation was introduced parallel to two panels and perpendicular to the other two. The attitude control jets and cabling were not simulated. The configuration was tested at

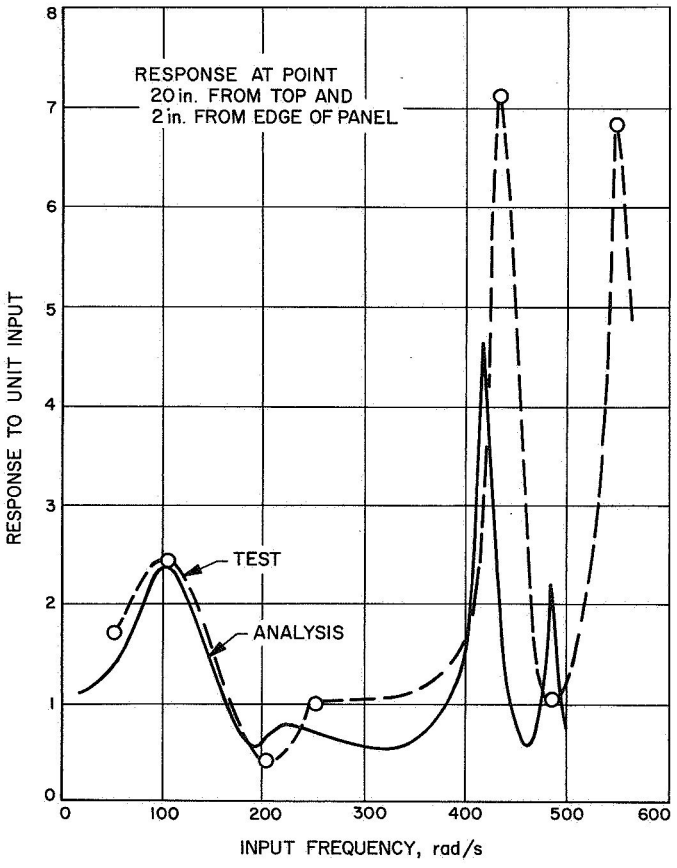

Fig. 46. Response of tip-latched *Mariner* Mars 1964 solar panels to unit acceleration

various levels up to the *Mariner* Mars 1964 structure type-approval dynamic test level in the lateral direction. Additional tests were conducted at an angle of 45 deg to the panels.

Test results. The test results were compared with analytical results in Fig. 46. The comparison between analysis and test was very good at low frequencies where the model was good.

The test demonstrated the soundness of the tip latching and damping approach and provided experimental verification of the suitability of the solar panel analysis approach.

d. Rod-end-monoball conductance test.

Description. A thermal vacuum test was conducted on August 9 and 10, 1966, to determine the thermal resistance of the monoball joint used to attach the solar

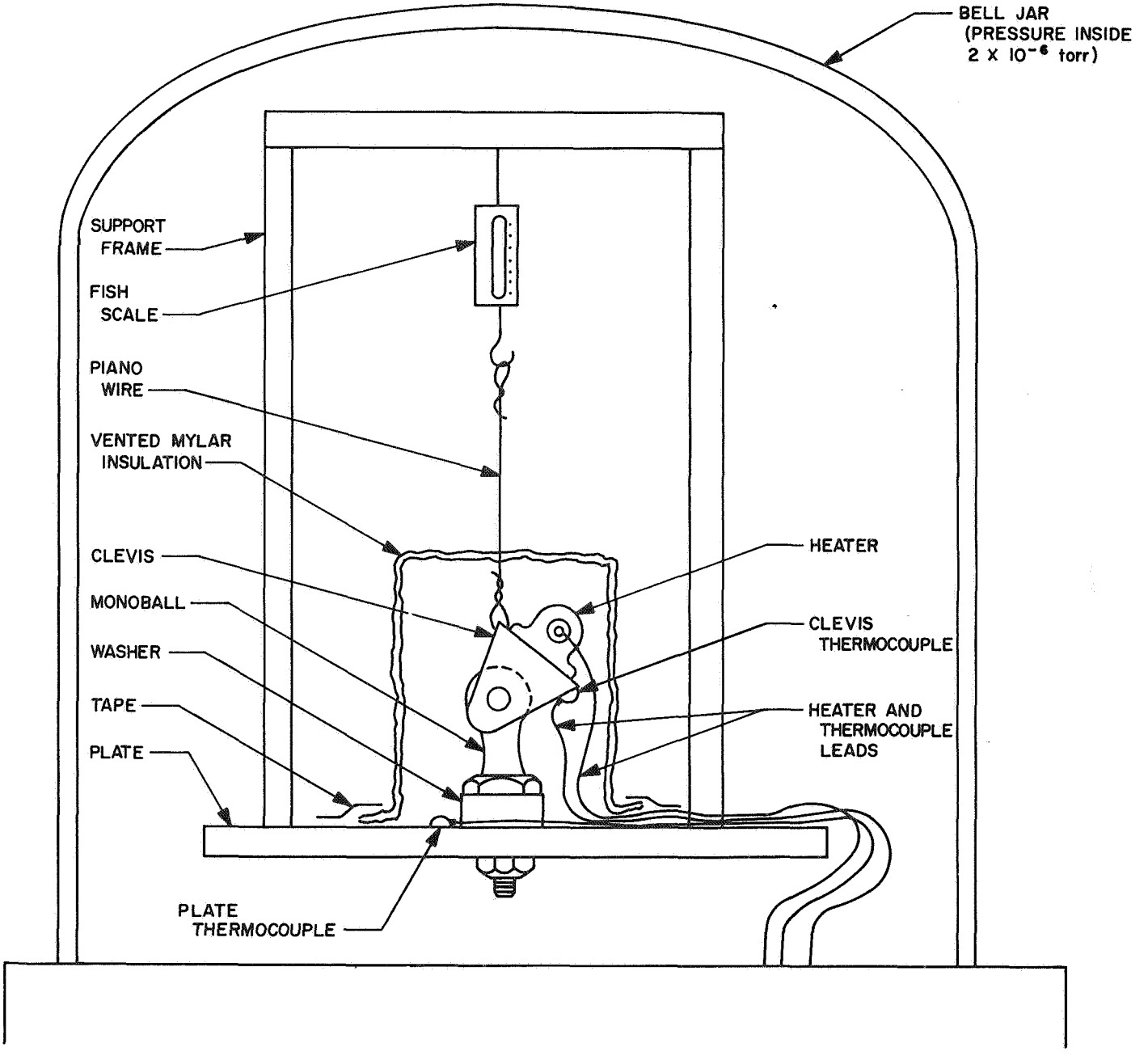

Fig. 47. Rod-end-monoball conductance test setup

panels to the bus. These data were to be used in evaluating TCM and flight spacecraft test errors caused by the use of dummy solar panels. The test setup used is shown in Fig. 47.

Test results. Data acquired from the test are given in Tables 19 and 20.

With the assumption of the heat transfer model shown below, the results are as follows:

Table 19. Thermal conductance of monoball joint

Mode	Monoball	Load, lb	E, V	I, A	Temperature, °F	
					Clevis	Plate
1	Mariner Venus 67	25	5.005	0.0499	74	51
2		25	10.003	0.0999	133	51
3		0	5.003	0.0499	80	51
4		0	10.003	0.1000	163	51
5	No Bolt	0	5.000	0.0499	118	51
6	Mariner Mars 1964	0	5.000	0.0499	84	51
7		0	10.004	0.1000	171	51

[a]Mariner Mars 1964 monoballs were used on the Mariner Venus 67 TCM.

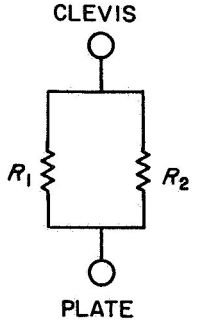

R_1 is the thermal resistance of the path from clevis-to-bolt-to-monoball-to-plate.

R_2 is the thermal resistance of the thermocouple and heater leads.

$$R = \frac{\Delta T}{q}$$

$$R_1 = \frac{R_2 R_{TOT}}{R_2 - R_{TOT}}$$

Table 20. Thermal resistance of monoball joint

Monoball	Load, lb	Thermal resistance, °F/W		
		R_{TOT}	R_2	R_1
Mariner Venus 67	25	92.2	268.5	140.4
	25	82.1	268.5	118.3
	0	116.2	268.5	204.9
	0	112.0	268.5	192.2
Mariner Mars 1964	0	132.3	268.5	260.8
	0	120.0	268.5	217.0

Conclusions. The use of *Mariner* Mars 1964 monoballs on the *Mariner* Venus 67 TCM caused a negligible decrease in thermal coupling between bus and panels. However, the total coupling is sufficiently large that flight spacecraft test data must be corrected for the effect of coupling the bus with the attitude control gas handling frames across these joints.

3. High-gain antenna and superstructure vibration test. The *Mariner V* spacecraft requirement of a two-position high-gain antenna with different pointing geometry necessitated the design of a new superstructure. In the new design, the antenna was attached to the superstructure at three locations – two were hinge points, one was a pyrotechnic pinpuller attachment. A test was conducted to determine the dynamic response characteristics of the new superstructure and the high-gain antenna.

a. Test description. A prototype high-gain antenna and superstructure, together with simulated pyrotechnics and associated hardware, was mounted to a slider plate (Fig. 48). Excitation was introduced along the spacecraft *X*, *X–Y*, and *Z* axes. The configuration was tested to the same input test levels as the *Mariner* Venus 67 STM.

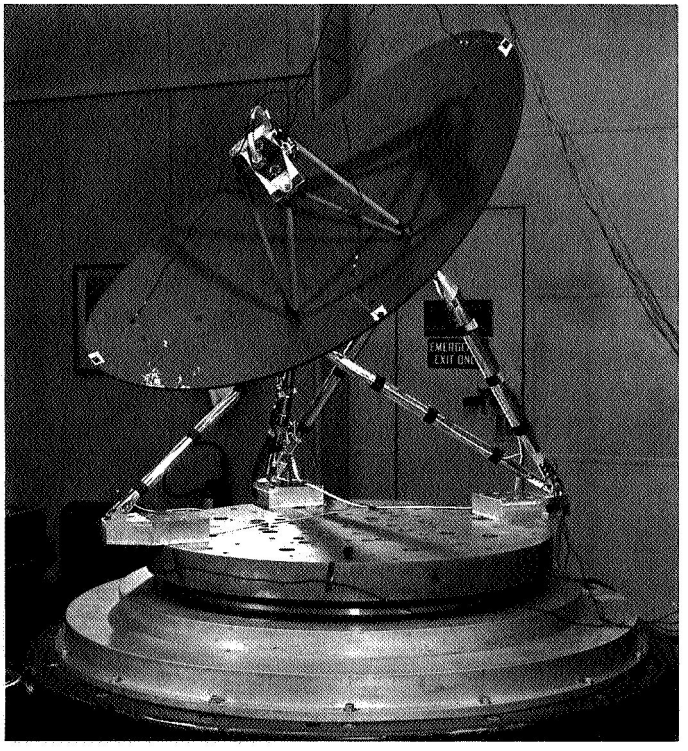

Fig. 48. High-gain antenna and superstructure vibration test setup

b. Test results. The axial loads measured in the superstructure were low, as expected, since the tubes were designed for local member resonance above 150 Hz. Designing for high, local-member resonance increased the diameter of the tube, which increased the area of the tube and decreased the axial load. The most pertinent part of the test was the high-acceleration response at the tip of the antenna dish. The response at the tip of the antenna for the first and second elastic bending modes is given in Table 21. The corresponding analytical results for the response at the tip of the antenna were 20 to 30% higher; however, this is reasonable since such a lightweight parabolic shell structure as the antenna is very difficult to analyze theoretically.

Table 21. Response levels of the tip of the high-gain antenna

Frequency of excitation, Hz	Input acceleration level and axis of excitation, g		
	1.0 g X-axis	1.0 g Z-axis	2.0 g Z-axis
114.0	22.0	25.0	27.0
127.0	27.6	48.0	88.0

4. High-gain-antenna low-temperature deployment testing. During the low temperature-vacuum type approval testing, to verify the high-gain-antenna deployment mechanism operation, a series of failures occurred. This resulted in an investigation of the flexible coaxial cable routing, across the antenna deployment hinge, and deployment torque requirements.

The purpose of this test was to determine the proper coaxial cable routing across the antenna deployment hinge (for minimum torque requirements) to determine the required torque, and to verify the total system met the design requirements.

a. Test configuration. The thermal–vacuum development testing of the antenna deployment mechanism was performed on a fixture that mounted the antenna-superstructure assembly in a 6-ft-diam cold-wall vacuum chamber (Fig. 49). The mounting fixture was oriented with the antenna hinge axis vertical, simulating a *zero* gravity condition. The RF energy supplied to the antenna was such that the flexible cable would be heated slightly by internal RF losses. Antenna deployment was initiated by firing a pinpuller (as in the flight configuration), and the elapsed time of deployment was recorded.

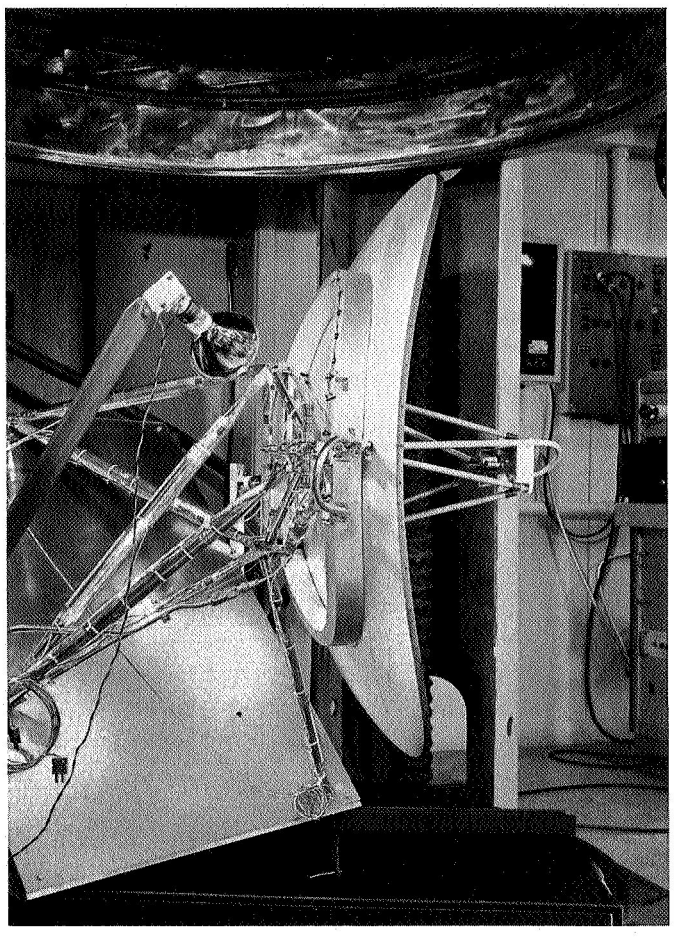

Fig. 49. High-gain antenna low-temperature-deployment test setup

Double-exposure photographs were made to study the displacement and configuration of the cable during the action, and they were used in conjunction with visual observation of the antenna deployment at the low temperatures to determine the best cable routing.

b. Test results. At the subsystem level, as a result of the developmental testing, it was learned the deployment springs were required to deliver a force of 12 in.-lb, which was more torque than was desired from design safety considerations. To ensure an adequate safety margin, the spring size was increased to deliver 16 in.-lb. Type approval testing following the modification was successful with a 250-ms deployment time at −230°F, as compared with a 200-ms deployment time at room temperature.

At the system level, a final FA cold-temperature antenna deployment was successfully performed on the spacecraft during the spacecraft thermal–vacuum test.

Because of the spacecraft orientation during the test, it was necessary to counterbalance the antenna to simulate a *zero* gravity condition. This test evaluated the pyrotechnic latch and antenna-deployment mechanism as an integral system.

5. Low-gain-antenna cable-clamp bonding test. During the low-gain antenna low-temperature TA testing, a portion of the epoxy-bonded viton cable clamps became detached from the antenna mast at −200°F. More exploratory testing was performed to understand the problem fully and to investigate possible solutions.

a. Test configuration. A test specimen was prepared, consisting of a short section of low-gain antenna mast to which viton cable clamps were attached with EC1614, EC2216,[12] and RTV 60[13] adhesives. Half of the EC1614 and EC2216 bonds were applied to the surface that was only cleaned. The other half were applied to the surface prepared with Bond Etch. The specimen was placed in a cold chamber and the temperature lowered from −125 to −250°F in 25°F increments, and at each step, the sample was observed to study any possible failures.

b. Results and conclusions. The test indicated no failure at temperatures above −200°F; the only failure during the test sequence occurred at −225°F with a clamp bonded with EC1614 on an unetched surface.

The test results indicated a potential problem with the flight antennas if the surface beneath the clamps had not been properly prepared. Since it was not possible to remove the clamps from the antenna without doing damage to the mast, a decision was made to rebond only those clamps that failed during testing. If any subsequent failures had occurred, it would have been repaired with EC2216 after proper surface preparation.

There were no clamp failures during subsequent low-temperature antenna FA system-level tests.

6. DFR 423-MHz antenna vibration test.

a. Test description. The objective of the test was to determine the dynamic response characteristics of the 423-MHz antenna test specimen. The specimen, which was identical in stiffness and mass distribution to the flight hardware, was mounted to a rigid fixture that, in turn, was mounted to a vibration exciter (Fig. 50). Excitation was introduced to the test structure along three orthogonal axes. The dynamic response was measured with small piezoelectric accelerometers mounted at the top of the main mast. Acceleration excitation input levels were derived from the results of the STM vibration test.

b. Test results. The discrete resonant frequencies of the DFR were separated from the response modes of the solar panel structure that were determined during the STM test. The antenna dynamic excursions were not large enough to violate the spacecraft dynamic envelope. The results from the development test verified the structural adequacy of the design.

7. Temperature-control-reference tests.

a. Vibration tests. The objective of these tests was to determine dynamic response characteristics and structural integrity of TCR design.

Description. The tests were conducted on a unit of standard construction – the same as that used for flight – and on a lightweight version.

The setup was mounted on a MB70 shaker; excited normal to the flat sensing area. Four test runs in

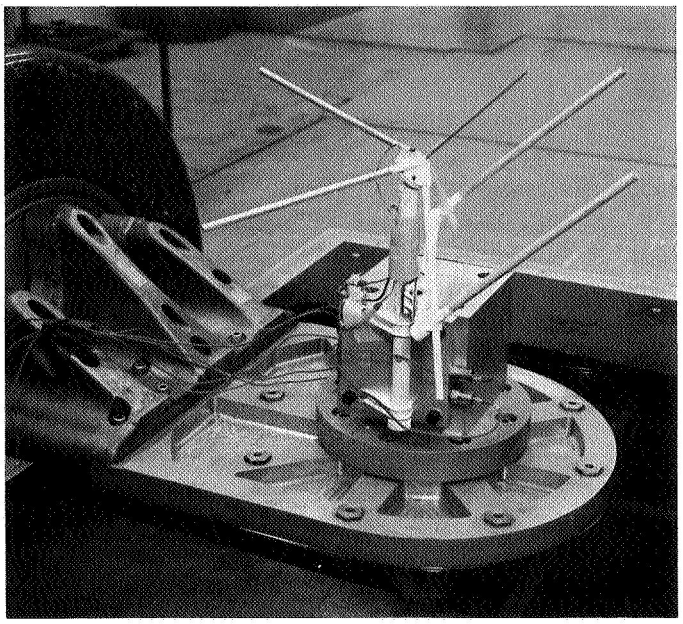

Fig. 50. Dual-frequency receiver vibration test setup

[12]EC1614 and EC2216 are Scotchweld epoxies, manufactured by Minnesota Mining.

[13]RTV 60 is room-temperature vulcanizing adhesive manufactured by General Electric.

frequency ranges between 20 and 400 Hz and in acceleration levels from 1 to 12 g were executed:

(1) Sweep 20 to 400 Hz at 1 g rms to determine resonant band.

(2) Sweep 20 to 55 Hz at 12 g rms, and
75 to 400 Hz at 12 g rms.

(3) Sweep 55 to 75 Hz at 2 g rms.

(4) Sweep 55 to 75 Hz at 2, 3, 4, 6, and 8 g rms to failure.

Results. There were two principal findings: (1) Structural integrity of TCR was more than sufficient. Larger excursion for the lightweight structure presented potential hazard to lead wires. (2) Resonant frequencies were not expected to couple with solar panels.

b. Thermal tests.

Developmental tests. A series of tests was conducted in the 2-ft diam horizontal chamber using a liquid nitrogen cold-wall, a quartz window and the spectrolab solar simulator. The test setup shown in Figs. 51 and 52 was also used for FA thermal–vacuum testing of the flight units.

The deviation of the sensor temperature from the true average of front and back temperatures was determined at various intensities by determining the equilibrium sensor temperature alternately illuminating the assembly from the front and back sides.

It was originally intended that the horizontal chamber tests and the FA tests provide a correlatable calibration comparison to the cone radiometer, as well as refine the edge-loss effects. Neither of these objectives was possible because of nonuniformities in the simulator beam at the test plane. Therefore, the best correlation with the cone or other instrumentation can be drawn from the radiometer comparison test (see Appendix E). The insignificance of the conduction along the web of the assembly was experimentally verified during the horizontal chamber test. With the 12-in.-diam simulator beam at 100 W/ft² illuminating all except the TCR bracket, the assembly was allowed to come to thermal equilibrium. A mask was then placed in the beam, external to the chamber, shadowing the support web down to approximately 3/4 in. from the 3-in. OD of the TCR sensor area. This masking produced a penumbra (partially shaded) area down to the 3-in. diameter. With this shadowing, the equilibrium sensor temperature was 2.5°F lower than the fully illuminated equilibrium temperature.

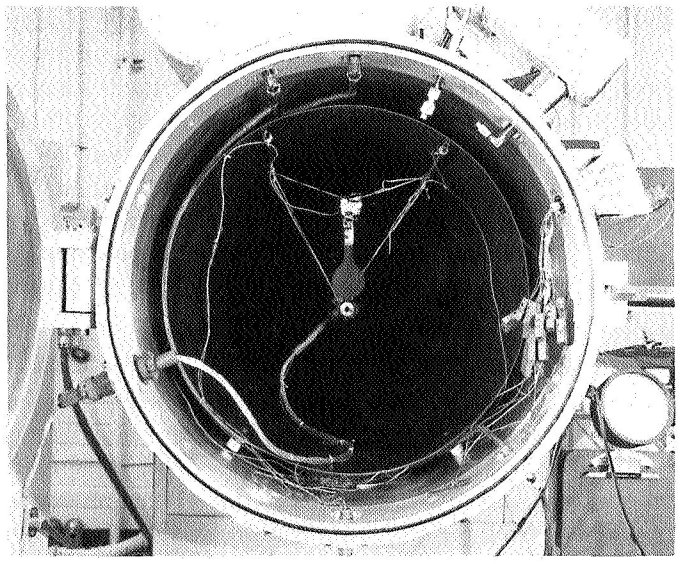

Fig. 51. Temperature-control reference test setup

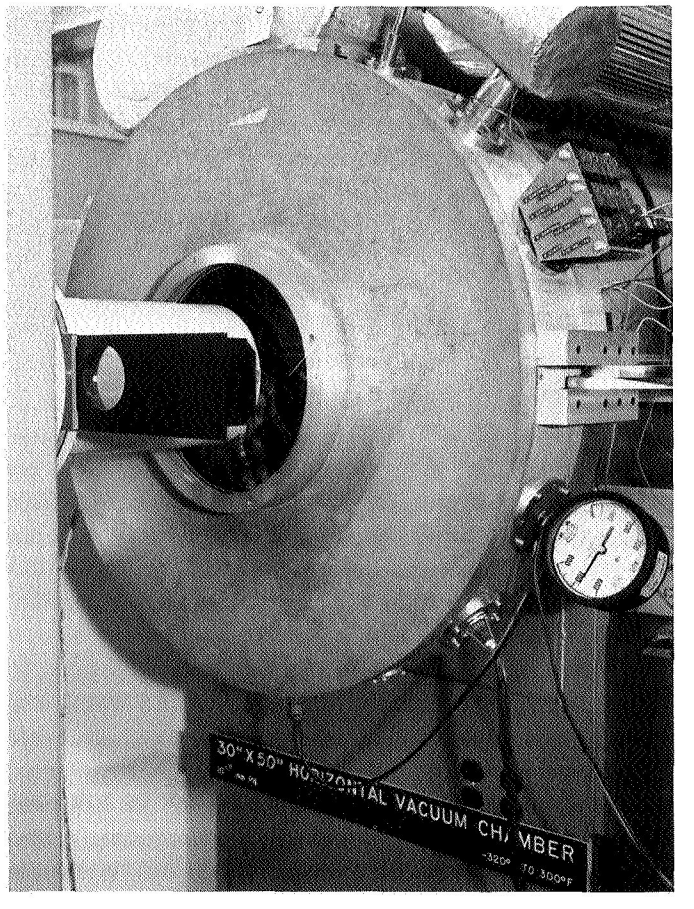

Fig. 52. TCR mounted in cold-wall chamber

An externally controlled heater was installed on the supporting equipment to permit varying the TCR bracket temperature. Varying the temperature of the bracket from −114 to ±150°F produced a 0.1°F increase in the sensor temperature, clearly demonstrating that excessive decoupling had been achieved.

Performance of TCR was verified and additional information necessary for flight data analysis was obtained.

Prototype test. A thermal prototype TCR mechanically similar to the final flight configuration, but containing thermocouples (resistance elements were not yet available), was included in the thermal test of the *Mariner* Venus 67 TA solar panel in the 10-ft simulator. This prototype included an aluminum-foil disk to provide temperature uniformity across the sensor surface. Following a scheduled thermal-shock cycle, temperature deviated substantially from the expected. When the panel was removed for some rework, it was noted that the aluminum foil had delaminated from the TCR assembly. When the foil was removed, there was evidence of air pockets under the foil. The foil was replaced with stainless mesh (no copper mesh was available), the assembly recoated and returned to the test along with the solar panel. Performance during the remainder of the solar-panel TA thermal test was nominal, including survival of a severe unscheduled thermal shock due to a complete electrical loss which resulted in the loss of the chamber lights.

In summary, aluminum foil was unsatisfactory; however, satisfactory performance of wire mesh was verified.

c. Sensor stability test. During the *Mariner V* mission, it was noted that annealing of platinum elements occurred during testing of some of the *Mariner* 1969 temperature-control flux monitor (TCFM) sensors. Since the effect of such annealing on the TCR flight data would be to produce an apparent bleaching, a stability test was initiated.

A prototype TCR (SN 22) that contained a sensor element from the same manufacturer's lot as that in the *Mariner V* black TCR (SN 19) was used. Since the initial assembly calibration, October 25, 1966, SN 22 has been used for a series of developmental tests including a 24-h total solar simulation in vacuum at various intensities and an additional approximately 24 h in vacuum without simulation.

The assembly was installed in the constant temperature oven in the JPL Standards Laboratory on July 31, 1967, and room temperature resistance was measured. Heat soak was initiated at 14:00 on that day and terminated at approximately 08:00 on August 4. No drift of resistivity was detected, and sensor-indicated temperature agreed with measured, control temperature at the initial ambient test and throughout the heat soak to within <0.1°C. To be responsible for the apparent degradation of the black TCR, a drift of the order of 1 Ω would be required during the time period of the test.

No evidence of sensor instability was found nor could it be inferred from the test.

8. Thermal-blanket-ballooning test.

a. Description. A series of tests were performed to verify the venting provisions in the multilayer Mylar upper and lower thermal blankets. The JPL 7- × 14-ft vacuum chamber was used for the test. Motion-picture and still-camera coverage was used to record shield behavior. Results verified that the shields were not damaged by the launch pressure profile and that possible ballooning will not interfere with such other spacecraft components as celestial sensors and science instruments or with such functions as solar-panel deployment and sunshade deployment.

b. Test summary. The STM upper and lower thermal C-102 shields were installed on the TCM bus and placed in the chamber with the Z axis horizontal and the bay 2 shear web installed to investigate any bus cavity venting problem. Six pumpdowns were performed, four of these were the 110-s profile of Fig. 53 and two more margin tests at the 80-s profile. Figure 54 shows the upper shield at atmospheric pressure of approximately 725 torr before the pumpdown; Fig. 55 shows the upper shield at 40 torr on an 80-s-profile margin test. Continuous motion pictures, at 24 frames/s, and still pictures, at approximately 200 torr intervals, were taken on three runs for each shield.

c. Conclusions. The photographs and visual inspection during and after the test revealed no problems in the shield venting provisions. The shields ballooned, as expected, and returned to a nominal position after each pumpdown. The 80-s-profile margin tests were conservative when compared with actual *Mariner IV* shroud cavity data, and no potential ballooning problems were indicated by these tests.

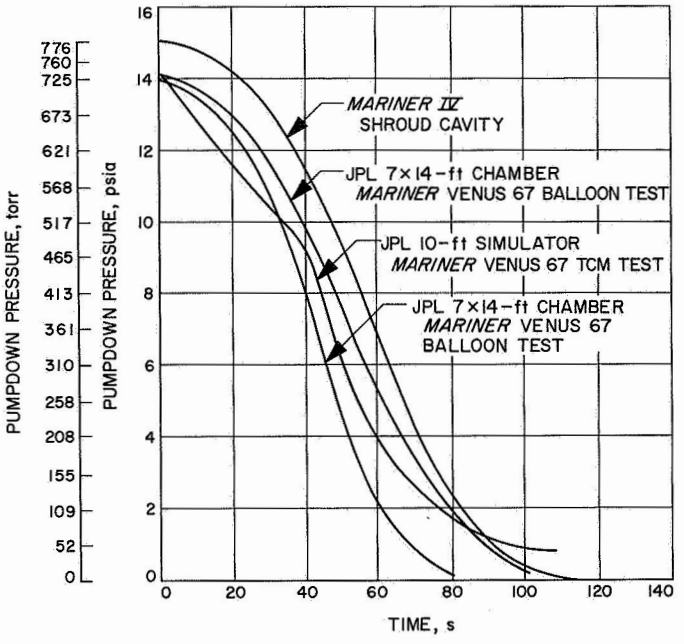

Fig. 53. Boost-environment pressure-decay curves

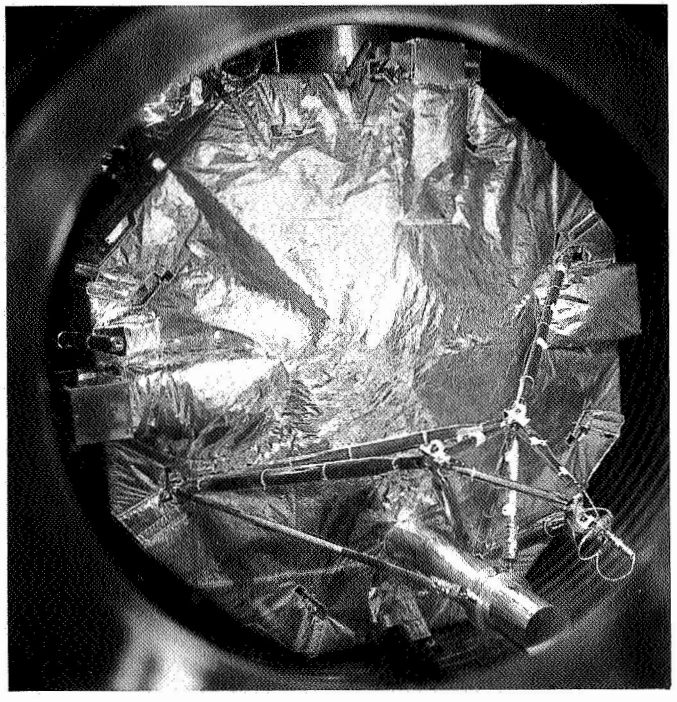

Fig. 54. Thermal-blanket ballooning test: upper thermal shield prior to pumpdown at 725 torr

9. *Magnetometer-sensor thermal tests.* Two separate thermal tests of the magnetometer were performed in small vacuum chambers. One test was carried out with cold walls, only, to empirically obtain a suitable thermal

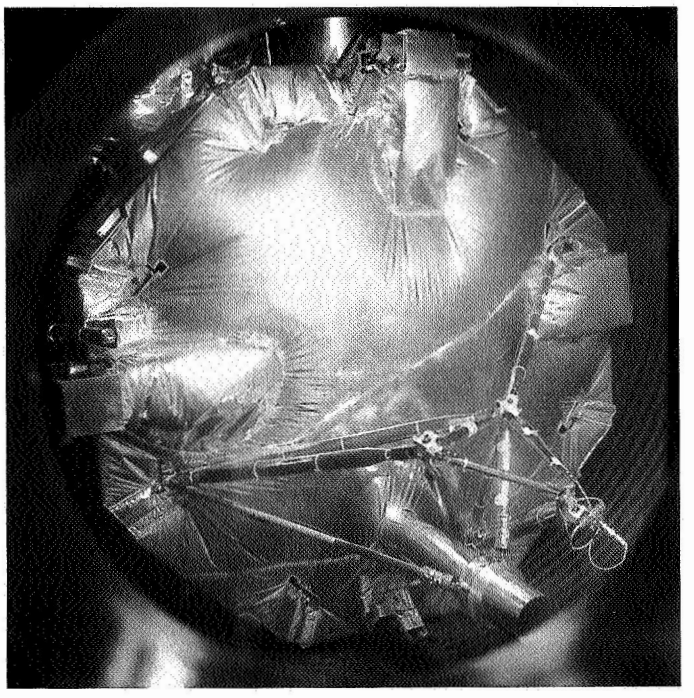

Fig. 55. Thermal blanket ballooning test: upper thermal shield at 40 torr on 80-s profile

design. The second test included solar simulation and was intended to establish the transient response of the sensor during sunlit midcourse maneuvers.

a. Temperature control test. The test objective was twofold: (1) to determine the magnitudes of the various parameters which affect the sensor heat balance in a flight-like environment; and (2) to minimize the thermal sensitivity of the sensor to solar inputs during a midcourse maneuver, to uncertainties in sensor heater power, to uncertainties in the equivalent black-emitting area of the sensor (emissivity ε and absorptivity α product), and to temperature uncertainties and excursions of the sensor mounting bracket.

Test configuration. The TCM magnetometer sensor was mounted in a flight-like configuration on an 18-in. section of omnidirectional antenna. This test package was then mounted in a 24- × 36-in. bell jar equipped with LN_2 cold walls (Fig. 56). Resistance heaters placed at appropriate locations within the sensor served as simulators for the temperature-control heater and the sensor electronics. A radiant heater was suspended within the mast to maintain the mast temperature at desired levels.

Test procedure. The variable parameters of interest were the conductive coupling between the sensor and

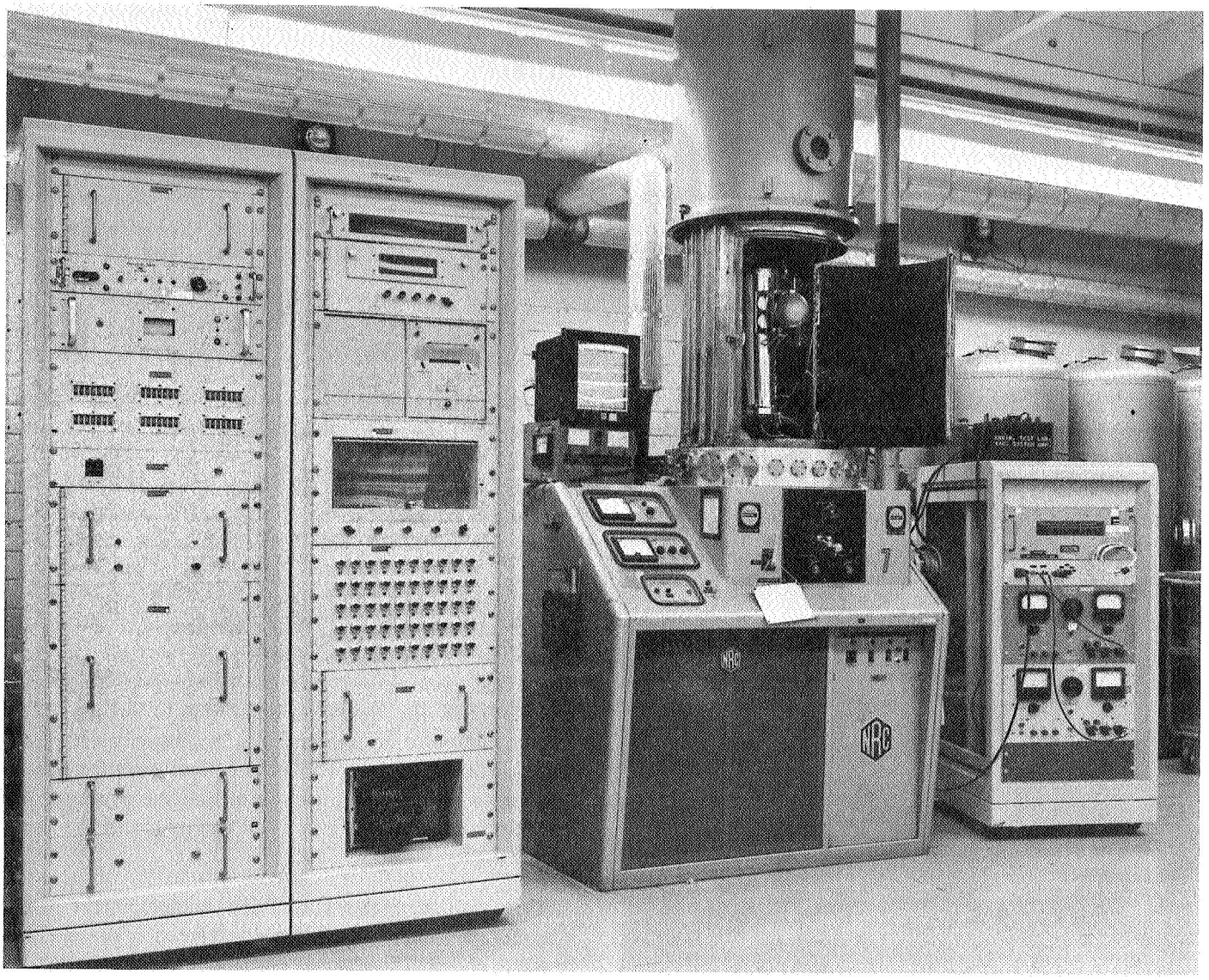

Fig. 56. TCM magnetometer sensor test setup

mounting bracket, the equivalent black emitting area of the sensor, and the power dissipated in the temperature-control heater.

With heater power as the independent parameter and the $\varepsilon\alpha$ product held constant, several test modes were run with variation only in the size and material of the thermal standoffs mounted between the sensor and the bracket. The standoffs that allowed negligible heat losses were then incorporated into the configuration.

The next series of test modes involved increasing the $\varepsilon\alpha$ product by means of PV-100 white paint[14] until the steady-state sensor temperature dropped to the proper level with 3 W of heater power. By raising the heater power and, consequently, increasing the $\varepsilon\alpha$ product, the sensor temperature becomes less sensitive to such perturbations as solar inputs during a midcourse maneuver. Also, percentage uncertainties in both the heater power and the $\varepsilon\alpha$ product are decreased. Since the emittance of PV-100 is well established and very reproducible, the effect of thermo-optical dissimilarities between the TCM sensor and the flight units is minimized.

To maintain a low-emittance surface on the epoxy sphere housing the Helmholz coil (the vacuum-deposited aluminum surface was beginning to degrade due to overhandling), a multilayer Teflon-Mylar thermal shield covering the sphere was installed. (This shield also helps to minimize solar inputs.) The final series of test modes involved altering the $\varepsilon\alpha$ product slightly to account for this modification.

Test results and conclusions. Test data indicated the optimum thermal configuration included a 3/8-in.-diam × 1/4-in. Kel-F washer between the sensor and mounting bracket with 3/8-in.-diam × 1/8-in. Kel-F washers under the bolt heads; 7.4 in.^{2} of PV-100 white paint on the ignitor housing; and a multilayer, aluminized Mylar shield with an aluminized Teflon facing covering the epoxy sphere that houses the Helmholz coil.

In flight, the solar panels provide raw dc power to the sensor heater. The panel voltage varies such that the heater power ranges from 3.0 W at earth to 2.19 W at Venus. For these power levels, the steady-state average sensor temperatures in the bell jar were 12 and −10°F, respectively. After correcting this data for the differences between the bell jar and space, the average sensor temperatures expected in flight became 12°F at earth intensities and −9°F at Venus intensities.

b. Midcourse thermal simulation test. The test objective was to determine the worst-case temperature response of the sensor to solar irradiation of known intensity.

Test configuration. The test package was essentially the same as that used for the magnetometer-sensor temperature-control test, namely, the TCM sensor mounted in a flight-like configuration on a short section of the omnidirectional antenna mast. The thermal configuration of the sensor itself was: 7.4 in.^{2} of PV-100 white paint on the ignitor housing; a multilayer aluminized Mylar insulation shield faced with aluminized Teflon covering the epoxy sphere which housed the Helmholz coil; and resistance heaters in the sensor to simulate the temperature-control heater and the sensor electronics. This was the optimum thermal configuration as determined by the initial magnetometer-sensor temperature-control test.

The test package (Fig. 57) was suspended in a 30 × 50-in. vacuum chamber equipped with LN_2 cold walls, along with an absolute cone radiometer (ACRAD) with which to accurately monitor the intensity of the simulated solar beam.

The test package was aligned with the 12-in.-diam quartz window in the end bell of the chamber such that the spectrolab portable solar source, positioned outside the chamber, would illuminate the entire sensor, the radiometer, and as much of the mast as possible. The sensor was suspended in what was estimated as the worst-case orientation with respect to the simulated solar beam — in other words, the sensor presented a maximum cross-sectional area to the beam.

Test procedure. Three test modes were run, one at an intensity of 65 mW/cm^2 (0.48 solar constant) and two at an intensity of 110 mW/cm^2 (0.81 solar constants). For one high- and one low-intensity mode, the lamp was turned *on* after the sensor temperatures had steadied out at earth cruise levels. The second high-intensity mode simulated a science-*off* maneuver. For this mode, once the sensor temperatures had steadied out, the power to the heater representing the sensor electronics was turned off for a 1-h period prior to turning the lamp *on*.

[14]Generic name for silicone white-solar-reflector temperature-control coating.

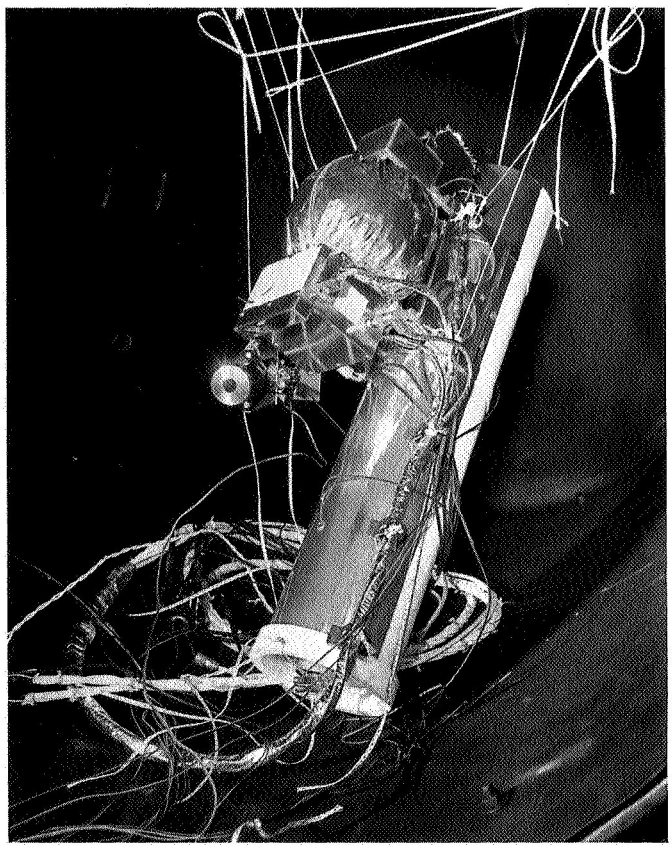

Fig. 57. Magnetometer sensor suspended in vacuum chamber

To accurately determine the simulated solar intensity at the test package, it was necessary to determine both the uniformity of the beam and the magnitude of any extraneous IR inputs to the radiometer due to the fact that neither the 12-in.-diam quartz window nor the end plate containing the window were directly LN_2 cooled.

The spatial variation of intensity through the beam was determined at the plane of the test package for both intensity levels by positioning a single, solar cell at various locations in the beam and accurately monitoring its output voltage. The data so acquired yielded the average intensity of the beam relative to the intensity measured by the radiometer.

The magnitude of background IR radiation present in the chamber was determined by taking two radiometer tares (intensity measurements with the lamp *off*). By taking one tare after the lamp had been *off* for a long period of time and another after the lamp had been *on* at maximum intensity for a considerable length of time, the significance of a *cold* or *hot* quartz window was also assessed. This difference was found to be negligible.

Test results and recommendations. Since the maximum intensity which the spectrolab solar source could provide was only 0.8 solar constants, it was necessary to extrapolate the test data to obtain worst-case transient information for both earth and Venus maneuvers. The data indicated that if the sensor were to remain fixed with respect to the sun for a period of 1 h in the worst case orientation, the sensor temperature would be 72°F at earth and 128°F at Venus intensities respectively. Although extrapolation tends to amplify any test errors or uncertainties, these numbers are felt to be accurate to within ±10°F at earth and ±30°F at Venus intensities.

The spectrolab portable solar source was found to be both convenient and appropriate for this type of test. Although its maximum capability of 0.8 solar constants in an 11-in.-diam beam, or approximately 1.7 solar constants in a 6-in.-diam beam, is something less than desirable, it remains a very useful tool for developmental tests of small sun-dependent or sun-prone components.

10. Data-automation-system 7-in. subchassis vibration test. To obtain the increased volume necessary for the new DAS subsystem design selected, the subchassis height was increased to 7 in. As a result of the combination of this increased cantilevered height, four large connector cutouts in the top subchassis web and the subchassis loading, the project packaging requirement for a 400-Hz minimum resonance in vibration was not met.

a. Test description. Several vibration tests were made to establish the best configuration to accomplish this requirement. Three test subassemblies configurations were made:

Test subassembly 1. The standard subchassis with increased height described in Figs. 58 and 62, configuration A.

Test subassembly 2. Similar to test subassembly 1, modified per Fig. 59, configuration B.

Test subassembly 3. Similar to test subassembly 1, modified per Fig. 59, configuration C.

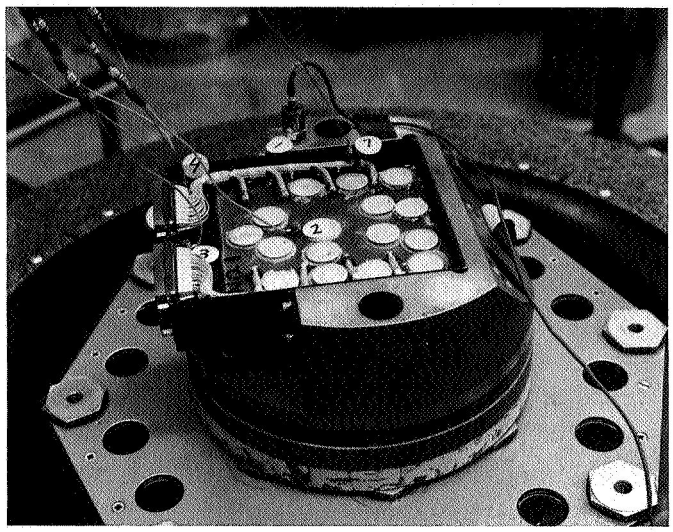

Fig. 58. Data automation system 7-in. chassis vibration test setup

Four, wired connectors were installed, and a simulated epoxy glass terminal board with dummy weights was bonded to the subchassis to make simulated a 1.5-lb subassembly. Accelerometers monitored the table input (location 1), the top of the subchassis between the connectors (location 2), and the center of subchassis between the mounting ears (location 3).

Table 22. Results of 7-in.-high subassembly vibration tests

Subchassis configuration	Number of screws in each mounting ear	Monitor location	Resonance, Hz and gain	
			1st	2nd
1	1	2	290/5.1	580/6.0
		3	290/7.6	570/3.6
1	2	2	390/2.5	650/9.5
		3	396/3.3	660/2.8
2	1	2	310/5.4	780/14.5
		3	310/1.6	780/11.5
3	1	2	320/4.7	750/10.7
		3	320/4.7	740/4.7
3	2	2	480/3.1	810/5.4
		3	480/6.4	810/3.2
3 (With dummy cable load)	2	2	480/1.8	800/7.5
		3	400/4.4	800/7.5

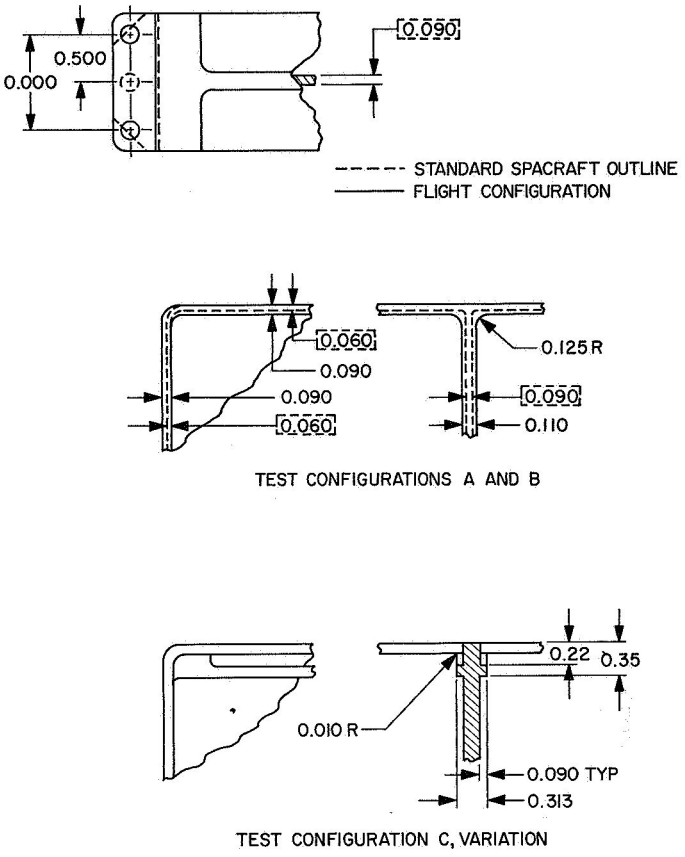

Fig. 59. Variations to 7-in. DAS subchassis

Tests were made using the three configurations with variations in the number of screws in the mounting ears. Only the axis perpendicular to the plane of the subchassis web were run for comparative worst-case comparisons. Test results are summarized in Table 22.

b. Results. As a result of the tests, the following changes were made to the standard subchassis for the DAS: two screws in each mounting ear, the top flange and the side flanges above the mounting ears increase 0.030 to 0.090 in., fillet radius between top flange and center web increased from 0.010 to 0.125 in. and each side of center web thickness increased 0.010 in. This increased the resonance to 480 Hz with a gain of 3.1. The old resonance was 290 Hz, with a gain of 5.1.

11. Plasma-probe cup-temperature test.

a. Objective. A developmental test was performed on the *Mariner IV* plasma probe unit (MC-3) to determine if the expected TA temperature levels would reduce the strength of the epoxy holding the collector plate to

the extent that arcing might occur. The test was also performed to determine the placement of the heat lamp from the front of the plasma probe cup such that there would be a 20°C difference in temperature between the collector plate and the outside wall of the cup, because a thermocouple could not be placed on the collector plate of the TA or flight units.

b. Description. The test was performed according to the general assembly level TA test specification, with the exception that the heat lamp distance was determined according to the above objective. The test was performed at JPL in a 30- × 50-in. horizontal chamber. A photograph of the test setup is shown in Fig. 60.

c. Results. The distance from the rim of the reflector on the heat lamp to the foot of the plasma probe was determined to be 4.5 in. by stabilizing the outside wall of the plasma probe cup to 135°C (275°F) and the collector plate at 155°C (311°F). The lamp intensity setting to obtain these temperatures was 88% of full scale, and the shroud temperature of the chamber was at 162°F. The test ran at these temperatures for about 3 days, and no adverse effects to the plasma probe were noted, either during or after the test.

d. Significant findings. It should be pointed out that when the TA test was performed on the plasma probe, a visual inspection following the test showed that the solder connection on the high-voltage grid ring had diffused during the test. A subsequent investigation failed to reveal the exact cause of this occurrence, but on any future test run in this type of setup, one should be very cautious, especially regarding the temperature of the shroud, because it is one of the most critical parameters.

It is also important to point out that this setup was to determine TA temperatures and that a linear interpolation of lamp power to obtain the FA test temperatures is not valid because of the fact that the test temperature not only is a function of the power of the intensity setting but, also, of the chamber shroud temperature.

12. Radio-relays test. At the Cape, just prior to launch, a relay failure occurred in the M67-2 radio. It was necessary to replace the relay, but it was not possible to obtain a relay with the same mounting bracket. Because of the different mounting technique, TA vibration tests were performed at JPL on two radio relays (SNs 870537 and 870547) similar to those onboard the M67-2 flight spacecraft. These two relays were previously subjected to screening per JPL specification. This specification includes a vibration test in each of the three orthogonal axes, 20 *g* rms, 50 to 2000-Hz sinusoidal sweep, 5 min/plane with coils de-energized. As a point of interest, the manufacturer's catalog data specifies a 30 *g*, 10 to 5000 Hz capability, energized or de-energized, for these relays.

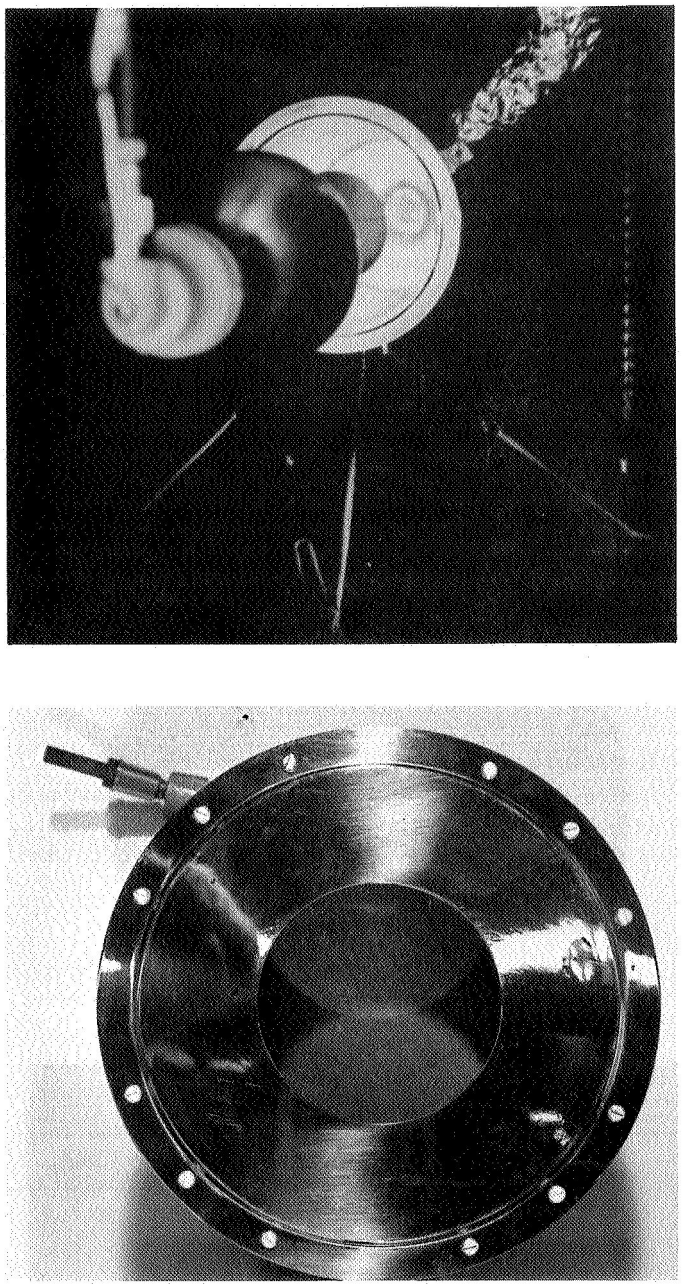

Fig. 60. Plasma probe test setup and plasma sensor

The relays were mounted in a dummy 2CC1 module in the same manner as was the relay in the flight radio—i.e., bonded and strapped. The dummy module was then mounted in a dummy radio case VI and placed on a vibration exciter. The relays were energized in the launch mode and a holding current of 13.5 mA was continuously applied. This simulates the actual conditions seen by the relay during the worst vibration of flight, which occurs during launch.

The two active contacts in each relay (four total) were current monitored (voltage drop across a resistance) on a 4-channel oscilloscope. The scope was externally triggered by sensing any current transient in the contact monitoring circuit in a leg common to all four contacts. The circuit values were adjusted so that approximately 21 V of triggering signal would be available should a contact open during vibration. The oscilloscope trigger was adjusted to its maximum sensitivity, about 1 V. This procedure assured reliable triggering in the event of contact chatter.

The relays were then vibration tested; two tests were completed for each orthogonal axis of the case. A high-frequency sinusoidal sweep at 2 octaves/min between 15 Hz and 2 kHz was performed at the following test levels: 2.0 *g* rms between 5 and 14 Hz; 9.0 *g* rms between 40 and 250 Hz; and 4.5 *g* rms between 250 and 2000 Hz. Random noise vibration followed with the TA shaped spectrum and a test level of 16.4 *g* rms. The final noise equalization plots were very accurate and well within the allowable test tolerances on the spectrum level of ±1.5 dB.

Relay circuitry was monitored during all testing to detect possible contact chatter. No chatter was detected and the test was completed without anomalies in the relay components.

13. Electron- and proton-radiation-test summary.

a. Electron radiation testing. Several *Mariner* Mars 1964 electronic subsystems were bombarded with 0.5 to 2.7 MeV electrons from a Dynamitron accelerator at fluxes in the range of 1×10^7 to 2×10^{11} electrons/cm²-s. Aluminum or copper foils were placed in the beam path upstream from the test item to scatter the beam uniformly (±20%) over the bombarded subsystem surface. The subsystems each exhibited a repeatable circuitry failure threshold. The failure thresholds

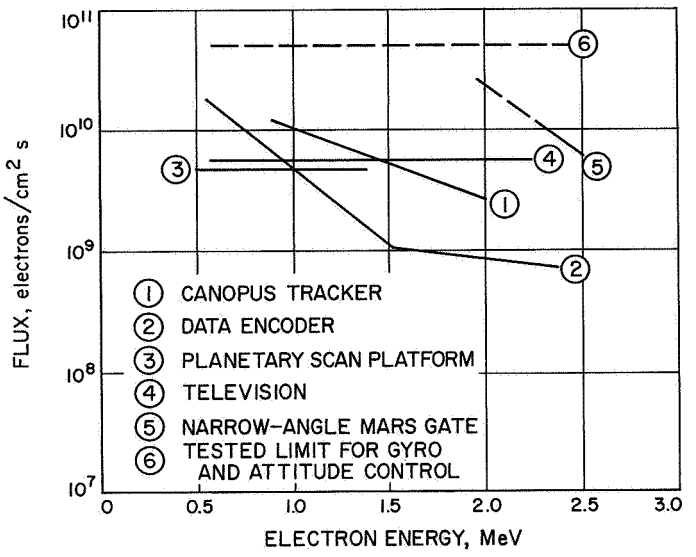

Fig. 61. Radiation thresholds of malfunction for various subsystems in test

were rather insensitive to either the electron energy or integrated flux, but very dependent on the flux rate. Failure thresholds for the subsystems tested ranged from 8×10^8 to 6×10^9 electrons/cm²-s. One subsystem was found to operate satisfactorily in a flux as high as 5×10^{10} electrons/cm²-s (see Fig. 61).

b. Proton radiation testing. The following *Mariner IV* components were irradiated with 20 to 137 MeV protons from the Harvard synchrocyclotron: (1) Canopus tracker, (2) data encoder, (3) squibs, (4) batteries, (5) solar cells, (6) central computer and sequencer circuitry, (7) sun sensor, (8) semiconductor devices and integrated circuits (Fig. 62). Flux rates used varied between 5×10^4 and 3×10^7 protons/cm²-s. All tested units were irradiated to an integrated flux of at least 2×10^{10} protons/cm². All components, except the solar cells and Canopus tracker, operated normally during irradiation. The power output of the solar cells permanently dropped to approximately 85% of the pre-irradiation value but was less than the predicted power loss. The tracker lost roll control at flux rates $>6 \times 10^5$ protons/cm²-s for energies >40 MeV, but recovered tracking ability immediately when the beam cut off, even after an integrated flux of 2.4×10^{10} protons/cm². Consequently, a high-energy, high-intensity solar flare could degrade tracker operation to a marginal region, but the system will recover after the flare. The tracker sensitivity was found to be due to an induced radioactivity in the image dissector tube (see Table 23).

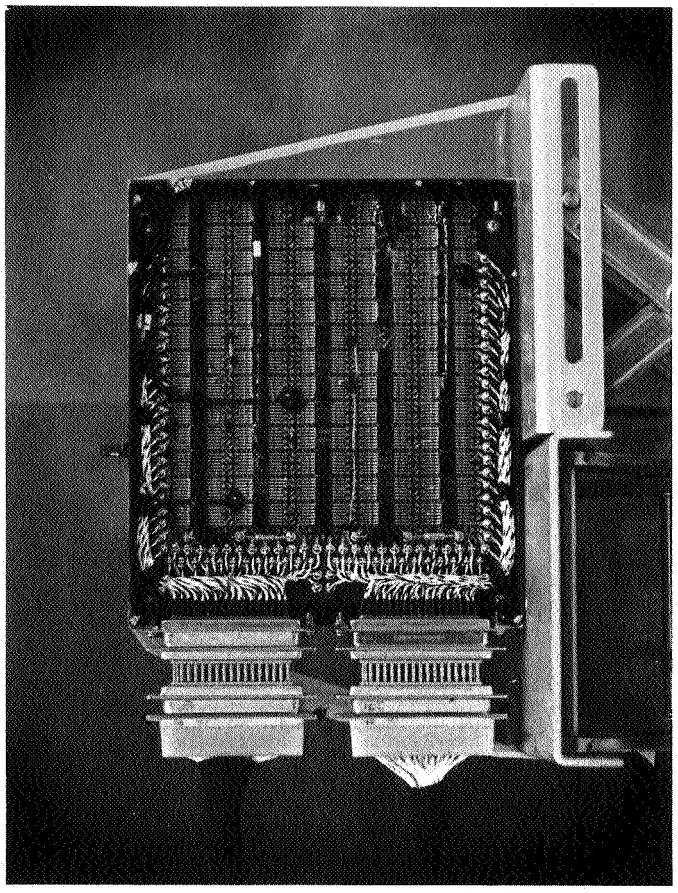

Fig. 62. Test setup for proton radiation of integrated circuits

C. Other Special and Developmental Testing

Various special environmental tests were performed during the *Mariner* Venus 67 program. However, some of these were not directly related to specific TA or FA subsystem tests. Therefore, resulting data have been included in appendix material. The following tests are documented in the noted Appendixes:

Shipping Container Environmental Testing, Appendix F

Truck Acceptance Testing and Transportation Environments, Appendix G

Battery Vibration Test, Appendix H

Effect of Configuration on Vibration Test of Electronic Chassis, Appendix I

Automatic 80 PSD vs Digital PSD Analytical Techniques, Appendix J

Table 23. Proton testing of *Mariner IV* circuits

Mariner IV test item	Fluxes used		Radiation effect
	Rate (protons/cm^2)	Total (protons/cm^2)	
Canopus tracker	6×10^5 ($E > 40$ MeV)	2.4×10^{10}	Loses roll control Dark current increase due to induced radioactivity, but can maintain roll control with beam off
Data encoder	10^7	1.7×10^{11}	No effect
Squibs	3.9×10^7	2.1×10^{10}	No effect
Batteries			
Ag–Zn, Ag–Cd, Ni–Cd	3.8×10^7	2.1×10^{10}	No change in open circuit voltage, cell capacity, or in internal cell pressure
Solar cells			
P/N	2.5×10^7	2.1×10^{10}	15% drop in power output
N/P	2.5×10^7	2.1×10^{10}	5% drop in power output
Central computer & sequencer			
Central clock, End counter, Maneuver duration	2.4×10^7	1.0×10^{11}	No effect
Sun sensor CdS cells	3.5×10^7	2.1×10^{10}	No change in cell resistance or in ability of sensor unit to lock on a light source
Integrated circuits	1×10^8	7.7×10^{11}	Slight degradation in analog circuits; no effect in digital circuits

IV. Spacecraft Flight-Acceptance (FA) Environmental Tests

Flight-acceptance (FA) environmental testing at the system level is performed to give assurance that the flight hardware configuration is representative of the design qualified by the type approval (TA) test and to identify any manufacturing defects that may be present in the flight hardware. In essence, the FA test is a certification of flightworthiness for each spacecraft. Flight-acceptance

testing at the subsystem level is performed to uncover major problems prior to system level testing.

The FA tests performed are primarily vibration, thermal–vacuum, and certain EMI investigative-type tests. The input levels are those estimated to be the actual operational environmental conditions. Passing tests that simulate these environments gives explicit and implicit evidence that the items can operate as required during the spacecraft's mission.

A meaningful FA environmental test is one that combines the environmental stimulus with the appropriate assembly performance tests necessary to determine satisfactory operation. The FA environmental tests complement FA functional tests, calibrations, and inspections.

Because there was no PTM for the *Mariner* Venus 67 program, the spare flight spacecraft (M67-1) often served a dual role – as a PTM and as a spare flight spacecraft. As a result of this dual role, the M67-1 spacecraft was subjected to limited qualification-type tests over and above those for the prime flight spacecraft (M67-2). In general, these test levels were some modest margin over the normal flight-acceptance test levels but were not equivalent to the *Mariner* Mars 1964 PTM test levels. These tests included additional margin in solar simulation, the firing of all spacecraft pyrotechnic devices, RF irradiation with live squibs installed, and an approximate 5-dB increase in random noise test levels below 800 Hz. These test levels do not invalidate the M67-1 spacecraft's flightworthiness.

A. Spare Flight Spacecraft, M67-1, System and Subsystem FA Environmental Tests

1. System level. The material presented here, which applies to the M67-1 spacecraft system, includes the reports of the system-level FA environmental tests and a history of subsystem experience in system-level environmental tests. The subsystem history permits examination as to whether or not a given subsystem experienced the system test, and if not, what was (or should have been) done to offset the deficiency.

a. Spacecraft FA vibration tests.

Configuration. The test configuration consisted of flight hardware with the exception of the post-injection propulsion system (PIPS), pyrotechnic actuators, and two solar panels. The FA vibration test setup is shown in Figs. 63 and 64.

Test description. Each test excitation direction was in one of the following spacecraft axes: (1) roll, (2) through bays II–VI, or (3) through bays IV–VIII. The nominal test sequence was a sinusoidal sweep at 2 octaves/min between 20 and 200 Hz and band-limited random noise with a shaped spectrum between approximately 100 and 2000 Hz. Table 24 displays the specified FA level test parameters for each test.

Test results.

(1) *Sinusoidal tests.* The ±5% specification tolerance was met in the tests. For the lateral axes tests (runs 2 and 4) this tolerance allows a test-level range of approximately 0.47 to 0.53 *g* rms; the actual average test-level bounds for runs 2 and 4 are given in Table 24. The allowable amplitude range in the roll-axis test is 0.95 to 1.05 *g* rms; the actual test-level bounds are given in the table.

(2) *Noise tests.* The average test levels (average of six control accelerometer outputs) were above nominal, but within the specified, tolerance of ±1 dB. The acceptable test range with this tolerance is 9.5 to 12.0 *g* rms. The

Table 24. M67-1 flight-acceptance vibration tests

Test No.	Spacecraft axis	Type of test	Frequency range, Hz	Test level, g rms		Test duration, s
				Specification	Actual	
2	XY (bay II–VI)	Sine sweep	200 to 20 to 200	0.50	0.50 to 0.48	200
3	XY (bay II–VI)	Shaped noise	100 to 2000	10.7	10.8	60
4	XY (bay IV–VIII)	Sine sweep	200 to 20 to 200	0.50	0.50 to 0.47	200
5	XY (bay IV–VIII)	Shaped noise	100 to 2000	10.7	11.7	60
6	Z	Sine sweep	200 to 20 to 200	1.00	0.99 to 0.95	200
7	Z	Shaped noise	100 to 2000	10.7	11.3	60

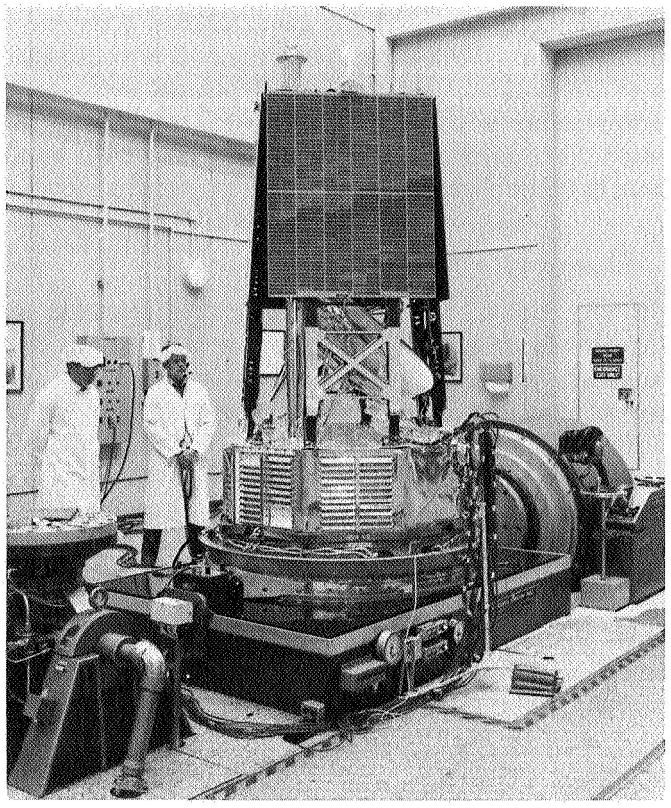

Fig. 63. FA vibration test setup for M67-1, view 1

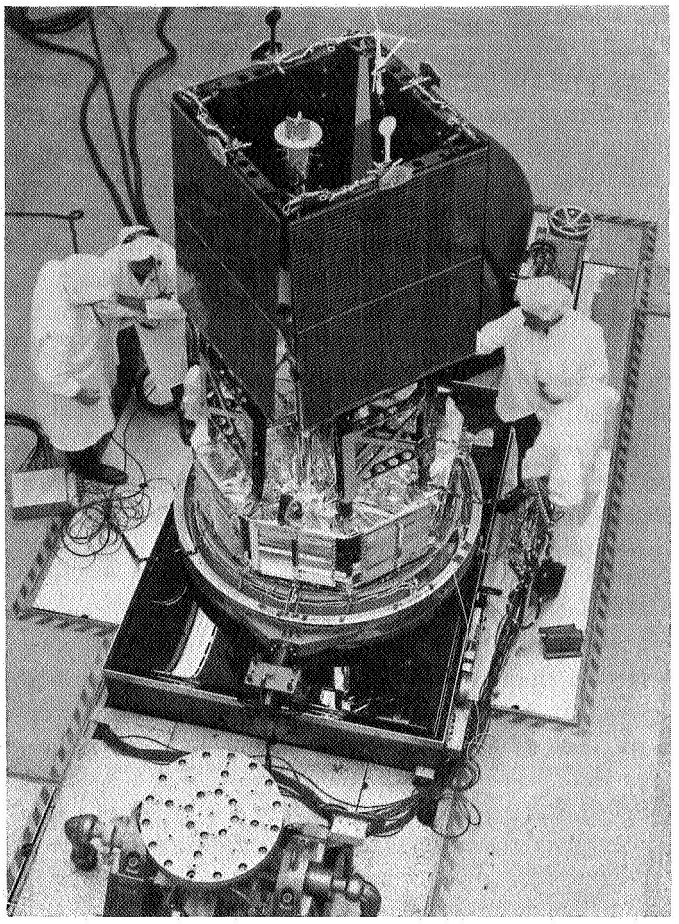

Fig. 64. FA vibration test setup for M67-1, view 2

actual average test levels from Table 24 are 10.8, 11.7, and 11.3 g rms for runs 3, 5, and 7, respectively.

Noise-spectrum-level control was adequate and satisfied the 3 dB peak-to-peak interpretation of the specification tolerances. The corresponding range of spectrum level is shown in each plot of Fig. 65, along with the actual test input acceleration spectral density (ASD) for each shake axis. Table 25 contains a summary of the peak-to-peak deviation for each axis.

Test anomalies.

(1) *DAS problem.* An anomaly was noted in the DAS during the first plane of shake. An intermittent signal was observed for one of the status bits. The problem did not occur in the remainder of the tests.

The post-test inspection at SAF revealed that the condition could be induced occasionally by moving the wire harness. A laboratory check of the assembly could not isolate the problem, but indications were that the problem was not vibration-induced. Although the reason for the anomalous operation was not fully understood, it was thought to be due to noise at the status bit OR gate (ASL 98). This expander gate input was not filtered, and it was not felt to be worthwhile to filter the expander, because the DAS status bits were designed as a trouble-shooting aid and were not part of the science data.

(2) *Operational problem.* Two test anomalies occurred that produced a negligible spacecraft excitation, as shown by the spacecraft response accelerometers.

Table 25. M67-1 maximum-noise spectrum-level deviations

Test No.	Spacecraft shake axis	Peak-to-peak test deviation, dB[a]
3	XY (bay II–VI)	2½
5	XY (bay IV–VIII)	3
7	Z	2½

[a]Reference 1 g^2/Hz.

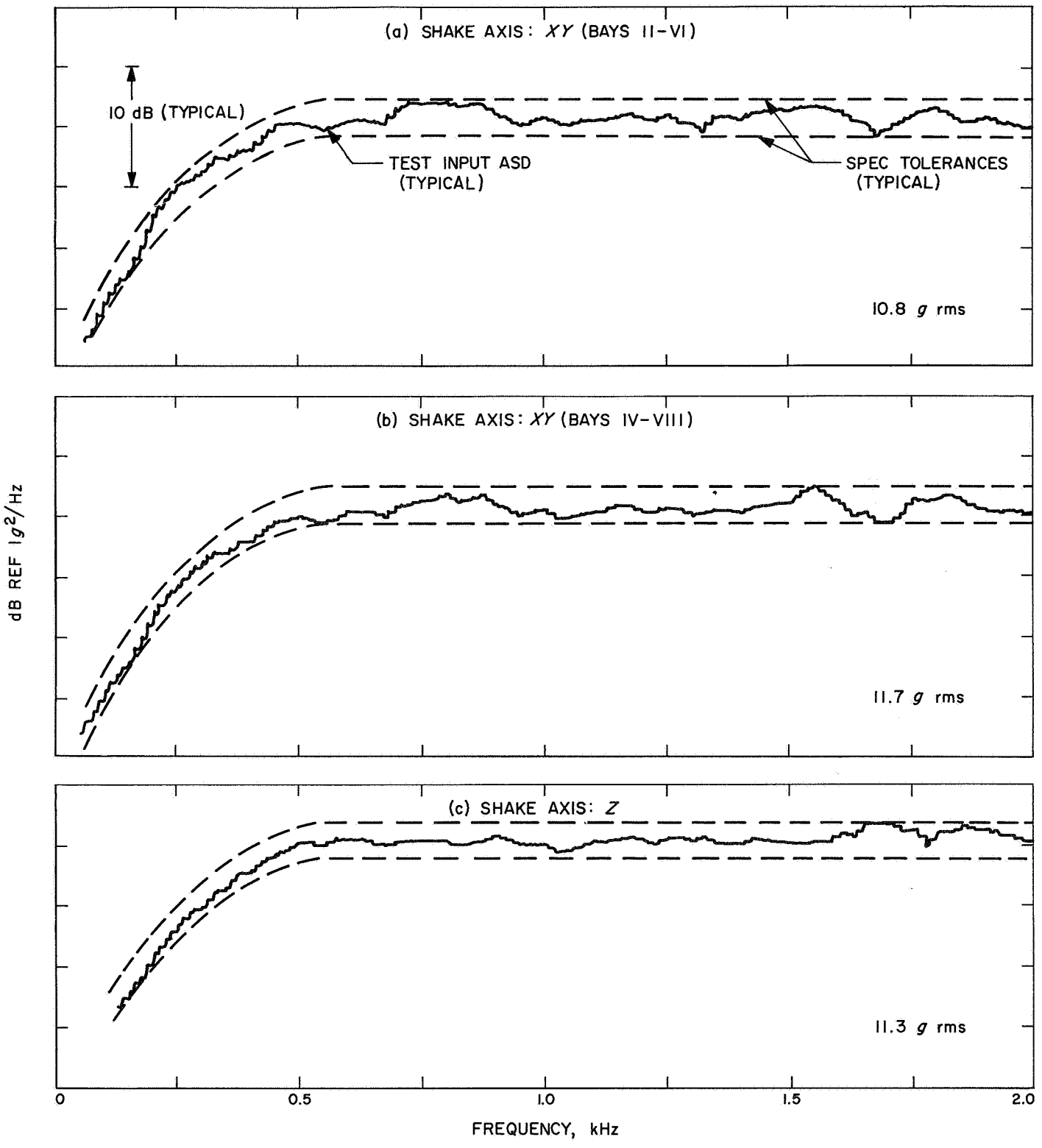

Fig. 65. M67-1 system level noise vibration

During run 2, an operator error caused a very low-level excitation, instead of the FA level, during the downsweep portion of the test, only, producing a negligible spacecraft response. A waiver was added to the procedure, signed by the cognizant engineers. The correction was made and the sweep was rerun with no incidents.

(3) *Structural problem.* During run 6, an audible transient occurred at approximately 35 Hz on the downsweep. The sound seemed to originate in the vicinity of the spacecraft bay II. An investigation of the recorded response-accelerometer data revealed no significant structural response. However, some spurious signals similar to tape *dropouts* were recorded throughout the run. These signals have been isolated as a problem with the instrumentation tape recorder.

The spacecraft was dismantled in the vicinity of bay II. No structural damage could be found. A loose nut was found in the adapter during the inspection, but it could not have originated in the spacecraft because of the lower thermal blanket configuration. The spacecraft was reassembled and the test continued.

b. Spacecraft FA pyrotechnic shock test.

Test events and comparison with specification requirements. The pyrotechnic shock test (Figs. 66 and 67) consisted of firing all pyrotechnic devices on or near the spacecraft; these consisted of (1) the shroud V-band release, (2) the spacecraft V-band release, (3) the solar-panel deploy, (4) the post-injection propulsion system, and (5) the antenna pointing-angle change (APAC). There was no deviation from the specified requirements.

Response data. The spacecraft and adapter[15] were instrumented with 24 accelerometers to record the shock events for later reduction to shock spectra and Fourier transform response data for determining the response characteristics of the structure, as well as to determine which pyrotechnic events resulted in maximum response spectra. Those pyro devices which produced maximum, or *enveloping*, shock spectra responses throughout the spacecraft (adapter excluded) were fired again during the M67-2 pyrotechnic shock test.

The pyrotechnic events that produced the maximum shock spectra throughout the spacecraft (adapter excluded) were (1) the spacecraft V-band release, (2) the solar-panel deploy, (3) the PIPS pyrotechnic units and (4) the APAC pyrotechnic devices.

The PIPS pyrotechnic event, however, produced a maximum response spectra at leg B and in the frequency range 2,000 to 20,000 Hz only. Below 2,000 Hz the spacecraft V-band release produced the maximum spectrum at this location. In addition, there was little difference

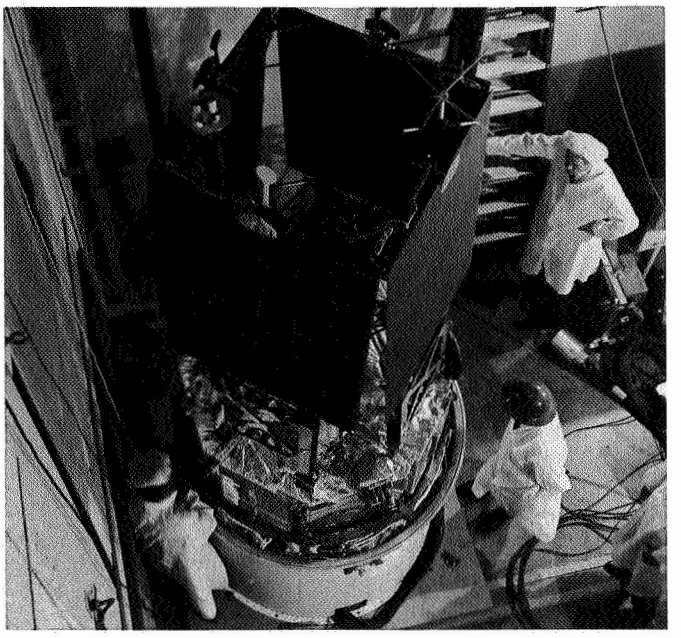

Fig. 66. Pyrotechnic shock test for M67-1

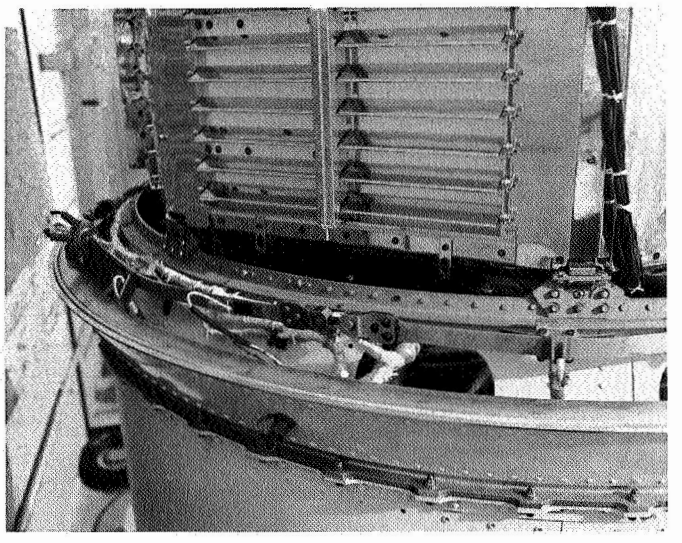

Fig. 67. Detail of M67-1 spacecraft FA pyrotechnic-units shock test

[15]Manufactured by Lockheed Missiles and Space Company, Sunnyvale, Calif.

between the maximum response produced by the PIPS event and the slightly lower response produced by the spacecraft V-band event in the 2,000 to 20,000 Hz bandwidth. Therefore, the spacecraft V-band release, solar-panel deploy, and APAC pyro devices were specified for the M67-2 test. All response data were of very high quality, and levels and spectra were comparable with the *Mariner* Mars 1964 data.

The high-speed Fastex film of the spacecraft V-band release showed that the V-band rebounded into the LMSC adapter, not into the spacecraft.

Test anomalies. There were no anomalies evident in this test.

Spacecraft test configuration. For this pyrotechnic test, the M67-1 spacecraft consisted of flight hardware, with the exception of the following: the attitude control system, the Canopus sensor, and the power subsystem in bay I were from the STM; solar panels 3 and 4 were flight spares—the other solar panels were from the STM.

Spacecraft failures. No failures occurred during this test.

c. Spacecraft FA thermal–vacuum test.

Comparison of test configuration with flight configuration. The M67-1 spacecraft had the following non-flight items during the systems test: the battery, solar

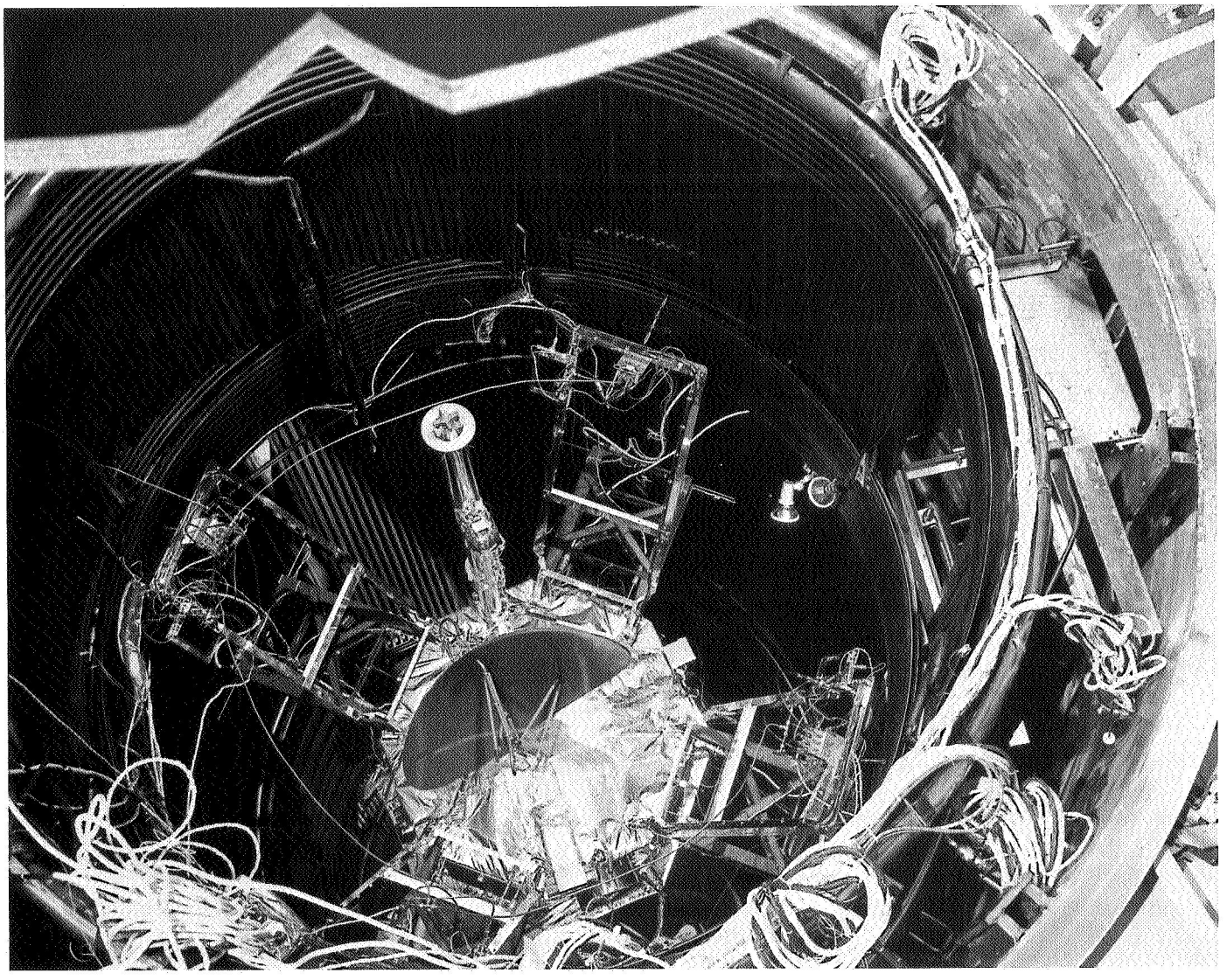

Fig. 68. M67-1 spacecraft thermal–vacuum test setup

panels, squibs, pinpullers, low-gain antenna dampers, unlatch motion sensors, and side thermal shields (cut-outs). The test setup is shown in Fig. 68.

Comparison of actual test with test requirements. A comparison of the requirements as set forth in the Test and Operation Plan (TOP), the M67-1 FA specification, and the M67-1 Detailed Test Procedure, as a function of the actual test, are presented in Tables 26 and 27. Table 26 covers phase I of the test. Significant phase I deviations are listed below:

(1) Actual time in earth cruise mode was longer than required, resulting primarily from the failure in the attitude control J box.

(2) Actual time spent in most of the other modes was significantly less than required as per request by Test Director in order that more time could be allotted to phase II.

(3) The high-gain antenna was not deployed as called for in the specification.

(4) Gyros were not on in the encounter mode because of the chamber vibration problem, which caused excessive gyro activity.

Table 27 covers Phase II of the M67-1 thermal–vacuum test. The significant phase II deviations are presented below:

(1) Considerably more time was actually spent in the earth cruise mode than was required primarily because the average internal bus temperature of the spacecraft was running about 7°F cooler than TCM data indicated was normal.

(2) The spacecraft was not tested at the 248 W/ft² intensity level. As a result of time lost for thermal-shield modifications (to raise the internal bus temperature), the test time remaining was spent at 126 W/ft² in mode 1 and at 290 W/ft² in mode 4 in an effort to bracket the extreme temperatures.

Problems and failures during test.

(1) *OSE problems.* Approximately 5 h after the initial pumpdown, a problem was incurred with the Canopus sensor; the Canopus simulation locked on one of the end relays such that its position could not be altered. The test activities were terminated by the Test Director, and the chamber was brought back to ambient conditions. It was determined that a diode had failed on one of the circuit boards in the attitude-control J box and, also, that this particular circuit board had been modified with certain resistors being changed for smaller ones than those on the original board. The board was replaced with one that met the original specifications. The chamber was again evacuated, and no further problem arose from this source.

(2) *Spacecraft problems.* Shortly after the second pumpdown of phase I, it was determined that the *gyros* were experiencing an abnormal amount of activity that caused the attitude-control jets to fire too frequently, thereby depleting the attitude-control gas supply. As a result of this problem, the first midcourse maneuver was shortened in duration. After it was determined to be a problem, the gyros-on mode was avoided – to prevent further depletion of the gas supply. The gyros experienced excursions of 3 mrad/s in pitch and yaw and 1.1 mrad/s in roll. It was determined that the gyro activity was a result of vibration inputs from the chamber through the spacecraft suspension system.

During phase I of the test, the *plasma probe* dropped from 109°F to about 12°F during the *lights off* midcourse maneuver. This was below the FA test levels but appeared to be no problem, since the plasma probe had undergone margin testing to lower temperatures.

The *secondary sun sensors* also experienced temperatures as low as 20°F during phase I, which is lower than FA requirements. This appeared to be no problem, since these sensors were margin-tested to much lower temperatures.

During phase I, an indication was received that the *sun gate* was always actuated. It was determined that this was due to light leaking through the hood from stray reflections.

The average *internal bus temperatures* on the M67-1 spacecraft were running approximately 7°F cooler during phase II than the corresponding temperatures on the TCM. To correct this problem, the chamber was returned to ambient conditions and thermal shields were added to the spacecraft. After pumping down again, the average internal bus temperatures were only about 2°F cooler than those on the TCM.

The high-gain antenna was not deployed during the M67-1 space simulation test, as called for in the specification. This deviation was approved by the Spacecraft Systems Manager in an internal office memo. The high-gain antenna was successfully deployed during the M67-2 space simulator test.

Table 26. Phase I of M67-1 thermal–vacuum FA test: Required and actual

Flight segment	Requirements									Actual test		
	Test and Operations Plan (TOP)			JPL Specification			Detail Test Procedure					
	Time, h	Intensity level, W/ft²	Operating mode	Time, h	Intensity level, W/ft²	Operating mode	Time, h	Intensity level, W/ft²	Operating mode	Time, h	Intensity level, W/ft²	Operating mode
Boost	—	—	—	0.5	0	Pressure profile	3	0	Pressure profile	3/2	0	Pressure profile
Earth cruise	24	126	—	24	126	[a, b]	24	126	[a, b]	42.5	126	[a, b]
Midcourse	6	0	—	4	0	Midcourse	2/2	0/126	Midcourse	1.5/2	0/126	Midcourse
Venus cruise	60	248	—	60	248	[a]	54	248	[a]	54	248	[a, b]
First encounter	12	248	—	16	248	[c, d]	7	248	[a]	7	248	[a, e, f]
First playback	48	263	—	48	263	[a]	17	263	[a]	17	263	[a]
Second encounter	12	248	—	12	275	4	7	275	[d]	7	275	[a, f]
Second playback	48	263	—	48	290	[a]	17	290	[a]	20	290	[a, d]
Post playback	24	263	—	0	—	Not required	18	290	[b]	18.5	290	[b]
Total, phase I	234	—	—	252	—	—	151	—	—	173.5	—	—

[a]Spacecraft on traveling-wave tube (TWT), broadcast *off*, gyros *off*.
[b]Spacecraft on TWT, broadcast *on*, gyros *off*.
[c]Spacecraft on TWT, broadcast *off*, gyros *off*, high-gain antenna deployed.
[d]Spacecraft on TWT, broadcast *off*, gyros *on*.
[e]High-gain antenna not deployed.
[f]Gyros *not on* because of chamber vibration.

Table 27. Phase II of M67-1 thermal–vacuum FA test: Required and actual

Flight segment	Requirements									Actual test		
	Test and Operations Plan (TOP)			JPL Specification			Detail Test Procedure					
	Time, h	Intensity level, W/ft²	Operating mode	Time, h	Intensity level, W/ft²	Operating mode	Time, h	Intensity level, W/ft²	Operating mode	Time, h	Intensity level, W/ft²	Operating mode
Boost	—	—	—	—	—	—	3	0	Pressure profile	1.5	0	Pressure profile
Earth cruise + margin	—	—	—	—	100	[a]	12	100	[a]	12	100	[a]
Earth cruise	20	126	—	—	126	[a, b]	24	126	[a, b]	60	126	[a, b, c]
Venus cruise	20	248	Gyros on	—	248	[b]	12	248	[b]	0	248	[d]
Venus cruise + margin	—	—	—	—	290	[b]	12	290	[b]	15.5	290	[e]
Special test mode	—	—	—	—	—	—	12	—	—	—	—	—
Total, phase I	40	—	—	—	—	—	75[f]	—	—	89.0	—	—
Total, phases I and II	274	—	—	250	—	—	226	—	—	262.5	—	—

[a]Spacecraft on cavity amplifier, battery charger *off*, gyros *off*.
[b]Spacecraft on TWT, battery charger *off*, gyros *off*.
[c]Spacecraft on cavity amplifier, battery charger *on*, gyros *off*.
[d]Because of redesign, spacecraft not tested in this mode.
[e]Spacecraft on TWT, battery charger *on*, gyros *on*.
[f]Reflects completion of phase I.

(3) *Facility.* Chamber *vibrations* caused excessive activity in the spacecraft gyros. It was determined that the fundamental frequency that affected the gyros was 3 Hz. The problem was partially resolved by altering the spacecraft suspension system.

On January 22, 1967, at approximately 12:00 a.m. a momentary (2 s) *power failure* occurred. The chamber was not under vacuum at the time.

Spacecraft environment during test. A discussion of four of the more salient features of the thermal–vacuum chamber is contained in the following paragraphs. Discussion of effects of deficiencies in these features is found in Section VI of this report.

(1) *Launch pressure profile simulation.* The simulated launch profiles for phases I and II are depicted in Figs. 69 and 70. The specified profiles for the transient pressure P, and the rate of change of pressure $\dot{P}$, are also included in these figures. The evaluation of the effect of differential pressures in enclosures, thermal blankets, etc., is the principal objective of launch pressure profile simulation. Since the condition which corresponds to the existence of this environment is the time rate of change of pressure, the range of maximum $\dot{P}$ (16.5 to 18.7) was the objective for the phase II pumpdown, rather than the profile bands as in phase I. From Fig. 70 one observes that the rates attained did not reach the maximum $\dot{P}$ range. Waivers were required for the failures to meet the specified profile bands. The $\dot{P}$ attained was accepted, and the test continued, since the rates in phases I and II did exceed the maximum expected flight value for a lofted trajectory ($\dot{P}$ = 15 torr/s), and it was advantageous to conserve test time.

(2) *Total irradiance levels.* The temporal sequence of total irradiance levels for phases I and II are included

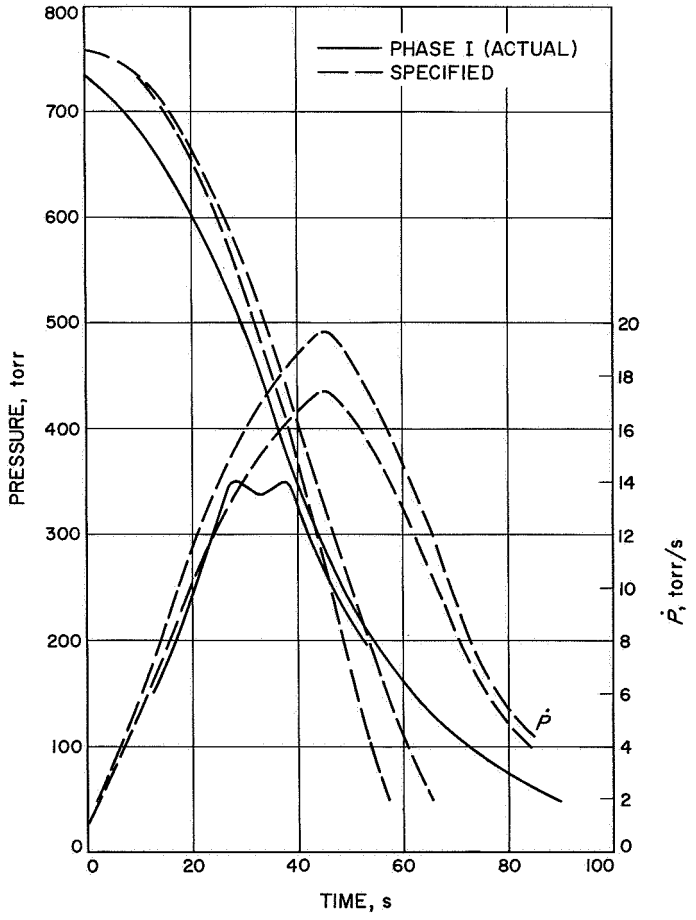

Fig. 69. Phase I, 10-ft space simulator pumpdown pressure profile for M67-1

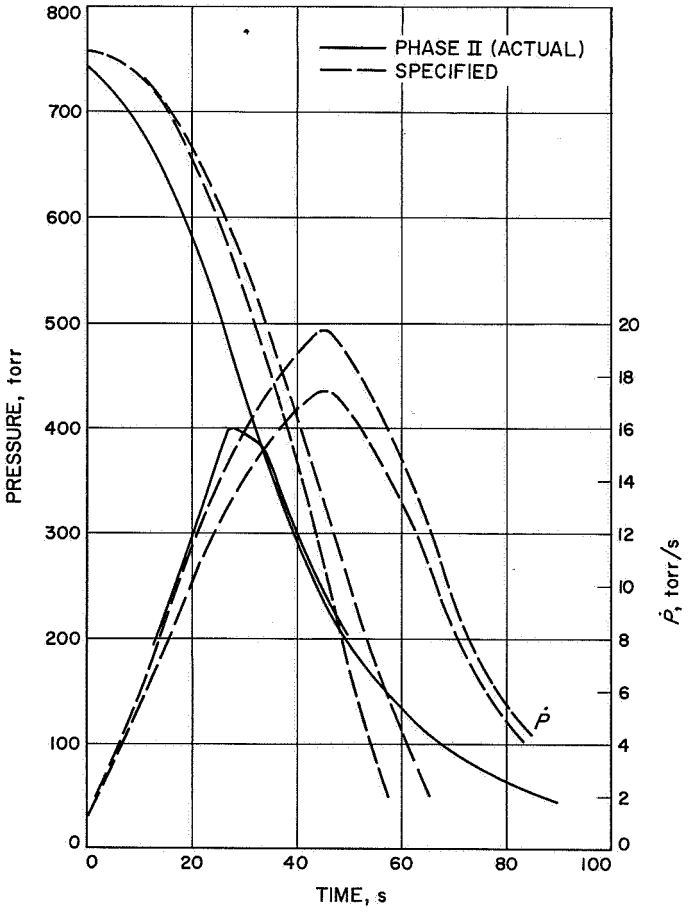

Fig. 70. Phase II, 10-ft space simulator pumpdown pressure profile for M67-1

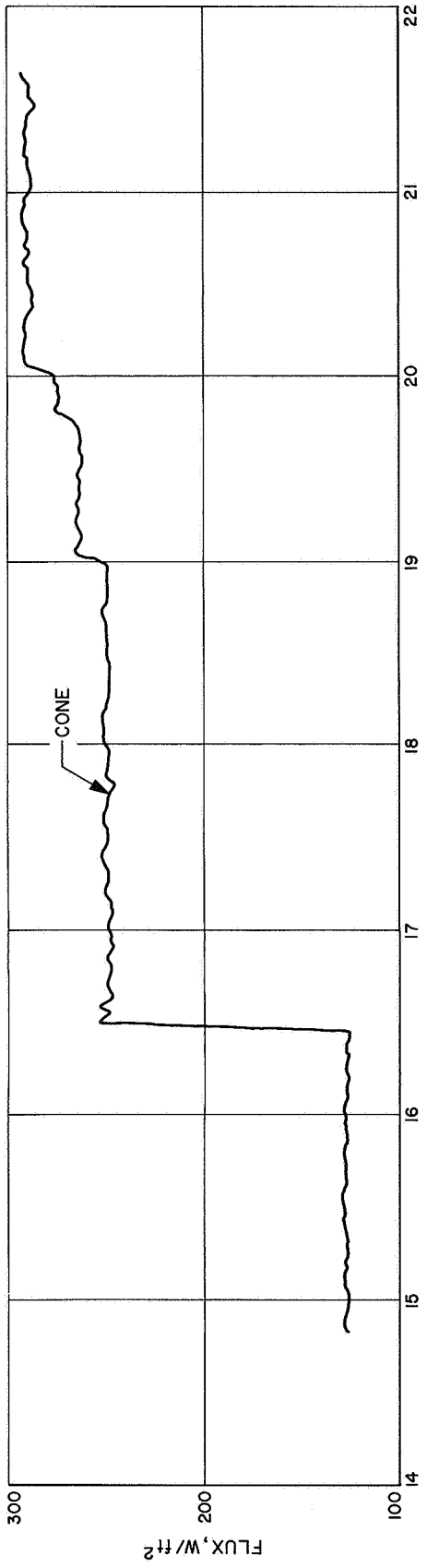

Fig. 71. Phase I, 10-ft space simulator radiometer flux for M67-1

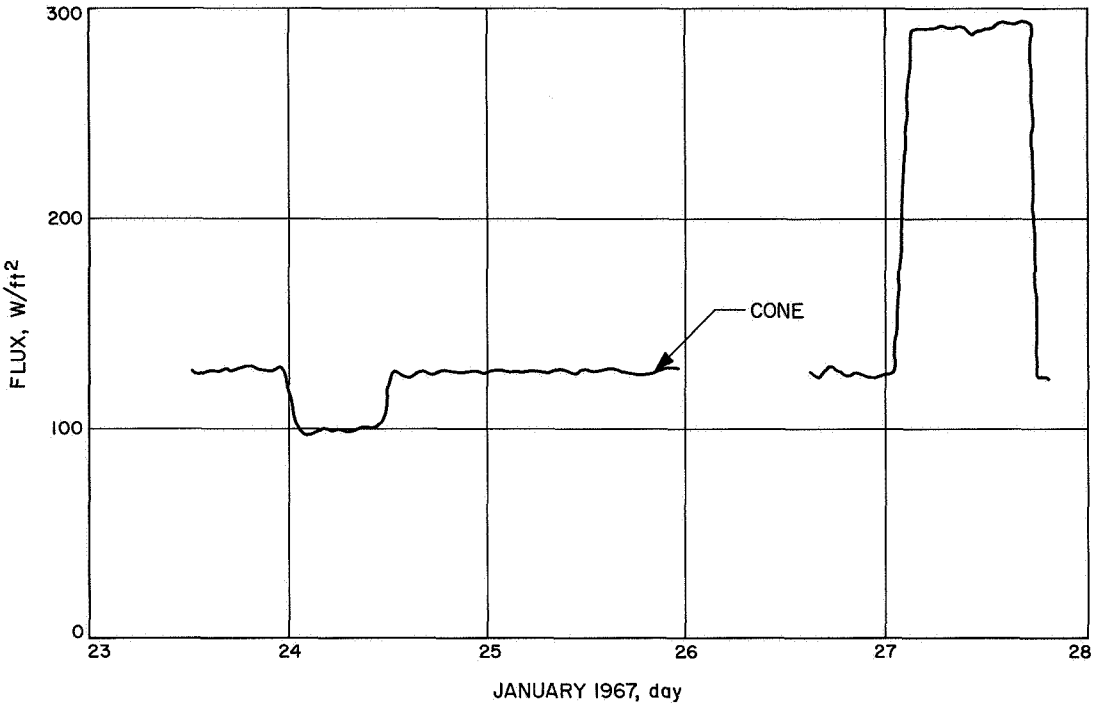

Fig. 72. Phase II, 10-ft space simulator radiometer flux for M67-1

in Figs. 71 and 72, respectively. The specified tolerance on the measurement of the required levels was ±2%. However, all of the levels measured were low by at least 3%, due to usage of incorrect infrared emittance data on the Parsons black used on the cone radiometer. This 3% deviation, plus the specified tolerance, could result in erroneous levels on the order of 5% for the M67-1 test. Because the *Mariner* Venus 67 configuration was relatively independent of the sun, the effects of this error are not considered critical. Table 28 illustrates the sun

Table 28. Correlation of spacecraft-temperature sensitivity to solar level

Telemetry channel	Location	Spacecraft temperature, °F	
		Earth cruise (126 W/ft² intensity)	Venus cruise (248 W/ft² intensity)
401	Bay I	60	68
421	Bay II	47	62
430	Bay II Primary sun sensor	42	70
402	Bay III	60	71
423	Bay IV	60	70
404	Bay V	62	69
405	Bay VI	71	76
426	Bay VII	58	62
407	Bay VIII Power regulator	87	86

Telemetry channel	Location	Spacecraft temperature, °F	
		Earth cruise (126 W/ft² intensity)	Venus cruise 248 W/ft² intensity)
422	Plasma probe	108	199
410	Canopus sensor	62	68
—	Bay II Secondary sun sensor	23	41
438	TRD chassis	38	50
—	Bay VI Primary sun sensor	57	89
—	Sun gate	58	85
—	Bay VI Secondary sun sensor	29	37

dependency when one observes the effects on the spacecraft bays, etc., when correlated to a change in irradiance level of 97% (126 and 248 W/ft²). It is easily observed from this table that, with the possible exception of the plasma probe, the spacecraft is only slightly affected by elevations in the solar irradiance level.

The plasma probe was tested, along with the entire spacecraft, at the 290 W/ft² level, which provides a 10% margin over the maximum expected mission level (playback at E + 10 days is 263 W/ft²) and reached temperatures of 232°F on the side of the probe and 221°F at the flight-sensor location. The plasma probe was FA tested at 115°C (239°F) and TA tested at 135°C (275°F) as measured at the flight-sensor location, so no problems were expected if the level of solar input was increased by 5%. (Note: The plasma probe side temperature at the E + 10 days irradiance level of 263 W/ft² was 214°F. The flight-sensor data were not available because engineering data were not obtained in that mode, but generally ran approximately 10°F lower than the side temperature.)

Therefore, the error in test irradiance level, although undesirable, was not considered to be a major problem.

(3) *Facility pressure levels.* The test of the M67-1 spacecraft was conducted, as desired, at pressure levels below the required maximum steady-state pressure of 1×10^{-5} torr. The test level was $\approx 6 \times 10^{-6}$ torr for phase I, and 9×10^{-6} torr for phase II. The automatic high-voltage cutoff was set at 5×10^{-5} torr, and no problems were encountered with the cutoff system as a result of the attitude-gas-jet operation.

(4) *Effective sink temperature.* The effective sink temperature specified was −250°F. No data are available on what the actual sink temperature is for the *Mariner* Venus 67 spacecraft–chamber configuration. The results of a previous test utilizing a small directionally sensitive arrangement of isolated flat plates indicated effective sink temperatures on the order of −200°F for the east, west, and south directions from the test volume, −225°F for the north, and −215°F for the chamber floor. It is expected that, with an arrangement such as the *Mariner* Venus 67 spacecraft–chamber configuration, the effective sink temperature would be much better. Since the actual level is unknown, it is difficult to assess the effect on the test. The estimated errors in test temperatures are a function of the temperature of the specific item and its thermal properties. In the case of *Mariner* Venus 67, it is considered unlikely that any errors due to the heat-sink error approached 10°F. More definition on what the sink temperature environment actually is should exist on future spacecraft tests.

d. Spacecraft FA electromagnetic interference tests.

M67-1 external environment simulation. The objective of this test was to verify the RF compatibility of the spacecraft, including pyrotechnics, when subjected to an RF environment similar to that expected at the AFETR launch complex.

(1) *Requirement vs test.* The RF simulation level requirements and the actual test levels are shown in Tables 29–31. The average power levels were met in the test; however, the peak power levels for two of the sources were not met because of equipment limitations. The omission is not considered serious, because each of the two simulated sources is a ground-based RF transmitter. The spacecraft is expected to have considerable protection from each of these sources afforded by the metallic shroud. In addition, two other sources that were simulated with peak levels are in the same frequency band. The situation is summarized in Table 32.

The expected shroud attenuation values were based on measurements made on the *Mariner IV* shroud with conductive paint. It is estimated that the metallic shroud of *Mariner* Venus 67 has at least the attenuation listed. The values in the table show that the ground RF peak level at 5.690 GHz are approximately in the order of magnitude of the simulated level and that the X-band peak level will be 30 dB below that used for the test.

The peak RF sources that would be present after the shroud is ejected were simulated with their expected levels. These sources are the two transponders listed in Table 32.

An additional requirement listed in the specification was for radiation of the VHF and UHF RF levels to the DFR experiment. This requirement was not met at this time in the testing, and it formed part of the DFR spacecraft compatibility tests. Because the DFR antennas were required to determine the appropriate RF levels for the DFR signals and the testing did not include installation of the solar panels for the antennas, the test was postponed. Each of these departures from the specification was noted, and very little compromise to the test resulted. The deviations were subsequently approved by the Spacecraft Systems Manager in an internal office memorandum.

Table 29. Requirements vs test, external environment simulation for M67-1: System test procedure

RF source simulated	RF simulation requirements				Test levels for system test procedure			
	Frequency, GHz	Peak power density at spacecraft, dBmW/m²	Average power density at spacecraft, dBmW/m²	Minimum pulse width, μs	Frequency, GHz	Peak power density at spacecraft, dBmW/m²	Average power density at spacecraft, dBmW/m²	Minimum pulse width, μs
Agena radar transmitter, FPS-16	5.690	59	21	1.0	5.690	[a]	20	CW
Atlas guidance track ground transmitter	Classified	20	−12	2.0	Classified	[b]	−12	CW
Atlas guidance rate ground transmitter	Classified	NA[c]	14	NA	Classified	NA	15	CW
Command destruct ground transmitter	Classified	NA	4	NA	Classified	NA	4	CW
Agena telemetry	0.2443	NA	23	NA	0.2443	NA	25	Subcarrier modulated
Agena radar transponder	5.765	7	−8	0.7	5.765	7	−8	[b]
Atlas telemetry	229.9	NA	−6	NA	229.9	NA	−6	Subcarrier modulated
Atlas guidance track transponder	Classified	30	−1	2.0	Classified	[a, d]	30	CW
Atlas guidance rate transponder	Classified	NA	−5	NA	Classified	NA	−5	CW

[a]Equipment limitations prevented simulation of specification requirements for the peak levels.

[b]Two sources used, one on pulse to meet peak requirements and one on continuous wave (CW) to meet average level requirements.

[c]Not applicable.

[d]The required peak level was simulated with a CW signal level.

Table 30. Requirements vs test, external environment simulation for M67-1: Simulated countdown procedure

RF source simulated	RF simulation requirements				Test levels for simulated countdown procedure			
	Frequency, GHz	Peak power density at spacecraft, dBmW/m²	Average power density at spacecraft, dBmW/m²	Minimum pulse width, μs	Frequency, GHz	Peak power density at spacecraft, dBmW/m²	Average power density at spacecraft, dBmW/m²	Minimum pulse width, μs
Agena radar transmitter FPS-16	5.690	59	21	1.0	5.690	[a]	20	CW
Atlas guidance track ground transmitter	Classified	20	−12	2.0	Classified	[a]	0	CW
Atlas guidance rate ground transmitter	Classified	NA[c]	14	NA	Classified	NA	15	CW
Command destruct ground transmitter	Classified	NA	4	NA	Classified	NA	4	CW
Agena telemetry	0.2443	NA	23	NA	0.2443	NA	25	Subcarrier modulated
Agena radar transponder	5.765	7	− 8	0.7	5.765	7.5	− 8	[a]
Atlas telemetry	229.9	NA	− 6	NA	229.9	NA	− 3	Subcarrier modulated
Atlas guidance track transponder	Classified	30	− 1	2.0	Classified	[a, d]	30	CW[d]
Atlas guidance rate transponder	Classified	NA	− 5	NA	Classified	NA	− 5	CW

[a]Equipment limitations prevented simulation of specification requirements for the peak levels.
[b]Two sources used, one on pulse to meet peak requirements and one on continuous wave (CW) to meet average level requirements.
[c]Not applicable.
[d]The required peak level was simulated with a CW signal level.

Table 31. Requirements vs test, external environment simulation for M67-1: Pyrotechnics and shock test procedure

RF source simulated	RF simulation requirements				Test levels for pyrotechnics and shock test procedure			
	Frequency, GHz	Peak power density at spacecraft, dBmW/m²	Average power density at spacecraft, dBmW/m²	Minimum pulse width, μs	Frequency, GHz	Peak power density at spacecraft, dBmW/m²	Average power density at spacecraft, dBmW/m²	Minimum pulse width, μs
Agena radar transmitter FPS-16	5.690	59	21	1.0	5.690	—	20	CW
Atlas guidance track ground transmitter	Classified	20	−12	2.0	Classified	—	−12	CW
Atlas guidance rate ground transmitter	Classified	NA[a]	14	NA	Classified	NA	15	CW
Command destruct ground transmitter	Classified	NA	4	NA	Classified	NA	4	CW
Agena telemetry	0.2443	NA	23	NA	0.2443	NA	25	Subcarrier modulated
Agena radar transponder	5.765	7	− 8	0.7	5.765	+11	− 6	[b]
Atlas telemetry	229.9	NA	− 6	NA	229.9	NA	− 6	Subcarrier modulated
Atlas guidance track transponder	Classified	30	− 1	2.0	Classified	—	30	CW
Atlas guidance rate transponder	Classified	NA	− 5	NA	Classified	NA	− 5	CW

[a]Not applicable.
[b]Two sources used, one on pulse to meet peak requirement and one on CW to meet the average level requirements.

Table 32. Requirements vs test, external environment simulation: Additional sources

RF source simulated	Frequency, GHz	Expected peak-power density external to shroud + 6 dB, dBmW/m²	Tested power density without shroud, dBmW/m²	Expected shroud attenuation, dB
Atlas radar ground transmitter	5.690	59	—	50
Agena radar transponder	5.765	7	7 peak	—
Atlas guidance ground track transponder	X-band	20	—	30
Atlas guidance track transponder	X-band	30	30 avg	—

(2) *Results.* The spacecraft systems were monitored by cognizant personnel, and no adverse effects due to any RF source were reported to the Test Director.

DFR/S-band/system-configuration EMC test. The objective of this test was to verify the compatibility between the DFR experiment, the S-band communications transponder, and the spacecraft in general.

(1) *Spacecraft noise environment at DFR receiver frequencies: Requirement vs test.* The permissible noise environment was determined on the basis of minimum acceptable space degradation levels specified by the experiment scientist and on the basis of cosmic noise temperature levels and receiver noise temperatures as stated in the functional specification.

(2) *DFR operation threshold degradation: Requirement vs test.* The degradation threshold requirements versus the procedure test implementation is summarized in Table I. It was not feasible in practice to perform the sweep test because the support test equipment instrumentation does not possess that capability. A manual performance of a sweep test was not considered meaningful.

Table 33. DFR/spacecraft compatibility comparison of requirements vs JPL test, M67-1

Item	Specification	JPL test procedure
Threshold degradation	49.8 MHz The performance degradation of the 49.8 MHz receiver required to be <3 dB with the receiver locked on a −125.7 dBmW signal.	Degradation threshold measured for various spacecraft modes, including required conditions
	The receiver shall maintain lock when a received signal of −120 dBmW (total power) is swept at a maximum rate of 224 Hz/s through a 5.48 kHz band centered at 49.8 MHz.	Not included because unfeasible to perform because of instrumentation limitations
	423.3 MHz The performance degradation of the 423.3 MHz receiver shall be less than 1 dB with the receiver locked on a −134.2 dBmW signal at 423.3 MHz.	Degradation threshold measured for various spacecraft modes, including required conditions
	The 423.3 MHz receiver shall maintain lock when a received signal of −130 dBmW (total power) is swept at a maximum rate of 1900 Hz through a 15.8433 kHz band centered at 423.3 MHz.	Not included because unfeasible to perform due to instrumentation limitations
Acquisition threshold	49.8 MHz The 49.8 MHz receiver required to acquire lock with a −125.7 dBmW signal applied at 49.8 MHz and at 49.8 MHz ±3 kHz, respectively.	Acquisition threshold tests included for various spacecraft modes
	423.3 MHz The 423.3 MHz receiver shall acquire lock with a −134.2 dBmW signal applied at 423.3 MHz and 423.3 MHz ±3 kHz, respectively.	Acquisition threshold tests included for various spacecraft modes
Spacecraft environment	49.8 MHz Noise levels not to exceed limits of specification for 49.8 MHz ±50 kHz. Constraints (1) Spacecraft flight configuration, suspended in SAF.	(1) As required; solar panels 4A1, 4A3 flight; 4A5 TA; 4A7 TM
	(2) Noise environment plus receiver not to exceed 21,850°K.	(2) Noise temperature approximately 2500°K with spacecraft *off*
	(3) Various spacecraft modes specified with various subsystems *on* and *off*.	(3) Spacecraft modes included specified conditions
	423.3 MHz Noise levels not to exceed limits of specification for 423.3 MHz ±50 kHz. Constraints (1) Spacecraft flight configuration, suspended in SAF.	(1) As required
	(2) Noise environment plus RCVR not to exceed 1025°K.	(2) System noise temperature approximately 200°K
	(3) Various spacecraft modes specified with various subsystems *on* and *off*.	(3) Spacecraft modes included specified conditions

(3) *DFR acquisition threshold degradation: Requirement vs test.* The acquisition threshold tests were implemented in the procedure.

(4) *Spacecraft noise environment at S-band receiver center and image frequencies and operation degradation tests: Requirement vs test.* The requirements of the specification were incorporated in the procedure (see Table 33) with the exception that the spacecraft was not elevated for the S-band test sequence for two reasons: First, the RF losses in the test cables would be too great; and second, it was decided to radiate the VHF and UHF radio frequency levels to the spacecraft from a direction that approximated that expected for flight and if the spacecraft were elevated the VHF and UHF antennas would have had to be suspended from the rafters.

Table 33 (contd)

Item	Specification	JPL test procedure
Spacecraft environment (contd)	473.1 MHz Noise levels not to exceed limits of specification for 473.1 MHz ±50 kHz. Constraints: (1) Spacecraft flight configuration, suspended in SAF (2) Noise environment plus test receiver not to exceed 1025°K (3) Various spacecraft modes specified with various subsystems on and off No spacecraft system-generated interference to appear at the S-band antennas input terminals within a 3.43 MHz bandwidth centered at the receiver frequency or centered at the image frequency This requirement to apply to the spacecraft when physically and operationally configured, as follows: (1) Spacecraft in flight configuration, suspended above test area floor (A non-conducting suspension is a prerequisite.) (2) Spacecraft operation in the encounter mode with the following specific constraints: Battery charger on Tape recorder operated in its record mode Stabilization jets actuated Spacecraft gyros energized Isotropic antenna and high-gain antenna in initial and deployed positions utilized, respectively (Two runs required)	(1) As required (2) System noise temperature approximately 200°K (3) Spacecraft modes included specified conditions Noise measurements outlined in Procedure for the center and the image frequency Various specified test modes listed
Threshold degradation	S-band receiver to maintain tracking loop acquisition and lock capability when operated in the spacecraft system environment S-band receiver to maintain lock when an applied signal 6 dB greater than threshold at best-lock frequency (determined from above) is swept at a rate of 30 Hz/s over a 10-kHz band centered at the best-lock frequency. Spacecraft in flight configuration, suspended above the test area floor (non-conducting suspension is a prerequisite). Spacecraft operation in the encounter mode with the following specific constraints: Battery charger on Tape recorder operated in record mode Stabilization jets actuated Spacecraft gyros energized Low-gain antenna and the high-gain antenna in initial and deployed positions, respectively, utilized (Two runs required)	Test sequence 4, description of tests to be performed (1) Condition spacecraft to noisiest mode determined with the EMI receiver; with TWT on and high-gain antenna to initial position, transponder evaluation tests of the following performed: Threshold S-band command (modulation on) Ranging Command lockup threshold Above performed for: Transmit low, receive low Transmit high, receive low Transmit high, receive high Repeat with high-gain antenna deployed to position 2 (2) Sweep test not feasible because of instrumentation limitations

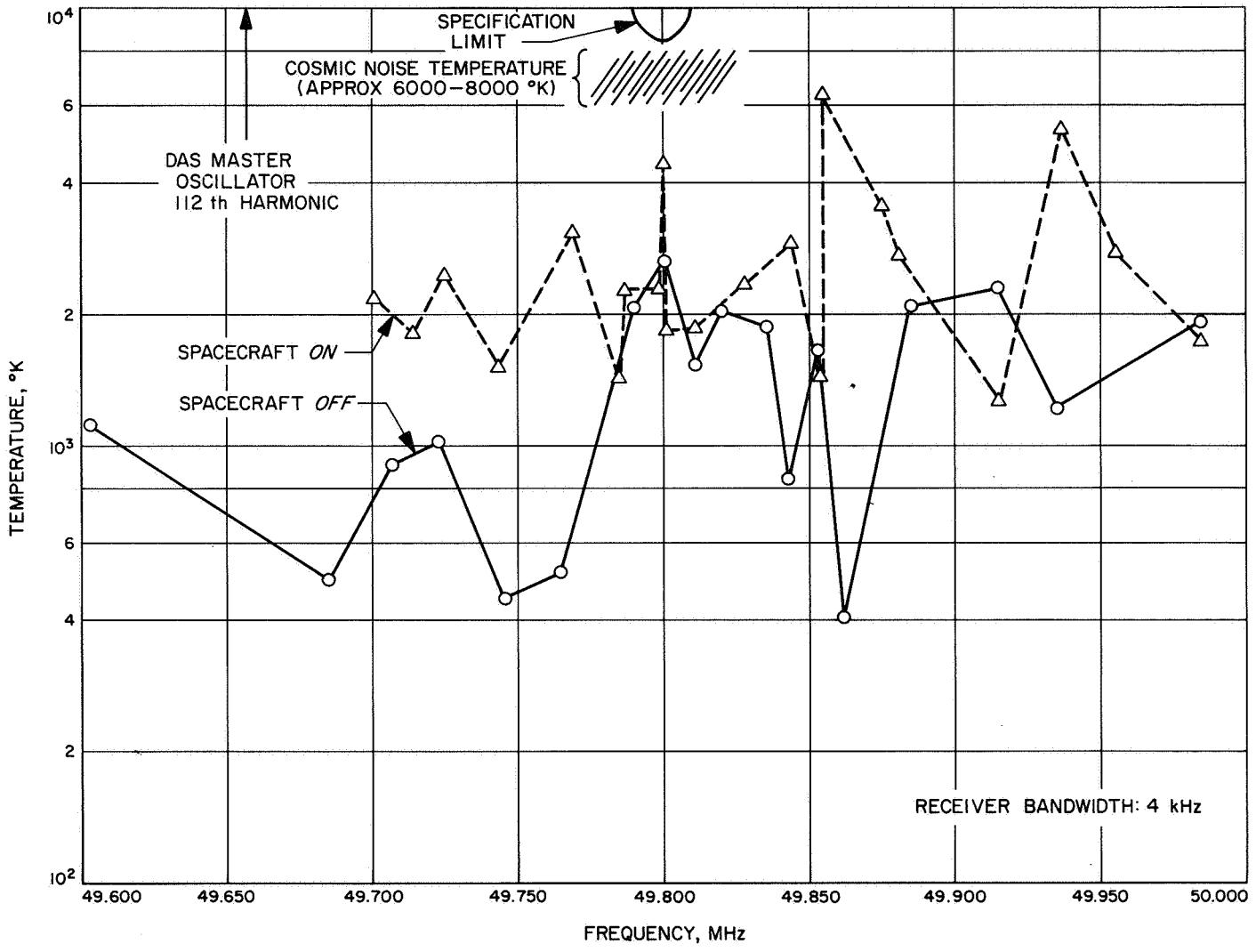

Fig. 73. EMI test, M67-1 dual-frequency receiver VHF antenna

Time schedules did not permit placement of the radiating antennas if the spacecraft were to have been elevated. It was considered that the intent of the specification would not be jeopardized with the spacecraft placed on the tripod used for the test assembly and that the characteristics of the S-band antennas would not be affected in this position.

(5) *Spacecraft environment results.* The results of the noise temperature survey at VHF are shown in Fig. 73. Included in the figure are the specified maximum permissible noise levels converted to temperature levels and the expected range of cosmic noise temperature for this mission. The documented expected cosmic noise temperature is 8000°K; however, some estimates have been mentioned from 6000 to 7000°K. The spacecraft *on* curve is not above the spacecraft *off* curve at all points, because the background noise was decreasing during the test period.

No RF levels contributed by the spacecraft were observed at 423.3 and 473.1 MHz with a receiver system that had a noise figure of approximately 2.3 dB. This noise figure would have permitted an observation (approximately an easily observed 0.8 dB deflection) for a spacecraft-contributed noise that would cause a 1 dB degradation in space.

Figure 74 is a block diagram of the test configuration used for the VHF noise level measurements. Figure 75 describes the test configuration used in the UHF noise level measurements.

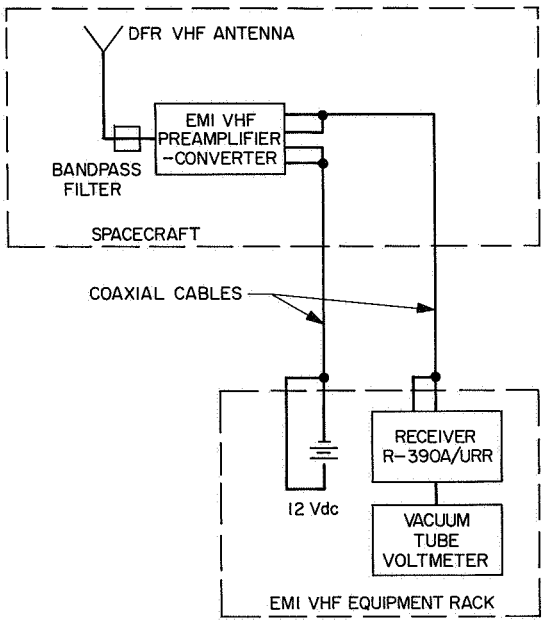

Fig. 74. Electromagnetic VHF test-receiver configuration

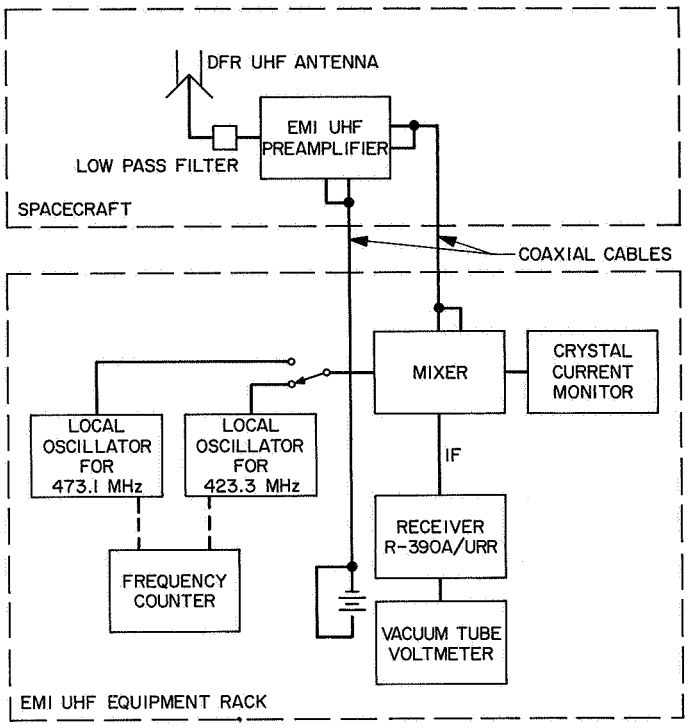

Fig. 75. Electromagnetic UHF test-receiver configuration

(6) *DFR operation threshold degradation results.* The data obtained in this test are shown in Table 34. The maximum threshold degradation noted was 7 dB determined by the DFR checkout equipment for the VHF receiver (Table 35). When this 7 dB value is converted to degradation in a space environment, the value of expected degradation is less than 1 dB. No appreciable degradation at the UHF frequency was noted. Figure 76 describes the configuration.

The data for the DFR VHF channel (at 49.8 MHz), which have been converted to RF levels present at the DFR receiver input, is included in Table 36. These levels were obtained by subtracting the RF losses shown in Fig. 73 from the 0-dBmW signal generated in the bench checkout equipment (BCE). The levels indicate the required RF power to maintain a constant signal to noise ratio at the DFR. Changes in signal level required to maintain a constant ratio provide a measure of noise at the operating frequency.

The degradation experienced by the DFR VHF receiver for the diverse spacecraft modes was either 5, 6,

Table 34. DFR degradation data for M67-1

Procedure step	Condition	VHF		UHF	
		Carrier, V	Attenuation, dB	Carrier, V	Attenuation, dB
	Spacecraft *off*, 50 Ω terminator *on*	0.71	46	0.72	34
	Spacecraft *off* and raised to test position				
(RF leakage problems occurred in steps prior to step 222)					
222	RF power *down*/RF power *up*	0.7	41	0.65	35
224		0.68	41	0.65	35
226	DC-V19 (Gyros *off*, normal control)	0.67	40	0.65	35
		0.72	39		
	DFR threshold	0.1	59	0.1	45
232	Valves blown	0.66	40	0.65	35
236	DC-V10 (Transmit high, receive low)	0.66	40	0.65	35
242	DC-V15 (Canopus gate inhibit override)	0.75	40	0.65	35
	Gyros *off*	0.70			
248	DC-V24 (Begin DAS encounter mode)	0.69	41	0.67	35
252	Isolation panel on (OSE)	0.65	31	0.6±0.2	33
252	Planet sensor output	0.66	41	0.67	35
254	Threshold	0.1	55	0.1	45
	Return to nominal	0.67	41	0.66	35
256	Deploy high-gain antenna	0.7	56	0.1	45
260	Threshold	0.1	40	0.66	35
262	DC-V19 (Gyros *off*, normal control)	0.71	40	0.68	35
	Drifting	0.7	41	0.68	35
	Science *off*	0.6	40	0.68	35
	Science *on*	0.7	40	0.67	35
276	Magnetometer ignition	>10 dB reduction in signal (Out of lock).			

Table 35. Dual-frequency receiver VHF test, RF levels, M67-1

Procedure step	Condition	Carrier, V	Signal level, dBmW	Change from 50 Ω reference, dB
	Spacecraft *off*, 50 Ω terminator *on*	0.71	−127.9	
	Spacecraft *off* and raised to test position	0.60	−123.9	4
222	RF power *down*/RF power *up*	0.7	−122.9	5
224		0.68	−122.9	5
226	DC-V19 (Gyros *off*, normal control)	0.67	−121.9	6
		0.72	−120.9	7
	DFR threshold	0.1	−140.9	
232	Valves blown	0.66	−121.9	6
236	DC-V10 (Transmit high, receive low)	0.66	−121.9	6
242	DC-V15 (Canopus gate inhibit override, gyros *off*)		−121.9	6
			−122.9	5
248	DC-V24 (Begin DAS encounter mode)	0.69	−122.9	5
252	Isolation panel *on* (OSE)	0.65	−112.9	15
252	Planet sensor output	0.66	−122.9	5
254	Threshold	0.1	−136.9	
	Return to nominal	0.67	−122.9	5
256	Deploy to high-gain antenna	0.7	−122.9	5
260	Threshold	0.1	−137.9	
262	DC-V19	0.71	−121.9	6
	Drifting	0.7	−122.9	5
	Science *off*	0.6	−121.9	6
	Science *on*	0.7	−121.9	6
276	Magnetometer ignition	Loss of Lock		

Table 36. Degradation determined with DFR, VHF receiver *on*, M67-1

Measured change, dB	Spacecraft-contributed effective noise temperature, °K	Space degradation for various cosmic temperatures, dB		
		For 6000°K	For 7000°K	For 8000°K
5	375	0.2	0.2	0.2
6	855	0.6	0.5	0.4
7	1445	0.9	0.8	0.7

or 7 dB. This degradation occurred in the presence of a background-noise level of the Spacecraft Assembly Facility. Before the data can be used, the test area background-noise level must be found. The background-noise-level temperature is determined from the data of Table 35 by noting the degradation of the DFR VHF channel when connected to the spacecraft antenna referenced to a 50 Ω termination at the DFR input. From the data it is seen that the change in required RF signal was 4 dB. The background effective antenna noise temperature with the spacecraft *off*, is then found from the following relationship:

$$4\,\text{dB} = 10 \log \frac{T_{DFR} + T_{SAF}}{T_{DFR} + T_{Term}}$$

With

T_{DFR} = 290°K for the DFR VHF receiver noise temperature (3-dB noise figure)

T_{Term} = 290°K for the 50 Ω termination at ambient temperature

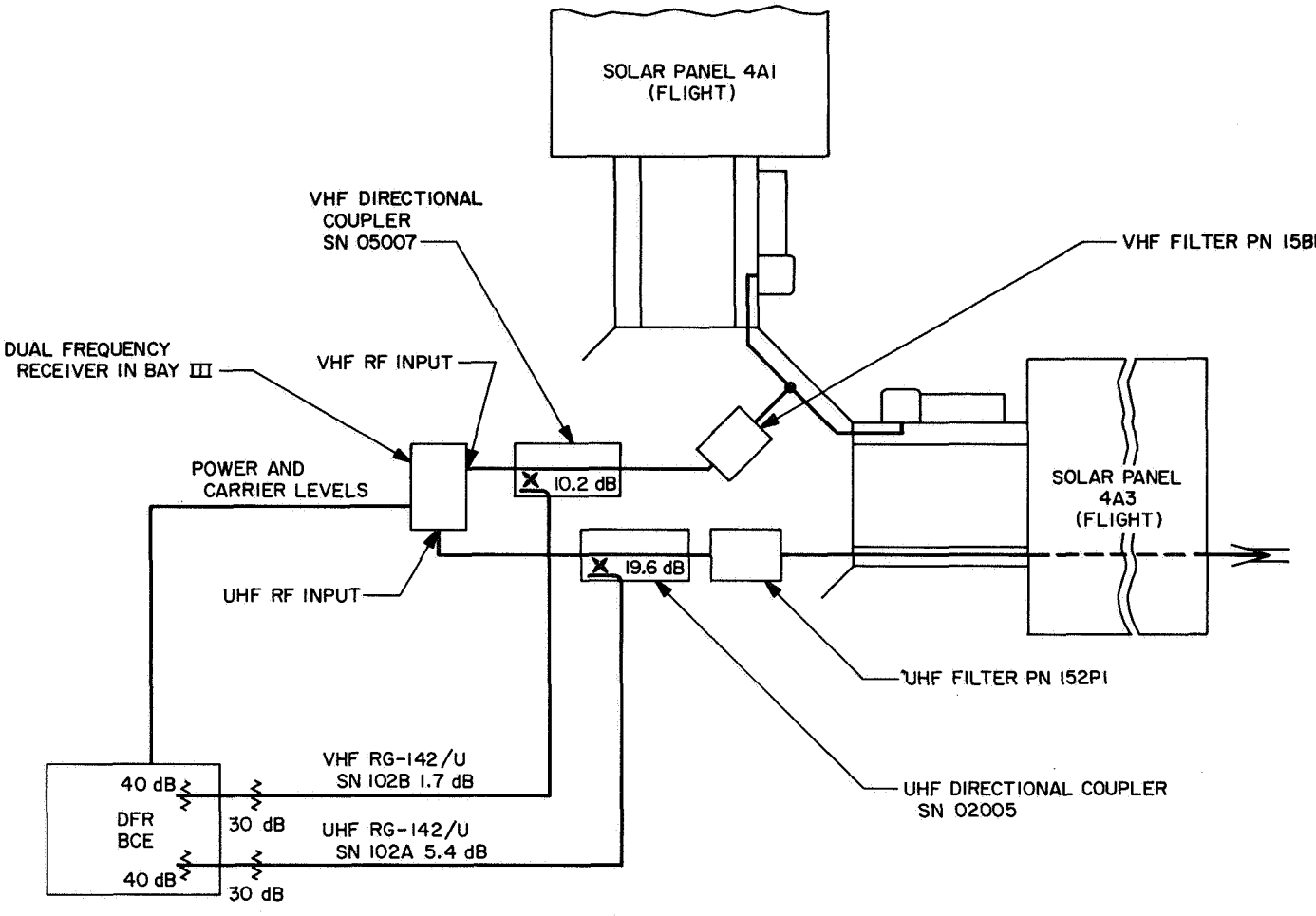

Fig. 76. Dual-frequency receiver test configuration

The effective antenna noise temperature T_{SAF} for SAF with the spacecraft *off* is, then, 1165°K. For the remainder of these tests, this background temperature level is assumed to remain constant.

The values of effective antenna temperature $T_{S/C}$ with the spacecraft *on* are determined from the following expression:

Measured degradation in decibels is

$$\text{dB} = 10 \log \frac{T_{DFR} + T_{SAF} + T_{S/C}}{T_{DFR} + T_{Term}}$$

Three separate effective antenna temperatures contributed by the spacecraft in various modes are determined from the 5, 6, and 7 dB degradation levels. Table 36 summarizes the effect of each spacecraft noise mode in the presence of cosmic noise expected during the mission. These levels are determined from:

Expected degradation in space in decibels is

$$\text{dB} = 10 \log \frac{T_{DFR} + T_{COSMIC} + T_{S/C}}{T_{DFR} + T_{COSMIC}}$$

The data show that there is no degradation to the VHF channel of the DFR.

No DFR acquisition threshold degradation results were obtained, since this test was not performed because of operator misinterpretation of the test procedure.

The test for spacecraft noise environment at S-band was not performed during the spacecraft/DFR electromagnetic compatibility test. Limited available test time was one of the factors considered by the Test Manager in eliminating this portion of the test at this time. The RF survey with EMI test receivers was performed on a non-interference basis during portions of the final system test. No RF levels were observed at either the center

frequency or the image. The low-gain antenna was used, as well as the high-gain antenna in its initial position.

(7) *Anomalies.*

Spacecraft Noise Environment at DFR Receiver Frequencies. None. The test configuration and RF line losses are shown in Fig. 75. Immediately prior to the performance of this test, the DFR bench checkout equipment cognizant personnel encountered RF leakage problems between the spacecraft and the test equipment. Considerable adjustment of equipment and an exchange of coaxial cables, in addition to shielding attempts, were made so that the test could be performed. The test was able to proceed after sufficient isolation was obtained.

DFR Operation Threshold Degradation. This test was not performed due to operator misinterpretation of the test procedure.

DFR Acquisition Threshold Degradation. None. The intent of this portion of the test was not carried out. Instead of gradually increasing the BCE signal to determine the acquisition level a strong signal was employed to lock the receiver.

Spacecraft Noise Environment at S-Band Receiver Center and Image Frequencies and Operation Degradation Tests. This test was not performed during the spacecraft/SFR electromagnetic compatibility test. Limited available test time was one of the factors considered by the Test Manager in eliminating this portion of the test at this time. The RF survey with EMI test receivers was performed on a non-interference basis during portions of the final system test. No RF levels were observed at either the center frequency or the image. The low-gain antenna was used, as well as the high-gain antenna in its initial position.

(8) *Follow-up activity.* There were no follow-up activities relative to the M67-1 DFR/S-band/system-configuration EMC test.

(9) *Recommendations.* If the decision had been made to launch the M67-1 spare spacecraft, it was recommended that the DFR acquisition threshold degradation test, as well as the spacecraft noise environment at S-band receiver center and image frequencies and operation degradation tests be made part of the flight qualifying requirements.

e. M67-1 subsystems requalification following systems-level testing. This material is presented to consider subsystems that did not receive a valid system-level environmental test history – from such possible causes as late delivery or subsequent rework, after systems test, which invalidated system flight status – and to describe what was done to offset that deficiency.

There were five M67-1 subsystems whose systems-test qualification was invalidated because of rework necessary following the spare spacecraft's systems environmental testing. The following information was extracted from two internal publications on the subject of retesting the subsystems. Because of the differences in the extent of rework, the time available, mission profile, and subsystem history, the retest plans for each of the subsystems were not identical but, in general, they required some degree of FA retesting, plus 200 to 300 h operating time.

Data Automation Subsystem. There were two reasons for retesting the DAS:

(1) The master clock frequency of the DAS was changed as a part of the DFR EMI fix by replacing the clock crystals.

(2) As a result of two failures caused by unsoldered transformer leads, a detailed X-ray examination of all transformers was performed, and 48 suspect DAS transformers (PE 6161) were replaced.

Three retesting requirements were made for the M67-1 DAS:

(1) Modules 20A2, 20A3, and 20A4 were subjected to the FA vibration levels specified in the axis which is perpendicular to the plane of the module circuit boards. The modules were mounted in the dummy-loaded vibration test case for the test.

(2) Upon completion of the vibration test, the complete DAS was retested in accordance with the specifications requirement for performance test with PDP-4 computer nominal and marginal voltages at room temperature.

(3) The entire DAS subsystem was subjected to the FA thermal–vacuum levels specified. Following FA thermal–vacuum test, the unit was subjected to 200 h of operating time in thermal–vacuum prior to redelivery to SAF, schedule permitting.

Radio Subsystem. Cavity amplifier power supply (2PS2, SN 14353), TWT power supply (2PS3, SN 14346), and transponder ×30 frequency multipliers (SN 11 and 12) were modified in accordance with ECRs: three tantalum capacitors were replaced in the 2PS2 and two tantalum capacitors in the 2PS3, by units with improved terminal seals. The transponder modification consisted of fillet-bonding the output cavity to the ×30 multiplier module cover.

The M67-1 radio subsystem had completed FA environmental tests as a subsystem in accordance with the requirements before undergoing spacecraft FA testing.

After modifications were completed, the specified requirements for retesting the radio subsystem were waived, and the following tests were performed to establish a satisfactory confidence level:

2PS2: FA vibration test in Z plane only. Power down (Launch Mode) condition. Outputs connected to a dummy load were monitored and recorded.

FA vacuum-temperature test with 1 h at 0°C and 20-h operation after stabilizing at +55°C. Power up condition with outputs connected to dummy load and monitored.

Operation at room ambient pressure and temperature in power up condition with outputs connected to a dummy load for a minimum of 100 h, 200-h goal. Performance was monitored.

2PS3: FA vibration test in Z plane only. Power down (Launch Mode) condition. Outputs connected to a dummy load. Monitor and record output voltage and current.

FA vacuum-temperature test with 1 h at 0°C and 20-h operation after stabilizing at +55°C. Power up condition. Outputs connected to dummy load and monitored.

Operation at room pressure and temperature. Power up condition. Outputs connected to dummy load. Test time: 100-h minimum, 200-h goal. Performance was monitored.

×30 Module: Bench test with complete radio subsystem after foregoing power supply tests. Bench test to demonstrate satisfactory performance in accordance with the requirements of the specification.

Tape recorder subsystem.

(1) *Vibration.* The 16A2 was vibrated in a bay V dummy module to FA limits at JPL in one plane only. 16A1 was vibrator tested at Raymond Engineering Laboratory, Inc. (REL), as part of the rework effort.

(2) *Thermal–vacuum.* The entire tape recorder system (TRS) was tested at FA temperature limits at REL. This test lasted approximately 4 h at each temperature and was not in a vacuum. A leak test of 16A1 was performed at REL in a vacuum, but only at ambient temperature; the REL vacuum test does not have temperature cycle capability. The JPL margin and acceptance testing were performed by JPL personnel in parallel with the REL test to expedite delivery to the spacecraft. The entire TRS was subjected to a total of 200-h operating time prior to redelivery.

Power subsystem. During a life test that was being performed on the TA power supply unit, a capacitor failure occurred in the three-phase inverter subassembly (4A18). This capacitor was replaced, and the replaced capacitor then failed. It was determined that these failures were independent of one another, and the decision was made to change capacitor type in each power supply subsystem.

The retesting requirements for the M67-1 power supply (4A18) were the following:

(1) Perform FA shake in 3 axes and 40 h in FA thermal–vacuum per specification with the flight 4A18 installed in the TA unit.

(2) The unit (still in the TA unit) was subjected to 250 h of testing under vacuum conditions at room temperature with power *on.*

DFR subsystem. After the 7-MHz crystal had been replaced in DFRs 2 and 3, the FA tests were performed at JPL. The requirements of the JPL specification were modified, as follows, for this retest only:

(1) The vibration test was on one axis only (spacecraft roll).

(2) Vacuum temperature test time was 30 min, or more, at 0°C and 4 h, or more, at 55°C.

Testing was satisfactorily completed. The only anomaly was a correction to a tuning circuit.

Additional information regarding these subsystems can be found in the following paragraphs on subsystem-level FA testing.

2. Subsystem level.

a. Spacecraft M67-1 flight-acceptance testing. A summary of the M67-1 flight-acceptance subsystem testing is presented in Table 37. This table shows each of the subsystems that were on the M67-1 spacecraft and discusses any significant past test history experienced by that unit during the *Mariner* Mars 1964 test program. The table also depicts the dates on which the units underwent vibration and thermal–vacuum testing and whether they passed or failed; and notes describe all of the problems and/or failures that resulted from the flight acceptance subsystem testing associated with the M67-1 spacecraft.

Summaries of all waivers and test deviations which were written against M67-1 hardware during the *Mariner* Venus 67 flight acceptance testing program and of the M67-1 flight equipment which was flight-acceptance tested during the *Mariner* Mars 1964 program is included. The flight equipment listed in this summary passed all of the flight acceptance requirements on the *Mariner* Mars 1964 program without any failures or anomalies and was accepted as flightworthy for the *Mariner* Venus 67 program. All other equipment was modified either to increase its reliability or because the functional requirements were changed by the difference in the science payloads between the two missions.

Summary of FA waivers and test deviations for M67-1 spacecraft subsystems.

(1) *Data automation subsystem.* The DAS was retested after the M67-1 spacecraft had gone through system environmental testing because the crystals in the DAS master clock were changed as part of the DFR EMI fix. The retest requirements were as follows: (1) Modules 20A2, 20A3 and 20A4 were subjected to partial FA vibration levels; (2) upon completion, the entire DAS was subjected to a partial FA vibration test and (3) following this, the entire DAS was FA thermal–vacuum. tested, which consisted of 200 h of operating time in thermal–vacuum prior to redelivery to the spacecraft.

(2) *Trapped radiation detector.* There were no waivers or deviations on this unit.

(3) *Plasma probe.* There were no waivers or deviations on this unit.

(4) *Magnetometer.* There were no waivers or deviations on this unit.

(5) *UV photometer.* An internal memorandum waived the requalification testing of replacement filters for the UV photometer.

(6) *Dual-frequency receiver.* Flight-acceptance testing of the DFR filters was waived on a subsystem level because they were qualified on the M67-1 spacecraft at the system level. The DFR was retested after the 7-MHz crystals were replaced. The retest consisted of one plane of vibration, only, and a thermal–vacuum test of 30 min at 0°C and 4 h at +55°C. This is the only M67-1 subsystem which had to be requalified after the M67-2 spacecraft system environmental testing was completed.

(7) *Transponder (radio): Cases V and VI.* Flight-acceptance testing of the radio after modification in accordance with ECRs occurred after the M67-1 spacecraft had gone through system environmental testing. The modification consisted of replacing three capacitors in the 2PS2 unit and two capacitors in the 2PS3 unit and, also, of fillet-bonding the ×30 multiplier module. The retest consisted of the following: (1) FA vibration, Z axis only, of 2PS2 and 2PS3; thermal–vacuum testing for 1 h at 0°C and 20 h at +55°C; also, a minimum of 100 h at room ambient pressures and temperature. (2) The ×30 module was bench tested with the complete radio subsystem after foregoing the power-supply test.

(8) *Data encoder.* There were no waivers or deviations on this unit.

(9) *Command subsystem.* There were no waivers or deviations on this unit.

(10) *Tape recorder.* An internal memorandum covers the FA retesting of the tape recorder after modification in accordance with ECRs. This occurred after the M67-1 spacecraft had gone through system environmental testing. The modification consisted of potting of 16A1 and 16A2 modules with new potting compound and the replacement of a diode in the 16A4 module. The retest consisted of the following: (1) FA vibration was run on one plane, only, of 16A1 and 16A2. (2) FA temperature test was conducted of the entire TRS at ambient pressures for 4 h at each specified temperature.

(11) *High-gain antenna.* A waiver permitted changing FA thermal–vacuum test temperature from −260°F for 2 h to −245°F ±5°F for 2 h.

Table 37. Summary of M67-1 flight-acceptance testing

Subsystem or assembly	Serial No.	Significant *Mariner* Mars 1964 FA test history	Design changes for *Mariner* Venus 67	M67-1 FA testing summary				
				Vibration test		Thermal–vacuum test		Comments
				Date	Results	Date	Results	
Data automation system 20A1-9	071	None.	New design	11/29/66 2/13/67	Passed Passed (4)	12/2/66 3/10/67	Passed Passed (4)	(1) Retest of 20A2 and 20A4 at FA vibration levels and retest of complete DAS at FA vibration levels due to replacement of crystals. (2) PFR written against subchassis that started to corrode. (3) Three PFRs for damaged 20A5, 20A7, and 20A8 during troubleshooting; retest at same time as crystals. (4) Changed crystal and changed resistor.
Trapped radiation detector 25A1	MC-1	MC-1 had three FA tests. This unit now on 67-1.	Significant	10/12/66 11/2/66	Passed Passed (1)	10/20/66 11/5/66	Passed Passed (1)	(1) Due to fractured GM tube, unit was reworked—which necessitated FA retesting. (2) Unit tested using nonstandard test temperatures, per specification.
Plasma probe 32A1-4	M67-1	No history found. Life test unit used as MC-4 spare; no known problems.	Significant	10/6/66 11/10/66	Passed Passed (1)	10/13/66 11/14/66	Passed Passed (1)	(1) Due to change of high voltage cable and 2 resistors, unit was FA retested. (2) PFR for high noise readings. (3) Unit tested using nonstandard test temperatures, per specification. (4) PFR written because unit exceeded lower TA levels.
Magnetometer 33A1-3	M67-1	33A1 and 33A2 were prototype units, and 33A3 a TA unit on *Mariner* C.	Small	9/28/66	Passed	9/18/66* 9/20/66	Failed (1) Passed	(1) PFR written for thermal–vacuum failure; sensor lamp and cell would not ignite at +40°C. (2) Unit tested using nonstandard test temperatures, per specification.
UV photometer 34A1 and 2	M67-2	MC-2 unit, no history.	Small	8/19/66	Passed	8/21/66	Passed	
Dual-frequency receiver 35A1 and 2	2	None.	New design	12/5/66 4/18/67	Passed Passed (2)	12/10/66 4/19/67 4/20/67	Passed Failed (3) Passed (3)	(1) PFR recorded abnormal values during space simulation test. (2) Abbreviated FA test was run because of crystal replacement. (3) Per PFR 7992—Retest because retuning of RF assembly required.

Radio bays V and VI	7	This system, known as unit 7, went through vibration, part I of thermal–vacuum test, and was on MC-4 when chamber lost vacuum. Also, this system was overstressed in thermal–vacuum FA testing. Case V heated to +165°F, Case VI cooled to −208°F.	Significant	10/29/66 10/31/66 11/1/66 3/10/67 3/22/67	Failed (2) Passed Passed (3) Passed (5) Passed (5)	11/5/66 3/17/67	Passed Passed (5)	(1) T/R unit dropped on floor. (2) PFR written for vibration failure. (3) Re-ran mode 3, Y axis only, for rework that involved this circuit. (4) ECRs for replaced capacitor and cavity bonding. (5) Retest per memo.
Data encoder 6A1-13	201	This system went through all MC-4 tests up to flight. It was on MC-4 when chamber failed. This system went through two FA vibration tests.	Small	9/20/66	Passed	9/26/66	Passed	None.
Command subsystem 3A1-7	5, 6	3A1, 3A2, and 3A3 tested on MC-4 spacecraft; was on MC-4 when chamber failed.	Significant	10/17/66	Passed	1/25/66	Passed	None.
Tape recorder 16A1-6	6	16A1 SN on MC-4 through first system test at AFETR; also on MC-4 during chamber failure. 16A3 SN 2 on *Mariner* Mars 1964 PTM. This unit did not go through FA vibration on *Mariner* Mars 1964. 16A6 new to *Mariner* Venus 67. Balance of units on MC-5.	Major	11/4/66 3/7/67	Passed Passed (1)	11/3/66.	Passed	(1) Three ECRs incorporated in 16A2; one plane of vibration only.

Table 37 (contd)

Subsystem or assembly	Serial No.	Significant *Mariner* Mars 1964 FA test history	Design changes for *Mariner* Venus 67	M67-1 FA testing summary				
				Vibration test		Thermal–vacuum test		Comments
				Date	Results	Date	Results	
High-gain antenna 2E1	9	No record found.	New support structure	10/28/66	Passed	11/1/66	Passed	(1) Unit tested using nonstandard test temperatures, per specification. (2) PFR written for thermal paint that cracked. ECR written for removal of paint.
Low-gain antenna 2E2	C120	No record found.	None	8/21/66	Passed	Waiver deleting thermal–vacuum test		
DFR antenna 423.3 MHz 15E3	4	None.	New design	11/30/66 12/12/66	Failed (1) Passed	Not required		(1) 15E3 SN 4 retested for FA vibration—Failure of bonding noticed after FA test was completed. ECR accomplished rework. SN3 experienced same failure but was a spare unit not assigned to a spacecraft.
DFR antenna 49.8 MHz 15E2F1 and 2	C102	None.	New design	Not required				There is no FA testing of DFR antenna 15E2F1 and 2; configuration precludes assembly-level test.
A/C Electronic-Control System 7A1	006	Originally a spare; replaced SN 003 on MC-4 after chamber failed. Continued with MC-4 through final system test at AFETR.	Small	8/22/66	Passed (2)	See comments	Passed	(1) Unit tested in air. (2) Partial FA test required of qualified *Mariner* Mars 1964 system after incorporation of ECRs.
A/C gyros and Electronic control 7A2	017	Originally a spare —used on MC-4 at AFETR.	No change in *Mariner* Mars 1964 design	Tested on *Mariner* C (1)				(1) M67-1 spacecraft failure during vibration. Gyro rate reading 13% off (non-critical). (2) Unit qualified on *Mariner* Mars 1964.
A/C gas system 7GA1 and 2	M67-1	This system used as spare, only, on *Mariner* Mars 1964.	Significant	8/20/66	Passed	8/1/66	Passed	(1) FA testing for valves only. (2) Units tested using non-standard test temperature, per specification.
Canopus sensor 7CS8	107	No record found.	Major	9/29/66	Passed	9/24/66	Passed	Unit tested using nonstandard test temperatures. PFR written against relay K2 hangup during FA vibration test.

Sun sensor 7PS2 and 6 7SS2 and 6	8	This system used as spare only on *Mariner* Mars 1964.	None	Tested on *Mariner* Mars 1964				(1) Unit qualified on *Mariner* Mars 1964.
Sun gate sensor 7SG2	8	This unit used as spare only on *Mariner* Mars 1964.	None	Tested on *Mariner* Mars 1964				(1) Unit qualified on *Mariner* Mars 1964.
Earth sensor 7ED6	3	This unit used as spare only on *Mariner* Mars 1964.	Significant	9/12/66	Passed	9/11/66	Passed	Unit tested using nonstandard test temperatures, per specification.
Planet sensor 7LS8	002	None.	New design	9/23/66	Passed	9/28/66	Passed	Unit tested using nonstandard test temperatures, per specification.
Terminator sensor 7TS2	04	NAMG used as spare only on *Mariner* Mars 1964.	Significant	9/12/66	Passed	9/8/66	Passed	None.
Jet-vane actuators, vanes, and support ring 7JV5-6	C108	Used on *Mariner* Mars 1964.	No change	8/8/66 8/22/66 8/25/66 3/24/67	Passed Passed Passed Passed	8/4/66 8/10/66 8/23/66 8/26/66 3/27/67	Failed (1) Failed (1) Passed (2) Passed (2) Passed	(1) PFR written for assembly action that froze. (2) Three vibration and two thermal–vacuum tests required because all four actuators did not pass FA at the same time. (3) Units tested using nonstandard test temperatures, per specification.
Central computer and sequencer 5A1-9	M67-2	This unit was used as MC-5 spare only.	Small	7/21/66	Passed	9/28/66	Passed	None.
Power (bay I) 4A11-13 4A15-18	05	It appears that this system was used as spare only on *Mariner* Mars 1964.	Significant	10/24/66 3/20/67	Passed Passed	10/26/66 3/17/67	Passed Passed (1)	(1) PFR written for capacitor failure, FA test re-run on 4A18.
Power (bay VIII) 4A8	06	This unit used as spare only on *Mariner* Mars 1964.	Significant	10/21/66	Passed	10/14/66 10/19/66	Failed (1) Passed	(1) PFR written for transformer lead fractured at solder joint.
Battery 4A14	31	None.	Small	12/12/66	Passed	Not required		None.

Table 37 (contd)

Subsystem or assembly	Serial No.	Significant *Mariner* Mars 1964 FA test history	Design changes for *Mariner* Venus 67	M67-1 FA testing summary				
				Vibration test		Thermal–vacuum test		Comments
				Date	Results	Date	Results	
Solar panels 4A1 4A2 4A3 4A4	003 004	None.	Major	12/12/66 12/15/66	Passed Passed	12/4/66 12/12/66	Passed Passed	(1) PFR written for responses of SN 003, 004, and 005 during FA vibration not as required or as predicted. (2) Unit tested using nonstandard test temperatures, per specification.
Louver assemblies	17 18 19 20 21 38	Five of the louvers, SN 17 through 21, used on MC-1. SN 38 MC-5 spare.	None	Temperature calibrated in air only (all required) completed 7/16/66				None.
Temperature-control reference unit	M67-1	None.	New design	Not required		11/18/66* 11/19/66 11/21/66	Passed Passed Passed	(1) PFR written because SN 14 delaminated during thermal–vacuum test; unit scrapped. No other units exhibited this problem.
Low-gain antenna dampers	C101 C101		Nonflight	Hardware				Flight units SN 102 on M67-1 spacecraft during spacecraft vibration.
Solar-panel-tip dampers 4A1 4A3 4A5 4A7	111, 112 113, 114 115, 116 117, 118	None.	New design	Not required				Same dampers used on STM.

Solar panel cruise dampers Bay I Bay III Bay V Bay VII	C-119 C-120 C-121 C-122	Used on MC-1 PTM.	No change	Tested on *Mariner* Mars 1964				(1) Units qualified on *Mariner* Mars 1964.
Separation-initiated timer 8M1	C106	Used on MC-4.	No change	9/15/66	Passed	Not required		None.
Pyro arming switch 8AS1	C110	Used on MC-4.	None	9/7/66 9/8/66 9/12/66	Passed Failed (1) Passed	Not required		(1) Z-axis vibration, only, retest to see if it would remain acceptable. One switch point seemed marginal.
PIPS 10A	M67-1	This unit assigned to MC-4.	Small	*Mariner* C FA tests still valid				(1) Covers flow test of pneumatic regulator.
Pyro control 8A1 and 2	1009, 1010	Used as spares, only, on *Mariner* Mars 1964.	Small	10/6/66	Passed	10/1/66	Passed	None.

(12) *Low-gain antenna.* The requirement to do FA thermal–vacuum testing of the low-gain antenna was waived by an internal memorandum.

(13) *DFR antenna.* There were no waivers or deviations on this unit.

(14) *Attitude-control electronics.* Two ECRs cover FA retesting of the unit after design change. The test consisted of one plane, Z axis only, of vibration.

(15) *Attitude-control gyro.* There were no waivers or deviations on this unit.

(16) *Attitude-control gas.* There were no waivers or deviations on this unit.

(17) *Canopus sensor.* An internal communication waived the FA demagnetization requirement for the Canopus sensor.

(18) *Sun sensors.* An internal communication waived the FA lower temperature limits. The waiver was based on special test results.

(19) *Earth and terminator sensors.* A waiver revised the lower FA test temperature to 0°F.

(20) *Planet sensor.* There were no waivers or deviations on this unit.

(21) *Jet vane actuators.* An internal communication waived the +20°F temperature test on SN 108. The unit passed FA at +32°F before specific action was changed. The waiver was based on special test results.

(22) *Central computer and sequencer.* There were no waivers or deviations on this unit.

(23) *Power bays I and VIII.* The FA retesting of the 4A18 power conversion unit after replacement of a capacitor in the unit was accomplished after the M67-1 spacecraft had gone through system environmental testing. Retest consisted of the following: Flight unit 4A18 was installed in the FA subsystem and FA vibration-tested in all three axes; it was then subjected to 40 h of FA thermal–vacuum testing. In addition, unit was tested for 250 h at room temperature with power *on.*

(24) *Battery.* There were no waivers or deviations on this unit.

(25) *Solar panels.* An internal memorandum waived FA acoustic testing of flight solar panels. Another waived FA vibration of flight solar panels.

(26) *Thermal control assembly.* There were no waivers or deviations on this unit.

(27) *Dampers.* There were no waivers or deviations on this unit.

(28) *Separation-initiated timer.* There were no waivers or deviations on this unit.

(29) *Pyro arming switch.* There were no waivers or deviations on this unit.

(30) *Post-injection propulsion system.* There were no waivers or deviations on this unit.

(31) *Pyrotechnic control.* There were no waivers or deviations on this unit.

Mariner Mars 1964 flight-acceptance testing of MV67-1 flight equipment. The flight equipment listed below passed all flight-acceptance requirements on the *Mariner* Mars 1964 program without any failures or anomalies and was accepted as flightworthy for the *Mariner* Venus 67 program.

(1) *Attitude-control gyros.* The attitude-control gyros and control assembly, 7A2, SN 017, passed all flight-acceptance requirements on the *Mariner* Mars 1964 program without any failures or anomalies.

(2) *Sun sensors.* The sun sensors, 7PS2 and 7PS6, SN 8; 7SS2 and 7SS6, SN 8; and the sun gate sensor 7SG2, SN 8, passed all FA requirements on the *Mariner* Mars 1964 program without any failures or anomalies. All test results can be found on TRSFs on file in the Environmental Requirements Group.

(3) *Solar panel cruise dampers.* The solar panel cruise dampers, bays I, III, V and VII, SN C-119 through C-122, passed all FA requirements on *Mariner* Mars 1964 program without any failures or anomalies. All test results can be found on TRSFs on file in the Environmental Requirements Group.

(4) *Post-injection propulsion system.* The PIPS, which was originally SN MC-64, now SN M67-1, passed all FA requirements on *Mariner* Mars 1964 program without any failures or anomalies.

b. Special subsystem tests.

Dual-frequency receiver (SN 02) EMI testing. Dual-frequency receiver electromagnetic interference testing was performed to verify that the DFR would function properly when subjected to an electromagnetic environment similar to that expected to exist on the *Mariner* Venus 67 spacecraft.

(1) *Requirements vs test.* The *Mariner* Venus 67 DFR used a configuration that had not flown on a spacecraft nor had been subjected to an electromagnetic environment similar to that expected for the *Mariner* Venus 67 spacecraft. The EMI testing levels that were used to verify that the DFR would function properly were derived from data acquired during the testing sequence of the *Mariner* Mars 1964 spacecraft and the expected electromagnetic environment for the *Mariner* Venus 67 spacecraft. In accordance with the specification, the DFR was tested per JPL procedure. Listed in Table 38 are the required tests and the defined test limits.

Table 38. M67-1 dual-frequency receiver EMI tests and test limits

Electromagnetic interference	Interference limits	
	Specification	JPL procedure
Generated interference		
Generated conducted transient	$<\pm 0.5$ V max	$<\pm 0.5$ V max
Generated sinusoidal		
30 Hz to 150 kHz	<0.5 V peak to peak	<0.5 V peak to peak
15 to 150 kHz	<0.5 V peak to peak, decreasing at 20 dB/octave to 0.05 V peak to peak at 150 kHz	<0.5 V peak to peak
150 kHz to 25 MHz	<0.05 V peak to peak	0.05 V peak to peak
Conducted interference susceptibility power leads		
Transients	± 8 V amplitude ≤ 20 μs wide ≤ 7 μs rise time Repetition rate: 0.5 to 500 pps	± 8 V amplitude
Sinusoidal		
30 Hz to 15 kHz	0.5 V peak to peak	0.5 V peak to peak
15 kHz to 150 kHz	0.5 V peak to peak at 15 kHz, decreasing at 20 dB/decade to 0.05 V peak to peak at 150 kHz.	0.5 V peak to peak
150 kHz to 25 MHz	0.05 V peak to peak	0.05 V peak to peak
Conducted interference susceptibility-signal lines		
Transients	± 200 mV amplitude ≤ 20μs wide ≤ 7 μs rise time Repetition rate: 0.5 to 500 pps	± 200 mV amplitude

Electromagnetic interference	Interference limits	
	Specification	JPL procedure
Sinusoidal		
30 Hz to 15 kHz	0.05 V peak to peak	0.05 V peak to peak
15 to 150 kHz	0.05 V peak to peak at 15 kHz, decreasing at 20 dB/decade to 0.005 V peak to peak at 150 kHz	0.05 V peak to peak
150 kHz to 25 MHz	0.005 V peak to peak	0.005 V peak to peak
Equipment enclosure radiated interference susceptibility test		
Frequency, MHz	**Power density, dBmW/m²**	**Power density, dBmW/m²**
229.9	− 8	—
244.3	−19	—
2297.5	− 2	—
5765	−18	—
8000	− 9	—
9000	−12	—
Spurious response susceptibility test		
Frequency, MHz	**Signal level, dBmW**	**Signal level, dBmW**
27.5	−65	—
2000	−75	—
2150	−65	—
2220	−78	—
2297.5	− 2	—
2450	−59	—
2600	−73	—
4590	−62	—
9210	−76	—
Oscillator radiation test		
2115–2116	−100	—

(2) *Results.* The DFR (SN 02) was subjected to EMI testing for flight acceptance as outlined in the JPL procedure. The DFR successfully passed the tests as specified and operated within the prescribed limits, with no degradation to operation during all electromagnetic interference testing.

Solar panel single-panel FA testing.

(1) *Test plan.* The TA vibration test plan (see Section II) was intended to lead to proper FA test levels. The FA single panel test configuration was a vibration input to the hinged end of the panel with the damper attachment points attached to struts rigidly fastened at the other end to the floor of the test facility. Input levels were selected to result in a single panel response in two corrugation modes that would produce panel stresses equal to those that would result on the panel during part of the FA spacecraft test. The desired response at a control location (on the corrugation side of the panel) and an estimate of the required input at the hinges were derived during the TA test program. The test was to be conducted by sweeping over the specified frequencies at the estimated input level with a limiting accelerometer mounted at the response control location. If an instantaneous acceleration exceeding a level of 10% above the desired response were reached, the test would automatically, and instantly, be stopped. The test would then be repeated with the input level reduced by 3 dB. This procedure was necessary because the panel damping might vary (from panel to panel) sufficiently to cause the response to exceed the desired value. At a later date (prior to FA testing), the allowable response was loosened up to 20% above the nominal value in an attempt to make test limiting less likely.

It was clear that these tests were nonstandard and would require the presence of cognizant environmental requirements and structural engineers. On-the-spot action determinations were quite likely to be required by test phenomena that could not be anticipated prior to the actual test.

(2) *Test results.* Three flight solar panels (SNs 003, 004, and 005) were FA tested to the required input level without activating the response limiter. *No* cognizant environmental requirements nor structural engineers were present, and the results of the test could only be evaluated in retrospect. For this test, the adequacy criteria was not the attainment of specified input levels but, rather, the attainment of desired responses. The response at the response control location is plotted on Fig. 77. Interpretation of the indicated responses is complicated by two factors.

First, on panel SN 003, the response-control accelerometer was mounted on the cell face, while on SNs 004 and 005 the accelerometer was mounted on the rear of the panel in a valley of the corrugation. The specified location for the response accelerometer was on a peak of the corrugation inside the central channel member running the length of the panel.

Second, the peak of the fast-changing responses may be 1.4 to 1.8 times higher than indicated, due to excessive time constants in the analysis system discovered in later tests. It is known, however, that the response did not exceed the limit value (3.35-*g* peak) so the real response is between the indicated value and 3.35-*g* peak.

The desired response at the lower frequency resonance was 2.8-*g* peak; at the higher, it was 6.6-*g* peak. One of the panels (SN 005) did respond to a value between the indicated 2.0-*g* peak and the limit value 3.35-*g* peak. The other two panels may not have quite reached full resonance response. Since the objectives of the FA test requirements were not met, a PFR was written on these three tests, and reconsideration of the entire FA test program was undertaken.

The TA panel was retested in the single-panel configuration to measure the effect of (1) the location of the response accelerometer (cell side or peak of corrugation), (2) the torque of the hinge bolts, and (3) sweep direction. These data were to be used in understanding what happened during the three FA tests and how the future tests might be more properly performed. The test results showed that the measurement on the corrugations was about double that on the cells over the entire FA test frequency range and that sweep direction affected the apparent resonance in the classic manner (lower for downsweep). No effect of torque at the hinges was uncovered. This test proved that the previous assumption that the cell-side and corrugation-side accelerometers should agree was very much in error, because the peak of the corrugation accelerometer indicated a response about double that on the cell side.

Following a meeting between all cognizant engineers and Project personnel, it was concluded that the panels should not be FA tested in the single-panel configuration but, rather, that all panels (including those already FA tested) should be included as part of the system-level FA test.

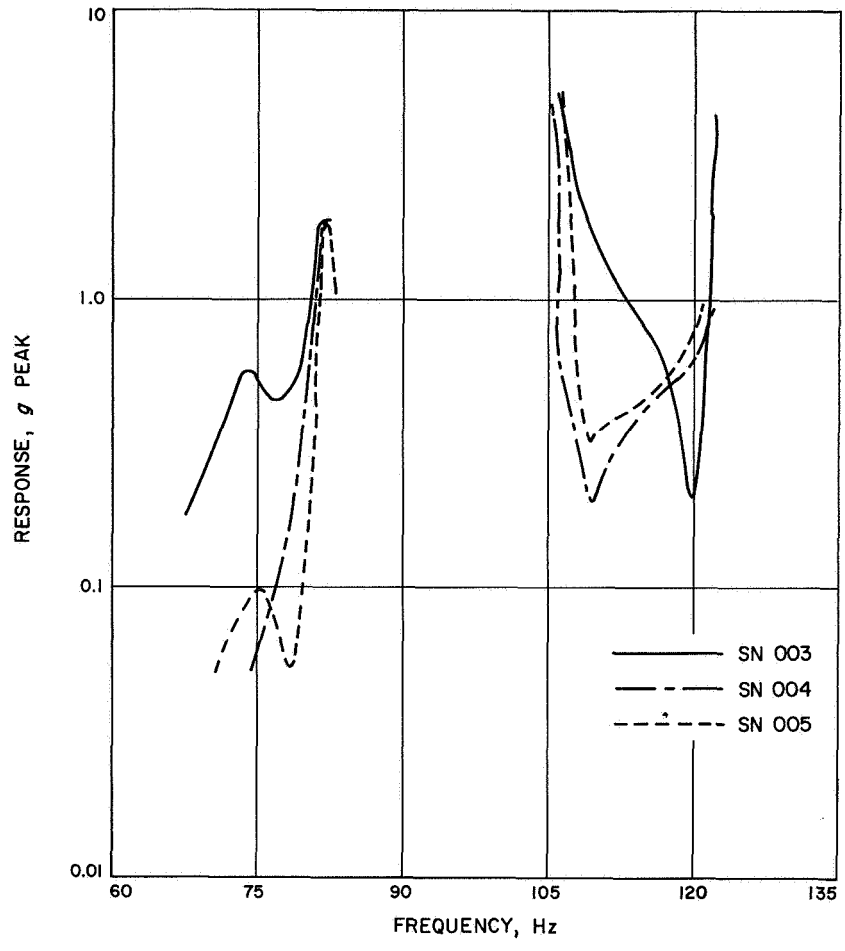

Fig. 77. *Mariner* Venus 67 single solar panel FA vibration test response at limit location

However, while this decision was being reached, another panel (SN 006) was inadvertently being FA tested.

For this panel (SN 006), the response-control accelerometer was located on the peak of the corrugation, as was originally intended. As a result of the higher output of this location, the test could not be conducted at the high-frequency sweep range (due to limiting). The test was conducted over the low-frequency range, but the limiter circuit was not correctly mechanized. Therefore, again due to the higher output on the corrugations, the specified limit value was exceeded (a response of 6.5-*g* peak compared with the limit value of 3.35-*g* peak). A modal test was conducted (at very low stress levels) on this panel and it was concluded that this response level would not be detrimental to the panel.

(3) *FA testing on the system FA tests.* All six flight panels were tested as part of a spacecraft system test. Panels SNs 003 and 004 were on M67-1, while 005, 006, 007, and 008 were on M67-2 (bays V, VII, I and III, respectively). No FA panel vibration was monitored on M67-1, but a response accelerometer was mounted on all panels on M67-2 (at the corrugation-peak location). Data from panels SNs 007 and 008 were lost during the *XY* bay II test. The maximum response during the low-frequency sine sweeps (all input axes) are shown on Figs. 78 through 81. The high-level resonance at 100 to 110 Hz (allowing a level of 50-*g* peak on SN 007) is not the one intended to be excited during single panel testing. The low-frequency resonance appears at 82 Hz on all panels and at about 80 to 82 Hz on the single panel FA test (Fig. 77). The high-frequency resonance appears at about 124 Hz. Apparently, the single panel FA high-frequency sine sweep was started just past the 100- to 110-Hz resonance and did not quite reach the 124 Hz resonance. The data in Figs. 78 through 81 show that the 82 Hz resonance was excited to 10- to 15-*g* peak. This would compare with the desired response of 2.8-*g* peak.

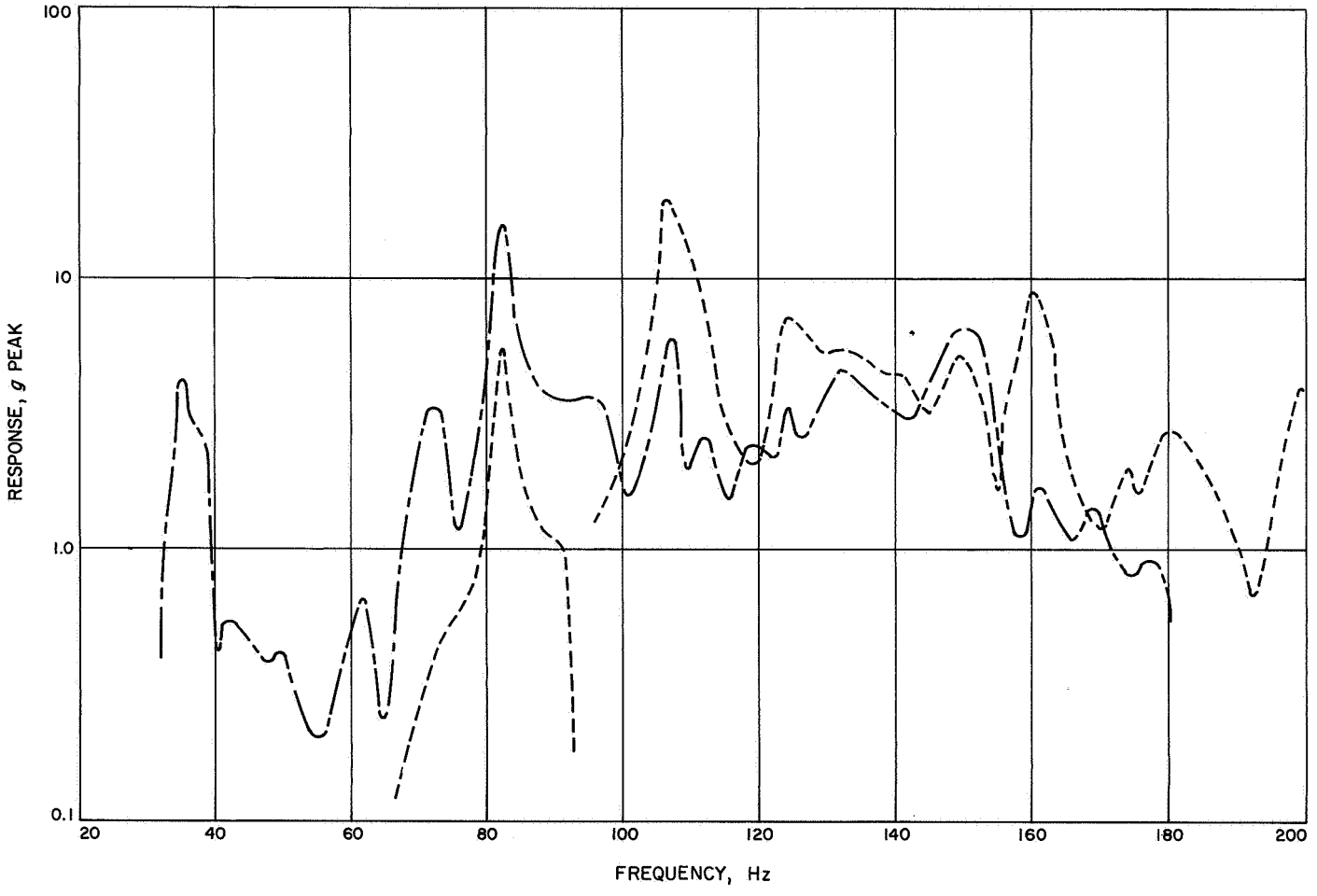

Fig. 78. *Mariner* Venus 67 maximum solar panel response at limit location during M67-2 system vibration test, SN 005

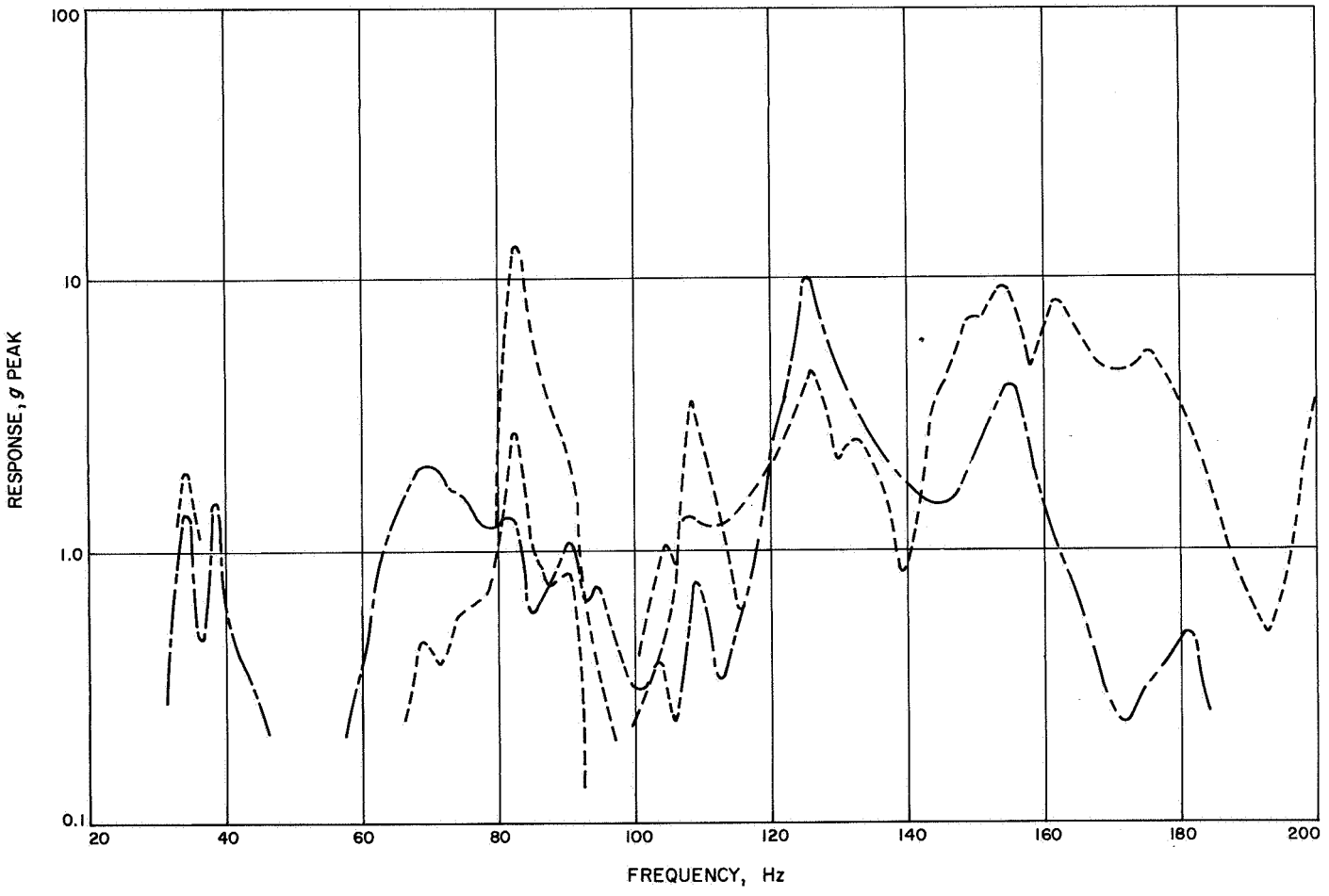

Fig. 79. *Mariner* Venus 67 maximum solar panel response at limit location during M67-2 system vibration test, SN 006

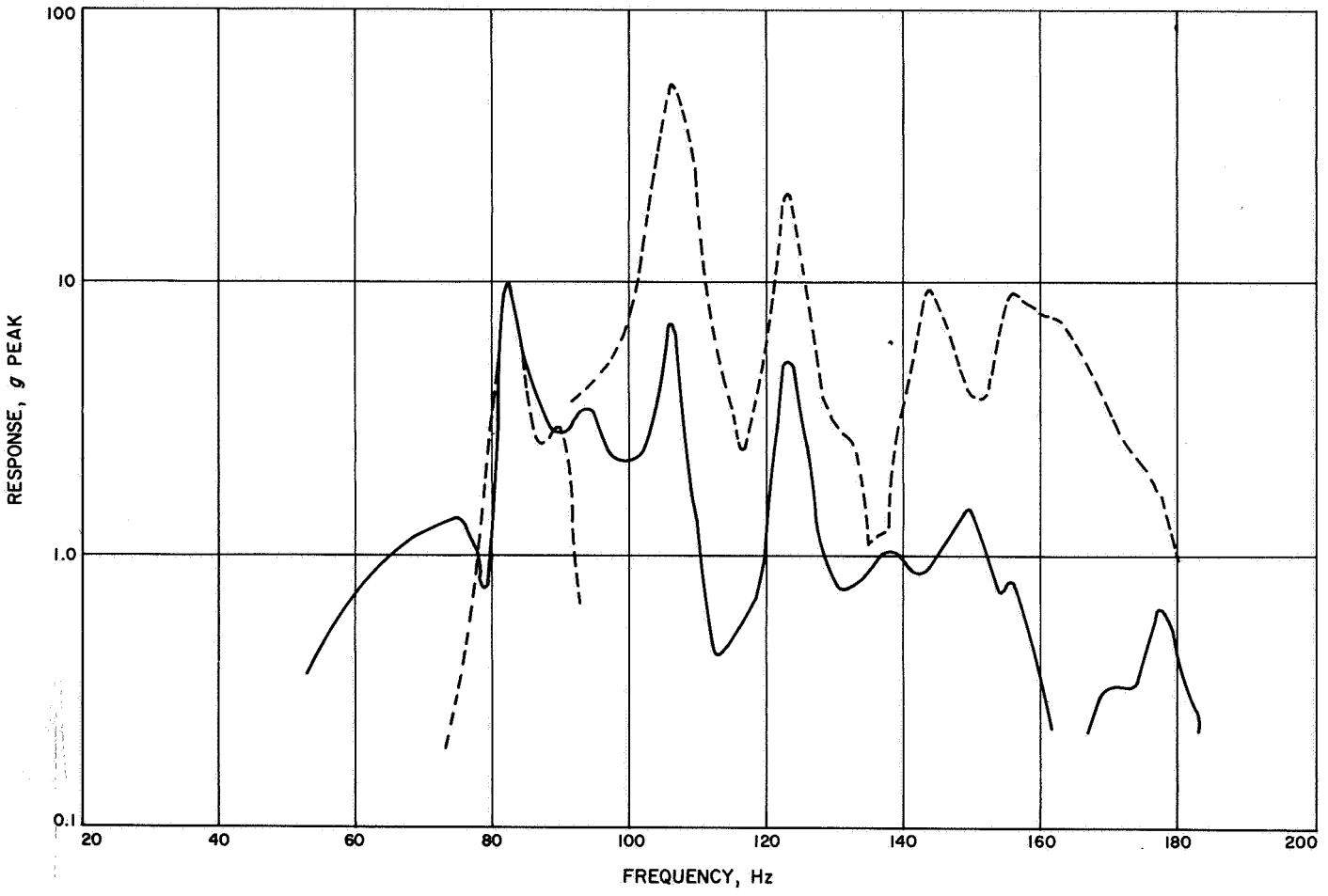

Fig. 80. *Mariner* Venus 67 maximum solar panel response at limit location during M67-2 system vibration test, SN 007

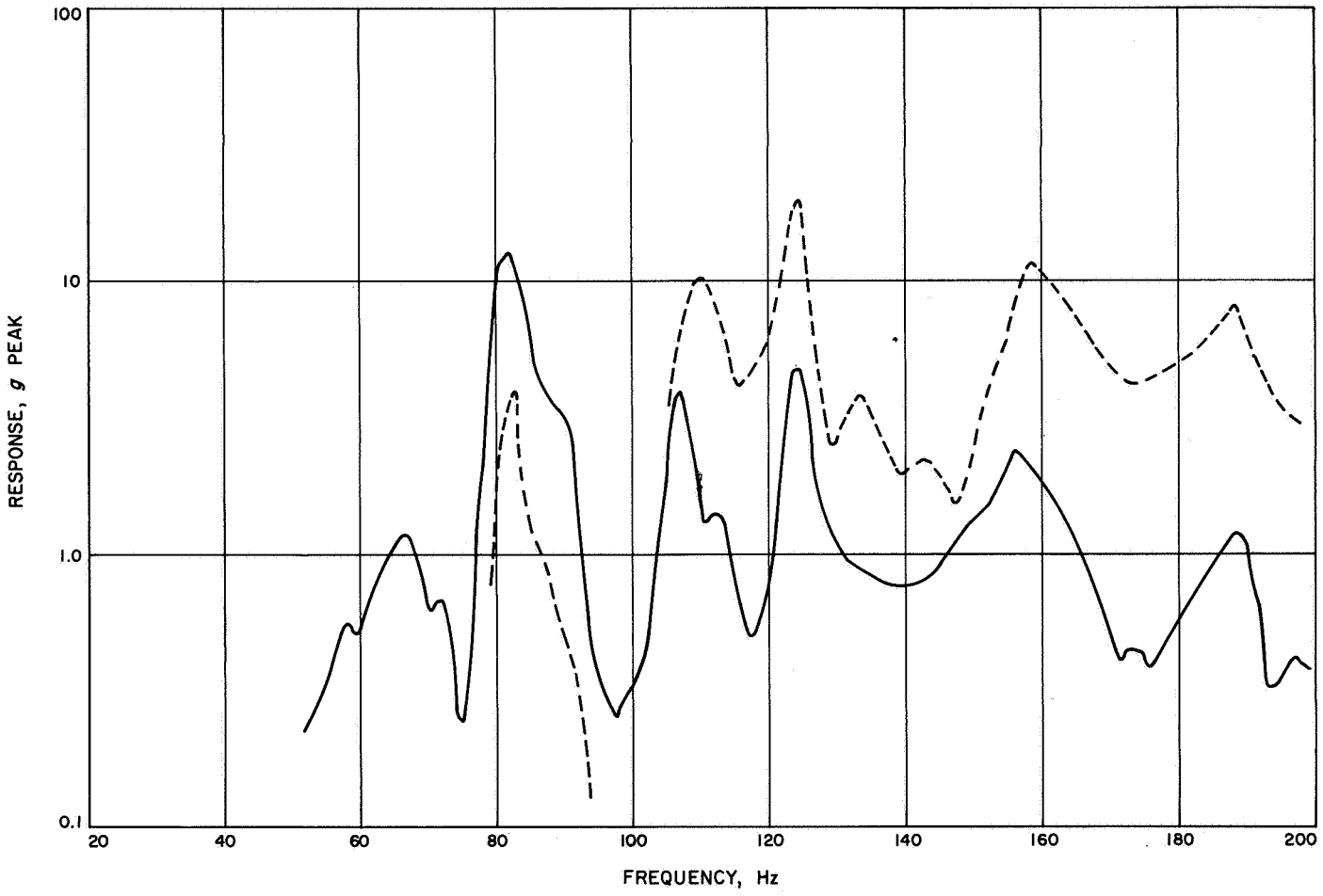

Fig. 81. *Mariner* Venus 67 maximum solar panel response at limit location during M67-2 system vibration test, SN 008

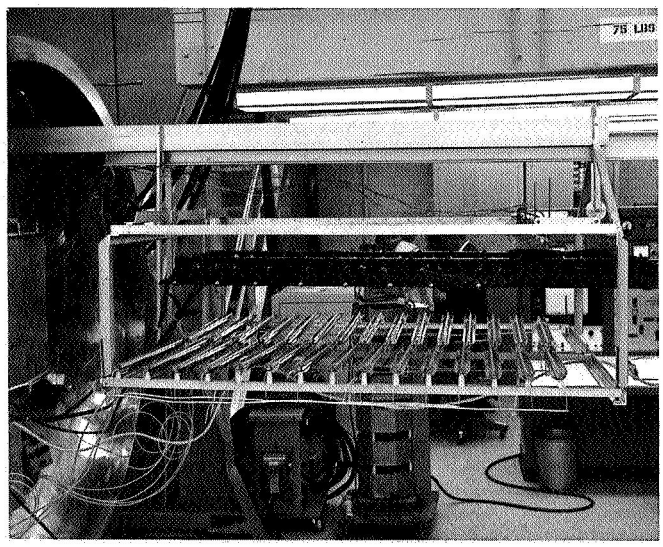

Fig. 82. Solar panel thermal gradient test

Part of this deficiency is due to the effect of the corrugation location on the spacecraft test measurement compared with the cell location on the STM test used in developing the desired response. The story at the 124-Hz resonance is similar; the response in the system test runs between 8- and 20-*g* peak compared with a single panel desired response of 6.6-*g* peak. Again, considering the effect of the corrugation mounting, the response during system test was close to the desired response.

Solar panel thermal–vacuum testing.

(1) *Test plan.* It was intended that the *Mariner* Venus 67 flight solar panels be tested in the JPL 7- × 14-ft thermal–vacuum chamber per JPL specification. A quartz heater, infrared radiant-heat source (Fig. 82) was employed to control panel temperature. A total of 30 thermocouples were employed to monitor the panel's temperature — one on each of the panel's 18 zener

Fig. 83. Typical plot of control thermocouple for *Mariner* Venus 67 solar panels, FA thermal–vacuum test

diodes, the remaining thermocouples uniformly distributed over the cell area. Figure 83 shows a typical plot of control thermocouples. Each panel was required to be exposed to a 239°F temperature for 2 h and to a 140°F temperature for 38 h. Maximum thermal gradient across the panel was to be limited to less than 10°F. The maximum thermal shock to be experienced by the panel was to be limited to less than 9°F/min.

(2) *Test results.* All *Mariner* Venus 67 flight-spacecraft solar panel SNs 3 through 8 were thermal–vacuum tested in the JPL 7- × 14-ft chamber, as specified. No anomalies were detected during this period in panel or chamber performance. On several of the panels, one or two of the thermocouples were found to be operating suspiciously. Subsequent investigations indicated that the difficulty was always traced to broken thermocouple wiring or improper bonding of the thermocouple to the panel. There were no difficulties encountered in this test and the sunlight electrical performance of the panels before and after FA thermal–vacuum testing did not reveal any degradation.

The maximum thermal gradient measured across the panels was <8°F.

c. Special subsystem environmental test anomalies.

Attitude-control jet valves vibration test anomaly. The results of the *Mariner* Venus 67 jet valve FA vibration tests displayed test anomalies that have been described as a fixture problem. The ASDs of the control transducers used on both the FA and TA tests were compared in an attempt to demonstrate the margin of safety provided by the TA testing.

Figure 84 is an example of the actual test data from the FA and TA tests with the shake axis perpendicular

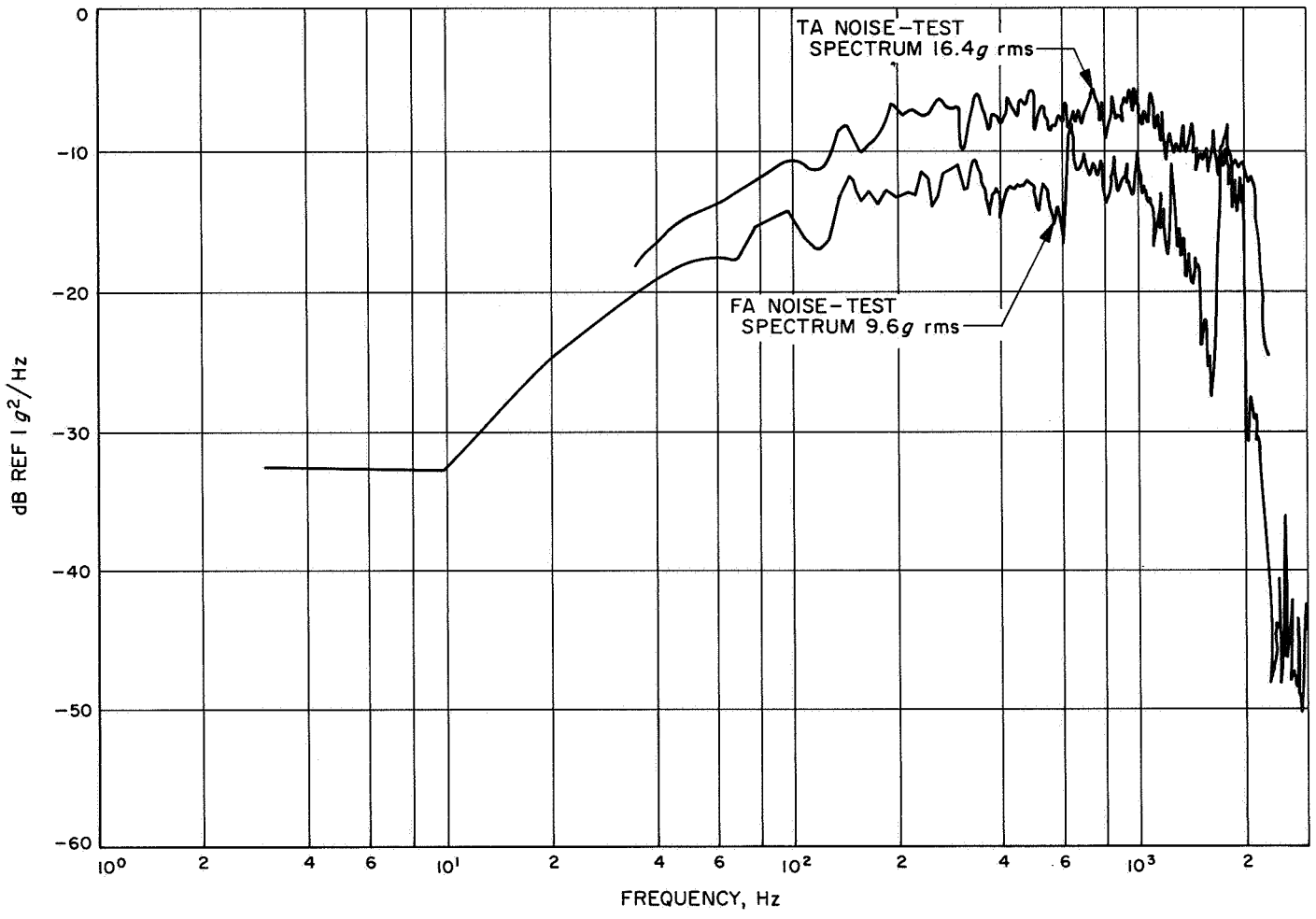

Fig. 84. Jet-valve-noise vibration data, shake axis perpendicular to valve axis

to the valve axis. The ASD of the TA test envelops the FA spectrum levels in the entire test frequency band. In particular, the FA test anomaly between 1700 and 2000 Hz was covered by the TA levels in this range.

Figure 85 presents similar data with the shake axis parallel to the valve axis. The TA spectrum levels cover the FA levels over most of the test frequency band. However, in the range of 1500 to 1600 Hz, two narrow-band spikes, caused by the FA test anomaly, are above the TA levels. However, since the natural frequency of the valve-spring-retainer system is approximately 3 Hz, the high-frequency over-test probably had no deleterious effect on this system.

Considering the overall test level (*g* rms) differences, the TA level of 16.4 *g* rms displays a large safety margin compared to the 9.1 *g* rms of the FA test. The valves have never displayed degradation from TA vibration testing.

Based on the information presented above, it was concluded that the FA test anomalies on the *Mariner* Venus 67 attitude-control jet valves produced no deleterious effects on the valves, and that they were acceptable for flight.

DAS vibration test anomaly. Two planes of vibration were completed on the M67-1 data automation system assembly (SN 071) on March 3, 1967. The third plane could not be equalized to the properly shaped random noise input spectrum at ⅓ level. A full-level run was not attempted until the source of the equalization problem was identified and corrected. The third plane (spacecraft *X* axis) of shake was completed on March 21, 1967.

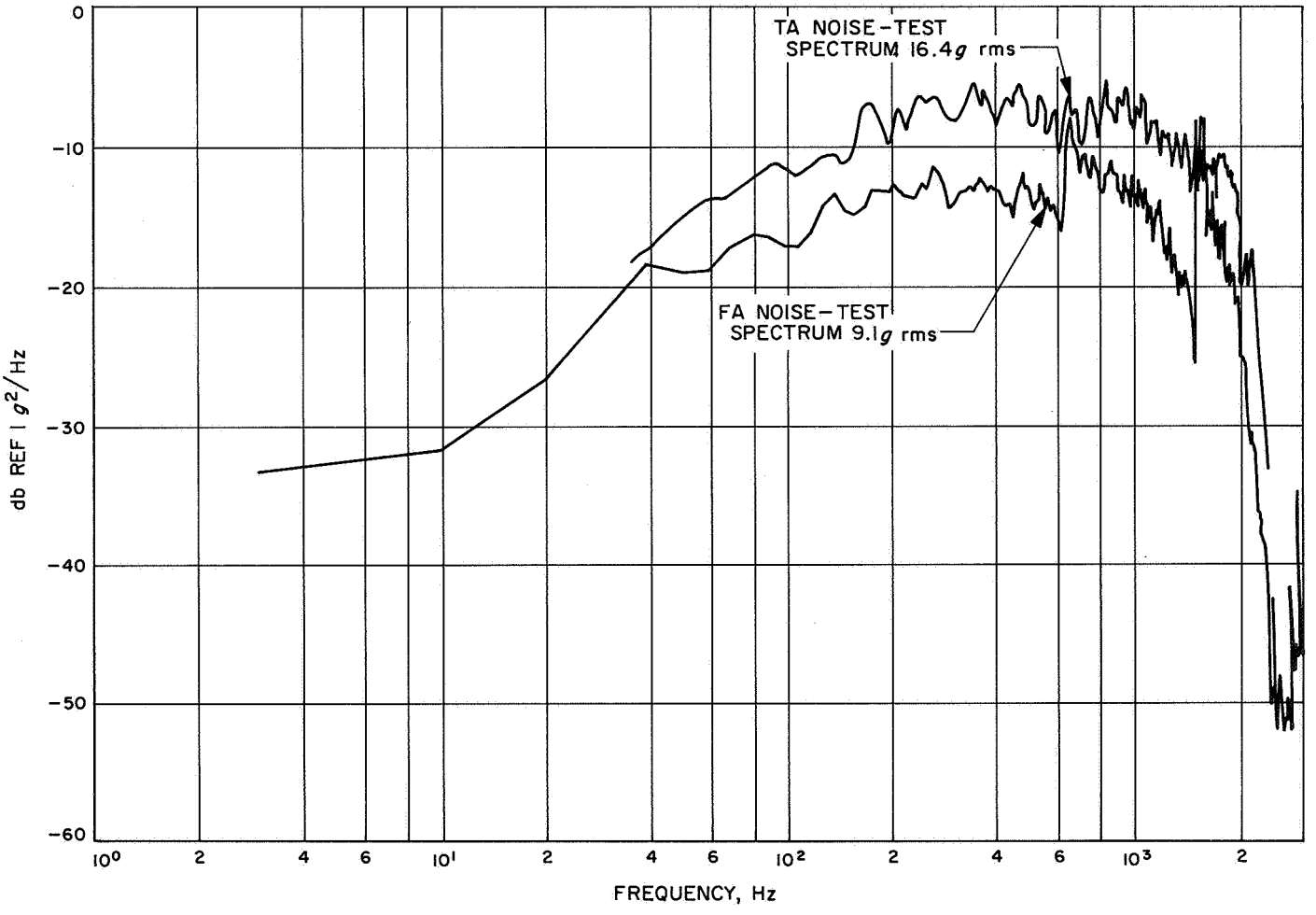

Fig. 85. Jet-valve-noise vibration data, shake axis parallel to valve axis

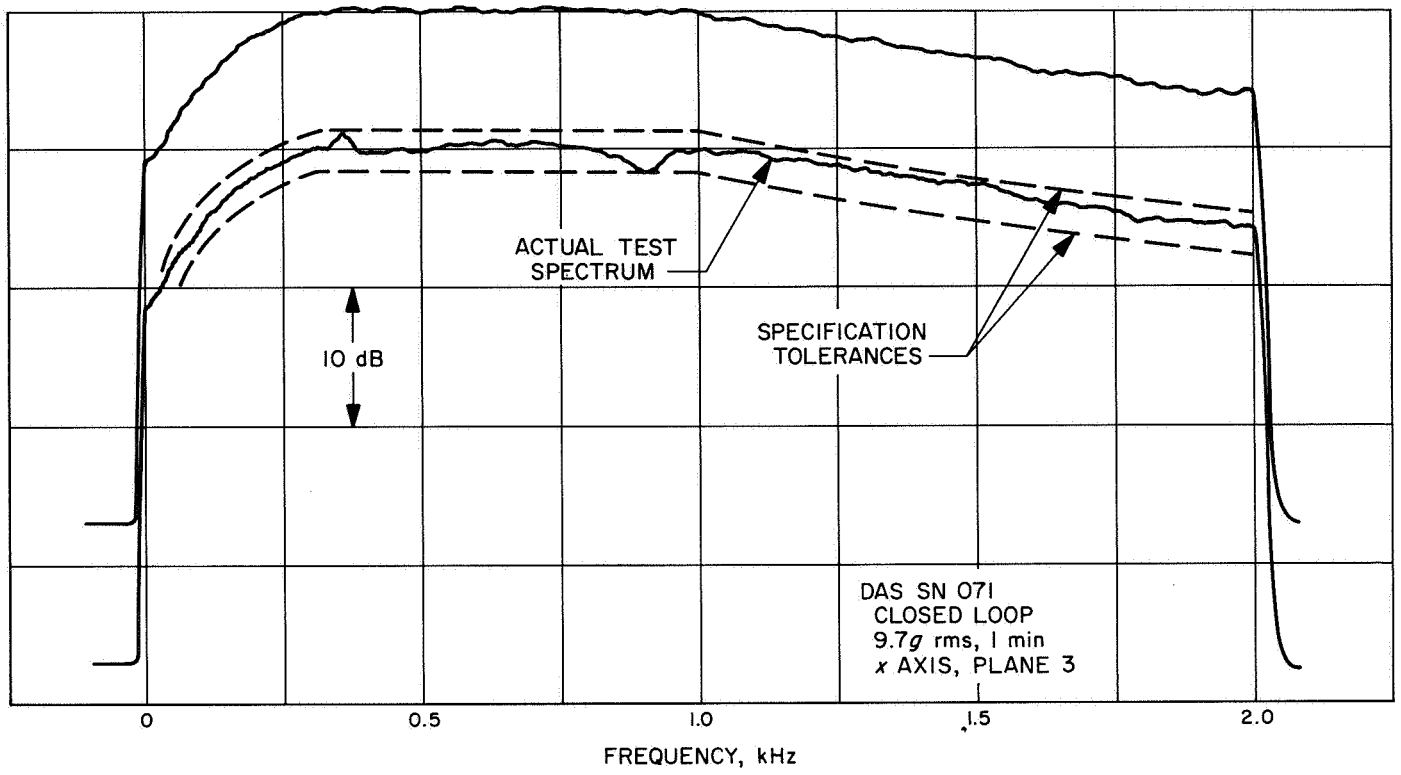

Fig. 86. DAS vibration test, X axis

Figure 86 displays the actual test spectrum and the allowable tolerances. At the referenced frequency, a peak can be seen that is $<1\frac{1}{2}$ dB and is within the allowable tolerance.

Canopus sensor anomaly: EMI test. All Canopus sensor EMI testing relating to the intensity output anomaly that occurred at Cape Kennedy just prior to launch is discussed in full in Section III.

B. Spacecraft M67-2 Flight-Acceptance Environmental Tests

1. System level. This material is applicable to the M67-2 spacecraft system. Included are the reports of the system-level FA environmental tests, and a history of subsystem experience in system-level environmental tests. The subsystem history examines whether a given subsystem experienced the system test, and if not, what was (or should have been) done to offset the deficiency.

a. Spacecraft FA vibration tests.

Configuration. The test configuration consisted of flight hardware, with the exception of the PIPS and pyrotechnic actuators.

Test description. The spacecraft structure was excited through each of the following axes: (1) roll, (2) through bays II–VI, and through bays IV–VIII. The nominal test sequence was a sinusoidal sweep at 2 octaves/min between 20 and 200 Hz, and band-limited random noise with a shaped spectrum between approximately 100 and 2000 Hz.

Figure 87 shows the M67-2 FA vibration test setup. Table 39 displays the specified FA level test parameters for all tests.

Test results.

(1) *Sinusoidal tests.* Test level control during each of the sweep tests was within the specified tolerance of $\pm 5\%$ with one minor exception. The tolerance results in a specified test level range of approximately 0.47 to 0.53 g rms for the lateral axes test runs 2 and 4. Table 39 contains the actual average test level bounds for these runs. The test level range for the roll axis test is 0.95 to 1.05 g rms and the actual test level bounds are given in run 6, Table 39.

(2) *Noise tests.* The actual average test levels were higher than nominal, but within the specified tolerance

Table 39. M67-2 flight-acceptance vibration tests

Test No.	Spacecraft axis	Type of test	Frequency range, Hz	Test level, g rms		Test duration, s
				Specification	Actual	
2	XY (bay II–VI)	Sine sweep	200 to 20 to 200	0.50	0.53 to 0.47[a]	200
3	XY (bay II–VI)	Shaped noise	100 to 2000	9.7	9.9	60
4	XY (bay VI–VIII)	Sine sweep	200 to 20 to 200	0.50	0.51 to 0.48[a]	200
5	XY (bay VI–VIII)	Shaped noise	100 to 2000	9.7	10.0	60
6	Z	Sine sweep	200 to 20 to 200	1.00	1.02 to 0.97[a]	200
7	Z	Shaped noise	100 to 2000	9.7	10.1	60

[a]Except at a discrete frequency; see Test Anomalies, following.

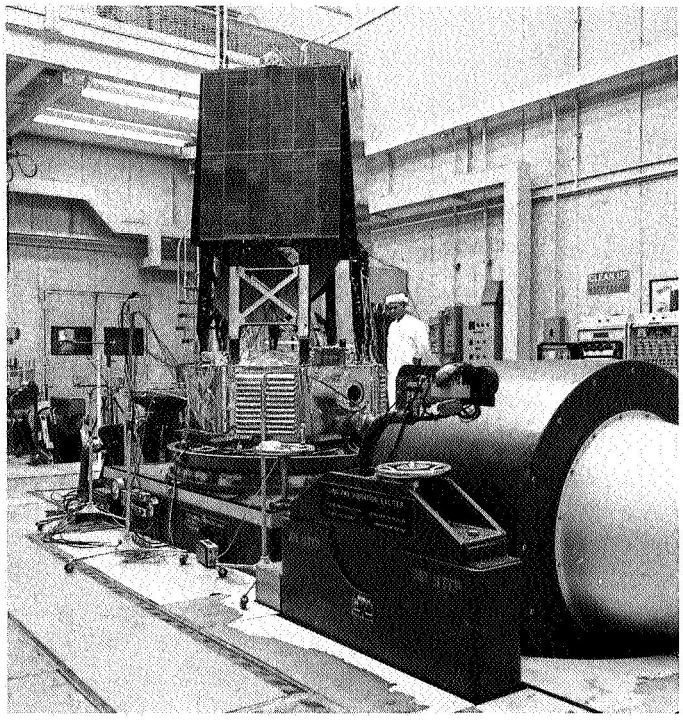

Fig. 87. FA vibration test setup for M67-2

of ±1 dB. Table 39 displays a comparison of the test results with the nominal specified level. The tolerance on the specified 9.7 *g* rms level allows a range of 8.6 to 10.7 *g* rms for the actual test levels. Reference to the table shows runs 3, 5, and 7 had resulting average levels of 9.9, 10.0, and 10.1 *g* rms, respectively.

Noise-spectrum-level control was well within the specified tolerances of ±1½ dB, as shown in Fig. 88. The figure displays the actual test power spectrum (test input ASD) for each shake axis and the range allowed by the specified tolerance. The final test equalization acceptance of each shake axis was based on a plot in this figure. Table 40 contains the maximum deviations from the nominal test spectrum for each shake axis.

Test anomalies. Transient signals detected by the fail-safe peak limiter circuit caused three sinusoidal tests to be terminated. The spacecraft response to these transients was negligible in all cases as shown by the spacecraft accelerometer data.

A transient terminated the pretest integrity sinusoidal sweep through *XY* bays II–VI at approximately 115 Hz. Since only one control circuit displayed this transient, it was concluded that a loose connection in a circuit terminal was the cause. When the terminal was repaired, the test was rerun to completion per procedure waiver.

The first FA sinusoidal sweep in the Z axis was terminated by a mechanical transient at 112 Hz. This transient was distinctly different from the first anomaly. Its source was clearly mechanical, as indicated by the response of all of the control accelerometers and the

Table 40. M67-2 maximum-noise spectrum-level deviations

Test No.	Spacecraft shake axis	Maximum test deviation, dB[a]	Frequency of deviation, Hz
3	XY (bay II–VI)	1¼	820
		−1¼	1700
5	XY (bay IV–VIII)	1½	820
		−1¼	1700
7	Z	¾	900
		−1¼	1920

[a]Reference 1 g^2/Hz.

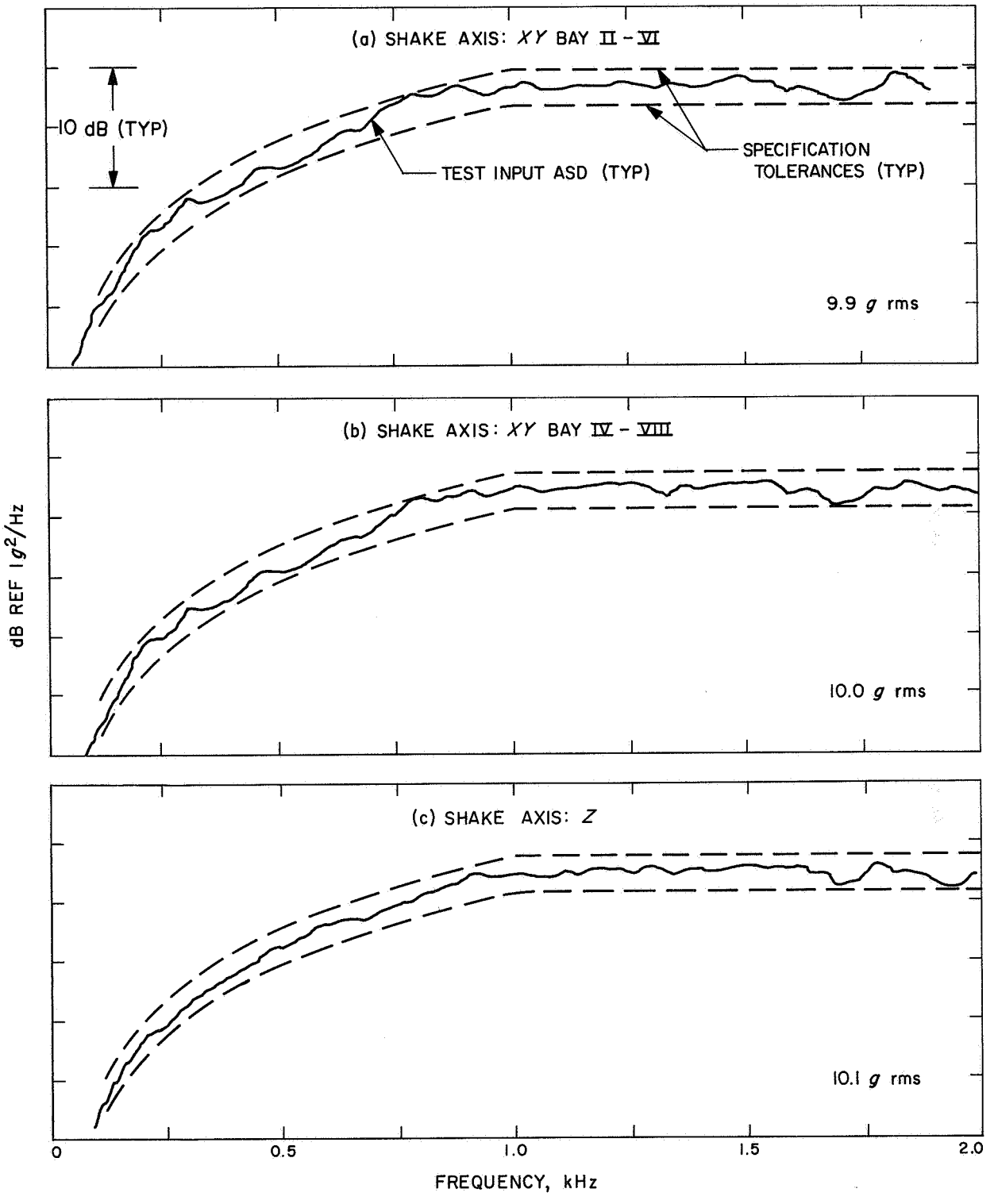

Fig. 88. M67-2 system FA noise vibration acceleration spectral density

adapter response accelerometers. The spacecraft response to this transient was negligible.

Retaining the same peak limiter setting but adding fixture instrumentation, the test was rerun, beginning at 125 Hz instead of 200 Hz per procedure waiver. A similar transient occurred, and this test was terminated. The source of the transient was not identified; however, spacecraft response to this transient was again insignificant.

Because the source of the transient could not be found and the spacecraft response to the transient was negligible, it was decided to raise the peak limiter setting in an effort to pass the anomalous signal. Upon reviewing the data, a transient amplitude of 3.6 g peak was causing the peak limiting. This transient level produced no spacecraft response, and it was assumed that raising the peak limiter to 5.6 g peak (4 g rms) would pass the transient but would not effect a significant response. For safety reasons, it was decided to use this higher peak limiter setting in the high-frequency range of 90 to 200 Hz, only, per procedure waiver. The test run in this frequency range was completed with no significant spacecraft transient response.

Resetting the peak limiter to the nominal 2.8 g peak, the low-frequency (90 to 20 Hz) test was completed with no incidents, per procedure waiver.

In each of the sinusoidal tests, an input level exceeding the specified tolerance existed at a discrete frequency. The deviation produced as much as a 21% increase in the input test level at this frequency, but the magnitude was less than the peak limiter setting. Specifically, the percentage of input level increase for runs 2, 4, and 6 were, respectively, 19%, 21%, and 10% (compared with the allowable tolerance of 5%).

During the M67-2 testing, the acceptability of the tests was based on the similarity in the M67-2 response as compared with the M67-1 when measured by the spacecraft response accelerometers. The accelerometer in the direction of shake on the secondary structure was used as a common reference. The test was considered acceptable if the M67-2 responses were within approximately 10% of the M67-1 response at that location. (This number was based on the maximum possible deviation of 10% allowed by the $\pm 5\%$ tolerance on the spacecraft inputs.)

At no time did the response level, as defined previously, exceed 10% above the M67-1 tests at the discrete frequencies in question. This slight difference in response levels was and is considered negligible.

On completion of the testing, no spacecraft problems were noted.

b. Spacecraft FA pyrotechnic shock test.

Test events and comparison with specification requirements. The pyrotechnic shock test (test setup shown in Fig. 89) consisted of firing those pyrotechnic devices

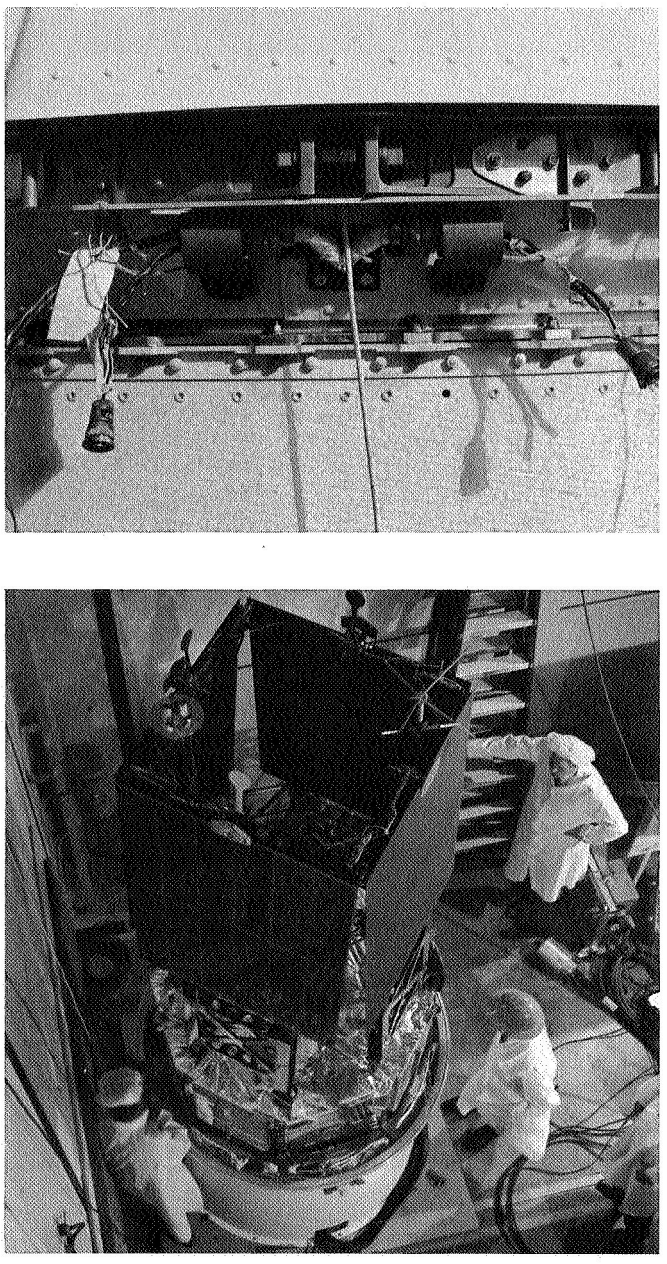

Fig. 89. Pyrotechnic shock test setup

that would produce the maximum primary shock spectra response throughout the spacecraft. These events were selected after analysis of the shock spectra response recorded during the M67-1 pyrotechnic test in which all spacecraft pyrotechnic events, including the shroud V-band release, were initiated. The pyrotechnic events specified and performed were (1) the spacecraft V-band release, (2) the solar-panel deploy, and (3) the antenna pointing angle change (APAC). There was no deviation from the specified requirements.

Comparison with M67-1 data. Since there can be no control of the spacecraft shock response parameters other than the selection and utilization of accepted squibs and pinpullers for each of the pyrotechnic events, there are no specified shock response parameters to compare with the measured response data. However, a comparison of shock spectra for the previously performed M67-1 spacecraft and this M67-2 test can be made.

Measurement and comparison of shock spectra recorded at comparable locations on the M67-1 and M67-2 spacecraft (flight location on bus Z axis) and in the LMSC adapter for the same pyrotechnic events indicate that the tests produced very similar shock spectra responses. A typical comparison (flight locations in bus and adapter for spacecraft V-band release pyrotechnics) is shown in Figs. 90 and 91, respectively.

Test anomalies. There were no test anomalies.

Spacecraft test configuration. For this pyrotechnic test, the M67-2 spacecraft consisted of flight hardware with the exception of the following units: The PIPS and attitude-control system were from the STM; solar panels 3 and 4 were from flight spares, and the others were flight spares.

Spacecraft failures during test. No spacecraft failures occurred.

c. Spacecraft FA thermal–vacuum test.

Comparison of test configuration with flight configuration. The thermal–vacuum test setup for the M67-2 is shown in Fig. 92. The M67-2 spacecraft had the following nonflight items during the systems test:

(1) Low-gain antenna damper

(2) Battery assembly

(3) Thermal shields (corners A, B, C, D, E, F, G, H)

(4) Solar panels

(5) All squibs (except high-gain antenna)

(6) Pinpullers (except high-gain antenna)

Comparison of actual test with test requirements. A comparison of the requirements as set forth in the TOP, the M67-2 FA specification, and the M67-1 Detail Test Procedure as a function of the actual test is presented in

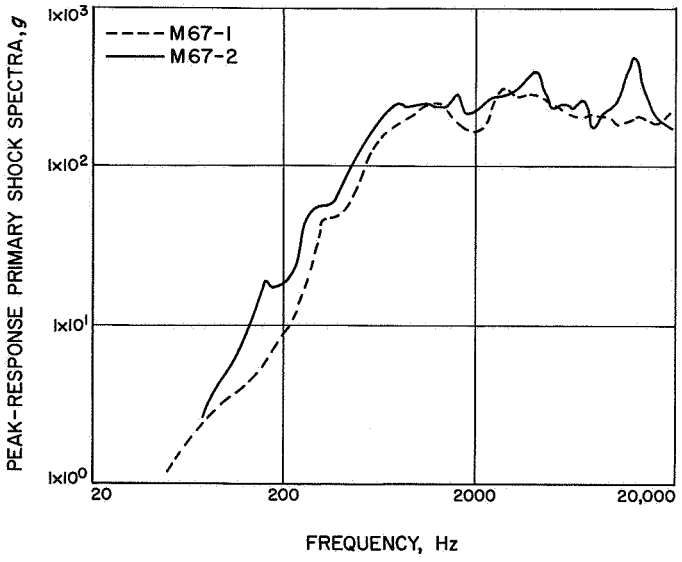

Fig. 90. Pyrotechnic shock spectra comparison, M67-1 and M67-2, acceleration code B3

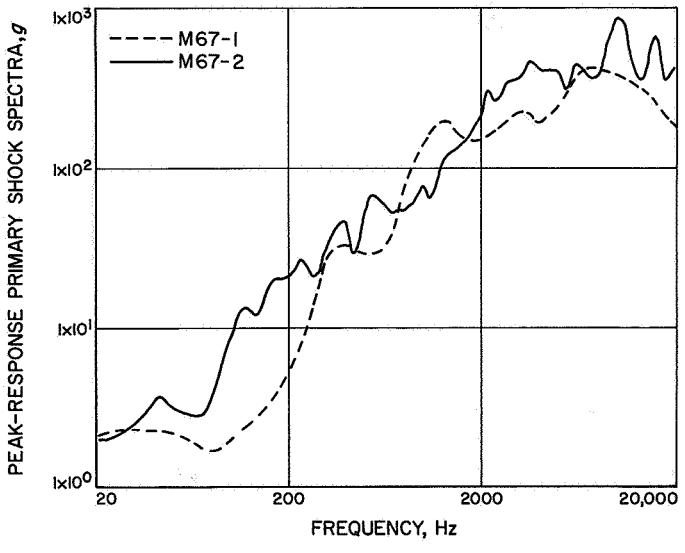

Fig. 91. Pyrotechnic shock spectra comparison, M67-1 and M67-2, acceleration code F4

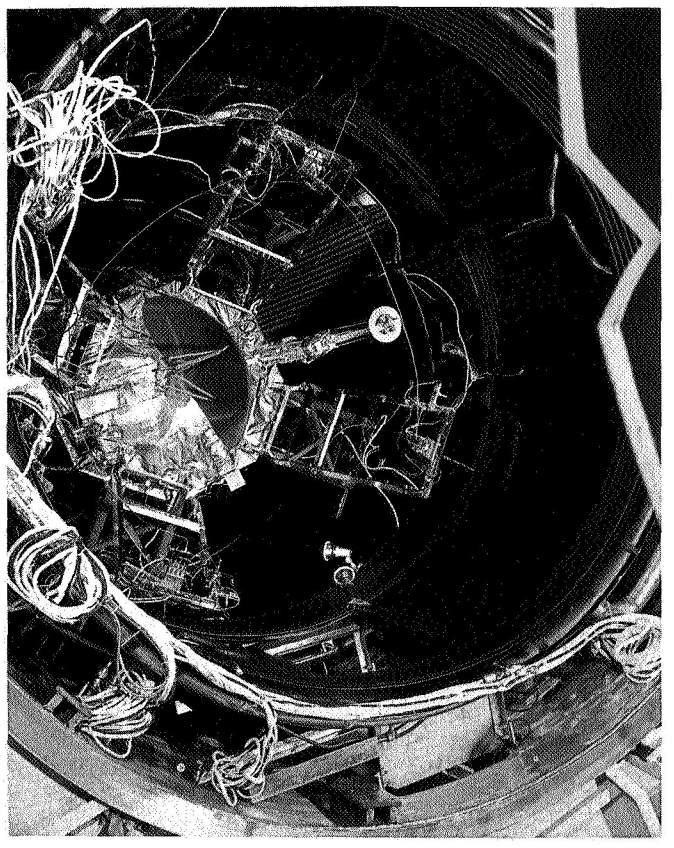

Fig. 92. FA thermal–vacuum test setup for M67-2

Tables 41 and 42. Table 41 covers phase I of the test. The phase I deviations worthy of mention were as follows:

(1) Earth-cruise mode with TWT, battery charger *on*, gyros *off*, I = 126 W/ft², was deleted as requested by thermal control group, in order to correlate data with M67-1 spacecraft turning battery charger *off*.

(2) Gyros were turned *off* for first encounter mode, I = 248 W/ft², because gas supply was low from improper functioning of relay inhibit switch while chamber leak check was being performed.

(3) Intensity during second playback and post-playback was 275 W/ft² instead of 290 W/ft² because of several lamp failures in chamber.

(4) Deployment of the high-gain antenna was postponed until phase II of test.

Table 42 covers phase II of the M67-2 thermal–vacuum test. Phase II deviations are presented below:

(1) The earth-cruise mode with cavity amplifier, battery charger *off*, gyros *off*, was not performed because the spacecraft is fairly insensitive to intensity changes and it was felt that very little information would be gained.

(2) Time at 290 W/ft² was shortened because test requirements had been satisfied.

(3) Deployment of high-gain antenna caused pressure to increase by 0.3 of a decade with a rapid recovery. Pinpuller temperature increased from −5 to 25°F.

Problem/failures during test.

(1) *Spacecraft-related.* A second pumpdown occurred in phase I because the UV stimulus for the UV photometer was not removed from the chamber prior to pumpdown, and it was possible that outgassing from the stimulus had caused arcing in the photometer. An examination of the UV photometer and associated data did not reveal any major damage, and a decision was made by the Spacecraft Systems Manager to proceed with the test without recalibrating the photometer. A problem/failure report was written to cover this mishap. Following the thermal–vacuum test, the unit was sent back to the University of Colorado to be recalibrated.

The M67-2 plasma probe was considerably less noisy than that of the M67-1. The ion gage that was installed near the plasma probe to monitor its environment caused an increase in noise whenever it was turned on.

Gyros were noisy during phase I of the test and initially showed a −5 V offset, which was later corrected by adjusting the line amplifiers. Attitude-control gas supply became very low during phase I because the spacecraft was placed in launch mode during a chamber-leak checkout and the stepping relay that shuts off the gas system did not function properly, so that the gas system continued to operate.

During the midcourse maneuver (lights *off*) in phase I, the bay II secondary sun sensor reached 17°F, the bay VI secondary sun sensor reached 23°F, and the plasma probe reached 14°F. During phase II, prior to lights-*on*, the plasma probe reached 7°F. The lower FA temperature requirement of 32°F was exceeded for each of these instruments. These instruments were TA tested to 14°F. A PFR was written against the M67-1 spacecraft regarding the same problem. A waiver, dated April 10, 1967, waived the lower limits of all sun-sensor assemblies for FA and TA testing.

Table 41. Phase I of M67-2 thermal–vacuum FA test: required and actual

Flight segment	Test and Operations Plan (TOP)			Requirements						Actual test		
				JPL Specification			Detail Test Procedure					
	Time, h	Intensity level, W/ft²	Operating mode	Time, h	Intensity level, W/ft²	Operating mode	Time, h	Intensity level, W/ft²	Operating mode	Time, h	Intensity level, W/ft²	Operating mode
Boost	—	—	—	0.5	0	Pressure profile	3	0	Pressure profile	2	0	Pressure profile
Earth cruise	24	126	—	24	126	[a, b]	24	126	[a, e, g]	37	126	[a, e]
Midcourse	6	0	—	4	0	Midcourse	2/2	0/126	[d, f]	1/3	0/126	[d, f]
Venus cruise	60	248	—	60	248	1	56	248	[a, b, d]	52	248	[a, b, i]
First encounter	12	248	—	16	248	[c, d]	7	248	[a, h, i]	6	248	[a]
First playback	48	263	—	48	263	[a]	17	263	[a]	18	263	[a]
Second encounter	12	248	—	12	275	[d]	7	275	[a, i]	7	275	[a]
Second playback	48	263	—	48	290	[a]	17	290	[a]	18.5	275[j]	[a]
Post playback	24	263	—	0	—	Not reqd	8	290	[a]	20.5	275[j]	[a]
Total phase I	234	—	—	212.5	—	—	143	—	—	164	—	—

[a]Spacecraft on TWT: battery charger *off*, gyros *off*.
[b]Spacecraft on TWT: battery charger *on*, gyros *off*.
[c]Spacecraft on TWT: battery charger *off*, gyros *off*; high-gain antenna deployed.
[d]Spacecraft on TWT: battery charger *off*, gyros *on*.
[e]Spacecraft on cavity amplifier: battery charger *off*, gyros *off*.
[f]Spacecraft on cavity amplifier: battery charger *off*, gyros *on*.
[g]Mode 2 with battery charger *on* deleted, as requested by thermal group, to correlate data with M67-1 spacecraft.
[h]High-gain antenna deployment planned for phase II.
[i]Mode 4 with gyros *on* deleted because gas supply was low, due to improper functioning of relay inhibit switch while chamber-leak check was being performed.
[j]Decision made to finish at 275 W/ft² because of several lamp failures in chamber.

The average internal bus temperatures on the M67-2 spacecraft ran approximately 3°F cooler than on the M67-1 spacecraft and 5°F cooler than the corresponding temperatures on the TCM. The design fix would have been to remove aluminum mylar from top of the thermal shield; however, it was decided by the Spacecraft Systems Manager that a fix was not necessary, since the internal bus power could always be increased to offset any low bus temperatures.

The M67-2 spacecraft was operated with the battery charger *off* during a mode of the test where the specification called for the battery charger to be *on* for part of the mode and *off* for the balance. The omission was not important, and very little compromise to the test data resulted. A pre-Canopus acquisition was also substituted for a cruise condition but did not compromise the test data. These deviations were approved by the Spacecraft Systems Manager in an internal memorandum.

(2) *Facility-related.* During phase I, a leak developed in the chamber and was isolated to the facility cabling going into the chamber. The pressure increased to 7×10^{-4} torr and remained at that level until the leak was fixed.

During phase I, one lamp exploded and fell on another lamp, causing it to short-circuit. Flying glass broke two other lamps which were not on at the time. At the time of the explosion a 20% decrease in solar power was noted. Approximately 24 h later, another lamp blew out. This left a total of 20 lamps, of which one lamp was questionable. The test was finished with a total of 19 lamps driven to 5200 W, which is slightly above their

Table 42. Phase II of M67-2 thermal–vacuum test

Flight segment	Test and Operations Plan (TOP)			Requirements						Actual test		
				JPL Specification			Detail Test Procedure					
	Time, h	Intensity level, W/ft²	Operating mode	Time, h	Intensity level, W/ft²	Operating mode	Time, h	Intensity level, W/ft²	Operating mode	Time, h	Intensity level, W/ft²	Operating mode
Boost	—	—	—	—	—	—	3	0	Pressure profile	3	0	Pressure profile
Earth cruise + margin	—	—	—	—	112	[a]	18	112	[a]	18	112	[a]
Earth cruise	20	126	—	—	126	[a, b]	36	126	[b, c, d, e]	36	126	[b, c, d]
Venus cruise	20	248	Gyros on	—	248	[b]	12	248	[b]	12	248	[b]
Venus cruise + margin	—	—	—	—	290	[b]	24	290	[b, f]	21[g]		[b, h, i, j]
Total, phase II	40	—	—	—	—	—	93	—	—	90	—	—
Total, phases I and II	274	—	—	212.5	—	—	236[k]	—	—	254	—	—

[a]Spacecraft on cavity amplifier: battery charger *off*, gyros *off*.

[b]Spacecraft on TWT: battery charger *off*, gyros *off*.

[c]Spacecraft on cavity amplifier: battery charger *on*, gyros *off*.

[d]Spacecraft on cavity amplifier: battery charger *on*, gyros *on*.

[e]Mode 1 not performed because spacecraft fairly insensitive to intensity change and information to be gained considered slight. Pre-Canopus acquisition mode performed, instead.

[f]Spacecraft on TWT: battery charger *on*, gyros *on*.

[g]Total test time requirement satisfied and test was terminated.

[h]Spacecraft on TWT. battery charger *off*, gyros *on*.

[i]Antenna pointing angle change.

[j]Mode 7 substituted for mode 6, as requested by test director.

[k]Reflects actual hours completed in phase I.

normal rating of 5000 W. Because of this problem it was decided to finish phase I of the test at an intensity level of 275 W/ft² instead of 290 W/ft² as planned.

Shortly after phase II pumpdown, another leak occurred in the chamber around one of the chamber ion gages in the top of the chamber. It was necessary to return to ambient pressure to make the fix, and a second pumpdown was also required in phase II.

An LN_2 pump failed during phase II of the test, and an auxiliary pump was turned on with only negligible variations in the chamber parameters.

During phase I of the thermal–vacuum test, facility personnel decided that an effective emittance for the cone radiometer of 1.0 (which was being used at that time to read the intensity in the chamber) was in error. Prior to raising the intensity to 248 W/ft², it was decided to use 0.97 for the effective emittance of the cone radiometer. As a result, the M67-2 spacecraft was tested to intensities that were 3% higher than were experienced by the M67-1 spacecraft.

Spacecraft environment during test. A discussion of the more salient features of the chamber is in the immediately following paragraphs. Discussion of effects of deficiencies in these is found in Section VI of this report.

(1) *Launch pressure-profile simulation.* The pressure P profile and the rate of change of pressure $\dot{P}$ profile for phases I and II are presented in Figs. 93 and 94. The evaluation of the effect of differential pressures in enclosures, thermal blankets, etc., is the principal objective of launch pressure-profile simulation. The condition that corresponds to the existence of this environment is $\dot{P}$. A window is used to specify that the maximum $\dot{P}$ during the period between 25 and 60 s from initiation of pumpdown shall attain a rate of 16.5 to 18.7 torr/s. The 25 s chosen for the starting time of the window was based on an estimate of the maximum capability of the pumping system. The extended window in Fig. 93 indicates that

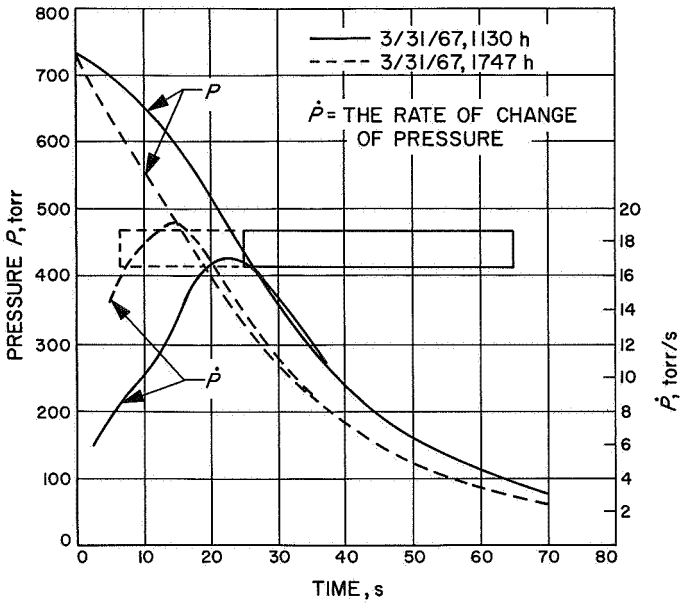

Fig. 93. Pumpdown pressure profile for 10-ft space simulator test M67-2, phase I

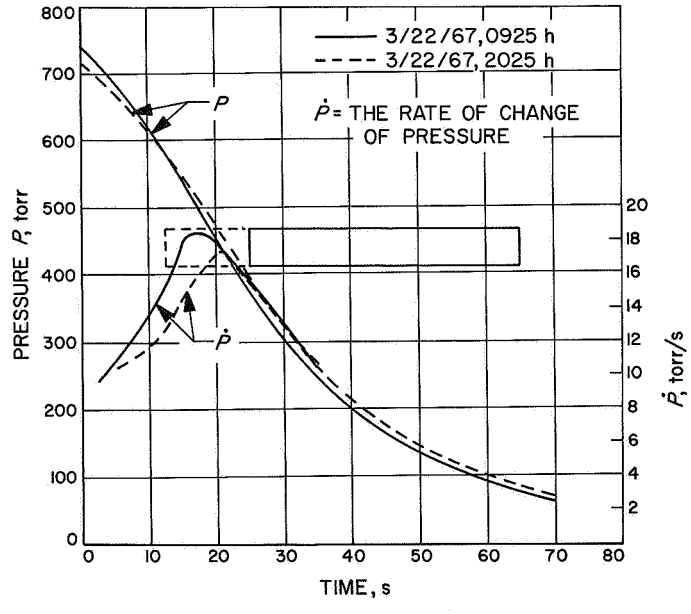

Fig. 94. Pumpdown pressure profile for 10-ft space simulator test M67-2, phase II

maximum $\dot{P}$ of 18.4 torr/s and 17.4 torr/s were attained for the two pumpdowns during phase I in <25 s, which demonstrates that the pumping capability is better than previously indicated. There were some scattering of $\dot{P}$ points due to data reduction technique. A smooth curve was drawn through the neighborhood of these points. The $\dot{P}$ requirement was more important for phase II than for phase I because the heat shield (thermal blanket) was not vented in phase II. Figure 94 shows that the requirement for phase II was met.

(2) *Total irradiance level.* The temporal sequence of total irradiance levels for phases I and II is included in Figs. 95 and 96, respectively. The instrumentation error (noted for the M67-1 under *Total irradiance levels* in IV-A-1-c) experienced previously was corrected. The specified tolerance on the required levels was ±2%. The data indicated that the requirement was met.

(3) *Facility pressure levels.* The test of the M67-2 spacecraft was conducted, as desired, at pressure levels below the required maximum steady-state pressure of 1×10^{-5} torr. The test level was 4.5×10^{-6} torr for phase I and 5×10^{-6} torr for phase II. During phase I pumpdown, at 14:30 March 23, 1967, a leak was detected in the feed-through connection. At 17:00, the leak was stopped and the test was resumed. The automatic high-voltage cutoff was set at 5×10^{-5} torr and no problems were encountered with the cutoff system as a result of the attitude gas jet operation.

(4) *Effective-sink temperature.* The effective-sink temperature specified was −250°F. No data are available on what the actual sink temperature is for the *Mariner* Venus 67 spacecraft-chamber configuration.

The estimated errors in test temperatures are a function of the temperature of the specific item and its thermal properties. In the case of *Mariner* Venus 67, it is considered unlikely that any errors due to the heat-sink error would approach 10°F; therefore, this was not considered as a compromise to the test. More definition on what the sink-temperature environment actually is should exist on future spacecraft tests.

d. Spacecraft FA electromagnetic interference tests.

External environmental simulation. The objective of this test was to verify the RF compatibility of the spacecraft, including pyrotechnics, when subjected to an RF environment similar to that expected at the AFETR launch complex.

Requirements vs test. The RF simulation-level requirements and the actual test levels are shown in Table 43. The average power levels were met in the test; however, the peak power levels for two of the sources were not met because of equipment limitations. The omission is not considered serious because each of

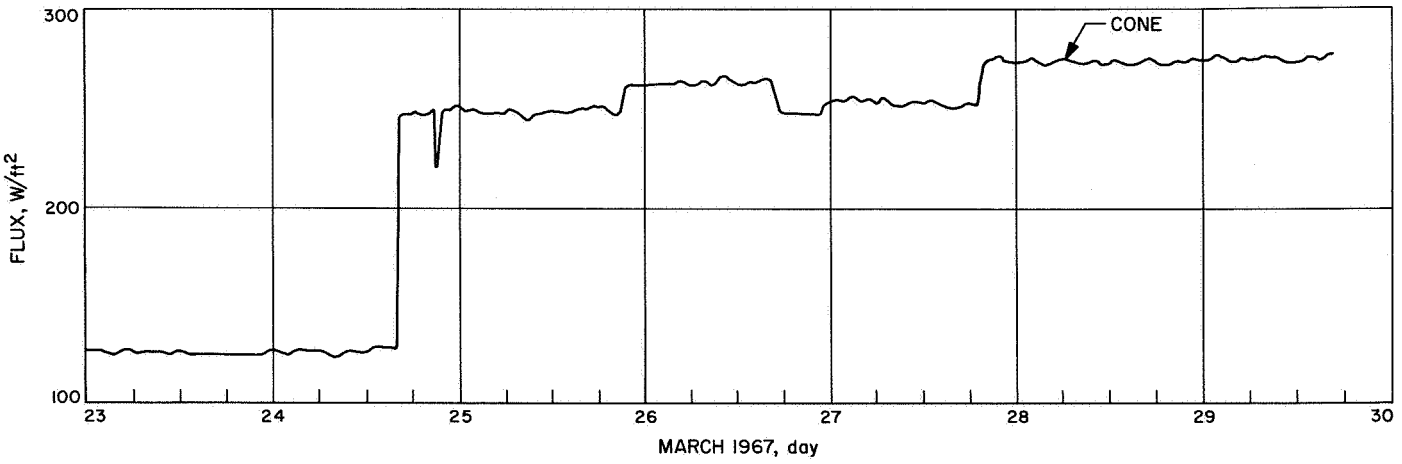

Fig. 95. Radiometer flux for 10-ft space simulator, M67-2, phase I

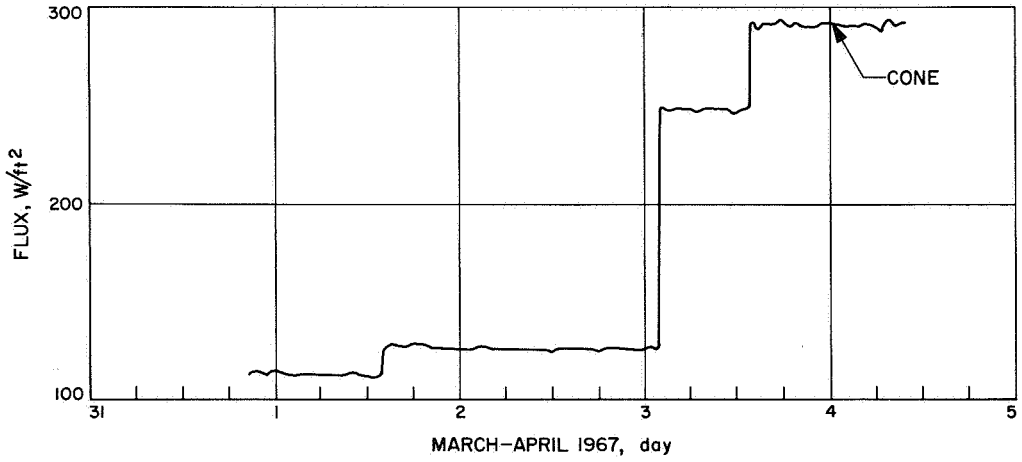

Fig. 96. Radiometer flux for 10-ft space simulator, M67-2, phase II

the two simulated sources is a ground-based RF transmitter. The spacecraft is expected to have considerable protection from each of these sources afforded by the metallic shroud. In addition, two other sources that were simulated with peak levels are in the same frequency band. The situation is summarized in Table 44.

The expected shroud attenuation values are based on measurements made on the *Mariner C* shroud with conductive paint. It was estimated that the metallic shroud of *Mariner* Venus 67 would have at least the attenuation listed. The values in the table show that the ground RF peak level at 5.690 kHz was approximately in the order of magnitude of the simulated level and that the X-band peak level would be 30 dB below that used for the test.

The peak RF sources that were to have been present after the shroud was ejected were simulated with their expected levels. These sources were the two transponders listed in Table 44.

An additional requirement listed in the specification was for radiation of the VHF and UHF radio frequency levels to the DFR experiment. This requirement was not met at this time in the testing and it formed part of the DFR/spacecraft compatibility tests. Because the DFR antennas were required to determine the appropriate RF levels for the DFR signals and the testing did not include installation of the solar panels for the antennas, the test was postponed.

After tests had been performed on M67-1 it was learned that the *Atlas* telemetry frequency had been changed from 229.9 to 249.9 MHz. The test of M67-2 reflected this change.

Table 43. Requirements vs test, external environment simulation

RF source simulated	RF simulation requirements				Test levels for System Test Procedure			
	Frequency, GHz	Peak power density at spacecraft, dBmW/m²	Average power density at spacecraft, dBmW/m²	Minimum pulse width, μs	Frequency, GHz	Peak power density at spacecraft, dBmW/m²	Average power density at spacecraft, dBmW/m²	Minimum pulse width, μs
Atlas radar transmitter (FPS-16)	5.690	59	21	1.0	5.690	[a]	20	CW
Atlas guidance track ground transmitter	Classified	20	−12	2.0	Classified	[a]	−12	CW
Atlas guidance rate ground transmitter	Classified	NA[b]	14	NA	Classified	NA	14	CW
Command destruct ground transmitter	Classified	NA	4	NA	Classified	NA	4	CW
Agena telemetry	0.2443	NA	23	NA	0.2443	NA	23	Subcarrier modulated
Agena radar transponder	5.765	7	−8	0.7	5.765	7.5	−8	[c]
Atlas telemetry	0.2299	NA	−6	NA	0.2499	NA	−6	CW
Atlas guidance track transponder	Classified	30	−1	2.0	Classified	[a, d]	30	CW
Atlas guidance rate transponder	Classified	NA	−5	NA	Classified	NA	−5	CW

[a]Equipment limitations prevented simulation of specification requirements for the peak levels.
[b]Not applicable.
[c]Two sources used, one on pulse to meet peak requirements and one on CW to meet average level requirements.
[d]The required peak level was simulated with a CW signal level.

Table 44. Comparison of test levels vs expected external environment

RF source simulated	Frequency, GHz	Expected peak power density external to shroud (+ 6 dB), dBmW/m²	Tested power density without shroud, dBmW/m²	Expected shroud attenuation, dB
Agena radar ground transmitter	5.690	59		50
Agena radar transponder	5.765	7	7.5 peak	—
Atlas guidance ground track transponder	X-band	20		30
Atlas guidance track transponder	X-band	30	30 avg	—

Each of these departures from the specification was noted, and very little compromise to the test data resulted. These deviations were subsequently approved by the Spacecraft Systems Manager in an internal memorandum.

Results. The spacecraft systems were monitored by cognizant personnel and no adverse effects were reported to the Test Director as resulting from any RF source.

DFR/S-band/system configuration EMC test. The objective of this test was to verify the compatibility between the DFR experiment, the S-band communications transponder, and the spacecraft in general.

(1) *Spacecraft noise environment at DFR receiver frequencies, requirement vs test.* The permissible noise environment was determined on the basis of minimum

acceptable space degradation levels specified by the experiment scientist and on the basis of cosmic noise temperature levels and receiver noise temperatures as stated in the Functional Specification.

(2) *DFR operation threshold degradation, requirement vs test.* The degradation threshold requirements vs the procedure test implementation is summarized in Table 45. It was not feasible in practice to perform the sweep test because the support test equipment instrumentation does not possess that capability. A manual performance of a sweep test was not considered meaningful.

(3) *DFR acquisition threshold degradation, requirement vs test.* The acquisition threshold tests were implemented in the procedure.

Table 45. DFR/spacecraft compatibility comparison of requirements vs JPL test procedure, M67-2

Item	Specification	Test procedure
Threshold degradation 49.8 MHz	Performance degradation of the 49.8-MHz receiver to be less than 3 dB with the receiver locked on a −125.7 dBmW signal	Degradation threshold measured for various spacecraft modes including required conditions
	Receiver to maintain lock when a received signal of −120 dBmW (total power) is swept at a maximum rate of 224 Hz/s through a 5.48-kHz band centered at 49.8 MHz	Not included because unfeasible to perform because of instrumentation limitations
Threshold degradation 423.3 MHz	Performance degradation of the 423.3-MHz receiver to be less than 1 dB with the receiver locked on a −134.2 dBmW signal at 423.3 MHz	Degradation threshold measured for various spacecraft modes including required conditions
	The 423.3-MHz receiver to maintain lock when a received signal of −130 dBmW (total power) is swept at a maximum rate of 1900 Hz through a 15.8433-kHz band centered at 423.3 MHz	Not included because unfeasible to perform due to instrumentation limitations
Acquisition threshold 49.8 MHz	The 49.8-MHz receiver required to acquire lock with a −125.7 dBmW signal applied at 49.8 MHz and at 49.8 MHz ±3 kHz, respectively	Acquisition threshold tests included for various spacecraft modes
Acquisition threshold 423.3 MHz	The 423.3-MHz receiver to acquire lock with a −134.2 dBmW signal applied at 423.3 MHz and 423.3 MHz ±3 kHz, respectively	Acquisition threshold tests included for various spacecraft modes
Spacecraft environment 49.8 MHz	Noise levels not to exceed limits of Fig. 2 of specification for 49.8 MHz ±50 kHz	
	Constraints:	
	Spacecraft flight configuration, suspended in SAF	As required; solar panels 4A1, 4A3 flight; 4A5 TA; 4A7 TM
	Noise environment plus test receiver not to exceed 21,850°K	Noise temperature approximately 2500°K with spacecraft *off*
	Various spacecraft modes with various subsystems *on* or *off* are specified	Spacecraft modes included specified conditions
Spacecraft environment 423.3 MHz	Noise levels not to exceed limits of Fig. 3 of specification for 423.3 MHz ±50 kHz	
	Constraints:	
	Spacecraft flight configuration, suspended in SAF	As required
	Noise environment plus test receiver not to exceed 1025°K	System noise temperature approximately 200°K
	Various spacecraft modes with various subsystems *on* and *off* are specified	Spacecraft modes included specified conditions
Spacecraft environment 473.1 MHz	Noise levels not to exceed limits of Fig. 3 of specification for 473.1 MHz ±50 kHz	
	Constraints:	
	Spacecraft flight configuration, suspended in SAF	As required
	Noise environment plus test receiver not to exceed 1025°K	System noise temperature approximately 200°K
	Various spacecraft modes with various subsystems *on* and *off* are specified	Spacecraft modes included specified conditions

Table 45 (contd)

Item	Specification	Test procedure
Spacecraft environment S-band	No spacecraft system-generated interference to appear at the S-band antenna input terminals within a 3.43-MHz bandwidth centered at the receiver frequency or centered at the image frequency Requirement to apply to the spacecraft when physically and operationally configured as follows: Spacecraft in flight configuration suspended above the test area floor; nonconducting suspension prerequisite The spacecraft operation to be in the *encounter* mode with the following specific constraints: Battery charger on Tape recorder to be operated in its record mode Stabilization jets to be actuated Spacecraft gyros to be energized Isotropic antenna and the high-gain antenna in its initial and deployed positions to be utilized respectively. (Two runs required)	Noise measurements outlined in procedure for the center and the image frequency The various specified test modes listed
Threshold degradation S-band	S-Band receiver to maintain its tracking loop acquisition and lock capability when operated in the spacecraft system environment S-band receiver to maintain lock when an applied signal 6-dB greater than threshold at best-lock frequency is swept at a rate of 30 Hz/s over a 10-kHz band centered at the best lock frequency Spacecraft to be in flight configuration suspended above the test area floor; nonconducting suspension prerequisite Spacecraft operation to be in the *encounter* mode with the following specific constraints: Battery charger on Tape recorder operated in its record mode Stabilization jets actuated Spacecraft gyros energized The low-gain antenna and the high-gain antenna in its initial and deployed positions to be utilized, respectively. (Two runs required)	Test sequence 4 describes tests to be performed: Condition the spacecraft to the noisiest mode determined with the EMI receiver. With the TWT on and the high-gain antenna to initial position, perform transponder evaluation tests of the following: Threshold S-band command (modulation on) Ranging Command lockup threshold Perform above for: Transmit *low*, receive *low* Transmit *high*, receive *low* Transmit *high*, receive *high* Repeat with the high-gain antenna deployed to position 2 Sweep test not feasible because of instrumentation limitations

(4) *Spacecraft noise environment at S-band receiver center and image frequencies and operation degradation tests, requirements vs test.* The requirements of the specification were incorporated in the procedure (see Table 45) with the exception that the spacecraft was not elevated for the S-band test sequence for two reasons: First, the RF losses in the test cables would be too great; and second, it was decided to radiate the VHF and UHF radio frequency levels to the spacecraft from a direction that approximated that expected for flight and if the spacecraft were elevated the VHF and UHF antennas would have had to be suspended from the rafters.

Time schedules did not permit placement of the radiating antennas if the spacecraft were to have been elevated. It was considered that the intent of the specification would not be jeopardized with the spacecraft placed on the tripod used for the test assembly and that the characteristics of the S-band antennas would not be affected in this position.

Spacecraft noise environment at DFR receiver frequencies, results.

(1) *Background noise measurements, VHF.* The background noise temperatures with the spacecraft *off* was found to vary between 650 and 950°K over a bandwidth from 49.2 to 50.1 MHz. A change from 650 to 950°K is a change of approximately 1.7 dB. The background noise level was also observed to vary by approximately 1.7 dB during the period of observation at the center frequency.

(2) *DFR operation threshold degradation.* After the background noise level was determined, the spacecraft was conditioned to various modes. The data obtained in this exercise for a frequency of 49.8 MHz is illustrated in Fig. 97. The noise is described in terms of temperature (°K) and is shown as covering a range, rather than a particular level. This was done because the background noise temperature varied between 650 and 950°K at this frequency. The SAF background noise has been subtracted from the total noise temperature.

By use of the data displayed in Fig. 97, the maximum spacecraft noise that the DFR would receive at the VHF receiver input at encounter would be approximately 1840°K in the following mode:

Battery charger *off*	Gas jets *on*
TWT *on*	Tape recorder drive *on*
Gyros *on*	Science *on*

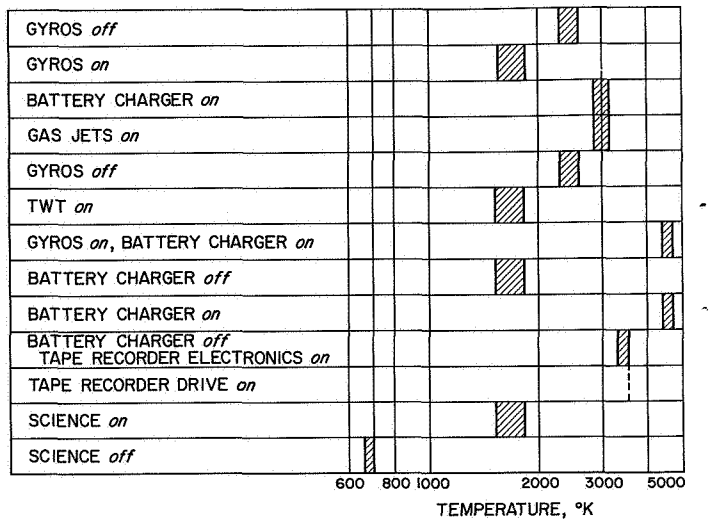

Fig. 97. Spacecraft-contributed noise at 49.8 MHz, without SAF ambient temperature of 620 to 950°K

Degradations of the DFR VHF receiver for various possible background cosmic noise temperatures are shown in Table 46. The values were determined from the following relationship:

Degradation in decibels is

$$\text{dB} = 10 \log \frac{T_{S/C} + T_{REC} + T_{COSMIC}}{T_{REC} + T_{COSMIC}}$$

where:

$T_{S/C}$ = the noise temperature of the spacecraft

T_{REC} = the receiver noise temperature, 290°K

T_{COSMIC} = the cosmic noise temperature at 50 MHz

(3) *Test results of 423.3 MHz.* In making background noise measurements with the spacecraft power *off*, at the UHF center frequency, background noise levels

Table 46. Calculated signal degradation in space, using measured noise values

Unit	Degradation from spacecraft noise for cosmic noise temperature, dB		
	For 6000°K	For 7000°K	For 8000°K
Dual-frequency receiver	1.1	1.0	0.9

from 250 to 268°K were observed within 423.3 MHz ±50 kHz. At the UHF image, the noise temperatures were observed to vary from 217 to 237°K within ±50 kHz of 473.1 MHz.

No noise was observed to be emitted by the spacecraft at either the UHF center frequency or the image. Spacecraft noise levels that would degrade the UHF receiver by 1 dB at a receiver system noise temperature of 1500°K (as could be expected for space) could have easily been observed with the test receiver. Such a noise level would cause an indication of 2.9 dB. Since noise was not observed, degradation to the UHF channel was not expected.

DFR operation threshold degradation, results.

(1) *Noise level measurements with DFR.* The degradation that the DFR system would experience due to spacecraft generated noise was measured on the second night of the tests. The test configuration was that shown in Fig. 98.

(2) *Test description.* With 50 Ω terminations placed at the inputs to the DFR bandpass and high pass filters, reference levels were established for each receiver. A test RF level of −130 dBmW was used for the UHF receiver and −125 dBmW for the VHF receiver. Because of the RF losses incurred in the test configuration, the levels at the DFR BCE were −62 dBmW with a carrier reading of 0.71 V at the UHF frequency and −78 dBmW with a carrier reading of 0.78 V at the VHF frequency. The reference levels were obtained while the DFR was powered by the BCE. For the remainder of the tests, the DFR was powered from the spacecraft. The configurations for these tests are described in Figs. 99 through 102.

The test data obtained in this test for different spacecraft modes is listed in Table 47.

Table 47 shows that a maximum value of 8-dB change in attenuator setting was required between a 50 Ω termination at the DFR VHF receiver input and the noisiest spacecraft condition. The noise represented by this change in the required RF level would degrade the DFR

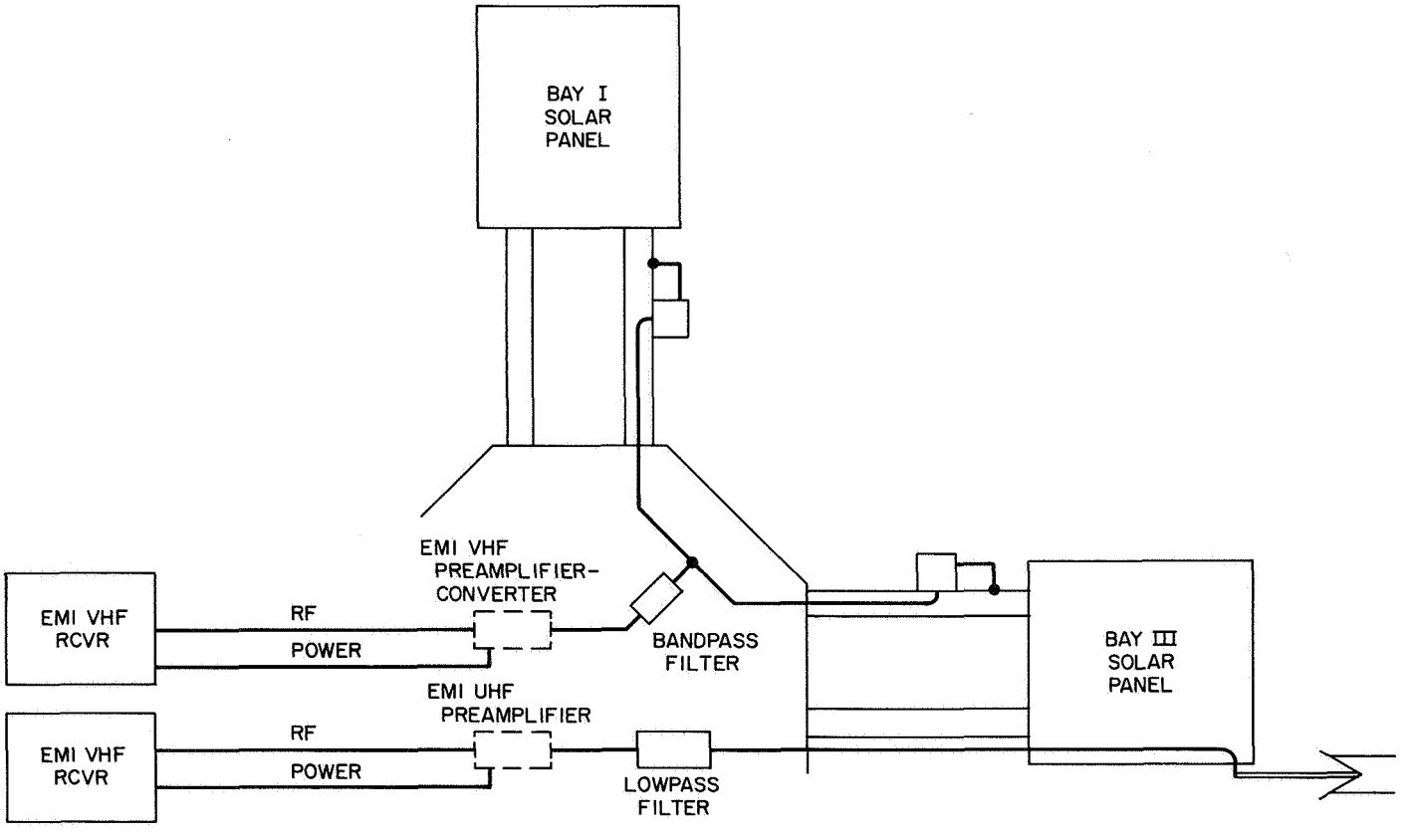

Fig. 98. Dual-frequency receiver EMI test

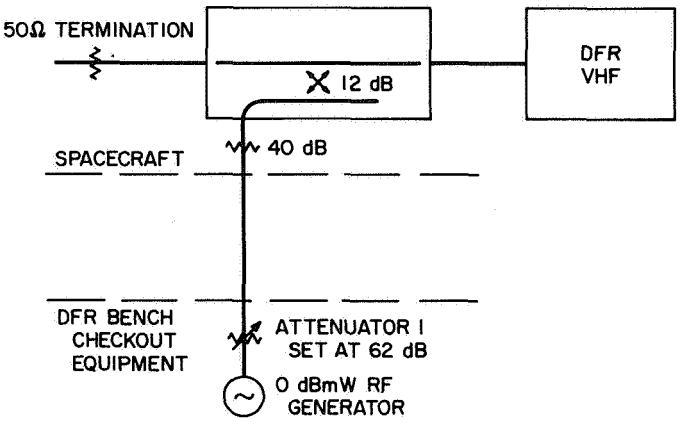

Fig. 99. Configuration to establish reference level on VHF dual-frequency receiver channel

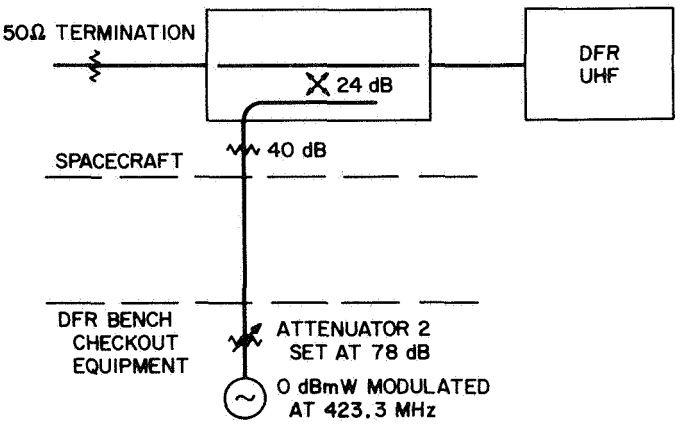

Fig. 101. Configuration to establish reference level on UHF dual-frequency receiver channel

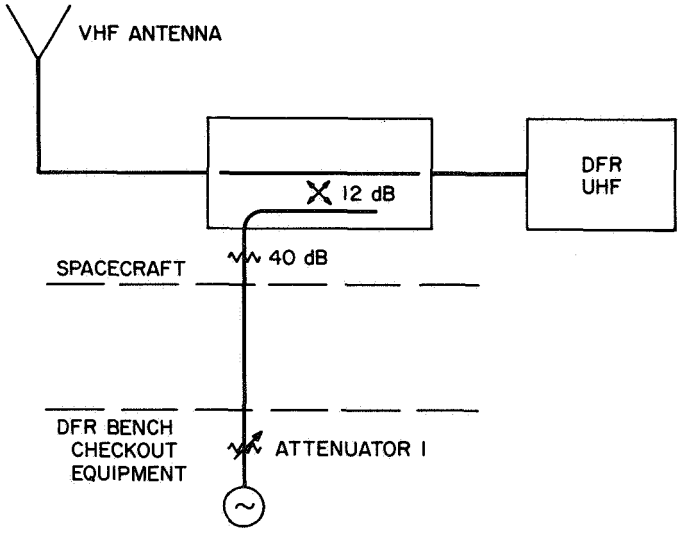

Fig. 100. Configuration for measuring noise degradation on VHF dual-frequency receiver channel

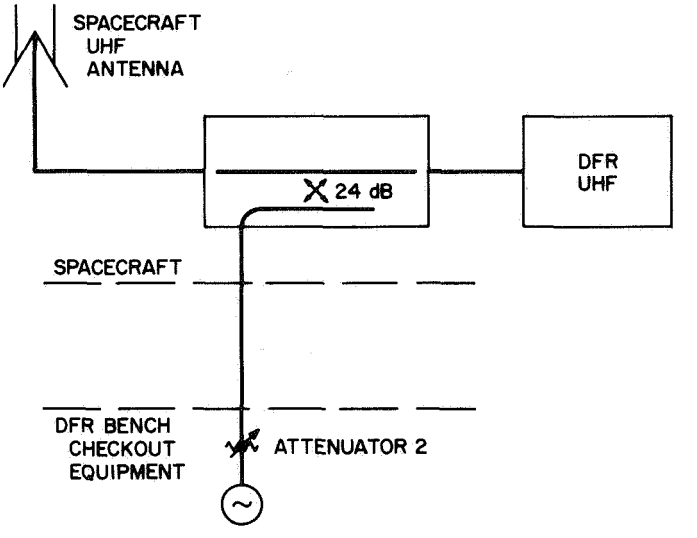

Fig. 102. Configuration for measuring noise degradation on UHF dual-frequency receiver channel

by approximately 1.4 dB in space, for a cosmic noise temperature of 8000°K. This degradation was determined in the following described way.

First, the RF level of the test signal from the DFR bench checkout equipment (BCE) must be adjusted when different noise levels enter the receiver. The RF test level is adjusted to provide a constant signal/noise ratio in the DFR. Therefore, if an RF signal increase of 3 dB (a factor of two) is required, the noise entering the receiver has increased by a factor of two. The RF level difference of 3 dB was noted between the test condition of a 50 Ω termination (at 290°K) at the receiver input and that for the VHF receiver connected to its antenna with the spacecraft *off*. For this case, the antenna temperature is then equal to the 50 Ω termination temperature of 290°K. This was a very low temperature when compared with that acquired during other days when tests were attempted.

Second, when the spacecraft was turned *on*, the greatest RF level change required to maintain a constant signal/noise ratio was 8 dB. A certain amount of noise is represented by this change in required RF test signal.

Table 47. Bench checkout equipment test data

Spacecraft condition	VHF		UHF	
	Carrier, V	Attenuation, dB	Carrier, V	Attenuation, dB
50 Ω termination on input	0.78	78	0.71	62
DFR antennas connected Spacecraft *off*	0.75	75	0.71	61
Spacecraft *on* TWT *on* Transmit low Receive low	0.80	70	0.70	62
Cavity *on* Transmit low Receive low Gyros *off*	0.78	73	0.70	62
Cavity amplifier high power Transmit low Receive low Gyros *on* Battery charger *on*	0.78	73	0.70	62
Battery charger *off*	0.78	73	0.70	62
Battery charger *on*	1/2-dB degradation		0.70	62
TWT *on (noisiest case)*	0.75	73	0.65	62
Cavity *on*	—	72	—	62
TWT *on*	No change			
Transmit high, receive low (DC-V10)	No change			
Tape electronics *on* (DC-V12, DC-V25)	0.80	73	0.65	62
Battery charger *off*	0.75	73	0.75	61
Antenna pointing angle change 2	0.74	72.5	0.60	61

Table 48. Calculated signal degradation in space from DFR VHF test data

Unit computed for	Degradation from spacecraft noise for cosmic noise temperature, dB		
	6000°K	7000°K	8000°K
Dual-frequency receiver	1.72	1.68	1.37

That noise level ($T_{S/C} + T_A$) can be found from the following expression:

$$8 \text{ dB change} = 10 \log \frac{T_{REC} + (T_{S/C} + T_A)}{T_{REC} + T_0}$$

where

T_{REC} = the VHF receiver noise temperature, 290°K

$T_{S/C}$ = the spacecraft contributed noise temperature

T_0 = the temperature of the 50 Ω input termination at ambient temperature: 290°K

T_A = the antenna temperature with the spacecraft *off*. (This temperature was determined to be 290°K, above.)

Using the stated temperature values a spacecraft noise temperature ($T_{S/C}$) of 3070°K was calculated.

Third, the degradation that the VHF receiver would suffer in space under various possible cosmic noise temperatures is calculated from:

$$\text{Degradation in dB} = 10 \log \frac{T_{S/C} + T_{REC} + T_{COSMIC}}{T_{REC} + T_{COSMIC}}$$

Table 48 shows the expected calculated space degradations for various cosmic noise temperatures.

It was determined that the degradation of the DFR VHF and UHF receivers did not exceed the levels specified under the test conditions of the test procedure.

DFR acquisition threshold degradation, results. The acquisition threshold degradation tests were performed successfully, as required in the specification.

Spacecraft noise environment at S-band receiver frequency, results. A frequency range of 7.5 MHz, centered at the receiver frequency, was examined with a bandwidth of 4 kHz for the presence of noise levels. With a bandwidth of 100 Hz, a range of 100 kHz, again centered at the receiver frequency, was examined for the presence of noise. None was observed in either case. The test receiver had a noise figure of 7.0 for this test, including cable losses. During this test, the spacecraft was maintained on its tripod stand without raising to the test level, as was done in the DFR tests. The reason for this was that RF levels were radiated to the spacecraft at the DFR frequencies (49.8 and 423.3 MHz) and it was

desired to have the radiation from the direction close to that expected for flight.

After the center frequency measurements were performed, the S-band receiver required reconfiguration to measure RF levels at the image frequency. Because it was not possible to perform the receiver change immediately, a performance test of the S-band transponder was started, as specified.

This test involved the illumination of the spacecraft with the DFR frequencies but – because of RF leakage problems encountered in the S-band OSE – this test could not be performed that night. A subsequent test was performed by personnel of the Systems Test and Launch Operations Section, and it was determined that the transponder operated without any observable degradation from either the DFR or the signals at 49.8 and 423.3 MHz.

On March 10, 1967 the final portion of the tests was completed by the measurement of RF levels at the S-band receiver image frequency. The image-frequency measurements were made in a 6.86-MHz band, centered at the image frequency, with a test-receiver bandwidth setting of 4.0 kHz. With a bandwidth setting of 100 Hz a bandwidth of 100 kHz was also examined. No noise was observed to be emitted by the spacecraft in any of the modes specified in the specification. This test portion could not be performed in a full flight configured spacecraft, because other spacecraft system tests required that the solar panels be removed and, in addition, the spacecraft was placed in the mechanical positioner. Because of special tests being performed with the spacecraft, the deployed position of the high-gain antenna was not monitored. However, the low-gain and the initial high-gain positions were examined. No RF noise at the image frequency was observed. Each of the required spacecraft modes was exercised on the spacecraft during the noise measurements.

Conclusions. The S-band transponder apparently is compatible with the DFR experiment, and there appears to be no degradation from 49.8- and 423.3-MHz signals of the OSE transmitter. No S-band noise at the receiver center or image frequencies was observed in the testing.

e. M67-2 subsystem requalification following systems-level testing. The intent of this material is to consider any subsystem that did not receive a valid system level environmental test history from such possible causes as late delivery or subsequent rework after systems test which invalidated system flight status, and describe what was done to offset that deficiency. The only M67-2 subsystem whose system-level-test qualification was invalidated following the M67-2 spacecraft systems environmental testing was the DFR subsystem. This subsystem was reworked to enable replacing the 7-MHz crystals.

The vibration test during requalification was on the spacecraft's roll axis, only; the vacuum-temperature test time was for approximately 30 min at 0°C and for approximately 4 h at 55°C.

Additional information regarding this subsystem appears under the following heading, *Subsystem level.*

2. *Subsystem level.*

a. Spacecraft M67-2 flight-acceptance testing. A summary of the M67-2 flight-acceptance subsystem testing is presented in Table 49. The table includes each of the subsystems on the M67-2 spacecraft and gives pertinent test data, as well as significant past test history experienced by the units during the *Mariner* Mars 1964 test program.

Summary of FA waivers and deviations (M67-2 spacecraft subsystems).

(1) *Data automation subsystem.* An ECR covered the design change and established the FA retest requirements. The reason for the retest was that the crystals in the DAS master clock were changed as part of the DFR EMI fix. Retest requirements included modules 20A2, 20A3, and 20A4 being subjected to partial FA vibration levels. On completion, the entire DAS was subjected to a partial FA vibration test. Following this, the entire DAS was FA thermal–vacuum tested, which consisted of 200 h of operating time in thermal–vacuum prior to redelivery to the spacecraft. This testing was completed prior to the M67-2 spacecraft system environmental test.

(2) *Trapped radiation detector.* There were no waivers or deviations on this unit.

(3) *Plasma probe.* There were no waivers or deviations on this unit.

(4) *Magnetometer.* There were no waivers or deviations on this unit.

(5) *UV photometer.* There were no waivers or deviations on this unit.

Table 49. Summary of M67-2 flight-acceptance testing

Subsystem or assembly	Serial No.	Significant *Mariner* Mars 1964 FA test history	Design changes for *Mariner* Venus 67	M67-2 FA testing summary				
				Vibration test		Thermal–vacuum test		Comments
				Date	Results	Date	Results	
Data automation subsystem 20A1-9	072	None.	New design	12/19/66 2/13/67	Passed Passed (1)	12/20/66	Passed	(1) Retest of 20A2, 3, and 4 for Z-axis, only, after incorporation of ECRs.
Trapped radiation detector 25A1	M67-2	MC-5 spare unit. No known problems.	Significant	12/16/66	Passed	12/18/66	Passed	(1) Unit tested during nonstandard test temperatures, per specification.
Plasma probe 32A1-4	M67-2	This unit went through system environmental test on MC-3 and MC-4.	Significant	12/2/66	Passed	12/8/66	Passed	(1) Unit tested using nonstandard test temperatures, per specification.
Magnetometer 33A1-3	M67-2	Most of this unit was on MC-4 for second part of chamber test and all AFETR operations.	Small	10/26/66 1/7/67	Passed Passed (1)	10/23/66 12/28/66	Passed Passed (1)	(1) PFR called for FA retesting because of a failure not related to environmental tests. (2) Unit tested using nonstandard test temperatures, per specification.
UV photometer 34A1 and 2	MC-4	No history. Dropped from list of experiments before FA test time.	Small	8/15/66	Passed	8/18/66	Passed	(1) PFR written: unit dropped 6 in. (2) Severe outgassing of aromatic ethers during thermal–vacuum test.
Dual-frequency receiver 35A1 and 2	3	None.	New	1/11/67 4/10/67	Passed Passed	1/14/67 4/10/67	Passed Passed	(1) Abbreviated FA test run after crystal replacement.
Radio bays V and VI	8	New.	Significant	12/8/66 12/15/66 12/21/66 1/27/67	Failed (1) Failed (1) Failed (1) Passed	2/1/67	Passed	(1) PFR written for 90°F phase spikes observed during vibration.
Data encoder 6A1-13	401	New.	Small	12/7/66 1/6/67	Passed Passed (1)	12/10/66	Passed	(1) PFR written for replacement of ladder switch; retested in one plane of vibration only.
Command subsystem 3A1-7	8	New.	Significant	11/21/66 1/7/67	Passed Passed (1)	12/6/66 1/3/67	Passed Passed (1)	(1) PFR against switch in 345 SN 8 module, which was replaced. Module, only, was retested.

Table 49 (contd)

Subsystem or assembly	Serial No.	Significant *Mariner* Mars 1964 FA test history	Design changes for *Mariner* Venus 67	M67-2 FA testing summary				
				Vibration test		Thermal–vacuum test		Comments
				Date	Results	Date	Results	
Tape recorder 16A1-6	4	Used on MC-4.	Major	12/8/66 2/15/67	Passed Passed (2)	12/8/66 2/16/67	Failed (1) Passed (2)	(1) PFR written against intermittent oscillation; retest performed at vendor. (2) Unit 16A2 vibration-tested in one plane; entire TRS tested at FA temperature in air at Raymond Engineering, in lieu of thermal–vacuum test.
High-gain antenna 2E1	7	New.	New	10/4/66	Passed	10/31/66	Passed (1)	(1) PFR for spot bonds pulled loose; no retest required. (2) Unit tested using nonstandard test temperatures, per specification.
Low-gain antenna 2E2	C-113	No record found.	None	8/24/66	Passed	Waiver deleting thermal–vacuum		None.
DFR antenna, 423.3 MHz 15E3	5	None.	New design	12/12/66	Passed (1)	Not required		(1) Rework per ECR accomplished before test.
DFR antenna, 49.8 MHz 15E2F1 and 2	C-104	None.	New design		Not required			(1) No FA testing required for DFR antenna 15E2F 1 and 2; configuration precludes assembly-level testing.
A/C electronic-control subsystem 7A1	7	This was an MC-5 spare.	Small	8/22/66	Passed (2)	See Remarks	Passed	(1) Unit tested in air. (2) Partial FA test required of qualified *Mariner Mars* 1964 system after incorporation of ECRs.
A/C gyro 7A2	12	New.	None	3/4/67	Passed (3)	Not required		(1) One axis vibration only.
A/C gas subsystem 7GA1 and 7GA2	28 & 29	This unit used on MC-4 through to final system test at AFETR and was on MC-4 during chamber failure.	Significant	9/9/66 10/21/66	Passed Passed	9/13/66 11/11/66 10/16/66 11/10/66	Passed Passed (1) Passed Passed (1)	(1) Test was rerun due to change of some of the A/C valves. (2) FA test on A/C valves, only. (3) Unit tested using nonstandard test temperatures, per specification.
Canopus sensor	106	No record found.	Major	11/9/66	Passed	11/7/66	Passed	
Sun sensor 7PS2 and 6 7SS2 and 6	7	This system used on MC-4 through final system test at AFETR and was on MC-4 when chamber failed.	None		Tested on *Mariner* Mars 1964			(1) Unit qualified on *Mariner* Mars 1964.

Sun gate 7SG2	7	This system used on MC-4 through final system test at AFETR and was on MC-4 when chamber failed.	None		Tested on *Mariner* Mars 1964			(1) Unit qualified on *Mariner* Mars 1964.
Earth sensor 7ED6	4	This system used on MC-4 through final system test at AFETR and was on MC-4 when chamber failed.	Significant	11/15/66	Passed	11/17/66	Passed	(1) Unit tested using nonstandard test temperatures, per specification.
Planet sensor 7LS8	003	None.	New design	10/13/66	Passed	12/12/66	Passed	(1) Unit tested using nonstandard test temperatures, per specification.
Terminator sensor 7TS2	6	No record found.	Significant	11/14/66	Passed	11/17/66	Passed	None.
Jet-vane actuator, vanes and support ring 7JV5 & 6	C-104	Used as MC-5 spare.	No change	10/21/66 11/4/66	Failed (1) Passed	11/5/66	Passed	(1) Two PFRs written for shift in zero position. (2) Unit tested using nonstandard test temperatures, per specification.
Central computer and sequencer 5A1-9	M67-1	This grouping of subsystem SNs referred to on MC-64 as SN MC-004. System was on MC-4 from start to final system test at AFETR, and was on MC-4 when chamber failed.	Small	9/22/66	Passed	7/27/66	Passed	None.
Power (bay I) 4A11-13 4A15-18	4	This unit used on MC-4.	Significant	12/5/66 2/27/67	Passed Passed (1)	12/8/66 3/3/67	Passed Passed	(1) PFR written for capacitor failure. FA test rerun on 4A18. (2) Unit 4A16 SN 06 was originally *Mariner* C 4A15. When *Mariner* Venus 67 SN 07 was damaged, the *Mariner* C unit (FA tested but not used) was substituted. No FA retest of assembly was done (verbal waiver), since spacecraft was ready to begin system-level FA testing.
Power (bay VIII) 4A8	3	This unit was used on MC-4 and had 8 planes of vibration on MC-64.	Significant	12/13/66	Passed	12/16/66	Passed	None.
Battery 4A14	34	None.	Small	1/20/67	Passed	Not required		None.
Solar panels 4A1–4	005 006 007 008	None.	Major	12/28/66 2/10/67	Passed Passed (1)	12/22/66 2/8/67 2/16/67 2/18/67	Passed Passed Passed Passed	(1) FA vibration of solar panels discontinued. (2) Units tested using nonstandard test temperatures, per specification.
Louver assembly	32–36, 39	All units used on MC-4 through to final system test at AFETR.	None	Temperature calibration in air only (all required) completed 10/4/66.				None.

Table 49 (contd)

Subsystem or assembly	Serial No.	Significant *Mariner* Mars 1964 FA test history	Design changes for *Mariner* Venus 67	M67-2 FA testing summary				
				Vibration test		Thermal–vacuum test		Comments
				Date	Results	Date	Results	
Temperature-control reference unit	M67-2	None.	New design	Not required		11/30/66 2/3/67 2/4/67	Passed Passed Passed	None.
Low-gain antenna dampers	C103, C111			Not required				(1) Units on M67-2 spacecraft for vibration.
Solar-panel-tip dampers 4A1, 3, 5, 7	119/120 121/122 123/124 125/126	None.	New design	Not required				(1) Units on M67-2 spacecraft for vibration and thermal–vacuum testing.
Solar-panel cruise dampers	C115–C118	All units used on MC-4 through to final system test at AFETR.	No change		Tested on MC-64			(1) Units on M67-2 spacecraft for vibration and thermal–vacuum testing.
Separation-initiated timer 8M1	107	No record found.	No change	9/15/66 10/7/66	Failed (1) Passed	Not required Waived (2)		(1) PFR written for dimensional problem on bracket, which allowed switch contacts to chatter; bracket was replaced and unit passed retesting. (2) PFR written against slow piston release due to viscosity of oil in damper; temperature, only cause. No concern; specification considered unrealistic.
Pyro arming switch 8AS1	C111	MC-5 spare only.	None	9/7/66 9/8/66 9/12/66	Failed Passed Passed (1)	Not required		(1) Z axis only. Retested to see if it would remain acceptable. One switch point seemed marginal.
PIPS 10A	67-2	All new except fuel tank.	Small	Not tested as subsystem; tested at component level. 5/11/67	Passed (2)			(1) Retest of start cartridge C-107 after transducer SN 46300 was replaced and welded into the cartridge.
Pyro control 8A1 & 2	1013 1014	Used on MC-4 through to final system test at AFETR.	Small	12/12/66	Passed	12/9/66	Passed	None.

(6) *Dual-frequency receiver.* The DFR was retested after 7-MHz crystals were replaced. Retest consisted of one plane of vibration, only, and a thermal–vacuum test of 30 min at 0°C and 4 h at 55°C.

(7) *Transponder (radio), Cases V and VI.* The radio was retested after modification, in accordance with ECRs. The modification consisted of replacing three capacitors in the 2PS2 unit and two capacitors in the 2PS3 unit, also fillet bonding of the ×30 multiplier module. The retest consisted of the following for 2PS2 and 2PS3: FA vibration Z axis only, thermal–vacuum 1 h at 0°C and 20 h at 55°C; also a minimum of 100 h at room ambient pressures and temperature. For the ×30 module, retesting consisted of bench test with complete radio subsystem, after foregoing the power-supply test. Vibration time on SN 8 radio was reduced from 60 to 30 s per axis. This testing was completed prior to the M67-2 spacecraft systems environmental test.

(8) *Data encoder.* A problem/failure report covered the FA vibration retesting, Z axis only, after replacement of bad ladder switch.

(9) *Command.* Flight-acceptance retesting of unit 3A5 SN 8, only (covered by a PFR), was accomplished after replacement of the transformer. Test consisted of one plane of vibration, only, for 1 min, 30 s and thermal–vacuum test for 41 h, 49 min. This testing was completed prior to the M67-2 spacecraft systems environmental test.

(10) *Tape recorder.* FA retesting of the tape recorder was accomplished after modification in accordance with ECRs. The modification consisted of potting of 16A1 and 16A2 modules with new potting compound and the replacement of a diode in the 16A4 module. The retest consisted (for 16A1 and 16A2) of FA vibration on one plane, only. For the entire TRS, retesting included FA temperature test at ambient pressures for 4 h at each specified temperature. This testing was completed prior to the M67-2 spacecraft systems environmental test.

(11) *High-gain antenna.* A waiver changed FA thermal–vacuum test temperature requirements from −260°F for 2 h to −245 ±5°F for 2 h.

(12) *Low-gain antenna.* The requirement to do FA thermal–vacuum testing of the low-gain antenna was waived.

(13) *DFR antenna.* There were no waivers or deviations on this unit.

(14) *A/C electronics.* Two ECRs cover FA retesting of the unit after design change. The test consisted of one plane, Z axis only, of vibration.

(15) *A/C gyro.* Modified FA test of the replacement gyro was made. The test consisted of one plane of vibration, only. Vibration equipment failures and schedule requirement caused bypass of planes 2 and 3.

(16) *A/C gas.* This gas system was FA retested. A waiver covered the testing of the A/C valves in the assembled configuration.

(17) *Canopus sensor.* The FA demagnetization requirement for the Canopus sensor was waived.

(18) *Sun sensors.* The FA lower temperature limits were waived.

(19) *Earth and terminator sensors.* A waiver revised the lower FA test temperature to 0°F.

(20) *Planet sensor.* There were no waivers or deviations on this unit.

(21) *Jet vane actuator.* A PFR covered the FA vibration retest of the actuator. The actuator pot was rezeroed; the unit then passed full FA vibration test.

(22) *Central computer and sequencer.* There were no waivers or deviations on this unit.

(23) *Power bays I and VIII.* The 4A18 power conversion unit was FA retested after replacement of a capacitor in the unit. For 4A18, this flight unit was installed in the FA subsystem and FA vibration-tested in all three axes and was then subjected to 40 h of FA thermal–vacuum. In addition, the unit was tested for 250 h at room temperature with power *on.* This testing was completed prior to the M67-2 spacecraft systems environmental tests.

(24) *Battery.* There were no waivers or deviations on this unit.

(25) *Solar panels.* The FA acoustic testing, as well as the FA vibration of flight solar panels, was waived (by two internal memorandums).

(26) *Thermal-control assembly.* There were no waivers or deviations on this unit.

(27) *Dampers.* There were no waivers or deviations on this unit.

(28) *Separation-initiated timer.* There were no waivers or deviations on this unit.

(29) *Pyro arming switch.* There were no waivers or deviations on this unit.

(30) *PIPS.* There was modified FA retesting of the oxidizer start cartridge after rewelding; the test consisted of vibration, only, in three planes. This testing occurred just prior to launch and did not include the complete PIPS subsystem.

(31) *Pyro control.* There were no waivers or deviations on this unit.

Mariner Mars 1964 flight-acceptance testing of Mariner Venus 67 flight equipment. The flight equipment listed below passed all flight-acceptance requirements on the *Mariner* Mars 1964 program without any failure or anomalies and was accepted as flightworthy for the *Mariner* Venus 67 program.

(1) Sun sensors 7PS2 (SN 7), 7SS2 and 7SS6 (SN 7), and the sun gate sensors 7SG2 (SN 7)

(2) Solar panel cruise dampers in bays I, III, V, and VII (SNs C-115 through C-118)

b. Special subsystem tests.

Dual-frequency receiver (SN 03) EMI testing. Dual-frequency receiver electromagnetic interference testing was performed to verify that the DFR would function

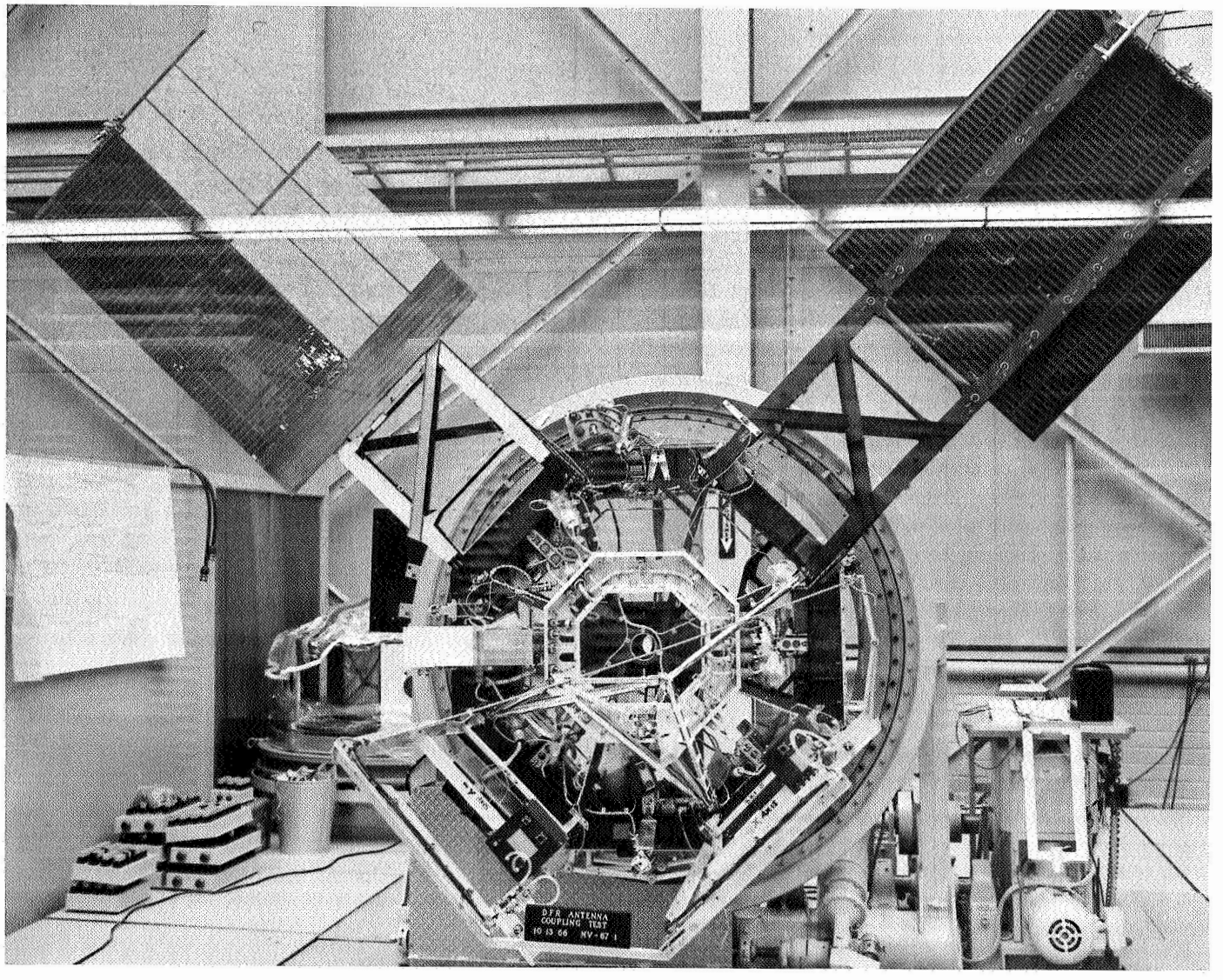

Fig. 103. Dual-frequency receiver antenna coupling test

properly when subjected to an electromagnetic environment similar to *twice* that expected to exist on the *Mariner* Venus 67 spacecraft. The test setup is shown in Fig. 103.

(1) *Requirements vs tests.* The electromagnetic interference testing levels that were used to verify that the DFR would function properly were derived from data acquired during the testing sequence of the *Mariner* Mars 1964 spacecraft and the expected electromagnetic environment for the *Mariner* Venus 67 spacecraft. The interference levels to which the DFR was subjected are specified in the Environmental Specification. In accordance with the specification, the DAS was tested per JPL Procedure. Listed in Table 50 are the required tests and the test limits as defined in the procedure.

Table 50. M67-2 dual-frequency receiver EMI tests and test limits

Electromagnetic interference	Interference limits	
	Specification	JPL procedure
Generated interference		
Generated conducted transients:	$<\pm 0.5$ V max	± 0.5 V max
Generated sinusoidal:		
30 Hz to 15 kHz	<0.5 V peak to peak	<0.5 V peak to peak
15 to 150 kHz	<0.5 V peak to peak, decreasing at 20 dB/octave to 0.05 V peak to peak	<0.5 V peak to peak
150 kHz to 25 MHz	<0.05 V peak to peak	<0.05 V peak to peak
Conducted interference susceptibility—power leads		
Transients	± 8 V amplitude ≤ 20 μs wide ≤ 7 μs rise time Repetition Rate: 0.5 to 500 pps	± 8 V amplitude
Sinusoidal		
30 Hz to 15 kHz	0.5 V peak to peak	0.5 V peak to peak
15 to 150 kHz	0.5 V peak to peak at 15 kHz, decreasing at 20 dB/decade to 0.05 V peak to peak	0.5 V peak to peak
150 kHz to 25 MHz	0.05 V peak to peak	0.05 V peak to peak
Conducted interference susceptibility—signal lines		
Transients	± 200 mV amplitude ≤ 20 μs wide ≤ 7 μs rise time Repetition Rate: 0.5 to 500 pps	± 200 mV amplitude
Sinusoidal		
30 Hz to 15 kHz	0.05 V peak to peak	0.05 V peak to peak

Electromagnetic interference	Interference limits	
	Specification	JPL procedure
Conducted interference susceptibility—signal lines (contd)		
15 to 150 kHz	0.05 V peak to peak at 15 kHz, decreasing at 20 dB/decade to 0.005 V peak to peak	0.05 V peak to peak
150 kHz to 25 MHz	0.005 V peak to peak	0.005 V peak to peak
Equipment enclosure radiated interference susceptibility		
Frequency, MHz	**Power density, dBmW/m²**	**Power density, dBmW/m²**
229.9	− 8	—
244.3	19	—
2297.5	− 2	—
5765	−18	—
8000	− 9	—
9000	−12	—
Spurious response susceptibility test		
Frequency, MHz	**Level of signal, dBmW**	**Level of signal, dBmW**
27.5	−65	—
2000	−75	—
2150	−65	—
2220	−78	—
2297.5	− 2	—
2450	−59	—
2600	−73	—
4590	−62	—
9210	−76	—
Oscillator radiation test		
2115-2116	−100	—

(2) *Results.* The dual-frequency receiver (SN 03) was subjected to EMI testing per the flight-acceptance procedures as outlined in a JPL Procedure. The DFR successfully passed the tests, as specified, and operated within the prescribed limits with no degradation to operation during all electromagnetic interference testing.

Solar panel single-panel FA test. All solar panel FA testing is discussed in the earlier part of this section, under M67-1, *Special subsystem tests* (IV-A-2-b).

c. Special subsystem environmental test anomalies.

PIPS oxidizer start subsystem test anomaly. Following a leakage repair in the M67-2 spacecraft oxidizer start subsystem (SN C-107), an FA vibration test was run to requalify it for flight. During the first plane of shake, some moderate-level transients were detected by the control transducer. A playback of the recorded transient signals revealed peak acceleration levels of approximately 60 g, with frequencies in the range of 5 to 10 kHz. The effect of these transients on the hardware was analyzed, as follows.

Comparison of the structural transient response of the hardware was attempted by use of a shock-spectrum equivalence. Figure 104 displays the shock spectra both from the M67-2 PIPS subsystem vibration test and from the M67-1 PIPS pyro firings that occurred during M67-1

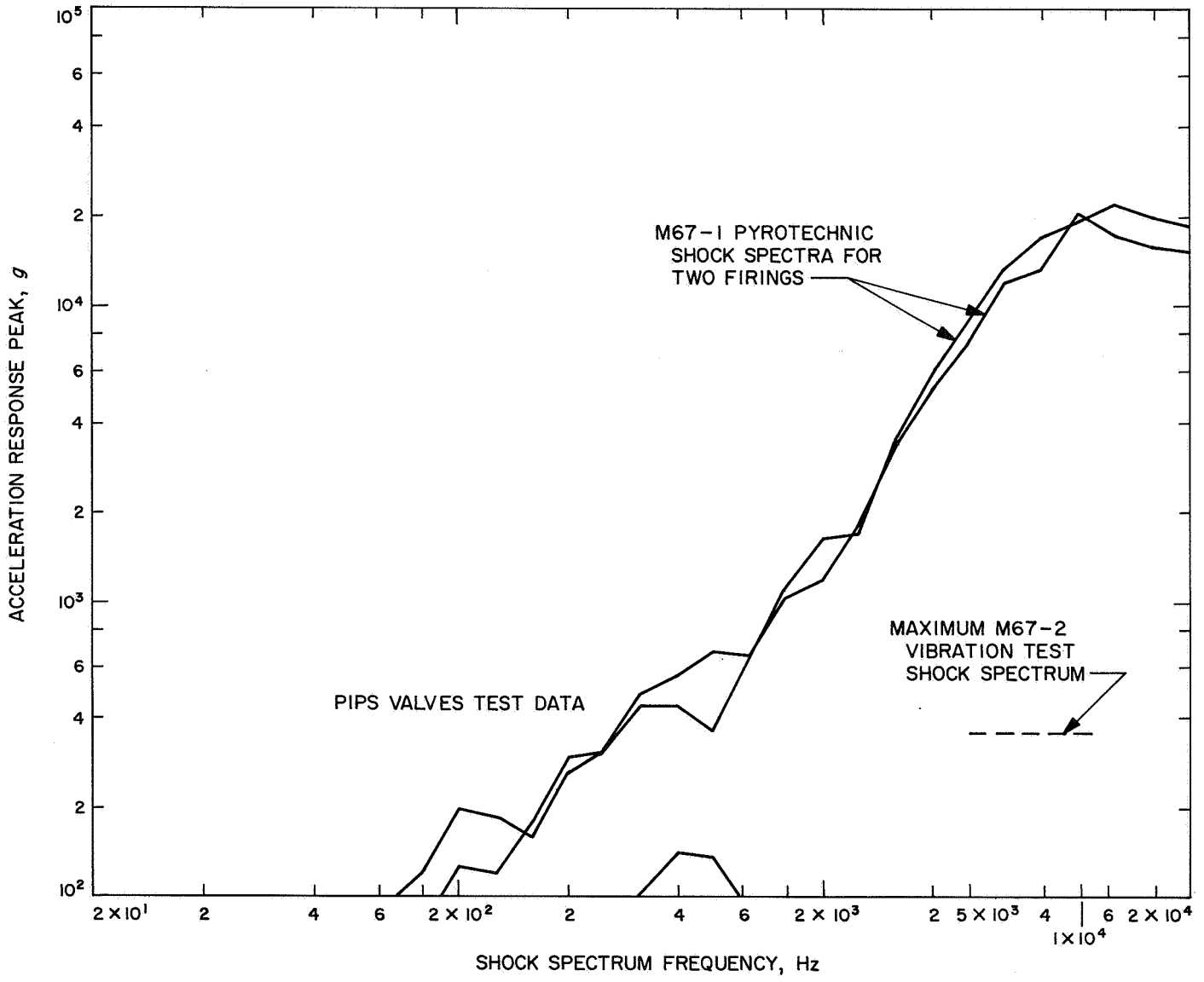

Fig. 104. Comparison of M67-1 and M67-2 structural transient response

spacecraft FA environmental testing. The reason for making this comparison with the M67-1 pyrotechnic environmental ground test, instead of the M67-2 pyrotechnic environmental ground test, is that the prime spacecraft (M67-2) was not instrumented as heavily as the spare spacecraft (M67-1), and this particular measurement location was not recorded. However, data recorded on each of the spacecraft show that a close correlation exists between the response levels of the two spacecraft.

The maximum M67-2 vibration-test shock spectrum in Fig. 101 is an upper bound derived from the actual peak g test level and frequencies using the criteria established in an internal communication. A maximum amplification factor of 6 times the peak g level has been used here. The resultant maximum-shock-spectrum level of 360 peak g (6×60 g) is shown as the dashed line between 5 and 10 kHz.

The pyrotechnic shock spectra in Fig. 104 display the results obtained from the transient response of a valve body transducer recorded during the M67-1 PIPS valve squib firings. A more comprehensive analysis of the M67-1 pyrotechnic tests is reported in an internal document. The higher level response of a typical shock spectrum level is at least an order of magnitude higher than any transient level experienced during the subject vibration test.

It has been shown repeatedly that the PIPS remains functional following the squib valve firings. Based on this fact and the difference in response levels discussed here, SN C-107 was considered acceptable for flight.

Canopus sensor anomaly: EMI test. All Canopus sensor EMI testing relating to the intensity output anomaly that occurred at Cape Kennedy just prior to launch is discussed in full in Section III.

V. Magnetic Control Program

A. Policy and Requirements

The Mariner Venus 67 Project Policy and Requirements document specified (1) that the magnetic quality of the *Mariner* Venus 67 spacecraft be at least equal to that of the *Mariner* Mars 1964, and (2) that an attempt be made to improve the quality with techniques possible within the fiscal restraints and time limits of the schedule. In support of these general requirements, it called for demagnetization of flight hardware at disassembly inspection on a subsystem (or assembly) basis, following demonstration of acceptability of the technique using TA or equivalent hardware.

The *Mariner* Venus 67 magnetic control program was initiated to reduce and stabilize the spacecraft perm field by demagnetization. To improve on the *Mariner* Mars 1964 PTM demagnetizing results, *Mariner* Venus 67 hardware was demagnetized on the assembly level, insofar as possible. Demagnetization and mapping were performed in a coil system that reduced the ambient field. All demagnetization was at 1/20 Hz, except for solar panels, which were at 60 Hz. The maximum peak field applied to TA hardware was 80 G. Following spacecraft demagnetization on this component basis, tool boxes were periodically monitored and demagnetized as required. The assembled spacecraft and the individual solar panels were mapped at JPL, only, in the earth's field.

To qualify the demagnetization process for the flight hardware, TA hardware was subjected to more extensive tests to encompass demagnetization to a peak level twice that to which the flight hardware was exposed. These tests included exposure to a standard 25-G field and two demagnetizations, each followed by a mapping to verify the safety and effectiveness of the operation and to provide a measure of the perm field stability.

1. Magnetic control plan. To meet the requirements, in March 1966, a magnetic control plan that detailed the necessary procedures was developed, approved, and distributed to those concerned. The main features of this plan, as it was actually carried out for *Mariner* Venus 67, are described here.

a. ECR review. All engineering change requests were reviewed, and discussions were held with cognizant engineers concerning hardware on which the magnetic quality might be affected by requested changes. If the magnetic quality of any item were questioned, it was checked.

b. Magnetic evaluation of hardware. At least one prototype or TA model of all flight hardware was subjected to an extensive magnetic evaluation, involving the following operations:

(1) Initial as-received mapping.

(2) Demagnetization in three orthogonal axes at a 1/20-Hz alternating frequency with a decreasing magnetic field that had an initial peak value of

40 G. This demagnetization was followed by a second mapping.

(3) Exposure of the hardware to a peak magnetic field of 25 G in the axis having the highest field component in the initial mapping. A third mapping was made following this exposure. In a few cases, the hardware was reexposed in a different axis and remapped.

(4) Demagnetization of the hardware as in (2), above, but with an initial peak magnetic field of 80 G. A fourth magnetic mapping was then obtained.

(5) Determination of the effect of an inducing field of 0.26 G in each of the three coordinate axes. Interpretation of these results was not entirely satisfactory.

c. Demagnetization of all FA hardware. All flight-approval hardware for the spacecraft was demagnetized in three orthogonal axes with a 1/20-Hz decreasing alternating field having a peak initial value of 40 G, and this action was followed by a magnetic mapping. The demagnetization and mapping were performed on the subassembly or, insofar as possible, on the assembly level during the disassembly of the spacecraft for final inspection – which is after all vibration and shock testing of the hardware.

d. Redemagnetization and remapping of hardware. Any hardware that was removed from the Spacecraft Assembly Facility subsequent to the demagnetization was remapped upon its return to the SAF and subjected to redemagnetization and remapping if the magnetic field had changed by more than 10%, or 1 γ, whichever was greater.

e. Solar panel demagnetization. A TA solar panel was mapped, permed and demagnetized several times with a 20-G, 60-Hz demagnetizing field. All flight solar panels were magnetically mapped and found to have such a low field as to not require demagnetization.

f. Solar panel examination for current flow fields. A single flight solar panel was examined for magnetic fields resulting from the flow of current in the panel.

g. Repeated checking of tools. All tools used on the flight spacecraft in SAF or at ESF were examined for magnetic fields and demagnetized if the field on the surface of the tool exceeded 5 G. Periodic rechecking of the tools was also made.

2. Safety aspects of magnetic control program. The safety aspects of the magnetic control program were carefully considered. To ensure that all potential personnel and material hazards associated with magnetic test operations were fully understood and that adequate measures were taken to avoid or minimize the hazard, four operations considered potential hazards – either to personnel or the spacecraft flight hardware – were presented to the *Mariner* Venus 67 safety task team for consideration. Measures were taken to minimize these hazards, and cognizant personnel were made aware of the necessary precautions to be taken. These four potential hazards are listed below:

(1) Physical damage to hardware by dropping or falling while being introduced into, or being removed from, the demagnetizing and mapping facility.

(2) Possible demagnetization of permanent magnet devices in the spacecraft during demagnetization of the assemblies or subassemblies. (Refer to relay study under V-C-1.)

(3) Induction of excessive and damaging voltages in spacecraft circuitry caused by changing demagnetizing fields. (These voltages were calculated to be negligible at frequencies below 1 Hz.)

(4) High voltage during 60-Hz operation of demagnetizing coils for solar panel demagnetizing. (Precautions continue to be necessary when demagnetizing at 60 Hz because of the series resonant circuit employed.)

Because the solar panels made up the only subsystem that required high voltage during demagnetization – and since the above hazards (2) and (3) were shown to be of minimum danger – the first item, then, remained the only real concern for precaution in handling operations.

B. Type-Approval (TA) Testing

1. System level. There was no TA demagnetization effort performed at the system level.

2. Subsystem level. The reasons for TA hardware evaluations were (1) to qualify the demagnetization process for the flight hardware, (2) to determine the effectiveness of the demagnetization, and (3) to obtain an indication of the relative stability of the resultant residual field.

a. Requirements vs tests. Type-approval magnetic testing was accomplished in accordance with the specification, with the following exceptions:

(1) Because of the small sizes of some hardware items, it was necessary to map at distances other than those specified. Mappings were made at 6 in., at 12 in., and at 2 ft, in addition to those stipulated in the test specification.

(2) Because induced field effects were difficult to interpret, deviation from specification was sometimes necessary for this test.

b. Results. It generally was found that hardware, as received, had a relatively high residual field that could be effectively reduced by demagnetization. The results indicated that some assemblies were not sufficiently demagnetized by the 40-G deperm.

The magnetic mapping results are summarized in Table 51, in which the data have been extrapolated to give the maximum residual radial field at a distance of 3 ft from the approximate center of the hardware under the following four conditions:

(1) Initial mapping of as-received hardware

(2) Mapping following 25-G exposure in the axis most nearly parallel to the dipole moment observed in the as-received hardware mapping

(3) Mapping following 80-G (peak field) demagnetization at 1/20 Hz

(4) Mapping following 40-G demagnetization at 1/20 Hz

The above results are comparable to results obtained from similar tests for the *Mariner* Mars 1964 spacecraft, for

Table 51. Type-approval hardware magnetic test results

Hardware	Designation	Serial No.	Maximum radial field at 3 ft, γ				40-G deperm residual field components at magnetometer, γ		
			As recd	25-G exposure	80-G deperm	40-G deperm	X	Y	Z
Bay I (less 8A1/2)	4A Series	02	17.5	26.8	14.4	14.7	−0.99	−0.36	−0.23
Pyro control	8A1/2	1005	10.9	8.0	11.0	11.1	0.82	0.34	0.26
		1006	10.0	7.9	10.7	9.9	−0.77	−0.10	−0.29
Midcourse motor	10	MC002	7.4	15.1	5.0	5.7	0.33	0.24	−0.36
Umbilical connector	600153	11	0	0	0.1	0	0	0	0
Bay III DAS	20A Series	073	1.3	39.5	0.2	0.7	0	−0.02	0.04
Trapped radiation detector	25A1	C101	12.8	5.1	0.5	0.6	0	0.08	−0.05
Plasma probe	32A1	397	18.8	32.1	2.2	0.6	−0.05	0.01	0.01
	32A2	02	3.6	8.5	0.3	2.4	−0.06	−0.11	−0.05
	32A3	02	0.4	0.4	0.1	0.2	−0.01	−0.01	0
	32A4	03	2.5	8.2	0.3	0.3	−0.01	−0.01	0.02
Magnetometer	33A1	Life Test	0	0	0	0	0	0	0
	33A2	Life Test	31.3	25.2	0.4	1.1	0.04	−0.07	0.08
	33A3	Life Test	0.5	38.1	0.6	0.5	−0.05	−0.02	0.01
UV photometer	34A1	MC3	2.0	13.1	0.3	0.4	−0.02	−0.04	0.04
	34A2	MC3	2.3	3.8	0.2	0.6	−0.03	0.01	0.04
DFR	35A1/2	1	1.1	4.9	0.1	0.4	0.01	0.04	0
DFR filters		A165-4 A251-1	0.7	4.4	0.9	4.2	0.56	−0.11	−0.09
Bay IV data encoder and command	3A & 6A Series	2/3	51.4	136.1	12.1	13.8	1.06	0.60	−0.61
Bay V radio	—	—	23.4[a]	100.7[a]	10.3[a]	10.5[a]	−0.34[a]	−1.06[a]	0.34[a]
Tape recorder system	16A Series	2	17.6	25.6	8.8	9.1	1.04	−0.38	0.22
Bay VI transponder		3	41.9	262.1	10.9	12.0	1.17	−0.96	0.03

Table 51 (contd)

Hardware	Designation	Serial No.	Maximum radial field at 3 ft, γ				40-G deperm residual field components at magnetometer, γ		
			As recd	25-G exposure	80-G deperm	40-G deperm	X	Y	Z
Bay VII CC&S		TA	97.4	123.8	82.7	81.5	0.49	9.56	3.31
Gyro assembly	7A2	PTM011	0.8	38.8	1.0	0.6	0.01	−0.02	0.03
Bay VIII power		02	3.3	8.3	3.6	4.9	0.33	−0.31	−0.26
Battery	4A14	26	0.1	0	0	0	0	0	0
Canopus sensor	7CS8	107	21.6	—	—	—	1.32[b]	−2.21[b]	−2.46[b]
	7CS8	103	17.8	16.9	14.2	15.1	1.43	−1.39	−1.73
Planet sensor	7LS8	002	1.6	2.5	0.1	0.1	0.01	0	0
Terminator sensor	7MG1	01	0.3	0.6	0	0.1	0	0	0
Earth sensor	7ED6	01	0	0	0	0	0	0	0
Primary sun sensor	7PS6	3	0	0.1	0	0	0	0	0
Secondary sun sensor	7SS2	3	0	0	0	0	0	0	0
Sun gate	7SG7	D420	0	0.3	0	0	0	0	0
Separation-initiated timer	8M1	103	0	0.2[c]	0.1	0	0	0	0
Pyro arming switch	8AS1	C106	0.1	0.1	0	0.1	0	0	0
Louver	4101330	2	11.8	30.0	0.0	0.5	−0.01[d]	−0.01[d]	−0.04[d]
A/C 4-jet valve assy	7GM41/411	—	2.0	3.2	0.8	1.5	−0.02[e]	0.04[e]	−0.02[e]
A/C 2-jet valve assy	7GM21/211	72/94	2.2	2.5	1.1	1.0	−0.02[f]	0.01[f]	0.03[f]
High-gain antenna	2E1	4	1.2	0.9	0.8	1.2	−0.62	−0.19	0.44
Low-gain antenna		C106	0	0	0	0	0	0	0
DFR UHF antenna	15E3	STM	0	0	0	0	0	0	0
DFR VHF antenna									
Bay I Ins	15E2F1		0.2	1.3	0.1	0	0	0	0
Bay I Metal			0	0.8	0.2	0	0	0	0
Bay III Ins	15E2F3		0	0	0.2	0	0	0	0
Bay III Metal			0.3	0.4	0.3	0.4	0.01	−0.01	0.02
Temperature-control reference	410363	11-1	0.2	0.4	0	0.1	0	0	0
	410363	13-2	0	0	0	0	0	0	0
Solar-panel-tip boost damper	4110009	C106	0.6	0.5	0.4	0.5	0.01[g]	−0.01[g]	−0.01[g]
Solar-panel-deploy assy	[h]		0.1	0.2	0.1	0.1	0	−0.01	0.01
Accelerometer	2217	HB52	0.1	0.1	0	0.0	0	0	0
	2217	HC66	0.3	0.1	0	0.1	0	0	0.01

[a]This bay V mapping includes tape recorder units, but not same units shown on next line.

[b]As the Canopus sensor was granted a waiver on magnetization and demagnetization, these components of the residual field are for the as-received condition.

[c]Separation initiated timer safety pin (nonflight) has a field of 2 γ at 3 ft.

[d]Only a single louver was given TA testing. Field at spacecraft magnetometer is shown for louver in bay VI position, which is closest to magnetometer and, consequently, the worst-case situation.

[e]A single 4-jet roll-and-yaw valve assembly was tested and is shown for the $-x$ position, which is closer to the magnetometer sensor.

[f]A single 2-jet pitch-valve assembly was tested and is shown for closer $-y$ position.

[g]A single boost damper was tested. Valves shown are worst-case for damper closest to magnetometer position.

[h]Solar-panel-deployment assembly consisted of two springs, microswitch assembly, and spherical bearing on stud bolt.

which was specified a field $<5\ \gamma$ at 3 ft. However, those results were obtained, generally, following vibration testing, only – which in most cases, should be compared only with the as-received mapping for *Mariner* Venus 67 hardware. Although the mappings are listed in the table in the above sequence, this is not the order in which the mappings were made. The last three columns of the table give the extrapolated rectangular components of the residual field at the relative position of the science magnetometer sensor, in spacecraft coordinates, for the mapping following the 40-G demagnetization – which is the comparable mapping that was made on *Mariner* Venus 67 flight hardware.

Note that in a few cases, the field after an 80-G demagnetization is greater than the field determined from the as-received or 40-G deperm mapping. This is usually caused by a permanent-magnet component in the hardware. Magnetic stability can best be inferred by comparing the 25-G exposure mapping and the 40-G deperm mapping. A large difference is indicative of relative instability in the magnetic field.

Investigation of the change in field due to the attitude control jets being in flight configuration, rather than on the dummy solar panel racks, indicated negligible effect.

In addition to the items listed in Table 51 the following items of hardware were also partially evaluated.

(1) The spacecraft octagon structure with one-half attitude-control gas system was demagnetized in the X and Y axes. Attempts to measure the resultant fields were unsuccessful, because of the size of the structure.

(2) The lower ring harness from the *Mariner* Mars 1964 PTM spacecraft was mounted on a plywood board in the form it is installed on the spacecraft. The following fields, extrapolated to 3 ft, were obtained: As-received, 2.0 γ; 40-G deperm, 1.1 γ; 25-G exposure, 19.2 γ.

(3) Sunshade deployment springs (SNs C-179 and C-180) were found to be entirely nonmagnetic.

(4) Low-gain antenna SN 3 was permed and depermed in two axes normal to the long axis of the antenna and was mapped about the antenna axis, only. This operation was performed on each end of the antenna. Although these results are not conclusive, no magnetic field could be detected. An 18-in. section of the low-gain antenna was more thoroughly evaluated in all three axes and, again, no magnetic field could be detected.

(5) Two pinpullers, D4901125B-1 SNs C-132 and -331, were tested and found to be nonmagnetic.

(6) A 10-in. section of coaxial cables (RG142B/U, representative of spacecraft cables 2W2 and 2W45; and RG188, representative of 2W47) was evaluated and found to be magnetic with results shown in Table 52.

(7) Two temperature transducers, T-4086S1 SNs 65746 and 65749, were evaluated and found to have a negligible magnetic field.

c. Anomalies. It was found that demagnetization of the science magnetometer sensor resulted in approximately a 1-γ change in the sensor offset. As the demagnetized condition was believed to be the more stable, the sensor was given a 40-G demagnetization before being calibrated.

Demagnetization of the Canopus sensor resulted in a ½-deg error in the look angle. The exact cause of the offset has not yet been determined, but is related to the magnetic shield surrounding the tube. Because of the difficulty in aligning the sensor, magnetization and demagnetization of the sensor was subsequently waived.

3. Solar panel tests. These tests were made to verify solar-panel demagnetizing and mapping procedures.

a. Requirements vs tests. Based on demagnetization tests on a small section of panel, the demagnetization facility was modified from that used for *Mariner* Mars 1964 panels so that the *Mariner* Venus 67 panels could be inserted into the demagnetizing coil system from the side, normal to the axis of the coils. With this arrangement, the solar panel Kovar buses were aligned with their long axes parallel to the demagnetizing field. As the initial mapping of the panel disclosed a negligible magnetic field in the panel, the panel was permed with permanent

Table 52. Coaxial cable magnetic mapping results

Coaxial cable	Maximum radial field at 3 ft, γ			
	As recd	40-G deperm	25-G exposure	80-G deperm
RG142B/U	4.3	5.5	65.3	2.1
RG188	2.0	2.0	17.3	2.1

magnets to verify the demagnetization process. All demagnetization of the solar panel was performed with a 60-Hz alternating field.

b. Results. Type-approval solar panel SN 002 was initially mapped following vibration testing, and it was found to have a negligible field. The panel was then permed by demagnetizing in the presence of a biasing dc field. The field of the panel at the spacecraft magnetometer location for a panel in the $-Y$ position following this perming was:

X component	Y component	Z component
6.0 γ	0.8 γ	-0.5 γ

The panel was next demagnetized with a decreasing magnetic field having an initial value of 20 G rms. Following this demagnetization, the components of the residual field of the panel were $<\frac{1}{2}$ γ.

c. Anomalies. This panel was reported to have been electrically damaged in an earlier environmental test, so could not be electrically checked to verify that performance had not been degraded by demagnetization. Subsequent mappings of flight panels indicated that demagnetization of *Mariner* Venus 67 panels was unnecessary, because their particular configuration was not conducive to acquiring a residual field in the vibration testing.

C. Development Testing

Magnetic tests that were instituted on request, or because of concern by the cognizant hardware engineer, are included in this section.

1. Relay study. With the decision that assemblies and subassemblies would be demagnetized, concern was expressed about the effect of the demagnetization on permanent magnets, which are a part of the latching relays employed in the CC&S, as well as other units. The CC&S, alone, employs approximately 25 of these relays. Therefore, this study was conducted to determine if normal spacecraft hardware demagnetizing fields cause degradation of latching relay performance and to determine what magnitude of demagnetizing fields do adversely affect latching relay magnets.

a. Requirements vs tests. Relays were tested by determining the maximum radial magnetic field at 8 in. and by measuring the minimum current required to cause a switching of the relay. These tests were made on a number of relays, following their exposure to various peak demagnetizing field levels.

Tests were conducted on Sigma type 32 and 33 relays and on the Potter and Bromfield SLG11D relay.

b. Results. The initial demagnetization of a latching relay appears to stabilize the relay magnetic field. This effect is independent of the demagnetizing field level up to several hundred gauss. This initial stabilization results in a decrease of a few percent in the magnetic field. After this initial effect, the relay magnetic field is relatively unaffected up to a magnetic field of about 500-G peak. Beyond this field level, the residual external field of the relay rapidly decreases, and the relay fails to latch after demagnetizing field levels of about 600-G peak.

When the ceramic, permanent magnet element of a relay was subjected to a demagnetizing field by itself, the maximum residual external field decreased by about 35% after a 100-G rms demagnetizing field. Since the magnet element consists of two opposing coaxial dipoles, this decrease may be a change in relationship of the two individual dipoles. It does indicate, however, that the magnet receives considerable protection in the assembled condition where the magnetic circuit is more complete.

Tests of the current that is necessary to cause tripping of the relay showed considerably more variation between similar relays than was evident due to demagnetization below about a 500-G peak. Individual tripping or latching currents varied by as much as 15% from the mean tripping current, while deviation due to demagnetization was less than 10%, up to 565-G peak demagnetizing fields.

The results of this study are summarized in Figs. 105 and 106 showing the results for two Sigma type 32RJD latching relays.

2. Solar panel demagnetization study. This study was made because of changes in the *Mariner* Mars 1964 solar panel design necessitated by the *Mariner* Venus 67 mission and because of constraints imposed by the existing solar panel demagnetization facility. Factors significant to this study were:

(1) Structural changes in the *Mariner* Mars 1964 solar panel design affected the magnetic quality of the *Mariner* Venus 67 panels. In particular, each of the Kovar buses was placed with its long axis perpendicular to the panel, rather than parallel to it as on *Mariner* Mars 1964 panels.

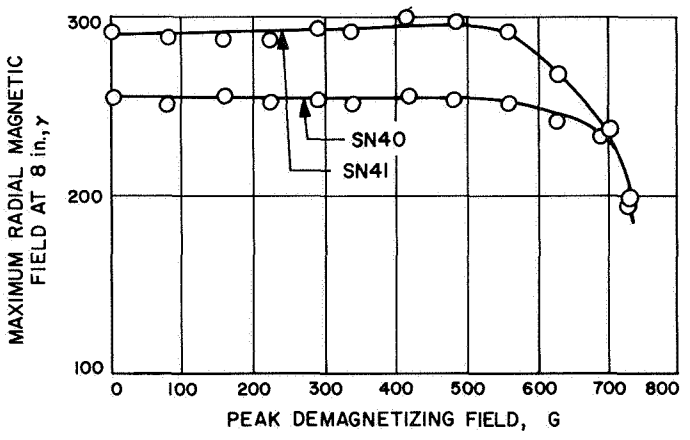

Fig. 105. Latching relay residual field test

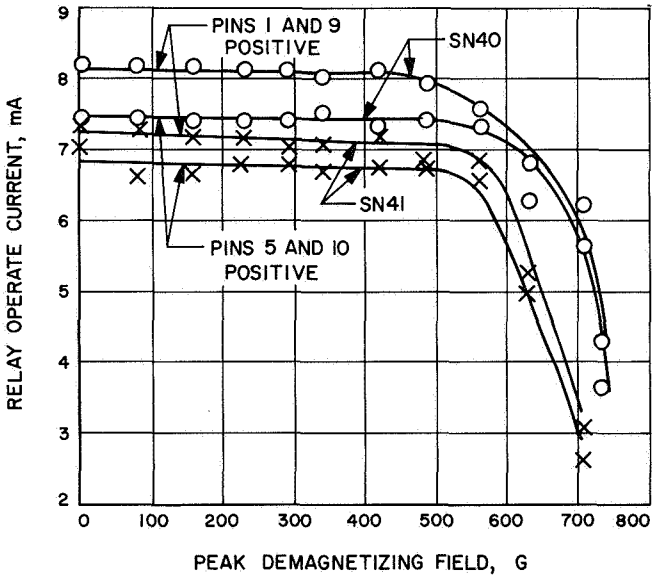

Fig. 106. Latching relay trip current test

(2) The test techniques and facilities were designed for demagnetization of the *Mariner* Mars 1964 panels parallel to the long panel axis (axis of buses). Reorientation of the Kovar buses (orthogonal to the *Mariner* Mars 1964 design) required major changes in the techniques and facilities.

(3) *Mariner* Mars 1964 panels were successfully demagnetized at 60 Hz. With the *Mariner* Venus 67 electronic subassemblies being demagnetized at 1/20 Hz, it would be necessary to change the facility from 60 to 1/20 Hz and back again.

To possibly minimize time and effort required – and yet adequately demagnetize *Mariner* Venus 67 solar panels – this special study was conducted in September 1966 on a solar panel substrate and a small section of a panel (1) to determine if such a small section could be demagnetized with a field perpendicular to the long axis of the Kovar bus bars and (2) to provide a comparison of 60-Hz and 1/20-Hz demagnetization.

a. Requirements vs tests. Tests were performed on a 10- × 12-in. section of solar panel substrates, but because of a limitation in the demagnetizing field level, the solar panel section could not be effectively demagnetized with the Kovar bus bars perpendicular to the demagnetizing field.

b. Results. These tests disclosed that while a demagnetizing field of about 20 G (peak) parallel to the Kovar bus bars would effectively demagnetize the Kovar, demagnetization normal to the bus bars was impracticable. As a result, modification of the demagnetizing facility was necessary so that the *Mariner* Venus 67 solar panels could be accommodated with the Kovar bus bars parallel to the demagnetizing field.

It was also found that 60-Hz demagnetization is slightly more effective than 1/20-Hz demagnetization. The results are shown in Fig. 107.

c. Follow-up test. While theoretical considerations indicate that demagnetization should be more effective in the long axis, the reason for more effective demagnetization at the higher frequency is not known. These later results have also been supported by tests at Goddard Space Flight Center where they found that 60-Hz demagnetization was more effective than so-called *dc pulse* demagnetization. It appears that further study is warranted in this area.

3. Canopus sensor relocation study. Because the *Mariner* Venus 67 spacecraft was oriented with the bottom of the spacecraft facing the sun, it was considered necessary to relocate the Canopus sensor from the bottom to the top of the bus structure. Since the sensor is sensitive to changing magnetic fields, a magnetic survey was made of the area of the *Mariner* Mars 1964 PTM spacecraft in which it was proposed to relocate the Canopus sensor for the *Mariner* Venus spacecraft.

Contrary to all other magnetic control effort on the spacecraft, which has as its goal the reduction and stabilization of the spacecraft magnetic field as an aid to

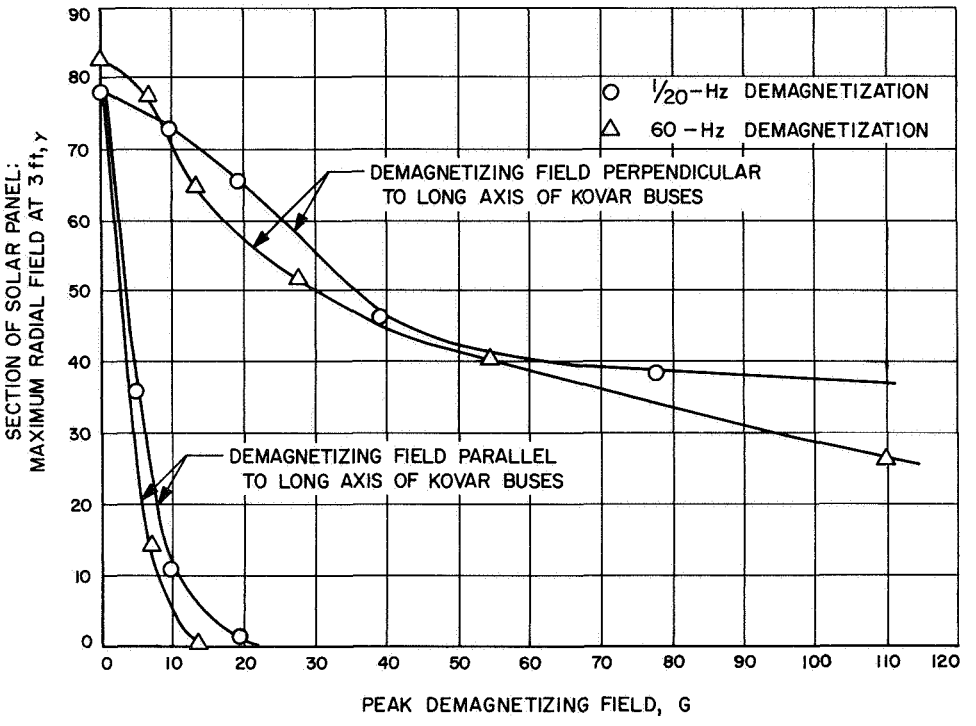

Fig. 107. Solar panel demagnetization tests

the magnetometer experiment, this study was to determine if there were magnetic fields caused by the spacecraft that would be detrimental to the proper performance of the Canopus sensor. Tests were conducted to determine the level of the magnetic field caused by operation of the *Mariner* spacecraft in the vicinity of the top of bay VIII.

a. Requirements vs tests. Tests of magnetic fields resulting from spacecraft operation were made on the face of and above bay VIII from dc through 30 kHz. Perm and induced fields caused by the earth's field were not determined. Fields $<1000\ \gamma$ were not considered detrimental to Canopus sensor operation and were not further investigated.

b. Results. On March 1, 1966, measurements were made on the *Mariner* Mars 1964 PTM spacecraft in the area above bay VIII to determine the magnetic fields caused by an energized spacecraft. Measurements were made with a Foerster Hoover model 5050 magnetometer from dc through about 80 Hz (utilizing an oscilloscope for ac indication) and with a Bell model 350 gaussmeter with magnaprobe from 9 Hz to 30 kHz.

No detrimental ac fields were observed in the vicinity of bay VIII.

The only fields $>1000\ \gamma$ in the vicinity of the proposed relocation site, were observed directly on the frame, immediately above the center of bay VIII, where the field was about $3000\ \gamma$. Approximately 3 in. above this point on the frame, the field had decreased to $1000\ \gamma$.

On the face of bay VIII, the field reached approximately $20{,}000\ \gamma$ about 5 in. from the upper edge. This was considered to result from an unshielded Kinetics power-transfer switch mounted in this bay. At the top edge of the bay, the field was down to $8000\ \gamma$.

In spite of these large fields, since the flight Kinetics switch is shielded, these fields were not considered detrimental to the proper operation of the Canopus sensor.

D. Flight-Acceptance (FA) Testing

Flight acceptance magnetic testing is considered to encompass those tests that were officially documented or directed by the *Mariner* Venus 67 Project Office. These tests were primarily governed by three test documents: (1) a JPL procedure on spacecraft subassembly demagnetization and magnetic mapping, (2) a JPL specification on Type-Approval Magnetic Test Requirements for assembly and subassembly levels, and (3) a JPL specification on the general requirements for magnetic

testing and demagnetization of type-approval and flight-acceptance solar panels.

Required tests associated with the *Agena* vehicle, spacecraft adapter, and shroud are defined in a Project Office document and letters. The remaining tests and the safety review were established by interoffice memorandums from the Project Office.

1. System level. In magnetics control, the distinction between system and subsystem level testing is not clearly defined. Generally, the flight-hardware demagnetization and mapping was conducted as a system procedure in the SAF. In this report, all efforts conducted on an assembly or subassembly basis are considered as on the subsystem level.

a. Spacecraft perm field mapping for M67-1. Each of the two flight spacecraft, M67-1 and M67-2, was magnetically mapped to determine the spacecraft residual field at the science magnetometer sensor at JPL, under the cognizance of the magnetometer experiment cognizant scientist, as an aid to interpreting the magnetometer data. The first flight spacecraft, M67-1, was mapped twice – the first time, immediately following demagnetization of its hardware, and the second time, approximately a month and a half later. A comparison of the two mappings was to have verified the magnetic stability of the demagnetized spacecraft to qualify the omission of an additional magnetic mapping at Cape Kennedy just before launch. The M67-2 flight spacecraft was magnetically mapped only once, on April 13, 1967, at Pasadena. (Figure 108 shows the spacecraft mapping fixture.)

(1) *Requirements vs tests.* Tests were conducted to determine the residual magnetic field at the location of the spacecraft magnetometer sensor with the spacecraft in as near flight configuration as practical and to verify the stability of the spacecraft magnetic field by a second mapping after an interval of one or two months. The spacecraft was magnetically mapped in the earth's field on the evenings of February 15, 1967, and March 31, 1967. In both cases, the spacecraft was approximately similarly configured with the following items not installed on the spacecraft either time:

Tape recorder subassemblies	16A1–16A6
Gyro subassembly	7A2
Solar panels	4A1, 3, 5, 7
DFR antennas	15E3, 15E2F1, 15E2F3
Low-gain antenna	2E2
Thermal shields and shades	

During the interval between the two mappings, the spacecraft underwent system testing and a gas-leak check. The following assemblies and subassemblies were removed from the spacecraft and taken from the SAF to be reworked during this period.

Subassembly 4A18 in bay I was removed for rework.

The midcourse motor was removed from SAF for rework, and torque check of jet-vane actuators was performed in high bay.

Bay III was disassembled, and all subassemblies were removed from SAF for rework.

Bay IV data encoder and command subassemblies were removed from SAF for rework.

Bay V tape recorder subassemblies were not demagnetized or installed in spacecraft during first spacecraft mapping; Bay V radio was reworked in SAF with undemagnetized tools.

Bay VI was reworked in SAF with undemagnetized tools, except 2RE1, 2PS2, and 2PS3 subassemblies, which were removed from SAF for rework.

The 7A1 subassembly was removed from SAF for rework.

All louvers were removed from SAF for polishing.

The trapped radiation detector was sent to University of Iowa.

The ultraviolet photometer was sent to University of Colorado.

The magnetometer was removed from SAF for rework.

Canopus sensor SN 001 was installed for first spacecraft mapping while SN 107 was installed for second mapping.

The high-gain antenna was removed from SAF for rework.

Magnetic control was not adequate, and hardware was reinstalled on the spacecraft without undergoing required magnetic mapping or redemagnetizing. Consequently, the results of the two mappings are not directly comparable.

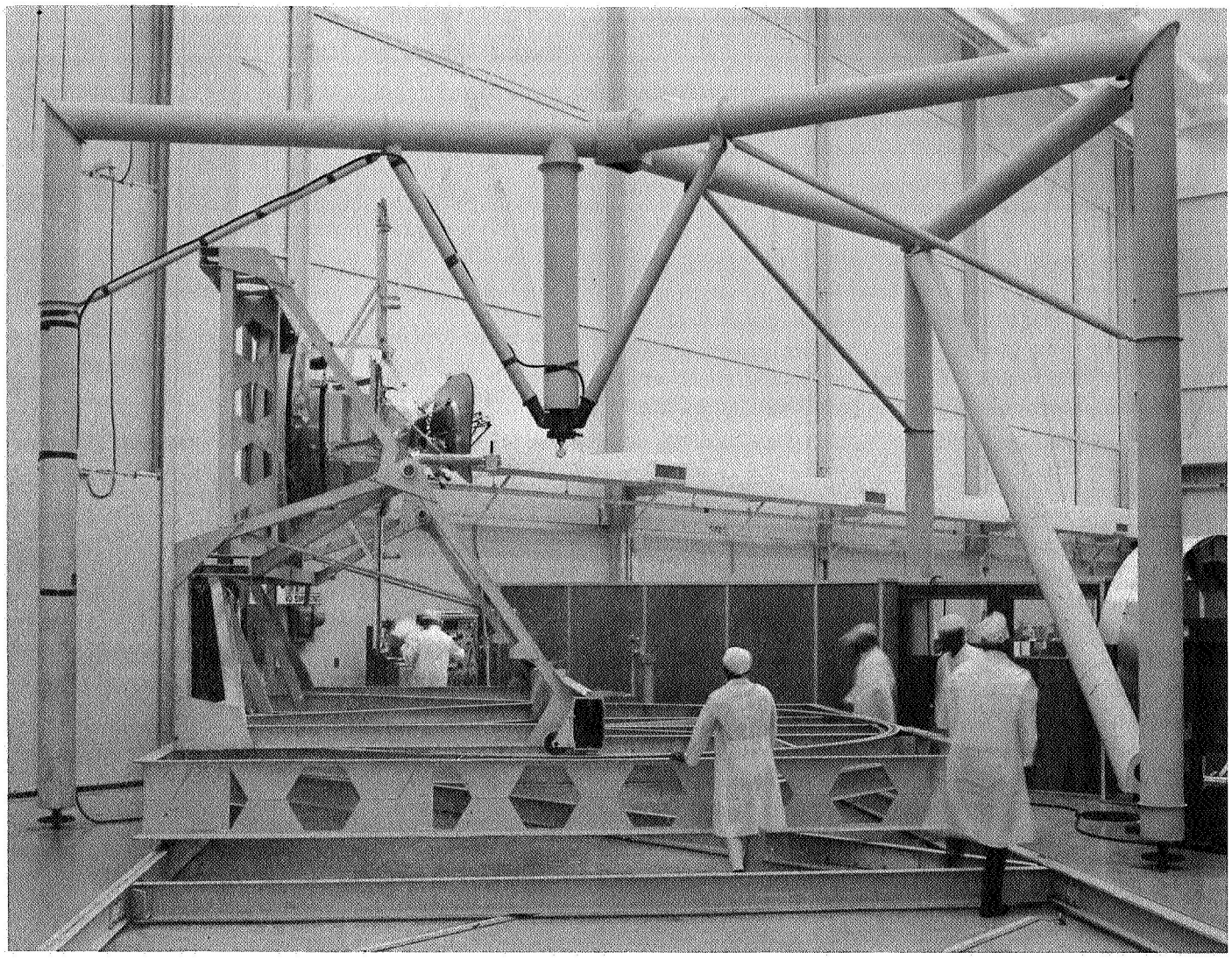

Fig. 108. Spacecraft mapping fixture: mapping in earth's field

(2) *Results.* The magnetic field components shown in Table 53 were determined for the perm field at the spacecraft magnetometer position on each of the two mappings.

Table 53. M67-1 perm field mappings

Mapping date	Value for component of spacecraft field at spacecraft magnetometer position, γ		
	P_x	P_y	P_z
February 15, 1967	1.5	3.9	3.1
March 31, 1967	−1.0	3.3	6.9

b. M67-2 spacecraft perm field mapping.

(1) *Requirements vs tests.* The M67-2 spacecraft was magnetically mapped without solar panels or their fittings, but with the attitude-control gas system mounted on extended solar panel frames. The high-gain antenna (2E1) which had earlier been found to be nonmagnetic, was not installed. The receiver T-R (2TR1), which was being modified, was not installed in bay V. As with the M67-1 spacecraft, the low-gain antenna and thermal shields and shades were not installed on the spacecraft. For this mapping, the gyro unit (7A2) and the tape recorder units (16A1–16) were installed, necessitating increased care in handling the spacecraft and mapping fixture to avoid excessive accelerations on these units.

(2) *Results.* The M67-2 flight spacecraft was magnetically mapped in the earth's field in the early morning of April 13, 1967 to determine the residual magnetic field at the location of the spacecraft magnetometer sensor, with the spacecraft in as near flight configuration as practical. Ambient magnetic conditions were relatively quiet for this mapping, and good results were obtained, in spite of the necessary cautious move of the fixture.

The following gamma values for the components of the residual magnetic field of the spacecraft at the science magnetometer position were obtained:

P_x	P_y	P_z
$-1.0\ \gamma$	$2.6\ \gamma$	$7.1\ \gamma$

This spacecraft was successfully launched from Cape Kennedy on June 14, 1967. While the spacecraft was rolling in space following sun acquisition, it was possible to determine the X and Y components of the residual field of the spacecraft. These values are compared with the components of the total field for the spacecraft including all perm and current-loop fields for the particular operating condition of the spacecraft. It was also subsequently possible to statistically obtain a value for the Z component of the residual field. This comparison is made in Table 54.

The differences between these values cannot be definitely explained, but they are probably due to two main causes: (1) Several subassemblies were removed from the spacecraft for rework following the spacecraft mapping, with a consequent change in the subassembly field; even though in some cases, the subassembly was redemagnetized. (2) Some subassemblies exhibit sufficient magnetic instability as to be affected by the launch environment.

c. Spacecraft current-loop-field mapping. The determination of the spacecraft current-loop fields was under the direction of the magnetometer experiment cognizant scientist. The current-loop fields (also commonly called *stray fields*) are those magnetic fields caused by the flow of current in the spacecraft circuitry during various modes of operation and the change in field resulting from the actuation of magnetic mechanical devices. The tests were conducted to determine the spacecraft magnetic field contribution due to operation of the spacecraft in its several operational modes in order to permit analysis of the inflight magnetometer data. Although the two spacecraft were checked for current-loop fields, minor differences and test conditions necessitated using a weighted average of the two results.

Table 54. M67-2 residual field

Computation	Residual field component value, γ		
	X	Y	Z
Preflight estimate of spacecraft field	−0.6	1.0	7.1
Inflight spacecraft field determination	4.8	0.8	8.7

(1) *Requirements vs tests.* The current-loop tests were conducted in accordance with the JPL procedure during the late evening hours when external magnetic disturbances were at a minimum. Changes in the magnetic field were monitored during spacecraft system tests. Those changes resulting in a measurable effect are listed in the following paragraphs.

(2) *Results.* Results were obtained for the four normal operational modes. The values shown are for the magnetic field components in spacecraft coordinates at the spacecraft magnetometer sensor, in gamma values, and do not include solar panel current-loop fields.

	X, γ	Y, γ	Z, γ
Pre-Canopus acquisition (solar power)	−3.0	−0.7	+0.4
Cruise mode (solar power, gyros *off*)	−1.6	−1.4	+1.8
After switch to TWT amplifier	−1.1	−0.9	+2.2
Encounter mode	−0.6	−0.9	+1.9

The following are the current loop field changes associated with the operation of the various subsystems that yielded measurable effects.

	$\Delta X, \gamma$	$\Delta Y, \gamma$	$\Delta Z, \gamma$
Switch from solar to battery power	−1.2	+1.6	+1.6
Switch from cavity to TWT amplifier	+0.5	+0.3	+0.3
Switch from exciter A to B	+0.4	+0.7	+0.4
Switch battery charger to boost mode	−0.4	0	−0.3
Turn gyros *on*	−1.4	+0.7	−1.4

d. Summation of spacecraft fields for M67-1. As an aid to future magnetic control programs, it was desired to determine the relationship between the summations of the magnetic fields of the individual assemblies or subassemblies and the total magnetic field of the spacecraft at the science magnetometer sensor. To this end, the magnetic field of the *Mariner* Venus 67 spacecraft subassemblies was extrapolated to the position of the magnetometer sensor on the spacecraft, and the spacecraft rectangular components of the field were summed. This resultant field was then compared with the field of the spacecraft as it was actually mapped in its entirety at Pasadena.

The sum of the magnetic fields of the various M67-1 spacecraft assemblies and subassemblies were made and compared with the actual spacecraft magnetic mapping; and the total field of the M67-1 spacecraft was estimated. The components of the total field of the M67-1 spacecraft, as determined by a summation of the subassembly magnetic field measurements as initially obtained, were:

X component	*Y* component	*Z* component
1.7 γ	7.2 γ	2.6 γ

The above values were for the complete spacecraft with the four flight solar panels and all other flight hardware included.

If a summation were to be made of only the hardware that was mounted on the spacecraft at the time it was magnetically mapped on February 15, 1967, the following values would be obtained for the components of the field at the flight sensor.

X component	*Y* component	*Z* component
0.9 γ	7.4 γ	2.2 γ

These values are compared with those obtained in the spacecraft mapping reported earlier in this section, as

X component	*Y* component	*Z* component
1.5 γ	3.9 γ	3.1 γ

Attempts to explain these large differences were not entirely successful. However, it appeared that, when summed, the individual field of several subassemblies would be greater than the mapped values for the subassemblies as a group.

The effect of both angular and magnitude errors in interpreting the bay VII data were analyzed because this assembly is several times more magnetic than any other system on the spacecraft. It was found that the errors in bay VII measurements could not have exceeded 1 γ and, consequently, did not account for the discrepancy between the summed and measured fields.

There were two major problems associated with attempts to sum the magnetic field components:

(1) To be able to extrapolate magnetic field data, it must be assumed that all sources can be represented by a simple dipole. In the case of actual hardware, this is not necessarily true. Although most hardware appeared to be a simple diode at the measurement distance, a few exhibited multipolar characteristics. In general, mapping a field that is distinctly multipolar results in a dipolar field component which is lower than would be expected from a simple dipolar field mapping. This results because the higher order components tend to reduce the net field and fall off more rapidly with distance. Similarly, if the mapping rotation is not about the dipole center, a greater-than-actual field magnitude is obtained.

(2) Subassembly magnetic fields are materially altered by ferromagnetic material in adjacent subassemblies. This apparently has the effect of shunting the subassembly field through the magnetic material so that the external fields of the assembly are reduced.

The M67-1 spacecraft, which was mapped twice – the second time after an interval of about six weeks – should have shown very little change in the magnetic field components. The fact that there was a rather large change resulted in a remapping of the assemblies that had been removed from SAF for rework and had not been rechecked subsequently for magnetic changes. The spacecraft fields were again summed in an effort to explain the difference in the two spacecraft mappings. While the new summed field did show changes in the proper direction, still the magnitudes of the Y and Z components differed by some 3 γ each.

The final value for the summed field changed as hardware was removed from the spacecraft for rework and was remapped on reintroduction into SAF for reinstallation on the spacecraft. The components of this final

summed field of the spacecraft as it was shipped to AFETR, not including solar panels, are the following:

X component	Y component	Z component
−1.4 γ	6.9 γ	3.2 γ

It appeared that the direct summation of magnetic fields or the consideration of the effect of a change in field of a subassembly on the overall spacecraft field was not an entirely valid procedure. It was believed, however, that this procedure was of use in setting upper limits on subassemblies and in establishing magnetic restraints on hardware.

e. Summation of spacecraft fields for M67-2. The sum of the components of the magnetic fields of the various spacecraft assemblies and subassemblies was made to obtain an estimate of the total field of the M67-2 spacecraft and to compare these results with the measured magnetic field of the spacecraft.

The components of the total field of the M67-2 spacecraft, as estimated from the subassembly magnetic field measurements initially obtained between April 6 and 12, 1967, were:

X component	Y component	Z component
−1.5 γ	+2.7 γ	+5.9 γ

The above values are for the complete spacecraft, including the solar panels and attached antennas and boost dampers.

If only those items of hardware that were on the spacecraft as it was mapped on April 13, 1967 are considered, the summed field components are:

X component	Y component	Z component
−1.3 γ	+2.5 γ	+5.7 γ

These values compare very well with those for the mapped field of the spacecraft which are given below:

X component	Y component	Z component
−1.0 γ	+2.6 γ	+7.1 γ

In view of the results of M67-1, these results are not considered conclusive. In fact, it is now believed that only a very general comparison can be made. It appears that, in general, the field of several assembled units will be less than the sum of the individually mapped subassemblies. This latter is supported by comparison of measurements made on completely assembled bays III and V and the summed fields of the equivalent individual subassemblies and subsystems making up these bays.

f. Exposure recorders. During November 1966, it was learned that the Ames Research Center was working on the development of a magnetic-field exposure recording device for use in connection with the *Apollo* Program. As it was felt that this device might be of some value to magnetic control in the *Mariner* Venus 67 Program, its use was recommended, and was approved by the Project Office. Two of these devices – that consisted of three 2- × 0.005-in.-diam dumet wires, imbedded in three nylon blocks such that, when the three blocks are fastened together, the three wires are normal to each other – were furnished by E. A. Iufer of Ames Research Center for use on *Mariner* Venus 67 flight spacecraft.

One of these devices was installed on each of the two flight spacecraft after reassembly of the spacecraft, following final inspection and demagnetization. These devices were installed inside the spacecraft bus structure on the support structure for the attitude control gas system, as shown in Fig. 109.

The magnetic field exposure recorder was used to determine if any excessive magnetic field was encountered by the spacecraft following demagnetization, until the time the spacecraft was enclosed in its shroud, prior to launch. In particular, it was desired to know if the spacecraft were exposed to excessive fields incident to shipment to Cape Kennedy from Pasadena.

The use of the exposure recorder on both spacecraft resulted in essentially negative results. Exposure of the recorder to a magnetic field above the threshold level of the recorder was observed at no time.

The calibration curves for each of the *Mariner* Venus 67 recorders are shown in Fig. 110. It was estimated that the recorder – as utilized – would not detect changes in the exposure field below about 2.7 G. In addition, it was possible that the recorder memory could be altered by subsequent exposures and conceivably be demagnetized by a proper sequence of exposures. Consequently, the above results are not necessarily conclusive.

Table 55 contains a summary history of each of the two exposure recorders installed on the *Mariner* Venus 67 spacecraft.

To make this device more useful for the purpose, its sensitivity must be increased by mapping at a shorter

Fig. 109. Magnetic exposure recorder installed inside spacecraft bus structure

Table 55. Exposure recorder histories

Event	M67-1 exposure recorder	M67-2 exposure recorder
Recorder calibrated	Feb. 16, 1967	April 14, 1967
Recorder first installed on spacecraft	Feb. 16, 1967	April 14, 1967
First monitoring of recorder at JPL	March 3, 1967	—
Second monitoring of recorder at JPL	March 24, 1967	—
Monitoring of recorder prior to shipment of spacecraft to AFETR	April 17, 1967	—
Initial monitoring of recorder at AFETR	April 28, 1967	May 2, 1967
Final monitoring of recorder at AFETR and removal from spacecraft	June 8, 1967	May 25, 1967

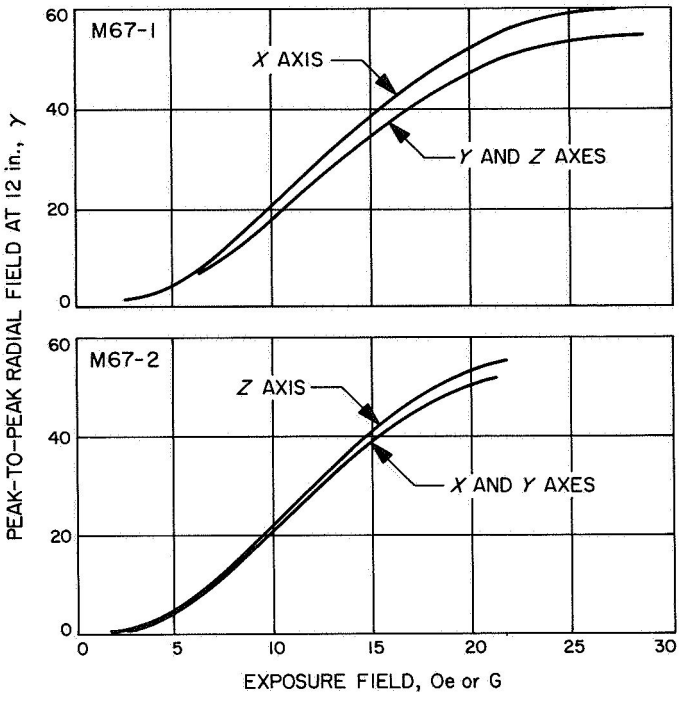

Fig. 110. Exposure recorder calibration curves

distance (possibly 6 in.) and/or using a softer magnetic material. Some of these areas have been explored by Ames, and several different materials to eliminate the possibility of loss of memory by the device have been investigated.

With just a single device on the spacecraft, the recorder can be expected to indicate only ambient field changes or the presence of concentrated fields in the immediate vicinity of the device.

g. Agena mappings. The magnetic requirements necessitated knowledge of the magnetic fields of matchmate tools and equipment and of the *Agena* adapter forward of the *Agena* station 247. In addition, demagnetization of these items was required under certain circumstances. As the Lockheed Missile and Space Company did not have adequate facilities for making these measurements or performing the necessary demagnetization, Lewis Research Center requested that JPL perform the operations for Lockheed. In addition, JPL was given the opportunity to perform a magnetic survey of the *Agena* forward equipment rack during the operation of the *Agena* subsystems.

On February 23, 1967, a magnetic survey was made of the *Agena* forward equipment rack at Lockheed, Sunnyvale, California. Approximately 35 Lockheed

V-band tools at JPL were checked on February 15, 1967, and 7 (that exceeded 5 G on the surface) were demagnetized to reduce the field below this level. On March 2, 1967, the *Agena* adapter and spacecraft shroud were checked for magnetic fields. The adapter spacecraft ejection springs were rechecked and demagnetized at AFETR on May 23, 1967.

(1) *Magnetic survey of Agena forward equipment rack.* A study was made to determine if the *Agena* vehicle had magnetic fields in the vicinity of the spacecraft adapter that might cause magnetic contamination of the spacecraft. In the *Agena* forward equipment rack there were three items that had a measurable field above the ambient level on the surface of the component:

FM telemetry unit	20 G
Power-distribution box	10 G
C-band-beacon adapter kit	8 G

These fields were very concentrated and did not extend beyond *Agena* station 247. The ac magnetic fields and dc magnetic fields due to operating modes of the *Agena* were minimal.

(2) *Magnetic control on spacecraft adapter and shroud.* Work was undertaken to locate sources of magnetic fields on the spacecraft adapter and shroud and demagnetize those items causing an excessive field which are within 6 inches of the spacecraft.

Interface hardware originally was required to be demagnetized if its field were >1 G within 6 in. of the spacecraft. Tests indicated that this requirement was too restrictive because (1) earth's induced field effects may be as large as 3 G, and (2) tests on a nickel-ribbon-connected module indicate that a field >5 G was necessary to cause a measurable perm in the module. Consequently, the requirements were revised to reflect the 5-G limit, in place of 1 G.

The following items on the spacecraft adapter and shroud were found to be magnetic and exceeded 5 G on the surface of the item:

(1) Approximately one-third of the bolts securing the adapter ring to the GSE ring (*Agena* station 247) exceeded 5 G.

(2) One of four spacecraft separation pistons had a field across the stem of the piston of 9 G.

(3) The large screw drive in the shroud spring cocking device exceeded 10 G and some of the screws holding the cocking devices to the shroud exceeded 5 G.

(4) The two pins in some shroud harness buckles exceeded 10 G.

Only the pushoff piston of item 2 was within 6 in. of the spacecraft and required demagnetization. These pistons were rechecked at AFETR. Two pistons on one shroud and one on another required demagnetization. The screws, item (1) above, were reported by a Lockheed engineer to be replaced by nonmagnetic screws when the adapter is secured to the *Agena* vehicle; however, this was not verified.

(3) *Lockheed matchmate tool control.* Any tools used near the spacecraft and not under direct JPL control are monitored and demagnetized as required to prevent spacecraft magnetic contamination. Initially, demagnetization of tools with fields >1 G was required. This requirement was modified to be consistent with the JPL tool requirement calling for demagnetization if the field exceeds 5 G.

All tools used by Lockheed in matchmate of the spacecraft and adapter were monitored at the Explosive Safe Facility at AFETR on May 25, 1967, immediately prior to matchmate. Approximately 25% of the tools required demagnetization to reduce their residual field to an acceptable level.

h. Spacecraft assembly tools. Steps were taken to ensure no magnetized tools being used on the flight spacecraft after demagnetization of the flight hardware unless the hardware was rechecked for a change in its magnetic field.

All tools used on the spacecraft in the spacecraft assembly area were examined for a magnetic field. This included two complete roll-away cabinets (designated G-5080 and G-5266) with a separate Kennedy tool box mounted on top of each. The tool boxes were initially checked between January 19 and February 16, 1967, with the results tabulated in Table 56.

Each tool box was rechecked between April 14 and 17, 1967. Box G-5060 had 52 tools requiring redemagnetization; box G-5266 had 27 tools requiring redemagnetization. These boxes were again checked at AFETR on

Table 56. Assembly tool magnetic monitoring results

Measurement	Spacecraft tool box	
	G-5080 (Approx. 1000 tools)	G-5266 (Approx. 800 tools)
Number of tools with field ≥5 G	370	326
Number of tools with field ≥20 G	89	73
Number of tools with field ≥100 G	8	3

May 5, 1967, and about six tools in each box required redemagnetization.

In addition to the two sets of tools regularly used in SAF, special division tools used on the attitude-control gas system and on the propulsion system were also checked. This was, approximately, an additional 500 tools.

During the initial survey, it was found that approximately one-third of the tools required demagnetization. No particular tool was found to be more susceptible; however, of the tools that were magnetic, the long thin tools had the higher fields. Although it had been expected that the tools would generally perm in the long axis, many wrenches were found with the field across the open jaws, and sockets were permed across the diameter of the socket.

2. Subsystem level testing and demagnetization. The major magnetic control effort on the *Mariner* Venus 67 spacecraft was on the subsystem level. As a result of tests on the *Mariner* Mars 1964 PTM spacecraft, it was believed that the most effective demagnetization could be accomplished on the assembly and subassembly level, where the ambient field could be more effectively reduced. As a consequence, procedures were established for demagnetizing the spacecraft hardware and determining the effectiveness of the demagnetization.

A facility was erected at JPL for accomplishing the required mapping, magnetization, and demagnetization, as shown in Fig. 111. A similar, but smaller, facility, capable of FA demagnetization, only, was erected at AFETR, Cape Kennedy, as shown in Fig. 112.

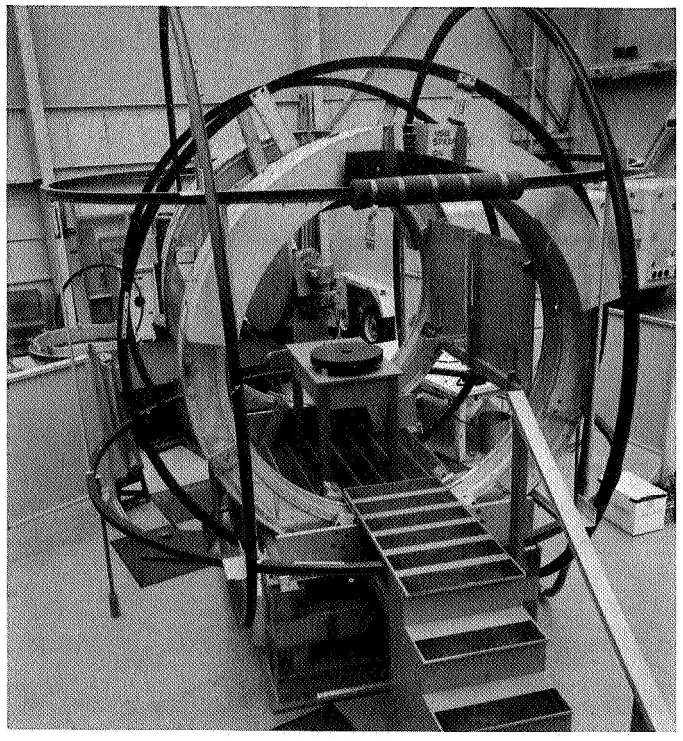

Fig. 111. Demagnetization and mapping fixture used at JPL

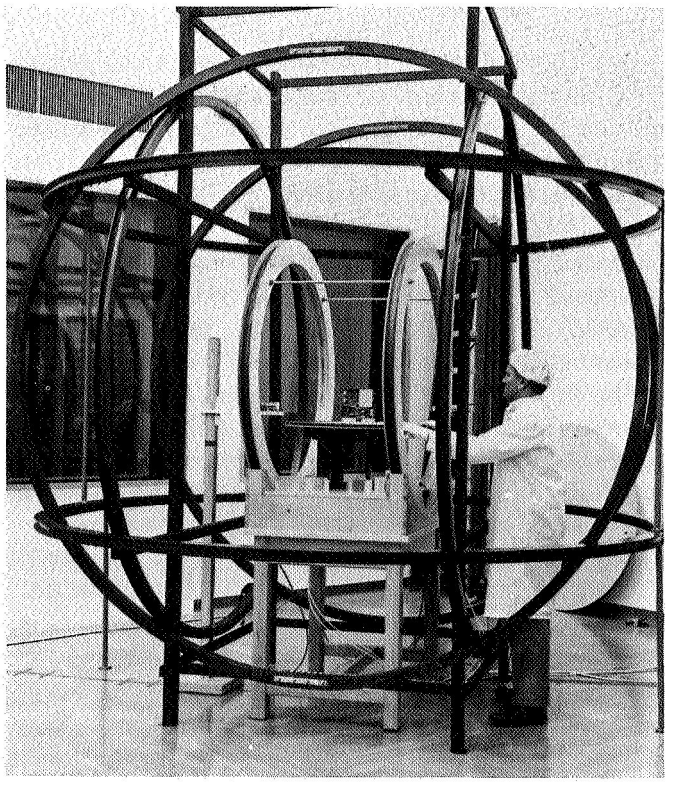

Fig. 112. Magnetic mapping and demagnetization facility at AFETR

The demagnetization and subsequent mapping of flight hardware was performed to erase the residual magnetization acquired by the hardware during vibration testing and to verify that the demagnetization was effective by comparing these results and the TA mapping results, following a similar demagnetization. It was also believed that the demagnetized state of the hardware would be more stable than the partially magnetized state acquired due to the vibration testing.

Flight hardware testing and demagnetization accomplished as part of the final disassembly and inspection of the spacecraft were performed in accordance with the JPL procedure. As a means of comparing the values obtained in each of the mappings of flight hardware, Table 57 has been prepared to show the maximum radial magnetic field component at a standard distance of 3 ft (this was the distance at which all *Mariner C* hardware magnetic fields were determined), and the three components of the magnetic field at the relative position of the science magnetometer.

a. M67-1 subsystem testing. The M67-1 assemblies and subassemblies were demagnetized to reduce and stabilize the residual magnetic field. They were mapped to verify the effectiveness of the demagnetization and to provide a reference value for possible future requalification or redemagnetization.

Requirements vs tests. All items of spacecraft hardware were demagnetized in accordance with the JPL procedure, with the exception of items that were obviously nonmagnetic; they are identified in Table 58. Solar panels were individually mapped and found not to require demagnetization. The Canopus sensor, which suffered an alignment error of ½ deg when demagnetized, was granted a waiver on the demagnetization requirement.

Results. Table 58 gives the results of the magnetic mapping and subsequent remapping of M67-1 hardware. The following items of hardware were checked for a magnetic field by passing them within a few inches of the magnetometer sensor and were found to be nonmagnetic:

(1) Solar panel pyro harnesses, 9W38, SNs V113, V114, V115, 11V6

(2) Low-gain antenna dampers, SN C101

(3) Solar panel cruise dampers, SNs C119, C121, C122

(4) Cable harness, 9W6, SN V101

(5) Cable harness, 9W3, SN V101

(6) Cable, 2W46, SN 01

b. M67-2 subsystem testing. Work was accomplished to demagnetize the assemblies and subassemblies, to reduce and stabilize the residual magnetic field, to verify the effectiveness of the demagnetization based on similar earlier results on M67-1 hardware and, after initial demagnetization, to maintain integrity of the magnetic quality.

Requirements vs tests. All items of flight hardware were demagnetized in accordance with the JPL procedure, and subsequent control was maintained. A waiver on demagnetization was granted the Canopus sensor because demagnetization caused alignment errors.

Results. The results of the magnetic mapping of M67-2 flight hardware are shown in Table 59. The following items were checked by passing them within a few inches of the magnetometer sensor and found to be nonmagnetic.

(1) Solar panel pyro harnesses, 9W38, SNs V117, V118, V119, V120

(2) Solar panel cruise dampers, SNs C115, C118

(3) Low-gain antenna dampers, SNs C103, C111, respectively

(4) DFR UHF antenna, 15E3, SN5

(5) Coaxial cable, 2W46, SN 02

In demagnetizing the 2W2, 2W45, and 2W47 cables with a tape demagnetizer in the earth's field, it was found that they became more magnetic. It was impossible to demagnetize them in the earth's field. When they were demagnetized with the tape demagnetizer in the earth's field bucking coil system, they readily demagnetized.

c. Solar panel perm fields.

Requirements vs tests. Tests on the flight solar panels were conducted in accordance with the JPL procedure to ensure that the residual perm field of the flight solar panels are less than 1 γ at the flight magnetometer sensor. Because of the low residual field in all of the flight solar panels, it was unnecessary to demagnetize the panels.

Table 57. Comparison of assembly and subassembly mapping results

Hardware nomenclature	M67-1 mapping results (2/13/67), γ				M67-1 mapping results (4/3/67), γ				M67-2 mapping results (4/12/67), γ			
	Maximum radial field @ 3 ft	Field at magnetometer sensor			Maximum radial field @ 3 ft	Field at magnetometer sensor			Maximum radial field @ 3 ft	Field at magnetometer sensor		
		B_x	B_y	B_z		B_x	B_y	B_z		B_x	B_y	B_z
Bay I Power	15.8	−0.72	−0.54	−0.33	16.2	−0.91	−0.42	−0.31	14.4	−0.86	−0.44	−0.22
8A1/2 Pyro control	11.5	−0.72	0	−0.48					10.4	−1.07	0.09	−0.07
8A1/2 Pyro control	10.7	1.01	0.18	0.09					10.9	0.28	0.34	0.59
Bay II PIPS	21.4	−0.98	−0.98	1.48	28.8	−1.65	−0.95	1.97	18.2	−0.88	−1.63	0.28
Bay III subassemblies					4.3	−0.19	0.09	0.20	0.6	0.01	0.02	0.02
20A1-9 DAS	1.2	−0.01	−0.05	0.07					1.4	0.04	−0.08	0.07
32A2 (Plasma probe)	0.9	−0.08	0.01	0.01					0.3	0	0.02	−0.01
32A3 (Plasma probe)	0.2	0	−0.01	0.01					0.4	0	0.03	−0.01
32A4 (Plasma probe)	0.4	−0.01	−0.02	0.02					0.1	0	0	0
33A2 (Magnetometer)	0.3	−0.01	−0.01	0.03					0.6	−0.02	0.06	0.03
33A3 (Magnetometer)	1.1	−0.04	−0.06	0.08					0.6	0.04	−0.06	0.03
34A2 UV photometer	0.3	0.01	−0.03	0.01					0.4	−0.03	0.01	0.02
35A1/2 DFR	0.5	0.01	0.03	0.01					0.4	0.01	−0.01	−0.01
DFR filters	4.9	0.67	−0.04	−0.09					1.0	0.11	−0.07	0.03
Bay IV data encoder and command	16.0	1.43	0.33	−0.58	15.1	1.44	0.04	−0.43	11.7	1.29	0.42	−0.08
Bay V radio	4.0	0.47	0.09	0.05								
Radio tape	16.2	−1.76	−0.70	−0.40	19.6	−2.23	−0.99	0.02	24.3	−2.84	−1.69	−0.54
Bay VI transponder	14.5	−0.96	0.69	0.76	14.6	−1.18	0.64	0.68	22.0	0.56	−2.41	0.66
Bay VII CC&S	78.9	−0.05	9.71	2.57	85.8	0.84	10.50	2.78	86.4	1.50	10.41	2.93
7A2 gyro	1.1	−0.03	0.08	0.06	0.8	−0.05	−0.06	0.01	0.9	−0.05	0.04	0.04
Bay VIII (4A8) power regulator	3.0	0.22	−0.10	0.19					3.8	0.22	−0.33	−0.16
4A14 battery	0	0	0	0					0	0	0	0
7CS8 Canopus sensor	23.7	0.96	−2.15	−2.71	21.0	1.52	−2.38	−2.31	14.3	1.58	−1.59	−1.44
25A1 TRD	0.4	0.03	−0.03	0.04					0.3	0.04	0	0.02
32A1 Plasma probe	0.3	−0.02	−0.01	0.01					0	0	0	0
34A1 UV photometer	0.5	0	−0.06	0.03					0.3	0	0.02	0.01
Spacecraft bus with gas system	—	−0.23	0.56	1.16					—	0.38	0.13	3.63
Louver Bay I	0.3	0	0.01	0.01					0.4	0	0.01	0.02
Bay III	0.5	0.04	−0.01	0.02					0.5	0.01	−0.01	0.03
Bay V	0.6	0.04	0.07	0					0.5	0.02	0.03	0.03
Bay VI	0.4	−0.05	0	−0.01					0.4	0.01	−0.02	−0.02
Bay VII	0.1	0.01	0.01	0.01					0.2	−0.02	−0.01	−0.01
Bay VIII	0.3	−0.02	−0.01	0.02					0.3	0.01	0.02	0.02

Table 58. M67-1 assembly and subassembly mappings

Hardware	Serial No.	Maximum radial field at 3 ft, γ	Component of magnetic field at spacecraft science magnetometer, γ		
			X	Y	Z
Bay I, 4A11-4A18	V16	15.8	−0.72	−0.54	−0.33
	V16[a]	16.2	−0.86	−0.54	−0.30
	V16[b]	16.2	−0.91	−0.42	−0.31
8A1/2, Pyro control	1009	11.5	−0.72	0	−0.48
	1010	10.7	1.01	0.18	0.09
Bay II, PIPS	MC-006	21.4	−0.98	−0.98	1.48
	MC-006[a]	27.0	−1.36	−1.47	1.82
	MC-006[b]	28.8	−1.65	−0.95	1.97
Bay III	[a]	4.3	−0.19	0.09	0.20
20A1-9 DAS	071	1.2	−0.01	−0.05	0.07
32A2 plasma probe electronics	5	0.9	−0.08	0.01	0.01
32A3 plasma probe electronics	5	0.2	0	−0.01	0.01
32A4 plasma probe electronics	6	0.4	−0.01	−0.02	0.02
33A2 magnetometer electronics	0	0.3	−0.01	−0.01	0.03
33A3 magnetometer electronics	1	1.1	−0.04	−0.06	0.08
34A2 UV photometer electronics	4	0.3	0.01	−0.03	0.01
35A1 and 2 DFR	2	0.5	0	−0.03	−0.01
	2[a]	0.5	0.01	−0.03	−0.01
	2[c]	0.5	0	−0.03	−0.01
DFR low-pass filter	A165-1	4.9	0.67	−0.04	−0.09
DFR high-pass filter	A251-4	0.3	0.02	−0.03	0.01
Bay IV, data encoder and command	201/V5/V6	16.0	1.43	0.33	−0.58
	201/V5/V6[a]	15.1	1.44	0.04	−0.43
Bay V, radio and tape recorder	Sys 7/8[a]	36.2	−4.55	−0.43	−0.73
	Sys 7/8[b]	19.6	−2.23	−0.99	0.02
Bay V, radio system only	V7/V5[d]	4.0	0.47	0.09	0.05
Bay VI, *transponder*	Sys 7[e]	14.5	−0.96	0.69	0.76
	Sys 7[a, e]	14.6	−1.18	0.64	0.68
Bay VII, CC&S	006/004/005	78.9	−0.05	9.71	2.57
	006/004/005[a]	83.4	1.49	9.56	2.94
	006/004/005[b]	85.8	0.84	10.50	2.78

[a]Remapped approximately 7 wk after initial deperm and mapping due to change in mapped field of spacecraft.

[b]Redemagnetized and remapped due to excessive change in field as a result of rework of hardware.

[c]Hardware remapped at AFETR due to rework.

[d]Initial mapping and demagnetization of Bay V did not include tape recorder subsystem.

[e]Mapping displays multipole characteristic.

Table 58 (contd)

Hardware	Serial No.	Maximum radial field at 3 ft, γ	Component of magnetic field at spacecraft science magnetometer, γ		
			X	Y	Z
7A2 gyro	013	1.1	−0.03	0.08	0.06
	017	0.8	−0.05	−0.06	0.01
	017[c]	3.3	−0.21	0.26	0.09
	017[b]	0.3	−0.01	−0.01	0.02
Bay VIII, 4A8 power	06	3.0	0.22	−0.10	−0.19
4A14 battery	17	0	0	0	0
7CS8 Canopus sensor	001[f]	23.7	0.96	−2.15	−2.71
	001[c]	18.8	1.01	−1.95	−2.13
	107[a, f]	21.0	1.52	−2.38	−2.31
	107[c, f]	19.8	1.55	−2.19	−2.19
	107[c]	20.3	1.59	−2.24	−2.24
7LS8 planet sensor	002	0.0	0	0	0
	002[c]	0.0	0	0	0
25A1 TRD	MC-1	0.4	0.03	−0.03	0.04
	MC-1[a]	0.3	0	−0.04	0.03
	MC-1[c]	0.4	0	−0.05	0.04
32A1 plasma probe	438	0.3	−0.02	−0.01	0.01
34A1 UV photometer	MC-4[c]	0.5	0	−0.06	0.03
	MC-4[a, e]	0.4	0.01	−0.05	0.02
33A1 magnetometer sensor	0[g]	0.0	0	0	0
Bay I louver	17	0.3	0	0.01	0.01
	17[a]	0.2	−0.02	0	0.01
Bay III louver	18	0.5	0.04	−0.01	0.02
	18[a]	0.9	0.06	−0.01	0.03
Bay V louver	19	0.6	0.04	0.07	0
	19[a]	0.6	0.06	0.01	0.04
Bay VI louver	38	0.4	−0.05	0	−0.01
	20[a]	0.9	−0.10	0.01	0.02
Bay VII louver	20	0.1	0.01	0.02	0.01
	20[a]	0.5	0.01	0.05	−0.01
Bay VIII louver	21	0.3	−0.02	−0.01	0.02
	21[a]	2.9	−0.23	0.16	0
	21[b]	0.7	0.04	−0.01	0.02
8M1 separation-initiated timer	106	0.2	−0.01	0	0

[a]Remapped approximately 7 wk after initial deperm and mapping due to change in mapped field of spacecraft.
[b]Redemagnetized and remapped due to excessive change in field as a result of rework of hardware.
[c]Hardware remapped at AFETR due to rework.
[d]Initial mapping and demagnetization of Bay V did not include tape recorder subsystem.
[e]Mapping displays multipole characteristic.
[f]Mapped only; granted waiver on demagnetization.
[g]Magnetometer sensor demagnetized prior to calibration to eliminate offset in reading.

Table 58 (contd)

Hardware	Serial No.	Maximum radial field at 3 ft, γ	Component of magnetic field at spacecraft science magnetometer, γ		
			X	Y	Z
8AS1 pyro arm switch	110	0.0	0	0	0
Temp control reference bay I	15	0.1	0	0	0
Temp control reference bay V	17	0.1	0	0	0
Temp control reference bay VII	19	0.1	0	0	0
Coax cable 2W2		0.2	−0.02	−0.02	0
Coax cable 2W45		0.3	−0.08	−0.08	−0.01
Tip (boost) damper	C-111[h]	0.3	0	0	0.01
	C-111[a]	0.2	0	0	0
Tip damper	C-112[h]	0.3	0	−0.01	0
	C-112[a]	0.3	0	−0.01	0
Tip damper	C-113[h]	0.3	0.01	0	0
	C-113[a]	0.2	0.01	0	0
Tip damper	C-114[h]	0.1	0	0	0
	C-114[a]	0.1	0	0	0
Tip damper	C-115[h]	0.3	0	−0.01	0
	C-115[a]	0.3	0	−0.01	0
Tip damper	C-116[h]	0.3	0.01	0.01	0
	C-116[a]	0.3	0.01	0.01	0
Tip damper	C-117[h]	0.3	0.01	0	0.01
	C-117[a]	0.4	0.01	0.01	0.01
Tip damper	C-118[h]	0.7	−0.02	0.02	0.02
	C-118[a]	0.7	−0.01	0.02	0.01
15E2F1 DFR antenna					
Metal end		0.2	0	0	0.01
Insulated		0.0	0	0	0
15E2F3 DFR antenna					
Metal end		0.0	0	0	0
Insulated		0.0	0	0	0
Spacecraft structure with sun and earth sensors	[i]		−0.23	0.56	1.16

[a]Remapped approximately 7 wk after initial deperm and mapping due to change in mapped field of spacecraft.

[h]Solar-panel-tip dampers may not necessarily be installed in position for which computations are made. These values should be considered typical only.

[i]Spacecraft structure includes two A/C gas systems, sun gate and sensors, earth sensor, terminator sensor, upper and lower ring harnesses, accelerometer, and high-gain antenna. Structure demagnetized in X and Y axes, only, and mapped in earth's field.

Table 59. M67-2 assembly and subassembly mappings

Hardware	Serial No.	Maximum radial field at 3 ft, γ	Component of magnetic field at spacecraft science magnetometer, γ		
			X	Y	Z
Bay I, 4A11–4A18	V17	14.5	−0.84	−0.55	−0.20
	V17[a]	14.4	−0.86	−0.44	−0.22
8A1/2, pyro control	1013	10.6	−1.16	−0.08	−0.03
	1013[a]	10.4	−1.07	0.09	−0.07
	1014	10.7	0.40	0.17	0.55
	1014[a]	10.9	0.28	0.34	0.59
Bay II, PIPS	M67-2	25.9	−0.86	−2.47	1.26
	M67-2[a]	19.6	−0.27	−2.08	0.43
	M67-2[b]	18.2	−0.88	−1.63	0.28
Bay III	[c]	0.6	0.01	0.02	0.02
20A1-9 DAS	072	1.4	0.04	−0.08	0.07
32A2 plasma probe electronics	6	0.3	0	0.02	−0.01
32A3 plasma probe electronics	6	0.4	0	0.03	−0.01
32A4 plasma probe electronics	7	0.1	0	0	0
33A2 magnetometer electronics	5	0.6	−0.02	0.06	−0.04
	5[d]	0.7	−0.05	0.08	−0.03
	5[b]	0.6	−0.02	0.07	−0.04
33A3 magnetometer electronics	2	0.6	0.04	−0.05	0.03
	2[a]	0.6	0.04	−0.06	0.03
	2[d]	0.6	0.03	−0.05	0.04
34A2 UV photometer electronics	MC2	0.4	−0.03	0.01	0.02
	MC2[d]	0.4	−0.03	0.01	0.03
	MC2[b]	0.3	−0.02	0	0.02
35A1&2 DFR	3	0.4	0.01	−0.01	−0.01
DFR low-pass filter	A165-5	1.0	0.11	−0.07	0.03
DFR high-pass filter	A251-3	0.2	−0.02	0	0.01
Bay IV, data encoder and command	V401/8[e]	11.7	1.29	0.42	−0.08
Bay V, radio and tape recorder	Sys 8[e]	24.3	−2.84	−1.69	−0.54
	Sys 8[e]	21.4	−2.63	−1.29	−0.42
	Sys 8[e]	19.3	−2.28	−1.38	−0.25
Bay VI, transponder	Sys 8	22.0	0.56	−2.41	0.66
	Sys 8[d]	25.4	1.17	−2.48	0.91

[a]Remapped due to rework on hardware.
[b]Redemagnetized due to variance of field following rework.
[c]Mapping indicates multipole field.
[d]Remapped at AFETR due to rework on hardware.
[e]2TR1 T-R unit not installed for this mapping.

Table 59 (contd)

Hardware	Serial No.	Maximum radial field at 3 ft, γ	Component of magnetic field at spacecraft science magnetometer, γ		
			X	Y	Z
Bay VII, CC&S	[f]	209.5	−1.40	25.49	8.41
		86.4	1.50	10.41	2.93
	[g]	80.0	−0.23	9.70	2.88
7A2 gyro	016	0.9	−0.05	0.04	0.04
	016[d]	2.0	−0.12	0.12	0.09
	016[b]	0.4	−0.02	0.02	0.02
Bay VIII, 4A8 power	03	3.8	0.22	−0.33	−0.16
4A14 battery	20	0.0	0	0	0
7CS8 Canopus sensor	106	14.3	1.58	−1.59	−1.44
	106[d]	17.9	0.56	−1.52	−2.04
7LS8 planet sensor	003	0.1	0.01	0.01	0
	003[d]	0.0	0.01	0	0
25A1 TRD	MC5	0.3	0.04	0	0.02
	MC6[d]	0.1	0.01	0.01	0
32A1 plasma probe	408	0.0	0	0	0
34A1 UV photometer	2[c]	0.3	0	0.02	0.01
	2[d]	0.3	−0.01	0.01	0.02
33A1 *magnetometer sensor*	1	0.0	0	0	0
	1[d]	0.0	0	0	0
Bay I louver	34	0.4	0	0.01	0.02
	34[d]	0.5	−0.02	0.02	0.03
Bay III louver	36	0.5	0.01	−0.01	0.03
	36[d]	0.4	−0.04	0.02	−0.01
Bay V louver	39	0.5	0.02	0.03	0.03
	39[d]	0.4	0.04	0	0.01
Bay VI louver	35	0.4	0.01	−0.02	−0.02
	35[d]	0.5	−0.04	−0.04	−0.03
Bay VII louver	32	0.2	−0.02	−0.01	−0.01
	32[d]	0.4	0	−0.03	−0.02
Bay VIII louver	33	0.3	0.01	0.02	0.02
	33[d]	0.7	0	0.02	0.04
8M1 separation-initiated timer	C-107	0.0	0	0	0
8AS1 pyro arm switch	C-111	0.0	0	0	0

[b]Redemagnetized due to variance of field following rework.
[c]Mapping indicates multipole field.
[d]Remapped at AFETR due to rework on hardware.
[e]2TR1 T-R unit not installed for this mapping.
[f]Mapped as initially received and before demagnetization.
[g]M67-1 CC&S installed with M67-2 A/C electronics 7A1.

Table 59 (contd)

Hardware	Serial No.	Maximum radial field at 3 ft, γ	Component of magnetic field at spacecraft science magnetometer, γ		
			X	Y	Z
15E2F1 DFR Antenna					
Metal end	C104	0.0	0	0	0
Insulated	C104	0.0	0	0	0
15E2F3 DFR Antenna					
Metal End	C104	0.0	0	0	0
Insulated	C104	0.0	0	0	0
Tip (boost) damper	C119[h]	0.2	0	0	0
Tip damper	C120[h]	0.2	0	0	0
Tip damper	C121[h]	0.3	−0.01	0	0
Tip damper	C122[h]	0.2	0	0	0
Tip damper	C123[h]	0.1	0	0	0
Tip damper	C124[h]	0.2	0	0	0
Tip damper	C125[h]	0.4	0.01	0	0.01
Tip damper	C126[h]	0.6	0.01	−0.01	0
2E1 high-gain antenna	10	0.0	0	0	0
Temp control reference—Bay V	17	0.1	0	0	0
Temp control reference—Bay VII	19	0.1	0	0	0
Temp control reference—Bay I	20	0.2	0	0	0
Spacecraft structure	[i]	—	0.38	0.13	3.63
2W2 coax cable	02	0.2			
2W45 coax cable	03	0.1			
2W47 coax cable	02	0.0			

[h]Tip dampers may not necessarily be installed in position for which computations are made.

[i]Spacecraft structure includes two A/C gas systems, sun gate and sensors, earth sensor, terminator sensor, upper and lower ring harnesses and accelerometer. Structure demagnetized in X and Y axes, only, and mapped in earth's field.

Results. On March 9, 1967, two spare flight solar panels, SNs 003 and 004, were magnetically mapped and found not to require subsequent demagnetization due to their low field. The remaining flight solar panels, SNs 005 through 008, were mapped on March 24, 1967, with similar results. In the case of the latter four panels, each panel was mapped three times in its assigned spacecraft position and once in the symmetrically located position. These four sets of readings were averaged – necessary because of the extremely low readings obtained – to obtain the results given in Table 60. The values in the table are estimated to be accurate to about 0.3 γ.

d. Solar panel current-loop fields. The objective of the solar panel current-loop tests was to determine the stray field caused by the flow of a known current in the panel. Because of the possibility that a portion of the panel may be damaged, it was also desirable to know the field caused by each of the three individually connected electrical sections of the panel.

Table 60. Solar panel perm field mapping results

Solar panel and location on spacecraft	Magnetic field components at spacecraft magnetometer, γ		
	B_x	B_y	B_z
SN 003 (Spare), +X	0	0.1	0.1
−X	0.2	−0.1	0.2
SN 004 (Spare), +X	0	−0.1	−0.1
−X	0	0	0
SN 005, 4A5	0	−0.1	0
SN 006, 4A7	−0.3	0	0
SN 007, 4A1	0.2	0.2	0.2
SN 008, 4A3	−0.1	0	0
Total field, SNs 005 through 008	−0.2	0.2	0.2

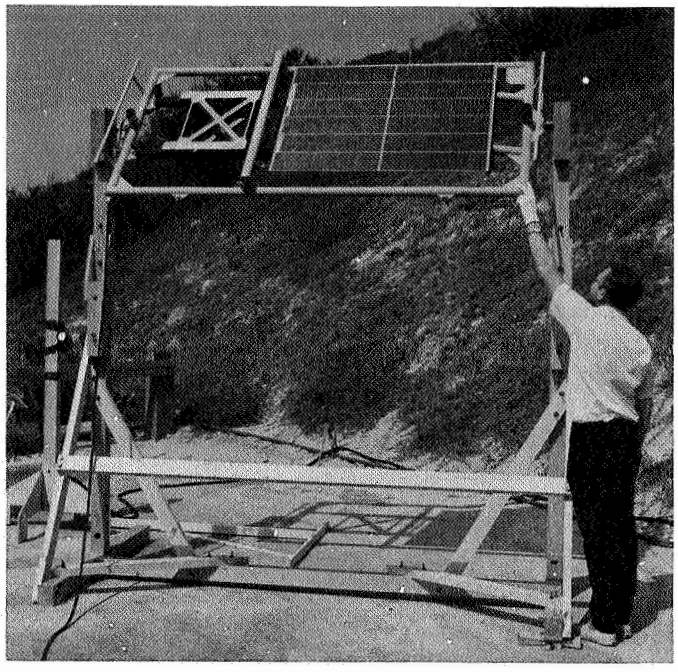

Fig. 113. Solar panel current loop testing

A spare flight solar panel SN 003 (shown in Fig. 113), was tested on March 24, 1967, to determine the stray magnetic fields at the spacecraft magnetometer sensor position as a result of current flow in the panel. The panel was separated into three similar electrical sections across the width of the panel with each section having a clockwise current flow as viewed from the cell side of

Table 61. Solar panel current-loop fields

Solar panel position on spacecraft	Results for solar panel section A, γ			Results for solar panel section B, γ			Results for solar panel section C, γ		
	X	Y	Z	X	Y	Z	X	Y	Z
Bay I 4A1 +x	−1.1	0.3	0	−1.7	0.2	−0.4	−0.9	0	0
Bay III 4A3 +y	0	−0.9	−0.2	−0.3	−1.7	−0.6	0	−0.9	−0.2
Bay V 4A5 −x	1.5	0	−0.4	2.4	−0.7	−1.0	1.3	−0.5	0
Bay VII 4A7 −y	0	1.8	0	0	2.3	−1.1	0	1.4	−0.5

Field components in spacecraft coordinates in γ for 600 mA current/panel section.

the panel. The field of each section, as well as the field of the whole panel, was determined for a panel in each of the four possible positions on the spacecraft. The values for each panel for each of the four spacecraft solar panel positions are shown in Table 61. With the $+X$ and $+Y$ panels and, also, the $-X$ and $-Y$ panels being symmetrically located about the sensor, the positive axes panels should have similar values with the X and Y components interchanged. The negative axes panels will likewise have similar values. These values have been averaged and extrapolated to provide the information in Table 62.

Table 62. Solar panel current-loop tests

Test condition solar panel SN 003	Stray field component at spacecraft magnetometer location, γ		
	X	Y	Z
Panel in +X position, 1.8 A	−3.1	0	−0.7
Panel in −X position, 1.8 A	5.2	−0.1	−1.7
Four panels on spacecraft cruise load 228 W	1.5	1.3	−3.4

VI. Evaluation of Test Requirements

In this section, the environmental test requirements that were used in the *Mariner* Venus 67 test program are evaluated to make a post-program assessment of the adequacy of the test program. Where possible, ground test environments are compared with actual *Mariner* Venus 67 flight environments. In addition, spacecraft response in the test environment is compared with response in the flight environment.

The total environment is divided into two broad categories; dynamics — i.e., shock, vibration, and acoustics — and the thermal–vacuum environment. The electromagnetic environment is not discussed in this section because it has been covered in other sections of this report; in addition, it was not possible to measure this aspect of the flight environment.

A. Dynamics

The significant dynamic environment occurs during the spacecraft launch prior to spacecraft separation and consists of (1) acoustic-induced vibration at liftoff and the transonic period, (2) booster-induced transient vibration associated with staging, motor ignition and shutdown, etc., and (3) spacecraft pyrotechnic shocks.

Each of these environments is discussed below and compared with some ground test environment. The tests that are compared with the flight data are system tests — mainly, the M67-2 system tests. This is the only level at which meaningful direct comparisons of data can be made. When possible, flight measurements of the dynamic environment (two accelerometers) are compared directly with the identical measurements during ground test.

Detailed results of the flight measurements are reported in Ref. 3 and detailed results of the ground vibration tests are reported in two Project documents. In addition, the results of ground tests of pyrotechnics and the V-band are reported in Ref. 4.

1. Random vibration. The random vibration test is intended to simulate, at somewhat higher levels, the high-frequency random vibration that occurs at liftoff and, also, the transonic portion of flight. The test levels for *Mariner* Venus 67 were based on data collected on the *Mariner III* and *IV* launches. These test levels, shown in Fig. 114, are the values to which the system test was controlled. The control scheme is described below. During these system tests, measurements of acceleration response were made at several locations, including the flight measurement positions B3 and F4, also described below. The comparisons that follow are direct comparisons of these two transducers during the M67-2 ground test and launch. With only two flight measurements, a minimum definition of the flight vibration is available; however, a qualitative evaluation of the test requirements is made below, which shows the requirements for random vibration tests were generally adequate.

a. Ground test configuration and control. Ground tests were performed with the *Mariner* Venus 67 spacecraft mounted on an *Agena* adapter which, in turn, was mounted on a vibration fixture. The vibration level at the fixture–adapter interface was controlled by monitoring six accelerometers, placed around the circumference of the attach plane, and measuring in the direction of applied excitation. The parameter controlled was the average power spectrum level in 25-Hz bands.

b. Flight measurements. Two piezoelectric accelerometers were used to monitor the flight vibration environment. One was located in the *Agena*–spacecraft adapter, with its sensitive axis in the thrust (Z axis) direction. The second was located at the top of the spacecraft bus on the foot B corner and also monitored Z axis vibration.

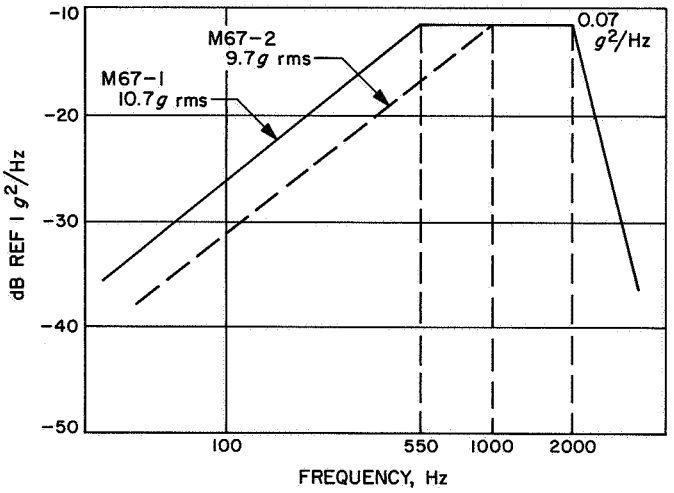

Fig. 114. Random-vibration test specification

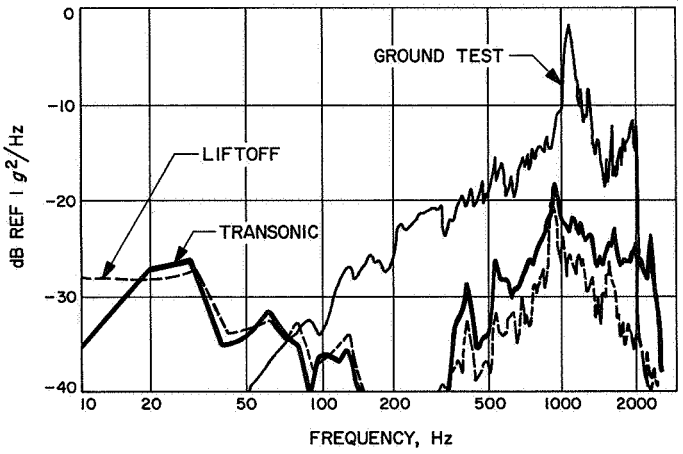

Fig. 115. Comparison of random vibration at F4 for ground test and flight

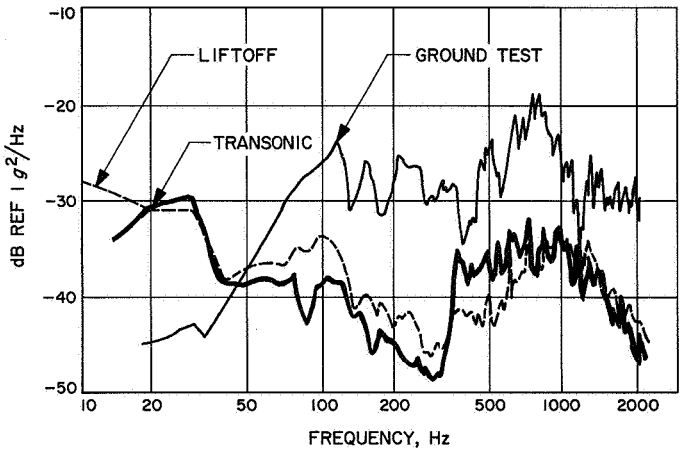

Fig. 116. Comparison of random vibration at B3 for ground test and flight

Nomenclature and channel assignment were as shown in Table 63.

c. Comparison of flight and ground test results. The comparison made below is based on the response vibration at the B3 and F4 measurement positions during ground test and flight. Ground tests were conducted in three orthogonal axes to identical test levels. However, during each test, the spacecraft response is generally omnidirectional at any point. The criteria for considering test adequacy in the following comparisons will be the maximum response of the two flight transducers for all three shake axes. This maximum response is compared, for each transducer, to what was observed in flight in Figs. 115 and 116.

It is observed that the transonic event generally causes slightly higher vibration levels than does the liftoff acoustic environment. Also, the maximum ground test response of each of the flight transducers is seen to be approximately 10 dB higher than any flight vibration. Exceptions to this occur at a few rather narrow frequency bands and at low frequencies ($f < 100$ Hz) where the random test input was very low.

Table 63. Flight vibration instrumentation

Location	Code	Telemetry channel No.	Nominal information bandwidth[a], Hz
Adapter	F4	18	3000
Top of bus	B3	17	2100

[a] Cutoff frequencies of discriminator low-pass filters.

Although a limited amount of data is available for definition of the spacecraft vibration, and although significant boundary condition differences exist between ground test and flight, it is concluded that the random vibration test created a vibration response of the spacecraft that was greater than that which existed during launch – either for liftoff or transonic periods. It is also concluded that within the ranges of uncertainty that exist for environmental definition, ground test simulation, and test control, the margin by which ground test exceeds flight was not overly conservative.

2. Sine vibration. The sinusoidal vibration test on the *Mariner* Venus 67 spacecraft consisted of a 1-*g* rms sine swept between 20 and 200 Hz at 0.5 octave/min. This

test served primarily to excite structural modes and to provide confidence in the structural integrity of the spacecraft. It was noted, previously, that some low-frequency energy was observed at liftoff and transonic times that was not covered by the random vibration test. In addition, various flight transient vibrations occurred that contained such low-frequency energy. However, there is no sine or sweeping sine in the flight vibration environment.

For purposes of comparison, the *transient* flight events will be compared to the sweeping sine ground tests by overlaying the maximum shock spectra of the data measured at each flight transducer in the flight and ground tests. These data are shown in Figs. 117 and 118.

Control of the ground test was based on the maximum acceleration at six instrumented locations at the shake fixture–adapter interface. The test configuration was the same as described above for the random vibration. The curves representing the ground test in Figs. 117 and 118 were obtained by multiplying the sinusoidal response at B3 and F4 by 20 (the assumed Q value of the shock spectrum). The flight data are the maximum envelopes of the shock spectra from all transient events as observed at these same measurement points.

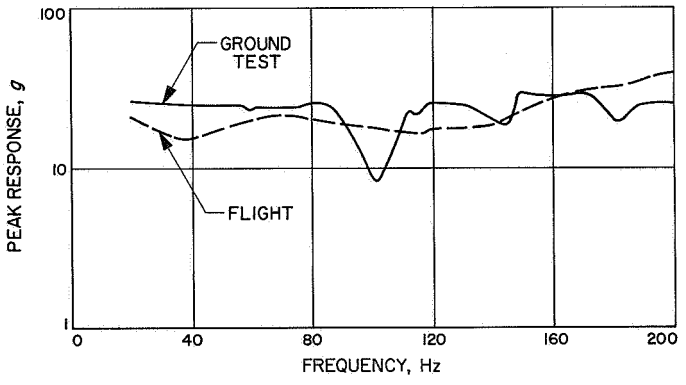

Fig. 117. Shock-spectrum comparison of ground sine vibration and flight transient vibration at F4

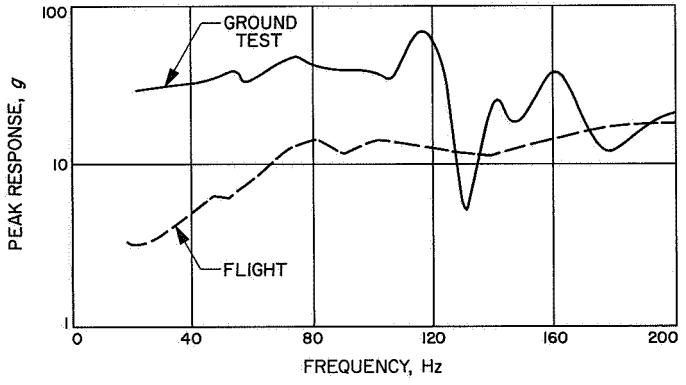

Fig. 118. Shock-spectrum comparison of ground sine vibration and flight transient vibration at B3

Surprisingly good agreement is shown between the ground and flight results. This should not be interpreted as indicating that the ground test was a good simulation of the flight transient environment; however, to the extent that it is meaningful to compare sweeping sine and transient vibrations, it is concluded that the level of the ground test was at least the correct magnitude.

3. Shock. The shock environment discussed in this section is that which results from release of the V-band and the actuation of pyrotechnic devices. The ground test program consisted of exercising the following events on the respective spacecraft.

M67-1	M67-2
1. V-band	1. V-band
2. Shroud separation	2. Solar-panel deploy
3. Solar-panel deploy	3. High-gain antenna
4. Midcourse *on* and *off*	
5. High-gain antenna	

The two events omitted in the M67-2 testing were found, following review of the M67-1 data, to create a shock environment that was enveloped by the other events for most spacecraft measurements. During these ground tests, several measurements (approximately 24 on M67-1 and 5 on M67-2) of spacecraft response were obtained. However, again, only the flight transducers are used for comparison. In ground test the most severe shock at the B3 location resulted from V-band release. At the F4 location, the most severe ground test shock was the shroud separation event.

During flight, several shock events originating in the booster created significant shocks at the spacecraft. For each of the events monitored in flight, a shock spectrum was computed, and the maximum envelope spectrum for each transducer was determined. These are compared on Figs. 119 and 120 to the maximum envelope of ground test results. Fig. 119 shows ground test results from both M67-1 and M67-2 tests. This was necessary since the shroud separation test was only done on the M67-1 spacecraft.

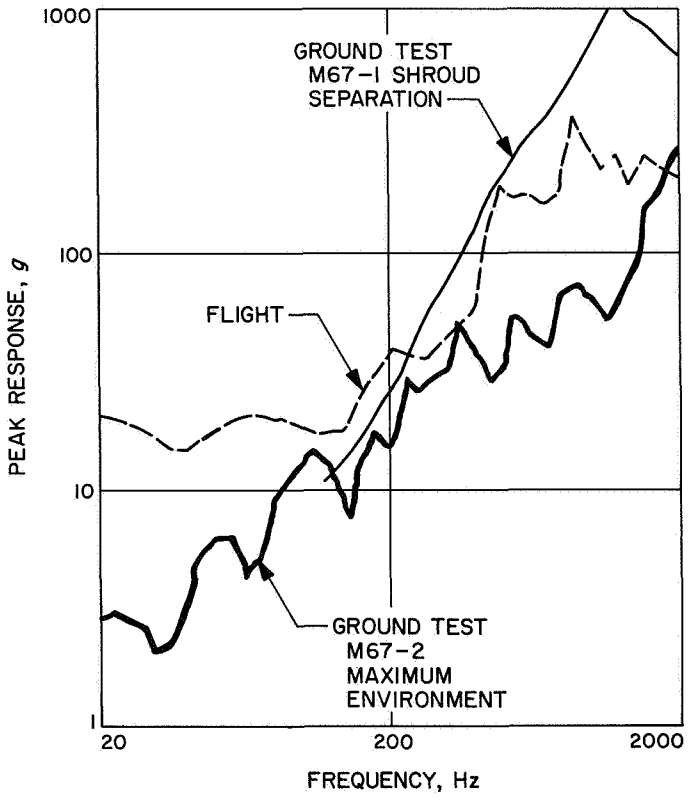

Fig. 119. Comparison of responses at F4 for ground test and flight shock

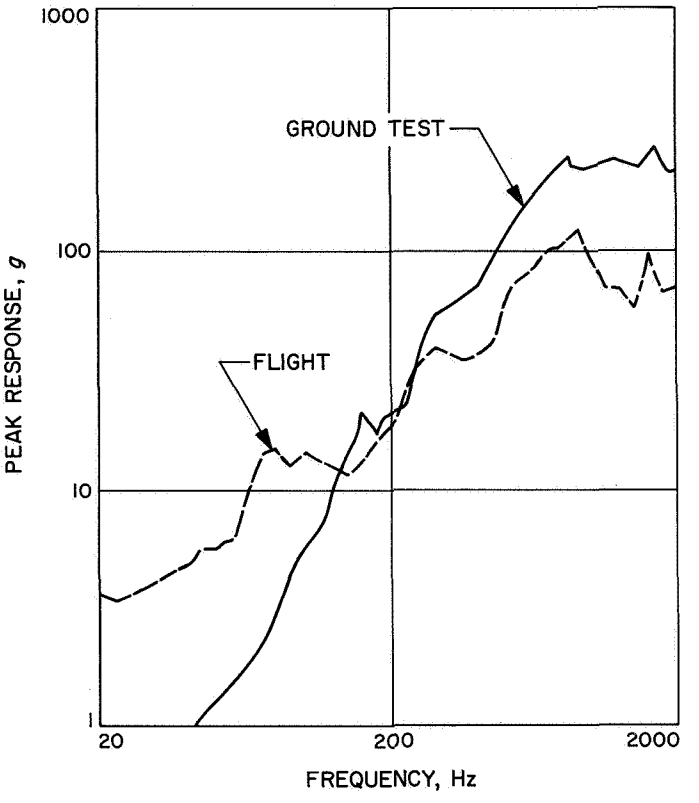

Fig. 120. Comparison of responses at B3 for ground test and flight shock

It is concluded from Figs. 119 and 120 that the operation of pyrotechnic devices and the V-band release generally produce a realistic test for the spacecraft at high frequencies. However, no margin over the expected environment is achieved as it is in random vibration testing. It is noted that, at low frequencies, the flight environment is higher than the ground environment during *these* tests. One explanation is that the low-frequency response is suppressed in ground test by the manner in which the spacecraft adapter was restrained. The ground test configuration was somewhat more rigid than the flight configuration. It is also noted that the low frequencies are additionally excited by the sweeping sine test.

4. Acoustics. During the *Mariner* Venus 67 liftoff, the acoustic field was monitored with microphones on the umbilical tower boom. Fig. 121 shows the measured sound pressure level compared with the acoustic spectrum used for the ground test on the structural test model (STM). It should be noted that the measured data represents the *external* acoustic field approximately 10 ft from the adapter skin, while the intent of the STM test was to simulate the acoustics *internal* to the spacecraft shroud.

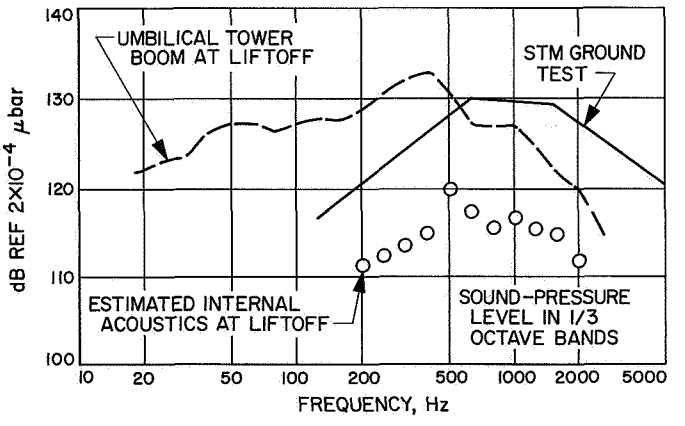

Fig. 121. Comparison of acoustic fields at launch and ground test

The ground test levels were based on acoustic measurements taken on the *Ranger* program, internal to the shroud. On the basis of an estimated shroud transmissibility (also based on *Ranger* data) the predicted internal acoustic field for the *Mariner* Venus 67 vehicle is shown with circles on Fig. 121. The ground test is seen to envelop with a pad the estimated flight environment.

The pad is appropriate, since the STM test was performed at TA (type approval) levels.

During this acoustic test the vibration responses at the flight measurement positions were monitored. These responses are compared with the liftoff vibration in Figs. 122 and 123. It is noted that the STM acoustic test caused generally higher vibration than occurred at liftoff for the bus location but not at the adapter. Of course, the acoustic test is most significant for those items which are acoustically sensitive (solar panels, antennas, etc.) and, consequently, the above comparisons are not the most meaningful. However, it is noteworthy that vibration levels can be generated at the top of the bus with acoustics that are more severe than vibration levels observed during launch.

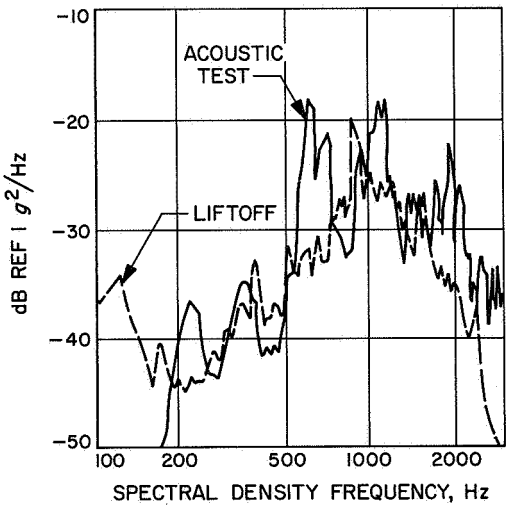

Fig. 122. Comparison of vibration responses at F4 for liftoff and acoustic test

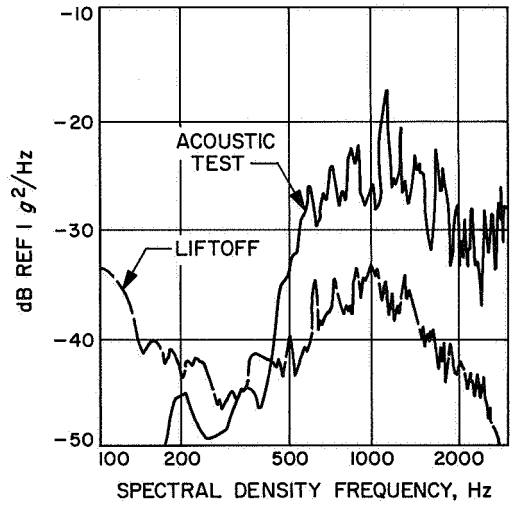

Fig. 123. Comparison of vibration responses at B3 for liftoff and acoustic test

5. Conclusions and recommendations. It is concluded in the preceding sections that the dynamic test levels used on the *Mariner* Venus 67 spacecraft system were generally adequate to provide confidence that the spacecraft was compatible with its environment. To the extent that meaningful comparisons can be made between ground test and flight, it has been shown that the spacecraft's response to ground test was equivalent to, or in excess of, its flight response. This is generally true for both prolonged random vibration and transient vibration. However, these statements are intentionally general and should not be construed to indicate that all aspects of the dynamic testing provided the best possible simulation of the actual environments.

One significant weakness in the test program concerns ground test simulation of the pyrotechnic environment. This is not so much a weakness in the *Mariner* Venus 67 program as it is a weakness in the state of the art. The problem is that a margin over the expected flight environment was not demonstrated prior to launch. (See Figs. 117 and 118.) An environment roughly *equivalent* to the launch environment was generated by ground test of the pyrotechnics. However, it is highly desirable to generate an environment having a controlled severity somewhat in *excess* of that anticipated. This area requires research to define such a test technique or procedure.

Another weakness concerns the ground test simulation of the transient vibration environment, either low frequency or high frequency. The sweeping sine vibration test exists in present test programs largely because of precedent and its use as a diagnostic tool; however, as has already been pointed out, no sine or sweeping sine vibration occurs in an actual launch environment. Better definition of transient vibration can be attained only through more extensive flight instrumentation to define low-frequency modal response. In addition, test techniques to simulate the transient vibrations require much refinement, both for the low-frequency and high-frequency environments.

References 3 and 4 include additional data on the dynamic environment and dynamic testing program for *Mariner* Venus 67.

B. Thermal–Vacuum

1. System level.

a. Comparison of systems-level test temperatures with actual flight temperatures. Systems-level space-simulator thermal–vacuum testing is intended to demonstrate the spacecraft's ability to operate under the various thermal environmental conditions associated with the various flight modes (launch, midcourse maneuver, cruise, encounter, and postencounter playback). To compare systems test temperatures with flight temperatures, it is necessary that the representative temperatures used in the comparison – i.e., solar irradiance level and spacecraft mode of operation – occurred as a result of the same flight mode. Presented in Table 64 are test and flight temperatures obtained during the earth cruise mode (minimum temperatures) and the Venus cruise post-playback flight mode (maximum temperatures). These flight modes represent the coldest and hottest mission modes.

The data in Table 64 show a close correlation between test and flight temperatures and indicate that test temperatures were higher than flight temperatures, on the average (e.g., the bus equipment had a 4°F average temperature difference at earth cruise, and an 8°F average temperature difference at Venus post playback). However, the temperature differences for equipment external to the bus vary from 36°F to −21°F. The exact causes of these larger temperature discrepancies on external bus items have not been determined, but testing errors due to the facility simulation or spacecraft interactions are contributing factors.

A number of error sources exist; and while every effort has been made to make these errors small and understood, still they must be considered in any comparison of this sort. A brief discussion of primary error sources is given below:

(1) *Louver hysteresis in a 1-g field.* This effect is small, typically about 1 or 2°F, and is only significant during test.

(2) *Telemetry accuracy.* Quoted flight temperature telemetry channel accuracy is within 5% of the total range (about 7°F). Comparison of telemetry and thermocouple data during test indicate much better accuracy, however.

(3) *Steady-state considerations.* The spacecraft is very slow in reaching thermal equilibrium, especially when going from cold to hot modes. Thus, if the test mode were terminated early, the bus would be cooler than the corresponding flight mode.

(4) *Nonflight spacecraft configuration.* Although this condition was minimized in the systems tests considered, a significant departure from flight configuration existed because of the substitution of dummy solar panels and A/C gas system handling frames.

(5) *Cabling effects.* The only cables attached to the spacecraft during the systems tests considered were the upper and lower support cables and minimal electrical cabling. The upper support cables were estimated to conduct 4 W *out* of the spacecraft at earth intensities and 2 W *in* at Venus intensities. Heat loss from the other cables was negligible.

(6) *Chamber heat inputs.* One of the test errors considered to be of high, although undefined, significance is that error induced by extraneous heat inputs to the spacecraft from the test chamber. Current estimates indicate about 9 W net input to the bus at earth-cruise intensities.

(7) *Solar intensity variations.* Except for sunlit assemblies, the spacecraft is insensitive to possible errors in solar irradiance. A 10% error in solar intensity would amount to <3 W in the bus.

(8) *Net effect.* A tabulation of known test error sources with an estimate of their effect on bus temperature is given below. The tabulation applies only to the earth-cruise, louvers-closed mode of test, which is the mode most sensitive to test errors. The *bias* is the calculated offset in bus temperature due to this effect; the *uncertainty* is the estimated maximum deviation from the test temperature after correction for the bias. Flight temperature is taken as reference; positive values in Table 65 indicate that the spacecraft is warmer in the chamber than in flight.

Thus, the worst-case flight deviation from test results should be 12½°F cooler. This corresponds to an actual worst-case deviation for bus equipment of 16°F cooler and an average deviation of 4°F cooler.

The following conclusions can be made with regard to *Mariner* Venus 67 flight results in comparison with systems level testing:

(1) In general, bus temperatures during test show a remarkably good correlation to flight temperatures.

Table 64. Systems-level test temperatures and actual flight temperatures

Item	T/M chan	M67-1 systems test temperature		M67-2 systems test temperature		Flight temperatures		
		Earth cruise (min. temp) $I = 126$	Venus cruise (post-playback mode, max) $I = 290$	Earth cruise (min. temp) $I = 126$	Venus cruise (post-playback mode, max) $I = 290$	Earth cruise (pre-midcourse maneuver)	Venus cruise (post-playback mode, max)	Midcourse maneuver
Bay I flight location	401	62	84	63	75	68	67	95
Bay II flight location	421	46	69	48	65	47	57	119
Midcourse fuel	217	57	80	59	73	56	67	79
Propulsion N_2	408	52	76	54	69	52	62	112
Primary sun sensor	430	48	93	50	95	49	105	98
UV photometer	437	57	78	47[a]	64[a]	46	61	77
Bay III flight location	402	59	74	64	72	59	69	74
Plasma probe	422	101	204	108	217	105	222	78
Bay IV flight location	423	56	76	63	74	56	70	63
$-X/+Y$ N_2 bottle	219	59	81	63	75	57	69	63
TRD chassis	438	45	64	51	63	45	59	57
Bay V flight location	404	54	70	65	72	53	68	56
Bay V VCO (2RA2)	424	60	78	74	80	59	76	65
Bay V tape (16A1)	436	55	73	64	73	54	69	56
Bay VI flight location	405	60	79	73	78	57	75	60
Bay VI aux. oscillator 1	414	67	81	72	79	62	74	66
Bay VI aux. oscillator 2	418	67	80	73	79	62	75	66
Bay VII flight location	426	61	76	58	70	54	60	64
Bay VIII power regulator	407	86	109	84	97	85	85	105
Battery	428	63	86	64	77	62	65	70
$+X/-Y$ N_2 bottle	218	61	83	62	76	59	66	67
Canopus sensor	410	60	78	59	70	57	61	67
High-gain dish	419	−184	−147	−188	−133	−197	−130	−5
Upper shield	434	−165	−134	−167	−136	−197	−170	−186
Lower shield	435	47	152	45	158	37	173	−25
Magnetometer preamp end	439	−12	−4	−11	−15	7	6	25
Mast at magnetometer	431	−94	−60	−83	−64	−90	−68	25

[a]New UV calibration curve.

Table 65. Error sources and effects on bus temperature

Error source	Bias, °F	Uncertainty, °F
Sticky louvers	−1	±1
Measurement inaccuracy	0	±2
Failure to achieve steady state	− ½	± ½
Inaccuracies in solar panel mockups	0	±1
Cabling effects	−3	±1½
Chamber heat inputs	+7	±2
Solar intensity	0	±2
Net effect	+2½	±10

This is a further indication of the insensitivity of the spacecraft bus to solar irradiance errors.

(2) Continuing investigation of effective heat sink temperature in the space simulator, as well as other error studies, is needed to improve the correlation of external bus assembly test temperatures and flight temperatures.

b. Significance of non-space environment for M67-1 thermal–vacuum test. A space simulator is appropriately named — it must not be called a *space duplicator*. Notably, it is inferior in solar radiation uniformity, collimation, and spectral distribution. The effect of these deficiencies is considered.

Uniformity of total irradiance. The specified requirement was that, for a 4-cm² sensor, the uniformity would be within ±5% of the mean level for three reference planes. Figures 124 through 127 present the data taken prior to, and after, the M67-1 test. Comparisons are made at two reference planes, rather than three, since the test plane is very close (approximately 6 in.) to the 12-ft measurement plane. Figure 124 compares uniformity mappings in polar coordinates taken before and after the test at the 4-ft elevation. Figure 125 compares the mappings taken before and after the test at the 12-ft elevation. Figures 126 and 127 compare the 12-ft to the 4-ft mappings taken before and after the test, respectively. The purpose of the comparisons is to evaluate the stability of the distribution of solar energy with respect to time and is dependent on the accuracy of the data supplied, which is supposed to be ±2%. The comparisons also yield information on the variation in a plane and with depth. In a plane, the variation of solar energy for a 4-cm² sensor as indicated directly from the data is only slightly greater than 5%, being 6% at the worst-case measurement for the extreme edge and the center of the beam (see Fig. 128).

The stability of the energy distribution with respect to time varied to a maximum 4 to 5% for certain areas in the planes of measurement (see Fig. 124). The temporal variation in Fig. 125 was less severe than in Fig. 124. NOTE: The greater-than implications in the data have been interpreted to imply that the level is $>(X)$ W/ft² but less than $(X + 1)$ W/ft².

The depth change with respect to position is illustrated in Figs. 126 and 127. For example, from Fig. 127 one observes that the maximum depth percentage difference is ~7 to 8% (94 to 102 W/ft²).

To summarize the data presented, one can conclude that the variation in a plane is less than 5% in most of the beam and less than 6% in all of the plane. In depth, a percentage difference of 7 to 8% is possible. This means that the maximum volumetric percentage difference is on the order of 14%. From Fig. 127, one notes the difference is as much as 16% at the very edge but is 14% for the beam for all practical purposes.

The significance of these variations is minor for the *Mariner* Venus 67 configuration, since the spacecraft presents essentially a plane-intercepting disc (except for the trapped radiation detector, plasma probe, sun sensors, and sun gate), at about the 12-ft elevation (see Fig. 128). Variation with depth is not critical for this spacecraft, and the uniformity in the 12-ft plane is better than ±5%. The change of energy distribution with time remained within the 6% band and is not significant as long as a post- and pretest spacecraft mapping is performed for evaluation of the effect (spacecraft mapping was performed on M67-1). The beam, for all practical purposes, met the specification (±5%) in a plane, although a very small portion of the outside edge of the 6-ft-diam beam had a variation of about 6%. A waiver was not required.

Angle of incidence. The specified angle of incidence for the worst ray to the plane of the spacecraft was 2 deg. The measured values are presented in Table 66, along with two figures that illustrate the measurement location/orientation.

The angles measured were accepted for the *Mariner* Venus 67 testing, and the 2-deg requirement was waived.

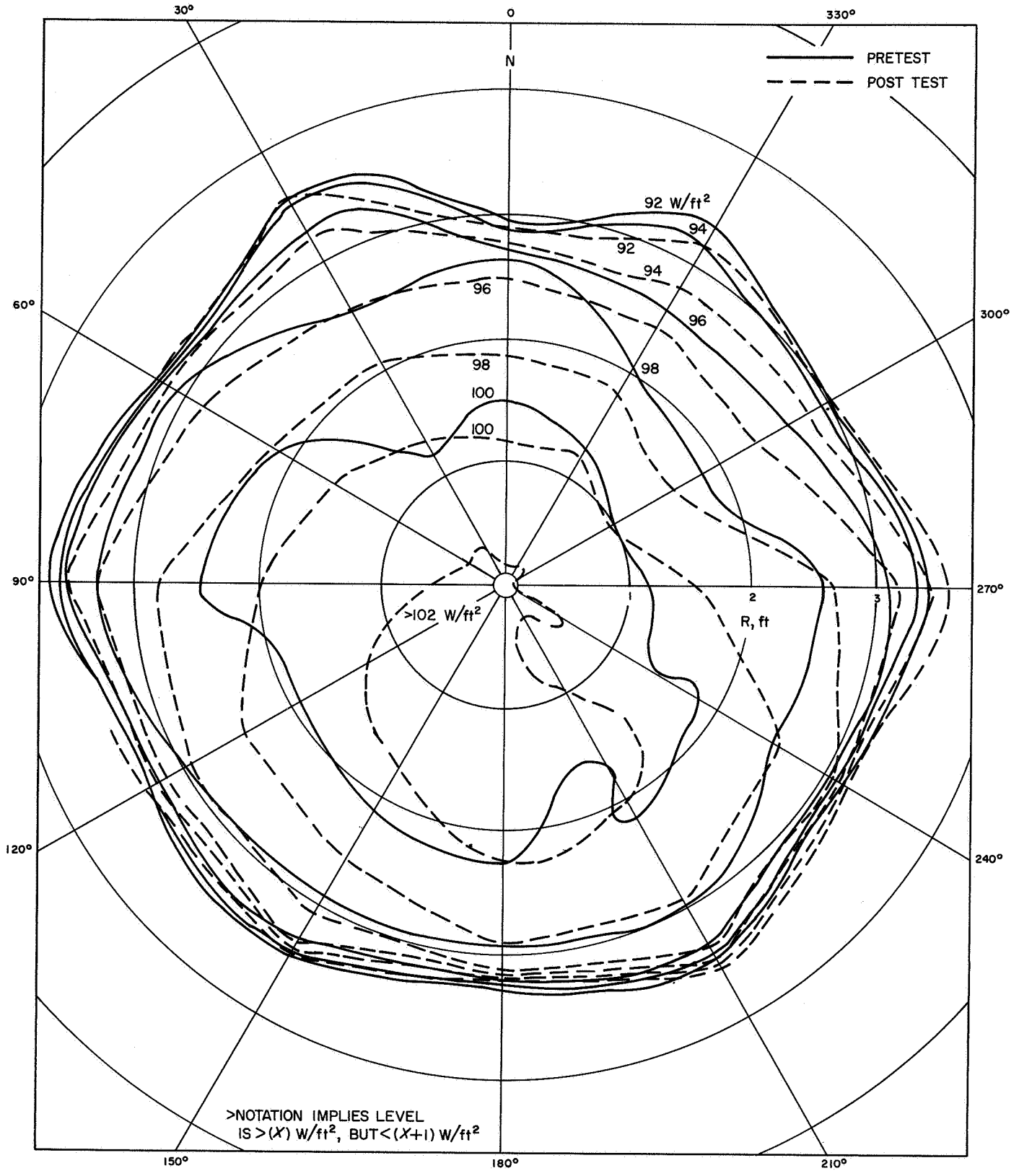

Fig. 124. Total irradiance uniformity mapping for 4-ft elevation, thermal–vacuum pretest and post-test of M67-1

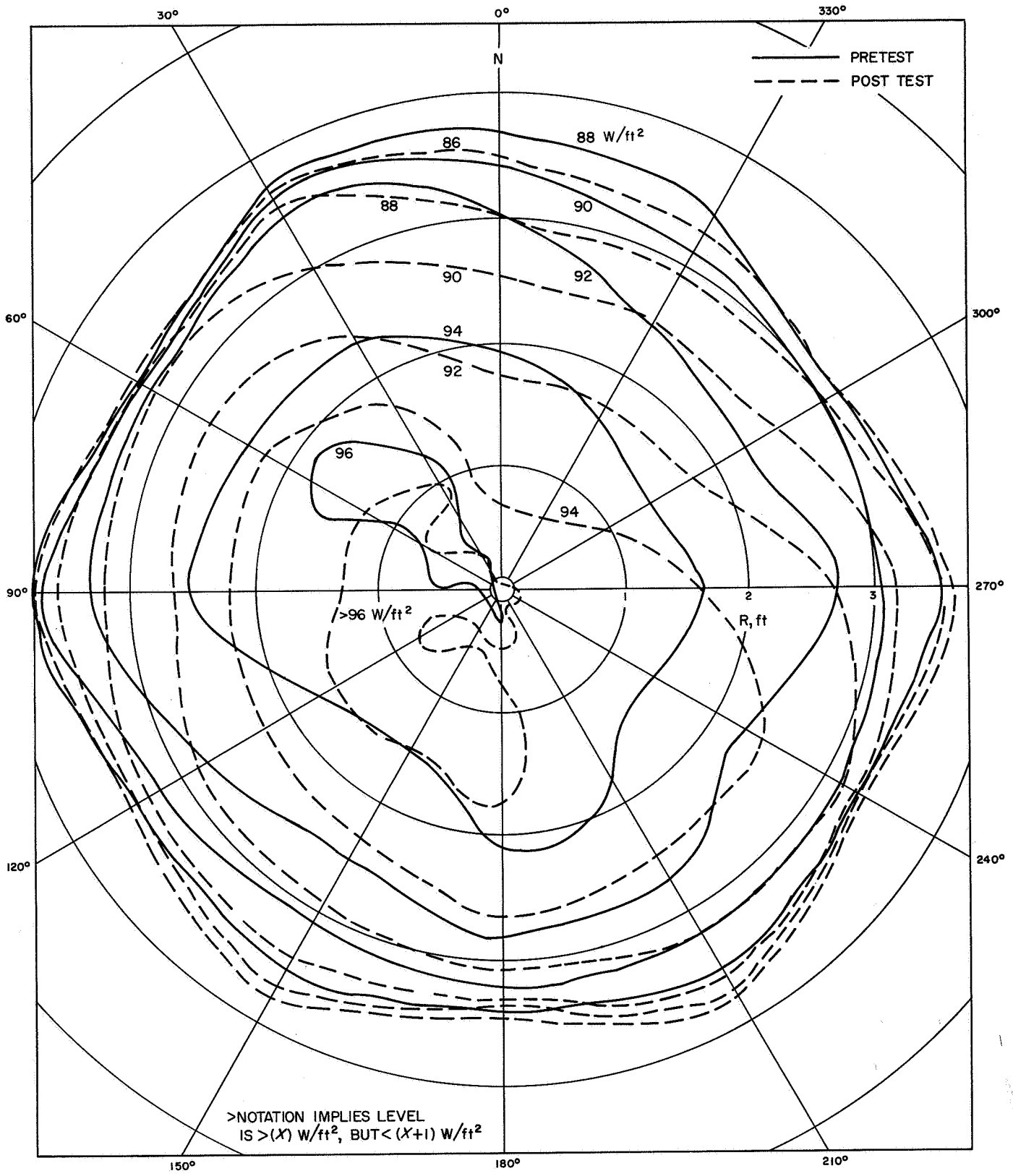

Fig. 125. Total irradiance uniformity mapping for 12-ft elevation, thermal–vacuum pretest and post-test of M67-1

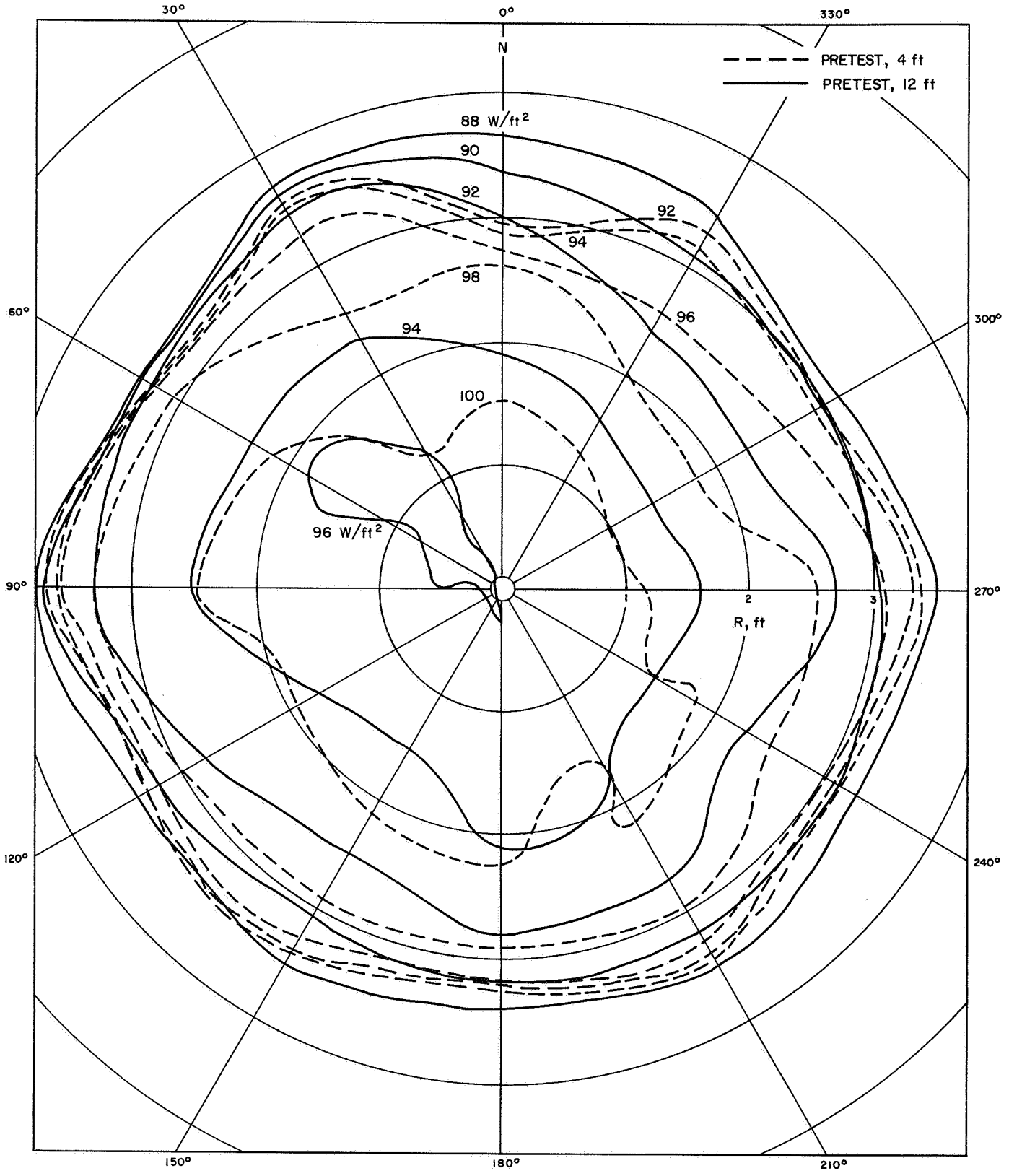

Fig. 126. Total irradiance uniformity mapping for 4- and 12-ft elevations, thermal–vacuum pretest of M67-1

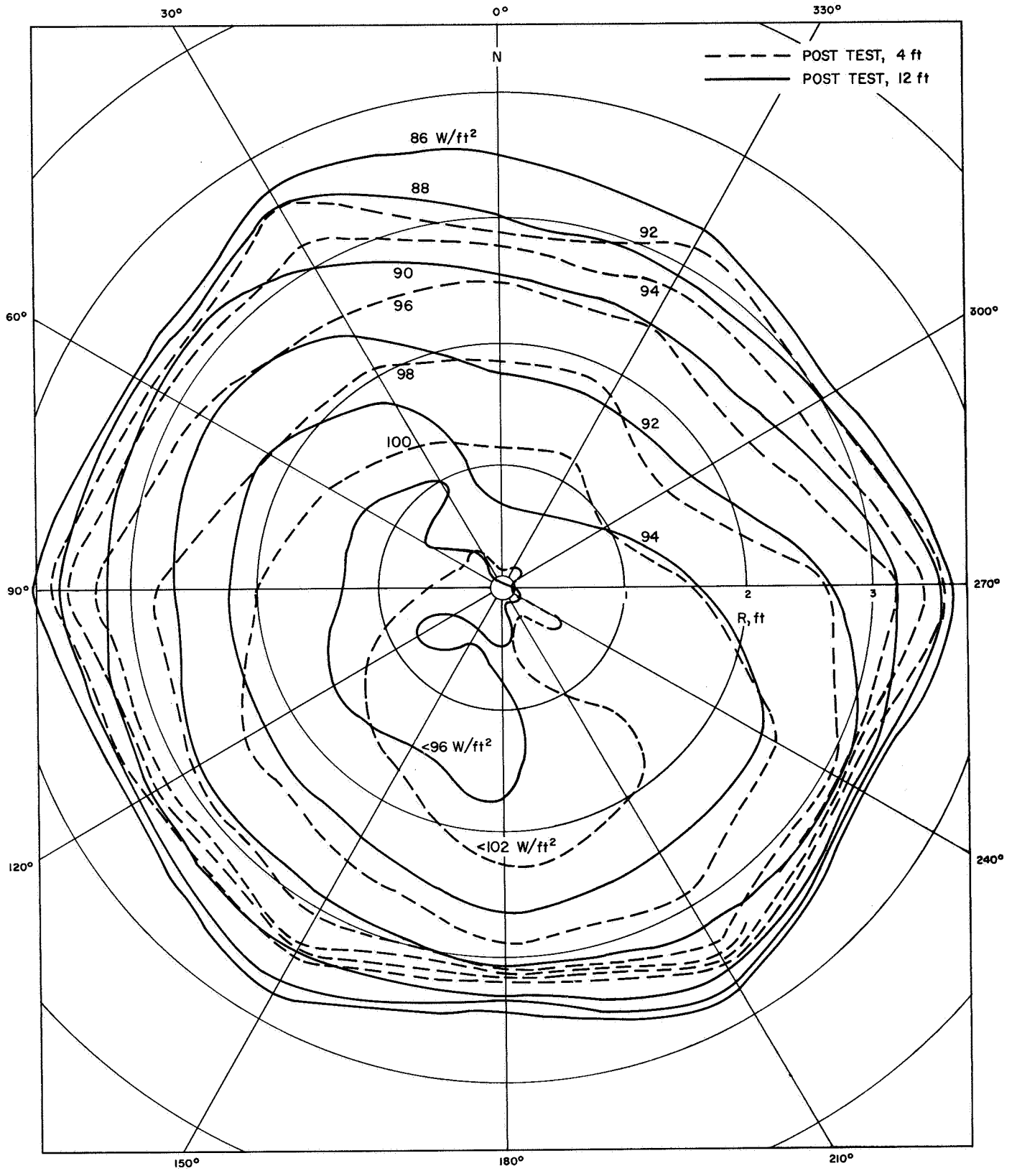

Fig. 127. Total irradiance uniformity mapping for 4- and 12-ft elevations, thermal–vacuum post-test of M67-1

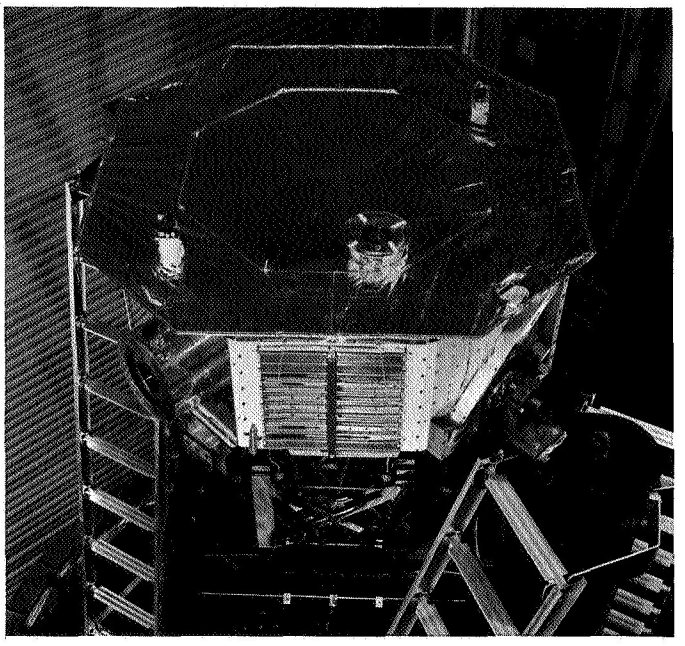

Fig. 128. *Mariner* Venus 67 TCM chamber installation

The purpose of the 2-deg requirement was to minimize the significance of thermal errors – e.g., an L-shaped intercepting structure with an α/ε of 1 would experience thermal errors of $+10°F$ on the vertical leg and $-10°F$ on the horizontal in a 2-deg off angle light source. The principal *Mariner* Venus 67 spacecraft item affected by radiation at the angles obtained is considered negligible. As a result, the M67-2 specification was changed to 3 deg.

Spectral irradiance uniformity. The spectral distribution was not specified; instead, a maximum variation in spectral irradiance of $\pm 2\%$ at each defined location for each filter was specified. Tables 67 and 68 reveal the data as reduced through several normalizations in terms of 100% for each reading. The data, although not of high quality, indicates the spectral uniformity is acceptable. The data quality is affected by the following two factors:

(1) Measurements in the UV (filters 1, 2 and 3) are difficult to make, and the variations indicated are believed due to the measurement error, rather than spectral non-uniformity.

(2) Variations at other levels are probably due to the fact that the ratio

$$\frac{\int J_\lambda \tau_\lambda d_\lambda}{\int J_\lambda d_\lambda}$$

was obtained with an average $\int J_\lambda d_\lambda$ for each twelve-filter scan, rather than an individual $\int J_\lambda d_\lambda$ for each filter. Therefore, fluctuations at the time of each filter reading would not be discernible.

J_λ = spectral radiant intensity

τ_λ = spectral transmittance

The uniformity of spectral irradiance requirement, as far as can be determined from the data, was met in the M67-1 testing.

Table 66. Measured values for angles of incidence, M67-1

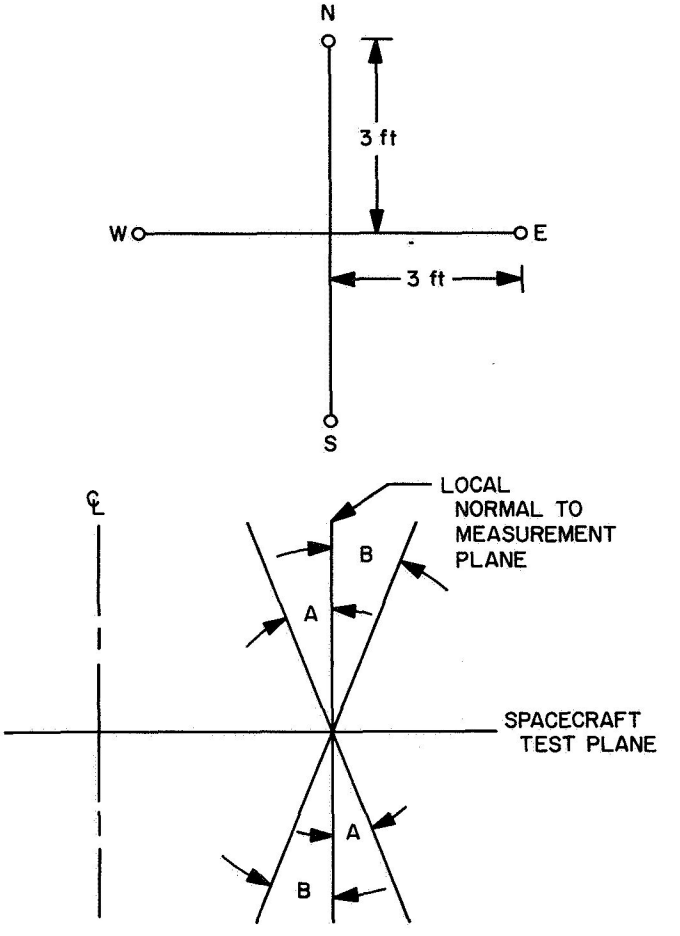

Position	Measured angles of incidence, deg			
	Pretest M67-1, angle A	Post-test M67-1, angle A	Pretest M67-1, angle B	Post-test M67-1, angle B
North	1°57′6″	1°57′48″	2°7′42″	2°7′16″
South	1°40′11″	1°40′44″	2°37′35″	2°36′46″
East	1°28′10″	1°31′	2°4′6″	2°1′15″
West	1°49′36″	1°49′3″	1°43′30″	1°44′6″

Table 67. Pretest spectral irradiance uniformity measurements for M67-1 thermal–vacuum test

Filter No.	1% transmission bandpass, μ	Normalized variation in spectral irradiance										
		4-ft elevation						12-ft elevation				
		1	2	3	4	5	6	2	3	4	5	6
Clear avg		5.889	5.916	5.958	6.058	6.097	5.997	5.803	5.805	5.683	5.722	5.634
1	0.240 to 0.300	201.7	135.1	135.9	103.8	83.5	137.0	99.4	79.6	97.3	97.9	128.5
2	0.300 to 0.355	100.9	105.6	102.0	99.8	104.5	107.1	99.4	99.5	97.4	106.6	100.6
3	0.340 to 0.380	103.7	104.3	102.1	101.1	104.5	105.7	99.4	99.5	97.4	100.8	102.0
4	0.376 to 0.425	100.9	100.2	100.9	101.4	100.8	102.8	99.5	98.3	98.6	99.3	101.4
5	0.430 to 0.510	101.3	101.0	98.6	100.5	100.8	101.9	99.4	99.5	100.2	99.7	100.2
6	0.525 to 0.610	101.4	101.0	101.6	100.9	101.0	101.8	99.4	98.9	99.8	100.0	99.9
7	0.610 to 0.720	100.9	100.3	101.0	100.6	100.7	101.7	100.0	99.4	100.1	99.7	100.3
8	0.710 to 0.810	100.9	101.4	101.1	100.7	101.4	100.7	100.5	100.5	100.0	100.1	100.2
9	0.750 to 0.900	100.4	100.5	100.4	100.3	100.7	100.7	100.7	100.5	100.3	100.8	100.9
10	0.800 to 1.000	98.6	99.4	99.6	99.7	99.5	99.0	102.8	102.8	101.8	101.7	101.1
11	1.025 to 1.600	100.3	100.8	100.9	101.4	100.9	100.4	100.7	100.4	100.4	100.5	99.5
12	1.500 to 2.200	100.9	100.6	100.4	101.2	101.8	101.0	100.3	99.5	99.1	100.7	99.1

The expression

$$\frac{\int_{\lambda_a}^{\lambda_b} J_\lambda \tau_\lambda d_\lambda}{\int_{\lambda_a}^{\lambda_b} J_\lambda d_\lambda}$$

is reduced from empirical measurements presented in the data package. This ratio is taken for each filter at each location which then is normalized to a percentage of the average ratio for that filter. The principal assumption made in this analysis is that the variation in the clear reading is small. This assumption could be avoided if a clear reading were taken with each filter reading.

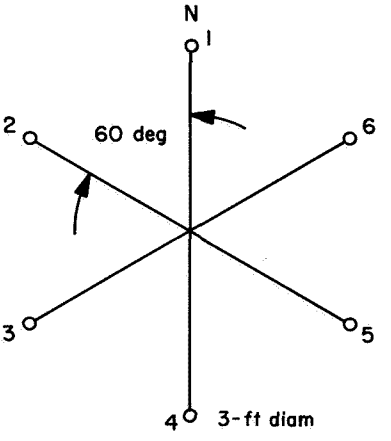

RADIOMETER POSITION

Table 68. Post-test spectral irradiance uniformity measurements for M67-1 thermal–vacuum test

Filter No.	1% transmission bandpass, μ	Normalized variation in spectral irradiance										
		4-ft elevation						12-ft elevation				
		1	2	3	4	5	6	2	3	4	5	6
Clear avg		5.716	5.820	5.772	5.835	5.847	5.777	5.725	5.620	5.525	5.504	5.431
1	0.240 to 0.300	67.0	102.5	81.2	102.6	102.9	101.7	100.7	99.0	97.2	96.8	127.5
2	0.300 to 0.355	92.9	102.7	106.2	98.8	103.2	97.7	101.0	99.1	97.5	97.0	104.4
3	0.340 to 0.380	95.6	97.3	99.1	97.6	97.8	101.9	103.7	96.4	103.0	102.5	101.2
4	0.376 to 0.425	96.9	99.9	100.4	97.7	101.6	100.4	102.2	101.6	99.7	101.2	99.5
5	0.430 to 0.510	98.5	99.8	99.0	99.3	99.8	101.3	100.2	99.8	100.8	95.9	100.9
6	0.525 to 0.610	98.8	100.3	99.7	99.4	100.0	100.6	101.2	99.1	100.6	99.7	100.1
7	0.610 to 0.720	98.7	99.3	99.7	99.7	100.0	101.0	99.7	100.0	100.0	99.0	99.6
8	0.710 to 0.810	99.4	99.1	99.7	100.0	99.7	100.0	99.7	100.0	100.6	99.1	100.0
9	0.750 to 0.900	99.6	99.6	99.8	99.5	99.7	99.9	100.3	100.1	100.5	100.3	99.9
10	0.800 to 1.000	99.4	99.6	100.5	100.3	100.2	100.1	100.9	100.8	100.0	99.3	98.8
11	1.025 to 1.600	100.0	100.6	100.9	100.2	100.4	99.8	100.9	100.4	100.6	99.5	98.8
12	1.500 to 2.200	101.4	101.4	99.6	100.7	100.0	98.8	100.6	100.5	99.7	99.4	98.0

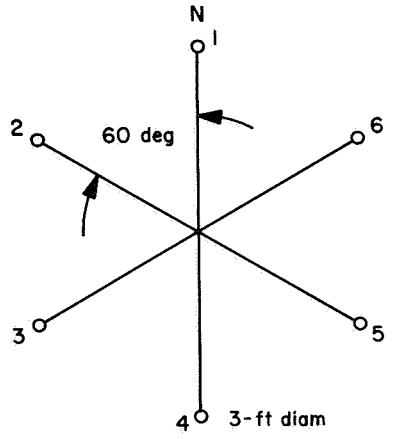

RADIOMETER POSITION

Summary. In Table 69, the environmental specification is compared in summary form with all the environmental parameters attained, as presented in the data packages. The requirements as presented are intended to provide test control to specified conditions to ensure compatibility with the mission environments. The requirements include margins based on uncertainty in the test conditions and knowledge of the space environment. The purpose of the margins in the requirements is to ensure that the spacecraft-design configuration is adequate for flight in both a functional sense, for electronic and mechanical equipment, and in a thermal sense, to provide assurance that the proper temperatures exist for the equipment to function.

Several minor changes were made in the M67-2 specification, where the integrity of the test was unaffected. Specifically, the changes were in the method of specifying launch pressure profiles and the angle of incidence, as discussed previously.

Table 69. Specified and actual M67-1 systems FA solar thermal–vacuum test environments

Test requirement	M67-1 requirements	Pretest M67-1, data package measurements	Post-test M67-1, data package measurements
Chamber launch-pressure-profile simulation	Profiles: $\dot{P} \approx$ 16.5 to 18.7 @ 45 s P of 50 torr in 58 to 66 s	For profile simulation Max $\dot{P}$ = 15.5 torr/s (Criteria changed to try to *attain* $\dot{P}$)	Phase I, $\dot{P}$ = 14.5 @ 30 s Phase II, $\dot{P}$ = 15.8 @ 30 s Actual M67-1 rates
Vacuum level	Continuous $< 1 \times 10^{-5}$ torr	NA	Actual M67-1 data: 5 to 9 $\times 10^{-6}$ in all phases. No anomalies identified
Chamber effective heat-sink temperature	$< -250°F$	Not measured for *Mariner* Venus 67 configuration; previous data indicated −200 to −210°F (HAC *birdcage*)	Not measured for *Mariner* Venus 67 configuration
Total irradiance level Tolerance on level or measurement	Variable 100 to 290 W/ft^2 Measurement ±2%	NA	110 to 294 W/ft^2 (Actual measurement by cone) $> \pm 2\%$
Uniformity of total irradiance	±5% at three defined reference planes	4-ft elevation: 92 to 102 W/ft^2, $\approx \pm 5\%$ 12-ft elevation: 88 to 96 W/ft^2, $\approx \pm 5\%$	4-ft elevation: 92 to 102 W/ft^2, $\approx \pm 5\%$ 12-ft elevation: 88 to 96 W/ft^2, $\approx \pm 5\%$
Beam geometry Angle between any incident solar radiation and the surface normal to the test plane (test plane parallel to top of spacecraft bus)	6-ft diam $< 2°$	6-ft diam 2°37′35″ max measured angle	6-ft diam 2°36′46″ max measured angle
Uniformity of spectral irradiance	$<$ 2% spatial and temporal for each filter	Measurements not accurate in UV. Specification met as far as can be determined from the data	Measurements not accurate in UV. Specification met as far as can be determined from the data
Instrumentation Irradiance monitor sensor size Spectral uniformity filter requirements Calibration period	 $\leq$ 4 cm^2 Nos. 4 to 6 from 0.2 to 0.4 μ Nos. 3 to 4 from 0.4 to 0.75 μ Nos. 3 to 4 from 0.75 to 2 μ at defined locations $<$ 3 mo prior to test all instruments		

c. Significance of non-space environment for M67-2 thermal–vacuum test.

Uniformity of total irradiance. The specified requirement for a 4-cm² sensor was for uniformity within ±5% of the mean level for two reference planes. Figures 129 through 132 present the data taken prior to, and after, the M67-2 test. Figure 129 compares uniformity mappings in polar coordinates taken before and after the test at the 4-ft elevation. Figure 130 compares the mappings taken before and after the test at the 12-ft elevation. Figures 131 and 132 compare the 12-ft to the 4-ft mappings taken before and after the test, respectively. The purpose of the comparisons is to evaluate the stability of the distribution of solar energy with respect to time. The comparisons also yield information on the variation in a plane and with depth. In a plane, the variation of solar energy for a 4-cm² sensor, which is dependent on the accuracy of the data supplied (supposedly, ±2%), is only slightly >5%, being 6% at the worst case measurement for the extreme edge and the center of the beam (see Fig. 129).

The stability of the energy distribution with respect to time, as indicated from the supplied data, varied to a maximum 4 to 5% for certain areas in the planes of measurement (see Fig. 129). The temporal variation in Fig. 130 was less severe than in Fig. 129.

The depth change with respect to position is illustrated in Figs. 131 and 132. For example, from Fig. 132, one observes that the maximum depth percentage difference is ≈7 to 8% (94 to 102 W/ft²).

To summarize the data presented, one can conclude that the variation in a plane is <5% in most of the beam and <6% in all of the plane. In depth, a percentage difference of 7 to 8% is possible. This means that the maximum volumetric percentage difference is on the order of 14%. From Fig. 131, one notes the difference is as much as 16% at the very edge but is 14% for the beam for all practical purposes.

The significance of these variations is minor for the *Mariner* Venus 67 configuration, since the spacecraft presents essentially a plane intercepting disc at about the 12-ft elevation. Variation with depth is not critical for this spacecraft, and the uniformity in the 12-ft plane is within ±6%. The change of energy distribution with time remained within the 6% band and is not significant as long as post- and pretest spacecraft mappings are performed for evaluation of the effect. The beam, for all practical purposes, met the specification (±5%) in a plane. A waiver was not written for the 6% band, since it represented only a very small portion of the outside edge of the 6-ft-diam beam.

Angle of incidence. The specified angle of incidence for the worst ray to the plane of the spacecraft was 3 deg. The measured values are presented in Table 70, along with two figures that illustrate the measurement location/orientation. The requirement was met.

Table 70. Measured values for angles of incidence, M67-2

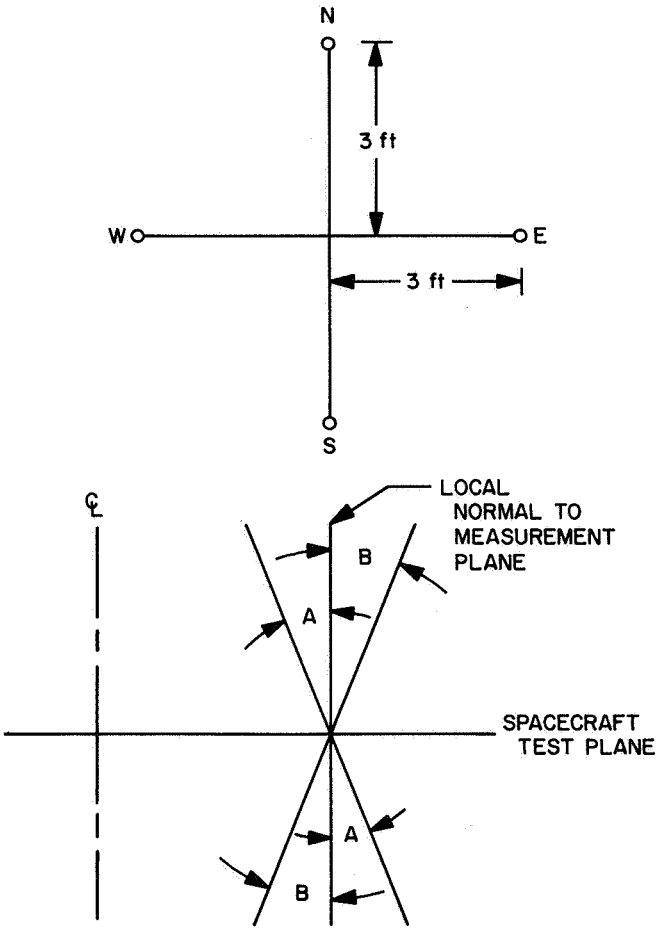

Position	Angle of incidence, deg			
	Pretest M67-2, angle A	Post-test M67-2, angle A	Pretest M67-2, angle B	Post-test M67-2, angle B
North	1°57′48″	2°4′6″	2°7′16″	2°12′6″
South	1°40′44″	1°49′18″	2°36′46″	2°46′27″
East	1°31′	1°56′43″	2°1′15″	2°4′54″
West	1°49′3″	1°38′6″	1°44′6″	2°33′56″

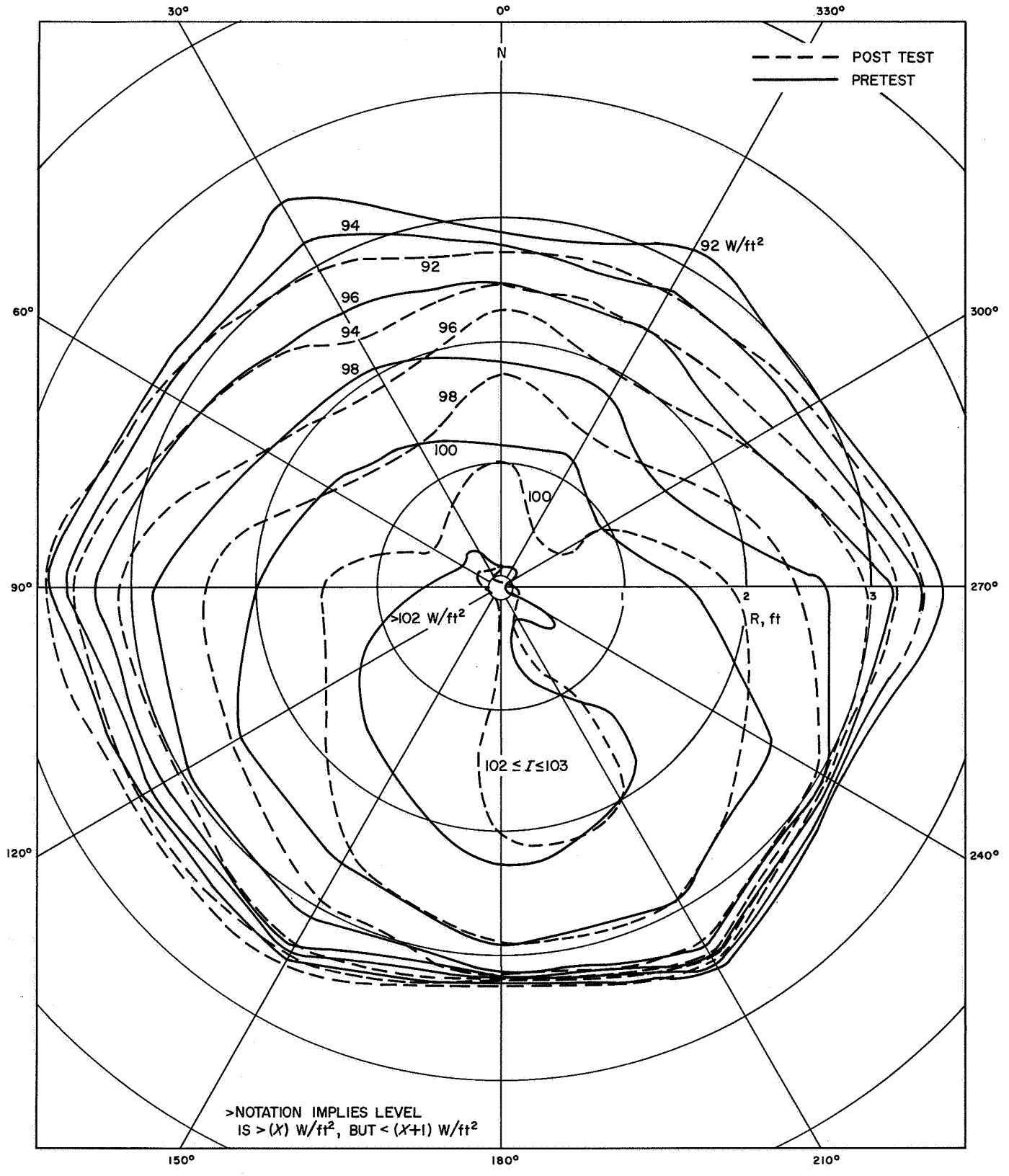

Fig. 129. Total irradiance uniformity mapping for 4-ft elevation, thermal–vacuum pretest and post-test of M67-2

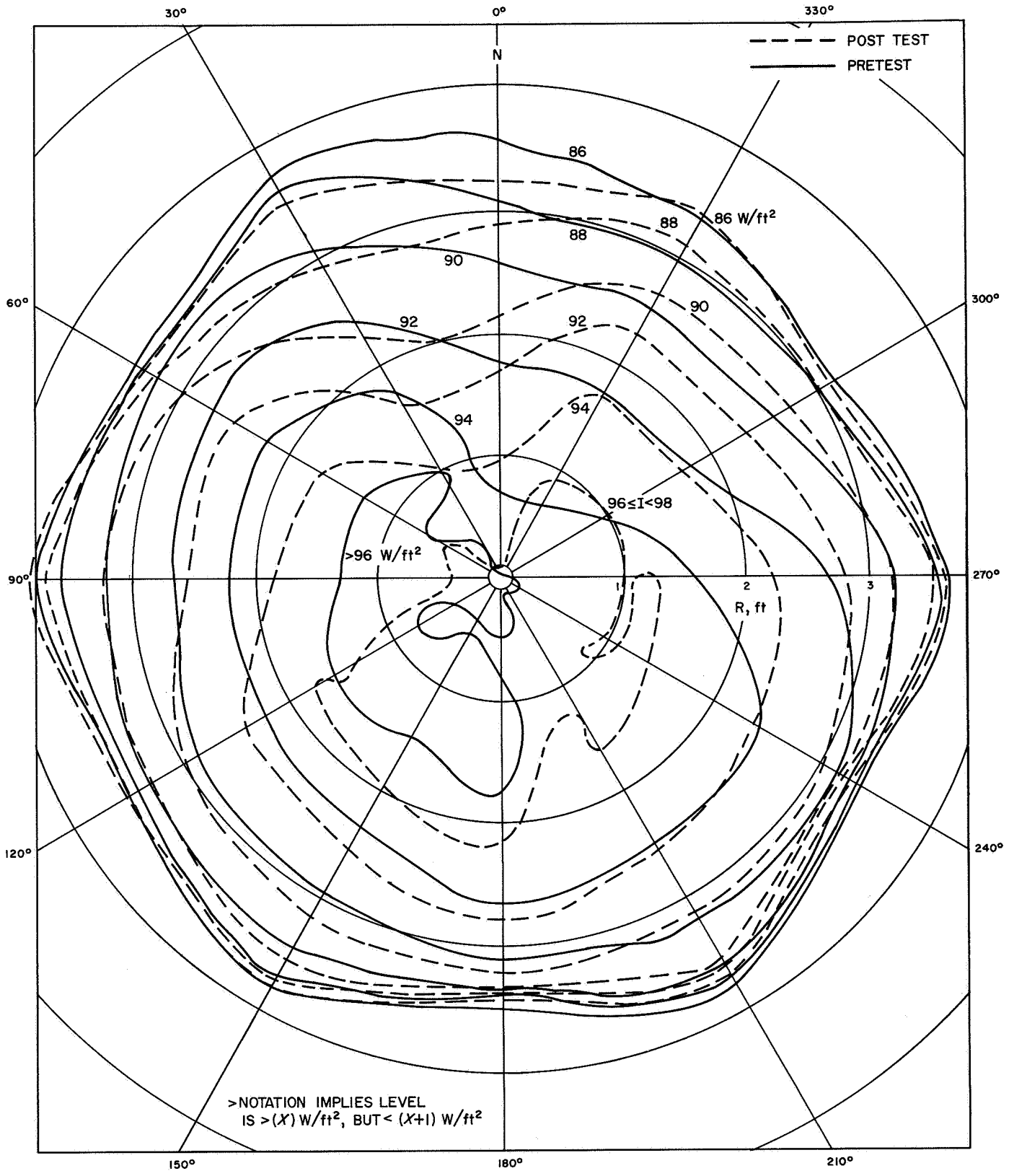

Fig. 130. Total irradiance uniformity mapping for 12-ft elevation, thermal–vacuum pretest and post-test of M67-2

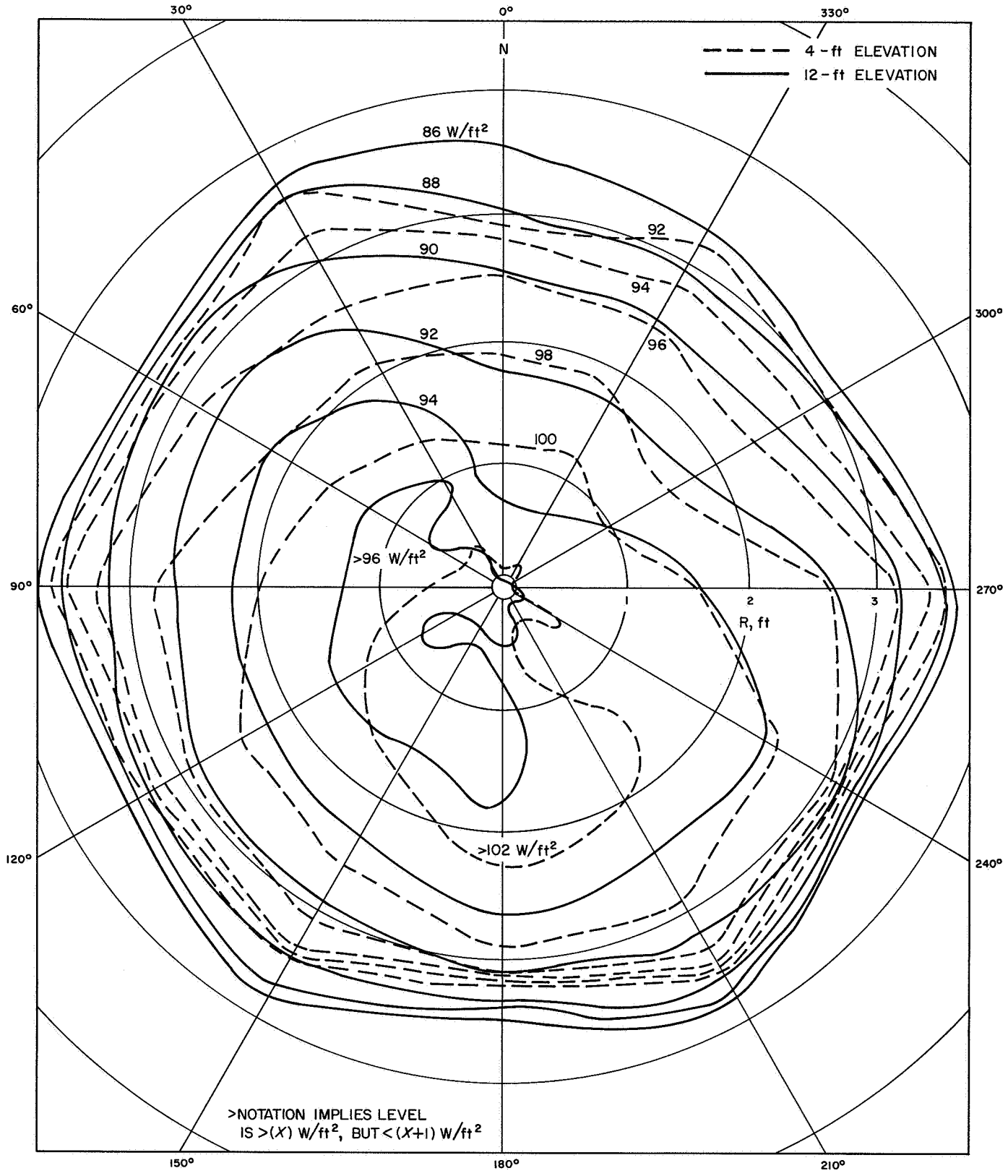

Fig. 131. Total irradiance uniformity mapping for 4- and 12-ft elevations, thermal–vacuum pretests of M67-2

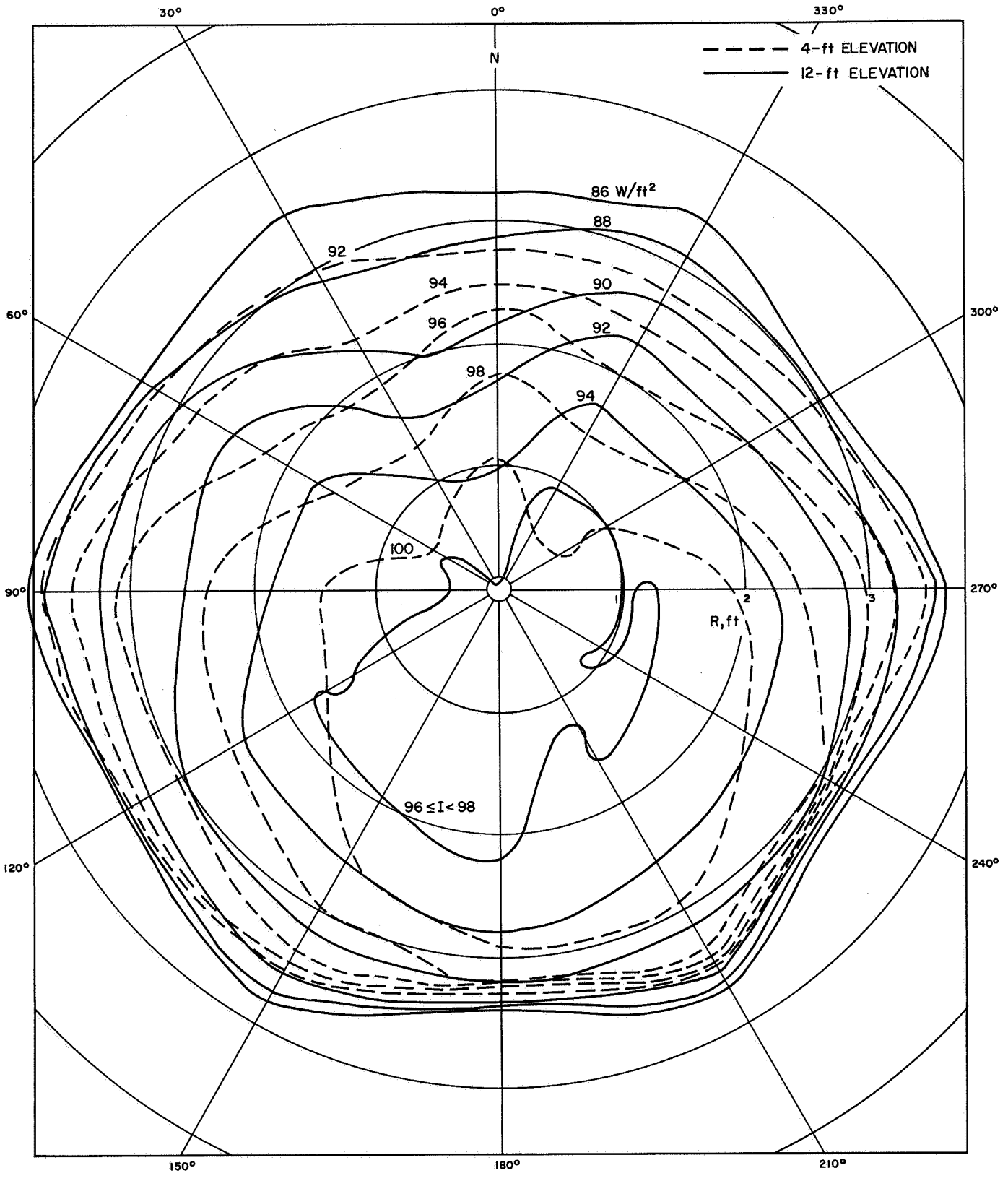

Fig. 132. Total irradiance uniformity mapping for 4- and 12-ft elevations, thermal–vacuum post-test of M67-2

Spectral irradiance uniformity. The generally accepted variation in spectral irradiance is ±2% at each defined location for each filter. Tables 71 and 72 reveal the data as reduced through several normalizations in terms of 100% for each reading. The data quality is affected by the following two factors:

(1) Measurements in the UV (filters 1, 2 and 3) are difficult to make, and the variations indicated are believed due to the measurement error rather than spectral non-uniformity.

(2) Variations at other levels on pretest M67-2 data are probably due to the fact that the ratio

$$\frac{\int J_\lambda \tau_\lambda d_\lambda}{\int J_\lambda d_\lambda}$$

was obtained with an average $\int J_\lambda d_\lambda$ for each twelve-filter scan, rather than an individual $\int J_\lambda d_\lambda$ for each filter. Therefore, fluctuations at the time of each filter reading would not be discernible.

J_λ = spectral radiant intensity

τ_λ = spectral transmittance

The data, given in Tables 71 and 72, although not of high quality, indicate good uniformity of spectral irradiance, in general. Nevertheless, in M67-2 pretest measurements, readings taken at positions 2 and 3 for filter 10 at 12-ft elevation were marginal. In M67-2 post-test measurements, readings taken at positions 4 and 6 for filter 8 at 12-ft elevation were also marginal. At position 5, the readings for filter 4 at 12-ft elevation were questionable. These questions might well be due to the error in measurement, rather than to shifts in spectral uniformity.

Summary. In Table 73 the thermal–vacuum environment specification is compared in summary form with all the environmental parameters attained, as presented in the data package.

The requirements, as presented, are intended to provide test control to specified conditions to ensure compatibility with the mission requirements. The requirements include margins based on uncertainty in the test conditions and knowledge of the space environment. The purpose of the margins in the requirements is to ensure that the spacecraft-design configuration is adequate for flight in both a functional sense for electronic and mechanical equipment and, in a thermal sense, to provide assurance that the proper temperatures exist for the equipment to function.

d. Significance of no TA systems test. For the *Mariner* Venus 67 mission, there was no system level TA thermal testing. This was because no PTM spacecraft was assembled. The non-existence of a TA systems level test seems to be in conflict with the normal environmental test philosophy; however, when one examines the origin of the *Mariner* Venus 67 mission and the specific hardware utilized, the testing approach implemented is adequate. Since the *Mariner* Venus 67 spacecraft was a vehicle whose design had been proven by extensive testing for the *Mariner* Mars 1964 mission, as well as by over 2 yr of actual space exposure, the TA systems test objectives had already been accomplished; that is to say, a qualified design existed. Under these circumstances, the decision not to run a TA test on a systems level is a logical conclusion, as long as the following conditions exist:

(1) The functional operation of the assemblies and system is no more severe than that which was previously qualified.

(2) The variations from the *Mariner* Mars 1964 mission in the conditions under which the assemblies would be expected to operate are minimal in number, and affected items can be adequately requalified in assembly testing.

(3) The FA systems level testing is extensive and verifies items (1) and (2) above, as well as the normal FA objectives – namely, verification of the quality of the flight hardware consistent with the previously qualified design.

The conditions were all met by the testing program performed for *Mariner* Venus 67. As a consequence, the significance of not having run a thermal–vacuum TA systems level test was that a minimum risk existed. The thermal testing on the TCM provided confidence in the thermal control configuration, and although some of the internal power dissipation levels were in error, testing condition 2 above was indicated as no problem. The backup flight spacecraft essentially validated all of the conditions, as well as provided assurance that there would be no major concerns about testing the intended flight vehicle in a new facility under a Venus solar simulation.

Table 71. Pretest spectral irradiance uniformity measurements for M67-2 thermal–vacuum test

Filter No.	1% transmission bandpass, μ	Normalized variation in spectral irradiance										
		4-ft elevation						12-ft elevation				
		1	2	3	4	5	6	2	3	4	5	6
Clear avg		5.889	5.916	5.958	6.058	6.097	5.997	5.803	5.805	5.683	5.722	5.634
1	0.240 to 0.300	201.7	135.1	135.9	103.8	83.5	137.0	99.4	79.6	97.3	97.9	128.5
2	0.300 to 0.355	100.9	105.6	102.0	99.8	104.5	107.1	99.4	99.5	97.4	106.6	100.6
3	0.340 to 0.380	103.7	104.3	102.1	101.1	104.5	105.7	99.4	99.5	97.4	100.8	102.0
4	0.376 to 0.425	100.9	100.2	100.9	101.4	100.8	102.8	99.5	98.3	98.6	99.3	101.4
5	0.430 to 0.510	101.3	101.0	98.6	100.5	100.8	101.9	99.4	99.5	100.2	99.7	100.2
6	0.525 to 0.610	101.4	101.0	101.6	100.9	101.0	101.8	99.4	98.9	99.8	100.0	99.9
7	0.610 to 0.720	100.9	100.3	101.0	100.6	100.7	101.7	100.0	99.4	100.1	99.7	100.3
8	0.710 to 0.810	100.9	101.4	101.1	100.7	101.4	100.7	100.5	100.5	100.0	100.1	100.2
9	0.750 to 0.900	100.4	100.5	100.4	100.3	100.7	100.7	100.7	100.5	100.3	100.8	100.9
10	0.800 to 1.000	98.6	99.4	99.6	99.7	99.5	99.0	102.8	102.8	101.8	101.7	101.1
11	1.025 to 1.600	100.3	100.8	100.9	101.4	100.9	100.4	100.7	100.4	100.4	100.5	99.5
12	1.500 to 2.200	100.9	100.6	100.4	101.2	101.8	101.0	100.3	99.5	99.1	100.7	99.1

The expression

$$\frac{\int_{\lambda_a}^{\lambda_b} J_\lambda \tau_\lambda d_\lambda}{\int_{\lambda_a}^{\lambda_b} J_\lambda d_\lambda}$$

is reduced from empirical measurements presented in the data package. This ratio is taken for each filter at each location which then is normalized to a percentage of the average ratio for that filter. The principal assumption made in this analysis is that the variation in the clear reading is small. This assumption could be avoided if a clear reading were taken with each filter reading.

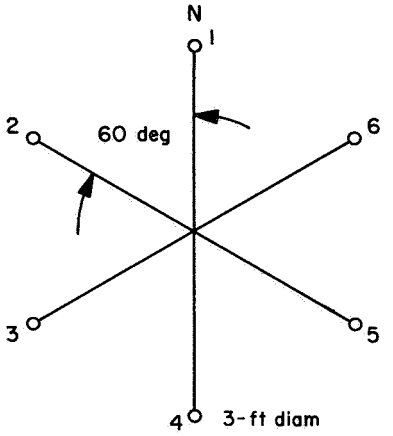

RADIOMETER POSITION

Table 72. Post-test spectral irradiance uniformity measurements for M67-2 thermal–vacuum test

Filter No.	1% transmission bandpass, μ	Normalized variation in spectral irradiance										
		4-ft elevation						12-ft elevation				
		1	2	3	4	5	6	2	3	4	5	6
Clear avg		5.773	5.820	5.941	5.995	5.910	5.752	5.606	5.690	5.728	5.717	5.558
1	0.240 to 0.300	105.9	107.5	109.1	82.6	93.0	105.6	123.6	179.0	83.9	78.8	87.1
2	0.300 to 0.355	91.9	107.6	101.2	96.8	100.5	104.9	97.9	96.8	95.9	110.4	99.5
3	0.340 to 0.380	89.1	100.0	100.2	96.5	102.3	104.6	97.9	95.8	104.6	95.5	117.2
4	0.376 to 0.425	100.4	102.1	100.6	98.0	99.9	101.0	99.6	99.9	100.1	96.8	101.6
5	0.430 to 0.510	98.4	99.6	101.1	98.9	99.7	100.4	100.9	99.9	101.2	98.7	101.1
6	0.525 to 0.610	100.0	98.9	98.8	100.3	99.9	100.1	100.5	101.4	100.4	98.2	101.2
7	0.610 to 0.720	99.6	100.8	98.8	100.4	99.9	99.5	101.1	100.2	100.3	98.5	100.9
8	0.710 to 0.810	98.9	99.4	100.1	98.5	99.6	99.4	100.5	100.3	102.4	98.9	102.3
9	0.750 to 0.900	101.0	101.2	101.3	101.4	100.1	100.0	99.9	99.9	100.4	99.4	100.4
10	0.800 to 1.000	100.2	100.9	100.6	101.2	101.2	100.8	98.9	99.5	99.6	98.9	99.2
11	1.025 to 1.600	99.8	100.3	101.4	100.4	100.6	99.6	100.0	99.8	99.8	98.9	99.4
12	1.500 to 2.200	100.0	100.9	100.9	100.6	99.3	99.5	100.0	100.5	99.9	99.6	98.9

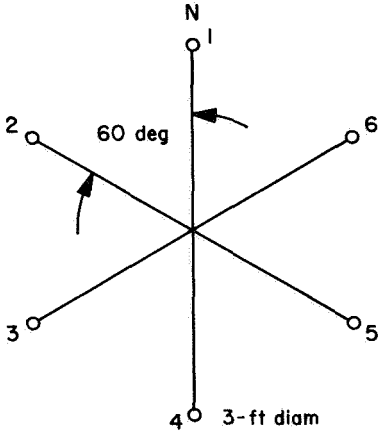

RADIOMETER POSITION

Table 73. Specified and actual M67-2 systems FA solar thermal–vacuum test environments

Test requirement	M67-2	Pretest M67-2 data package	Post-test M67-2 data package
Chamber launch-pressure-profile simulation	Max $\dot{P}$ is 16.5 to 18.7 torr/s in 25 to 65 s	Phase I $\dot{P}$ = 14.5 torr/s @ 30 s Phase II $\dot{P}$ = 15.8 torr/s @ 30 s Actual M67-2 rates	Phase I $\dot{P}$ = 18.4 torr/s @ 17.5 s; $\dot{P}$ = 17.4 torr/s @ 21 s Phase II $\dot{P}$ = 16.8 torr/s @ 25 s; $\dot{P}$ = 19.2 torr/s @ 15 s Actual M67-2 rates
Vacuum level	Continuous $< 1 \times 10^{-5}$ torr	Actual M67-2 data: 5.9×10^{-6} torr in all phases. No anomalies identified	Actual M67-2 data: 4.5 to 5.0×10^{-6} torr in all phases; leak detected in Phase I
Chamber effective heat-sink temperature	$< -250°F$	Not measured for *Mariner* Venus 67 configuration	Not properly measured for *Mariner* Venus 67
Total irradiance level Tolerance on level or measurement	Variable 112 to 290 W/ft^2 ±2% on level required	110 to 294 W/ft^2 (Actual measurement by cone) $> \pm 2\%$	110 to 294 W/ft^2
Uniformity of total irradiance	±5% at two defined reference planes	4-ft elevation: 92 to >102 W/ft^2 12-ft elevation: 86 to >96 W/ft^2	
Beam geometry Angle between any incident solar radiation and the surface normal to the test plane (test plane parallel to top of spacecraft bus)	6-ft diam < 3 deg	6-ft diam 2°46′27″ max measured angle	
Uniformity of spectral irradiance	Measured; no requirement	Measurements not accurate in UV; in general, data acceptable	
Instrumentation Irradiance monitor sensor size Spectral uniformity filter requirements Calibration period	≤ 4 cm^2 Nos. 4 to 6 from 0.2 to 0.4 μ Nos. 3 to 4 from 0.4 to 0.75 μ Nos. 3 to 4 from 0.75 to 2 μ at defined locations Same unless controlled by another Lab standard		

2. Comparison of assembly level TA and FA test temperatures with actual flight temperatures. The assembly-level thermal–vacuum tests performed consisted of two types with differing objectives. Type-approval tests were intended to qualify designs and were intentionally severe to ensure design margins over flight predictions. Flight acceptance tests were intended to be as severe as the most extreme flight environment and to verify the quality of the flight equipment. To determine whether these objectives have been accomplished, it is necessary to compare test temperatures with actual flight temperatures. Presented in Table 74 are *Mariner* Venus 67 maximum- and minimum-flight temperatures from initial earth cruise to Venus cruise post-playback, as well as assembly level TA and FA test temperatures.

The data in Table 74 indicate that the flight temperatures experienced were well within the assembly level FA and TA test limits, with one exception – the solar panel FA temperatures. This is not altogether unexpected, since the FA test margins were deliberately set near the expected flight extremes to prevent possible degradation of the flight solar panels. Battery FA thermal–vacuum tests were not performed for the same reason. The margins of FAT levels over flight levels ran approximately 60 and −30°F for the bus equipment,

Table 74. Assembly-level test temperatures and actual flight temperatures

Item	Telemetry channel	Assembly FAT levels		Assembly TAT levels		Flight temperatures		
						Cruise		Midcourse
		Min	Max	Min	Max	Min	Max	
Bay I power & pyro (flight location)	401	32	131	14	167	61	67	95
Bay II PIPS (flight location)	421	Not req.		40	167	46	57	119
Midcourse motor fuel	217	32	131	14	167	56	67	79
Propulsion N_2	408	32	131	14	167	52	62	112
Primary sun sensor	430	32	131	14	167	47	105	98
UV photometer	437	32	131	14	167	46	61	77
Bay III DAS (flight location)	402	32	131	14	167	59	69	74
Plasma probe	422	32	239	14	275	105	222	78
Bay IV data encoder & command (flight location)	423	32	131	14	167	56	70	63
$-X/+Y$ N_2 bottle	219	32	131	14	167	57	69	63
TRD chassis	438	−4	122	14	122	45	59	57
Bay V data storage & radio (flight location)	404	32	122	14	158	53	68	56
Bay V VCO (2RA2)	424	32	131	14	167	59	76	65
Bay V tape (16A1)	436	32	122	14	158	54	69	56
Bay VI radio (flight location)	405	32	131	14	167	57	75	60
Bay VI aux. oscillator 1	414	32	131	14	167	62	74	66
Bay VI aux. oscillator 2	418	32	131	14	167	62	75	66
Bay VII A/C & CC&S (flight location)	426	32	131	14	167	54	60	64
Bay VIII power regulator	407	32	131	14	167	80	85	105
Battery	428	Not req.		32	140	61	65	70
$+X/-Y$ N_2 bottle	218	32	131	14	167	59	66	67
Canopus sensor	410	0	100	14	167	56	61	67
High-gain antenna	419	−245	131	−285	167	−198	−130	−5
Magnetometer preamp end	439	−40	122	−50	167	2	7	25
Low-gain antenna mast (at magnetometer)	431	−160	131	−200	167	−90	−68	25
Solar panel 4A1	409	140	239	−180[a]	284	119	245	48
Solar panel 4A5	429	140	239	−180[a]	284	118	245	50
A/C jet, $-Y$ *P*	425	−45	215	−65	255	−12	56	−23
A/C jet, $+X$ *RY*	406	−45	215	−65	255	−25	50	21
A/C jet, $-X$ *RY*	433	−45	215	−65	255	−24	49	−32

[a]During thermal shock.

with larger margins for external equipment. These temperature ΔTs can be attributed to *margin factors* added as a quality verification tool and to account for uncertainties in the predicted flight and test thermal environments.

Figure 133 compares the flight midcourse thermal shock and the assembly level TA thermal shock test on the solar panels. The test thermal shock, based on the worst-case environment of complete loss of sun on the solar panel, attained a much lower temperature than the flight thermal shock in which at most only partial shadowing occurred. Also, the rate of temperature change is higher during the test shock than during the slow pitch and roll turns of the midcourse maneuver. This is a result of the simplified mechanization of the lights-*off*, lights-*on* test environment and is considered to be a reasonable margin over the flight rate of temperature change.

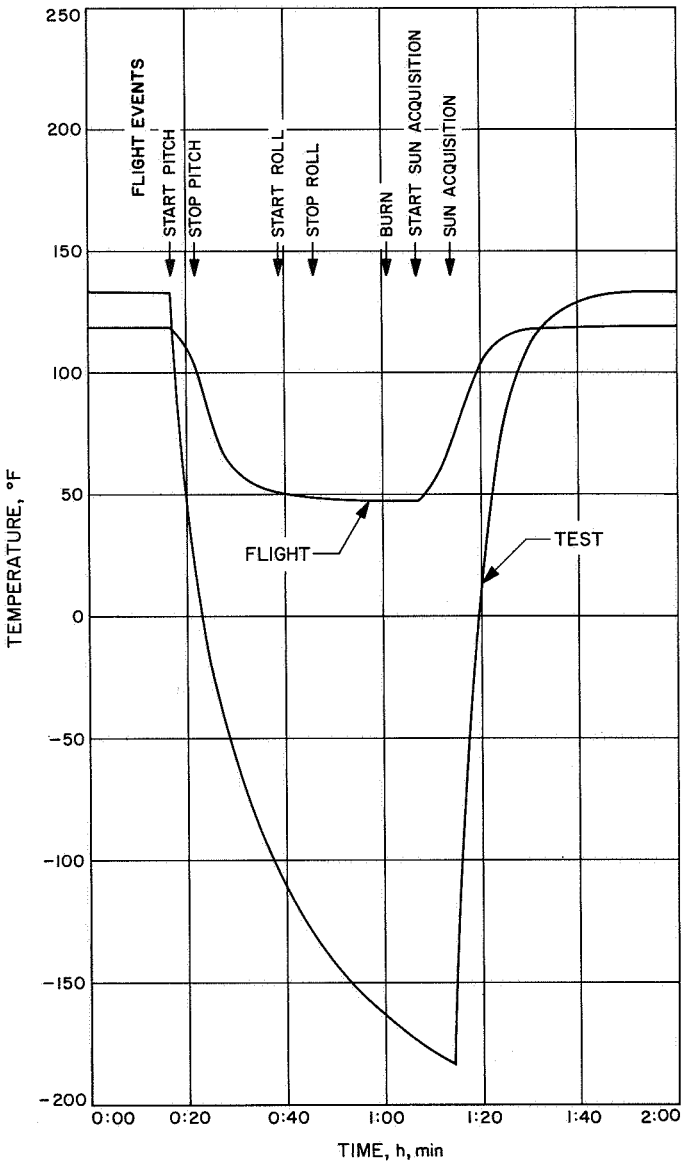

Fig. 133. Comparison of thermal shocks for flight midcourse and assembly-level TA test

Thus, the following conclusions can be made with regard to *Mariner* Venus 67 flight results in comparison with assembly level testing:

(1) TAT and FAT levels were adequate.

(2) In general, test levels for external assemblies were more conservative than bus assemblies, but necessarily so, because of uncertainties in the expected flight environment.

VII. Recommendations for Future Programs

A. General

It can be said that, in general, the *vibration* test requirements for a spacecraft depend on the *launch vehicle* environment. On the other hand, the *thermal–vacuum* test requirements depend primarily on the *particular mission* requirements. Design and mission changes that occur during the course of a Project affect the qualification of the spacecraft system. *Design changes* usually mean *requalifying a part* of a subsystem, whereas a *mission change* requires a *complete requalification* of the system. During the *Mariner* Venus 67 program, there were four major design changes and one major mission change.

For a project based on modification of hardware that was developed or fabricated for a previous project, it is essential to determine early in the program the appropriate amounts of repetitive TA testing desired. This is especially important since the decision not to repeat TA testing of an item implies high expectation that the item will pass, if subjected to, the test. One can infer the skill in such decision making *a posteriori* from TA failure rates. The fact that *Mariner* Venus 67 TA failure rates were $<50\%$ would indicate that the tests were very conservatively selected. The fact that TA failure rates were higher than FA failure rates can be construed to justify that assumption.

One of the more significant considerations during the *Mariner* Venus 67 testing program was what tests were

required to requalify a subsystem that had failed and had been reworked to some degree. The *retest philosophy* that evolved from the *Mariner* Mars 1964 and the *Mariner* Venus 67 testing programs is recommended for future programs. If a subsystem has a failure, it is certainly necessary to requalify that portion of the subsystem that has had to be reworked. If the subsystem is a TA unit, it is recommended that the reworked portion of the subsystem be required to pass a TA test and, also, multiple FA tests if time permits. If the subsystem is an FA unit, then the reworked portion of the unit should be required to pass an FA test. However, if during the requalification, a failure occurs in the non-reworked portion of the subsystem, then it should not necessarily invalidate the test, because that portion of the subsystem would have already been qualified. In each case, though, one should evaluate the failure to ascertain whether or not a possible design deficiency has been uncovered.

B. Dynamics

Response-controlled testing of the solar panels constituted part of the overall solar panel vibration test program for the *Mariner* Venus 67. Response control (producing a desired response amplitude), rather than input control (producing a desired input at the mounting points), was required for the panels due to input-point loading caused (1) by the relatively large size and distinct resonances and (2) by fixturing problems caused by the interconnection between panels by dampers at the tips. At the low-frequency (high-mass) resonances, the panels interact with one another at the tips (through the dampers) and load the input (mounting) points, because of their relatively heavy weight. For these reasons, a pure input test could not properly reflect the effect on both the input and response of these two interactions. The response test was designed to produce a desired response in selected modes of the panel in its test configuration that resulted in panel stresses equal to the stresses experienced by the panel during the system test.

1. Need for response tests on future programs. If there is significant interaction of an assembly at resonance with its supporting structure at *identifiable* and important assembly resonances, then some form of response control should be considered for a program. The complexity of test procedures resulting from response control testing with the more physically desirable test produced should be weighed against the simpler test procedure of input control and the possibly improper test it produces. It may be sufficient (as has been done on many *Mariner* Venus 67 assemblies) to specify an input test with the input adjusted to produce proper response in the assembly at important resonances in its test configuration. (This type of test is actually a pseudoresponse test based on calculated or measured gains and a desired response.) If actual response control is required for a unit, then by using careful procedures and considering the lessons learned for *Mariner* Venus 67, it should be possible to conduct proper and safe tests.

2. Guidelines for conducting response-control tests. The capability to conduct response-control testing has not, in fact, been demonstrated. Valuable lessons were learned and some precautions and procedures required for future applications of this method are clearly evident. Details of the attempted solar panel test are applicable only to other similar solar panel tests, but the following recommendations apply, in general, to any response-control testing:

(1) The need for *detailed pre-planning* is evident. Of necessity, such a test involves several interdependent sectional responsibilities, and it is essential that all concerned understand the test purpose, the plan, and the required contributions.

(2) Response tests can *not* be treated as *production tests.* The presence of cognizant personnel during tests is a definite requirement.

(3) *Complete documentation* of all requirements in test procedures and test specification is a necessity. The results of tests must be completely documented.

Some conclusions applicable specifically to solar panels can be derived from the test history:

(1) Low-level modal testing of each panel to be tested is required to *identify* exactly the *modes* to be excited.

(2) The very lightweight structure of the panel requires the *careful locating* of the response control *accelerometer* at a point with a known response relationship to all other significant panel locations.

(3) *Knowledgeable personnel* must be *present* during testing to assure proper test procedure and to determine the proper disposition of test anomalies and deviations.

C. Thermal–Vacuum

The sensitivity of the *Mariner* Venus 67 spacecraft to the testing environment was noticeably small, especially the significance of solar irradiance changes. However, there are several test-associated deficiencies related to thermal–vacuum that became evident during the *Mariner* Venus 67 testing and which will be discussed in the following paragraphs. While the impact on *Mariner* Venus 67 was not felt, the importance to future testing could be significant. This section will address itself to two areas: (1) the thermal–vacuum facility at JPL and (2) the manner of conducting the test.

The JPL thermal–vacuum facility provides perhaps the finest simulation of the space environment available in the world today. However, future projects need to concern themselves with obtaining accurate information as to what the environment really is and the significance of the nonduplicated parameters. For example, one cannot assess the significance of either heat sink or solar spectrum errors due to lack of information defining the effective sink or the spectrum. It is not known what part the sink error played in the implemented design change to the thermal control configuration, although it was recognized as a possible contributor. It is essential that the facility parameters be documented for each test program and that the stability of the parameters be verified. When this is done, then meaningful test comparisons can be made and the effects on the vehicle determined. One of the major problems in getting adequate measurements is having adequate instrumentation. Adequate instrumentation should be made available to the facility for the environment to be properly evaluated.

The simulator testing should be performed with better control on conditions and with best information to avoid risk of having to redo testing or possible damage to the spacecraft. For example, the solar irradiance levels were altered because of calculation errors midway in the testing, and the information was not properly distributed. The information was obtained through observation of the temperature data, rather than by an announced and discussed change. This could have resulted in lost test time had the *Mariner* Venus 67 spacecraft not been so insensitive to the solar changes. It is recommended that complete and certified procedures be utilized for all functions and that deviations from them be allowed only after consultation with the appropriate personnel, one of whom should be the test director.

It has been observed that some of the spacecraft test performance in the past has not exercised the TA systems level test vehicle in conditions that provide a sufficient test margin over FA testing. This can, and should, be accomplished by utilizing an internal heat source — either the emergency heaters or some other appropriate device — to raise the assemblies to temperatures near the TA assembly levels and the spacecraft operated in normal, high- and low-power test modes.

Due to some of the transients experienced during midcourse, it appears desirable to consider the merits of using some means of simulating the manner in which the environment interacts with the spacecraft to determine the adequacy of the design to accommodate the changes. To date, these effects have been handled analytically or by TCM testing.

D. Electromagnetic Interference

1. Breadboard or prototype subsystem testing. During the DFR *Mariner V* testing period, it became evident that an early delivery of a prototype subsystem would have helped considerably in the integration effort. Since time is a vital element in spacecraft programs, the time gained in the early portions of a test program is of great value. It is recommended that, in future programs, a breadboard or *prototype* model of any *new electronic subsystem* added to a spacecraft system be made available for inter-subsystem evaluation and tests.

2. Adequately shielded RF test facility. An adequately shielded RF test facility should be provided for future radio subsystem integration efforts. The merits of such a test facility should be evaluated by considering its overall contribution to the effectiveness of a test program. Among alternatives that should be evaluated are: RF shielding the Spacecraft Assembly Facility (SAF) and erecting a large shielded enclosure within that building.

Experience on the *Mariner V* program has shown that a noise-free environment cannot always be obtained during any given 24-h period. As a consequence of the changing ambient noise environment, the spacecraft test sequences must be revised in short notice; this, in turn, can minimize the effective use of the allotted test time.

3. Low-noise components. It is recommended that all subsystem cognizant personnel attempt to replace known noise-generating components in their equipment with

lower-noise substitutes, whenever it is feasible, to reduce the spacecraft background noise level. The individual cognizant personnel on spacecraft subsystems develop an intimate knowledge of their electronic equipment and its components. In the course of their work they will at times determine that acceptable less noisy component substitutes have been developed and are on the market. Each cognizant person should thus be urged to contribute to an incremental noise level reduction by his suggestion of specific component changes.

4. Interference to spacecraft radio subsystems. It is recommended that the following steps be followed early in a spacecraft program to assure the successful integration of communications equipment or radio experiments:

(1) Determine the permissible noise levels in the receiver and transmitter bandwidths of both the spacecraft radio equipment and the OSE.

(2) Specify that adequate filters be incorporated in all radio subsystems before they are incorporated into the spacecraft.

(3) Specify and procure noise-measurement equipment required to make noise measurements at levels and frequencies determined in (1), above.

E. Magnetic Control

Magnetic control efforts in the *Mariner* Venus 67 Program were severely restricted by the fact that virtually all hardware design, and even some items of hardware, were taken directly from the *Mariner* Mars 1964 Program. While that program had magnetic restraints, in general they were imposed too late in the program or with insufficient enforcement to be effective. Consequently, even with the majority of the *Mariner* Mars 1964 hardware not meeting its design requirements, there was very little opportunity to improve this situation on the *Mariner* Venus 67 spacecraft.

The magnetic field of this spacecraft was made lower by demagnetization, which was also believed to result in a slight improvement in magnetic stability. To make a significant improvement in magnetic control efforts, four principal recommendations are made.

First, develop a general design specification for low magnetic field hardware to contain design restraints and guidelines. Such a specification should be developed as part of a supporting research and advanced development program and should be made applicable to all JPL spacecraft in varying degree, based on the probability that the spacecraft or its hardware will be used for a magnetometer-carrying spacecraft.

Second, conduct studies in the following areas of magnetic control to improve the quality of these efforts:

(1) Thoroughly investigate the nature of magnetic stability. Develop definition and means of measuring this characteristic. Determine effects of vibration and weak magnetic fields on stability.

(2) Study magnetic shielding techniques, with special emphasis on shielding pieceparts, to contain high fields. Investigate external field stability as a consequence of these shielded sources.

(3) Develop techniques for estimating and predicting the magnetic field of subassemblies or pieceparts on the basis of their constituent materials.

(4) Develop improved mapping and data handling techniques that will permit extrapolation of multipolar fields to different points in space.

(5) Develop improved material and piecepart lists that will categorize the low magnetic field characteristics of such commonly used items. Categories should include susceptibility to perming, magnetic hardness, and magnetic stability.

These studies should not be delayed, waiting for a future program requiring magnetic control but, rather, should be established as a supporting research or advanced development program. They are essential to maintaining a state-of-the-art capability in magnetic control and as preparation for new programs with these requirements.

Third, establish a permanent, but not necessarily permanently staffed, magnetic facility for support of advanced hardware development programs involving magnetic restraints or test requirements.

Fourth, include magnetic control engineer on conceptual design team of future spacecraft programs that might carry fields and particle experiments.

Successful magnetic control is dependent on early injection into the initial design efforts. Magnetic control should be approached on the *systems level* where it could influence the arrangement of hardware on the spacecraft and where magnetic control costs could be developed to establish the degree of magnetic control costs to be supported by the program.

Appendix A

Mariner Venus 67 Environment Test Specifications

Extensive environmental tests were used in qualifying *Mariner* Venus 67 for its flight. The following subject-list of the tests performed indicates the thoroughness of the tests.

MCB-50138-ETS-A	Environmental Test, Low-Gain Antenna Damper
MCB-50317-ETS	Environmental Test, Solar Panel Cruise Dampers
MCK-50146-TAT	TA Test, Flight Command Subsystem
MCS-50254-TST	TST, High-Gain Antenna
MCV-50095-ETS	Pressure Transducer
MCV-50566-ETS	CC&S Test, FA
MCX-50243-TST	TST, Low-Gain Antenna
MCX-50259-TST	Antenna Cable (2W1–2W2)
MCX-50320-ETS	TA and FA Hybrid Radio Subsystem
MCX-50347-TAT	S-Band Cavity Amplifier and Power Supply
MVA-50640-TST	Qualification Test Requirements
MVA-50657-FAT	DFR Ultra-High Frequency Antenna
MVA-50658-FAT	DFR VHF Antenna
MVA-50659-TAT	DFR UHF Antenna
MVA-50660-TAT	DFR VHF Antenna
MVB-50587-TST	Vibration Qualification Test
MVD-50600-ETS	Planet Sensor Attitude Control
MVD-50619-TAT	Bipolar Analog-to-Pulse-Width Converter, Mark II
MVD-50644-ETS	Science Data Automation System
MVE-50593-ETS	Pyrotechnic Subsystem, TA and FA
MVE-50605-ETS	Separation Initiated Timer, FA
MVE-50606-ETS	Pyrotechnic Arming Switch, FA
MVF-50652	TA and FA Temperature Control
MVF-50652-ETS	Temperature-Control Reference, TA and FA
MVF-50592-FAT-A	Temperature-Control Louvers, TA and FA
MVK-50626-FAT-A	Flight Command Subsystem, FA
MVM-50596-ETS	Postinjection Propulsion Subsystem, TA and FA
MVM-50597-ETS	Pneumatic Regulator, TA and FA
MVM-50598-ETS	Rocket Engine, TA and FA

MVM-50599-ETS-A	Oxidizer Start Subsystem, TA and FA
MVN-50627-ETS	Data Encoder Subsystem, FA
MVP-50578-ETS	Power Supply System Case I, TA and FA
MVP-50579-ETS	Power Supply System Case VIII, TA and FA
MVP-50602-TST	System Level Qualification Testing
MVP-50622-FAT	Power Subsystem, Mark VI Battery, FA
MVP-50623-TAT	Power Subsystem, Mark VI Battery, TA
MVP-50661-ETS	Magnetic Testing & Demagnetization of Solar Panels
MVR-50641-ETS	Tape Recorder Subsystem, TA and FA
MVS-50595-ETS	UV Photometers, TA and FA
MVS-50612-FAT	Magnetometer
MVS-50620-ETS	Environmental Test, Plasma Probe
MVS-50625-ETS	Trapped Radiation Detector, TA and FA
MVV-50568-ETS-A	Attitude-Control Jet Assemblies
MVV-50590-FAT-A	Terminator Sensor
MVV-50591-FAT-A	Earth Sensor, FA
MVV-50594-ETS	Canopus Star Sensor
MVV-50601-ETS	Thrust Vector Control Actuator, TA and FA
MVV-50624-FAT	Attitude-Control Electronics, FA
MVV-50635-ETS	Attitude-Control Gas Actuator System
MVV-50645-TST	Sun Gate
MVV-50648-TST	A/C Acquisition and Cruise Sun Sensors, TA and FA
MVX-50631-FAT	FA Test, Low-Gain Antenna
MVX-50632-FAT	FA Test, High-Gain Antenna
MVX-50636-TAT	TA Test, Low-Gain Antenna
MVX-50637-TAT	TA Test, High-Gain Antenna
MVX-50649-FAT	Flight Acceptance Radio Subsystem, Cases V and VI
MVX-50653-ETS-B	DFR Subsystem, TA and FA
MVX-50662-FAT	S-Band Cavity Amplifier
MVX-50668-TAT	TA Radio Subsystem
SS 500103B	Environmental Test Specification, *Mariner* Venus 67 Flight Equipment, Power Subsystem, Solar Panel TA Requirements
SS 500104B	Environmental Test Specification, *Mariner* Venus 67 Flight Equipment, Power Subsystem, Solar Panel FA Requirements

30025	TA and FA Temperature Transducer
50595-ETS-AM-1	UV Photometers, TA and FA
50625-ETS-AM-1	Trapped Radiation Detector, TA and FA

Appendix B

Change in Assembly Sinusoidal Vibration From *Mariner* Mars 1964

For the *Mariner* Venus 67 Program, separate sinusoidal and noise vibration testing of TA assemblies replaced the combined sine-noise tests used for *Mariner* Mars 1964. The change permitted the test implementation to be simplified. Individual tests had two advantages – they required less test preparation and permitted more accurate control of the test input.

The noise portion of the *Mariner* Mars 1964 combined test was adequately covered in the *Mariner* Venus 67 random noise tests. The latter spectrum levels are between 2 and 12 dB higher than the former noise levels of the combined test of the earlier *Mariner*.

To compare subsystem response to the *Mariner* Mars 1964 and *Mariner* Venus 67 specifications, an equivalence based on the response of an ideal single-degree-of-freedom structural system with a Q of 20 was used. Figure B-1 displays the response spectra of the system to both the *Mariner* Mars 1964 and the *Mariner* Venus 67 inputs. In the low-frequency range (<250 Hz), the levels are almost identical to the maximum difference of <0.5%. Between 250 and 2000 Hz, the difference is <4.7%.

Mariner Venus 67 FA vibration tests consisted of random noise, only.

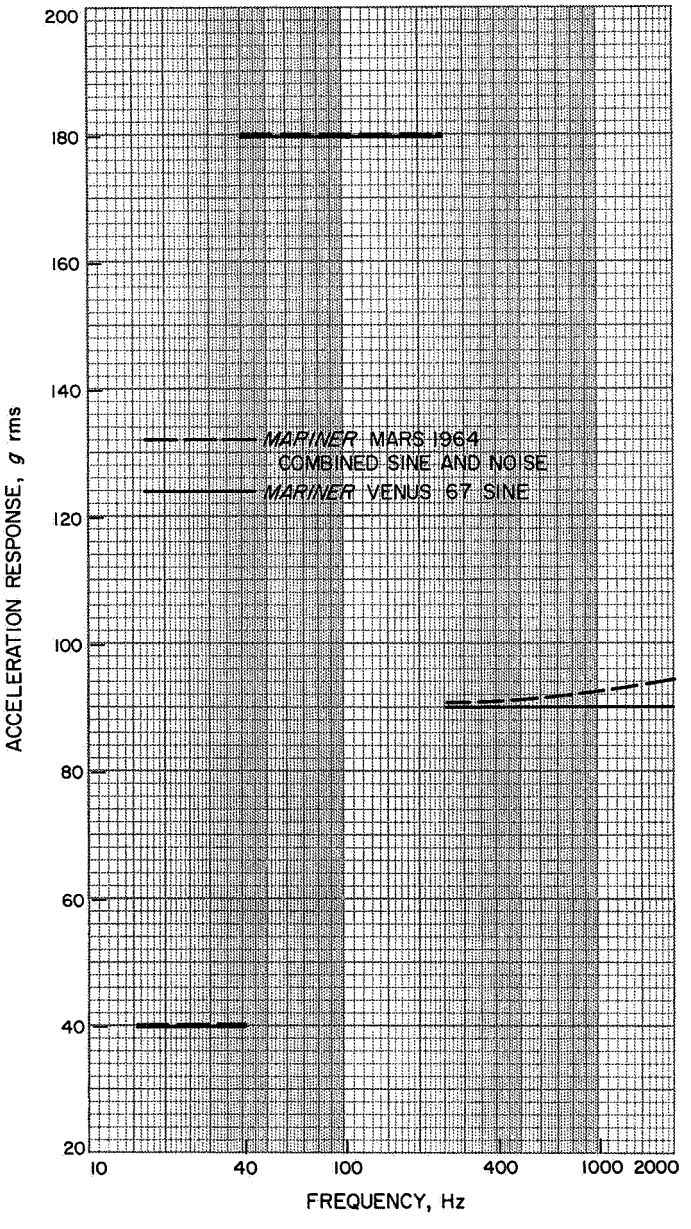

Fig. B-1. Response of a single-degree-of-freedom system to TA assembly vibration

Appendix C

Mariner Mars 1964 Life Test Results

Item	Ref. No.	Serial No.	Test duration		Start of regular reporting	Test environment				Observed effects	
			Start	End		Vac.	Temperature			Failures	Degradation
							Low	High	Cycling		
Trapped radiation detector	25A1	TA	6/18/65	7/30/65	2/25/65	—	—	—	x	—	—
Magnetometer	33A1	2	10/12/64	7/30/65	2/26/65	x	—	—	—	—	x[a]
	33A2	2									
	33A3	0									
Plasma probe	32A1	MC-0	12/22/64	12/20/67	2/23/65	x	—	x	—	x	—
	32A2	MC-0									
	32A3	MC-0									
	32A4	MC-0									
Data automation system	20A1	2	12/23/64	7/30/65	2/24/65	—	—	—	—	—	—
	20A2	MC-7	2/12/65								
	20A3	TAW	1/23/64								
	20A4	MC-7	2/12/65								
	20A5	3	12/23/64								
Data encoder	6A1-13	3	7/10/64	7/31/65	—	—	—	x	—	—	—
Command	3A1-7	2	7/9/64	7/31/65	3/29/65	—	—	x	—	—	x
Radio	2	MC-0	1/27/65	12/20/67	2/28/65	x	—	x	—	x	x
Tape machine	16A1-5	2	8/4/64	2/23/65	—	x	—	x	—	—	—[b]
Power	4A	02	8/17/64	7/16/65	2/16/65	x	—	—	x	x	—
Battery	4A14	6	2/11/64	11/2/64		x	x	—	—	—	x[c]
		7	2/11/64	4/27/64		—	—	x	—	x	x
		8	8/19/64	5/3/65	2/16/65	x	—	x	—	—	x
		9	5/1/64	12/18/64		x	—	x	—	x	x
		18	11/28/64	7/28/65		x	—	x	—	—	x
A/C electronics	7A1	002	6/15/64	8/30/65	3/3/65	—	—	x	—	—	—
Sun sensors	7PS6	2	6/15/64	5/3/65	1/4/65	—	—	—	—	—	—
Earth detector	7ED6	2	5/12/64	6/18/65	2/2/65	—	—	—	—	—	—
Canopus sensor	7CS8	004	12/18/64	7/31/65	2/1/65	x	—	—	—	—	—
		103	12/3/65	7/31/65		—	—	—	—	—	—
Jet vane actuators	7JV	2,4,7,32	8/24/64	8/30/65	3/1/65	—	—	x	—	—	—
Attitude/control gyros	7A2	012	4/1/64	8/6/65	3/1/65	x	—	x	—	—	x
Central computer and sequencer	5A	MC-TA	4/1/64	8/15/65	2/17/65	—	—	—	x	x	—
Pyrotechnics control	8A1	1003	8/31/64	7/30/65	1/29/65	x	—	x	—	—	—
	8A2	1004									
Post-injection propulsion system		003	2/10/64	12/30/65	—	—	—	x	—	—	x

[a] Unit operated at approximately flight temperatures.

[b] Some set observed as result of prolonged storage.

[c] Degradation was normal aging process.

Appendix D

Environmental Test Waivers

Subsystem	Test type	Waiver No.	Date	JPL Div[a]	Description of waiver
DAS	TA	001	3/31/67	32	Acceptance of TA thermal–vacuum testing by the Project Office.
Trapped radiation detector	TA, FA	002	8/1/66	32	Change TA and FA testing temperatures.
Plasma probe	TA	003	9/20/66	32	Correct paragraph reference in TA vibration specification.
Plasma probe	TA	004	10/6/66	32	Waiver of TA thermal shock.
Plasma probe	TA, FA	005	10/7/66	32	Additional requirements for test setup.
UV photometer	—	006	3/31/67	32	Waive requalification testing of UV filters.
DFR filters	FA	007	2/3/67	32	Waive FA testing of M67-1 DFR filters (were qualified on M67-2 spacecraft).
Dual frequency receiver	FA	008	3/23/67	32	Repeat modified FA test on flight DFRs.
Radio	FA	009	2/15/67	33	Repeat modified FA test on M67-1 radio.
Radio	FA	010	2/22/67	33	Waiver to reduce vibration test time on SN 8 radio.
Radio	TA	011	2/24/67	33	Waiver to rerun only X axis vibration after minor failure of radio during TA test.
Radio	FA	012	3/20/67	33	Repeat modified FA vibration on M67-1 TWT power supply.
Radio	TA	013	4/26/67	33	Acceptance of TA testing of radio by Project Office.
Low-gain antennas	FA	014	8/22/66	35	Waive FA testing of *Mariner* Mars 1964 low-gain antenna for use on *Mariner* Venus 67 spacecraft.
High- and low-gain antennas	TA, FA	015	9/2/66	35	Modification of TA and FA testing of radio antennas.
High- and low-gain antennas	TA, FA	016	9/13/66	35	Modification of TA and FA testing of radio antennas.
Low-gain antenna	TA	017	10/3/66	35	Waiver for deletion of TA vibration of low-gain antenna.
High-gain antenna	TA, FA	018	10/31/66	35	Change TA and FA thermal–vacuum temperature levels.
Low-gain antenna	TA	019	4/4/67	35	Waive retest of TA low-gain antenna after failure of cable clamp bonding during thermal–vacuum test.
High-gain antenna	FA	020	4/12/67	35	Repeat modified FA vibration test after repair of bond joint on antenna SN 7.
Tape recorder	FA	021	3/3/67	33	Repeat modified FA test after module replacement on units SN 4 and SN 6.
Tape recorder	FA	022	2/15/67	33	Modification of test configuration for FA retesting.
Tape recorder	TA	023	4/10/67	33	Repeat modified TA test after design change.
Power (4A11)	TA	024	8/22/66	34	Waiver to use unit 4A11 SN 002 for TA test; this unit is not the same configuration as flight units.
Power	TA	025	1/24/67	34	Waiver of TA low-frequency sine sweep of power subsystem.
Power (case VIII)	TA	026	2/3/67	34	Waiver for controlling heat exchanger at 167°F.
Power (4A18)	FA	027	2/27/67	34	Repeat of modified FA after rework.
Battery	Life	028	12/6/66	34	Modification of battery life-test time.
Battery	TA	029	2/3/67	34	Waive battery static acceleration test.
Solar panel	FA	030	11/28/66	34	Waive solar panel acoustic test.

[a]Division 32, Space Sciences.
Division 33, Telecommunications.
Division 34, Guidance and Control.
Division 35, Engineering Mechanics.

Appendix D (contd)

Subsystem	Test type	Waiver No.	Date	JPL Div[a]	Description of waiver
Solar panel	FA	031	3/27/67	34	Waive FA vibration test on solar panels.
Power (4A18)	TA	032	4/5/67	34	Waiver to retest TA unit to modified FA levels.
A/C gyro	FA	033	1/27/67	34	Waiver to depart from FA test specification for qualification of replacement gyro.
A/C gyro	FA	034	3/1/67	34	Clarification of waiver No. 33.
A/C jet valve	TA, FA	035	9/27/66	34	Waiver to change TA and FA lower test temperatures.
A/C jet valve	TA, FA	036	10/3/66	34	Waiver to delete thermal shock test and state new TA and FA test temperatures.
A/C jet valve	FA	037	11/8/66	34	Modification of configuration for temperature test.
A/C jet valve	FA	038	11/23/66	34	Waive FA retest of 12 valves that were delivered to SAF.
Earth and terminator sensors	FA	039	9/6/66	34	Change FA lower temperatures to 0°F.
Canopus sensor	FA	040	3/8/67	34	Waiver to delete demagnetization of Canopus sensor.
Primary and secondary sun sensor	TA, FA	041	4/10/67	34	Waiver to lower TA and FA test temperatures.
Jet-vane actuator	FA	042	8/10/66	34	Waiver to rerun FA low temperature test.
Jet-vane actuator	TA, FA	043	9/22/66	34	Change TA and FA temperatures to 0°F and 20°F, respectively.
Jet-vane actuator	FA	044	3/8/67	34	Waiver of FA +20°F testing of JVA SN C-108.
Temperature-control reference	TA	045	11/29/66	35	Waiver for modification of TCR test duration.
Temperature-control reference	—	046	2/14/67	35	Waiver for utilization of TA (SN 13) TCR for flight.
Oxidizer-start cartridge	FA	047	5/11/67	38	Waiver to rerun modified FA vibration test.
M67-1 subsystems	FA	048	2/17/67	29	Waiver to rerun modified FA test on M67-1 subsystems: radio, tape recorder, power bay I, and DAS.
Space simulator	FA	049	4/4/67	29	Waive $\dot{P}$ requirements.
M67-1 spacecraft	FA	050	1/13/67	29	Seven waivers to the M67-1 test specification.
Structural test model	TA	051	8/8/66	35	Waiver to revise TA noise test length.

[a]Division 29, Project Engineering.
Division 34, Guidance and Control.
Division 38, Propulsion.
Division 35, Engineering Mechanics.

Appendix E

Space Simulator Radiometer Comparison Test

During the temperature control model test in the 10-ft space simulator, the Eppley and absolute cavity (cone) radiometers used to monitor solar intensity differed by about 15% at Venus intensities. Although the cone radiometer had been believed to be the more accurate instrument, it was observed that the ratio of the measured intensity to the lower thermal shield absolute temperature to the fourth power was not constant over the intensity range of the test. To resolve this anomaly and to increase the assurance that the flight spacecraft would be tested at the correct solar intensities, a radiometer comparison test was conducted in the 10-ft space simulator during October 1966.

The comparison test included the below listed items:

Item	Description
1	Eppley radiometer with 7-deg view limiter
2–7	Hycal radiometers
8–9	Cone radiometers
10	TCM lower thermal shield
11–12	Relative intensity monitors (RIM)
13–15	Temperature-control references
16–17	Black plates
18	Cone radiometer facing down

The test results are plotted in Figs. E-1 and E-2. These graphs compare the measured intensity of each device to that measured by cone 8 (TCM cone). Two discrepancies are apparent: A departure of the ratio from 1.00 indicates a difference in absolute intensity; a nonhorizontal line indicates a difference in intensity ratio at various intensity levels. The results plotted in Fig. E-2 were deduced from simple temperature measurement devices. Except for the cone radiometers, Fig. E-1 presents results for commercially available instruments.

Figure E-2 shows good agreement among all test items (excluding the cone), except at low intensities. The high data values at low intensities are unexplained, but they appear to be associated with low temperature.

The lower thermal shield data were in considerably better agreement with cone 8 during this test than during the TCM test. There was scatter in shield temperatures for the TCM test at 125 W/ft^2 intensity. This fact – combined with the agreement among plates, TCRs, and the shield in the comparison test – suggests that the comparison test data are the more reliable.

It was concluded that the TCM test levels as measured by the cone were substantially correct. The cone radiometer was, therefore, used to set intensity levels for the flight spacecraft tests.

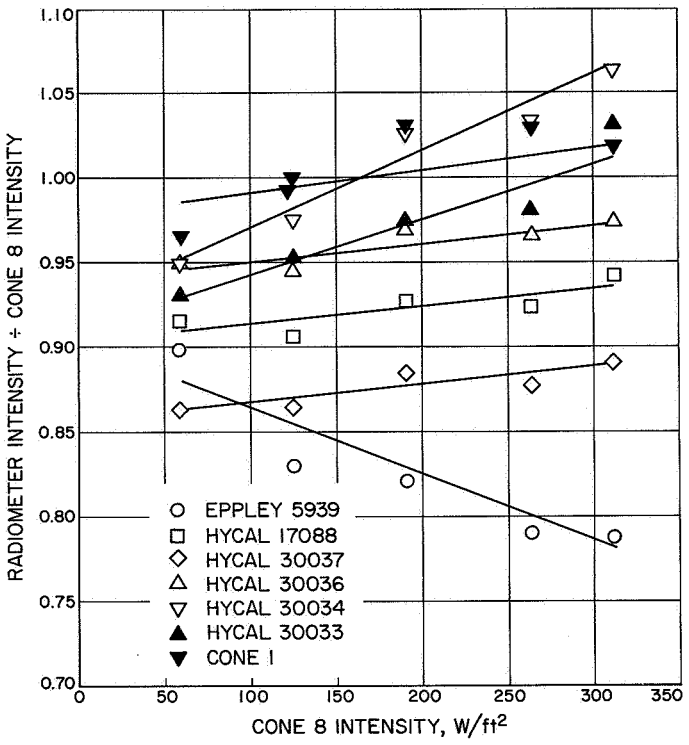

Fig. E-1. Radiometer relative-intensity comparison test

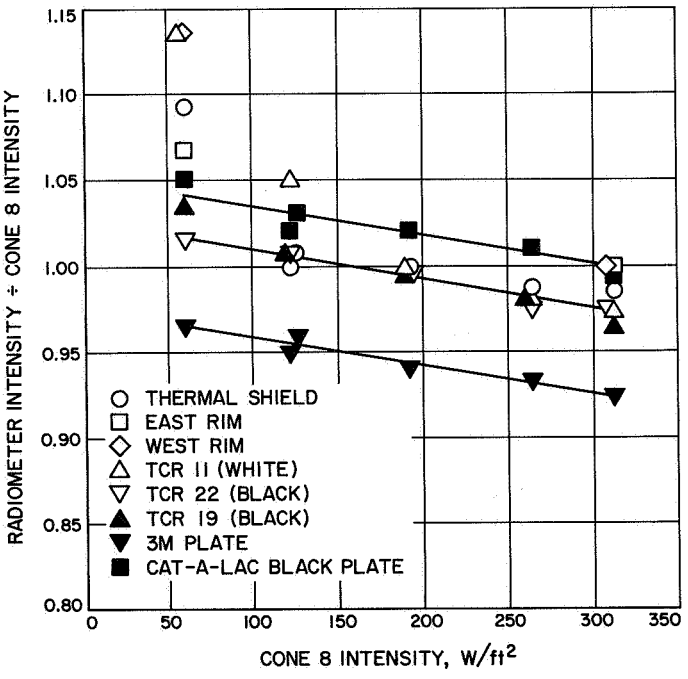

Fig. E-2. Temperature measurement item relative-intensity comparison test

Appendix F

Shipping Container Environmental Testing

A series of vibration and drop qualification tests was performed on the electronic assembly and battery shipping containers, because doubts were expressed about the acceptability of the *Mariner C* container system. After initial tests, hardware modifications were required to qualify the containers.

I. Electronic Assembly Shipping Container Tests

A. *Mariner C* Container Vibration Test

Weighted dummy subchassis were mounted in an electronic assembly chassis and assembled into the shipping system per specification to provide the worst-case condition of a 54-lb electronic assembly.

Triaxial accelerometers were located on the inner container handling fixture, chassis and subchassis. A control accelerometer was located on the vibration table head. The container assembly was mounted to the vibration table as shown in Fig. F-1 to simulate truck bed transportation mounting and vibration tested; and peak g test recordings were taken.

The test proved the shipping system did not adequately support the electronic equipment to meet the requirements of the JPL specification. A program was generated to upgrade all old containers and design new fixtures and containers wherever necessary.

B. *Mariner* Venus 67 Container Vibration Test

After the shipping containers were modified as described in the electronic packaging portion of the *Mariner* Venus 67 final Project report, the modified design (Figs. F-2 and F-3) was tested by the same procedure described above. The test results are shown in the curves of Figs. F-4, F-5, and F-6.

The electronic assembly modified shipping system passed the specification acceptance requirements. The only point where the system response exceeds the input was at the 9-Hz resonance; this resonant point was still well within the acceptable limit.

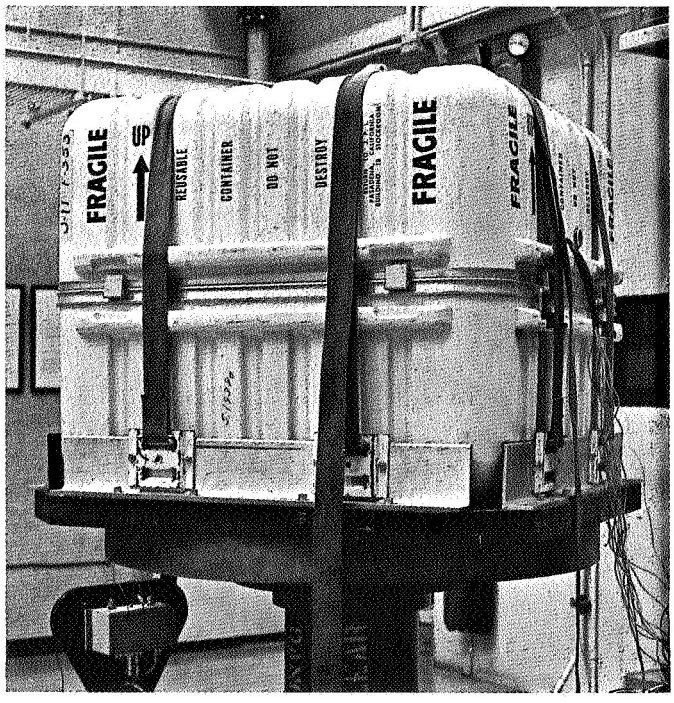

Fig. F-1. *Mariner* Venus 67 electronic assembly shipping container vibration test, vertical axis

Fig. F-2. *Mariner* Venus 67 electronic assembly shipping container vibration test, lateral axis

Fig. F-3. Test setup for electronic compartment shipping container evaluation

C. Drop Test (Impact) of *Mariner* Venus 67 Shipping Container

To determine if the electronic assembly shipping system design would withstand and attenuate shock levels produced by drop test per JPL specification, drop tests were conducted with the complete electronic assembly shipping system and with the inner container only.

1. Test Procedure. A dummy, weighted, electronic assembly was assembled to a *Mariner* Venus 67 handling and assembly frame per specification. Weight of this total assembly was 77 lb. When assembled to inner container, foam liner, and outer container, the total weight was 144 lb.

Triaxial accelerometers were used to record shock input at the outer container and the response of the dummy load. One accelerometer was mounted to the middle

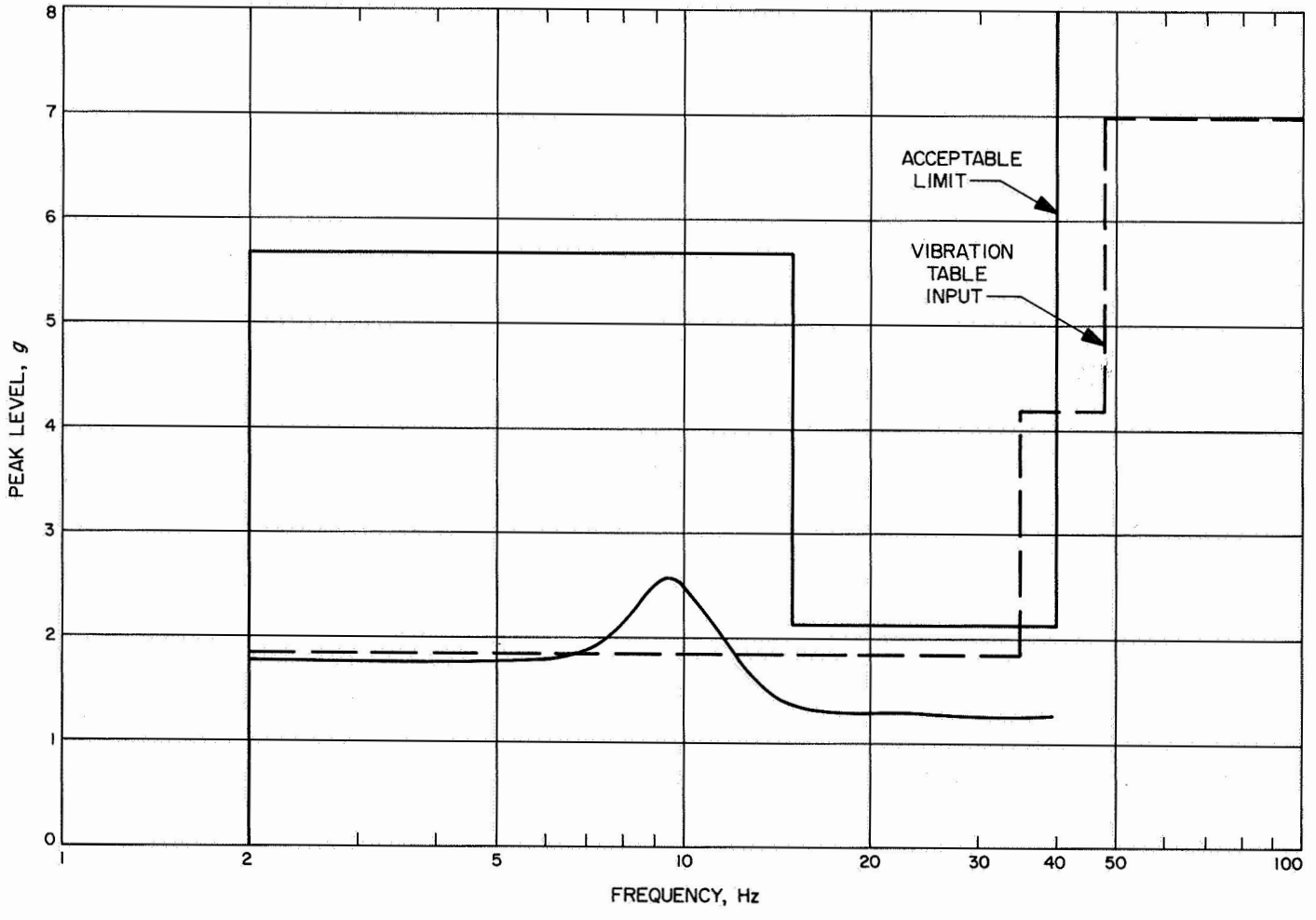

Fig. F-4. Response of encased electronic assembly, 54-lb chassis, to X-axis, 0 to 48-Hz vibration

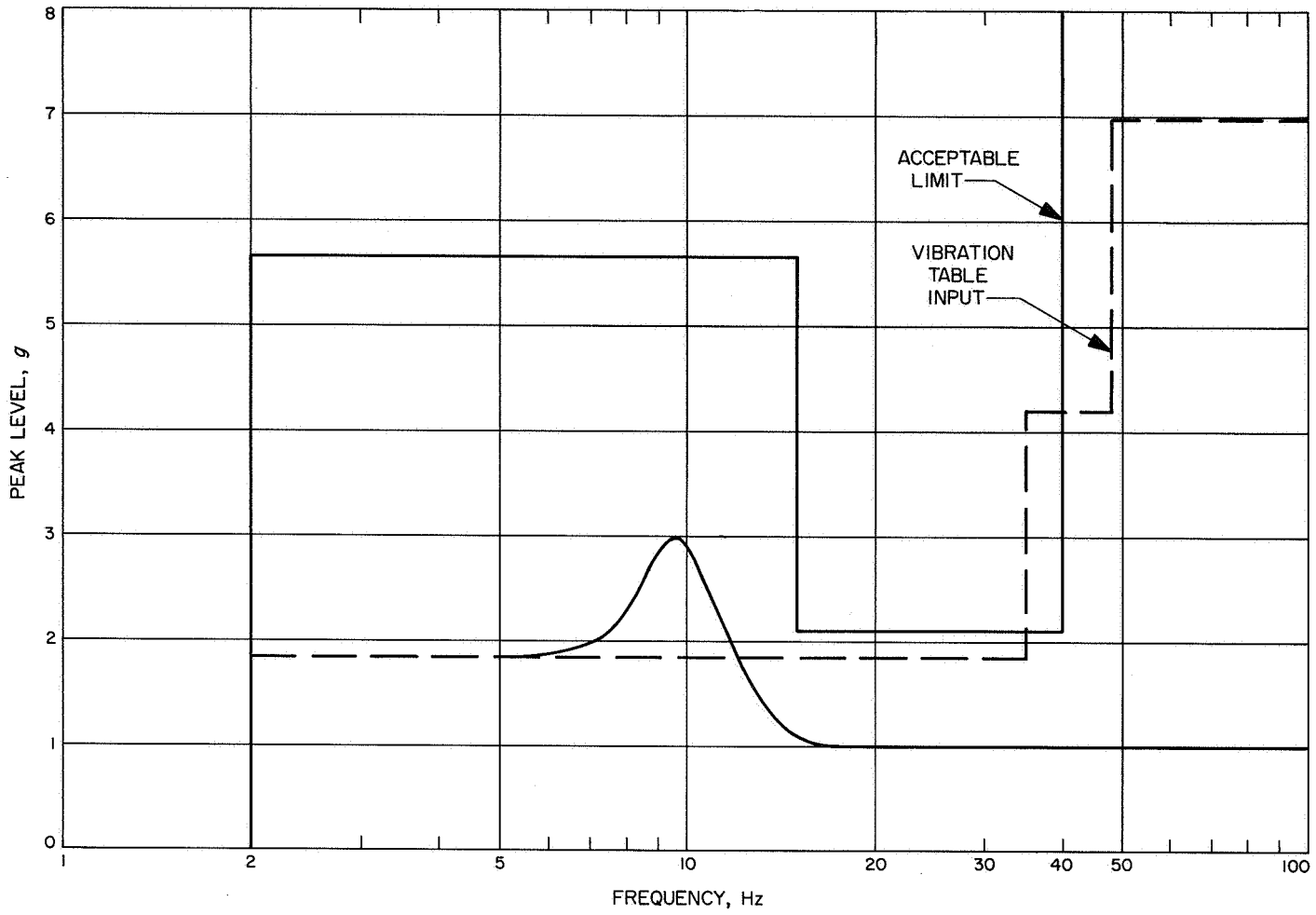

Fig. F-5. Response of encased electronic assembly, 54-lb chassis, to Y-axis, 0 to 48-Hz vibration

of the electronic assembly and the other close to the aluminum extrusion on the outer container, near an edge.

All drop distances were measured from the lowest point on the container to the concrete driveway. Visual inspection of the shipping container and its contents was performed after each series of impacts to determine damage and contamination, if any.

The following tests were performed, in sequence:

(1) Flat bottom drop

(2) 45-deg side-edge drop (length of edge)

(3) Bottom corner drop

(4) Flat side drop

(5) 45-deg top-edge drop (length of edge)

(6) Top corner drop

(7) Flat bottom drop

(8) Flat side drop

(9) Flat bottom drop, pivoting along the axis of one bottom edge with the opposite edge 12 in. from the floor

(10) *Non*-flat bottom drop – two-stage impact: bottom corner first, then flat bottom

The electronic assembly shipping container exhibited dented corners on the outer container, but no cracks were visible. The dents could be removed by applying pressure from the inside. When the inner container was dropped, no physical damage was noted on containers, fixture, or chassis and no contamination was found in any portion of this container system after drop tests were completed.

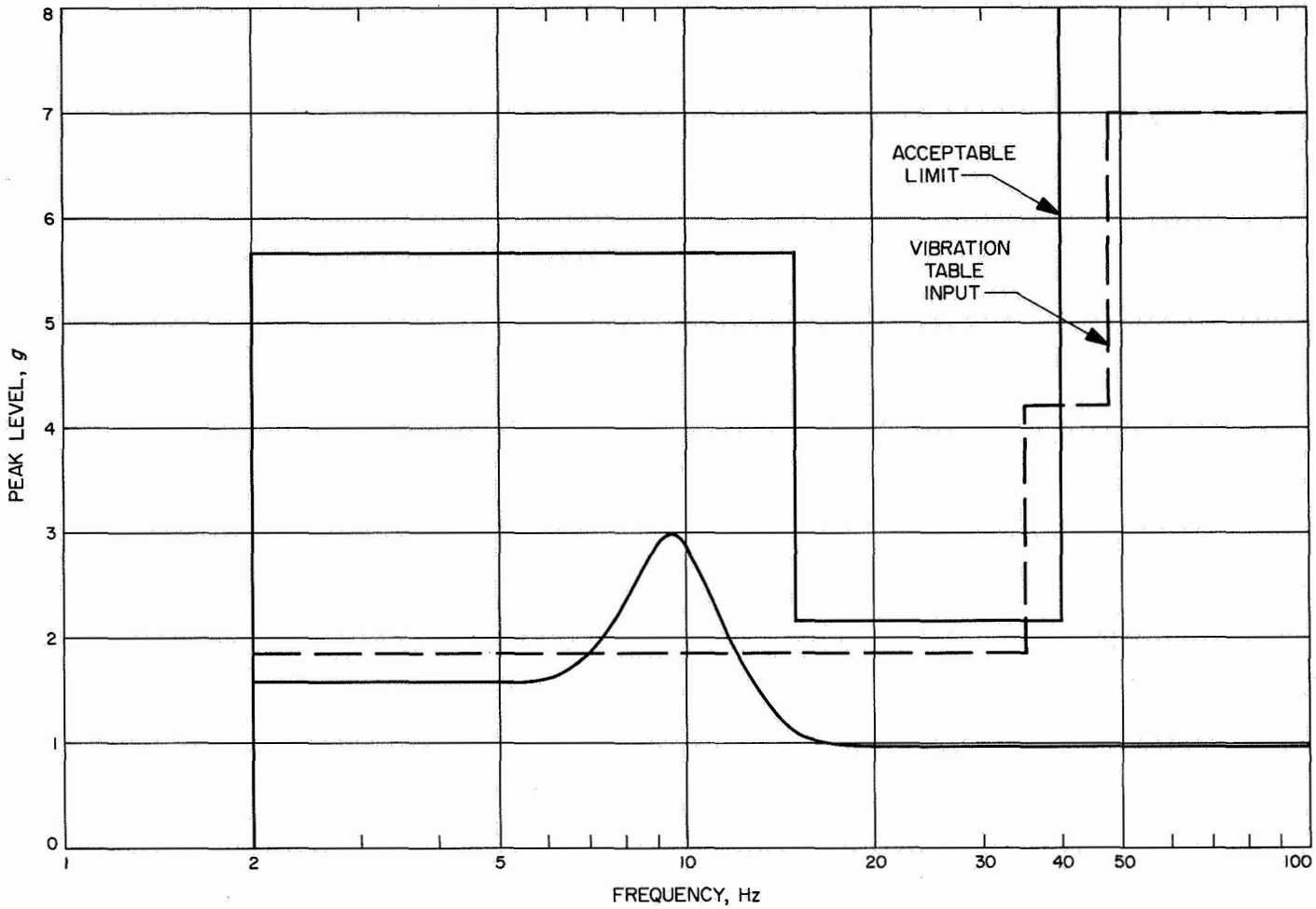

Fig. F-6. Response of encased electronic assembly, 54-lb chassis, to Z-axis, 0 to 48-Hz vibration

2. Conclusion. The *Mariner* Venus 67 electronic assembly shipping container design concept is acceptable from a drop, or impact, test standpoint. Response is within the tentative requirement of 30-*g* peak when assembled per specification. The range of attenuation was dropped simulating a handling error without the foam liner or outer container, and the level reached a 67-*g* peak.

II. Battery Shipping Container Qualification Tests

Because the batteries were handled and shipped more frequently than the electronic assemblies, a separate handling and shipping system was designed to simplify the handling at JPL.

A. Battery Shipping System Vibration Test

For the environmental test of the battery shipping system, the batteries were mounted as shown in Fig. F-7.

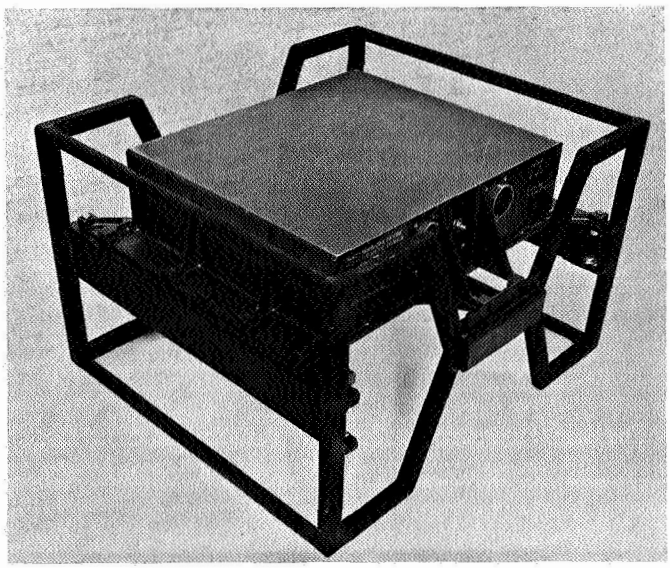

Fig. F-7. Battery installed in shipping fixture

Accelerometers (triaxial) were placed in the middle of the battery bottom and on the fixture channel. A control accelerometer was mounted to the vibration table head. This assembly was then placed into the modified *Ranger* shipping container and strapped to the vibration table in the same manner as the electronic shipping container. It was noted that two batteries were the worst case for the shipping containers, which required the design and test effort to be concentrated on this configuration.

Test recordings were taken in peak g to show spikes that would not be evident using rms instrumentation. The test indicated that the batteries would withstand the shipping environment.

B. Battery Drop Test

Because of the decision to use the *Ranger* shipping case and a new handling fixture for *Mariner* Venus 67, drop qualification tests were required to determine if the battery container design concept could withstand and attenuate shock levels produced by drop testing. Tests were performed per JPL specification. Three configurations were drop tested:

Configuration 1. Battery handling fixture, modified *Ranger* shipping container with neoprene corner pads

Configuration 2. Battery handling fixture, modified *Ranger* shipping container without neoprene corner pads

Configuration 3. Battery handling fixture, modified *Ranger* container without neoprene corner pads and *Mariner* Venus 67 outer container

1. Test Procedure. A dummy weighted battery was assembled to a *Mariner* Venus 67 handling and assembly frame, per specification. The battery shipping system was assembled to the handling frame, using an inoperative battery of the configuration used on *Mariner* Venus 67. Weight at this point was 75 lb.

The three battery container configurations were tested by the same general procedure and technique as used for electronic assembly shipping container. Triaxial accelerometers were used to record shock input at the outer container and the response of the dummy load. A bomb release mechanism was suspended from the fork lift by a chain. The shipping system was then suspended from the bomb release. After each drop test, visual inspection of the shipping container and its contents was performed to determine damage and contamination, if any.

Configuration 1 of the battery shipping system exhibited dented corners and a severely marred surface finish. Welds on the modified *Ranger* container seemed to be intact after the first drop sequence with rubber corner pads. Some contamination consisting of silicone rubber cement, sand, and dust was found after this drop sequence. No damage to the exterior of the battery was noticed, and the handling frame was undamaged.

The drop sequence performed on configuration 2 proved fatal to both the battery and the container after 5 drops. Several bad cracks were found in the battery chassis and part of the battery structure was bent. Contamination was considerable and consisted of sand, dust, screw heads, sheared bolts, rubber pads, silicone rubber cement residue and pieces of phenolic washers. Corner welds on the container were cracked.

Tests per configuration 3 on the *Mariner* Venus 67 battery shipping system exhibited no scratches or damage of any type and, in any event, none of the impact levels exceeded 20 g.

2. Conclusion. The modified *Ranger* battery container as tested was not considered adequate protection for the *Mariner* Mars 67 spacecraft battery.

It was decided to remove the corner pads from all the modified *Ranger* shipping containers and place these in the new heavier-gaged outer container designed for the *Mariner* Venus 67 electronic shipping system. The *Mariner* Venus 67 battery assembly shipping container system design (configuration 3) was acceptable from a drop-test standpoint for use on the *Mariner* Venus 67 program. Response was within the tentative requirement of 30 g peak when assembled per specification and tested. The range of attenuation was, for the worst case, from 80 to 99%.

Appendix G

Truck Acceptance Testing and Transportation Environment

It has been JPL practice to monitor the dynamic environment of spacecraft during ground transportation from Pasadena to Cape Kennedy.

The *Surveyor* SC-3 spacecraft was returned to California from Cape Kennedy. Inspection of the spacecraft revealed a damaged component, possibly due to the transportation environment. Analysis of the data recorded on the trip showed that the environment was much more severe than on previous runs. The vibration severity was traced to an abnormal suspension system.

As a result of the above experience, it was decided to subject all vans used for transporting the M67-1 and M67-2 spacecraft and equipment to a qualification test. Figures in this appendix show the data that were used in determining the acceleration limits for truck acceptance testing. These data were measured on *good* and *bad* vans used to transport *Surveyor* equipment. Figures G-1 and G-2 show instantaneous accelerations and Figs. G-3 and G-4 are the corresponding acceleration spectral densities (ASDs) for a nominal ride in a good van; whereas, Figs. G-5 and G-6 show the instantaneous acceleration and ASD from a rough-road ride in a good van. In no case does the instantaneous acceleration exceed ± 1 *g*, nor does the rms value exceed 0.25 *g*. Figures G-7 and G-8 show typical instantaneous accelerations and ASDs for a smooth-road ride in a van with a faulty suspension system. Measurements from abnormal suspension vans revealed peak accelerations ranging to ± 4 *g* and rms values ranging to 0.6 *g*.

During each evaluation run, an accelerometer was attached to the floor of the van over the rear wheels, with its sensitive axis in the vertical direction. The output was measured on an oscilloscope and a voltmeter, as the van was driven over a prescribed course at various speeds. The test criterion was that the rms acceleration be less than 0.25 *g* and that the instantaneous amplitude be less than 1 *g*. This criterion proved to be slightly conservative, and some subjectivity had to be included. With all trucks, some severe bumps produced instantaneous measurement exceeding 1 *g*. But with good vans, the response was low-frequency, highly damped excitation. Abnormal suspension systems responded with higher frequency vibration and lower damping.

As a result of these tests, several vans were rejected. These were reworked by the van company and subsequently qualified. This fact demonstrates that the test was adequate and not unreasonable, in that it was within the ability of the trackers to qualify all vans.

The van floors and the spacecraft transporters used in transporting the *Mariner* Venus 67 spacecraft to the Cape were instrumented with 12 accelerometers that were located in strategic locations and were continuously recorded during the trip. In addition, a warning device was included that would sound a 4-s tone over the radio in the lead car whenever the dynamic vertical acceleration of the floor of the van exceeded a level of 1 *g*.

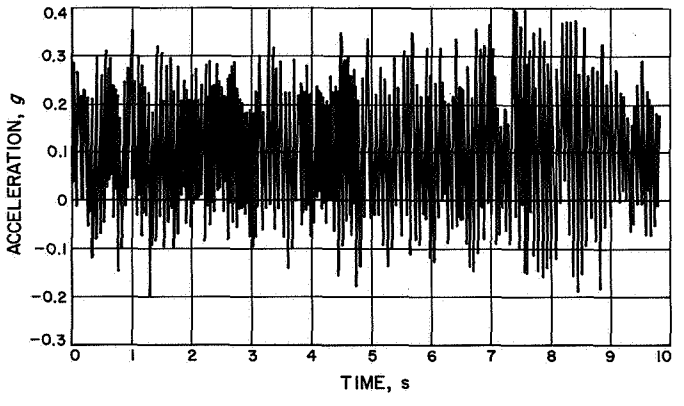

Fig. G-1. Typical van vibration, 10-s sample: good van, normal road

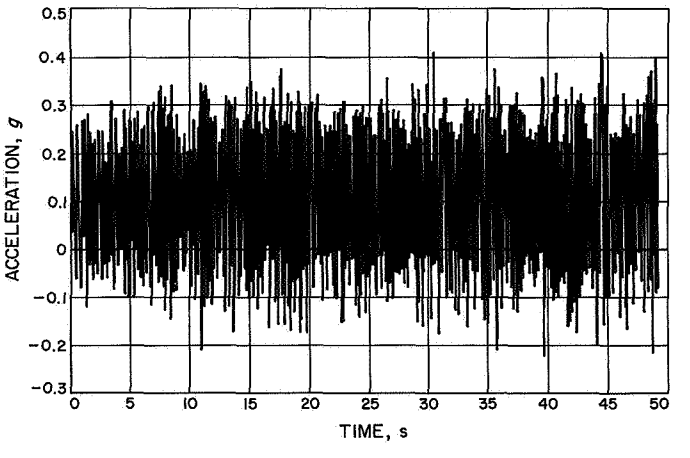

Fig. G-2. Typical van vibration, 50-s sample: good van, normal road

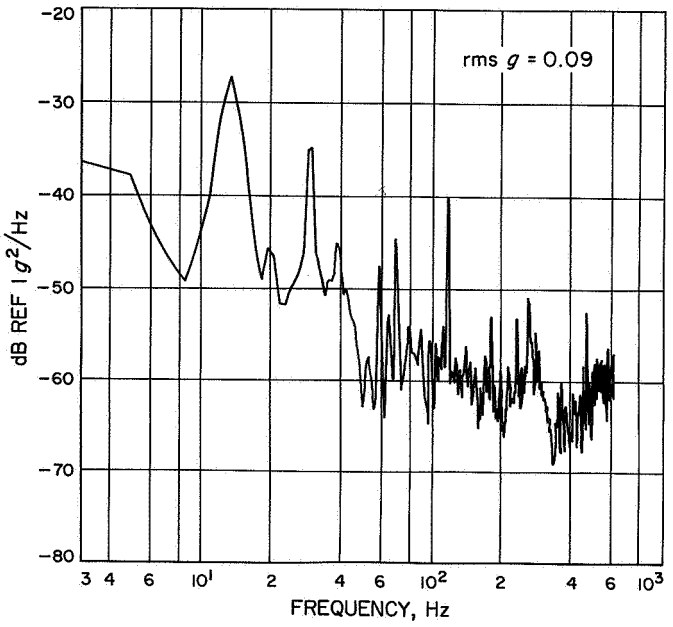

Fig. G-3. Acceleration spectral density, 10-s sample: good van, normal road

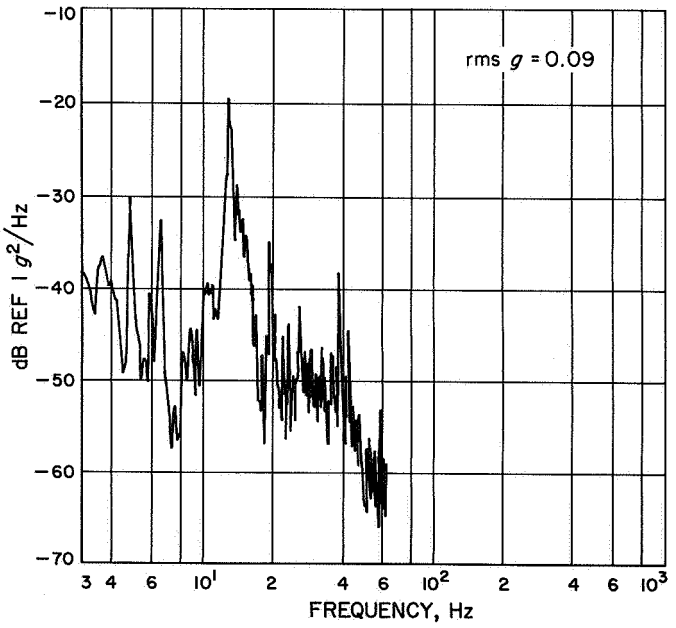

Fig. G-4. Acceleration spectral density, 50-s sample: good van, normal road

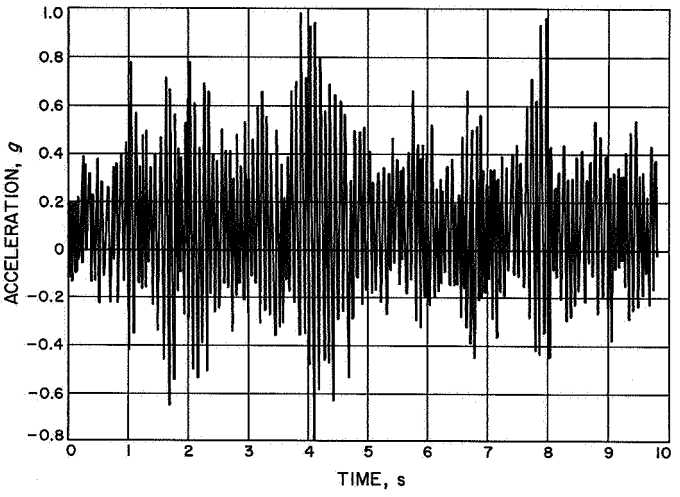

Fig. G-5. Typical van vibration, 10-s sample: good van, rough road

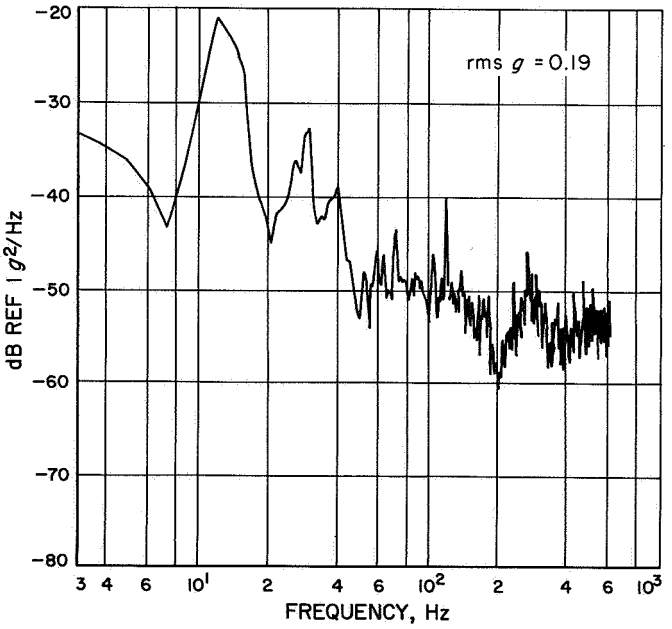

Fig. G-6. Acceleration spectral density, 10-s sample: good van, rough road

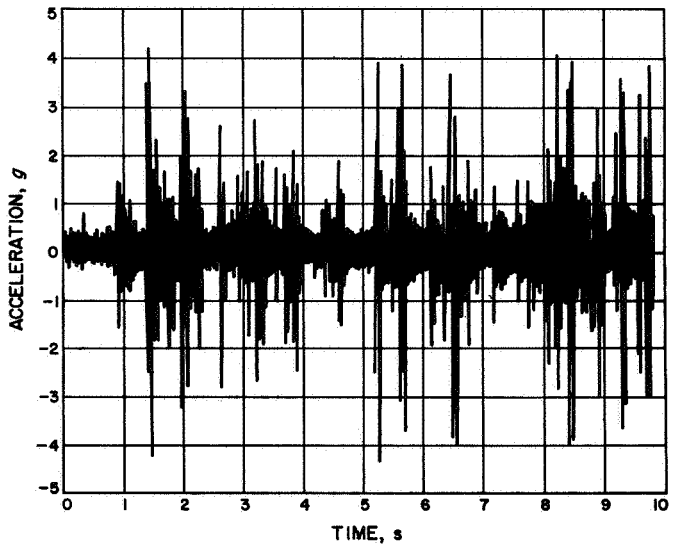

Fig. G-7. Typical van vibration, 10-s sample: faulty van

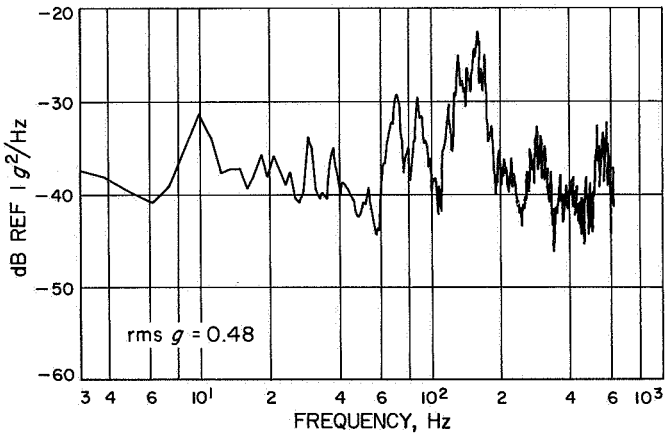

Fig. G-8. Acceleration spectral density, 10-s sample: faulty van

Due to a failure in the truck's power generating system outside of Monroe, Louisiana, the environment of the M67-1 spacecraft was monitored only to this point. The alarm sounded six times before this power failure. The environment of the M67-2 spacecraft was monitored throughout the entire trip, except during a 30-min period near Yuma, Arizona. The alarm sounded five times. However, subsequent analysis of the data showed all alarm soundings were caused by electrical transients, due apparently to the air-condition system turning on. The maximum vibration amplitude was approximately 0.75 *g*. Figures G-9 and G-10 show ASD analyses of the data measured at the time of maximum excitation for the M67-1 and M67-2 environments, respectively.

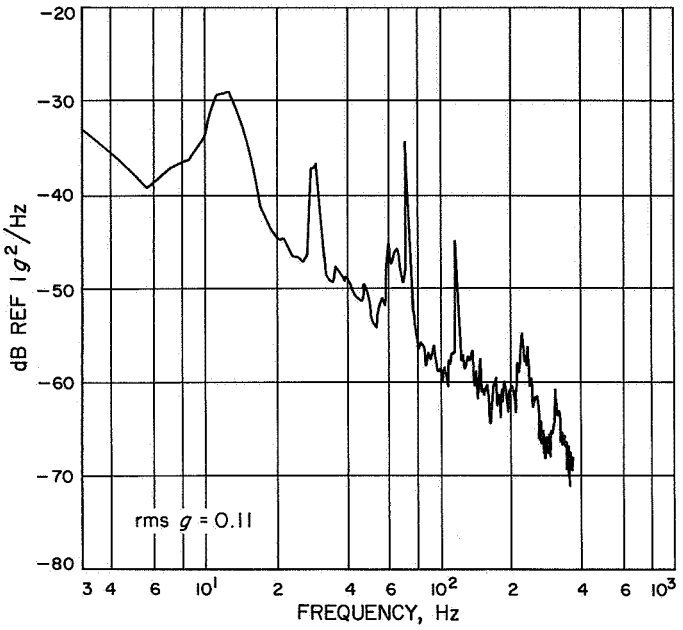

Fig. G-9. Maximum excitation for M67-1 spacecraft during transportation

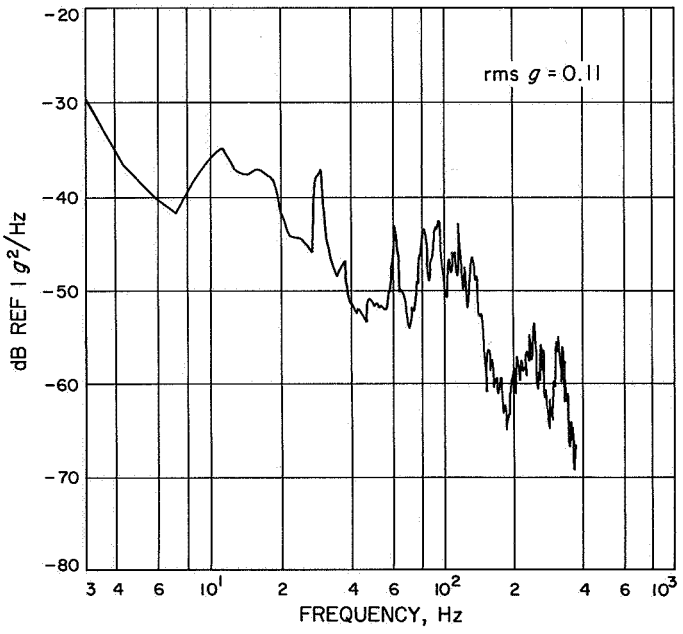

Fig. G-10. Maximum excitation for M67-2 spacecraft during transportation

Appendix H

Battery Test

This appendix presents a summary of the dynamic data acquired during vibration tests of a *Mariner* TA battery subsystem (SN 26) on March 8, 1967. High-frequency sinusoidal sweeps and shaped random noise were the induced environments as given in the JPL specification.

The test was proposed to attempt to correlate cell circuit failures with vibration test levels. Post-test results displayed a test anomaly interpreted as cell–14 circuit failure after the third axis of shake (spacecraft Z axis).

The test configuration was designed such that localized vibration levels could be associated directly with cell failures in that area. Ten response accelerometers were mounted on the face plate supporting the cells on one side of the battery. The 18 battery cells were divided electrically into 6 groups of 3 cells and were monitored and recorded during the testing. At least one accelerometer was located near each group of cells with its sensitive acceleration axis perpendicular to the face plate. In addition, the lateral vibration of the two center groups of cells, including cell 14, was monitored with triaxial accelerometers.

An initial look at the accelerometer data suggested little correlation between the cell wire failure and acceleration levels. Transient excitation was suspected as the cause of the cell failure. Some transient signals were recorded on the accelerometer channels during the Z axis run; however, no time correlation existed between the cell circuit transients and the accelerometer channel transients. A more detailed study of the accelerometer transient signals has shown that vibration transients could not have caused this type of signal. It is concluded that these accelerometer transients were associated with spurious signals in the electronics.

Data results presented are from the center triaxial accelerometer located on the battery plate near the failed cell 14. The random-noise data from each orthogonal shake axis are discussed separately. Analysis parameters for the power spectra include a resolution of 20 Hz and a time sample of 2.5 s which leads to a 100-degree-of-freedom acceleration spectral density (ASD) analysis.

The first shake axis (X) was perpendicular to the plane of the face plate. Figure H-1 displays the ASDs of the control and X axis (near cell 14) accelerometers. A significant wideband gain exists through most of the spectrum with a maximum gain of 8 dB at about 1200 Hz. This is clearly displayed in Fig. H-2, with high-gain

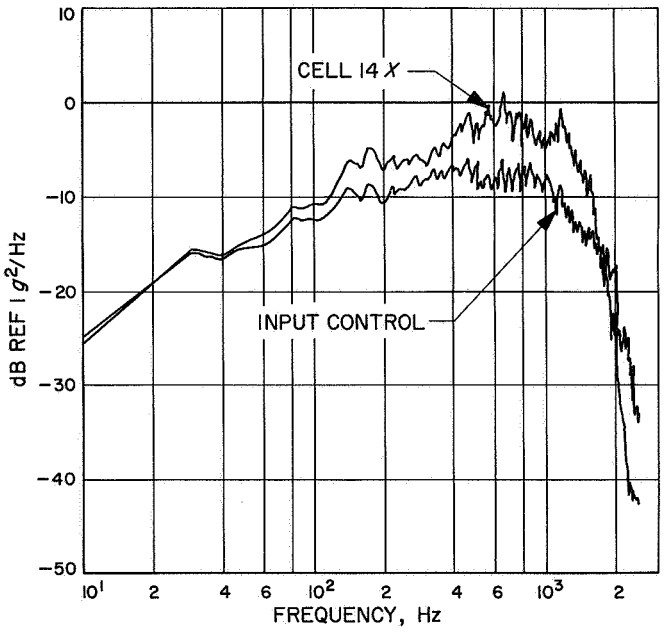

Fig. H-1. Comparison of battery cell 14X response with X-axis input excitation

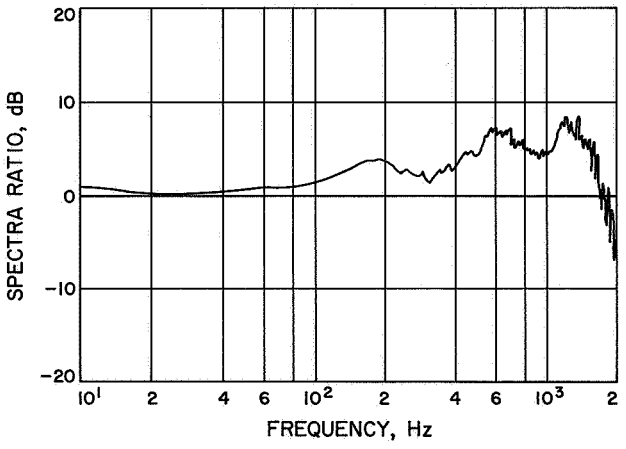

Fig. H-2. Ratio of 14X battery cell response to input excitation

ranges in the spectrum near 500 to 700 Hz and 1000 to 1500 Hz. These suggest modally *rich* ranges associated with base plate modes. The data verified an intuitive assumption that the overall wideband vibration response of the battery primary structure is a maximum in this shake direction. No failures were detected during the test in this axis.

Vibration in the *Y* axis, parallel to the axes of the battery cell groups, followed. This was the first of the lateral axes of the battery and was expected to be the most likely failure axis. The data displayed an unusual result.

Figure H-3 contains the ASD data for the Y-axis accelerometer, located near cell 14, and the input control accelerometer. A glance reveals the gross gain range centered at approximately 1300 Hz. A detailed inspection discloses a marked similarity in the fine resolution peaks and notches in the spectrum. The spectra of Fig. H-3 have been ratioed to obtain Fig. H-4. The clearly defined single peak suggests a very simple system in this configuration. If it is caused by a single response mode of the structure, the damping is unusually high (approximately 20% of critical). Absence of secondary peaks and notches suggests an unusual response pattern for such a seemingly complex system. Rigid-body motion must exist near the cell-14 accelerometer throughout the

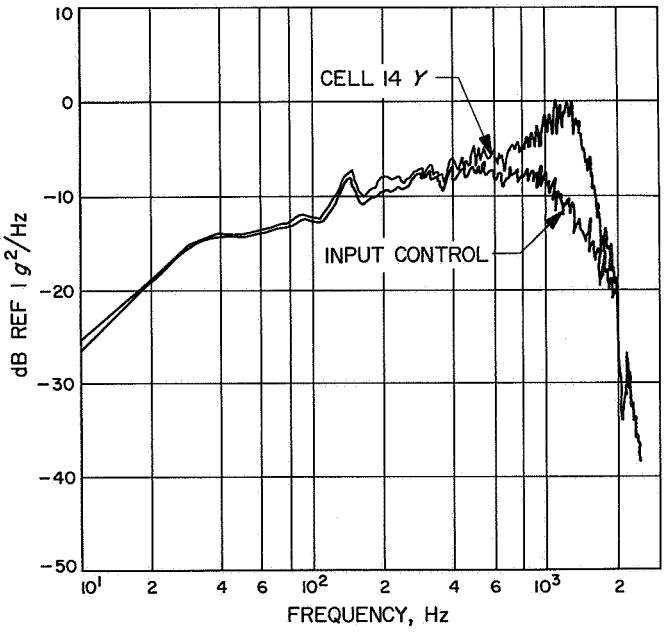

Fig. H-3. Comparison of battery cell 14Y response with Y-axis input excitation

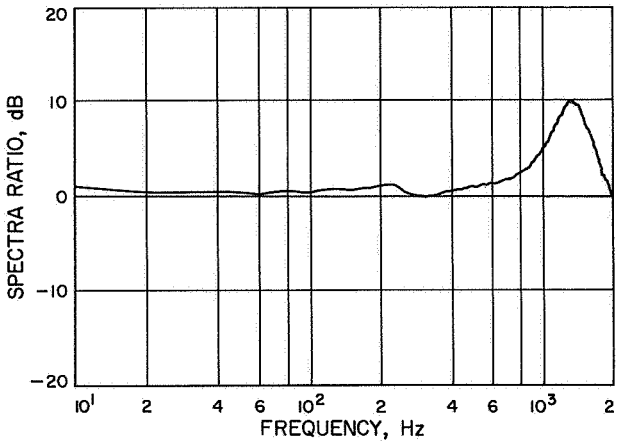

Fig. H-4. Ratio of 14Y battery cell response to input excitation

spectrum, with the exception of the highly damped response at 1300 Hz.

Correlation of similar sinusoidal data results is shown in Fig. H-5. The wideband peak plot sinusoidal data display nearly identical response characteristics and similar amplitude gains. (The plot format is different, however.)

The remaining lateral shake axis, or Z axis, was excited last. The axis is parallel to an individual cell plate. Figure H-6 contains the resulting ASD data from the cell-14 accelerometer in the Z axis and from the control accelerometer. The response data in this axis is quite different from the other lateral axis data (*Y* axis), particularly in the *cross-over* near 600 Hz.

The ratio of the ASDs in Fig. H-6 is given in Fig. H-7 to more clearly define the gains observed. Maximum response in this axis was less than in either of the previous axes. The ratio also suggests a modally rich response with a major primary structure mode near 450 Hz. The significant negative ratio between approximately 800 to 1200 Hz is unique to this shake axis. This ratio is displayed, also, in Fig. H-8 as the difference in wideband peak plot levels recorded during the high-frequency sinusoidal test. A possible failure environment associated with this negative ratio will be discussed later.

A summary of the response ratio data discussed is given in Fig. H-9. Figures H-2, H-4, and H-7 have been included in this composite plot as curves *X*, *Y*, and *Z*, respectively. The *X*, *Y*, and Z notation refers to each shake axis of the battery. It is clear that there is little

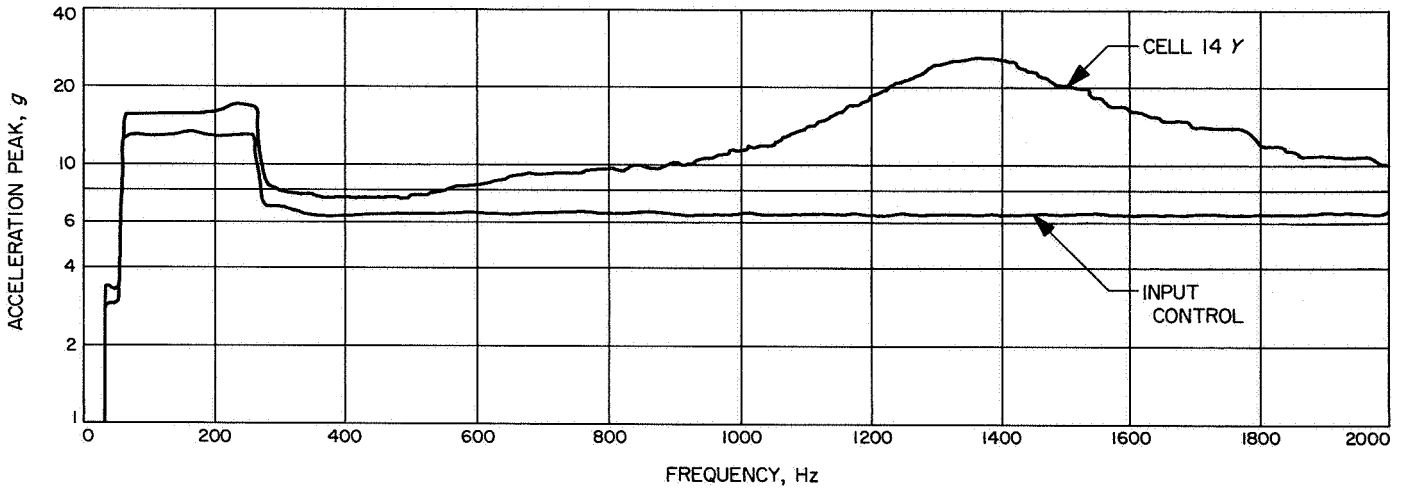

Fig. H-5. Comparison of battery cell 14Y response with Y-axis sinusoidal vibration input

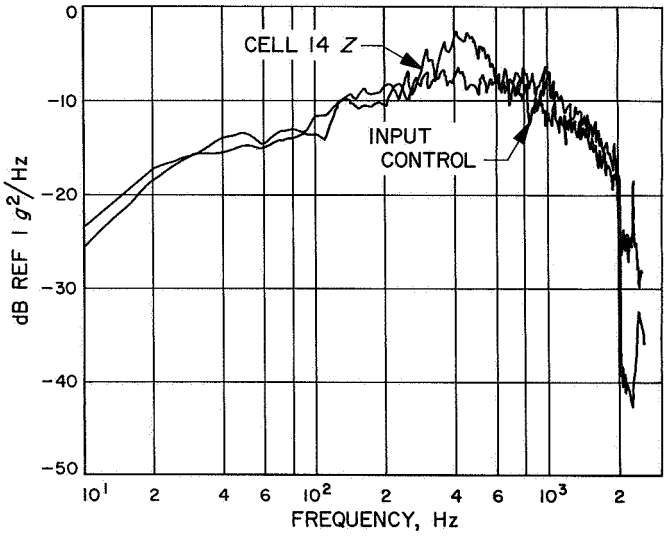

Fig. H-6. Comparison of battery cell 14Z response with Z-axis random vibration input

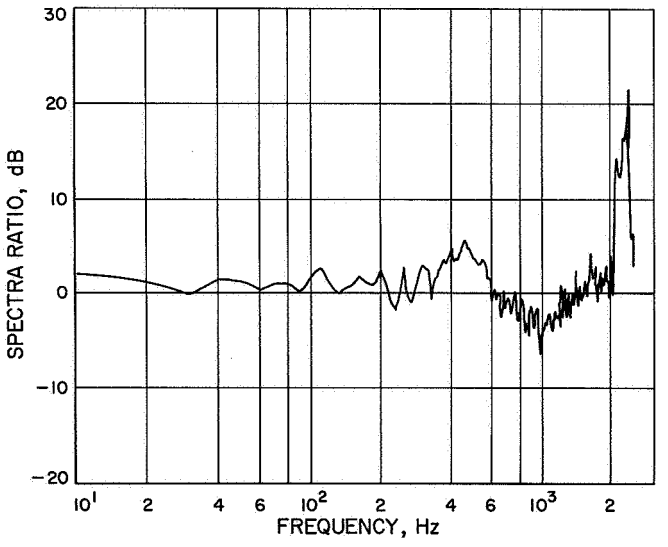

Fig. H-7. Ratio of cell 14Z response to Z-axis random vibration input

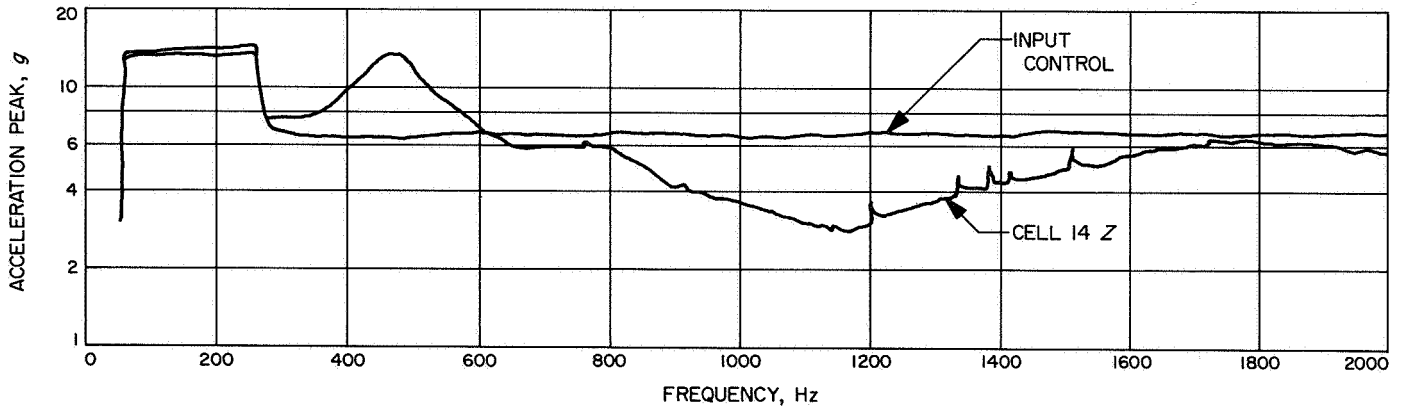

Fig. H-8. Comparison of battery cell 14Z response with Z-axis sinusoidal vibration input

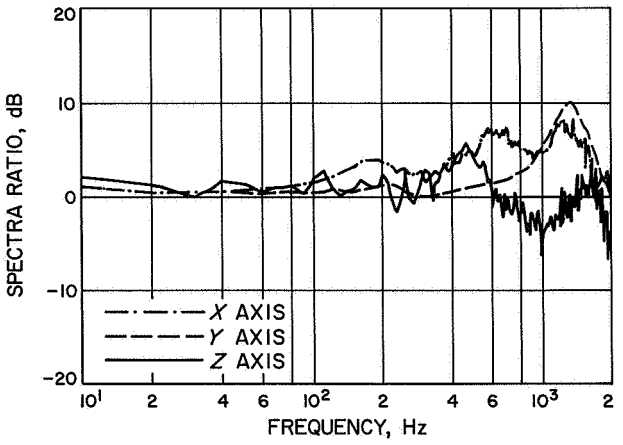

Fig. H-9. Composite plot of X, Y, and Z-axes spectral ratios

similarity in the response ratios for different excitation axes. There is little primary structural response below 100 Hz and significant response from approximately 300 to 1600 Hz. The unusual characteristic of the Y-axis ratio is clearly compared to the other modally rich ratios.

A possible cause of the cell failure is suggested by Fig. H-9. Curve Z displays a significant negative ratio in the 800 to 1200-Hz range that is unlike either of the other curves. It is recalled that each response accelerometer was located on the primary structure (face plate) near cell 14, and the gain curves display the frequency spectrum of this response with a normalized input. For this frequency range and shake configuration, the negative ratio suggests high mechanical impedance of the primary structure with possible low mechanical impedance of the internal battery structure. That is, the vibration energy was not dissipated by the primary structure as with the other axes, but may have been dissipated internally by the battery plates and cells. The possible high internal vibration of these components could have caused the failure. There may be a more direct path of internal excitation and very low internal damping in this shake configuration. However, it must be recalled that low-frequency and other high-frequency vibration tests preceded this testing. Therefore, the failure may have been caused by fatigue from cycling and becomes a more complex problem.

The data presented here make up only a small percentage of the total data acquired during this testing. An attempt was made to summarize the results by use of a method that suggests a possible failure mode. The data and result may be of value for future design and test predictions if it is used realistically, considering measurement and analysis limitations.

Appendix I

Effect of Configuration on Vibration Test of Electronic Modules

Vibration testing of spacecraft components in a noise environment has been accomplished in a case assembly configuration during the *Mariner IV* and *V* programs. On occasion, single-module testing was requested by cognizant personnel because cases were not available. Little valid information existed at the time to generate such a subassembly test.

It was the purpose of this investigation to define a specification to be used in a test of a single module not mounted in a case. A case is defined as a basic *Mariner* electronic chassis, as illustrated in Fig. I-1. A module is defined as a standard electronic subchassis, as illustrated in Figs. I-1 and -2. The modules were instrumented with accelerometers near each corner and on the face, as shown in the same two figures. Module response is defined as the acceleration recorded at the response accelerometer location shown in Fig. I-2.

A module specification is derived from the case-test data, using the corner accelerometers of each module as module input data. These corner accelerations are combined to give an average test-input spectrum for the module test.

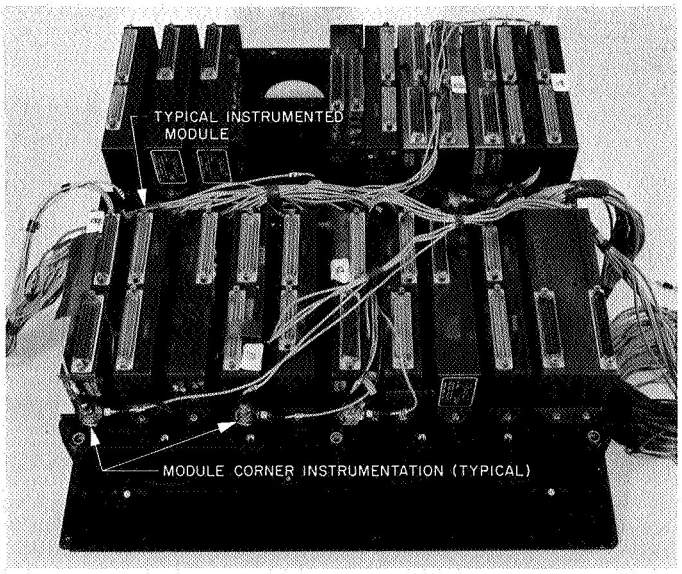

Fig. I-1. *Mariner* case IV, data encoder and command

With a *Mariner* Venus 67 assembly-test specification, a typical single-module-input spectrum is defined.

I. Configuration and Test

A case IV electronics chassis assembly was used as the basic hardware system. Three electronic modules were instrumented. Figure I-2 displays a typical, instrumented module with three response accelerometers located in the upper, center, and lower areas of the module. Other accelerometers were attached to the case chassis. Figures I-1, I-3, and I-4 display these monitoring locations. Figure I-2 also shows the relationship between the monitoring locations on the case near the corners of a typical module. These corner accelerometers are the primary sources of data for the following analysis.

The tests were run with a full case configuration. The case was excited in two directions in the same plane — through the web axis (Z) and perpendicular to that axis (*X*). All noise tests used manual equalization with peak-notch filters.

II. Limitations of the Data

The data used in this analysis were derived from 5-s time samples analyzed with 10-Hz resolution. The resulting BT product is 50, and the statistical error (normalized standard error, ε) is estimated to be

$$\varepsilon \approx \frac{1}{\sqrt{BT}} = 0.14$$

This may be interpreted to mean that the true spectrum value lies within $\pm 14\%$ of the computed spectrum with 67% confidence.

Additional errors occur at low frequency if the spectrum is not flat because of insufficient resolution (i.e., narrow peaks and valleys are not adequately defined with 10-Hz resolution).

To cover all errors, the final estimates in this analysis are bracketed by a 4-dB-wide band (i.e., estimate ± 2 dB). This is considered to be the best engineering estimate now available.

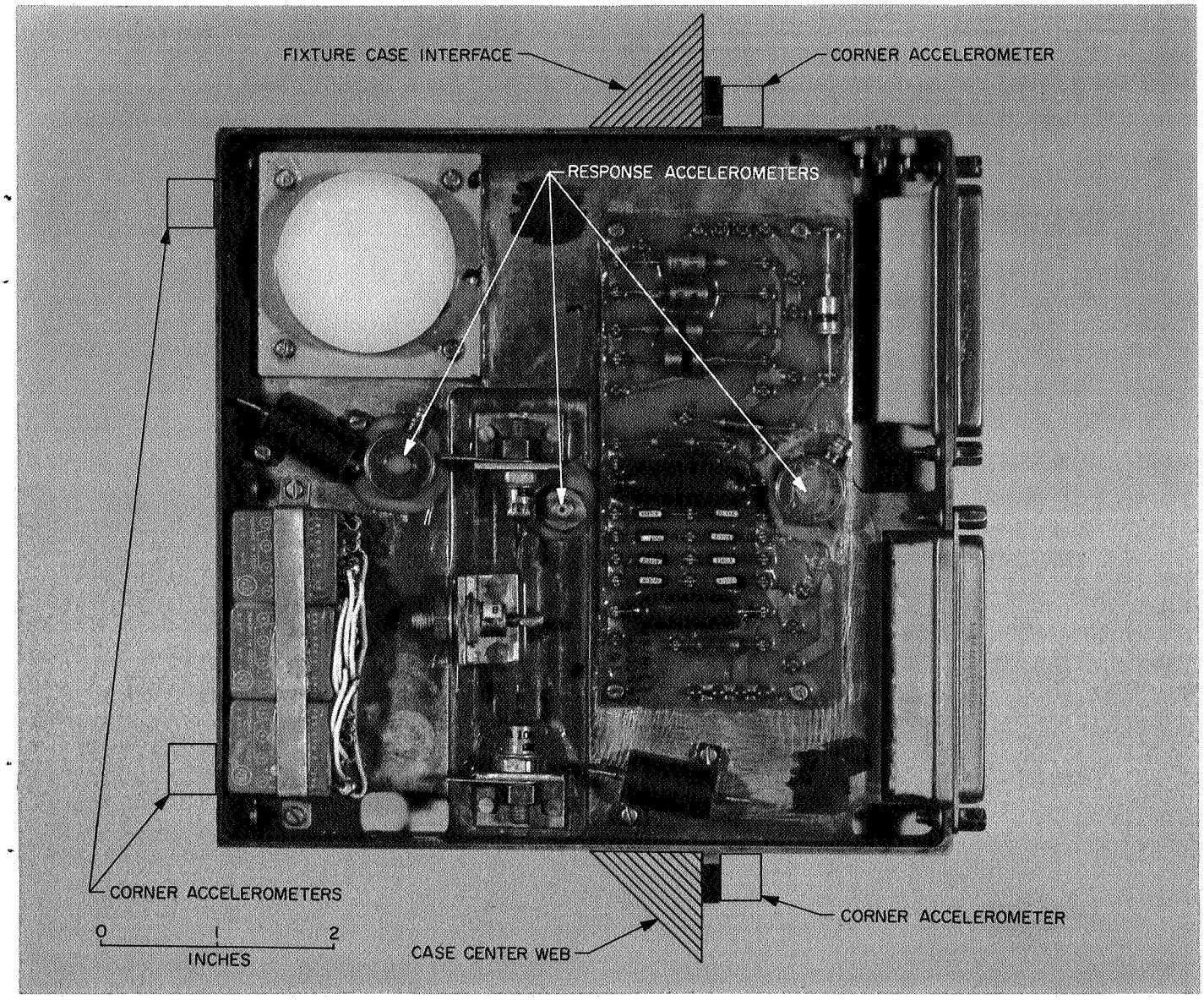

Fig. I-2. Typical case module

III. Test Analysis and Results

1. Module-input specification ratios. An input specification for individual modules can be developed from spectra ratios of the given data. The corner locations of each module are considered equivalent to a module input with a rigid module fixture. The ratios of the case-input spectra to each of these locations were averaged and are shown in Figs. I-5 and I-6.

Figure I-5 displays the mean spectra ratio for modules excited in a direction perpendicular to the module board plane. Below 500 Hz, the ratio is almost unity (0 dB), implying rigid-body motion in this range. From 500 to 1500 Hz, the data rolls off at approximately 3 dB/octave. Between 1500 and 2000 Hz, a significant gain occurs in the spectrum, probably caused by a localized case-fixture resonance not sensed by the case control accelerometer. A simplification of the ratio for practical application is

shown by the line segment envelope of Fig. I-5. Smoothing has been attempted in the envelope to facilitate actual test spectrum shaping to be discussed later.

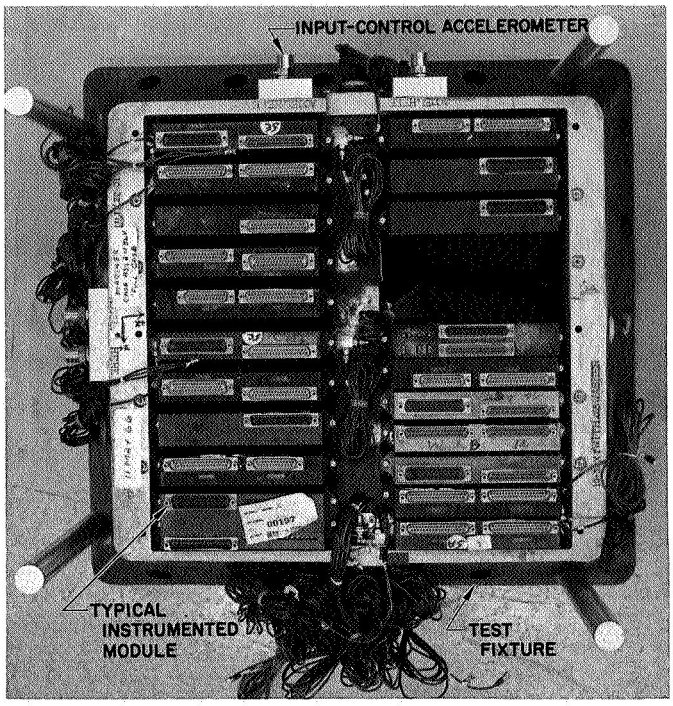

Fig. I-3. Typical case assembly test configuration

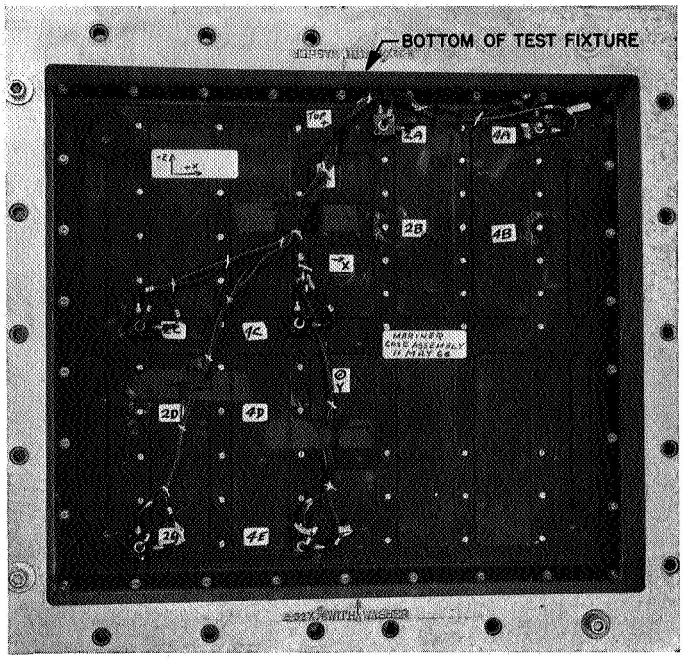

Fig. I-4. Accelerometer on lower case surface

Figure I-6 is a display of similar data with excitation parallel to a module board. Below 250 Hz, the gain is unity. Between 250 and 600 Hz, gain is near unity with the exception of a peak-notch resonance near 400 Hz that is probably caused by a module mode of vibration. From 600 to 1000 Hz, the ratio displays a significant peak-notch resonance probably attributed to a center

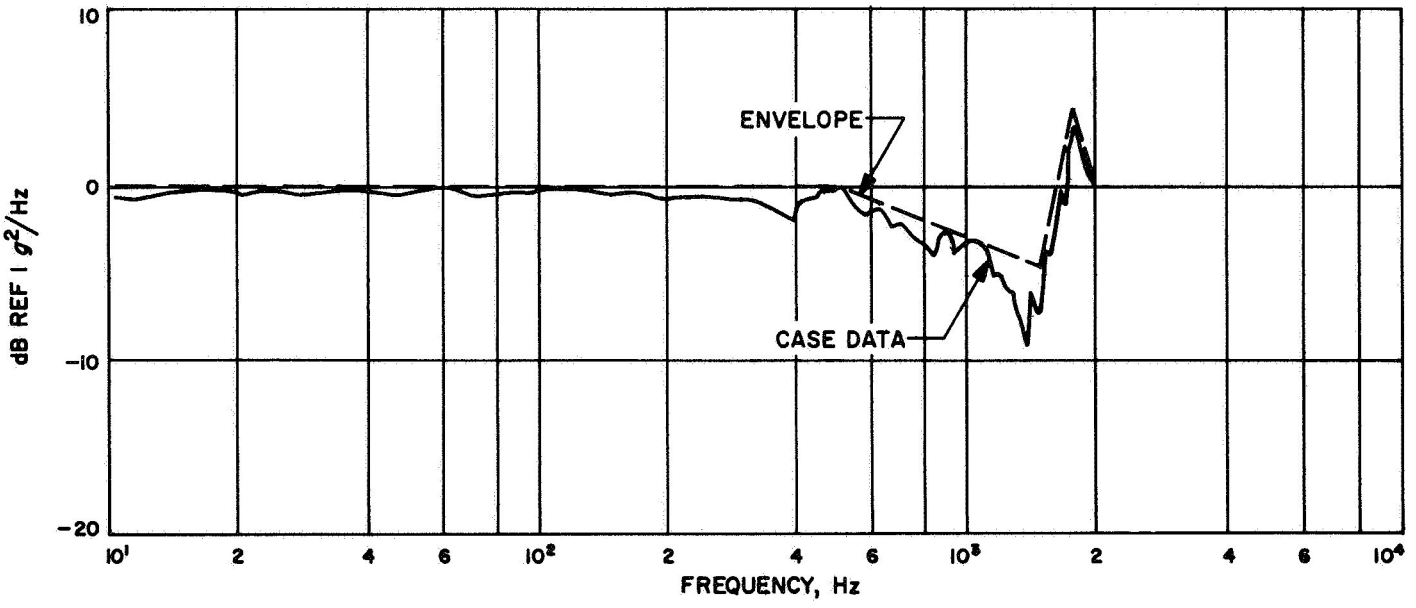

Fig. I-5. Mean spectra ratio of excitation perpendicular to module board, Z axis

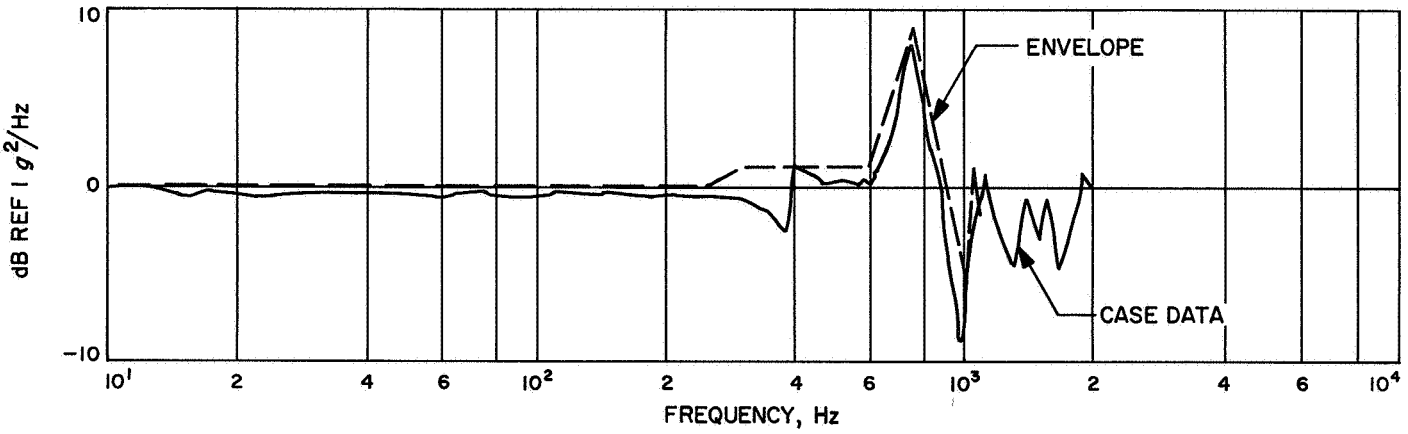

Fig. I-6. Mean spectra ratio of excitation parallel to module board, X axis

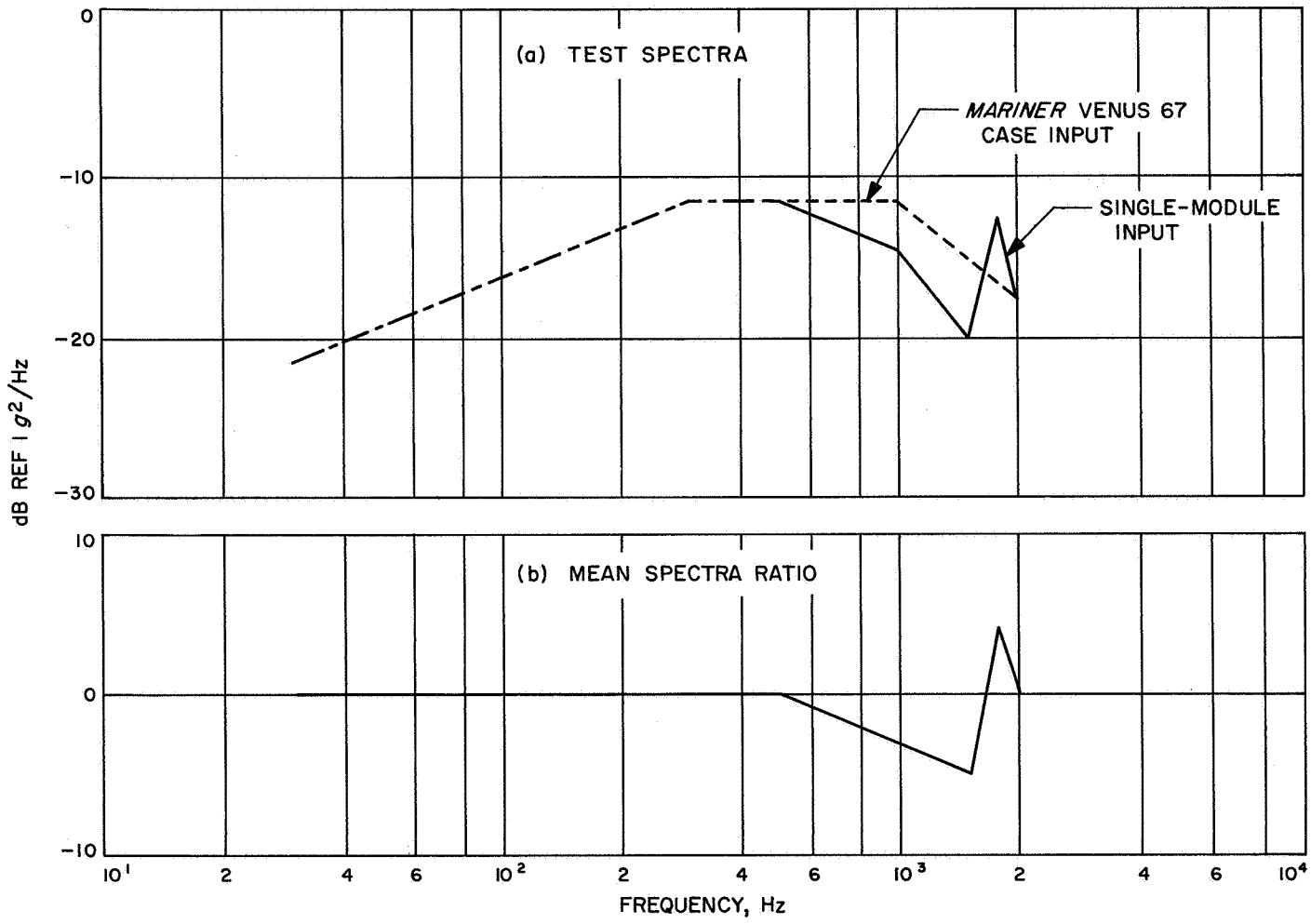

Fig. I-7. Derivation of single-module input specification for Z axis, from *Mariner* Venus 67 FA assembly spectrum

web mode of the case. The resonance is very consistent in the data samples. Above 1000 Hz, the ratio oscillates at different frequencies probably associated with modes of the fixture. The line segment envelope of Fig. I-6 smooths the data and is used for test input spectrum shaping. The envelope is more liberal than used in Fig. I-5 because of the known spread in the data for this excitation axis.

The spectra ratio envelopes are used to define a module test when given an input test spectrum for a case. Examples of this usage are given in the following paragraph.

2. Examples of single-module-input spectra. The following examples illustrate spectrum shaping of a single module input based on the derived spectra ratios and the *Mariner* Venus 67 FA assembly vibration spectrum (case-input spectrum).

Figure I-7 contains the module-input spectrum (I-7a) based on the derived spectra ratio envelope (I-7b) redrawn from Fig. I-6. The module-input spectrum is the product of the *Mariner* Venus 67 spectrum and the spectra ratio envelope at each frequency. Below 500 Hz, the input spectrum remains unchanged. Above 2000 Hz and below 30 Hz, the spectrum rolls off at 24 dB/octave.

Figure I-8 displays a similar derivation of a single-module-input excitation in the *X* axis, or parallel to a module board. The final input spectrum rolls off at 24 dB/octave above 2000 Hz and below 30 Hz.

The final single-module-input spectra are given in Fig. I-9. The desired or mean spectrum is given by the solid curves. The deviation allowed is given by the two dashed curves about each mean spectrum. Errors discussed earlier are accounted for by these tolerance bands. Above 2000 Hz, and below 30 Hz, the mean spectrum rolls off at least 24 dB/octave.

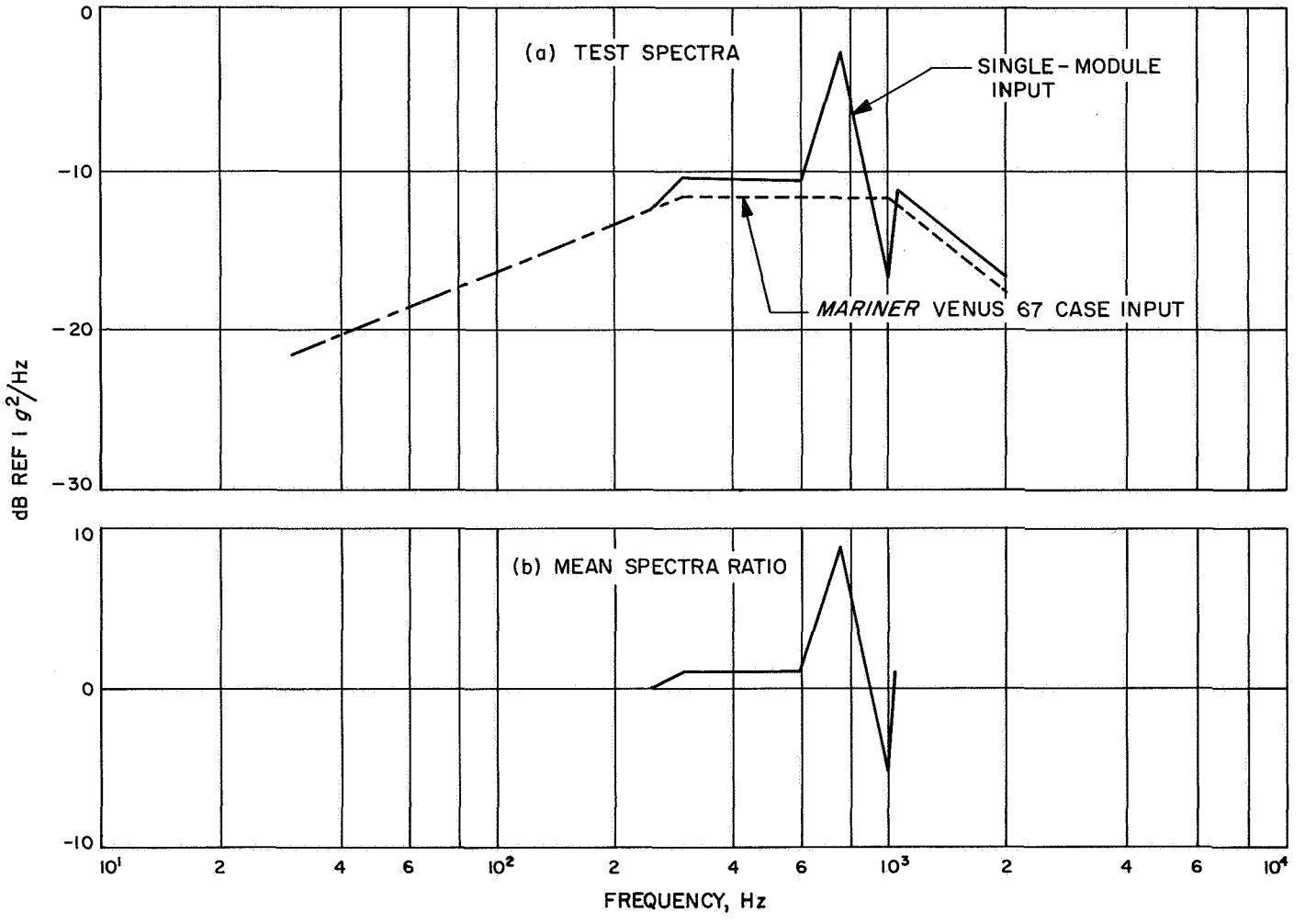

Fig. I-8. Derivation of single-module input specification for X axis, from *Mariner* Venus 67 FA assembly spectrum

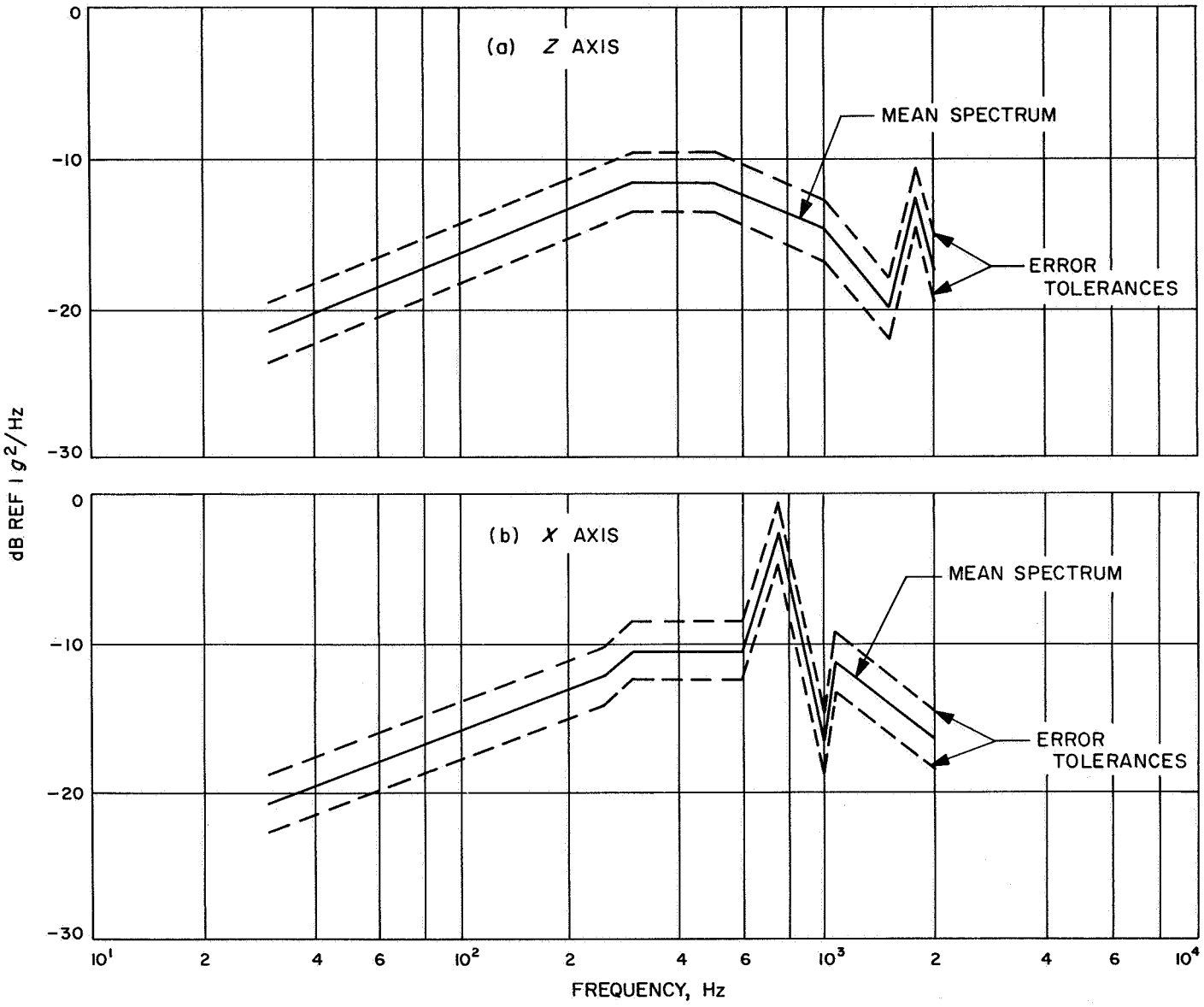

Fig. I-9. Single-module input noise spectra

IV. Conclusions

Single-module noise vibration testing can use the given curves of Fig. I-9. The final spectra seem to be discontinuous at certain frequencies, but the tolerances would allow smoothing in these areas. Implementation of the test is within the capability of the Auto 80 equalizer described in Appendix J.

Appendix J

Differences in Power Spectral Density Analyses Between IBM 7094 Digital Analysis and Auto 80 Analog Analysis

I. Analytical Comparison

Analysis of the control accelerometer data from this test showed noticeable differences in smoothness of the power spectral density curves for the two methods of data reduction. Onsite data reduction and test control was obtained using the MB T 588 automatic spectrum equalizer and analyzer (Auto 80) with a scanning device which sampled the response of the six control accelerometers in real time. Upon completion of the test, all accelerometer data, including the control accelerometer data, were analyzed digitally using the IBM 7094 computer. The fact that the two methods present a different analysis of the same phenomenon does not necessarily invalidate either method, but is cause to examine the capabilities, limitations, and relative merits of each method; and based upon desired confidence, available time, and resources, decide which method is best applied under the circumstances.

Figure J-1 is the onsite Auto 80 analysis of the scanned control accelerometer signal for the *XY* bay II (run 3) random noise test. Figure J-2 is the digital analysis of the six control accelerometers averaged in the frequency domain for the same test. It can be seen that around 800 to 900 Hz, the Auto 80 analysis shows a spread of approximately 1 dB. However, the IBM 7094 digital analysis shows a spread of approximately 10.5 dB. It should be noted, at this point, that test compliance is demonstrated with the Auto 80 analysis – not with the IBM 7094 digital analysis.

Smaller differences exist for the *XY* bay VIII axis random noise (run 5) controls – approximately a 2 dB spread for the Auto 80 analysis and 8 dB for the IBM 7094 analysis in the 800 to 900 Hz range. The differences in the apparent smoothness are not confined to the 800 to 900-Hz frequency range, where the maximum differences occur, but are evident throughout the frequency range of the analysis (20 to 2000 Hz). Since the analysis time (sample length) and resolution (bandwidth) for the power spectrum measurement was finite in both analysis methods, the resultant spectra are approximations to the actual spectra. The quality of the resultant spectra is primarily dependent on two analysis parameters: resolution (bandwidth) and analysis time (sample length).

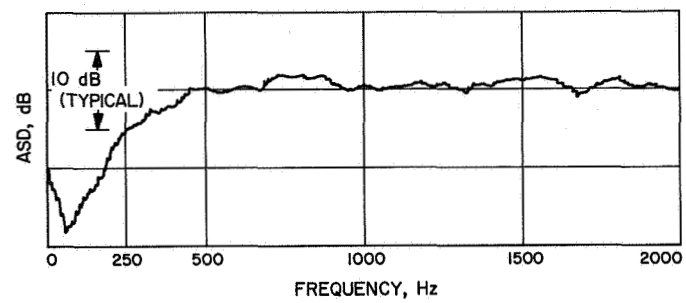

Fig. J-1. Auto 80 real-time analysis of vibration control, bay II *XY* axis, run 3

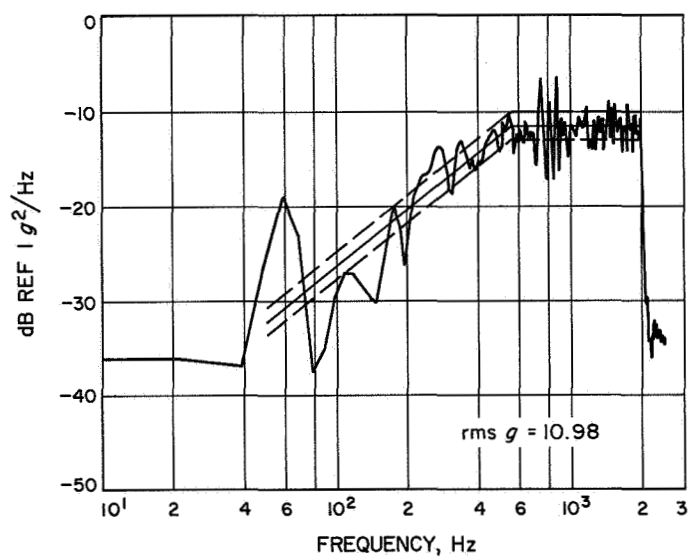

Fig. J-2. Average of six controls, 20-Hz resolution and 2.5-s sample length

The detector in the Auto 80 analyzer is a compromise between a peak and averaging detector. In addition, it is known that there are two time constants associated with the detector; a time constant T_c, which governs the rate of rise of the detector's response, and a time constant T_d, which governs the decay rate of the detector. These time constants for a random noise signal applied to the detector are known ($T_d \approx 23$ s and $T_c \approx 8$ s). It is not possible at this time to generate an exact equivalent analysis time or the number of statistical degrees of freedom associated with this analyzer. An equivalent

T_d time constant for this system, analyzing a random noise signal, is probably between 10 and 15 s. The 2.5-s sample length for the digital analysis represents the true averaging time for this method. The effective time constant of the Auto 80 detector, as represented by T_d ($10 < T_d < 15$ s), cannot be directly compared with the 2.5-s sample length of the digital analysis. For the same number of statistical degrees of freedom or for the same statistical reliability, the duration of the true average (sample length of the digital analysis) should be twice the time constant of the continuously averaging detector. Therefore, for a comparable Auto 80 and IBM 7094 analysis, the digital sample length should be between 20 and 30 s (for comparable bandwidths). Figure J-3 of this appendix is a digital analysis of the average of the six control accelerometers from run 3 (*XY* bay II axis), using the following analysis parameters:

Analysis time	20 s
Resolution	25 Hz

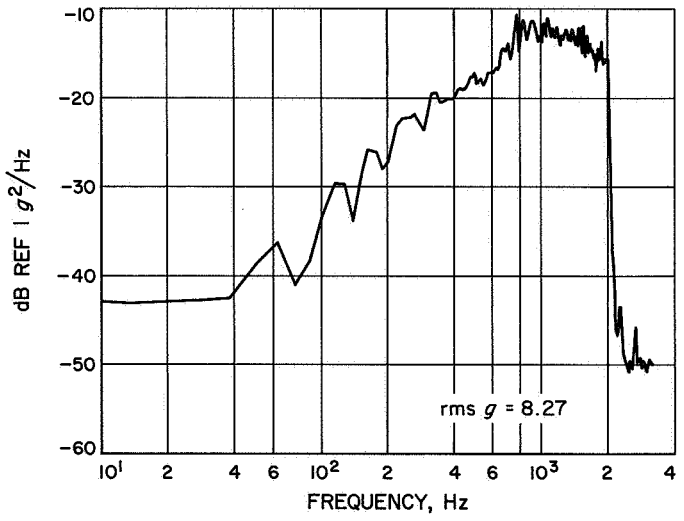

Fig. J-3. Average of six controls, 25-Hz resolution and 20-s sample length

Notice that this presentation is much smoother than Fig. J-2 curves (2.5-s sample and 20-Hz resolution) and approximates the smoothness of the Auto 80 analysis (Fig. J-1).

The effect of changing the bandwidth of the analysis can be seen by comparing the digital analyses of Figs. J-4 and J-5. Both analyses were derived from a 20-s sample length, but Fig. J-4 presents an analysis using a 25-Hz resolution, and Fig. J-5 represents a 20-Hz

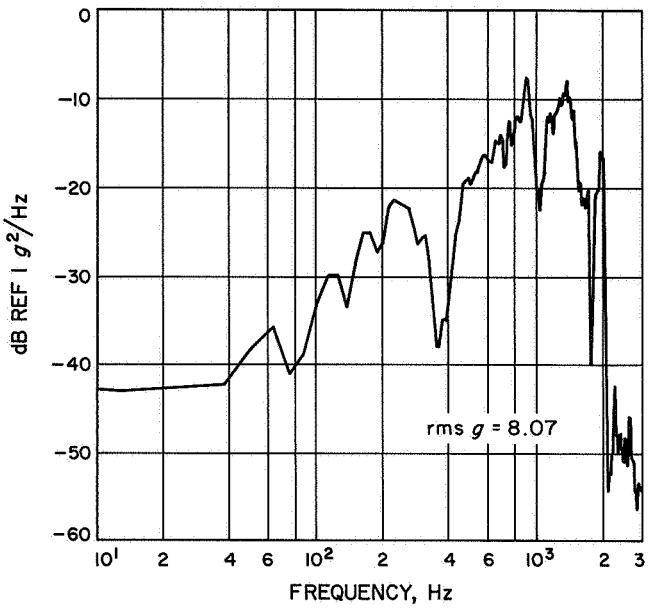

Fig. J-4. Sample analysis using a 25-Hz resolution and 20-s sample length

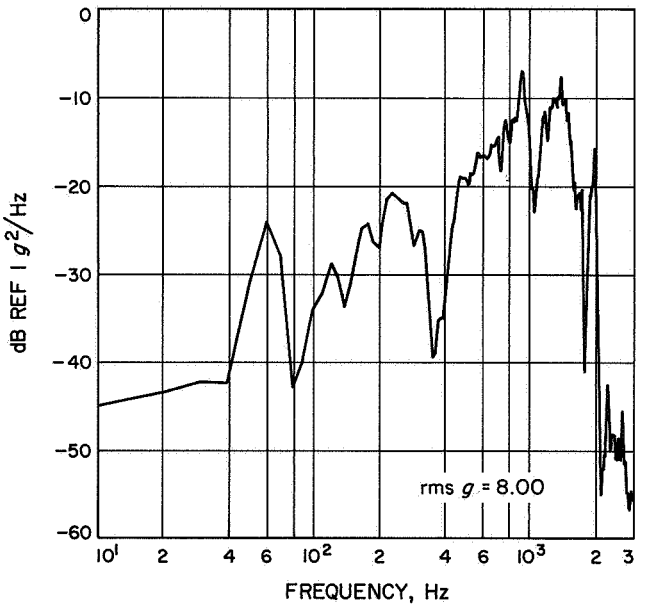

Fig. J-5. Sample analysis using a 20-Hz resolution and 20-s sample length

analysis. It can be seen that the 25-Hz analysis is only slightly smoother than the 20-Hz analysis.

II. Conclusions

The analyses provided by the Auto 80 analyzer used for this test presents a power spectral density curve that

more closely approximates the actual PSD than does the digital analysis with a 2.5-s sample length. Demonstration of specification compliance using the Auto 80 is adequate. To achieve closer agreement between the Auto 80 analysis and the IBM 7094 digital analysis, it would be necessary to use a sample length between 20 and 30 s. This would entail considerably more computer time than currently used, and therefore, greater expense. Considering the present application of the digitally reduced data, the 2.5-s sample length is adequate.

Nomenclature

A/C	attitude control
APAC	antenna pointing-angle change
ACRAD	absolute cone radiometer
ASD	acceleration spectral density
ATM	antenna test model
BCE	bench checkout equipment
CC&S	central computer & sequencer
DAS	data automation system
DFR	dual-frequency receiver
DTM	developmental test model
ECR	Environmental Change Request
EMC	electromagnetic compatibility
EMI	electromagnetic interference
f	frequency
FA	flight acceptance
IR	infrared
MC-1	*Mariner C* block PTM
MC-2	spacecraft became *Mariner III*
MC-3	spacecraft became *Mariner IV*
MC-4	*Mariner IV* spare
M67-1	*Mariner* Venus 67 flight-support spacecraft
M67-2	spacecraft became *Mariner V*
OSE	operational support equipment
PAS	pyrotechnic arming switch
PCU	pyrotechnic control unit
PFR	Problem/Failure Report
PIPS	post-injection propulsion system
PSD	power spectral density
PSO	planet sensor output
PTM	proof test model
RIM	relative intensity monitor
SAF	spacecraft assembly facility
SIT	separation-initiated timer
SN	serial number
SPSL	sound-pressure-spectrum level
STM	structural test model
TA	type approval
TCFM	temperature-control flux monitor
TCM	thermal control model
TCR	thermal control reference
TOP	Test and Operations Plan
TRD	trapped radiation detector
TRSF	Test Results Summary Form
TVCA	thrust-vector-control assembly
UHF	ultra-high frequency
UV	ultraviolet
VHF	very high frequency

References

1. Freeland, R. E., *Mariner Venus 67 Structural Development and Qualification Vibration Test Report,* Technical Report 32-1161. Jet Propulsion Laboratory, Pasadena, Calif., November 1, 1967.

2. Swenson, D. H., *Electromagnetic Interference Test Report of the Mariner Venus 67 Canopus Sensor,* Technical Memorandum 33-365. Jet Propulsion Laboratory, Pasadena, Calif., December 15, 1967.

3. Brand, D. O., *Mariner Venus 67 Dynamic Flight Data,* Technical Report 32-1185. Jet Propulsion Laboratory, Pasadena, Calif., March 15, 1968.

4. Barnett, P. M., *Mariner Venus 67 Flight Acceptance Pyrotechnic Test,* Technical Report 32-1218. Jet Propulsion Laboratory, Pasadena, Calif., December 15, 1967.

5. Forlifer, W. R., *The Effects of Filter Bandwidth in Spectrum Analysis of Random Vibration, DOD Shock and Vibration Bulletin, No. 33, Part II,* February 1964.

6. Bendat, J. S., and Piersol, A. G., *Measurement and Analysis of Random Data,* John Wiley & Sons, Inc., New York, 1966.